

Mechanotransduction in vascular development and disease

Edited by

Julia J. Mack, Brian Gene Coon and Nicolas Baeyens

Published in

Frontiers in Physiology



FRONTIERS EBOOK COPYRIGHT STATEMENT

The copyright in the text of individual articles in this ebook is the property of their respective authors or their respective institutions or funders. The copyright in graphics and images within each article may be subject to copyright of other parties. In both cases this is subject to a license granted to Frontiers.

The compilation of articles constituting this ebook is the property of Frontiers.

Each article within this ebook, and the ebook itself, are published under the most recent version of the Creative Commons CC-BY licence. The version current at the date of publication of this ebook is CC-BY 4.0. If the CC-BY licence is updated, the licence granted by Frontiers is automatically updated to the new version.

When exercising any right under the CC-BY licence, Frontiers must be attributed as the original publisher of the article or ebook, as applicable.

Authors have the responsibility of ensuring that any graphics or other materials which are the property of others may be included in the CC-BY licence, but this should be checked before relying on the CC-BY licence to reproduce those materials. Any copyright notices relating to those materials must be complied with.

Copyright and source acknowledgement notices may not be removed and must be displayed in any copy, derivative work or partial copy which includes the elements in question.

All copyright, and all rights therein, are protected by national and international copyright laws. The above represents a summary only. For further information please read Frontiers' Conditions for Website Use and Copyright Statement, and the applicable CC-BY licence.

ISSN 1664-8714
ISBN 978-2-8325-5816-4
DOI 10.3389/978-2-8325-5816-4

About Frontiers

Frontiers is more than just an open access publisher of scholarly articles: it is a pioneering approach to the world of academia, radically improving the way scholarly research is managed. The grand vision of Frontiers is a world where all people have an equal opportunity to seek, share and generate knowledge. Frontiers provides immediate and permanent online open access to all its publications, but this alone is not enough to realize our grand goals.

Frontiers journal series

The Frontiers journal series is a multi-tier and interdisciplinary set of open-access, online journals, promising a paradigm shift from the current review, selection and dissemination processes in academic publishing. All Frontiers journals are driven by researchers for researchers; therefore, they constitute a service to the scholarly community. At the same time, the *Frontiers journal series* operates on a revolutionary invention, the tiered publishing system, initially addressing specific communities of scholars, and gradually climbing up to broader public understanding, thus serving the interests of the lay society, too.

Dedication to quality

Each Frontiers article is a landmark of the highest quality, thanks to genuinely collaborative interactions between authors and review editors, who include some of the world's best academicians. Research must be certified by peers before entering a stream of knowledge that may eventually reach the public - and shape society; therefore, Frontiers only applies the most rigorous and unbiased reviews. Frontiers revolutionizes research publishing by freely delivering the most outstanding research, evaluated with no bias from both the academic and social point of view. By applying the most advanced information technologies, Frontiers is catapulting scholarly publishing into a new generation.

What are Frontiers Research Topics?

Frontiers Research Topics are very popular trademarks of the *Frontiers journals series*: they are collections of at least ten articles, all centered on a particular subject. With their unique mix of varied contributions from Original Research to Review Articles, Frontiers Research Topics unify the most influential researchers, the latest key findings and historical advances in a hot research area.

Find out more on how to host your own Frontiers Research Topic or contribute to one as an author by contacting the Frontiers editorial office: frontiersin.org/about/contact

Mechanotransduction in vascular development and disease

Topic editors

Julia J. Mack — UCLA Health System, United States

Brian Gene Coon — Oklahoma Medical Research Foundation, United States

Nicolas Baeyens — Université libre de Bruxelles, Belgium

Citation

Mack, J. J., Coon, B. G., Baeyens, N., eds. (2024). *Mechanotransduction in vascular development and disease*. Lausanne: Frontiers Media SA.

doi: 10.3389/978-2-8325-5816-4

Table of contents

- 04 **Editorial: Mechanotransduction in vascular development and disease**
Nicolas Baeyens, Brian G. Coon and Julia J. Mack
- 06 **Origin and flow-mediated remodeling of the murine and human extraembryonic circulation systems**
Kristof Van Schoor, Emmanuel Bruet, Elizabeth Anne Vincent Jones and Isabelle Migeotte
- 20 **Life at the crossroads: the nuclear LINC complex and vascular mechanotransduction**
Pauline Bougaran and Victoria L. Bautch
- 35 **Unraveling neurovascular mysteries: the role of endothelial glycocalyx dysfunction in Alzheimer's disease pathogenesis**
Nicholas O'Hare, Karina Millican and Eno E. Ebong
- 56 **Anatomical location, sex, and age modulate adipocyte progenitor populations in perivascular adipose tissues**
C. Javier Rendon, Lorenzo Sempere, Adam Lauver, Stephanie W. Watts and G. Andres Contreras
- 70 **Blood shear stress during the cardiac cycle and endothelial cell orientation and polarity in the carotid artery of male and female mice**
Nabil Nicolas, Alexandre de Tilly and Etienne Roux
- 82 **Flow-mediated modulation of the endothelial cell lipidome**
Soon-Gook Hong, John P. Kennelly, Kevin J. Williams, Steven J. Bensinger and Julia J. Mack
- 95 **Capturing physiological hemodynamic flow and mechanosensitive cell signaling in vessel-on-a-chip platforms**
A. Martier, Z. Chen, H. Schaps, M. J. Mondrinos and J. S. Fang
- 109 **Vicious cycle of oxidative stress and neuroinflammation in pathophysiology of chronic vascular encephalopathy**
Tetiana R. Dmytriv, Khrystyna V. Duve, Kenneth B. Storey and Volodymyr I. Lushchak
- 121 **Mechanotransduction of the vasculature in Hutchinson-Gilford Progeria Syndrome**
Kevin L. Shores and George A. Truskey
- 134 **Endothelial cell elongation and alignment in response to shear stress requires acetylation of microtubules**
Katiannah Moise, Keerthana M. Arun, Maalavika Pillai, Jocelynda Salvador, Aarya S. Mehta, Yogesh Goyal and M. Luisa Iruela-Arispe



OPEN ACCESS

EDITED AND REVIEWED BY

Irena Levitan,
University of Illinois Chicago, United States

*CORRESPONDENCE

Julia J. Mack,
✉ jmack@mednet.ucla.edu

RECEIVED 08 November 2024

ACCEPTED 25 November 2024

PUBLISHED 10 December 2024

CITATION

Baeyens N, Coon BG and Mack JJ (2024)
Editorial: Mechanotransduction in vascular
development and disease.
Front. Physiol. 15:1525184.
doi: 10.3389/fphys.2024.1525184

COPYRIGHT

© 2024 Baeyens, Coon and Mack. This is an
open-access article distributed under the terms
of the [Creative Commons Attribution License
\(CC BY\)](#). The use, distribution or reproduction in
other forums is permitted, provided the original
author(s) and the copyright owner(s) are
credited and that the original publication in this
journal is cited, in accordance with accepted
academic practice. No use, distribution or
reproduction is permitted which does not
comply with these terms.

Editorial: Mechanotransduction in vascular development and disease

Nicolas Baeyens¹, Brian G. Coon^{2,3} and Julia J. Mack^{4*}

¹Laboratoire de Physiologie et Pharmacologie, Faculté de Médecine, Université libre de Bruxelles, Brussels, Belgium, ²Cardiovascular Biology Program, Oklahoma Medical Research Foundation, Oklahoma City, OK, United States, ³Department of Cell Biology, University of Oklahoma Health Sciences Center, Oklahoma City, OK, United States, ⁴Department of Medicine, Division of Cardiology, University of California, Los Angeles, Los Angeles, CA, United States

KEYWORDS

blood flow, hemodynamics, shear stress, vascular disease, mechanotransduction, vascular development, endothelial

Editorial on the Research Topic

Mechanotransduction in vascular development and disease

This Research Topic of reviews and research articles focuses on the Research Topic of vascular mechanotransduction. Articles cover various aspects of vascular mechanobiology, but with special emphasis on understanding the role of the hemodynamic microenvironment on cell signaling, cellular organization, vascular inflammation, and physiological function.

Endothelial cell responses to blood flow depends on various environmental and intrinsic factors. However, a typical response involves cytoskeletal, nuclear, and Golgi apparatus orientation in line with the flow direction. Through a thorough *in vivo* experiment, [Nicolas et al.](#) accurately defined the hemodynamics parameters of the mouse carotid artery during systole and diastole, estimating wall shear stress by using a modified equation to estimate blood behavior in smaller vessels. They analyzed endothelial cell polarity by *en-face* staining, confirming that endothelial cells align against flow direction in small arteries. Continuing in the theme of endothelial cell polarity with flow, *in vitro* work from [Moise et al.](#) deciphered how physiological and unidirectional wall shear stress transduces endothelial cell polarization through acetylation of microtubules and increased polymerization, bridging flow-mediated cell polarity with all components of the cellular cytoskeleton.

Hemodynamic forces are not uniform through the vascular network and organotypic adaptation is a critical feature of organ function. Thus, there is increasing interest to model hemodynamics and vessel structure/function in organoids. The review by [Martier et al.](#) summarizes current platforms and discusses *in vitro* models that include a vascular compartment. Considering mechanosensitive signaling regulates the characteristics of a healthy vasculature, *in vitro* models that include hemodynamic flow will better recapitulate *in vivo* settings. In one example, [Hong et al.](#) use an *in vitro* system to recapitulate the different endothelial cell phenotypes associated with unidirectional laminar flow (UF) and disturbed flow (DF). Performing complementary RNA sequencing and lipidomics, the authors revealed that genes associated with lipid metabolism and specific lipid species are altered under DF. Interestingly, they found that the endothelial inflammatory state, induced by DF or an inflammatory agonist, increases total lipid abundance in cells. Whether this

lipid increase is a protective response of the cell is unknown. Ultimately, the work provides transcriptomic and lipidomic datasets of aortic endothelial cells to interrogate how the local flow pattern contributes to vascular inflammation.

Regarding fundamental cell responses to shear stress, [Bougaran and Bautch](#) review the roles of the nuclear LINC complex in endothelial mechanotransduction and force sensing. The review touches on key functions of the LINC complex components, including SUN and nesprin proteins. It describes recent evidence that SUN1 and SUN2 orchestrate a mechanosensing response that extends both inward to the nuclear chromatin and outward to cell-cell and cell-matrix junctions. The authors further discuss these findings with vascular pathologies such as Hutchinson-Gilford progeria syndrome (HGPS), a premature aging disorder with cardiovascular impairment. Following the importance of nuclear mechanosensing, [Shores and Truskey](#) review HGPS disease pathology and the disrupted mechanics of nuclear mechanotransduction. The disease, associated with the accumulation of progerin, a mutated form of the nuclear lamina protein lamin A, disrupts nuclear integrity and leads to cell senescence and overall dysfunction. The review focuses on the consequence of progerin accumulation in vascular cells, specifically endothelial and smooth muscle, and suggests that dysfunctional mechanotransduction plays a role in the pathobiology of HGPS.

The adventitia of the aorta is lined with connective tissue, fat, lymphatics, and microvasculature. As aortic segments have different developmental origins and propensity to disease, it is important to consider the local vessel composition. The study by [Rendon et al.](#) focuses on the spatial-temporal changes to adipocyte progenitor cell (APC) and APC-subtype populations along the aortic and mesenteric vascular systems. Using short-term labeling of APCs, the authors found that aged mice lose perivascular APCs in the thoracic aortas but gain them, preferentially in female mice, in the mesenteric vasculature without a significant change in blood pressure. Notably, the adventitia of the thoracic and abdominal aorta is associated with different expression of APC subtype markers.

Moving onto the cerebral vasculature, the review by [Dmytriv et al.](#) discusses the onset and progression of cognitive impairment associated with chronic vascular encephalopathy (CVE). CVE occurs after prolonged reduction of blood flow to the brain. The lack of cerebral blood flow causes insufficient oxygenation, leading to hypoxia and the development of oxidative/reductive stresses. The authors discuss how the hypoxia-induced challenges in CVE, specifically oxidative stress and inflammation, work in concert to advance degeneration. Interestingly, they highlight potential therapeutic approaches to treating CVE, to alleviate the cognitive impairments.

Considering the global population is aging along with an increase in aging-associated diseases such as Alzheimer's disease (AD), [O'Hare et al.](#) elaborate on their hypothesis that AD is linked to dysfunctional endothelial glycocalyx. The glycocalyx is a network of plasma membrane glycoproteins and proteoglycans that act as a structural and chemical barrier. In many vascular pathologies, such as sepsis, the glycocalyx is shed concurrently with disrupted cell function. There are also instances whereby the glycocalyx thins, which might be associated with endothelial impairment. The authors review the roles of the glycocalyx and discuss the importance of perfectly tuned endothelial function in

neurovascular coupling. As neurovascular coupling defects are likely major contributors to disease progression, the authors make a strong case for considering endothelial drivers of AD.

Finally, maternal vascular adaptation during pregnancy is critical for the developing fetus. For the treatment of medical complications of pregnancy, we need a better understanding of vascular remodeling during embryogenesis. Unfortunately, research in this area is complicated because human samples are difficult to obtain, and there are differences between human and mouse extraembryonic vascular structures. [Van Schoor et al.](#) review the development of the extra-embryonic circulatory systems of both mice and humans, the associated hemodynamics, and mechanosensitive signaling pathways likely to guide vascular remodeling. Since proper vascular network development involves blood flow-independent and blood flow-dependent pathways, further mechanistic studies are needed. The review brings insights into the role of hemodynamics as a cause or consequence of extraembryonic vascular remodeling.

In summary, the role of blood flow forces and cell mechanotransduction must be addressed in the context of vascular health. This Research Topic highlights the consequences of effective and defective mechanosensitive signaling and reminds us that healthy vessels are associated with healthy blood flow.

Author contributions

NB: Writing—original draft, Writing—review and editing. BC: Writing—original draft, Writing—review and editing. JM: Writing—original draft, Writing—review and editing.

Funding

The author(s) declare that no financial support was received for the research, authorship, and/or publication of this article.

Conflict of interest

The authors declare that the research was conducted in the absence of any commercial or financial relationships that could be construed as a potential conflict of interest.

Generative AI statement

The author(s) declare that no Generative AI was used in the creation of this manuscript.

Publisher's note

All claims expressed in this article are solely those of the authors and do not necessarily represent those of their affiliated organizations, or those of the publisher, the editors and the reviewers. Any product that may be evaluated in this article, or claim that may be made by its manufacturer, is not guaranteed or endorsed by the publisher.



OPEN ACCESS

EDITED BY

Brian Gene Coon,
Oklahoma Medical Research Foundation,
United States

REVIEWED BY

Ramón A. Lorca,
University of Colorado Anschutz Medical
Campus, United States
Kristina Haase,
European Molecular Biology Laboratory, Spain

*CORRESPONDENCE

Isabelle Migeotte,
✉ isabelle.migeotte@ulb.be

[†]These authors have contributed equally to this work

RECEIVED 02 March 2024

ACCEPTED 16 April 2024

PUBLISHED 16 May 2024

CITATION

Van Schoor K, Bruet E, Jones EAV and Migeotte I (2024), Origin and flow-mediated remodeling of the murine and human extraembryonic circulation systems.
Front. Physiol. 15:1395006.
doi: 10.3389/fphys.2024.1395006

COPYRIGHT

© 2024 Van Schoor, Bruet, Jones and Migeotte.
This is an open-access article distributed under the terms of the [Creative Commons Attribution License \(CC BY\)](#). The use, distribution or reproduction in other forums is permitted, provided the original author(s) and the copyright owner(s) are credited and that the original publication in this journal is cited, in accordance with accepted academic practice. No use, distribution or reproduction is permitted which does not comply with these terms.

Origin and flow-mediated remodeling of the murine and human extraembryonic circulation systems

Kristof Van Schoor^{1†}, Emmanuel Bruet^{1†},
Elizabeth Anne Vincent Jones^{2,3} and Isabelle Migeotte^{1*}

¹Institut de Recherche Interdisciplinaire Jacques E. Dumont, Université Libre de Bruxelles (ULB), Brussels, Belgium, ²Department of Cardiovascular Sciences, Centre for Molecular and Vascular Biology, Katholieke Universiteit Leuven (KU Leuven), Leuven, Belgium, ³Department of Cardiology CARIM School for Cardiovascular Diseases Maastricht University, Maastricht, Netherlands

The transduction of mechanical stimuli produced by blood flow is an important regulator of vascular development. The vitelline and umbilico-placental circulations are extraembryonic vascular systems that are required for proper embryonic development in mammalian embryos. The morphogenesis of the extraembryonic vasculature and the cardiovascular system of the embryo are hemodynamically and molecularly connected. Here we provide an overview of the establishment of the murine and human vitelline and umbilico-placental vascular systems and how blood flow influences various steps in their development. A deeper comprehension of extraembryonic vessel development may aid the establishment of stem-cell based embryo models and provide novel insights to understanding pregnancy complications related to the umbilical cord and placenta.

KEYWORDS

embryo development, allantois, umbilical cord, yolk sac, vitelline vessels, placenta, mechanotransduction, blood flow

1 Introduction

Mechanotransduction and vascular development are tightly linked together and the impact of mechanical stimuli on endothelial cells has been well documented (Campinho et al., 2020). Forces from blood flow affect endothelial cell polarization and migration, angiogenesis, lumen formation and vascular network remodeling. Three forces arise from blood flow: 1) shear stress, which is a consequence of shear flow, 2) circumferential stress, which is the force tangential to the vessel wall, and finally 3) axial stress, the force in the longitudinal axis of the vessel (Hofer et al., 2013; Campinho et al., 2020). Shear stress is influenced by flow, viscosity, and vessel diameter, but it can also in turn affect the diameter of the vessel. Circumferential stress is regulated by blood pressure, vessel diameter and wall thickness and changes in circumferential stretch impact the thickness of the vessel wall. Axial stress is changed by longitudinal force, vessel diameter and wall thickness and will regulate vessel length (Hofer et al., 2013). Mechanical stimuli from flow are sensed through several molecules including ion channels and cell-cell junctions (Table 1) (Rizzo et al., 1998; Tzima et al., 2005; Tarbell and Pahakis, 2006; Lucitti et al., 2007; Osol and Mandala, 2009; Li et al., 2014b; Li et al., 2014a; Garcia and Larina, 2014; Coon et al., 2015; Baeyens

TABLE 1 Currently identified mechanosensors of blood flow forces in endothelial cells.

Mechanosensor	Function	References
Caveolae	Mechanosensation and rapid adaptation to changes in membrane tension	Rizzo et al. (1998)
		Luse et al. (2023)
		Shin et al. (2019)
Glycocalyx	Sensation and transmission of shear stress to the actin cytoskeleton and plasma membrane	Tarbell and Pahakis (2006)
Pecam1	Mechanosensory complex	Tzima et al. (2005)
Piezo1	Mechanosensitive non-selective cation channel	Li et al. (2014a)
Plexin D1	Mechanosensor	Mehta et al. (2020)
Primary cilia	Ca ²⁺ -dependent mechanosensors	Luu et al. (2018)
VE-Cadherin	Mechanosensory complex	Tzima et al. (2005)
VEGFR2	Mechanosensory complex	Shay-Salit et al. (2002)
		Tzima et al. (2005)
VEGFR3	Mechanosensory complex	Coon et al. (2015)

and Schwartz, 2016; Luu et al., 2018; Shin et al., 2019; Campinho et al., 2020; Daems et al., 2020; Mehta et al., 2020; Luse et al., 2023).

The vessels of the vitelline and umbilico-placental circulations are required for embryo development, as they provide nutrients and gas exchange. In addition, these extraembryonic vascular systems are functionally linked to the embryonic cardiovascular system (Linask et al., 2014). Vitelline vessels rely on embryonic circulation for their morphogenesis and remodeling (Jauniaux et al., 1991; Lucitti et al., 2007; Burton and Jauniaux, 2018a). As for placental vessels, the maternal uterine vasculature plays a large role in regulating hemodynamic stimuli (Osol and Mandala, 2009).

The yolk sac is conserved in many species and is the oldest extraembryonic structure present in vertebrates. Before the development of the placenta and the onset of the umbilico-placental circulation, the yolk sac provides nutrition to the embryo (Martinelli et al., 2023). The yolk sac consists of three layers: mesothelium, mesoderm, and endoderm. The way these three layers are oriented is everted between human and mouse, with the endoderm facing the endometrium in mice. While the yolk sac and placenta in mouse are not exactly like those in human, similar cell types are present with analogous functions. The endodermal layer provides nutrition to the embryo, whereas the mesodermal layer is at the origin of haemato- and angiogenesis (Rossant and Cross, 2001; Linask et al., 2014; Martinelli et al., 2023). The mouse yolk sac envelops the entire conceptus; the parietal yolk sac deteriorates around mid-gestation while the visceral yolk sac (formed of the three layers described above) persists until term. In human, the primary yolk sac will split in two: the smaller part deteriorates while the larger portion, the secondary yolk sac, remains until the end of the 20th week of pregnancy. Different to mouse, the human yolk sac does not envelop the conceptus but extends into the extraembryonic coelom (Martinelli et al., 2023).

The allantois is the precursor for the umbilical cord in mouse (Inman and Downs, 2007; Arora and Papaioannou, 2012) and contributes to the umbilical cord in human (Spurway et al., 2012; Basta and Lipsett, 2023). The murine allantois is capable of developing its vasculature independently and can be isolated and cultured *ex vivo* or transplanted to study vascular development and

chorio-allantoic fusion (Downs and Harmann, 1997; Diehl et al., 2001; Downs et al., 2001; Downs, 2006; Arora and Papaioannou, 2012; Hou et al., 2016; Hadamek et al., 2018). In human, the umbilical cord contains one umbilical vein and two umbilical arteries (Spurway et al., 2012; Ramesh et al., 2015; Li et al., 2019; Ebbing et al., 2020), whereas the umbilical cord in mouse has single umbilical artery and vein (Inman and Downs, 2007). In human, the presence of only one umbilical artery may be associated with pregnancy and postnatal complications (Ramesh et al., 2015; Li et al., 2019; Ebbing et al., 2020).

The mesoderm layer of the yolk sac is the site where the first endothelial and blood cells form, in structures known as the blood islands, around embryonic day (E) 7 in mouse embryos (Lucitti et al., 2007; Linask et al., 2014; Martinelli et al., 2023). Primitive erythroblasts from the yolk sac enter the circulation after the heart starts beating, around E8 in mouse embryos (Lucitti et al., 2007). Live imaging data showed that endothelial cells originating from the yolk sac contribute to the endocardium, head vasculature and dorsal aortae in the mouse embryo (Collart et al., 2021), thereby confirming that the vitelline and embryonic vascular systems share cells of a similar origin. Aside from this cellular link, the extraembryonic vasculatures and the fetal cardiovascular system are also hemodynamically connected (Lucitti et al., 2007; Garcia and Larina, 2014; Linask et al., 2014; Burton and Jauniaux, 2018a; 2018b; Jauniaux et al., 2020). These connections will be the focus of this review, based on experimental data in mouse and findings from rare samples as well as functional analysis of pregnancies in human.

2 Mechanotransduction in the murine vitelline and umbilico-placental vasculatures

2.1 Vitelline vasculature

2.1.1 From blood islands to vessels

The blood islands arise around E7-E7.5 in the proximal yolk sac (Figures 1A, B); they consist of endothelial (angioblasts) and

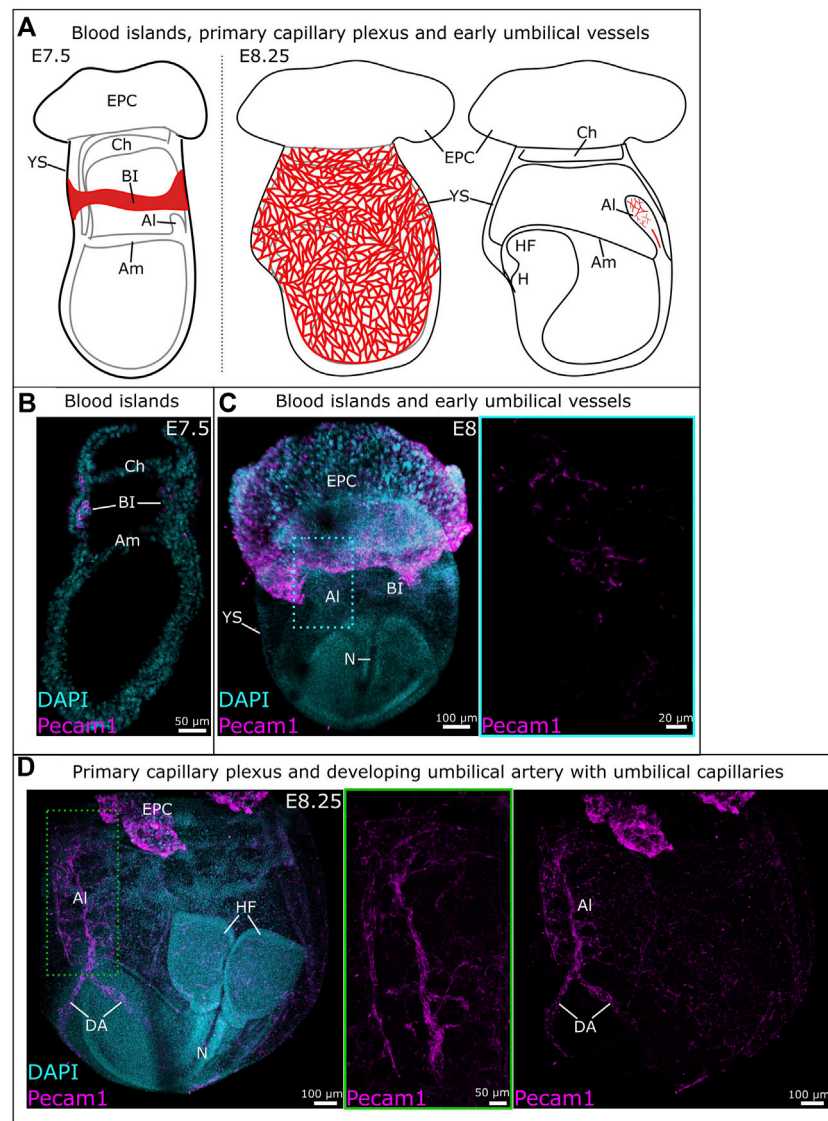


FIGURE 1

Development of vitelline and umbilical vessels between E7.5 and E8.25. **(A)** Schematic overview of vitelline vascular development from blood islands at E7.5 (left) to the primary capillary plexus at E8.25 (middle). Schematic representation of early umbilical vascular development at E8.25 (right). **(B)** Sagittal cryosection of an E7.5 mouse embryo. Blood islands were identified through immunofluorescent staining for Pecam1. **(C)** Whole mount E8 mouse embryo with vessels identified through Pecam1 staining. The blue frame provides a close-up of the umbilical vasculature. **(D)** Whole mount E8.25 mouse embryo with the umbilical vasculature (middle) and primary capillary plexus (right). A close-up of the umbilical vessels is provided in the green frame where the z-slices containing the vitelline vessels have been removed. AI: allantois; Am: amnion; BI: blood islands; Ch: chorion; DA: dorsal aorta; EPC: ectoplacental cone; H: heart; HF: headfold; N: notochord; YS: yolk sac.

hematopoietic progenitors. The first vessels are formed through vasculogenesis, prior to the start of hemodynamic forces (Lucitti et al., 2007; Garcia and Larina, 2014; Linask et al., 2014; Martinelli et al., 2023). Outer angioblasts proliferate and differentiate into endothelial cells that migrate distally into the yolk sac and organize into a rudimentary network of vessels (Ferkowicz et al., 2003). This network is known as the primary capillary plexus and is fully established around E8.5 (Figures 1A, C) (Udan et al., 2013a; Garcia and Larina, 2014). Around this same time (E8–E8.5), the embryonic heart starts beating, which triggers blood flow and thereby hemodynamic forces (Lucitti et al., 2007; Garcia and Larina, 2014; Linask et al., 2014).

Between E8.5 and E9.5, the vitelline vasculature remodels under the influence of mechanical stimuli originating from blood flow and circulating primitive erythroblasts (Lucitti et al., 2007). The remodeled vasculature of the yolk sac consists of a structured, hierarchical network of vessels with functional arteries and veins (Figures 2B, D, E) (Garcia and Larina, 2014). This remodeling is essential to the survival of the embryo, as demonstrated by the phenotype of several genetically modified mouse lines (Table 2). For example, impairment of TGF β (Carvalho et al., 2007) or Notch (Krebs et al., 2004) signaling prevent vitelline vasculature remodeling and result in embryonic death at E10.5. Yolk sac vessels in Neuropilin-1 knockout embryos have a large diameter

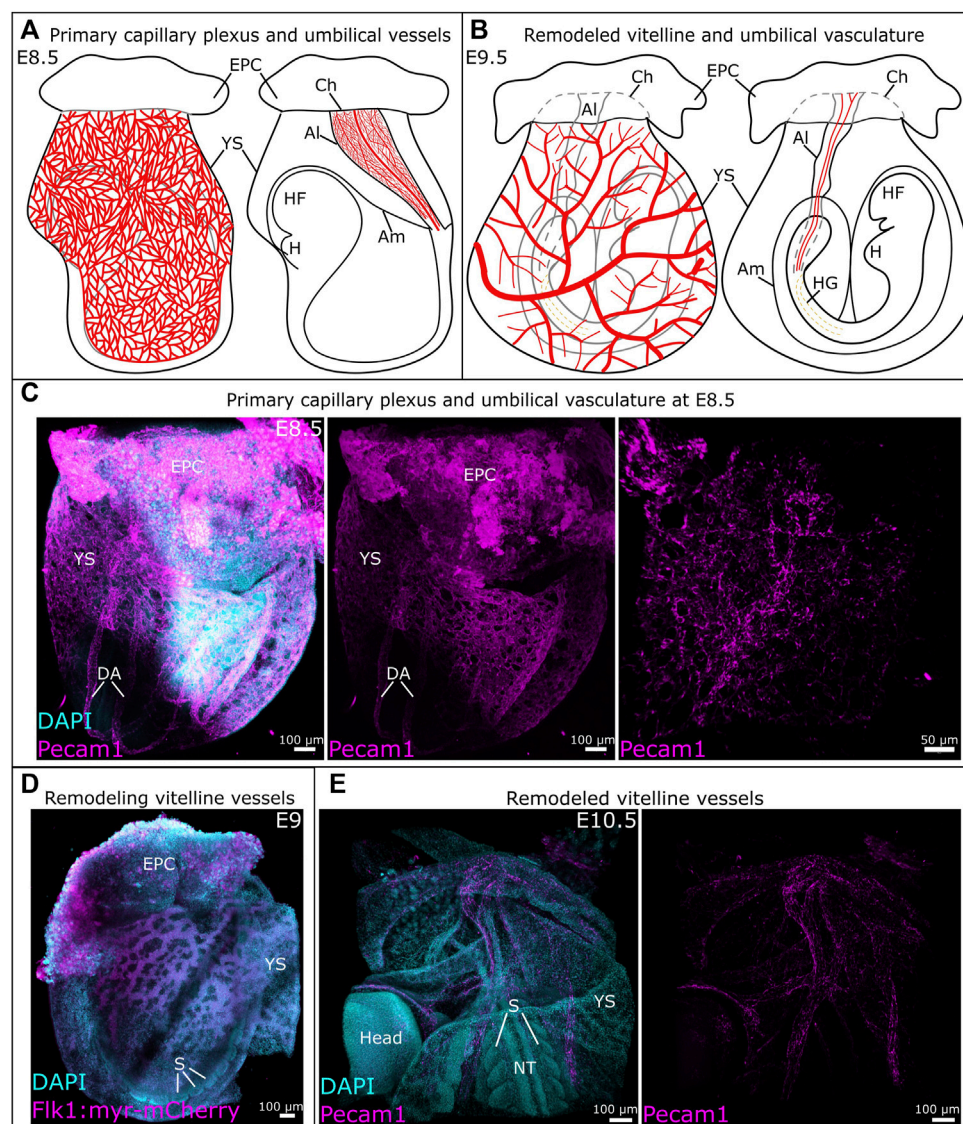


FIGURE 2

Development of vitelline and umbilical vessels between E8.5 and E10.5. (A) Schematic representation of the primary capillary plexus (left) and umbilical vessels (right) at E8.5. (B) Schematic overview of the remodeled vitelline vasculature (left) and umbilical vessels (right). (C) Whole mount E8.5 mouse embryo with vessels identified by Pecam1. A detailed view of the umbilical vessels is provided in the image on the right. (D) The remodeling vitelline vasculature in a Tg (Flk1::myr-mCherry) mouse embryo at E9. (E) The remodeled vitelline vascular system at E10.5, vessels are visualized through Pecam1. Al, allantois; Am, amnion; Ch, chorion; DA, dorsal aorta; EPC, ectoplacental cone; H, heart; HF, headfold; HG, hindgut; NT, neural tube; S, somite; YS, yolk sac.

and fail to remodel (Jones et al., 2008). Deletion of *Piezo1* impairs mechanosensation, which results in a failure to rearrange the network and ultimately embryonic death (Li et al., 2014a). In *Foxo1*^{-/-} embryos, even though blood flow is normal, failure to remodel leads to embryonic death by E10.5 (Li-Villarreal et al., 2022).

2.1.2 Blood flow forces drive the remodeling of the primary capillary plexus to a mature vascular system

Circulation of primitive erythroblasts from the yolk sac starts around E8.25, but their distribution in the vitelline and embryo

circulation is uneven until E10. The hematopoietic progenitors are also enriched in the yolk sac until E10.5. Those observations show that the yolk sac vasculature remains a site of progenitor production and preferential adhesion even after the liver becomes a site of hematopoiesis (McGrath et al., 2003; Jones et al., 2004). A fully functioning heart creating sufficient pulsatile flow is required to drive vascular remodeling in the yolk sac. Embryos defective for myosin light chain 2a (*Mlc2a*) did not remodel the vitelline vessels because of reduced laminar flow (Lucitti et al., 2007). *Mlc2a*^{-/-} embryos exhibited defects in atrial contraction and ventricular filling, resulting in slow and delayed blood circulation, and limited oscillatory movement of primitive erythroblasts. Although

TABLE 2 Summary of experimental models showing failure to remodel the vitelline vasculature.

Protein/ molecule	Model	Findings	References
Foxo1	Mouse embryo	KO results in failed vascular remodeling and embryonic death by E10.5	Li-Villarreal et al. (2022)
		Arterial fate specification through repression of <i>Sprouty2</i> and <i>Sprouty4</i>	
		Maintains <i>Vegfr2</i> expression on arterial endothelial cells	
Mlc2a	Mouse embryo	KO results in cardiac defects and failed remodeling of the primary capillary plexus, resulting in embryonic death	Huang et al. (2003)
Notch	Mouse embryo	Impairment prevents vitelline vascular remodeling and results in embryonic death by E10.5	Krebs et al. (2004)
TGFβ	Mouse embryo	Impairment prevents vitelline vascular remodeling and results in embryonic death by E10.5	Jones et al. (2004)
			Carvalho et al. (2007)

mutant embryos appeared normal at E8.5, the primary capillary plexus did not remodel by E9.5, so that their yolk sacs lacked both small and large vessels (Table 2) (Huang et al., 2003; Lucitti et al., 2007). Immobilizing the erythroblasts in the blood islands also prevented vascular remodeling and delayed embryo development. By artificially increasing the blood viscosity, without restoring erythroblast mobility, vascular remodeling and normal embryo development up to the axial rotation or turning stage (between E8 and E9) could be rescued (Lucitti et al., 2007).

Hematocrit levels influence laminar shear stress and correlate to vessel size, according to the Fåhræus-Lindqvist effect (Fåhræus and Lindqvist, 1931; Jones et al., 2004; Farina et al., 2021). In addition, laminar shear stress impacts various molecules that are known to be involved in development. For instance, laminar shear stress will induce platelet-derived growth factor A and B receptors, that are required for vessel stabilization via pericytes and mural cells (Jones et al., 2004). Furthermore, laminar shear stress can induce TGFβ signaling, which is required for the remodeling of the primary capillary plexus (Jones et al., 2004; Carvalho et al., 2007). *Vegfr2*, which is required prior to the appearance of flow for the formation of blood islands and the primary capillary plexus (Shalaby et al., 1995; Jones et al., 2004), is also a component of the mechanotransduction cascade (Shay-Salit et al., 2002; Lucitti et al., 2007; Osol and Mandala, 2009; Garcia and Larina, 2014; Campinho et al., 2020). *In vitro*, *Vegfr2* was shown to be activated by laminar flow (Shay-Salit et al., 2002; Baeyens and Schwartz, 2016). At E8.5, prior to remodeling, the levels of laminar shear stress vary between vessels of similar size in the yolk sac. Between E9.5 and E10.5, similar sized vessels possess similar shear stress levels (Jones et al., 2004). These data correlate with earlier findings showing that a steady-state hematocrit is not reached before E10 and changes in the distribution of primitive erythroblasts are temporally regulated (McGrath et al., 2003).

2.1.3 Piezo1 as a sensor for shear stress in endothelial cells

While it is well established that blood circulation is required to generate the hemodynamic forces that drive vascular remodeling (Lucitti et al., 2007), the exact mechanism by which endothelial cells sense these forces has long remained an enigma. In addition to adherens junctions (Shay-Salit et al., 2002; Lucitti et al., 2007; Osol

and Mandala, 2009; Garcia and Larina, 2014; Baeyens and Schwartz, 2016; Campinho et al., 2020), the role of mechanically sensitive Ca^{2+} cation channels is becoming increasingly clear, with Piezo1 being the most studied in vascular development. Piezo proteins are subunits and assemble in trimers to form the functional mechanically sensitive channels (Ge et al., 2015; Guo and MacKinnon, 2017; Saotome et al., 2018; Zhao et al., 2018). Global or endothelial cell-specific disruption of Piezo1 reduced the Ca^{2+} -entry evoked by shear stress, which resulted in vascular defects in the mouse yolk sac and embryonic lethality at E9.5 (Li et al., 2014a; Ranade et al., 2014), with a minority of embryos surviving up to E16.5 (Li et al., 2014a). Piezo1 complete or partial deletion reduced the number of large vessels in the vitelline vasculature (Li et al., 2014a; Ranade et al., 2014). Endothelial cells were organized in a cobblestone pattern in *Piezo1*^{+/-} embryos at E9.5, whereas they had a linear appearance in *Piezo1*^{+/+} control littermates, indicating that haploinsufficiency reduced the capacity of endothelial cells to align in the direction of flow (Li et al., 2014a). Calpain-2 impacts the actin cytoskeleton and focal adhesions and has also been suggested to be involved in endothelial cell alignment under shear stress (Lebart and Benyamin, 2006; Miyazaki et al., 2007; McHugh et al., 2010; Li et al., 2014a). Calpain-2 activity was significantly reduced in *Piezo1*^{-/-} embryos compared to controls. Proteomic analysis confirmed that Piezo1 regulates the calpain-2 system through Ca^{2+} -influx. Therefore, these experiments suggest that Piezo1 is required for shear stress sensing and regulates endothelial cell alignment to blood flow via the calpain-2 system (Li et al., 2014a). Deletion of *Capn4*, which encodes the regulatory subunit of Calpains, leads to embryonic lethality at E10.5, attributed to heart defects (Arthur et al., 2000). It is possible that disrupted vascular development in the yolk sac might play a role in embryo arrest in that model as well.

2.1.4 A common key transcription factor regulates arterial fate specification, mechano-sensing, and vascular remodeling in the yolk sac

Arterial and venous identities in the yolk sac are, to some extent, already established before blood flow starts (Herzog et al., 2005; Aitsebaomo et al., 2008; Chong et al., 2011; Li-Villarreal et al., 2022). However, arterio-venous specification remains somewhat ambiguous and plastic, and its completion is dependent on hemodynamical forces and blood flow (le Noble et al., 2004; le

Noble et al., 2005; Jones et al., 2006; Wragg et al., 2014; Li-Villarreal et al., 2022).

The transcription factor Forkhead box protein O1 (Foxo1) is required for pre-flow arterial specification and subsequent vascular remodeling, specifically in the yolk sac. Embryos deficient for *Foxo1* in endothelial cells (*Foxo1^{ECKO}*) are indistinguishable from wild type until E8.5, including blood flow velocity. At E9.5 the vitelline vessels fail to remodel, blood flow velocity has now slowed compared to the WT littermates, and mutant embryos show symptoms of heart failure, leading to embryonic lethality around E11.5. It is likely that the decrease in flow velocity in the mutants is a consequence of the heart beating against an immature vitelline network (Table 2) (Li-Villarreal et al., 2022). Germline defects in *Foxo1* display a similar phenotype, plus additional defects in allantois and chorio-allantoic fusion with partial penetrance (Ferdous et al., 2011; Li-Villarreal et al., 2022). Mechanistically, deep analysis of the mutant phenotype showed that *Foxo1*-mediated repression of *Sprouty2* and *Sprouty4* specifically in the yolk sac is necessary to maintain an arterial gene expression profile (notably *Dll4*) as well as the expression of *Vegfr2* (Li-Villarreal et al., 2022).

Remodeling of the vitelline vasculature relies on endothelial cell migration and fusion of vessels (Udan et al., 2013b; Campinho et al., 2020; Li-Villarreal et al., 2022). While arterial endothelial cells in the yolk sac showed directional migration to the hemodynamic stimuli, those under lower flow and those in the vitelline veins migrated in a random manner (Udan et al., 2013b). The disturbance of *Vegfr2* signaling in *Foxo1^{ECKO}* embryos might thus prevent arterial cells from properly responding to mechanical signals. Whether there is also a connection between the repression of arterial fate and failed remodeling requires further investigation. Thus, whether the defects in vascular remodeling in the yolk sac of *Foxo1^{ECKO}* embryos are solely related to reduced *Vegfr2* levels or also to the repression of arterial fate remains unclear (Li-Villarreal et al., 2022).

2.2 The murine umbilical cord and placenta

2.2.1 From gastrulation to the umbilical cord

The allantois is the precursor for the umbilical cord. While it was thought to develop solely from primitive streak-derived extraembryonic mesoderm (Inman and Downs, 2007; Arora and Papaioannou, 2012; Downs, 2022), recent studies unveiled a possible input from streak-associated extraembryonic visceral endoderm through an epithelial-to-mesenchymal transition (Rodriguez and Downs, 2017; Downs and Rodriguez, 2020; Downs, 2022). The allantois first appears as a bud at the posterior embryonic-extraembryonic border, then extends into the exocoelomic cavity towards the chorion (Figure 1A). Between E8.25 and E8.75, the allantois fuses to the chorion, which initiates the development of fetus-derived vessels of the placental labyrinth (Figures 2A, B) (Watson and Cross, 2005; Arora and Papaioannou, 2012; Downs, 2022; Elmore et al., 2022).

Blood vessels in the allantois develop *de novo*, like in the yolk sac. However, in contrast with the yolk sac, vasculogenesis in the allantois is not accompanied by erythropoiesis (Downs et al., 1998). The first angioblasts appear in the distal portion of the allantois around E7.75-E8 (Figures 1A, C) and vasculogenesis takes place in a distal-to-proximal path (Downs et al., 1998;

Downs, 2022). A branched vascular network develops distally while the umbilical artery forms without branches in the proximal third of the allantois (Figures 1A, C). At the base is the vessel of confluence, the site where the umbilical artery, omphalomesenteric artery and dorsal aorta meet. The unbranched nature of the developing umbilical artery is likely to ensure its proper connection to the vessel of confluence (Rodriguez and Downs, 2017; Rodriguez et al., 2017; Downs, 2022). Hedgehog is believed to be involved in the visceral endoderm epithelial-to-mesenchymal transition, and is required for the patterning of the arterial vessels of the allantois (Rodriguez and Downs, 2017).

2.2.2 The maternal-fetal interface

Placentation is a crucial step in the development of mammalian embryos. In mice and men, defective placentation causes pregnancy pathologies going from intrauterine growth restriction to embryonic death (Rossant and Cross, 2001; Burton and Jauniaux, 2018b; Perez-Garcia et al., 2018; Woods et al., 2018; Lu et al., 2019). Hypoxia is a strong driving force for placenta formation but also a consequence of placental defects (Soares et al., 2017; 2018).

The labyrinth arises by folding of the chorion and its invasion by the allantois. It develops after chorio-allantoic fusion, around E8.5, and has a branched vasculature by E9. The mesoderm-derived allantois promotes the formation of three distinct trophoblast cell lineages from the chorion ectoderm: the cytotrophoblasts and syncytiotrophoblasts type I and type II. These three cell types form the transport layer across which nutrients and waste are exchanged. In addition, they line the maternal blood sinusoids, where blood enters from the spiral arteries and canals, and are juxtaposed to the endothelial cells from the fetal vessels (Rossant and Cross, 2001; Watson and Cross, 2005; Woods et al., 2018; Hemberger et al., 2020; Elmore et al., 2022). By E10, the embryo becomes reliant on the umbilico-placental vasculature for its survival (Woods et al., 2018).

In mouse, the ectoplacental cone, derived from polar trophoblasts, is a structure that resembles a cap on top of the extraembryonic ectoderm and separates the conceptus from the decidua. From the core of the ectoplacental cone, the junctional zone of the placenta will develop. The junctional zone consists of two layers, formed by three cell types. The outer layer contacts the decidua and contains parietal giant cells, whereas the inner layer is constituted by spongiotrophoblasts and glycogen trophoblasts (Rossant and Cross, 2001; Watson and Cross, 2005; Woods et al., 2018; Hemberger et al., 2020; Panja and Paria, 2021).

The uterine arteries branch at the implantation site, dividing into the spiral arteries (Panja and Paria, 2021). The outer cells of the ectoplacental cone differentiate into secondary trophoblast giant cells. These cells penetrate the endometrial stroma and connect to the maternal spiral arteries where they erode the smooth muscle cell layer and replace the endothelial cells, forming the blood canals through which maternal blood enters the maternal sinusoids in the labyrinth. Because trophoblast cells replace the endothelial cells of the maternal vessels, maternal blood in the placenta is in contact with fetal-derived cells instead of maternal ones (Woods et al., 2018; Panja and Paria, 2021). Interestingly, this contact between maternal blood and fetal-derived cells does not elicit an immune response.

The placenta presents an essential role in inducing an immune-privileged environment (Erlebacher, 2013; Woods et al., 2018) at the

TABLE 3 Overview of the evolution of blood flow velocity throughout development.

Model	Tissue	Developmental stage	Velocity	References
Mouse	Uterine artery	Not pregnant	23 cm/s ^a	Mu and Adamson (2006)
	Uterine artery	E15.5	52 cm/s ^a	Mu and Adamson (2006)
	Uterine artery	E18.5	60 cm/s ^a	Mu and Adamson (2006)
	Umbilical artery	E14.5	10 cm/s ^a	Mu and Adamson (2006)
	Umbilical artery	E18.5	15 cm/s ^a	Mu and Adamson (2006)
	Ductus venosus	E17.5	14.65–17.71 cm/s ^a	Zhou et al. (2014)
	Intrahepatic umbilical vein	E17.5	4.95–5.93 cm/s ^c	Zhou et al. (2014)
Human	Uterine artery	Not pregnant	32–44 cm/s ^a	Bernstein et al. (2002)
				Mu and Adamson (2006)
	Uterine artery	18–20 weeks	70–130 cm/s ^a	Mu and Adamson (2006)
	Umbilical artery	18–20 weeks	27 cm/s ^a	Mu and Adamson (2006)
	Umbilical artery	38–40 weeks	36 cm/s ^a	Mu and Adamson (2006)
	Umbilical vein	20 weeks	63 mL/min ^b	Barbieri et al. (2023)
	Umbilical vein	38 weeks	373 mL/min ^b	Barbieri et al. (2023)

^aPeak velocity.

^bAbsolute flow volume.

^cTime-average maximal velocity over whole cardiac cycle.

maternal-fetal interface, through the regulation of maternal immune cells populating the decidua. These immune cells are highly specialized, avoiding any placental attack as a foreign organ transplant and protecting the embryo from infection. Specifically in the first trimester, the decidua is primarily populated by natural killer cells (~70%) and macrophages (~20%) in both human and mouse. In human, decidual natural killer cells first appear in the secretory endometrium prior to implantation and express high levels of chemokines and cytokines. In mouse however, natural killer cells only appear during pregnancy. These decidual natural killer cells play a major role in spiral arteriole remodeling to maximize maternal blood flow through the placenta (Chazara et al., 2011; Zhang et al., 2011). Interestingly, in human the cytolytic function of decidual natural killer cells is inhibited through the expression of non-classical class I molecules (i.e., HLA-E and HLA-G) expressed by extravillous trophoblasts. In addition, decidual natural killer cells express IL-10, which induces the differentiation of decidual macrophages and maintains a non-inflammatory state. Similarly to natural killer cells, decidual macrophages contribute to spiral arteriole remodeling and both cells express IL-15.

2.2.3 Hemodynamics in the umbilical cord and placenta throughout gestation

In 2006, Mu and Adamson measured blood flow in the mouse umbilical and placental arteries, using Doppler ultrasound (Table 3). As gestation progresses, the resistance to blood flow in the uterine arteries decreases and blood is allowed to flow more freely, as was indicated by an increase in peak systolic and end-diastolic velocities. Blood flow was detected in the maternal arterial canal from E10.5 on, and in its branches starting from E12.5. While initially slow, flow velocity increased over time. In the spiral arteries however, blood flow was not always detected (Bernstein et al., 2002; Mu and

Adamson, 2006). The slow pace of blood movement within the placenta helps facilitate adequate exchange of nutrients and waste between the maternal and fetal blood (Linask et al., 2014).

At late E8.5, blood flow becomes detectable in the umbilical artery. Flow velocity in the umbilical artery increases during gestation and is paired with a decrease in vascular resistance. In the umbilical veins, pulsatile flow was also detected. However, these pulsations likely originate from retrograde waves that are caused by the contractions of the heart (Mu and Adamson, 2006).

2.2.4 Remodeling of the umbilical vasculature

Piezo1 acts as a mechanosensor in the vitelline vasculature. It was also demonstrated *in vitro* that endothelial cells derived from human umbilical vein respond to shear stress through Piezo1 (Li et al., 2014a). Therefore, a similar role for Piezo1 in the murine umbilical vasculature seems not too farfetched. In addition, umbilical endothelial cells express Vegfr2, Pecam1, VE-cadherin and eNOS. These are involved in angio- and vasculogenesis, as well as the normal functioning of blood vessels, and are also involved in the mechanosensation of hemodynamic forces (Lucitti et al., 2007; Osol and Mandala, 2009; Garcia and Larina, 2014; Baeyens and Schwartz, 2016; Campinho et al., 2020).

Various *ex vivo* methods to study the allantois are available (Downs, 2006; Arora and Papaioannou, 2012; Hou et al., 2016; Hadamek et al., 2018). However, they do not readily provide a means to incorporate hemodynamic factors (Arora and Papaioannou, 2012). Blood flow in the umbilical cord only starts after chorio-allantoic fusion and after the umbilical artery has connected to the vessel of confluence (Linask et al., 2014). Perhaps it is because of these reasons that there is very little data available on the role of mechanotransduction in the development of the allantois and its vasculature in the mouse.

2.2.5 Remodeling of the utero-placental vasculature

The uterine arteries must expand to support the fetoplacental unit after the placenta is formed and until birth. The lumen of the uterine arteries expands and doubles in size during gestation in mice. Interestingly, and as opposed to other species, the tunica media of the uterine arteries expands as well (van der Heijden et al., 2005; Osol and Mandala, 2009). The uterine arteries grow in the longitudinal axis too, approximately doubling their length in comparison to a non-pregnant state. Considering Hagen-Poiseuille's law for laminar flow, extension of the artery increases its resistance to flow, whereas luminal expansion decreases this resistance. In case both parameters are doubled, resistance to flow would still decrease since length has a linear relationship to resistance while the radius has an inverse and quadratic relationship (Osol and Mandala, 2009). The uterine veins also expand (Forbes and Taku, 1975; Osol and Mandala, 2009).

Nitric oxide (NO) and eNOS are important factors in endothelial mechanosensation that can be influenced by progesterone and estrogen (Osol and Mandala, 2009). Estrogens stimulate vascular remodeling of the uterine arteries and invasion of the spiral arteries in humans, supporting an increased blood flow that is accompanied by an increase in shear stress. Estrogens drive NO and VEGF synthesis by ECs (Mandala, 2020). In addition, *in vitro* experiments on human umbilical vein endothelial cells (HUVECs) showed that progesterone causes a rapid increase of NO production through the PI3K/Akt pathway (Pang et al., 2015). Knockout of eNOS impairs uterine artery growth during pregnancy. However, uterine arteries in pregnant mutant animals were still larger than those from non-pregnant females, suggesting that other factors are also at play (van der Heijden et al., 2005; Osol and Mandala, 2009).

3 Mechanotransduction in the human vitelline and umbilico-placental vasculatures

Similar to mouse, the human extraembryonic vasculature is comprised of two circulation circuits: 1) the vitelline circulation in the secondary yolk sac during early development, and 2) the umbilico-placental circulation towards the end of the first trimester (Burton and Jauniaux, 2018a).

3.1 Human vitelline vasculature

3.1.1 Formation of the primary circulation system

In human, the yolk sac is a temporary organ, present only in early pregnancy. The human yolk sac was first described *in vivo* in 1979, as "a round, translucent, cyst-like structure" located in the exocoelomic cavity, by Mantoni and Pedersen, using ultrasound scanning (Mantoni and Pedersen, 1979). Due to difficult access to early human embryos and the fragile structure of the yolk sac (Jauniaux et al., 1991), it has rarely been studied and its biological functions are relatively poorly understood (Gulbis et al., 1998; Burton and Jauniaux, 2018a). Nonetheless, it is well established that the yolk sac plays an essential role as the first

circulatory system of the embryo. Starting during the second week of gestation (Jordan, 1910; Palis and Yoder, 2001; Tavian and Péault, 2005), the human yolk sac produces nucleated erythrocytes synthesizing hemoglobin (Luckett, 1978). Hematopoiesis takes place in extraembryonic mesoderm-derived cells that organize as blood islands in the mesenchymal layer of the secondary yolk sac. Most inner cells of the islands differentiate into blood cell progenitors, while peripheral cells become endothelial cells. Secondary to the start of heartbeats (around 3 somite stage) and the onset of blood flow (around 6 somite stage), blood islands angioblasts coalesce in a process called vasculogenesis to form the yolk sac primitive capillary plexus, which is then progressively remodeled. The primitive circulatory system is organized in a hierarchical network of large vessels ensuring high volumetric blood flow and small vessels carrying low flow. This vascular network connects the yolk sac to the embryo with a functional circulation via vitelline blood vessels between the yolk sac and the developing heart (Figure 3A). Until the placenta is sufficiently developed, this pre-portal system allows the transport of nutrients and O₂ extracted from extraembryonic coelomic fluid to the embryonic tissues via vitelline veins and the elimination of metabolic waste and CO₂ from the embryonic heart to the yolk sac via the vitelline artery (Martinelli et al., 2023). Therefore, aberrant formation of this primary circulation system could lead to growth retardation, cardiac failure, and embryonic death (Lucitti et al., 2007; Graupera et al., 2008; Culver and Dickinson, 2010).

3.2 Human umbilico-placental vasculature

3.2.1 Development of the human umbilico-placental vasculature

The definitive placenta is formed by the end of the first trimester, concomitant to the degeneration of the yolk sac, after a series of extensive remodeling steps (Jauniaux et al., 1991; Burton and Jauniaux, 2018a). Firstly, villi develop in the entire gestational sac. After 8 weeks of gestation, the villi from the superficial pole of the placenta regress, leaving a smooth membrane called chorion laeve (Figure 3A). This regression occurs simultaneously with the entry of the maternal arterial circulation to the placenta, initially in the periphery and then in the entire placenta (Burton and Jauniaux, 2018a). It requires the migration of extravillous trophoblastic cells into the placental bed, and is modulated by high level of oxidative stress within the villi (Jauniaux et al., 2003). As the endothelial cells forming the capillaries in the regressing villi lose integrity, they become avascular. This regression is important to determine the final size and shape of the placenta (Figure 3B) (Burton et al., 2010). Indeed, an excessive or asymmetric recession of the villi can lead to ellipsoid placentas or eccentric insertion of the umbilical cord, which restrict nutrient supply to the fetus and impact the developing heart (Burton and Jauniaux, 2018a).

3.2.2 Hemodynamic regulation in the human umbilical cord

Even though the precise molecular etiology and the direction of causality is often unclear, there is a clinical correlation between alterations of extraembryonic tissues and pregnancies characterized by intrauterine growth restriction and small babies at birth. For

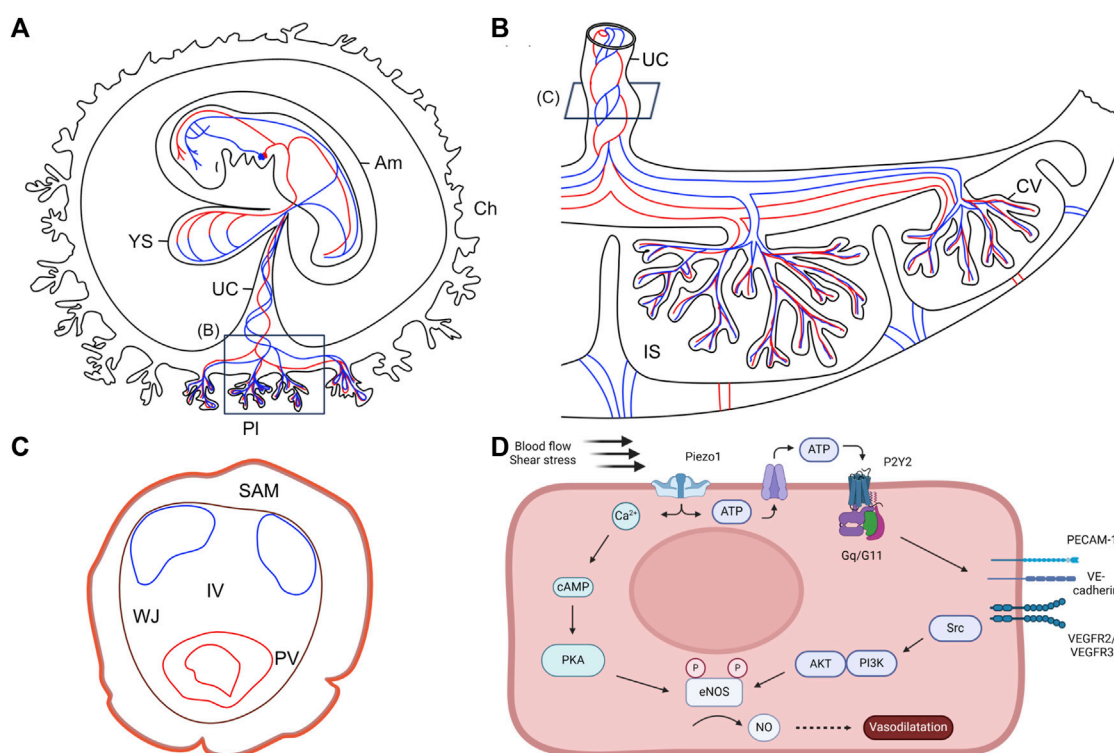


FIGURE 3

Anatomy of the human embryo and its extraembryonic structures. (A) Schematic representation of the human embryo and its extraembryonic structures during the fourth week of pregnancy. Adapted from [Martinelli et al., 2023](#), with permission from SNCSC. (B) Schematic representation of the human term placenta. Based on [Silini et al., 2020](#). (C) Schematic representation of the full-term human umbilical cord. Umbilical arteries are represented in blue and umbilical vein is represented in red. Based on [Blanco-Elices et al., 2022](#). (D) Schematic illustrating the molecular pathways of vascular remodeling mediated by shear stress. AKT: protein kinase; Am: amnion; Ca²⁺: calcium ions; cAMP: cyclic adenosine monophosphate; ATP: adenosine triphosphate; Ch: chorion; CV: chorionic villi; eNOS: endothelial nitric oxide synthase; IS: intervillous space; IV: intervascular zone; NO: nitric oxide; P2Y2: purinergic receptor; PECAM-1: platelet endothelial cell adhesion molecule 1; PI3K: phosphatidylinositol 3-kinase; PKA: protein kinase A; Pl: placenta; PV: perivascular zone; SAM: subamniotic zone; UC: umbilical cord; V-cad: vascular endothelial cadherin; VEGFR: vascular endothelial growth factor receptor; WJ: Wharton's jelly; YS: yolk sac.

instance, cases of intrauterine growth restriction may be associated with an abnormal placenta, displaying immature or less abundant villi, presumably secondary to impaired branching angiogenesis and endothelial dysfunction, and creating a hypoxic environment ([Kingdom et al., 2000](#)).

Fluid mechanics and shear stress have a major impact on both the fetal cardio-vascular system and the umbilico-placental vasculature. In general, a high blood flow increases wall shear stress and the diameter of blood vessels (vasodilation), while a low blood flow reduces wall shear stress and vessels diameter (vasoconstriction) ([Saw et al., 2018](#)). While there seems to be no correlation between shear stress and diameter in the umbilical arteries, a strong relationship was found between shear stress and the diameter of the umbilical vein. A reduced velocity of blood flow in the umbilical vein and/or an impaired blood viscosity resulting in increased resistance to flow both result in the insufficient transfer of nutrients and oxygen to the fetus. Since blood vessels in the placenta lack autonomic innervation ([Myatt, 1992](#)), the regulation of vessel diameter relies on the production of vasoactive agents by endothelial cells, such as NO ([Lu and Kassab, 2011](#)), endothelin 1 (ET1) ([Egorova et al., 2012](#)), VEGF ([dela Paz et al., 2012](#)), or placental growth factor (PlGF) ([Rashdan and Lloyd, 2015](#)) to maintain a homeostatic level. These homeostasis mechanisms were only

observed in umbilical arteries and seem to be absent or weak in umbilical vein, which could explain the lack of correlation between shear stress and umbilical arterial diameter ([Saw et al., 2018](#)).

The two umbilical arteries form helical structures as they coil around the umbilical vein. This helical geometry of the blood vessels in the umbilical cord is already visible at 7 weeks of gestation and appears important for the health of the pregnancy. Indeed, in about 2%–5% of human fetuses, an absence of blood vessel coiling, preventing hemodynamic changes, was observed and correlated with an increased incidence of fetal death ([Strong et al., 1994](#); [Saw et al., 2017](#)).

The umbilical vessels are embedded in Wharton's jelly, a protective mucous connective tissue, and contained within an outer layer of amnion ([Figure 3C](#)) ([Spurway et al., 2012](#); [Murphy et al., 2020](#)). Degeneration or absence of Wharton's jelly are risk factors for vessel compression, disruption of fetal blood flow, and eventually fetal hypoxia which can lead to fetal death ([Kulkarni et al., 2007](#); [Murphy et al., 2020](#)). Wharton's jelly degeneration is indicated by a decreased cord diameter in late gestation and is usually caused by a reduction of its water content. Absence of Wharton's jelly is an extremely rare and severe disorder of pregnancy which results in intrauterine growth retardation, fetal morbidity, or perinatal death ([Weissman et al., 1994](#); [Spurway et al., 2012](#)).

The two first cases of Wharton's jelly degeneration were described in 1961 by Bergman et al. Analysis of the cords revealed wide-spread mucoid degeneration with cyst formation and mucous masses. The fetus died in one of the cases (Bergman et al., 1961). In 1985, Labarrere et al. described three cases where the Wharton's jelly was only present around the umbilical vein, leaving the umbilical arteries hanging free. In all three cases, the newborn died with meconium found either in the amniotic fluid or in the respiratory tract (Labarrere et al., 1985). In 2007, Kulkarni et al. reported a case of absent Wharton's jelly associated with persistent vitello-intestinal duct (Kulkarni et al., 2007) and in 2020, Murphy et al. described a case of Wharton's jelly absence around all three umbilical vessels with fetal bradycardia, and meconium staining of all three umbilical vessels and of the placenta. The newborn survived but suffered from meconium aspiration syndrome (Murphy et al., 2020).

In humans and other mammals, while the umbilical arteries occlude rapidly after delivery of the newborn, the umbilical vein remains patent longer to allow placental infusion. Indeed, while the umbilical arteries have a bilaminar structure (Meyer et al., 1978) composed of an outer and an inner tunica media, with no elastic structure, no distinct inner layer is observed in the vein. Even though smooth muscle cells are observed equally within both tunica media of the arteries and of the vein, the latter contains fewer layers of smooth muscle cells. Thus, the umbilical arteries have a much thicker tunica media than the vein. In addition, the outer tunica media of umbilical arteries includes more contractile smooth muscle cells compared to the inner tunica media and the vein, allowing vasoconstriction of umbilical arteries through folding of the inner layer for lumen occlusion at birth. Furthermore, the proteoglycan composition of the extracellular matrix of the umbilical vessels plays a role in vasoconstriction. While the inner tunica media of the umbilical arteries is rich in proteoglycans, the expression of these proteoglycans is very weak in the arterial outer tunica media and the venous tunica media. This composition results from the expression of proteoglycanases called ADAMTS. ADAMTS are highly expressed in the venous tunica media, specifically prior to parturition, and in the arterial outer tunica media. ADAMTS proteolyzes the proteoglycans, thus reducing its level in the vein and the outer tunica media of the arteries. The low level of ADAMTS allows the maintenance of proteoglycans in the inner tunica media of the arteries, leading to rapid arterial occlusion at birth (Nandadasa et al., 2015; 2020).

3.2.3 Piezo1 as blood flow sensor in the human umbilical vasculature

Piezo proteins are essential determinants of vascular structures that act as sensors of blood flow through their dependence on shear stress-evoked ionic current and calcium influx (Figure 3D) (Li et al., 2014a; Ranade et al., 2014; Xiao et al., 2023). The importance of Piezo1 in the development of human umbilical veins was demonstrated notably through experiments in cultured HUVECs. Indeed, depletion of Piezo1 led to suppressed migration of endothelial cells, thus inhibiting umbilical vein tube formation (Li et al., 2014a). Li and colleagues performed mass spectrometry to identify proteins affected by Piezo1 depletion in static and shear stress conditions. Results showed reduction of endothelial nitric oxide synthase (eNOS) upon Piezo1 depletion in both static and

shear stress conditions. In addition, phosphorylation of eNOS at serine 1,177 by VEGF, which enhances eNOS activity, was abolished in static endothelial cells depleted of Piezo1. Endothelial cell migration was similarly affected by Piezo1 depletion, eNOS depletion, and NOS inhibition. The defective alignment observed in Piezo1 depleted HUVECs was not due to an effect on NO/eNOS, but rather on cytoskeletal regulation mediated through activation of calpain-mediated proteolytic cleavage of actin cytoskeleton and focal adhesion proteins (Li et al., 2014a).

In addition to the effect of shear stress on Piezo1 in the apical membrane of endothelial cells, Piezo1 also senses membrane tension at the junctional cell side through the adherens junction force sensing machinery. In this case, Piezo1 activity is regulated by PECAM1 in endothelial cells. In response to membrane tension, PECAM1 inhibits Piezo1 activity. The C-terminal structure of PECAM1, particularly Y713, interacts with N-terminal regions of Piezo1 to reduce its mechanical sensitivity. Thus, an increased abundance of PECAM1 reduces Piezo1 channel function and decreases calcium influx in endothelial cells (Figure 3D) (Chuntharpursat-Bon et al., 2023).

4 Discussion

The mouse is often used as a model to study human development. Due to its transient and fragile nature, the human yolk sac is challenging to study. The mouse yolk sac, however, remains throughout gestation; it has a similar histological makeup, and cells that cover equivalent functions (Martinelli et al., 2023), thereby offering a great opportunity to study early vascular and blood cell development.

There is still relatively little known on the development of the umbilical vessels. While blood flow velocity was measured in several species, including mouse and human (Table 3) (Mu and Adamson, 2006; Osol and Mandala, 2009; Linask et al., 2014; Zhou et al., 2014; Downs, 2022; Barbieri et al., 2023), a thorough investigation of hemodynamic forces and their impact on vascular development and remodeling in the umbilical cord and placenta is yet to be performed. To study vascular development quantitatively, one can measure vessel and blood flow parameters such as the pulsatility index and refractive index, as well as end-diastolic velocity, end-systolic velocity, and peak systolic velocity (Linask et al., 2014), among others. Various methods to study flow *in vivo* can be used to investigate its role in vascular development, remodeling and maturation (Daems et al., 2020).

Although there are differences between the murine and human umbilical cord and placenta, the mouse is a useful model (Soares et al., 2017; 2018; Woods et al., 2018). Blood flow in the umbilical cord only occurs after chorio-allantoic fusion and after the umbilical artery connects to the vessel of confluence (Linask et al., 2014). Therefore, the initial vascular development of the umbilical cord is likely independent from hemodynamic factors. Another non mechanical driver for placenta development is hypoxia (Soares et al., 2017). Several studies have shown the effect of fluid shear stress on vascular remodeling via NO production in mouse and human endothelial cells (Tao et al., 2006; Lucitti et al., 2007; Lu and Kassab, 2011; Li et al., 2014a; Wang et al., 2016; Albarrán-Juárez et al., 2018; Xiao et al., 2023). Shear stress activates the endothelial

mechanosensitive cation channel Piezo1 (Xiao et al., 2023), increasing the intracellular Ca^{2+} concentration and releasing ATP. ATP-release leads to the activation of the Gq/ G_{11} -coupled purinergic P2Y2 receptor on endothelial cells (Wang et al., 2016; Morley et al., 2019). The increased intracellular concentration of Ca^{2+} upregulates eNOS mRNA expression in a dose-dependent manner through Ca^{2+} /calmodulin, as well as phosphorylation of eNOS at Ser1176 and Ser320 sites by PKA or PI3K/AKT via the mechanosensory complex, consisting of PECAM1, VE-cadherin and VEGR2/VEGFR3 (Figure 3D) (Dimmeler et al., 1999; Balligand et al., 2009; Wang et al., 2016; Morley et al., 2019). Intracellular eNOS is subsequently translocated to the endothelial cell membrane (Lucitti et al., 2007) and increases the production of the key vasodilator NO. Overall, this downstream pathway results in vascular relaxation (Tao et al., 2006; Xiao et al., 2023). NO plays a critical role in systemic blood pressure regulation (Wang et al., 2016) and is required for normal vascular remodeling (Lucitti et al., 2007).

The development of the embryonic vascular system relies on the morphogenesis of the extraembryonic tissues. The study of the early steps of embryogenesis is crucial to understand the causes of pathologies of pregnancy, from first trimester loss to later anomalies. However, ethical and technical challenges are limiting factors. In human, negative pregnancy outcomes have been associated to ectopic insertion of the umbilical cord into the chorion (Jauniaux et al., 2020). Malperfusion of the uterus and/or placenta alter smooth muscle cell proliferation. A smooth muscle cell excess surrounding the placental arteries increases the umbilical resistance to flow, elevating the afterload on the developing heart (Burton and Jauniaux, 2018a). In addition, while hypoxia is a driving force for placental development, it can result from placental defects (Soares et al., 2017; 2018). Single umbilical artery, a condition where only one umbilical artery is present in human instead of the usual two, is most often benign but is a risk factor for defective nutrient and waste exchange between the mother and fetus and can lead to intrauterine growth restriction. Furthermore, single umbilical artery may cause hemodynamic changes that increase the afterload on the developing heart, resulting in right ventricular defects (Rossant and Cross, 2001; Burton and Jauniaux, 2018a; Woods et al., 2018; Li et al., 2019; Ebbing et al., 2020). The mouse has proven a valuable model to study both normal and aberrant placenta development (Rossant and Cross, 2001; Perez-Garcia et al., 2018; Woods et al., 2018).

The recent advances in mouse and human stem cell-based embryo models and organoids offer new opportunities to study the formation of embryonic but also extraembryonic structures and are likely to reduce the need for human tissues or laboratory animals. Recently, a mouse embryo model was created by combining embryonic, trophoblastic, and extraembryonic endoderm stem cells (Amadei et al., 2022). These embryoids develop from the first stages of embryogenesis (gastrulation, neurulation, and early organogenesis) up to a stage resembling E8.5. While placentation cannot be fully investigated, allantois- and YS-like structures are present. Furthermore, a beating heart develops even though no looping of the heart tube was observed.

While a vascular system was not described, Runx1^+ structures that are similar to blood islands are formed in the YS-like tissues and at the base of the structure that resembles the allantois. A human stem cell-based embryo model was also recently created from naïve pluripotent stem cells that act as totipotent stem cells (Oldak et al., 2023). Those initially present the epiblast and hypoblast lineages, and form the amniotic sac and YS cavities but do not go through a blastocyst stage. These self-assembling embryoids imitate the main developmental structures of natural human embryos until 13–14 days post-fertilization.

Although those stem cells-based models are not suitable to study extraembryonic circulation yet, it is likely that further research may offer the opportunity to uncover flow-related mechanisms of extraembryonic vascular development, notably through association with organoids reproducing the endometrium. Combining experiments on mouse embryos and stem cell-based models would be a powerful and ethical way to improve our knowledge of the establishment of the maternal/fetal interface.

Author contributions

KVS: Writing–original draft, Visualization, Data curation, Conceptualization. EB: Writing–original draft, Visualization, Conceptualization. EJ: Writing–review and editing. IM: Writing–review and editing, Validation, Supervision, Project administration, Funding acquisition, Conceptualization.

Funding

The author(s) declare that financial support was received for the research, authorship, and/or publication of this article. KVS and EB are financed by the Fonds de la Recherche Scientifique (FNRS) through a PDR Thema grant for cardiovascular research (PDR Thema IH CARDIO.P.C007.22). IM is a senior FNRS research associate. EJ is funded by FWO (G0B5920N), Horizon 2020 (848109) and HFSP (RGP015/2023).

Conflict of interest

The authors declare that the research was conducted in the absence of any commercial or financial relationships that could be construed as a potential conflict of interest.

Publisher's note

All claims expressed in this article are solely those of the authors and do not necessarily represent those of their affiliated organizations, or those of the publisher, the editors and the reviewers. Any product that may be evaluated in this article, or claim that may be made by its manufacturer, is not guaranteed or endorsed by the publisher.

References

- Aitsebaomo, J., Portbury, A. L., Schisler, J. C., and Patterson, C. (2008). Brothers and sisters: molecular insights into arterial-venous heterogeneity. *Circ. Res.* 103, 929–939. doi:10.1161/CIRCRESAHA.108.184937
- Albarrán-Juárez, J., Iring, A., Wang, S., Joseph, S., Grimm, M., Strlic, B., et al. (2012). Piezo1 and Gq/G11 promote endothelial inflammation depending on flow pattern and integrin activation. *J. Exp. Med.* 215, 2655–2672. doi:10.1084/jem.20180483
- Amadei, G., Handford, C. E., Qiu, C., De Jonghe, J., Greenfeld, H., Tran, M., et al. (2022). Embryo model completes gastrulation to neurulation and organogenesis. *Nature* 610, 143–153. doi:10.1038/s41586-022-05246-3
- Arora, R., and Papaioannou, V. E. (2012). The murine allantois: a model system for the study of blood vessel formation. *Blood* 120, 2562–2572. doi:10.1182/blood-2012-03-390070
- Arthur, J. S. C., Elce, J. S., Hegadorn, C., Williams, K., and Greer, P. A. (2000). Disruption of the murine calpain small subunit gene, *Capn4*: calpain is essential for embryonic development but not for cell growth and division. *Mol. Cell. Biol.* 20, 4474–4481. doi:10.1128/MCB.20.12.4474-4481.2000
- Baeyens, N., and Schwartz, M. A. (2016). Biomechanics of vascular mechanosensation and remodeling. *Mol. Biol. Cell* 27, 7–11. doi:10.1091/mbc.E14-11-1522
- Balligand, J.-L., Feron, O., and Dessy, C. (2009). eNOS activation by physical forces: from short-term regulation of contraction to chronic remodeling of cardiovascular tissues. *Physiol. Rev.* 89, 481–534. doi:10.1152/physrev.00042.2007
- Barbieri, M., Di Martino, D. D., Ferrazzi, E. M., and Stampalija, T. (2023). Umbilical vein blood flow: state-of-the-art. *J. Clin. Ultrasound* 51, 318–325. doi:10.1002/jcu.23412
- Basta, M., and Lipsett, B. J. (2023). *Anatomy, abdomen and pelvis: umbilical cord*. Treasure Island, FL: StatPearls Publishing Available at: <https://www.ncbi.nlm.nih.gov/books/NBK557389/>.
- Bergman, P., Lundin, P., and Malmström, T. (1961). Mucoid degeneration of Wharton's jelly. An umbilical cord anomaly threatening fetal life. *Acta Obstet. Gynecol. Scand.* 40, 372–378. doi:10.3109/00016346109159935
- Bernstein, I. M., Ziegler, W. F., Leavitt, T., and Badger, G. J. (2002). Uterine artery hemodynamic adaptations through the menstrual cycle into early pregnancy. *Obstet. Gynecol.* 99, 620–624. doi:10.1016/s0029-7844(01)01787-2
- Blanco-Elices, C., Chato-Astrain, J., González-González, A., Sánchez-Porras, D., Carriel, V., Fernández-Valadés, R., et al. (2022). Histological profiling of the human umbilical cord: a potential alternative cell source in tissue engineering. *J. Pers. Med.* 12. doi:10.3390/jpm12040648
- Burton, G. J., and Jauniaux, E. (2018a). Development of the human placenta and fetal heart: synergic or independent? *Front. Physiol.* 9, 373–410. doi:10.3389/fphys.2018.00373
- Burton, G. J., and Jauniaux, E. (2018b). Pathophysiology of placental-derived fetal growth restriction. *Am. J. Obstet. Gynecol.* 218, S745–S761. doi:10.1016/j.ajog.2017.11.577
- Burton, G. J., Jauniaux, E., and Charnock-Jones, D. S. (2010). The influence of the intrauterine environment on human placental development. *Int. J. Dev. Biol.* 54, 303–312. doi:10.1387/jidb.082764gb
- Campinho, P., Vilfan, A., and Vermot, J. (2020). Blood flow forces in shaping the vascular system: a focus on endothelial cell behavior. *Front. Physiol.* 11, 552–612. doi:10.3389/fphys.2020.00552
- Carvalho, R. L. C., Itoh, F., Goumans, M.-J., Lebrin, F., Kato, M., Takahashi, S., et al. (2007). Compensatory signalling induced in the yolk sac vasculature by deletion of TGFbeta receptors in mice. *J. Cell Sci.* 120, 4269–4277. doi:10.1242/jcs.013169
- Chazara, O., Xiong, S., and Moffett, A. (2011). Maternal KIR and fetal HLA-C: a fine balance. *J. Leukoc. Biol.* 90, 703–716. doi:10.1189/jlb.0511227
- Chong, D. C., Koo, Y., Xu, K., Fu, S., and Cleaver, O. (2011). Stepwise arteriovenous fate acquisition during mammalian vasculogenesis. *Dev. Dyn.* 240, 2153–2165. doi:10.1002/dvdy.22706
- Chuntharpursat-Bon, E., Povstyan, O. V., Ludlow, M. J., Carrier, D. J., Debant, M., Shi, J., et al. (2023). PIEZO1 and PECAM1 interact at cell-cell junctions and partner in endothelial force sensing. *Commun. Biol.* 6, 358. doi:10.1038/s42003-023-04706-4
- Collart, C., Ciccarelli, A., Ivanovitch, K., Rosewell, I., Kumar, S., Kelly, G., et al. (2021). The migratory pathways of the cells that form the endocardium, dorsal aortae, and head vasculature in the mouse embryo. *BMC Dev. Biol.* 21, 8–18. doi:10.1186/s12861-021-00239-3
- Coon, B. G., Baeyens, N., Han, J., Budatha, M., Ross, T. D., Fang, J. S., et al. (2015). Intramembrane binding of VE-cadherin to VEGFR2 and VEGFR3 assembles the endothelial mechanosensory complex. *J. Cell Biol.* 208, 975–986. doi:10.1083/jcb.201408103
- Culver, J. C., and Dickinson, M. E. (2010). The effects of hemodynamic force on embryonic development. *Microcirculation* 17, 164–178. doi:10.1111/j.1549-8719.2010.00025.x
- Daems, M., Peacock, H. M., and Jones, E. A. V. (2020). Fluid flow as a driver of embryonic morphogenesis. *Development* 147, dev185579. doi:10.1242/dev.185579
- delà Paz, N. G., Walshe, T. E., Leach, L. L., Saint-Geniez, M., and D'Amore, P. A. (2012). Role of shear-stress-induced VEGF expression in endothelial cell survival. *J. Cell Sci.* 125, 831–843. doi:10.1242/jcs.084301
- Diehl, K. H., Hull, R., Morton, D., Pfister, R., Rabemampianina, Y., Smith, D., et al. (2001). A good practice guide to the administration of substances and removal of blood, including routes and volumes. *J. Appl. Toxicol.* 21, 15–23. doi:10.1002/jat.727
- Dimmeler, S., Fleming, I., Fisslthaler, B., Hermann, C., Busse, R., and Zeiher, A. M. (1999). Activation of nitric oxide synthase in endothelial cells by Akt-dependent phosphorylation. *Nature* 399, 601–605. doi:10.1038/21224
- Downs, K. M. (2006). *In vitro* methods for studying vascularization of the murine allantois and allantoic union with the chorion. *Methods Mol. Med.* 121, 241–272. doi:10.1385/1-59259-983-4.239
- Downs, K. M. (2022). The mouse allantois: new insights at the embryonic-extraembryonic interface. *Philos. Trans. R. Soc. B Biol. Sci.* 377, 20210251. doi:10.1098/rstb.2021.0251
- Downs, K. M., Gifford, S., Blahnik, M., and Gardner, R. L. (1998). Vascularization in the murine allantois occurs by vasculogenesis without accompanying erythropoiesis. *Development* 125, 4507–4520. doi:10.1242/dev.125.22.4507
- Downs, K. M., and Harmann, C. (1997). Developmental potency of the murine allantois. *Development* 124, 2769–2780. doi:10.1242/dev.124.14.2769
- Downs, K. M., and Rodriguez, A. M. (2020). The mouse fetal-placental arterial connection: a paradigm involving the primitive streak and visceral endoderm with implications for human development. *WIREs Dev. Biol.* 9, 3622–e430. doi:10.1002/wdev.362
- Downs, K. M., Temkin, R., Gifford, S., and McHugh, J. (2001). Study of the murine allantois by allantoic explants. *Dev. Biol.* 233, 347–364. doi:10.1006/dbio.2001.0227
- Ebbing, C., Kessler, J., Moster, D., and Rasmussen, S. (2020). Isolated single umbilical artery and the risk of adverse perinatal outcome and third stage of labor complications: a population-based study. *Acta Obstet. Gynecol. Scand.* 99, 374–380. doi:10.1111/aogs.13747
- Egorova, A. D., DeRuiter, M. C., De Boer, H. C., Van De Pas, S., Gittenberger-De Groot, A. C., Van Zonneveld, A. J., et al. (2012). Endothelial colony-forming cells show a mature transcriptional response to shear stress. *Vitr. Cell. Dev. Biol. - Anim.* 48, 21–29. doi:10.1007/s11626-011-9470-z
- Elmore, S. A., Cochran, R. Z., Bolon, B., Lubeck, B., Mahler, B., Sabio, D., et al. (2022). Histology atlas of the developing mouse placenta. *Toxicol. Pathol.* 50, 60–117. doi:10.1177/01926232211042270
- Erlebacher, A. (2013). Immunology of the maternal-fetal interface. *Annu. Rev. Immunol.* 31, 387–411. doi:10.1146/annurev-immunol-032712-100003
- Fähræus, R., and Lindqvist, T. (1931). THE VISCOSITY OF THE BLOOD IN NARROW CAPILLARY TUBES. *Am. J. Physiol. Content* 96, 562–568. doi:10.1152/ajplegacy.1931.96.3.562
- Farina, A., Rosso, F., and Fasano, A. (2021). A continuum mechanics model for the Fähræus-Lindqvist effect. *J. Biol. Phys.* 47, 253–270. doi:10.1007/s10867-021-09575-8
- Ferdous, A., Morris, J., Abedin, M. J., Collins, S., Richardson, J. A., and Hill, J. A. (2011). Forkhead factor FoxO1 is essential for placental morphogenesis in the developing embryo. *Proc. Natl. Acad. Sci.* 108, 16307–16312. doi:10.1073/pnas.1107341108
- Ferkowicz, M. J., Starr, M., Xie, X., Li, W., Johnson, S. A., Shelley, W. C., et al. (2003). CD41 expression defines the onset of primitive and definitive hematopoiesis in the murine embryo. *Development* 130, 4393–4403. doi:10.1242/dev.00632
- Forbes, T. R., and Taku, E. (1975). Vein size in intact and hysterectomized mice during the estrous cycle and pregnancy. *Anat. Rec.* 182, 61–65. doi:10.1002/ar.1091820107
- Garcia, M. D., and Larina, I. V. (2014). Vascular development and hemodynamic force in the mouse yolk sac. *Front. Physiol.* 5 AUG, 308–310. doi:10.3389/fphys.2014.00308
- Ge, J., Li, W., Zhao, Q., Li, N., Chen, M., Zhi, P., et al. (2015). Architecture of the mammalian mechanosensitive Piezo1 channel. *Nature* 527, 64–69. doi:10.1038/nature15247
- Graupera, M., Guillermet-Guibert, J., Foukas, L. C., Phng, L. K., Cain, R. J., Salpekar, A., et al. (2008). Angiogenesis selectively requires the p110alpha isoform of PI3K to control endothelial cell migration. *Nature* 453, 662–666. doi:10.1038/nature06892
- Gulbis, B., Jauniaux, E., Cotton, F., and Stordeur, P. (1998). Protein and enzyme patterns in the fluid cavities of the first trimester gestational sac: relevance to the absorptive role of secondary yolk sac. *Mol. Hum. Reprod.* 4, 857–862. doi:10.1093/molehr/4.9.857
- Guo, Y. R., and MacKinnon, R. (2017). Structure-based membrane dome mechanism for Piezo mechanosensitivity. *Elife* 6, 336600–e33719. doi:10.7554/eLife.33660

- Hadamek, K., Keller, A., and Gohla, A. (2018). Dissection and explant culture of murine allantois for the *in vitro* analysis of allantoic attachment. *J. Vis. Exp.* 2018, 56712–56718. doi:10.3791/56712
- Hemberger, M., Hanna, C. W., and Dean, W. (2020). Mechanisms of early placental development in mouse and humans. *Nat. Rev. Genet.* 21, 27–43. doi:10.1038/s41576-019-0169-4
- Herzog, Y., Guttmann-Raviv, N., and Neufeld, G. (2005). Segregation of arterial and venous markers in subpopulations of blood islands before vessel formation. *Dev. Dyn.* 232, 1047–1055. doi:10.1002/dvdy.20257
- Hoefler, I. E., den Adel, B., and Daemen, M. J. A. P. (2013). Biomechanical factors as triggers of vascular growth. *Cardiovasc. Res.* 99, 276–283. doi:10.1093/cvr/cvt089
- Hou, W., Sarikaya, D. P., and Jerome-Majewska, L. A. (2016). *Ex vivo* culture of pre-placental tissues reveals that the allantois is required for maintained expression of Gcm1 and Tpbpa. *Placenta* 47, 12–23. doi:10.1016/j.placenta.2016.08.091
- Huang, C., Sheikh, F., Hollander, M., Cai, C., Becker, D., Chu, P.-H., et al. (2003). Embryonic atrial function is essential for mouse embryogenesis, cardiac morphogenesis and angiogenesis. *Development* 130, 6111–6119. doi:10.1242/dev.00831
- Inman, K. E., and Downs, K. M. (2007). The murine allantois: emerging paradigms in development of the mammalian umbilical cord and its relation to the fetus. *Genesis* 45, 237–258. doi:10.1002/dvg.20281
- Jauniaux, E., Hempstock, J., Greenwold, N., and Burton, G. J. (2003). Trophoblastic oxidative stress in relation to temporal and regional differences in maternal placental blood flow in normal and abnormal early pregnancies. *Am. J. Pathol.* 162, 115–125. doi:10.1016/S0002-9440(10)63803-5
- Jauniaux, E., Jurkovic, D., Henriet, Y., Rodesch, F., and Hustin, J. (1991). Development of the secondary human yolk sac: correlation of sonographic and anatomical features. *Hum. Reprod.* 6, 1160–1166. doi:10.1093/oxfordjournals.humrep.a137503
- Jauniaux, E., Moffett, A., and Burton, G. J. (2020). Placental implantation disorders. *Obstet. Gynecol. Clin. North Am.* 47, 117–132. doi:10.1016/j.ogc.2019.10.002
- Jones, E. A. V., Baron, M. H., Fraser, S. E., and Dickinson, M. E. (2004). Measuring hemodynamic changes during mammalian development. *Am. J. Physiol. - Hear. Circ. Physiol.* 287, 1561–1569. doi:10.1152/ajpheart.00081.2004
- Jones, E. A. V., Le Noble, F., and Eichmann, A. (2006). What determines blood vessel structure? Genetic prespecification vs. hemodynamics. *Physiology* 21, 388–395. doi:10.1152/physiol.00020.2006
- Jones, E. A. V., Yuan, L., Breant, C., Watts, R. J., and Eichmann, A. (2008). Separating genetic and hemodynamic defects in neuropilin 1 knockout embryos. *Development* 135, 2479–2488. doi:10.1242/dev.014902
- Jordan, H. E. (1910). A further study of the human umbilical vesicle. *Anat. Rec.* 4, 341–353. doi:10.1002/ar.1090040903
- Kingdom, J., Huppertz, B., Seaward, G., and Kaufmann, P. (2000). Development of the placental villous tree and its consequences for fetal growth. *Eur. J. Obstet. Gynecol. Reprod. Biol.* 92, 35–43. doi:10.1016/S0301-2115(00)00423-1
- Krebs, L. T., Shutter, J. R., Tanigaki, K., Honjo, T., Stark, K. L., and Gridley, T. (2004). Haploinsufficient lethality and formation of arteriovenous malformations in Notch pathway mutants. *Genes. Dev.* 18, 2469–2473. doi:10.1101/gad.1239204
- Kulkarni, M. L., Matadh, P. S., Ashok, C., Pradeep, N., Avinash, T., and Kulkarni, A. M. (2007). Absence of Wharton's jelly around the umbilical arteries. *Indian J. Pediatr.* 74, 787–789. doi:10.1007/s12098-007-0142-7
- Labarrere, C., Sebastiani, M., Siminovich, M., Torassa, E., and Althabe, O. (1985). Absence of Wharton's jelly around the umbilical arteries: an unusual cause of perinatal mortality. *Placenta* 6, 555–559. doi:10.1016/S0143-4004(85)80010-2
- Lebart, M., and Benyamin, Y. (2006). Calpain involvement in the remodeling of cytoskeletal anchorage complexes. *FEBS J.* 273, 3415–3426. doi:10.1111/j.1742-4658.2006.05350.x
- le Noble, F., Fleury, V., Pries, A., Corvol, P., Eichmann, A., and Reneman, R. S. (2005). Control of arterial branching morphogenesis in embryogenesis: go with the flow. *Cardiovasc. Res.* 65, 619–628. doi:10.1016/j.cardiores.2004.09.018
- le Noble, F., Moyon, D., Pardauna, L., Yuan, L., Djonov, V., Matthijsen, R., et al. (2004). Flow regulates arterial-venous differentiation in the chick embryo yolk sac. *Development* 131, 361–375. doi:10.1242/dev.00929
- Li, J., Hou, B., Tumova, S., Muraki, K., Bruns, A., Ludlow, M. J., et al. (2014a). Piezo1 integration of vascular architecture with physiological force. *Nature* 515, 279–282. doi:10.1038/nature13701
- Li, R., Beebe, T., Jen, N., Yu, F., Takabe, W., Harrison, M., et al. (2014b). Shear stress-activated wnt-angiopoietin-2 signaling recapitulates vascular repair in zebrafish embryos. *Arterioscler. Thromb. Vasc. Biol.* 34, 2268–2275. doi:10.1161/ATVBAHA.114.303345
- Li, T., Nie, F., Li, Z., Wang, Y., and Li, Q. (2019). Evaluation of right ventricular function in fetuses with isolated single umbilical artery using spatiotemporal image correlation M-mode. *Cardiovasc. Ultrasound* 17, 14. doi:10.1186/s12947-019-0164-0
- Linask, K. K., Han, M., and Bravo-Valenzuela, N. J. M. (2014). Changes in vitelline and utero-placental hemodynamics: implications for cardiovascular development. *Front. Physiol.* 5, 390–412. doi:10.3389/fphys.2014.00390
- Li-Villareal, N., Wong, R. L. Y., Garcia, M. D., Udan, R. S., Poché, R. A., Rasmussen, T. L., et al. (2022). FOXO1 represses sprouty 2 and sprouty 4 expression to promote arterial specification and vascular remodeling in the mouse yolk sac. *Development* 149, dev200131. doi:10.1242/dev.200131
- Lu, D., and Kassab, G. S. (2011). Role of shear stress and stretch in vascular mechanobiology. *J. R. Soc. Interface* 8, 1379–1385. doi:10.1098/rsif.2011.0177
- Lu, J., Wu, W., Xin, Q., Zhou, C., Wang, J., Ni, Z., et al. (2019). Spatiotemporal coordination of trophoblast and allantoic Rbpj signaling directs normal placental morphogenesis. *Cell Death Dis.* 10, 438–514. doi:10.1038/s41419-019-1683-1
- Lucitti, J. L., Jones, E. A. V., Huang, C., Chen, J., Fraser, S. E., and Dickinson, M. E. (2007). Vascular remodeling of the mouse yolk sac requires hemodynamic force. *Development* 134, 3317–3326. doi:10.1242/dev.02883
- Luckett, W. P. (1978). Origin and differentiation of the yolk sac and extraembryonic mesoderm in presomite human and rhesus monkey embryos. *Am. J. Anat.* 152, 59–97. doi:10.1002/aja.1001520106
- Luse, M. A., Jackson, M. G., Juszkiewicz, Z. J., and Isakson, B. E. (2023). Physiological functions of caveolae in endothelium. *Curr. Opin. Physiol.* 35, 100701. doi:10.1016/j.cophys.2023.100701
- Luu, V. Z., Chowdhury, B., Al-Omran, M., Hess, D. A., and Verma, S. (2018). Role of endothelial primary cilia as fluid mechanosensors on vascular health. *Atherosclerosis* 275, 196–204. doi:10.1016/j.atherosclerosis.2018.06.818
- Mandalà, M. (2020). Influence of estrogens on uterine vascular adaptation in normal and preeclamptic pregnancies. *Int. J. Mol. Sci.* 21, 2592. doi:10.3390/ijms21072592
- Mantoni, M., and Pedersen, J. F. (1979). Ultrasound visualization of the human yolk sac. *J. Clin. Ultrasound* 7, 459–460. doi:10.1002/jcu.1870070608
- Martinelli, L. M., Carucci, A., Payano, V. J. H., Connor, K. L., and Bloise, E. (2023). Translational comparison of the human and mouse yolk sac development and function. *Reprod. Sci.* 30, 41–53. doi:10.1007/s43032-022-00872-8
- McGrath, K. E., Koniski, A. D., Malik, J., and Palis, J. (2003). Circulation is established in a stepwise pattern in the mammalian embryo. *Blood* 101, 1669–1676. doi:10.1182/blood-2002-08-2531
- McHugh, B. J., Buttery, R., Lad, Y., Banks, S., Haslett, C., and Sethi, T. (2010). Integrin activation by Fam38A uses a novel mechanism of R-Ras targeting to the endoplasmic reticulum. *J. Cell Sci.* 123, 51–61. doi:10.1242/jcs.056424
- Mehta, V., Pang, K.-L., Rozbesky, D., Nather, K., Keen, A., Lachowski, D., et al. (2020). The guidance receptor plexin D1 is a mechanosensor in endothelial cells. *Nature* 578, 290–295. doi:10.1038/s41586-020-1979-4
- Meyer, W. W., Rumpelt, H. J., Yao, A. C., and Lind, J. (1978). Structure and closure mechanism of the human umbilical artery. *Eur. J. Pediatr.* 128, 247–259. doi:10.1007/BF00445610
- Miyazaki, T., Honda, K., and Ohata, H. (2007). Requirement of Ca²⁺ influx- and phosphatidylinositol 3-kinase-mediated m-calpain activity for shear stress-induced endothelial cell polarity. *Am. J. Physiol. Physiol.* 293, C1216–C1225. doi:10.1152/ajpcell.00083.2007
- Morley, L. C., Beech, D. J., Walker, J. J., and Simpson, N. A. B. (2019). Emerging concepts of shear stress in placental development and function. *Mol. Hum. Reprod.* 25, 329–339. doi:10.1093/molehr/gaz018
- Mu, J., and Adamson, S. L. (2006). Developmental changes in hemodynamics of uterine artery, utero- and umbilicoplacental, and vitelline circulations in mouse throughout gestation. *Am. J. Physiol. - Hear. Circ. Physiol.* 291, 1421–1428. doi:10.1152/ajpheart.00031.2006
- Murphy, S. J., Deegan, N., O'Leary, B. D., and McParland, P. (2020). Absence of Wharton's jelly. *BMJ Case Rep.* 13, e237222–e237223. doi:10.1136/bcr-2020-237222
- Myatt, L. (1992). Control of vascular resistance in the human placenta. *Placenta* 13, 329–341. doi:10.1016/0143-4004(92)90057-Z
- Nandadasa, S., Nelson, C. M., and Apte, S. S. (2015). ADAMTS9-Mediated extracellular matrix dynamics regulates umbilical cord vascular smooth muscle differentiation and rotation. *Cell Rep.* 11, 1519–1528. doi:10.1016/j.celrep.2015.05.005
- Nandadasa, S., Szafron, J. M., Pathak, V., Murtada, S., Kraft, C. M., O'donnell, A., et al. (2020). Vascular dimorphism ensured by regulated proteoglycan dynamics favors rapid umbilical artery closure at birth. *Elife* 9, e60633–e60730. doi:10.7554/ELIFE.60633
- Oldak, B., Wildschutz, E., Bondarenko, V., Comar, M. Y., Zhao, C., Aguilera-Castrejon, A., et al. (2023). Complete human day 14 post-implantation embryo models from naive ES cells. *Nature* 622, 562–573. doi:10.1038/s41586-023-06604-5
- Osol, G., and Mandalà, M. (2009). Maternal uterine vascular remodeling during pregnancy. *Physiology* 24, 58–71. doi:10.1152/physiol.00033.2008
- Palis, J., and Yoder, M. C. (2001). Yolk-sac hematopoiesis: the first blood cells of mouse and man. *Exp. Hematol.* 29, 927–936. doi:10.1016/S0301-472X(01)00669-5
- Pang, Y., Dong, J., and Thomas, P. (2015). Progesterone increases nitric oxide synthesis in human vascular endothelial cells through activation of membrane

- progesterone receptor- α . *Am. J. Physiol. Metab.* 308, E899–E911. doi:10.1152/ajpendo.00527.2014
- Panja, S., and Paria, B. C. (2021). Development of the mouse placenta. *Adv. Anat. Embryol. Cell Biol.* 234, 205–221. doi:10.1007/978-3-030-77360-1_10
- Perez-Garcia, V., Fineberg, E., Wilson, R., Murray, A., Mazzeo, C. I., Tudor, C., et al. (2018). Placentation defects are highly prevalent in embryonic lethal mouse mutants. *Nature* 555, 463–468. doi:10.1038/nature26002
- Ramesh, S., Hariprasath, S., Anandan, G., Solomon, P., and Vijayakumar, V. (2015). Single umbilical artery. *J. Pharm. Bioallied Sci.* 7, 83–S84. doi:10.4103/0975-7406.155815
- Ranade, S. S., Qiu, Z., Woo, S. H., Hur, S. S., Murthy, S. E., Cahalan, S. M., et al. (2014). Piezo1, a mechanically activated ion channel, is required for vascular development in mice. *Proc. Natl. Acad. Sci. U. S. A.* 111, 10347–10352. doi:10.1073/pnas.1409233111
- Rashdan, N. A., and Lloyd, P. G. (2015). Fluid shear stress upregulates placental growth factor in the vessel wall via NADPH oxidase 4. *Am. J. Physiol. - Hear. Circ. Physiol.* 309, H1655–H1666. doi:10.1152/ajpheart.00408.2015
- Rizzo, V., Sung, A., Oh, P., and Schnitzer, J. E. (1998). Rapid mechanotransduction *in situ* at the luminal cell surface of vascular endothelium and its caveolae. *J. Biol. Chem.* 273, 26323–26329. doi:10.1074/jbc.273.41.26323
- Rodriguez, A. M., and Downs, K. M. (2017). Visceral endoderm and the primitive streak interact to build the fetal-placental interface of the mouse gastrula. *Dev. Biol.* 432, 98–124. doi:10.1016/j.ydbio.2017.08.026
- Rodriguez, A. M., Jin, D. X., Wolfe, A. D., Mikedis, M. M., Wierenga, L., Hashmi, M. P., et al. (2017). Brachyury drives formation of a distinct vascular branchpoint critical for fetal-placental arterial union in the mouse gastrula. *Dev. Biol.* 425, 208–222. doi:10.1016/j.ydbio.2017.03.032
- Rossant, J., and Cross, J. C. (2001). Placental development: lessons from mouse mutants. *Nat. Rev. Genet.* 2, 538–548. doi:10.1038/35080570
- Saotome, K., Murthy, S. E., Kefauver, J. M., Whitwam, T., Patapoutian, A., and Ward, A. B. (2018). Structure of the mechanically activated ion channel Piezo1. *Nature* 554, 481–486. doi:10.1038/nature25453
- Saw, S. N., Dawn, C., Biswas, A., Mattar, C. N. Z., and Yap, C. H. (2017). Characterization of the *in vivo* wall shear stress environment of human fetus umbilical arteries and veins. *Biomech. Model. Mechanobiol.* 16, 197–211. doi:10.1007/s10237-016-0810-5
- Saw, S. N., Poh, Y. W., Chia, D., Biswas, A., Mattar, C. N. Z., and Yap, C. H. (2018). Characterization of the hemodynamic wall shear stresses in human umbilical vessels from normal and intrauterine growth restricted pregnancies. *Biomech. Model. Mechanobiol.* 17, 1107–1117. doi:10.1007/s10237-018-1017-8
- Shalaby, F., Rossant, J., Yamaguchi, T. P., Gertsenstein, M., Wu, X. F., Breitman, M. L., et al. (1995). Failure of blood-island formation and vasculogenesis in Flk-1-deficient mice. *Nature* 376, 62–66. doi:10.1038/376062a0
- Shay-Salit, A., Shushy, M., Wolfovitz, E., Yahav, H., Breviaro, F., Dejana, E., et al. (2002). VEGF receptor 2 and the adherens junction as a mechanical transducer in vascular endothelial cells. *Proc. Natl. Acad. Sci.* 99, 9462–9467. doi:10.1073/pnas.142224299
- Shin, H., Haga, J. H., Kosawada, T., Kimura, K., Li, Y. S., Chien, S., et al. (2019). Fine control of endothelial VEGFR-2 activation: caveolae as fluid shear stress shelters for membrane receptors. *Biomech. Model. Mechanobiol.* 18, 5–16. doi:10.1007/s10237-018-1063-2
- Silini, A. R., Di Pietro, R., Lang-Olip, I., Alviano, F., Banerjee, A., Basile, M., et al. (2020). Perinatal derivatives: Where do we stand? A roadmap of the human placenta and consensus for tissue and cell nomenclature. *Front. Bioeng. Biotechnol.* 8, 1–33. doi:10.3389/fbioe.2020.610544
- Soares, M. J., Iqbal, K., and Kozai, K. (2017). Hypoxia and placental development. *Birth Defects Res.* 109, 1309–1329. doi:10.1002/bdr2.1135
- Soares, M. J., Varberg, K. M., and Iqbal, K. (2018). Hemochorial placentation: development, function, and adaptations. *Biol. Reprod.* 99, 196–211. doi:10.1093/biolre/iy049
- Spurway, J., Logan, P., and Pak, S. (2012). The development, structure and blood flow within the umbilical cord with particular reference to the venous system. *Australas. J. Ultrasound Med.* 15, 97–102. doi:10.1002/j.2205-0140.2012.tb00013.x
- Strong, T. H., Jarles, D. L., Vega, J. S., and Feldman, D. B. (1994). The umbilical coiling index. *Am. J. Obstet. Gynecol.* 170, 29–32. doi:10.1016/S0002-9378(94)70378-7
- Tao, J., Yang, Z., Wang, J.-M., Tu, C., and Pan, S.-R. (2006). Effects of fluid shear stress on eNOS mRNA expression and NO production in human endothelial progenitor cells. *Cardiology* 106, 82–88. doi:10.1159/000092636
- Tarbell, J. M., and Pahakis, M. Y. (2006). Mechanotransduction and the glycocalyx. *J. Intern. Med.* 259, 339–350. doi:10.1111/j.1365-2796.2006.01620.x
- Tavian, M., and Péault, B. (2005). The changing cellular environments of hematopoiesis in human development *in utero*. *Exp. Hematol.* 33, 1062–1069. doi:10.1016/j.exphem.2005.06.025
- Tzima, E., Irani-Tehrani, M., Kiosses, W. B., Dejana, E., Schultz, D. A., Engelhardt, B., et al. (2005). A mechanosensory complex that mediates the endothelial cell response to fluid shear stress. *Nature* 437, 426–431. doi:10.1038/nature03952
- Udan, R. S., Culver, J. C., and Dickinson, M. E. (2013a). Understanding vascular development. *WIREs Dev. Biol.* 2, 327–346. doi:10.1002/wdev.91
- Udan, R. S., Vadakkan, T. J., and Dickinson, M. E. (2013b). Dynamic responses of endothelial cells to changes in blood flow during vascular remodeling of the mouse yolk sac. *Development* 140, 4041–4050. doi:10.1242/dev.096255
- van der Heijden, O. W. H., Essers, Y. P. G., Fazzi, G., Peeters, L. L. H., De Mey, J. G. R., and van Eys, G. J. M. (2005). Uterine artery remodeling and reproductive performance are impaired in endothelial nitric oxide synthase-deficient mice. *Biol. Reprod.* 72, 1161–1168. doi:10.1095/biolreprod.104.033985
- Wang, S., Chennupati, R., Kaur, H., Iring, A., Wettschurek, N., and Offermanns, S. (2016). Endothelial cation channel PIEZO1 controls blood pressure by mediating flow-induced ATP release. *J. Clin. Invest.* 126, 4527–4536. doi:10.1172/JCI87343
- Watson, E. D., and Cross, J. C. (2005). Development of structures and transport functions in the mouse placenta. *Physiology* 20, 180–193. doi:10.1152/physiol.00001.2005
- Weissman, A., Jakobi, P., Bronshtein, M., and Goldstein, I. (1994). Sonographic measurements of the umbilical cord and vessels during normal pregnancies. *J. Ultrasound Med.* 13, 11–14. doi:10.7863/jum.1994.13.1.11
- Woods, L., Perez-Garcia, V., and Hemberger, M. (2018). Regulation of placental development and its impact on fetal growth—new insights from mouse models. *Front. Endocrinol. (Lausanne)* 9, 570–618. doi:10.3389/fendo.2018.00570
- Wragg, J. W., Durant, S., McGettrick, H. M., Sample, K. M., Egginton, S., and Bicknell, R. (2014). Shear stress regulated gene expression and angiogenesis in vascular endothelium. *Microcirculation* 21, 290–300. doi:10.1111/micc.12119
- Xiao, R., Liu, J., and Shawn Xu, X. Z. (2023). Mechanosensitive GPCRs and ion channels in shear stress sensing. *Curr. Opin. Cell Biol.* 84, 102216. doi:10.1016/j.ceb.2023.102216
- Zhang, J., Chen, Z., Smith, G. N., and Croy, B. A. (2011). Natural killer cell-triggered vascular transformation: maternal care before birth? *Cell. Mol. Immunol.* 8, 1–11. doi:10.1038/cmi.2010.38
- Zhao, Q., Zhou, H., Chi, S., Wang, Y., Wang, J., Geng, J., et al. (2018). Structure and mechanogating mechanism of the Piezo1 channel. *Nature* 554, 487–492. doi:10.1038/nature25743
- Zhou, Y.-Q., Cahill, L. S., Wong, M. D., Seed, M., Macgowan, C. K., and Sled, J. G. (2014). Assessment of flow distribution in the mouse fetal circulation at late gestation by high-frequency Doppler ultrasound. *Physiol. Genomics* 46, 602–614. doi:10.1152/physiolgenomics.00049.2014



OPEN ACCESS

EDITED BY

Julia J. Mack,
UCLA Health System, United States

REVIEWED BY

Matthew Caporizzo,
University of Vermont, United States
Thomas M. Vondriska,
University of California, Los Angeles,
United States

*CORRESPONDENCE

Victoria L. Bautch,
✉ bautch@med.unc.edu

RECEIVED 03 April 2024

ACCEPTED 02 May 2024

PUBLISHED 20 May 2024

CITATION

Bougaran P and Bautch VL (2024), Life at the crossroads: the nuclear LINC complex and vascular mechanotransduction.
Front. Physiol. 15:1411995.
doi: 10.3389/fphys.2024.1411995

COPYRIGHT

© 2024 Bougaran and Bautch. This is an open-access article distributed under the terms of the [Creative Commons Attribution License \(CC BY\)](https://creativecommons.org/licenses/by/4.0/). The use, distribution or reproduction in other forums is permitted, provided the original author(s) and the copyright owner(s) are credited and that the original publication in this journal is cited, in accordance with accepted academic practice. No use, distribution or reproduction is permitted which does not comply with these terms.

Life at the crossroads: the nuclear LINC complex and vascular mechanotransduction

Pauline Bougaran¹ and Victoria L. Bautch^{1,2*}

¹Department of Biology, The University of North Carolina, Chapel Hill, NC, United States, ²McAllister Heart Institute, The University of North Carolina, Chapel Hill, NC, United States

Vascular endothelial cells line the inner surface of all blood vessels, where they are exposed to polarized mechanical forces throughout their lifespan. Both basal substrate interactions and apical blood flow-induced shear stress regulate blood vessel development, remodeling, and maintenance of vascular homeostasis. Disruption of these interactions leads to dysfunction and vascular pathologies, although how forces are sensed and integrated to affect endothelial cell behaviors is incompletely understood. Recently the endothelial cell nucleus has emerged as a prominent force-transducing organelle that participates in vascular mechanotransduction, via communication to and from cell-cell and cell-matrix junctions. The LINC complex, composed of SUN and nesprin proteins, spans the nuclear membranes and connects the nuclear lamina, the nuclear envelope, and the cytoskeleton. Here we review LINC complex involvement in endothelial cell mechanotransduction, describe unique and overlapping functions of each LINC complex component, and consider emerging evidence that two major SUN proteins, SUN1 and SUN2, orchestrate a complex interplay that extends outward to cell-cell and cell-matrix junctions and inward to interactions within the nucleus and chromatin. We discuss these findings in relation to vascular pathologies such as Hutchinson-Gilford progeria syndrome, a premature aging disorder with cardiovascular impairment. More knowledge of LINC complex regulation and function will help to understand how the nucleus participates in endothelial cell force sensing and how dysfunction leads to cardiovascular disease.

KEYWORDS

endothelial cell, nucleus, LINC complex, SUN protein, mechanotransduction, cytoskeleton, lamin, vascular disease

1 Introduction

Unlike many other tissues, blood vessels are exposed to mechanical forces that strongly influence both vessel development and vascular function (Roux et al., 2020), and inappropriate or incomplete responses to these forces trigger vascular disease (Marchuk et al., 2003; Baeyens et al., 2016; Humphrey and Schwartz, 2021; Tabosh et al., 2024). Early work showed that the endothelial cells lining all blood vessels align their cytoskeleton and nucleus-centrosome-Golgi axis to the shear stress vector imparted by laminar blood flow (Reidy and Langille, 1980; Dewey et al., 1981; Remuzzi et al., 1984). Other forces created by blood flow, including cyclic strain and outward pressure, also influence endothelial cell responses and those of support cells such as vascular smooth muscle (Hoefer et al., 2013; Campinho et al., 2020). Vascular flow patterns strongly coincide with disease development *in vivo*; for example, areas of disturbed flow such as vessel branch points are prone to

atherosclerotic plaque development. Plaque formation leads to reduced blood flow, additional turbulence, and in some cases, plaque rupture and the formation of blood clots.

Mechanical forces generated by laminar blood flow are crucial for vascular remodeling once a primitive vascular plexus forms during development. Vascular remodeling leads to large arterial conduits that branch into smaller arterioles, then into small diameter capillaries that eventually lead to larger caliber venules and veins that return blood to the heart on the venous side. This pattern results from the regression of early vessel segments that experience reduced flow, while segments with elevated blood flow remain and enlarge (Potente et al., 2011). Endothelial cell responses to blood flow strongly contribute to the hierarchical distribution of vessel diameters in most vascular beds, and several lines of evidence support the model that endothelial cells migrate from areas of low flow to areas of higher flow as the vascular network is remodeled and patterned (Udan et al., 2013; Xu et al., 2014; Franco et al., 2015; Pitulescu et al., 2017; Lee et al., 2022). Although initial arterial-venous identity is not flow-dependent, the maintenance of arterial-venous status relies on shear stress, and higher magnitude shear vectors maintain arterial identity while lower vectors maintain venous identity (le Noble et al., 2004; Chong et al., 2011). Finally, laminar flow is critical to maintain vascular homeostasis and an anti-inflammatory state in endothelial cells. Disturbed flow, or the inability of endothelial cells to respond to laminar flow, sets up a pro-inflammatory endothelial cell phenotype that often leads to disease. Thus, blood vessel formation and function are intimately linked to proper endothelial cell responses to mechanical signals.

Endothelial cells form a flattened monolayer on the inner vessel wall that is a single cell layer thick, with very little cytoplasm between the apical (luminal) and basal (abluminal) endothelial surfaces. In this topology, the endothelial cell nucleus extends above the apical plane of the cytoplasm, essentially leaving it exposed to shear forces created by blood flow. Despite this topology and evidence that the nucleus is required for flow-mediated endothelial cell functions and migration (Tkachenko et al., 2013; Guilluy et al., 2014; Graham et al., 2018), how the nucleus acts as a mechanotransducer in endothelial cells is poorly understood, and how the nucleus integrates cytoplasmic mechanotransduction inputs has not been extensively investigated. However, nuclear integrity in vascular cells is important for proper vessel function and maintenance, and human mutations in nuclear-localized proteins such as lamin-A lead to diseases with cardiovascular dysfunction such as Hutchinson-Gilford progeria Syndrome (Östlund et al., 2019).

Several molecules and molecular complexes that reside in the endothelial cell plasma membrane, often at cell-cell junctions, transduce flow-generated mechanical forces on the apical side. These structures, such as PECAM1/VE-cadherin/VEGFR2, Piezo channels, and plexin D1, translate mechanical inputs into cellular signaling readouts (Tzima et al., 2005; Duchemin et al., 2019; Mehta et al., 2020), that in turn regulate flow-responsive signaling pathways in endothelial cells. The BMP pathway is one example of a flow-responsive signaling axis, where key signaling components likely do not act as direct sensors but are strongly regulated by flow-mediated inputs (Han et al., 2021; Desroches-Castan et al., 2022; Kulikauskas et al., 2022). In contrast to the extensive literature on endothelial cell signaling in general, how the nucleus participates in mechanotransduction is poorly understood. The LINC (Linker of

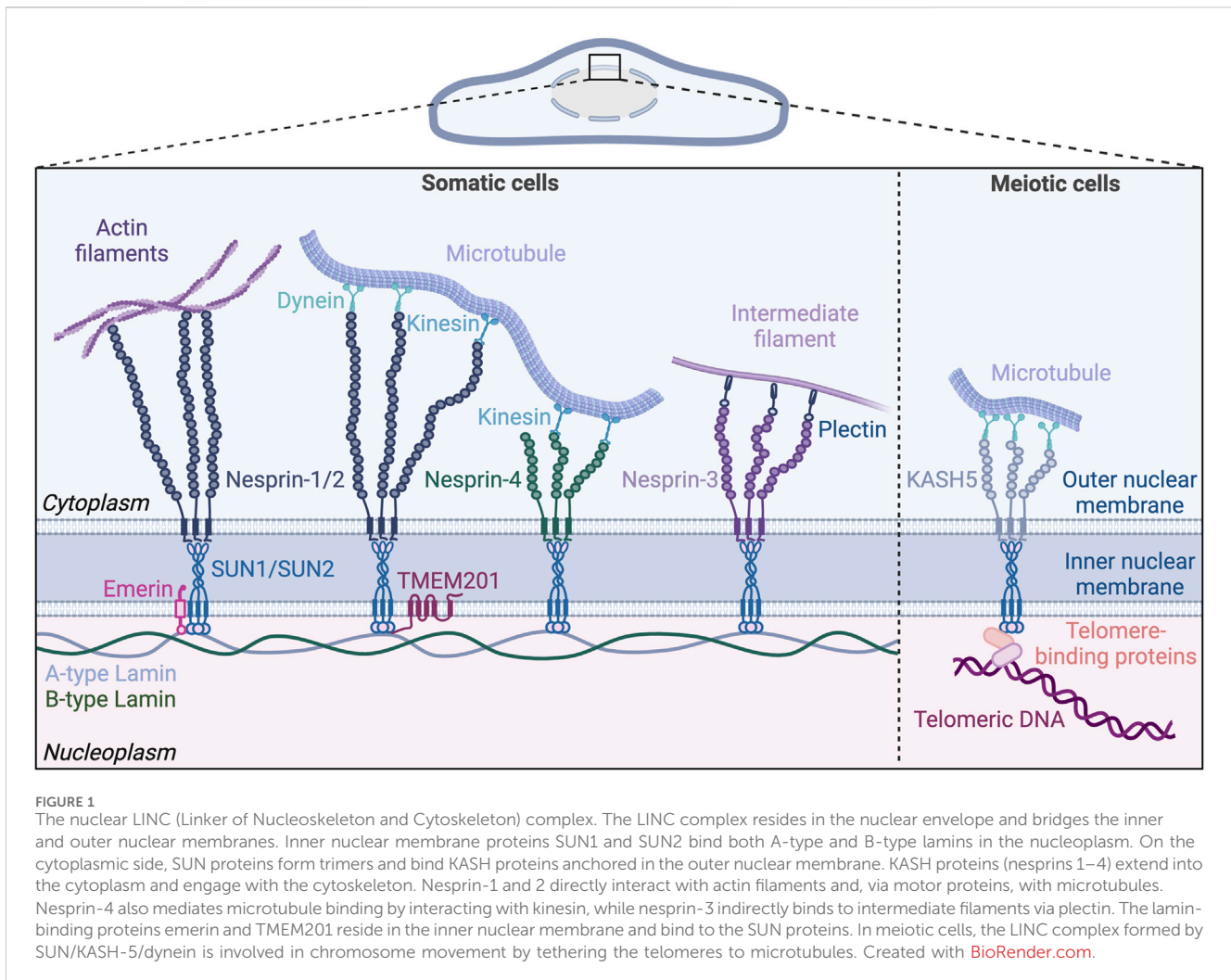
Nucleoskeleton and Cytoskeleton) complex resides in the nuclear envelope and bridges the nucleus and cytoskeleton, and it has recently been implicated in mechanotransduction processes (Janota et al., 2020; King, 2023). Although most of the published work is in non-vascular cells, some recent studies examine LINC complex functions in the vasculature (Mannion and Holmgren, 2023).

Here we provide a brief overview of the LINC complex, followed by a specific focus on its function in vascular endothelial cells. Other recent excellent reviews discuss the role of the LINC complex in non-vascular cells and in non-endothelial vascular cells (Iyer et al., 2021; Salvador and Iruela-Arispe, 2022). The LINC complex consists of inner nuclear membrane-localized SUN (Sad1, UNC84) proteins that interact with lamin intermediate filaments in the nucleus and KASH (Klarsicht/ANC-1/Syne Homology) proteins in the outer nuclear membrane that in turn interact with the actin, microtubule, and intermediate filament cytoskeletons outside the nucleus (Starr, 2019; McGillivray et al., 2023). Given the promiscuous nature of KASH protein interactions with SUN proteins and cytoskeletal components, this review primarily focuses on the two major SUN proteins. We picture the SUN proteins sitting in the inner nuclear membrane of the endothelial cell lining the blood vessel (Figure 1). Like Janus, they face both inward to the nucleus proper and outward to the cytoplasm via KASH interactions, with outside-in interactions transmitting cytoskeletal changes to the nucleus and chromatin, while inside-out interactions integrate nuclear inputs for transmission to the cytoplasm and plasma membrane (Hieda, 2019). We describe cell-based and *in vivo* studies that inform our current knowledge of endothelial cell SUN protein function, we discuss links to cardiovascular pathologies, and we highlight future directions that will inform how the endothelial cell integrates nuclear mechanotransduction to respond to forces that regulate vascular function and disease.

2 The LINC complex: a bridge between the nucleus and cytoskeleton

The mechanosensing properties of the nucleus are the focus of recent work (Kirby and Lammerding, 2018; Östlund et al., 2019). The nucleoplasm contains the genetic information of the cell, DNA, organized as chromatin. The nucleoplasm is enclosed by the nuclear envelope, which is a double membrane consisting of inner and outer layers separated by perinuclear space. Nuclear pore complexes span both membranes and facilitate exchange between the nucleoplasm and cytoplasm (Gerace et al., 1978; Gerace and Burke, 1988). On the nucleus side, the inner membrane is next to an interconnected network of A-type (lamin-A and C) and B-type (lamin-B1 and B2) lamin intermediate filaments that form the nuclear lamina (Gerace et al., 1984).

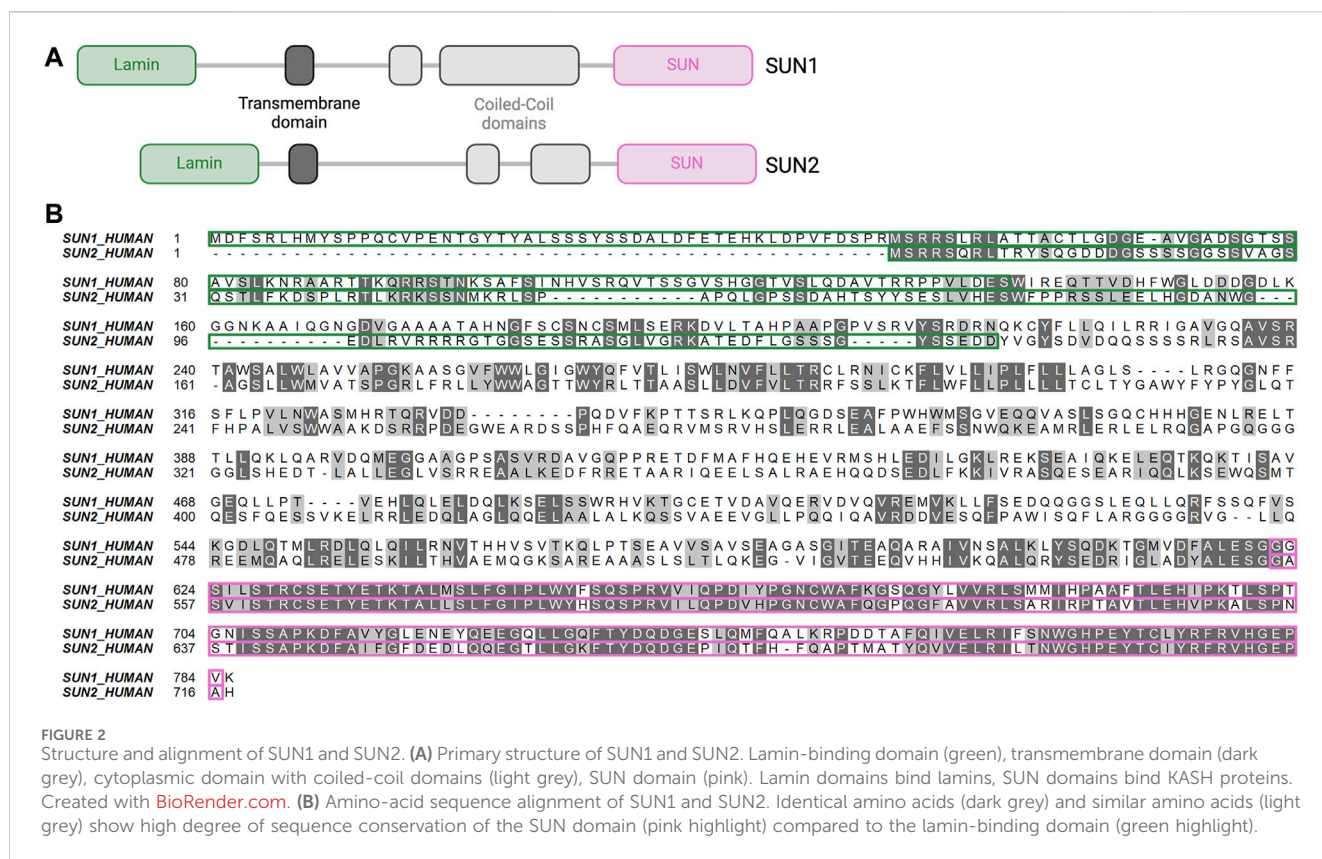
The LINC complex resides in the nuclear envelope and connects the inner nucleoplasm with cytoskeletal components (Figure 1). The LINC complex consists of SUN proteins located in the inner nuclear membrane and KASH proteins located in the outer nuclear membrane (Stroud et al., 2014). SUN proteins span the inner nuclear membrane via a single transmembrane domain, with their N-terminal and C-terminal domains exposed to the nucleoplasm and the perinuclear space, respectively



(Padmakumar et al., 2005; Crisp et al., 2006). The N-terminal domain of the SUN proteins binds nuclear lamins and chromatin-binding proteins in the nucleoplasm (Crisp et al., 2006; Haque et al., 2006; Chi et al., 2007; Wang et al., 2020) (Figure 2A). Lamin-associated proteins residing in the inner nuclear membrane, including emerlin and TMEM201 (also known as NET5 or Samp1) also interact with SUN proteins and anchor the LINC complex in the nuclear envelope (Haque et al., 2010; Zhang et al., 2022). C-terminal SUN domains bind the KASH domain of KASH proteins in the perinuclear space. On the cytoplasmic side of the outer nuclear membrane, N-terminal regions of KASH proteins interact with all major cytoskeletal components including microtubules, actin, and intermediate filaments (Luxton and Starr, 2014).

SUN1 and SUN2 are expressed in most mammalian cells, with three additional SUN proteins expressed primarily in male germ cells (Malone et al., 1999; Shao et al., 1999; Hodzic et al., 2004; Xing et al., 2004; Padmakumar et al., 2005; Göb et al., 2010). Mammals express six KASH domain-containing proteins, including the four nesprins (Nuclear envelope spectrin repeat proteins), nesprins-1 to 4, as well as KASH-5, and lymphoid-restricted membrane protein (LRMP, also known as Jaw-1 or KASH-6) (Behrens et al., 1994; Zhang et al., 2001; Wilhelmsen

et al., 2005; Roux et al., 2009; Morimoto et al., 2012; Horn et al., 2013b; Kim et al., 2015). Nesprin-1 and 2 are ubiquitously expressed and were originally believed to only associate with actin filaments via their N-terminal actin binding domains (Zhang et al., 2001; Zhang et al., 2002). However, further research showed that nesprin-1 and 2 also link to microtubules indirectly through motor proteins that bind both microtubules and nesprins (Zhang et al., 2009; Yu et al., 2011). Nesprin-3 is also ubiquitously expressed, and it has a plectin-binding domain that binds to intermediate filaments via plectin instead of an actin-binding domain (Wilhelmsen et al., 2005). Balanced forces from microtubules and intermediate filaments in cardiomyocytes act through nesprin-1/2 and nesprin-3, respectively, to maintain nuclear morphology and regulate gene expression (Heffler et al., 2020). Nesprin-4 is mainly expressed in secretory epithelial cells (Horn et al., 2013b) and can interact with the motor protein kinesin to mediate microtubule binding (Roux et al., 2009). KASH-5 expression is limited to germline cells where it interacts with the dynein/dynactin complex associated with microtubules during meiosis (Morimoto et al., 2012). LRMP, found in the outer nuclear membrane and in the endoplasmic reticulum (ER), interacts with microtubules, although the binding mechanism is unclear (Kozono et al., 2018; Okumura et al., 2023).



The LINC complex has a key role in force mechanotransduction between the nucleus and the cytoskeleton, although how this is accomplished mechanistically is not well understood. A wide range of cellular functions are attributed to the LINC complex, from regulation of DNA repair (Lawrence et al., 2016), chromatin architecture (Ghosh et al., 2021) and chromosome movement during meiosis (Ding et al., 2007), to functions far from the nucleus such as cell-substrate adhesion (Chancellor et al., 2010). The LINC complex regulates aspects of cell migration and polarization via poorly understood mechanisms that likely involve its control of nuclear shape and positioning, and the nucleus-centrosome connection (Lombardi et al., 2011; Banerjee et al., 2014; Heffler et al., 2020; Nishino et al., 2023). Consistent with their pivotal role in cellular functions, mutations in genes encoding LINC complex components or interacting partners are associated with pathological conditions known as nuclear envelopathies (Janin et al., 2017). Examples include Hutchinson-Gilford progeria syndrome (HGPS), Emery-Dreifuss muscular dystrophy (EDMD), and dilated cardiomyopathy (see below for more detail).

3 SUN proteins: key integrators of LINC complex function

SUN1 and SUN2 interact molecularly with the nucleus via their N-terminal domains, and with the cytoskeleton indirectly via interactions of their C-terminal domains with KASH proteins. Thus, they are key integrators in the LINC complex, but the interplay between these two major SUN proteins, and how they

interact with other binding partners, are incompletely understood. They are described as having both unique and overlapping functions.

3.1 SUN protein structure and function

SUN1 and SUN2 were first identified as homologues of the *C. elegans* proteins UNC-84A and UNC-84B, respectively (Malone et al., 1999). The SUN domain of SUN proteins is highly conserved throughout evolution (Fridkin et al., 2009). Human SUN1 and SUN2 share 46% overall amino acid sequence similarity that varies among domains, with the KASH-binding SUN domains having high conservation (82% similarity), while lamin-binding domains have low conservation (19.7% similarity) (Figure 2B). These sequence disparities and similarities likely account for the distinct vs. shared binding affinities of individual SUN proteins for lamins and nesprins, respectively. The precise mechanism by which the LINC complex links the cytoskeleton and the chromatin remains unclear. It is uncertain whether these interactions occur directly through the SUN proteins or indirectly via interactions with lamin-A or emerin, both of which can bind chromatin proteins (Lee et al., 2001; Gesson et al., 2016). SUN1 directly binds chromatin and DNA via its N-terminal domain in *Dictyostelium discoideum* (Xiong et al., 2008). Although SUN1 directly binds DNA in lower eucaryotes, there is no evidence of direct binding between SUN proteins and DNA in mammalian cells. However, chromatin binding and immunoprecipitation assays revealed interaction of SUN1 with histone H2B in HeLa cells (Chi et al., 2007) and of SUN1 and

SUN2 with DNA-dependent protein kinase complex in 293T cells (Lei et al., 2012). Both SUN1 and SUN2 interact with telomere-associated proteins such as MAJIN to tether telomeres to the nuclear envelope during meiosis (Schmitt et al., 2007; Wang et al., 2020; Chen et al., 2021). Both SUN1 and SUN2 interact with lamin-A and to a weaker degree with lamin-B1/C via their N-terminal domains (Crisp et al., 2006; Haque et al., 2006). However, SUN1 and SUN2 are differentially anchored to the nuclear lamina, with FRET (Fluorescence Resonance Energy Transfer) analysis revealing a stronger SUN1/lamin-A association than SUN2/lamin-A association (Östlund et al., 2009). Moreover, co-immunoprecipitation analysis in HeLa cells revealed that B-type lamins interact with SUN1 and not with SUN2 (Nishioka et al., 2016). Both SUN1 and SUN2 bind to type-A lamin-interacting proteins such as emerin (Haque et al., 2010). In addition, SUN1, and not SUN2, is closely associated with nuclear pore complexes and contributes to mRNA export in HeLa cells (Liu et al., 2007; Li et al., 2017). SUN1 association with nuclear pore complexes requires both SUN1 nucleoplasm and transmembrane domains (Liu et al., 2007).

The KASH-binding domains of human SUN1 and SUN2 are highly conserved, and both similar and distinct interactions between SUN and KASH proteins have been described. Both SUN1 and SUN2 bind all six mammalian nesprins (Padmakumar et al., 2005; Crisp et al., 2006; Ketema et al., 2007; Stewart-Hutchinson et al., 2008; Morimoto et al., 2012; Cruz et al., 2020; Gurusaran and Davies, 2021). Structural analysis showed that SUN1 and SUN2 form trimers in the nuclear membrane, with each trimer interacting with three KASH proteins (Sosa et al., 2012; Wang et al., 2012; Zhou et al., 2012; Jahed et al., 2021; McGillivray et al., 2023) (Figure 1). Early co-immunoprecipitation experiments suggested that SUN1 and SUN2 can bind each other and potentially form heterooligomers (Wang et al., 2006; Lu et al., 2008), while more recent crystallographic analysis suggested that SUN1 and SUN2 form homotrimers (Jahed et al., 2018a). Each SUN protein has two coiled-coil domains (CC1 and CC2), and these domains and the SUN domain extend into the perinuclear space (Nie et al., 2016; Gurusaran et al., 2023) (Figure 2A). The C-terminal SUN domain interacts with KASH proteins through a protruding structure in the SUN domain, called the KASH lid. In its monomeric state, the KASH lid of SUN proteins binds to CC2, which locks it in an autoinhibited conformation that prevents nesprin binding. Trimerization of the SUN proteins is likely mediated by CC1 and enables interaction between the KASH lid and nesprins (Nie et al., 2016). Although it is still unclear what triggers SUN protein trimerization, it may be dependent on calcium concentration (Jahed et al., 2018b; Majumder et al., 2022). Both SUN proteins form trimers and adopt an autoinhibited monomeric conformation. However, KASH lid inhibition of monomeric SUN1 is likely weaker than that of monomeric SUN2, suggesting that SUN1 may be more accessible for nesprin binding than SUN2 (Jahed et al., 2018a). These findings align with another study showing that SUN1 was consistently co-precipitated with both nesprin-1 and nesprin-2 while SUN2 was almost undetectable in nesprin immunoprecipitates, suggesting that SUN1 is more efficiently incorporated into the LINC complex (May and Carroll, 2018). However, plasmon surface resonance analysis did not reveal significant binding differences between SUN1 or SUN2 and the KASH domain of nesprin-2 (Östlund et al., 2009).

Although SUN1 and SUN2 have highly conserved KASH-binding domains, they differentially engage the cytoskeleton, suggesting that molecular differences in SUN-KASH interactions have consequences for cellular behaviors. SUN1 and SUN2 regulate nuclear positioning in fibroblasts via different mechanisms; SUN1/nesprin-2 complexes preferentially interact with microtubules to regulate forward nuclear movement, while SUN2/nesprin-2 complexes preferentially interact with the actin cytoskeleton to regulate rearward nuclear movement (Zhu et al., 2017). These findings align with another study showing that SUN2/nesprin-2 complexes assemble into Transmembrane Actin-associated Nuclear (TAN) lines that anchor nuclei to actin filaments during nuclear movement (Folker et al., 2011). Initial research indicated that LINC complex assembly into TAN lines was specific to SUN2/nesprin-2 complexes (Luxton and Starr, 2014), but subsequent work showed that other nuclear proteins such as nesprin-1, lamin-A/C, lamin-B1, and SUN1 are also concentrated in these lines (Versaev et al., 2014; Hoffman et al., 2020; Smith et al., 2022). The mechanism by which SUN proteins discern specific nesprin-associated cytoskeletal components remains unclear, since there is no apparent specificity to nesprin/SUN binding. It is hypothesized that SUN proteins perceive force differences exerted on nesprins by different cytoskeletal components (Zhu et al., 2017). The distinction in SUN/cytoskeletal binding may be cell- or context-dependent, as SUN1 also regulates actin cytoskeleton organization (Ueda et al., 2022), while SUN2 is involved in astral microtubule organization during mitosis (Belaadi et al., 2022). Each SUN protein appears to regulate both the actin and microtubule cytoskeletal networks, yet it remains unclear whether any given effect is direct or indirect.

3.2 Function of the SUN proteins: findings from *in vivo* models

Early studies in mouse models demonstrated both distinct and redundant functions of SUN1 and SUN2 in developmental processes. Mice globally lacking *Sun1* are completely sterile due to severe impairment of telomere attachment to the nuclear envelope during meiosis and repressed gametogenesis-related gene expression (Ding et al., 2007; Chi et al., 2009). Similar to SUN1, SUN2 also localizes to telomere attachment sites and contributes to telomere tethering to the nuclear envelope (Schmitt et al., 2007). However, although SUN2 is present at attachment sites, it does not compensate for *Sun1* loss during meiosis (Link et al., 2014), suggesting distinct SUN-telomere interactions. *Sun1* loss in mice also disrupts nuclear localization in outer hair cells of the ear and leads to progressive hearing loss (Horn et al., 2013a). In contrast to mice globally lacking *Sun1*, mice globally lacking *Sun2* are fertile and have no apparent abnormalities in growth and development (Lei et al., 2009). However, a recent aging study revealed that *Sun2* mutant mice developed cardiac hypertrophy characterized by enlarged cardiomyocytes with altered sarcomere structure and adhesion. Despite these changes, no cardiac-related deaths were observed. Interestingly the global loss of *Sun2* in mice did not induce cardiac fibrosis. Instead, it led to the downregulation of TGF β -associated profibrotic gene transcription in the left ventricle, attributed to elevated levels of MAN1, a negative

regulator of the TGF β signaling at the nuclear envelope (Stewart et al., 2019). The global loss of both *Sun1* and *Sun2* is lethal neonatally, indicating that SUN1 and SUN2 have overlapping functions developmentally. Redundant roles were found in regulating skeletal muscle nuclear anchorage (Lei et al., 2009) and coupling the centrosome and nucleus during neuronal migration in cerebral cortex neurogenesis (Zhang et al., 2009). Postnatally, decrease in cerebellar volume and impairment of motor coordination resulting from *Sun1* loss were exacerbated by the loss of one allele of *Sun2* (Wang et al., 2015). Embryonic fibroblasts isolated from mice globally lacking both *Sun1* and *Sun2* exhibited increased apoptosis and DNA damage due to compromised DNA damage response. This implies a redundant function of SUN1 and SUN2 in DNA repair, as no evident defects were observed in mice lacking either *Sun1* or *Sun2* individually (Lei et al., 2012).

3.3 LINC complex and SUN proteins in the vascular endothelium

The LINC complex is important for vascular development and homeostasis, and several recent studies address LINC complex functions in endothelial cell biology. Overall disruption of the LINC complex via dominant negative KASH (DN-KASH) over-expression *in vitro* revealed regulation of migration and responses to flow-mediated forces in Human Umbilical Vein Endothelial Cells (HUVEC) (Denis et al., 2021). LINC complex disruption through individual depletion of nesprin-1, 2 or 3 in endothelial cells revealed LINC complex involvement in endothelial cell behaviors. Depletion of nesprin-1 or nesprin-2 in HUVEC increased cell spreading and decreased endothelial cell network formation on Matrigel and collective endothelial cell migration (Chancellor et al., 2010; King et al., 2014). During collective cell migration, nesprin-1-depleted endothelial cells had impaired nuclear-centrosomal polarization at the leading edge and abnormal reorientation in response to cyclic strain that correlated with increased focal adhesion number. Traction force microscopy analysis showed increased traction forces in nesprin-1-depleted endothelial cells, leading to a model whereby disrupted nucleus-cytoskeleton connections downstream of nesprin-1 depletion led to reduced nuclear actomyosin forces and increased cytoskeletal tension on focal adhesions (Chancellor et al., 2010). Depletion of nesprin-1 and 2 in HUVEC demonstrated their necessity for shear stress-induced tight junction protein expression. Specifically, nesprin-1 and 2 co-depletion reduced the induction of ZO-1 (Zonula Occludens-1) and occludin protein expression by pulsatile shear stress (Yang et al., 2020). Nesprin-1 depletion in HUVEC rescued impaired barrier function resulting from *SUN1* depletion without showing obvious effects when depleted in the presence of *SUN1*, indicating a role for nesprin-1 in endothelial cell barrier function (Buglak et al., 2023). In rat aortic endothelial cells, both nesprin-2 and lamin-A protein expression decreased with exposure to low-shear stress (5 dynes/cm²) conditions, compared to arterial shear stress conditions (15 dynes/cm²), suggesting that these proteins respond to flow-mediated inputs. Lamin-A or nesprin-2 overexpression decreased cell proliferation and apoptosis under low-shear stress conditions (Han et al., 2015).

Dissecting the roles of nesprin-1 vs. nesprin-2 in endothelial cells has been challenging, as both proteins bind to SUN proteins and

interact with both actin and microtubule networks. Nesprin-3 binds both SUN proteins (Ketema et al., 2007), but interacts with vimentin-containing intermediate filaments on the cytoplasmic side, leading to some clarity regarding its function in endothelial cells. In nesprin-3-depleted Human Aortic Endothelial Cells (HAEC), perinuclear vimentin loss is associated with impaired nucleus-MTOC (Microtubule-Organizing Center) connectivity, leading to nucleus-MTOC polarization defects under shear stress conditions. Moreover, nesprin-3 silencing induced endothelial cell hyper-elongation in the absence of stimuli (Morgan et al., 2011). Thus, nesprins are crucial for proper endothelial cell behaviors and for flow-mediated responses *in vitro*; however, the redundancy in binding and function, and the lack of *in vivo* vascular manipulations, have hindered explicit understanding of their unique roles in vascular function and detailed mechanistic understanding.

Focused research to decipher SUN protein function in endothelial cell biology has also been complicated. In non-endothelial cell types, SUN1 and SUN2 have both overlapping and unique functions in cell behaviors that are also involved in blood vessel formation and function, such as nuclear positioning and movement (Zhang et al., 2009), nucleus-centrosome connection (Chang et al., 2019; Lima et al., 2024), Golgi organization (Hieda et al., 2021), focal adhesion assembly (Ueda et al., 2022) and cell migration (Nishioka et al., 2016; Nishino et al., 2023). Studies of isolated nuclei improved our understanding of nucleus-cytoskeleton force transmission, revealing that force applied to nesprin-1 in HUVEC nuclei induces nuclear stiffening (Guilluy et al., 2014). Further work in fibroblast nuclei demonstrated that co-depletion of both *SUN1* and *SUN2* affected force transduction via nesprin-1, whereas individual depletion of either *SUN1* or *SUN2* did not show significant effects, indicating overlapping function. Studies on enucleated HUVEC and fibroblasts highlighted the role of the nucleus in maintaining cell contractility and traction forces that were dependent on substrate rigidity (Graham et al., 2018). Enucleated HUVEC and *SUN1/SUN2* co-depleted fibroblasts showed similar cellular phenotypes, with a decrease in cell contractility and traction forces. The co-depletion of *SUN1/SUN2* affected traction forces differently than nesprin-1 depletion (Chancellor et al., 2010), perhaps due to cell type or experimental differences. These findings indicate that SUN proteins regulate force transmission between the substrate and the nucleus via the cytoskeleton.

Force transmission between the substrate and nucleus induces chromatin deformation, resulting in changes in gene transcription. In CHO (Chinese Hamster Ovary) cells, localized surface force application propagated a signal from integrins to the nucleus via the actin cytoskeleton, leading to chromatin stretching and gene transcription (Tajik et al., 2016). The LINC complex contributes to this force transmission, as depletion of both *SUN1* and *SUN2* inhibited force-induced chromatin stretching. Disrupting the LINC complex in cardiomyocytes through the overexpression of a truncated nesprin-3 protein interfered with chromatin reorganization during cardiomyocyte maturation by decreasing the nuclear peripheral accumulation of trimethylated H3K9-marked chromatin (Seelbinder et al., 2021). During mitosis, *SUN1* depletion in HeLa cells decreased histone acetylation and delayed chromosome de-condensation (Chi et al., 2007). *SUN2* modulates chromatin structure indirectly by interacting with lamin-A/C to maintain chromatin in a repressive state (Sun et al., 2018). Although SUN proteins regulate chromatin structure,

their impact on gene transcription remains unclear. Whole genome expression profiling revealed few significant differentially expressed genes following *SUN1* depletion in HeLa cells or HUVEC (Li et al., 2017; Buglak et al., 2023). However, in HeLa cells, *SUN1* regulates gene expression independently of its interaction with KASH proteins (May and Carroll, 2018). Moreover, disrupting the LINC complex in cultured fibroblasts using a *SUN1* dominant-negative construct revealed its role in regulating gene transcription in response to substrate rigidity (Alam et al., 2016).

We recently showed that endothelial cell-specific deletion of *Sun1* led to impaired vascular expansion and endothelial barrier function in the murine postnatal retina, and that vascular sprouting was compromised in zebrafish lacking *sun1* (Buglak et al., 2023). Live imaging of 3D angiogenic sprouting showed that *SUN1* negatively modulates sprout retractions, suggesting that depletion leads to increased contractility. The mechanism was revealed in HUVEC, where *SUN1* stabilized peripheral microtubules that in turn sequestered Rho GEF-H1 and negatively regulated Rho-mediated signaling. The effects of *SUN1* depletion on endothelial junctions were rescued by co-depletion of either Rho GEF-H1 or nesprin-1. Taken together, the findings suggest that endothelial *SUN1* functions as a decoy to negatively regulate nesprin-1-mediated LINC complex interactions that in turn regulate microtubule stability. Microtubule dynamics in turn regulate peripheral Rho signaling that modulates contractility, cell-cell junctions, and barrier function in endothelial cells. This model of nucleus-to-junctions molecular communication is consistent with other studies in non-endothelial cells; for example, *SUN1* inhibited RhoA activation and focal adhesion assembly in HeLa cells by antagonizing *SUN2*-LINC complexes (Thakar et al., 2017). Moreover, *SUN2* depletion rescued the Golgi dispersion of *SUN1*-depleted HeLa cells, suggesting that *SUN1* suppresses *SUN2*/nesprin-2 complexes to maintain proper Golgi structure (Hieda et al., 2021).

The role of *SUN2* is less investigated in endothelial cells, but several recent studies point to a required function in flow-mediated responses. *SUN2*/nesprin-1 interactions were increased in HUVEC exposed to pulsatile shear stress compared to oscillatory shear stress (Yang et al., 2020). It was hypothesized that the nuclear translocation of β -catenin is downstream of these interactions and regulates tight junction protein expression. TMEM201, an inner nuclear membrane-resident protein, interacts with *SUN2* and lamin-A in endothelial cells and functions in the regulation of endothelial cell migration and angiogenic processes *in vivo* (Zhang et al., 2022).

4 The LINC complex and cardiovascular pathologies

Mutations in LINC complex components and their binding partners, including *SUN1* and 2, nesprin-1 and 2, lamin-A and emerin, are associated with human disease. Hutchinson-Gilford progeria syndrome (HGPS), Emery-Dreifuss muscular dystrophy (EDMD), and dilated cardiomyopathy (DCM) are three diseases associated with mutations in components or interactors of the LINC complex that have cardiovascular pathology (Méjat and Misteli, 2010). The mutations affect vascular endothelial and smooth muscle cells in HGPS and primarily affect skeletal and cardiac muscle in EDMD and DCM, leading to cardiovascular disease.

4.1 LINC complex and Hutchinson-Gilford progeria syndrome (HGPS)

HGPS is a rare genetic disorder that causes premature aging, and children with HGPS have accelerated atherosclerosis, resulting in premature death in their early teens due to heart attack or stroke (Makous et al., 1962; Hennekam, 2006; Olive et al., 2010; Prakash et al., 2018). The disease results from an autosomal dominant mutation in the *LMNA* gene, leading to expression of a truncated and farnesylated form of lamin-A known as progerin (De Sandre-Giovannoli et al., 2003; Eriksson et al., 2003). Lamin-A is typically produced from a precursor protein called prelamin-A, which undergoes post-translational modifications, including farnesylation of the C-terminal region (Sinensky et al., 1994). Subsequently, the ZMPSTE24 (Zinc Metalloproteinase STE24) protease cleaves the C-terminal 15 amino acids, including the farnesyl group, resulting in the formation of mature lamin-A (Corrigan et al., 2005). Many HGPS patients carry a *de novo* mutation (c.1824C→T; p.G608G) in exon 11 of the *LMNA* gene. This mutation preserves the farnesylation site but activates a cryptic splice site, leading to the deletion of 150 nucleotides that includes the ZMPSTE24 proteolytic cleavage site in exon 11. Consequently, truncated and farnesylated progerin, without post-translational modification, accumulates at the nuclear envelope.

The cardiovascular deterioration observed in HGPS patients mirrors that of normal aging, although exposure to traditional risk factors is limited (Gordon et al., 2005; Merideth et al., 2008; Gerhard-Herman et al., 2012). Like aged individuals, HGPS patients develop atherosclerosis characterized by vascular smooth muscle cell (VSMC) loss in the media as well as vascular calcification and stiffening, leading to plaque erosion and rupture (Stehbens et al., 1999; Stehbens et al., 2001; Hamczyk and Andrés, 2019). Mouse models that recapitulate aspects of HGPS have been developed (Hamczyk et al., 2018a; Benedicto et al., 2021). Knock-in mouse models carrying a mutant *Lmna* allele deleted for exon 9 (*Lmna* Δ 9) (Mounkes et al., 2003; Hernandez et al., 2010) or with a deletion of intron 10, intron 11 and the last 150 nucleotides of exon 11 (*Lmna*^{HG}) (Yang et al., 2005; Yang et al., 2006) result in expression of a truncated form of lamin-A. Mice globally expressing the human G608G mutation were generated via transgenesis (G608G BAC) (Varga et al., 2006) or via mutation of the endogenous locus (*Lmna*^{G609G/G609G}) (Osorio et al., 2011). The breeding of *Lmna*^{G609G/G609G} mice to apolipoprotein E-deficient mice (*ApoE*^{-/-}) revealed progerin-induced acceleration of atherosclerosis (Hamczyk et al., 2018b). Two different *Zmpste24*-deficient mouse models (*Zmpste24*^{-/-}) have also been used to study HGPS (Bergo et al., 2002; Pendás et al., 2002).

Analysis of these models revealed that progerin expression affects both endothelial cells and vascular smooth muscle cells. While the effects of progerin expression on vascular smooth muscle cell properties are well documented, the effects of progerin on endothelial cell function, and the role of endothelial cells in HGPS development, is less understood. Mice with endothelial cell-specific expression of progerin had accelerated aging and a shortened life span associated with cardiac hypertrophy and fibrosis (Osmanagic-Myers et al., 2019; Sun et al., 2020), showing that endothelial cells contribute to the pathology of HGPS. Medial VSMC loss seen in some global

HGPS mutants was not documented in endothelial cell-expressing progerin mice, suggesting that some cardiovascular impairment in HGPS is due to progerin expression in medial VSMC (Osmanagic-Myers et al., 2019). These findings align with another study showing that progerin expression in VSMCs induced arterial stiffness and inward remodeling, which were not observed in mice expressing progerin exclusively in endothelial cells (del Campo et al., 2019).

Ubiquitous progerin expression in mice leads to endothelial dysfunction. *Ex vivo* aortic wire myography demonstrated that *Lmna*^{G609G/G609G} mice had impaired aortic contraction and endothelial-dependent relaxation (del Campo et al., 2020). However, restricting progerin expression to only VSMC or endothelial cells was not sufficient to induce impairment of endothelium-dependent relaxation, suggesting complex cell-cell interactions in the phenotype. Other *in vivo* studies showed that endothelial-specific progerin expression induced endothelial cell dysfunction characterized by cellular senescence, a pro-inflammatory profile, and downregulation of eNOS expression (Osmanagic-Myers et al., 2019; Sun et al., 2020; Manakanatas et al., 2022). Reduced eNOS activity and reduced nitric oxide levels were found in induced pluripotent stem cell (iPSC)-derived endothelial cells from HGPS patients, along with increased expression of pro-inflammatory molecules and reduced flow-induced gene expression (Atchison et al., 2020; Gete et al., 2021), suggesting that progerin perturbs endothelial flow-mediated responses and promotes inflammation. Progerin expression in endothelial cells also leads to reduced neovascularization following ischemia *in vivo* (Sun et al., 2020) and vascular network formation *in vitro* (Bonello-Palot et al., 2014; Gete et al., 2021).

Progerin-induced endothelial cell dysfunction in cultured cells has been studied using multiple approaches to induce progerin expression, including viral-mediated progerin expression, siRNA-mediated *ZMPSTE24* depletion, or treatment with Atazanavir, a protease inhibitor that results in accumulation of farnesylated prelamin-A. Progerin expression in cultured endothelial cells induced pro-inflammatory gene expression and increased oxidative stress leading to premature cellular senescence (Bonello-Palot et al., 2014; Bidault et al., 2020). Moreover, progerin-expressing endothelial cells displayed impaired shear stress responses. Progerin expression in HUVEC resulted in nuclear abnormalities and significant cell loss under laminar shear stress (Danielsson et al., 2022). Another study demonstrated decreased collective cell migration in progerin-expressing endothelial cells under laminar shear stress (Jiang and Ji, 2022). Thus, endothelial cell progerin expression induces dysfunction that likely contributes to cardiovascular alterations.

Although the precise mechanisms by which *LMNA* mutations impact endothelial cell function in HGPS remain unclear, they likely involve lamin-A interactions with the SUN proteins that disrupt LINC complex-mediated nucleus-cytoskeletal connections. SUN1 expression is upregulated in progerin-expressing endothelial cells (Osmanagic-Myers et al., 2019), and in HGPS fibroblasts (Chen et al., 2012). Moreover, progerin farnesylation increased its binding affinity for SUN1, resulting in abnormal clustering of SUN1 and progerin in the endoplasmic reticulum (Chen et al., 2014). In this study, progerin expression reduced SUN1 motility in the nuclear envelope of HeLa cells, although no effect on SUN1 diffusional mobility was reported in HGPS patient-derived fibroblasts (Chang et al., 2019). *In vivo*, genetic loss of *Sun1* reduced disease severity and extended the

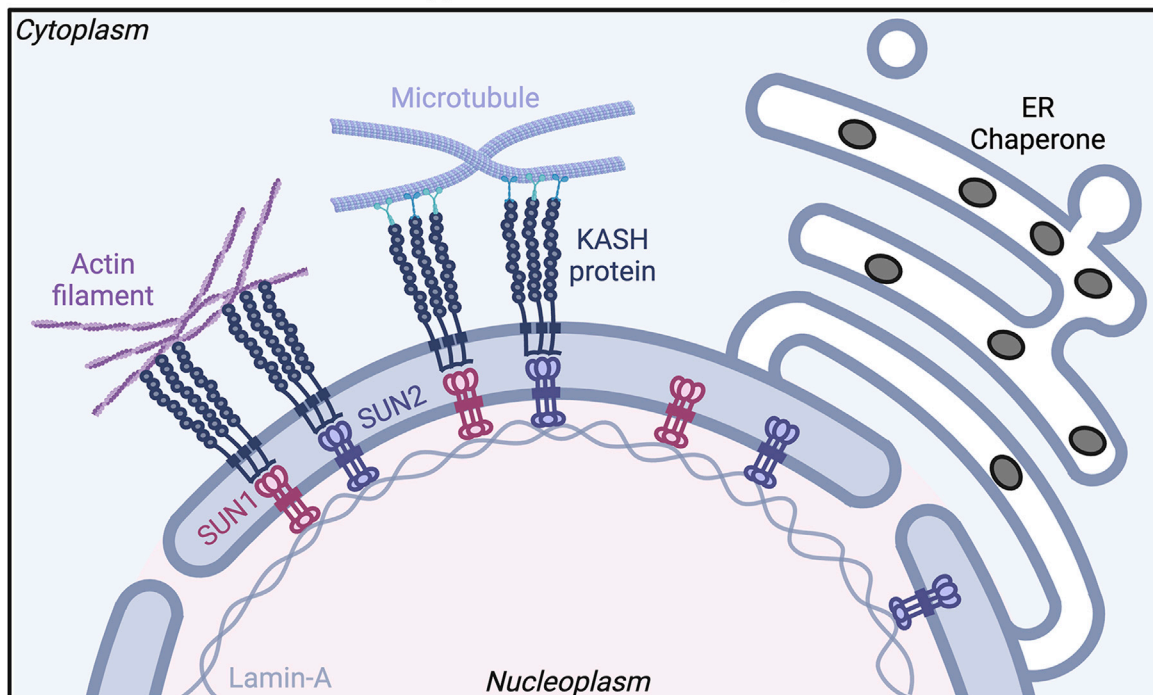
lifespan of *Lmna*^{Δ9} HGPS mice, indicating SUN1 involvement in HGPS pathology. Additionally, *SUN1* siRNA treatment rescued cellular senescence observed in fibroblasts from HGPS patients (Chen et al., 2012). Cell polarity defects of HGPS patient-derived fibroblasts in culture were rescued by siRNA-mediated depletion of *SUN1*, leading to a model whereby imbalanced LINC complexes downstream of *LMNA* defects resulted in impaired nucleus-cytoskeleton connections (Chang et al., 2019). In this model, increased levels of SUN1 compete with SUN2 for a limited pool of nesprin-2, thereby restricting the formation of SUN2/nesprin-2 complexes and changing the balance of LINC complex-mediated microtubule vs. actin cytoskeleton interactions (Figure 3).

SUN2 accumulates in progerin-expressing endothelial cells (Osmanagic-Myers et al., 2019) and in muscle cells from *Zmpste24*^{-/-} mice (Yue et al., 2023), although how this contributes to HGPS pathology is not understood. In mesenchymal stromal cells from *Zmpste24*^{-/-} mice, siRNA-mediated depletion of *Sun2* rescued the nuclear damage and cellular senescence induced by mechanical stress (Yue et al., 2023) suggesting that SUN2 mediates mechanotransduction. Progerin expression induces SUN2 clustering in the inner nuclear membrane in cultured fibroblasts. Moreover, SUN2 but not SUN1 depletion rescued an endoplasmic reticulum (ER) stress phenotype induced by progerin expression in fibroblasts. SUN2 clusters trigger ER stress inducing elevated UPR (Unfolded Protein Response) gene transcription downstream of progerin expression, leading to cell death. Interestingly, the UPR gene transcription induced by SUN2 clusters relies on the SUN2 C-terminal luminal domain rather than its nucleoplasmic and transmembrane domains (Vidak et al., 2023) (Figure 3).

4.2 LINC complex and Emery-Dreifuss muscular dystrophy (EDMD)

Patients with Emery-Dreifuss muscular dystrophy (EDMD) have muscle weakness and wasting that ultimately leads to premature death from cardiac abnormalities such as conduction defects and arrhythmia (Emery, 2000). Mutations in the *EMD* gene that encodes emerin, a LINC complex-associated protein, account for 60% of EDMD cases and are responsible for X-linked EDMD (Bione et al., 1994). Most *EMD* gene mutations are loss-of-function mutations resulting in the complete absence of emerin in the nuclear envelope (Koch and Holaska, 2014), while an autosomal dominant form of EDMD is associated with mutations in *LMNA* (Bonne et al., 1999). Screening of *SYNE1* (nesprin-1), *SYNE2* (nesprin-2), and *SUN1* and *SUN2* genes identified variants in patients with EDMD or related myopathies (Zhang et al., 2007; Meinke et al., 2014). Variants in LINC complex-encoding genes may explain the heterogeneity in disease severity, as EDMD patients with mutations in *SUN1* or *SUN2*, along with mutations in other genes like *EMD* or *LMNA*, had more severe symptoms compared to relatives without SUN gene mutations, although the *SUN* mutations alone were not linked to disease in other family members. Disruption of coupling between the nucleus and the cytoskeleton was highlighted by impaired centrosome reorientation in fibroblasts expressing SUN1 or SUN2 variant proteins (Meinke et al., 2014). Therefore, SUN1 and SUN2, by maintaining nuclear-cytoskeletal

Wild-Type : Balanced LINC complex



HGPS : Imbalanced LINC complex

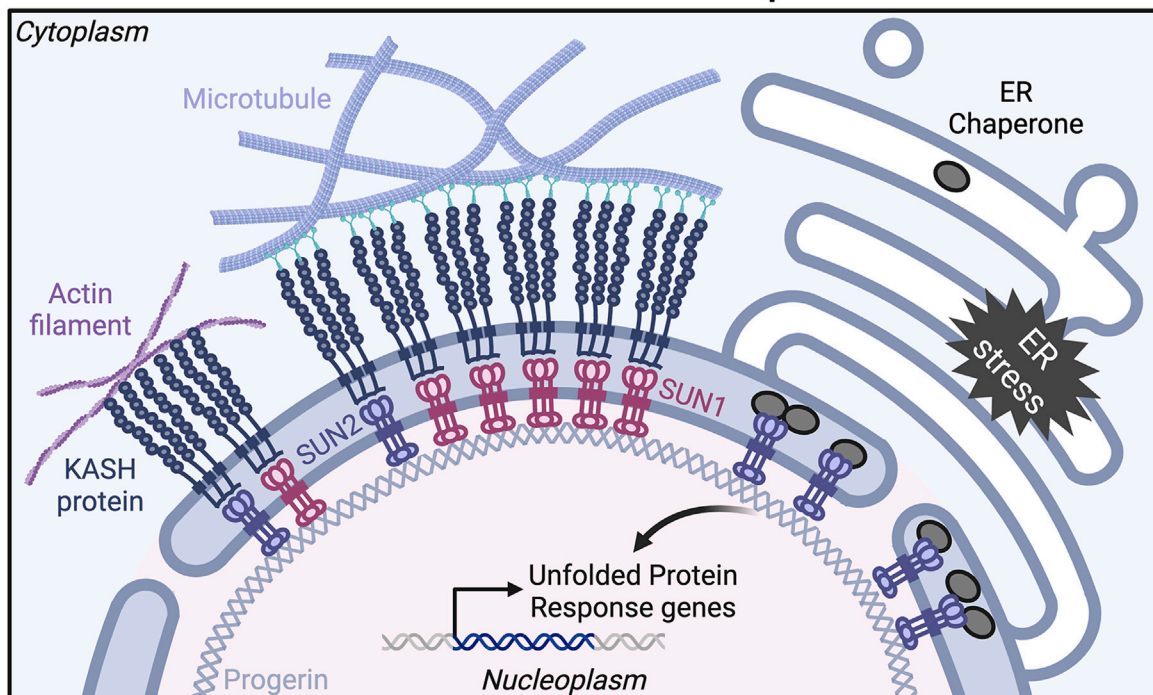


FIGURE 3

The nuclear LINC complex in health and disease. Model showing proposed interactions among LINC complex components in Wild-Type (top panel) and Hutchinson-Gilford progeria syndrome (HGPS) (bottom panel) cells. **Top:** In Wild-Type, SUN/KASH protein complexes engage similarly with actin filaments and microtubules, resulting in balanced interactions between the nucleus and the cytoskeleton. **Bottom:** In HGPS, progerin expression leads to SUN1 and SUN2 accumulation at the nuclear envelope, causing an imbalance in LINC complexes with a preference for interaction with microtubules over actin filaments. SUN2 also clusters at the nuclear envelope/ER interface, sequestering Endoplasmic Reticulum (ER) chaperone proteins and inducing an ER stress response. Created with BioRender.com.

connections, regulate nuclear positioning and contribute to the pathogenicity of EDMD.

4.3 LINC complex and dilated cardiomyopathy (DCM)

Dilated cardiomyopathy (DCM) is defined by reduced systolic cardiac function resulting from enlargement and thinning of the left ventricular wall. DCM patients often develop heart failure, which can lead to sudden cardiac arrest (Hershberger et al., 2010). While the genetic basis of much DCM is unknown, mutations in the *TTN* gene which encodes the sarcomeric protein titin are associated with some DCM (Herman et al., 2012), and *LMNA* mutations represent the second most common genetic cause of DCM (Goidescu, 2013). Cardiomyocyte-specific deletion of *Lmna* in mice led to cardiac failure and decreased lifespan (Chai et al., 2021). The expression of the *LMNA* mutations found in DCM patients in human iPSC-derived cardiomyocytes disrupts peripheral chromatin organization, leading to the expression of non-myocyte lineage genes (Shah et al., 2021). Similar to the HGPS model, the global loss of *Sun1* rescued cardiac function and increased life span in these mice while the global loss of *Sun2* did not affect their longevity (Chai et al., 2021). Adenovirus Associated Virus 9 (AAV9) mediated injection of a dominant negative SUN1 miniprotein that disrupted binding between endogenous SUN and KASH domains also improved cardiac function and extended lifespan. These findings indicate the potential for future therapeutic treatments that reduce SUN1 accumulation.

5 Future directions

The LINC complex resides in the nuclear membrane, where it mediates nucleus-to-cytoplasm and cytoplasm-to-nucleus mechanotransduction and communication in ways that are only partially understood. Although we understand aspects of how the LINC complex is regulated and in turn how it regulates cellular behaviors, there are still gaps in our knowledge. Our understanding of the LINC complex involvement in vascular processes and contributions to cardiovascular disease is in the beginning stages. Cutting-edge assays to measure and manipulate molecular forces, along with advances in high-resolution cellular imaging and genetic manipulations and techniques, present exciting prospects for cardiovascular biologists investigating LINC complex interactions.

The LINC complex contributes to endothelial cell mechanotransduction, which is crucial for vascular function and impaired in diseases with compromised vascular function. However, the specific mechanisms whereby the LINC complex perceives forces and integrates with other cellular inputs remain unclear. Numerous studies highlight the importance of the nucleus in cytoskeletal regulation of cell behaviors such as migration and cell-cell adhesion, and the cytoskeleton in turn regulates nuclear movement within the cell. We predict that enhanced understanding of the underlying mechanisms will result from precise force measurements in different cellular locales. It will be especially important that these assays utilize physiologically relevant endothelial cell micro-environments to better understand effects in the cardiovascular system, as force generation and transduction depend on parameters such as substrate stiffness.

Another important property that may be elucidated via high-resolution imaging is the exact topology of the SUN protein complexes in the nuclear membrane. Do SUN1 and SUN2 form heterodimers or only homodimers? When and how do they interact with partners such as emerin? This knowledge is relevant for understanding the respective roles of SUN1 and SUN2 in endothelial cells and blood vessels, as published data overall suggests interactions that are sometimes complementary/redundant and sometimes antagonistic. The different interaction outcomes may be influenced by the relative location of SUN proteins in the nuclear membrane, and the clustering observed in HGPS and related diseases may alter the relationship between SUN1 and SUN2.

Finally, it will be exciting and important to test the role of the LINC complex and SUN proteins more rigorously *in vivo* to understand their effects on the cardiovascular system. Live imaging in zebrafish will help determine how the LINC complex regulates cell behaviors dynamically *in vivo*. Selective genetic manipulations in endothelial cells or other vascular cells in mice will help to understand how each cell type contributes to premature aging and cardiovascular disease, and profiling of vascular cells from animal models will also help define roles. We anticipate that addition of other -omics (such as ATAC-seq, proteomics, etc.) will complement RNA profiling, and spatial -omics will add a further dimension of understanding to the pathologies resulting from nuclear and LINC complex perturbations. Once there is a more unifying concept of how the LINC complex participates in endothelial cell behaviors and blood vessel function, rational design of therapeutics to mitigate the effects of disease and perhaps normal aging will be closer to reality.

Author contributions

PB: Conceptualization, Visualization, Writing—original draft, Writing—review and editing. VB: Conceptualization, Funding acquisition, Writing—original draft, Writing—review and editing.

Funding

The author(s) declare that financial support was received for the research, authorship, and/or publication of this article. NIH R35 HL139950 (VB).

Acknowledgments

We thank Bautch lab members for productive discussions. We apologize to all authors whose work could not be cited due to space limitations. The figures were created with [Biorender.com](https://www.biorender.com).

Conflict of interest

The authors declare that the research was conducted in the absence of any commercial or financial relationships that could be construed as a potential conflict of interest.

Publisher's note

All claims expressed in this article are solely those of the authors and do not necessarily represent those of their affiliated

organizations, or those of the publisher, the editors and the reviewers. Any product that may be evaluated in this article, or claim that may be made by its manufacturer, is not guaranteed or endorsed by the publisher.

References

- Alam, S. G., Zhang, Q., Prasad, N., Li, Y., Chamala, S., Kuchibhotla, R., et al. (2016). The mammalian LINC complex regulates genome transcriptional responses to substrate rigidity. *Sci. Rep.* 6, 38063. doi:10.1038/srep38063
- Atchison, L., Abutaleb, N. O., Snyder-Mounts, E., Gete, Y., Ladha, A., Ribar, T., et al. (2020). iPSC-derived endothelial cells affect vascular function in a tissue-engineered blood vessel model of hutchinson-gilford progeria syndrome. *Stem Cell Rep.* 14, 325–337. doi:10.1016/j.stemcr.2020.01.005
- Baeyens, N., Bandyopadhyay, C., Coon, B. G., Yun, S., and Schwartz, M. A. (2016). Endothelial fluid shear stress sensing in vascular health and disease. *J. Clin. Invest.* 126, 821–828. doi:10.1172/JCI83083
- Banerjee, I., Zhang, J., Moore-Morris, T., Pfeiffer, E., Buchholz, K. S., Liu, A., et al. (2014). Targeted ablation of nesprin 1 and nesprin 2 from murine myocardium results in cardiomyopathy, altered nuclear morphology and inhibition of the biomechanical gene response. *PLoS Genet.* 10, e1004114. doi:10.1371/journal.pgen.1004114
- Behrens, T. W., Jagadeesh, J., Scherle, P., Kearns, G., Yewdell, J., and Staudt, L. M. (1994). Jaw1, A lymphoid-restricted membrane protein localized to the endoplasmic reticulum. *J. Immunol. Balt. Md* 150, 682–690. doi:10.4049/jimmunol.153.2.682
- Belaadi, N., Pernet, L., Aureille, J., Chadeuf, G., Rio, M., Vaillant, N., et al. (2022). SUN2 regulates mitotic duration in response to extracellular matrix rigidity. *Proc. Natl. Acad. Sci.* 119, e2116167119. doi:10.1073/pnas.2116167119
- Benedicto, I., Dorado, B., and Andrés, V. (2021). Molecular and cellular mechanisms driving cardiovascular disease in hutchinson-gilford progeria syndrome: lessons learned from animal models. *Cells* 10, 1157. doi:10.3390/cells10051157
- Bergo, M. O., Gavino, B., Ross, J., Schmidt, W. K., Hong, C., Kendall, L. V., et al. (2002). Zmpste24 deficiency in mice causes spontaneous bone fractures, muscle weakness, and a prelamin A processing defect. *Proc. Natl. Acad. Sci.* 99, 13049–13054. doi:10.1073/pnas.192460799
- Bidault, G., Garcia, M., Capeau, J., Morichon, R., Vigouroux, C., and Béréziat, V. (2020). Progerin expression induces inflammation, oxidative stress and senescence in human coronary endothelial cells. *Cells* 9, 1201. doi:10.3390/cells9051201
- Bione, S., Maestrini, E., Rivella, S., Mancini, M., Regis, S., Romeo, G., et al. (1994). Identification of a novel X-linked gene responsible for Emery-Dreifuss muscular dystrophy. *Nat. Genet.* 8, 323–327. doi:10.1038/ng1294-323
- Bonello-Palot, N., Simoncini, S., Robert, S., Bourgeois, P., Sabatier, F., Levy, N., et al. (2014). Prelamin A accumulation in endothelial cells induces premature senescence and functional impairment. *Atherosclerosis* 237, 45–52. doi:10.1016/j.atherosclerosis.2014.08.036
- Bonne, G., Di Barletta, M. R., Varnous, S., Bécane, H. M., Hammouda, E. H., Merlini, L., et al. (1999). Mutations in the gene encoding lamin A/C cause autosomal dominant Emery-Dreifuss muscular dystrophy. *Nat. Genet.* 21, 285–288. doi:10.1038/6799
- Buglak, D. B., Bougaran, P., Kulikauskas, M. R., Liu, Z., Monaghan-Benson, E., Gold, A. L., et al. (2023). Nuclear SUN1 stabilizes endothelial cell junctions via microtubules to regulate blood vessel formation. *eLife* 12, e83652. doi:10.7554/eLife.83652
- Campinho, P., Vilfan, A., and Vermot, J. (2020). Blood flow forces in shaping the vascular system: a focus on endothelial cell behavior. *Front. Physiol.* 11, 552. doi:10.3389/fphys.2020.00552
- Chai, R. J., Werner, H., Li, P. Y., Lee, Y. L., Nyein, K. T., Solovei, I., et al. (2021). Disrupting the LINC complex by AAV mediated gene transduction prevents progression of Lamin induced cardiomyopathy. *Nat. Commun.* 12, 4722. doi:10.1038/s41467-021-24849-4
- Chancellor, T. J., Lee, J., Thodeti, C. K., and Lele, T. (2010). Actomyosin tension exerted on the nucleus through nesprin-1 connections influences endothelial cell adhesion, migration, and cyclic strain-induced reorientation. *Biophys. J.* 99, 115–123. doi:10.1016/j.bpj.2010.04.011
- Chang, W., Wang, Y., Luxton, G. W. G., Östlund, C., Worman, H. J., and Gundersen, G. G. (2019). Imbalanced nucleocytoskeletal connections create common polarity defects in progeria and physiological aging. *Proc. Natl. Acad. Sci.* 116, 3578–3583. doi:10.1073/pnas.1809683116
- Chen, C.-Y., Chi, Y.-H., Matalif, R. A., Starost, M. F., Myers, T. G., Anderson, S. A., et al. (2012). Accumulation of the inner nuclear envelope protein Sun1 is pathogenic in progeric and dystrophic laminopathies. *Cell* 149, 565–577. doi:10.1016/j.cell.2012.01.059
- Chen, Y., Wang, Y., Chen, J., Zuo, W., Fan, Y., Huang, S., et al. (2021). The SUN1-SPDYA interaction plays an essential role in meiosis prophase I. *Nat. Commun.* 12, 3176. doi:10.1038/s41467-021-23550-w
- Chen, Z.-J., Wang, W.-P., Chen, Y.-C., Wang, J.-Y., Lin, W.-H., Tai, L.-A., et al. (2014). Dysregulated interactions between lamin A and SUN1 induce abnormalities in the nuclear envelope and endoplasmic reticulum in progeric laminopathies. *J. Cell Sci.* 127, 1792–1804. doi:10.1242/jcs.139683
- Chi, Y.-H., Cheng, L. I., Myers, T., Ward, J. M., Williams, E., Su, Q., et al. (2009). Requirement for Sun1 in the expression of meiotic reproductive genes and piRNA. *Dev. Camb. Engl.* 136, 965–973. doi:10.1242/dev.029868
- Chi, Y.-H., Haller, K., Peloponese, J.-M., and Jeang, K.-T. (2007). Histone acetyltransferase hALP and nuclear membrane protein hsSUN1 function in decondensation of mitotic chromosomes. *J. Biol. Chem.* 282, 27447–27458. doi:10.1074/jbc.M703098200
- Chong, D. C., Koo, Y., Xu, K., Fu, S., and Cleaver, O. (2011). Stepwise arteriovenous fate acquisition during mammalian vasculogenesis. *Dev. Dyn.* 240, 2153–2165. doi:10.1002/dvdy.22706
- Corrigan, D. P., Kuszczak, D., Rusinol, A. E., Thewke, D. P., Hrycyna, C. A., Michaelis, S., et al. (2005). Prelamin A endoproteolytic processing *in vitro* by recombinant Zmpste24. *Biochem. J.* 387, 129–138. doi:10.1042/BJ20041359
- Crisp, M., Liu, Q., Roux, K., Rattner, J. B., Shanahan, C., Burke, B., et al. (2006). Coupling of the nucleus and cytoplasm: role of the LINC complex. *J. Cell Biol.* 172, 41–53. doi:10.1083/jcb.200509124
- Cruz, V. E., Esra Demircioglu, F., and Schwartz, T. U. (2020). Structural analysis of different LINC complexes reveals distinct binding modes. *J. Mol. Biol.* 432, 6028–6041. doi:10.1016/j.jmb.2020.09.019
- Danielsson, B. E., Peters, H. C., Bathula, K., Spear, L. M., Noll, N. A., Dahl, K. N., et al. (2022). Progerin-expressing endothelial cells are unable to adapt to shear stress. *Biophys. J.* 121, 620–628. doi:10.1016/j.bpj.2022.01.004
- del Campo, L., Sánchez-López, A., González-Gómez, C., Andrés-Manzano, M. J., Dorado, B., and Andrés, V. (2020). Vascular smooth muscle cell-specific progerin expression provokes contractile impairment in a mouse model of hutchinson-gilford progeria syndrome that is ameliorated by nitrite treatment. *Cells* 9, 656. doi:10.3390/cells9030656
- del Campo, L., Sánchez-López, A., Salaices, M., von Kleck, R. A., Expósito, E., González-Gómez, C., et al. (2019). Vascular smooth muscle cell-specific progerin expression in a mouse model of Hutchinson-Gilford progeria syndrome promotes arterial stiffness: therapeutic effect of dietary nitrite. *Aging Cell* 18, e12936. doi:10.1111/acer.12936
- Denis, K. B., Cabe, J. I., Danielsson, B. E., Tieu, K. V., Mayer, C. R., and Conway, D. E. (2021). The LINC complex is required for endothelial cell adhesion and adaptation to shear stress and cyclic stretch. *Mol. Biol. Cell* 32, 1654–1663. doi:10.1091/mbc.E20-11-0698
- De Sandre-Giovannoli, A., Bernard, R., Cau, P., Navarro, C., Amiel, J., Boccaccio, I., et al. (2003). Lamin A truncation in hutchinson-gilford progeria. *Science* 300, 2055. doi:10.1126/science.1084125
- Desroches-Castan, A., Tillet, E., Bouvard, C., and Bailly, S. (2022). BMP9 and BMP10: two close vascular quiescence partners that stand out. *Dev. Dyn.* 251, 178–197. doi:10.1002/dvdy.395
- Dewey, C. F., Bussolari, S. R., Gimbrone, M. A., and Davies, P. F. (1981). The dynamic response of vascular endothelial cells to fluid shear stress. *J. Biomech. Eng.* 103, 177–185. doi:10.1115/1.3138276
- Ding, X., Xu, R., Yu, J., Xu, T., Zhuang, Y., and Han, M. (2007). SUN1 is required for telomere attachment to nuclear envelope and gametogenesis in mice. *Dev. Cell* 12, 863–872. doi:10.1016/j.devcel.2007.03.018
- Duchemin, A.-L., Vignes, H., and Vermot, J. (2019). Mechanically activated piezo channels modulate outflow tract valve development through the Yap1 and Klf2-Notch signaling axis. *eLife* 8, e44706. doi:10.7554/eLife.44706
- Emery, A. E. H. (2000). Emery-Dreifuss muscular dystrophy – a 40 year retrospective. *Neuromuscul. Disord.* 10, 228–232. doi:10.1016/S0960-8966(00)00105-X
- Eriksson, M., Brown, W. T., Gordon, L. B., Glynn, M. W., Singer, J., Scott, L., et al. (2003). Recurrent *de novo* point mutations in lamin A cause Hutchinson-Gilford progeria syndrome. *Nature* 423, 293–298. doi:10.1038/nature01629
- Folker, E. S., Östlund, C., Luxton, G. W. G., Worman, H. J., and Gundersen, G. G. (2011). Lamin A variants that cause striated muscle disease are defective in anchoring transmembrane actin-associated nuclear lines for nuclear movement. *Proc. Natl. Acad. Sci.* 108, 131–136. doi:10.1073/pnas.1000824108

- Franco, C. A., Jones, M. L., Bernabeu, M. O., Geudens, I., Mathivet, T., Rosa, A., et al. (2015). Dynamic endothelial cell rearrangements drive developmental vessel regression. *PLoS Biol.* 13, e1002125. doi:10.1371/journal.pbio.1002125
- Fridkin, A., Penkner, A., Jantsch, V., and Gruenbaum, Y. (2009). SUN-domain and KASH-domain proteins during development, meiosis and disease. *Cell. Mol. Life Sci. CMLS* 66, 1518–1533. doi:10.1007/s00018-008-8713-y
- Gerace, L., Blum, A., and Blobel, G. (1978). Immunocytochemical localization of the major polypeptides of the nuclear pore complex-lamina fraction. Interphase and mitotic distribution. *J. Cell Biol.* 79, 546–566. doi:10.1083/jcb.79.2.546
- Gerace, L., and Burke, B. (1988). Functional organization of the nuclear envelope. *Annu. Rev. Cell Biol.* 4, 335–374. doi:10.1146/annurev.cb.04.110188.002003
- Gerace, L., Comeau, C., and Benson, M. (1984). Organization and modulation of nuclear lamina structure. *J. Cell Sci.* 1984, 137–160. doi:10.1242/jcs.1984.Supplement_1.10
- Gerhard-Herman, M., Smoot, L. B., Wake, N., Kieran, M. W., Kleinman, M. E., Miller, D. T., et al. (2012). Mechanisms of premature vascular aging in children with hutchinson-gilford progeria syndrome. *Hypertension* 59, 92–97. doi:10.1161/HYPERTENSIONAHA.111.180919
- Gesson, K., Rescheneder, P., Skoruppa, M. P., von Haeseler, A., Dechat, T., and Foisner, R. (2016). A-type lamins bind both hetero- and euchromatin, the latter being regulated by lamina-associated polypeptide 2 alpha. *Genome Res.* 26, 462–473. doi:10.1101/gr.196220.115
- Gete, Y. G., Koblan, L. W., Mao, X., Trappio, M., Mahadik, B., Fisher, J. P., et al. (2021). Mechanisms of angiogenic incompetence in Hutchinson–Gilford progeria via downregulation of endothelial NOS. *Aging Cell* 20, e13388. doi:10.1111/ace1.13388
- Ghosh, S., Cuevas, V. C., Seelbinder, B., and Neu, C. P. (2021). Image-based elastography of heterochromatin and euchromatin domains in the deforming cell nucleus. *Small Weinheim. Bergstr.* 17, e2006109. doi:10.1002/sml.202006109
- Göb, E., Schmitt, J., Benavente, R., and Alsheimer, M. (2010). Mammalian sperm head formation involves different polarization of two novel LINC complexes. *PLoS ONE* 5, e12072. doi:10.1371/journal.pone.0012072
- Goidescu, C. M. (2013). Dilated cardiomyopathy produced by lamin A/C gene mutations. *Clujul Med.* 86 (4), 309–312.
- Gordon, L. B., Harten, I. A., Patti, M. E., and Lichtenstein, A. H. (2005). Reduced adiponectin and HDL cholesterol without elevated C-reactive protein: clues to the biology of premature atherosclerosis in Hutchinson–Gilford Progeria Syndrome. *J. Pediatr.* 146, 336–341. doi:10.1016/j.jpeds.2004.10.064
- Graham, D. M., Andersen, T., Sharek, L., Uzer, G., Rothenberg, K., Hoffman, B. D., et al. (2018). Enucleated cells reveal differential roles of the nucleus in cell migration, polarity, and mechanotransduction. *J. Cell Biol.* 217, 895–914. doi:10.1083/jcb.201706097
- Guilluy, C., Osborne, L. D., Van Landeghem, L., Sharek, L., Superfine, R., Garcia-Mata, R., et al. (2014). Isolated nuclei adapt to force and reveal a mechanotransduction pathway in the nucleus. *Nat. Cell Biol.* 16, 376–381. doi:10.1038/ncb2927
- Gurusaran, M., Biemans, J. J., Wood, C. W., and Davies, O. R. (2023). Molecular insights into LINC complex architecture through the crystal structure of a luminal trimeric coiled-coil domain of SUN1. *Front. Cell Dev. Biol.* 11, 1144277. doi:10.3389/fcell.2023.1144277
- Gurusaran, M., and Davies, O. R. (2021). A molecular mechanism for LINC complex branching by structurally diverse SUN-KASH 6:6 assemblies. *eLife* 10, e60175. doi:10.7554/eLife.60175
- Hamczyk, M. R., and Andrés, V. (2019). Vascular smooth muscle cell loss underpins the accelerated atherosclerosis in Hutchinson–Gilford progeria syndrome. *Nucleus* 10, 28–34. doi:10.1080/19491034.2019.1589359
- Hamczyk, M. R., del Campo, L., and Andrés, V. (2018a). Aging in the cardiovascular system: lessons from hutchinson-gilford progeria syndrome. *Annu. Rev. Physiol.* 80, 27–48. doi:10.1146/annurev-physiol-021317-121454
- Hamczyk, M. R., Villa-Bellosta, R., Gonzalo, P., Andrés-Manzano, M. J., Nogales, P., Bentzon, J. F., et al. (2018b). Vascular smooth muscle-specific progerin expression accelerates atherosclerosis and death in a mouse model of hutchinson-gilford progeria syndrome. *Circulation* 138, 266–282. doi:10.1161/CIRCULATIONAHA.117.030856
- Han, O., Pak, B., and Jin, S.-W. (2021). The role of BMP signaling in endothelial heterogeneity. *Front. Cell Dev. Biol.* 9, 673396. doi:10.3389/fcell.2021.673396
- Han, Y., Wang, L., Yao, Q.-P., Zhang, P., Liu, B., Wang, G.-L., et al. (2015). Nuclear envelope proteins Nesprin2 and LaminA regulate proliferation and apoptosis of vascular endothelial cells in response to shear stress. *Biochim. Biophys. Acta* 1853, 1165–1173. doi:10.1016/j.bbamer.2015.02.013
- Haque, F., Lloyd, D. J., Smallwood, D. T., Dent, C. L., Shanahan, C. M., Fry, A. M., et al. (2006). SUN1 interacts with nuclear lamin A and cytoplasmic nesprins to provide a physical connection between the nuclear lamina and the cytoskeleton. *Mol. Cell Biol.* 26, 3738–3751. doi:10.1128/MCB.26.10.3738-3751.2006
- Haque, F., Mazzeo, D., Patel, J. T., Smallwood, D. T., Ellis, J. A., Shanahan, C. M., et al. (2010). Mammalian SUN protein interaction networks at the inner nuclear membrane and their role in laminopathy disease processes. *J. Biol. Chem.* 285, 3487–3498. doi:10.1074/jbc.M109.071910
- Heffler, J., Shah, P. P., Robison, P., Phyto, S., Veliz, K., Uchida, K., et al. (2020). A balance between intermediate filaments and microtubules maintains nuclear architecture in the cardiomyocyte. *Circ. Res.* 126, e10–e26. doi:10.1161/CIRCRESAHA.119.315582
- Hennekam, R. C. M. (2006). Hutchinson–Gilford progeria syndrome: review of the phenotype. *Am. J. Med. Genet. A* 140, 2603–2624. doi:10.1002/ajmg.a.31346
- Herman, D. S., Lam, L., Taylor, M. R. G., Wang, L., Teekakirikul, P., Christodoulou, D., et al. (2012). Truncations of titin causing dilated cardiomyopathy. *N. Engl. J. Med.* 366, 619–628. doi:10.1056/NEJMoa1110186
- Hernandez, L., Roux, K. J., Wong, E. S. M., Mounkes, L. C., Mutalif, R., Navasankari, R., et al. (2010). Functional coupling between the extracellular matrix and nuclear lamina by wnt signaling in progeria. *Dev. Cell* 19, 413–425. doi:10.1016/j.devcel.2010.08.013
- Hershberger, R. E., Morales, A., and Siegfried, J. D. (2010). Clinical and genetic issues in dilated cardiomyopathy: a review for genetics professionals. *Genet. Med. Off. J. Am. Coll. Med. Genet.* 12, 655–667. doi:10.1097/GIM.0b013e3181f2481f
- Hieda, M. (2019). Signal transduction across the nuclear envelope: role of the LINC complex in bidirectional signaling. *Cells* 8, 124. doi:10.3390/cells8020124
- Hieda, M., Matsumoto, T., Isobe, M., Kurono, S., Yuka, K., Kametaka, S., et al. (2021). The SUN2–nesprin-2 LINC complex and KIF20A function in the Golgi dispersal. *Sci. Rep.* 11, 5358. doi:10.1038/s41598-021-84750-4
- Hodjic, D. M., Yeater, D. B., Bengtsson, L., Otto, H., and Stahl, P. D. (2004). Sun2 is a novel mammalian inner nuclear membrane protein. *J. Biol. Chem.* 279, 25805–25812. doi:10.1074/jbc.M313157200
- Hofer, I. E., den Adel, B., and Daemen, M. J. A. P. (2013). Biomechanical factors as triggers of vascular growth. *Cardiovasc. Res.* 99, 276–283. doi:10.1093/cvr/cvt089
- Hoffman, L. M., Smith, M. A., Jensen, C. C., Yoshigi, M., Blankman, E., Ullman, K. S., et al. (2020). Mechanical stress triggers nuclear remodeling and the formation of transmembrane actin nuclear lines with associated nuclear pore complexes. *Mol. Biol. Cell* 31, 1774–1787. doi:10.1091/mbc.E19-01-0027
- Horn, H. F., Brownstein, Z., Lenz, D. R., Shvartzki, S., Dror, A. A., Dagan-Rosenfeld, O., et al. (2013a). The LINC complex is essential for hearing. *J. Clin. Invest.* 123, 740–750. doi:10.1172/JCI66911
- Horn, H. F., Kim, D. I., Wright, G. D., Wong, E. S. M., Stewart, C. L., Burke, B., et al. (2013b). A mammalian KASH domain protein coupling meiotic chromosomes to the cytoskeleton. *J. Cell Biol.* 202, 1023–1039. doi:10.1083/jcb.201304004
- Humphrey, J. D., and Schwartz, M. A. (2021). Vascular mechanobiology: homeostasis, adaptation, and disease. *Annu. Rev. Biomed. Eng.* 23, 1–27. doi:10.1146/annurev-bioeng-092419-060810
- Iyer, S. R., Folker, E. S., and Lovering, R. M. (2021). The nucleoskeleton: crossroad of mechanotransduction in skeletal muscle. *Front. Physiol.* 12, 724010. doi:10.3389/fphys.2021.724010
- Jahed, Z., Domkam, N., Ornowski, J., Yerima, G., and Mofrad, M. R. K. (2021). Molecular models of LINC complex assembly at the nuclear envelope. *J. Cell Sci.* 134, jcs258194. doi:10.1242/jcs.258194
- Jahed, Z., Fadavi, D., Vu, U. T., Asgari, E., Luxton, G. W. G., and Mofrad, M. R. K. (2018a). Molecular insights into the mechanisms of SUN1 oligomerization in the nuclear envelope. *Biophys. J.* 114, 1190–1203. doi:10.1016/j.bpj.2018.01.015
- Jahed, Z., Vu, U. T., Fadavi, D., Ke, H., Rathish, A., Kim, S. C. J., et al. (2018b). A molecular model for LINC complex regulation: activation of SUN2 for KASH binding. *Mol. Biol. Cell* 29, 2012–2023. doi:10.1091/mbc.E18-04-0266
- Janin, A., Bauer, D., Ratti, F., Millat, G., and Méjat, A. (2017). Nuclear envelopopathies: a complex LINC between nuclear envelope and pathology. *Orphanet J. Rare Dis.* 12, 147. doi:10.1186/s13023-017-0698-x
- Janota, C. S., Calero-Cuenca, F. J., and Gomes, E. R. (2020). The role of the cell nucleus in mechanotransduction. *Curr. Opin. Cell Biol.* 63, 204–211. doi:10.1016/j.cob.2020.03.001
- Jiang, Y., and Ji, J. Y. (2022). Progerin-induced impairment in wound healing and proliferation in vascular endothelial cells. *Front. Aging* 3, 844885. doi:10.3389/fragi.2022.844885
- Ketema, M., Wilhelmsen, K., Kuikman, I., Janssen, H., Hodjic, D., and Sonnenberg, A. (2007). Requirements for the localization of nesprin-3 at the nuclear envelope and its interaction with plectin. *J. Cell Sci.* 120, 3384–3394. doi:10.1242/jcs.014191
- Kim, D. I., Birendra, K. C., and Roux, K. J. (2015). Making the LINC: SUN and KASH protein interactions. *Biol. Chem.* 396, 295–310. doi:10.1515/hsz-2014-0267
- King, M. C. (2023). Dynamic regulation of LINC complex composition and function across tissues and contexts. *FEBS Lett.* 597, 2823–2832. doi:10.1002/1873-3468.14757
- King, S. J., Nowak, K., Suryavanshi, N., Holt, I., Shanahan, C. M., and Ridley, A. J. (2014). Nesprin-1 and nesprin-2 regulate endothelial cell shape and migration. *Cytoskeleton* 71, 423–434. doi:10.1002/cm.21182
- Kirby, T. J., and Lammerding, J. (2018). Emerging views of the nucleus as a cellular mechanosensor. *Nat. Cell Biol.* 20, 373–381. doi:10.1038/s41556-018-0038-y
- Koch, A. J., and Holaska, J. M. (2014). Emerin in health and disease. *Semin. Cell Dev. Biol.* 29, 95–106. doi:10.1016/j.semedb.2013.12.008

- Kozono, T., Tadahira, K., Okumura, W., Itai, N., Tamura-Nakano, M., Dohi, T., et al. (2018). Jaw1/LRMP has a role in maintaining nuclear shape via interaction with SUN proteins. *J. Biochem. (Tokyo)* 164, 303–311. doi:10.1093/jb/mvy053
- Kulikauskas, M. R., X. S., and Bautch, V. L. (2022). The versatility and paradox of BMP signaling in endothelial cell behaviors and blood vessel function. *Cell. Mol. Life Sci. CMLS* 79, 77. doi:10.1007/s00018-021-04033-z
- Lawrence, K. S., Tapley, E. C., Cruz, V. E., Li, Q., Aung, K., Hart, K. C., et al. (2016). LINC complexes promote homologous recombination in part through inhibition of nonhomologous end joining. *J. Cell Biol.* 215, 801–821. doi:10.1083/jcb.201604112
- Lee, H.-W., Shin, J. H., and Simons, M. (2022). Flow goes forward and cells step backward: endothelial migration. *Exp. Mol. Med.* 54, 711–719. doi:10.1038/s12276-022-00785-1
- Lee, K. K., Haraguchi, T., Lee, R. S., Koujin, T., Hiraoka, Y., and Wilson, K. L. (2001). Distinct functional domains in emerin bind lamin A and DNA-bridging protein BAF. *J. Cell Sci.* 114, 4567–4573. doi:10.1242/jcs.114.24.4567
- Lei, K., Zhang, X., Ding, X., Guo, X., Chen, M., Zhu, B., et al. (2009). SUN1 and SUN2 play critical but partially redundant roles in anchoring nuclei in skeletal muscle cells in mice. *Proc. Natl. Acad. Sci. U. S. A.* 106, 10207–10212. doi:10.1073/pnas.0812037106
- Lei, K., Zhu, X., Xu, R., Xu, T., Zhuang, Y., Han, M., et al. (2012). Inner nuclear envelope proteins SUN1 and SUN2 play a prominent role in the DNA damage response. *Curr. Biol. CB* 22, 1609–1615. doi:10.1016/j.cub.2012.06.043
- le Noble, F., Moyon, D., Pardanaud, L., Yuan, L., Djonov, V., Matthijsen, R., et al. (2004). Flow regulates arterial-venous differentiation in the chick embryo yolk sac. *Dev. Camb. Engl.* 131, 361–375. doi:10.1242/dev.00929
- Li, P., Stumpf, M., Müller, R., Eichinger, L., Glöckner, G., and Noegel, A. A. (2017). The function of the inner nuclear envelope protein SUN1 in mRNA export is regulated by phosphorylation. *Sci. Rep.* 7, 9157. doi:10.1038/s41598-017-08837-7
- Lima, J. T., Pereira, A. J., and Ferreira, J. G. (2024). The LINC complex ensures accurate centrosome positioning during prophase. *Life Sci. Alliance* 7, e202302404. doi:10.26508/lsa.202302404
- Link, J., Leubner, M., Schmitt, J., Göb, E., Benavente, R., Jeang, K.-T., et al. (2014). Analysis of meiosis in SUN1 deficient mice reveals a distinct role of SUN2 in mammalian meiotic LINC complex formation and function. *PLoS Genet.* 10, e1004099. doi:10.1371/journal.pgen.1004099
- Liu, Q., Pante, N., Misteli, T., Elsagga, M., Crisp, M., Hodzic, D., et al. (2007). Functional association of Sun1 with nuclear pore complexes. *J. Cell Biol.* 178, 785–798. doi:10.1083/jcb.200704108
- Lombardi, M. L., Jaalouk, D. E., Shanahan, C. M., Burke, B., Roux, K. J., and Lammerding, J. (2011). The interaction between nesprins and sun proteins at the nuclear envelope is critical for force transmission between the nucleus and cytoskeleton. *J. Biol. Chem.* 286, 26743–26753. doi:10.1074/jbc.M111.233700
- Lu, W., Gotzmann, J., Sironi, L., Jaeger, V.-M., Schneider, M., Lücke, Y., et al. (2008). Sun1 forms immobile macromolecular assemblies at the nuclear envelope. *Biochim. Biophys. Acta BBA - Mol. Cell Res.* 1783, 2415–2426. doi:10.1016/j.bbamcr.2008.09.001
- Luxton, G. G., and Starr, D. A. (2014). KASHing up with the nucleus: novel functional roles of KASH proteins at the cytoplasmic surface of the nucleus. *Curr. Opin. Cell Biol.* 28, 69–75. doi:10.1016/j.ccb.2014.03.002
- Majumder, S., Hsu, Y.-Y., Moghianianavval, H., Andreas, M., Giessen, T. W., Luxton, G. W. G., et al. (2022). *In vitro* synthesis and reconstitution using mammalian cell-free lysates enables the systematic study of the regulation of LINC complex assembly. *Biochemistry* 61, 1495–1507. doi:10.1021/acs.biochem.2c00118
- Makous, N., Friedman, S., Yakovac, W., and Maris, E. P. (1962). Cardiovascular manifestations in progeria. Report of clinical and pathologic findings in a patient with severe arteriosclerotic heart disease and aortic stenosis. *Am. Heart J.* 64, 334–346. doi:10.1016/0002-8703(62)90148-5
- Malone, C. J., Fixsen, W. D., Horvitz, H. R., and Han, M. (1999). UNC-84 localizes to the nuclear envelope and is required for nuclear migration and anchoring during *C. elegans* development. *Development* 126, 3171–3181. doi:10.1242/dev.126.14.3171
- Manakanatas, C., Ghadge, S. K., Agic, A., Sarigol, F., Fichtinger, P., Fischer, I., et al. (2022). Endothelial and systemic upregulation of miR-34a-5p fine-tunes senescence in progeria. *Aging* 14, 195–224. doi:10.18632/aging.203820
- Mannion, A. J., and Holmgren, L. (2023). Nuclear mechanosensing of the aortic endothelium in health and disease. *Dis. Model. Mech.* 16, dmm050361. doi:10.1242/dmm.050361
- Marchuk, D. A., Srinivasan, S., Squire, T. L., and Zawistowski, J. S. (2003). Vascular morphogenesis: tales of two syndromes. *Hum. Mol. Genet.* 12, R97–R112. doi:10.1093/hmg/ddg103
- May, C. K., and Carroll, C. W. (2018). Differential incorporation of SUN-domain proteins into LINC complexes is coupled to gene expression. *PLoS ONE* 13, e0197621. doi:10.1371/journal.pone.0197621
- McGillivray, R. M., Starr, D. A., and Luxton, G. W. G. (2023). Building and breaking mechanical bridges between the nucleus and cytoskeleton: regulation of LINC complex assembly and disassembly. *Curr. Opin. Cell Biol.* 85, 102260. doi:10.1016/j.ccb.2023.102260
- Mehta, V., Pang, K.-L., Rozbesky, D., Nather, K., Keen, A., Lachowski, D., et al. (2020). The guidance receptor plexin D1 is a mechanosensor in endothelial cells. *Nature* 578, 290–295. doi:10.1038/s41586-020-1979-4
- Meinke, P., Mattioli, E., Haque, F., Antoku, S., Columbaro, M., Straatman, K. R., et al. (2014). Muscular dystrophy-associated SUN1 and SUN2 variants disrupt nuclear-cytoskeletal connections and myonuclear organization. *PLoS Genet.* 10, e1004605. doi:10.1371/journal.pgen.1004605
- Méjat, A., and Misteli, T. (2010). LINC complexes in health and disease. *Nucleus* 1, 40–52. doi:10.4161/nucl.1.1.10530
- Merideth, M. A., Gordon, L. B., Clauss, S., Sachdev, V., Smith, A. C. M., Perry, M. B., et al. (2008). Phenotype and course of hutchinson-gilford progeria syndrome. *N. Engl. J. Med.* 358, 592–604. doi:10.1056/NEJMoa0706898
- Morgan, J. T., Pfeiffer, E. R., Thirkill, T. L., Kumar, P., Peng, G., Fridolfsson, H. N., et al. (2011). Nesprin-3 regulates endothelial cell morphology, perinuclear cytoskeletal architecture, and flow-induced polarization. *Mol. Biol. Cell* 22, 4324–4334. doi:10.1091/mbc.E11-04-0287
- Morimoto, A., Shibuya, H., Zhu, X., Kim, J., Ishiguro, K., Han, M., et al. (2012). A conserved KASH domain protein associates with telomeres, SUN1, and dynactin during mammalian meiosis. *J. Cell Biol.* 198, 165–172. doi:10.1083/jcb.201204085
- Mounkes, L. C., Kozlov, S., Hernandez, L., Sullivan, T., and Stewart, C. L. (2003). A progeroid syndrome in mice is caused by defects in A-type lamins. *Nature* 423, 298–301. doi:10.1038/nature01631
- Nie, S., Ke, H., Gao, F., Ren, J., Wang, M., Huo, L., et al. (2016). Coiled-coil domains of SUN proteins as intrinsic dynamic regulators. *Structure* 24, 80–91. doi:10.1016/j.str.2015.10.024
- Nishino, M., Imaizumi, H., Yokoyama, Y., Katahira, J., Kimura, H., Matsuura, N., et al. (2023). Histone methyltransferase SUV39H1 regulates the Golgi complex via the nuclear envelope-spanning LINC complex. *PLOS ONE* 18, e0283490. doi:10.1371/journal.pone.0283490
- Nishioka, Y., Imaizumi, H., Imada, J., Katahira, J., Matsuura, N., and Hieda, M. (2016). SUN1 splice variants, SUN1_888, SUN1_785, and predominant SUN1_916, variably function in directional cell migration. *Nucleus* 7, 572–584. doi:10.1080/19491034.2016.1260802
- Okumura, W., Tadahira, K., Kozono, T., Tamura-Nakano, M., Sato, H., Matsui, H., et al. (2023). Jaw1/LRMP is associated with the maintenance of Golgi ribbon structure. *J. Biochem. (Tokyo)* 173, 383–392. doi:10.1093/jb/mvad004
- Olive, M., Harten, I., Mitchell, R., Beers, J. K., Djabali, K., Cao, K., et al. (2010). Cardiovascular pathology in hutchinson-gilford progeria: correlation with the vascular pathology of aging. *Arterioscler. Thromb. Vasc. Biol.* 30, 2301–2309. doi:10.1161/ATVBAHA.110.209460
- Osmanagic-Myers, S., Kiss, A., Manakanatas, C., Hamza, O., Sedlmayer, F., Szabo, P. L., et al. (2019). Endothelial progerin expression causes cardiovascular pathology through an impaired mechanoreponse. *J. Clin. Invest.* 129, 531–545. doi:10.1172/JCI121297
- Osorio, F. G., Navarro, C. L., Cadiñanos, J., López-Mejía, I. C., Quirós, P. M., Bartoli, C., et al. (2011). Splicing-directed therapy in a new mouse model of human accelerated aging. *Sci. Transl. Med.* 3, 106ra107. doi:10.1126/scitranslmed.3002847
- Östlund, C., Chang, W., Gundersen, G. G., and Worman, H. J. (2019). Pathogenic mutations in genes encoding nuclear envelope proteins and defective nucleocytoplasmic connections. *Exp. Biol. Med.* 244, 1333–1344. doi:10.1177/1535370219862243
- Östlund, C., Folker, E. S., Choi, J. C., Gomes, E. R., Gundersen, G. G., and Worman, H. J. (2009). Dynamics and molecular interactions of linker of nucleoskeleton and cytoskeleton (LINC) complex proteins. *J. Cell Sci.* 122, 4099–4108. doi:10.1242/jcs.057075
- Padmakumar, V. C., Libotte, T., Lu, W., Zaim, H., Abraham, S., Noegel, A. A., et al. (2005). The inner nuclear membrane protein Sun1 mediates the anchorage of Nesprin-2 to the nuclear envelope. *J. Cell Sci.* 118, 3419–3430. doi:10.1242/jcs.02471
- Pendás, A. M., Zhou, Z., Cadiñanos, J., Freije, J. M. P., Wang, J., Hultenby, K., et al. (2002). Defective prelamin A processing and muscular and adipocyte alterations in Zmpste24 metalloproteinase-deficient mice. *Nat. Genet.* 31, 94–99. doi:10.1038/ng871
- Pitulescu, M. E., Schmidt, I., Giaimo, B. D., Antoine, T., Berkenfeld, F., Ferrante, F., et al. (2017). DLL4 and Notch signalling couples sprouting angiogenesis and artery formation. *Nat. Cell Biol.* 19, 915–927. doi:10.1038/ncb3555
- Potente, M., Gerhardt, H., and Carmeliet, P. (2011). Basic and therapeutic aspects of angiogenesis. *Cell* 146, 873–887. doi:10.1016/j.cell.2011.08.039
- Prakash, A., Gordon, L. B., Kleinman, M. E., Gurary, E. B., Massaro, J., D'Agostino, R., et al. (2018). Cardiac abnormalities in patients with hutchinson-gilford progeria syndrome. *JAMA Cardiol.* 3, 326–334. doi:10.1001/jamacardio.2017.5235

- Reidy, M. A., and Langille, B. L. (1980). The effect of local blood flow patterns on endothelial cell morphology. *Exp. Mol. Pathol.* 32, 276–289. doi:10.1016/0014-4800(80)90061-1
- Remuzzi, A., Dewey, C. F., Davies, P. F., and Gimbrone, M. A. (1984). Orientation of endothelial cells in shear fields *in vitro*. *Biorheology* 21, 617–630. doi:10.3233/BIR-1984-21419
- Roux, E., Bougaran, P., Dufourcq, P., and Couffignal, T. (2020). Fluid shear stress sensing by the endothelial layer. *Front. Physiol.* 11, 861. doi:10.3389/fphys.2020.00861
- Roux, K. J., Crisp, M. L., Liu, Q., Kim, D., Kozlov, S., Stewart, C. L., et al. (2009). Nesprin 4 is an outer nuclear membrane protein that can induce kinesin-mediated cell polarization. *Proc. Natl. Acad. Sci. U. S. A.* 106, 2194–2199. doi:10.1073/pnas.0808602106
- Salvador, J., and Iruela-Arispe, M. L. (2022). Nuclear mechanosensation and mechanotransduction in vascular cells. *Front. Cell Dev. Biol.* 10, 905927. doi:10.3389/fcell.2022.905927
- Schmitt, J., Benavente, R., Hodzic, D., Höög, C., Stewart, C. L., and Alsheimer, M. (2007). Transmembrane protein Sun2 is involved in tethering mammalian meiotic telomeres to the nuclear envelope. *Proc. Natl. Acad. Sci. U. S. A.* 104, 7426–7431. doi:10.1073/pnas.0609198104
- Seelbinder, B., Ghosh, S., Schneider, S. E., Scott, A. K., Berman, A. G., Goergen, C. J., et al. (2021). Nuclear deformation guides chromatin reorganization in cardiac development and disease. *Nat. Biomed. Eng.* 5, 1500–1516. doi:10.1038/s41551-021-00823-9
- Shah, P. P., Lv, W., Rhoades, J. H., Poleshko, A., Abbey, D., Caporizzo, M. A., et al. (2021). Pathogenic LMNA variants disrupt cardiac lamina-chromatin interactions and de-repress alternative fate genes. *Cell Stem Cell* 28, 938–954.e9. doi:10.1016/j.stem.2020.12.016
- Shao, X., Tarnasky, H. A., Lee, J. P., Oko, R., and van der Hoorn, F. A. (1999). Spag4, a novel sperm protein, binds outer dense-fiber protein Odf1 and localizes to microtubules of manchette and axoneme. *Dev. Biol.* 211, 109–123. doi:10.1006/dbio.1999.9297
- Sinensky, M., Fantle, K., Trujillo, M., McLain, T., Kupfer, A., and Dalton, M. (1994). The processing pathway of prelamin A. *J. Cell Sci.* 107, 61–67. doi:10.1242/jcs.107.1.61
- Smith, M. A., Blankman, E., Jensen, C. C., Hoffman, L. M., Ullman, K. S., and Beckerle, M. C. (2022). Nuclear pore complexes concentrate on Actin/LINC/Lamin nuclear lines in response to mechanical stress in a SUN1 dependent manner. *Heliyon* 8, e12147. doi:10.1016/j.heliyon.2022.e12147
- Sosa, B. A., Rothballe, A., Kutay, U., and Schwartz, T. U. (2012). LINC complexes form by binding of three KASH peptides to domain interfaces of trimeric SUN proteins. *Cell* 149, 1035–1047. doi:10.1016/j.cell.2012.03.046
- Starr, D. A. (2019). A network of nuclear envelope proteins and cytoskeletal force generators mediates movements of and within nuclei throughout *Caenorhabditis elegans* development. *Exp. Biol. Med.* 244, 1323–1332. doi:10.1177/1535370219871965
- Stebbens, W. E., Delahunt, B., Shozawa, T., and Gilbert-Barness, E. (2001). Smooth muscle cell depletion and collagen types in progeric arteries. *Cardiovasc. Pathol.* 10, 133–136. doi:10.1016/S1054-8807(01)00069-2
- Stebbens, W. E., Wakefield, St. J., Gilbert-Barness, E., Olson, R. E., and Ackerman, J. (1999). Histological and ultrastructural features of atherosclerosis in progeria. *Cardiovasc. Pathol.* 8, 29–39. doi:10.1016/S1054-8807(98)00023-4
- Stewart, R. M., Rodriguez, E. C., and King, M. C. (2019). Ablation of SUN2-containing LINC complexes drives cardiac hypertrophy without interstitial fibrosis. *Mol. Biol. Cell* 30, 1664–1675. doi:10.1091/mbc.E18-07-0438
- Stewart-Hutchinson, P. J., Hale, C. M., Wirtz, D., and Hodzic, D. (2008). Structural requirements for the assembly of LINC complexes and their function in cellular mechanical stiffness. *Exp. Cell Res.* 314, 1892–1905. doi:10.1016/j.yexcr.2008.02.022
- Stroud, M. J., Banerjee, I., Lowe, J., and Chen, J. (2014). Linker of nucleoskeleton and cytoskeleton complex proteins in cardiac structure, function, and disease. *Circ. Res.* 114, 538–548. doi:10.1161/CIRCRESAHA.114.301236
- Sun, S., Qin, W., Tang, X., Meng, Y., Hu, W., Zhang, S., et al. (2020). Vascular endothelium-targeted Sirt7 gene therapy rejuvenates blood vessels and extends life span in a Hutchinson-Gilford progeria model. *Sci. Adv.* 6, eaay5556. doi:10.1126/sciadv.aay5556
- Sun, W.-W., Jiao, S., Sun, L., Zhou, Z., Jin, X., and Wang, J.-H. (2018). SUN2 modulates HIV-1 infection and latency through association with lamin A/C to maintain the repressive chromatin. *mBio* 9, e02408–e02417. doi:10.1128/mBio.02408-17
- Tabosh, T. A., Tarrass, M. A., Tourvieille, L., Guilhem, A., Dupuis-Girod, S., and Bailly, S. (2024). Hereditary hemorrhagic telangiectasia: from signaling insights to therapeutic advances. *J. Clin. Invest.* 134, e176379. doi:10.1172/JCI176379
- Tajik, A., Zhang, Y., Wei, F., Sun, J., Jia, Q., Zhou, W., et al. (2016). Transcription upregulation via force-induced direct stretching of chromatin. *Nat. Mat.* 15, 1287–1296. doi:10.1038/nmat4729
- Thakar, K., May, C. K., Rogers, A., and Carroll, C. W. (2017). Opposing roles for distinct LINC complexes in regulation of the small GTPase RhoA. *Mol. Biol. Cell* 28, 182–191. doi:10.1091/mbc.E16-06-0467
- Tkachenko, E., Gutierrez, E., Saikin, S. K., Fogelstrand, P., Kim, C., Groisman, A., et al. (2013). The nucleus of endothelial cell as a sensor of blood flow direction. *Biol. Open* 2, 1007–1012. doi:10.1242/bio.20134622
- Tzima, E., Irani-Tehrani, M., Kiosses, W. B., Dejana, E., Schultz, D. A., Engelhardt, B., et al. (2005). A mechanosensory complex that mediates the endothelial cell response to fluid shear stress. *Nature* 437, 426–431. doi:10.1038/nature03952
- Udan, R. S., Vadakkan, T. J., and Dickinson, M. E. (2013). Dynamic responses of endothelial cells to changes in blood flow during vascular remodeling of the mouse yolk sac. *Development* 140, 4041–4050. doi:10.1242/dev.096255
- Ueda, N., Maekawa, M., Matsui, T. S., Deguchi, S., Takata, T., Katahira, J., et al. (2022). Inner nuclear membrane protein, SUN1, is required for cytoskeletal force generation and focal adhesion maturation. *Front. Cell Dev. Biol.* 10, 885859. doi:10.3389/fcell.2022.885859
- Varga, R., Eriksson, M., Erdos, M. R., Olive, M., Harten, I., Kolodgie, F., et al. (2006). Progressive vascular smooth muscle cell defects in a mouse model of Hutchinson-Gilford progeria syndrome. *Proc. Natl. Acad. Sci. U. S. A.* 103, 3250–3255. doi:10.1073/pnas.0600012103
- Versaevel, M., Braquénier, J.-B., Riaz, M., Grevesse, T., Lantoine, J., and Gabriele, S. (2014). Super-resolution microscopy reveals LINC complex recruitment at nuclear indentation sites. *Sci. Rep.* 4, 7362. doi:10.1038/srep07362
- Vidak, S., Serebryanny, L. A., Pegoraro, G., and Misteli, T. (2023). Activation of endoplasmic reticulum stress in premature aging via the inner nuclear membrane protein SUN2. *Cell Rep.* 42, 112534. doi:10.1016/j.celrep.2023.112534
- Wang, G., Wu, X., Zhou, L., Gao, S., Yun, D., Liang, A., et al. (2020). Tethering of telomeres to the nuclear envelope is mediated by SUN1-MAJIN and possibly promoted by SPDYA-CDK2 during meiosis. *Front. Cell Dev. Biol.* 8, 845. doi:10.3389/fcell.2020.00845
- Wang, J.-Y., Yu, I.-S., Huang, C.-C., Chen, C.-Y., Wang, W.-P., Lin, S.-W., et al. (2015). Sun1 deficiency leads to cerebellar ataxia in mice. *Dis. Model. Mech.* 8, 957–967. doi:10.1242/dmm.019240
- Wang, Q., Du, X., Cai, Z., and Greene, M. I. (2006). Characterization of the structures involved in localization of the SUN proteins to the nuclear envelope and the centrosome. *DNA Cell Biol.* 25, 554–562. doi:10.1089/dna.2006.25.554
- Wang, W., Shi, Z., Jiao, S., Chen, C., Wang, H., Liu, G., et al. (2012). Structural insights into SUN-KASH complexes across the nuclear envelope. *Cell Res.* 22, 1440–1452. doi:10.1038/cr.2012.126
- Wilhelmsen, K., Litjens, S. H. M., Kuikman, I., Tshimbalanga, N., Janssen, H., Van Den Bout, I., et al. (2005). Nesprin-3, a novel outer nuclear membrane protein, associates with the cytoskeletal linker protein plectin. *J. Cell Biol.* 171, 799–810. doi:10.1083/jcb.200506083
- Xing, X.-W., Li, L.-Y., Liu, G., Fu, J.-J., Tan, X.-J., and Lu, G.-X. (2004). Identification of a novel gene SRG4 expressed at specific stages of mouse spermatogenesis. *Acta Biochim. Biophys. Sin.* 36, 351–359. doi:10.1093/abbs/36.5.351
- Xiong, H., Rivero, F., Euteneuer, U., Mondal, S., Mana-Capelli, S., Laroche, D., et al. (2008). Dictyostelium sun-1 connects the centrosome to chromatin and ensures genome stability. *Traffic* 9, 708–724. doi:10.1111/j.1600-0854.2008.009721.x
- Xu, C., Hasan, S. S., Schmidt, I., Rocha, S. F., Pitulescu, M. E., Bussmann, J., et al. (2014). Arteries are formed by vein-derived endothelial tip cells. *Nat. Commun.* 5, 5758. doi:10.1038/ncomms6758
- Yang, F., Zhang, Y., Zhu, J., Wang, J., Jiang, Z., Zhao, C., et al. (2020). Laminar flow protects vascular endothelial tight junctions and barrier function via maintaining the expression of long non-coding RNA MALAT1. *Front. Bioeng. Biotechnol.* 8, 647. doi:10.3389/fbioe.2020.00647
- Yang, S. H., Bergo, M. O., Toth, J. I., Qiao, X., Hu, Y., Sandoval, S., et al. (2005). Blocking protein farnesyltransferase improves nuclear blebbing in mouse fibroblasts with a targeted Hutchinson-Gilford progeria syndrome mutation. *Proc. Natl. Acad. Sci. U. S. A.* 102, 10291–10296. doi:10.1073/pnas.0504641102
- Yang, S. H., Meta, M., Qiao, X., Frost, D., Bauch, J., Coffinier, C., et al. (2006). A farnesyltransferase inhibitor improves disease phenotypes in mice with a Hutchinson-Gilford progeria syndrome mutation. *J. Clin. Invest.* 116, 2115–2121. doi:10.1172/JCI28968
- Yu, J., Lei, K., Zhou, M., Craft, C. M., Xu, G., Xu, T., et al. (2011). KASH protein Syne-2/Nesprin-2 and SUN proteins SUN1/2 mediate nuclear migration during mammalian retinal development. *Hum. Mol. Genet.* 20, 1061–1073. doi:10.1093/hmg/ddq549
- Yue, X., Cui, J., Sun, Z., Liu, L., Li, Y., Shao, L., et al. (2023). Nuclear softening mediated by Sun2 suppression delays mechanical stress-induced cellular senescence. *Cell Death Discov.* 9, 167–211. doi:10.1038/s41420-023-01467-1
- Zhang, Q., Bethmann, C., Worth, N. F., Davies, J. D., Wasner, C., Feuer, A., et al. (2007). Nesprin-1 and -2 are involved in the pathogenesis of Emery Dreifuss muscular

dystrophy and are critical for nuclear envelope integrity. *Hum. Mol. Genet.* 16, 2816–2833. doi:10.1093/hmg/ddm238

Zhang, Q., Ragnauth, C., Greener, M. J., Shanahan, C. M., and Roberts, R. G. (2002). The nesprins are giant actin-binding proteins, orthologous to *Drosophila melanogaster* muscle protein MSP-300. *Genomics* 80, 473–481. doi:10.1006/geno.2002.6859

Zhang, Q., Skepper, J. N., Yang, F., Davies, J. D., Hegyi, L., Roberts, R. G., et al. (2001). Nesprins: a novel family of spectrin-repeat-containing proteins that localize to the nuclear membrane in multiple tissues. *J. Cell Sci.* 114, 4485–4498. doi:10.1242/jcs.114.24.4485

Zhang, X., Lei, K., Yuan, X., Wu, X., Zhuang, Y., Xu, T., et al. (2009). SUN1/2 and Syne/Nesprin-1/2 complexes connect centrosome to the nucleus during neurogenesis and neuronal migration in mice. *Neuron* 64, 173–187. doi:10.1016/j.neuron.2009.08.018

Zhang, Y., Kong, Y., Guo, H., Liu, Y., Zang, Y., and Li, J. (2022). Inner nuclear membrane protein TMEM201 maintains endothelial cell migration and angiogenesis by interacting with the LINC complex. *J. Mol. Cell Biol.* 14, mjac017. doi:10.1093/jmcb/mjac017

Zhou, Z., Du, X., Cai, Z., Song, X., Zhang, H., Mizuno, T., et al. (2012). Structure of sad1-UNC84 Homology (SUN) domain defines features of molecular bridge in nuclear envelope. *J. Biol. Chem.* 287, 5317–5326. doi:10.1074/jbc.M111.304543

Zhu, R., Antoku, S., and Gundersen, G. G. (2017). Centrifugal displacement of nuclei reveals multiple LINC complex mechanisms for homeostatic nuclear positioning. *Curr. Biol.* 27, 3097–3110. doi:10.1016/j.cub.2017.08.073



OPEN ACCESS

EDITED BY

Brian Gene Coon,
Oklahoma Medical Research Foundation,
United States

REVIEWED BY

Audrey Cleuren,
Oklahoma Medical Research Foundation,
United States
Ran You,
Nanjing Children's Hospital, China

*CORRESPONDENCE

Eno E. Ebong,
✉ e.ebong@northeastern.edu

RECEIVED 02 March 2024

ACCEPTED 27 May 2024

PUBLISHED 04 July 2024

CITATION

O'Hare N, Millican K and Ebong EE (2024),
Unraveling neurovascular mysteries: the role of
endothelial glycocalyx dysfunction in
Alzheimer's disease pathogenesis.
Front. Physiol. 15:1394725.
doi: 10.3389/fphys.2024.1394725

COPYRIGHT

© 2024 O'Hare, Millican and Ebong. This is an
open-access article distributed under the terms
of the [Creative Commons Attribution License](#)
(CC BY). The use, distribution or reproduction in
other forums is permitted, provided the original
author(s) and the copyright owner(s) are
credited and that the original publication in this
journal is cited, in accordance with accepted
academic practice. No use, distribution or
reproduction is permitted which does not
comply with these terms.

Unraveling neurovascular mysteries: the role of endothelial glycocalyx dysfunction in Alzheimer's disease pathogenesis

Nicholas O'Hare¹, Karina Millican² and Eno E. Ebong^{1,2,3*}

¹Department of Chemical Engineering, Northeastern University, Boston, MA, United States, ²Department of Bioengineering, Northeastern University, Boston, MA, United States, ³Department of Neuroscience, Albert Einstein College of Medicine, New York, NY, United States

While cardiovascular disease, cancer, and human immunodeficiency virus (HIV) mortality rates have decreased over the past 20 years, Alzheimer's Disease (AD) deaths have risen by 145% since 2010. Despite significant research efforts, effective AD treatments remain elusive due to a poorly defined etiology and difficulty in targeting events that occur too downstream of disease onset. In hopes of elucidating alternative treatment pathways, now, AD is commonly being more broadly defined not only as a neurological disorder but also as a progression of a variety of cerebrovascular pathologies highlighted by the breakdown of the blood-brain barrier. The endothelial glycocalyx (GCX), which is an essential regulator of vascular physiology, plays a crucial role in the function of the neurovascular system, acting as an essential vascular mechanotransducer to facilitate ultimate blood-brain homeostasis. Shedding of the cerebrovascular GCX could be an early indication of neurovascular dysfunction and may subsequently progress neurodegenerative diseases like AD. Recent advances in in vitro modeling, gene/protein silencing, and imaging techniques offer new avenues of scrutinizing the GCX's effects on AD-related neurovascular pathology. Initial studies indicate GCX degradation in AD and other neurodegenerative diseases and have begun to demonstrate a possible link to GCX loss and cerebrovascular dysfunction. This review will scrutinize the GCX's contribution to known vascular etiologies of AD and propose future work aimed at continuing to uncover the relationship between GCX dysfunction and eventual AD-associated neurological deterioration.

KEYWORDS

endothelial glycocalyx, Alzheimer's disease, blood-brain barrier, neurovascular dysfunction, vascular mechanobiology, vascular etiology

Abbreviations: AD, Alzheimer's Disease; A β , Amyloid Beta; BBB, Blood Brain Barrier; CLSM, Confocal Laser Scanning Microscopy; CNS, Central Nervous System; DCE MRI, Dynamic Contrast-Enhanced Magnetic Resonance Imaging; eNOS, Endothelial Nitric Oxide Synthase; GAG, Glycosaminoglycan; GCX, Endothelial Glycocalyx; HA, Hyaluronic Acid; HS, Heparan Sulfate; ICAM-1, Intercellular adhesion molecule-1; IL, Interleukin; MMP, Matrix Metalloproteinase; NFT, Neurofibrillary Tangle; NO, Nitric Oxide; NVU, Neurovascular Unit; RF/FS, Rapid Freezing/Freeze Substitution; RNS, Reactive Nitrogen Species; ROS, Reactive Oxygen Species; SDF, Side-Stream Darkfield Microscopy; TEM, Transmission Electron Microscopy; TPLSM, Two-Photon Light Scanning Microscopy; QUTE-CE MRI, Quantitative Ultra-Short Time-To-Echo Contrast-Enhanced Magnetic Resonance Imaging.

1 Introduction: the role of vascular dysfunction in Alzheimer's disease

Alzheimer's disease (AD) is a neurodegenerative disorder that causes a gradual and irreversible loss of neuronal function in the brain, resulting in progressive impairment of cognitive abilities, such as memory, decision-making, and communication skills (Sheppard and Coleman, 2020). As the disease advances, it leads to increasingly severe symptoms and eventual loss of independence, leading to devastating effects not only for the individual but also their loved ones, caregivers, and society as a whole. In the United States alone, an estimated 6.2 million people over the age of 65 suffer from the condition as of 2021 (Alzheimer, 2021). Unfortunately, the number of cases of AD is projected to increase two to four times by 2050 without significant medical breakthroughs (Alzheimer's disease facts and figures, 2021; Kumar et al., 2022). There are currently no cures for AD, and the only clinical successes have been related to delaying the inevitable cognitive and behavioral decline associated with the disease.

Effective treatments for AD remain elusive due to the complex and poorly understood etiology of the disorder. Traditionally, Amyloid beta (A β) plaques and neurofibrillary tangles (NFTs) are considered the hallmark pathological features of AD (De-Paula et al., 2012). However, targeting these protein aggregates has been challenging, and clinical trials focused on these deposits have shown mixed results, suggesting other mechanisms contribute to the development and progression of AD (Braak and Braak, 1995; Korszyn, 2008; Korszyn, 2012). Thus, it is imperative to investigate additional disease factors for better treatments. This includes exploring the vascular hypothesis of AD, which could significantly advance research and therapies.

Redefining AD as not only a neurological disorder, but rather a combination of vascular abnormalities and neurodegeneration could provide a novel perspective on disease pathology. Despite AD being traditionally considered a non-vascular dementia, virtually all AD patients exhibit impaired vascular function in their brains (De La Torre, 2002). Although this correlation between vascular disease and AD was proposed nearly 30 years ago, the underlying link between vascular dysfunction and AD progression remains relatively understudied (de la Torre and Mussivand, 1993). Epidemiological studies indicate that neurovascular dysfunction often precedes conventional neuro-centric pathology in AD patients, offering a promising avenue for novel treatment of AD (Prohovnik et al., 1988; Ruitenberg et al., 2005; Li et al., 2010). This observation is critical to supporting the notion that not only do vascular abnormalities coincide with AD, but they may be promoting the accumulation of toxic protein aggregates in the brain, upstream of symptom manifestation. Future work aims to identify the causal impact of vascular dysfunction to AD symptoms and clarify the weight of these vascular events.

The vascular hypothesis proposes that AD development may originate from neurovascular unit (NVU) breakdown, leading to significant neuronal health changes characteristic of AD. This dysfunction is driven by various interconnected neurovascular pathologies including blood-brain barrier (BBB) breakdown, neurovascular decoupling, and endothelial dysfunction. Structurally, the BBB plays an essential role in facilitating the

transport of nutrients and waste products in and out of the brain's fragile environment (Hussain et al., 2021). When the BBB is damaged, it allows for neuroinflammatory compounds to enter while hindering the clearance of waste products such as AD-associated protein precursors. This leads to protein aggregation, glial inflammation, and neuronal death (Chen and Strickland, 1997; Mhatre et al., 2004; Schachtrup et al., 2007; Sweeney et al., 2018). Congruently, neurovascular decoupling, the process in which the vasculature cannot adequately adapt to the brain's demands, also promotes AD manifestation through inadequate nutrient delivery and impeded waste clearance (Zhu et al., 2022). Finally, endothelial dysfunction within the brain microvasculature induces oxidative stress and cellular inflammation while simultaneously further deteriorating BBB integrity and the responsiveness of blood vessels (Di Marco et al., 2015). All these vascular pathologies have been observed in patients presenting early-stage AD cognitive dysfunction, suggesting their contribution to disease progression (Di Marco et al., 2015; Montagne et al., 2015; van de Haar et al., 2016). Further investigating the impact of these pathologies to AD progression and uncovering the initial insult which causes cerebral vascular dysfunction could dramatically alter treatment approaches to AD.

Although a vascular role appears likely in the pathogenesis of AD, determining a therapeutic target to mitigate or reverse these vascular pathologies remains an unresolved question. Some of the structures at the neurovascular interface under investigation include tight junctions, intracellular transporters, nitric oxide (NO) regulators, and adhesion molecules (Govindpani et al., 2019; Soto-Rojas et al., 2021). However, as of now, no specific blood-vessel based target which significantly modifies the progression of AD has been identified. Thus, in this review, the focus will be drawn to the vascular endothelial glycocalyx (GCX), a relatively understudied structure which stands as a potential master regulator of neurovascular health. The GCX is a sugar-rich nano-structure that resembles a dense bush and lines the inner part of blood vessels (Reitsma et al., 2007). Due to its diverse functionality and structural diversity, it may play a role in regulating several vascular functions that are disrupted in AD, such as stabilizing vessel permeability, promoting neurovascular coupling, and maintaining physiological redox of the endothelium (Curry and Adamson, 2012; Yen et al., 2015; Qu et al., 2021). Research has already demonstrated the significant role of GCX health in preventing various vascular disorders in the body, and recent discoveries regarding its therapeutic potential are rapidly multiplying (Tarbell and Cancel, 2016; Dogné and Flamion, 2020; Zhao et al., 2021). Therefore here, we will present the current knowledge regarding the GCX and its connection to neurovascular health in the context of AD while also outlining future research directions aimed at unraveling its role in disease pathology. Overall, we will propose a GCX-vascular-hypothesis of AD progression where GCX degradation leads to neurovascular unit dysfunction, ultimately promoting abnormal protein accumulation in the brain resulting in AD manifestation (Figure 1). Although still in its early stages and primarily correlational, recent research has notably progressed our comprehension of the connection between cerebral vascular dysfunction and AD, while also shedding light on the involvement of the GCX (Figure 1) (van de Haar et al., 2016; Zhu et al., 2018; Smyth et al., 2022; Moon et al., 2023). However,

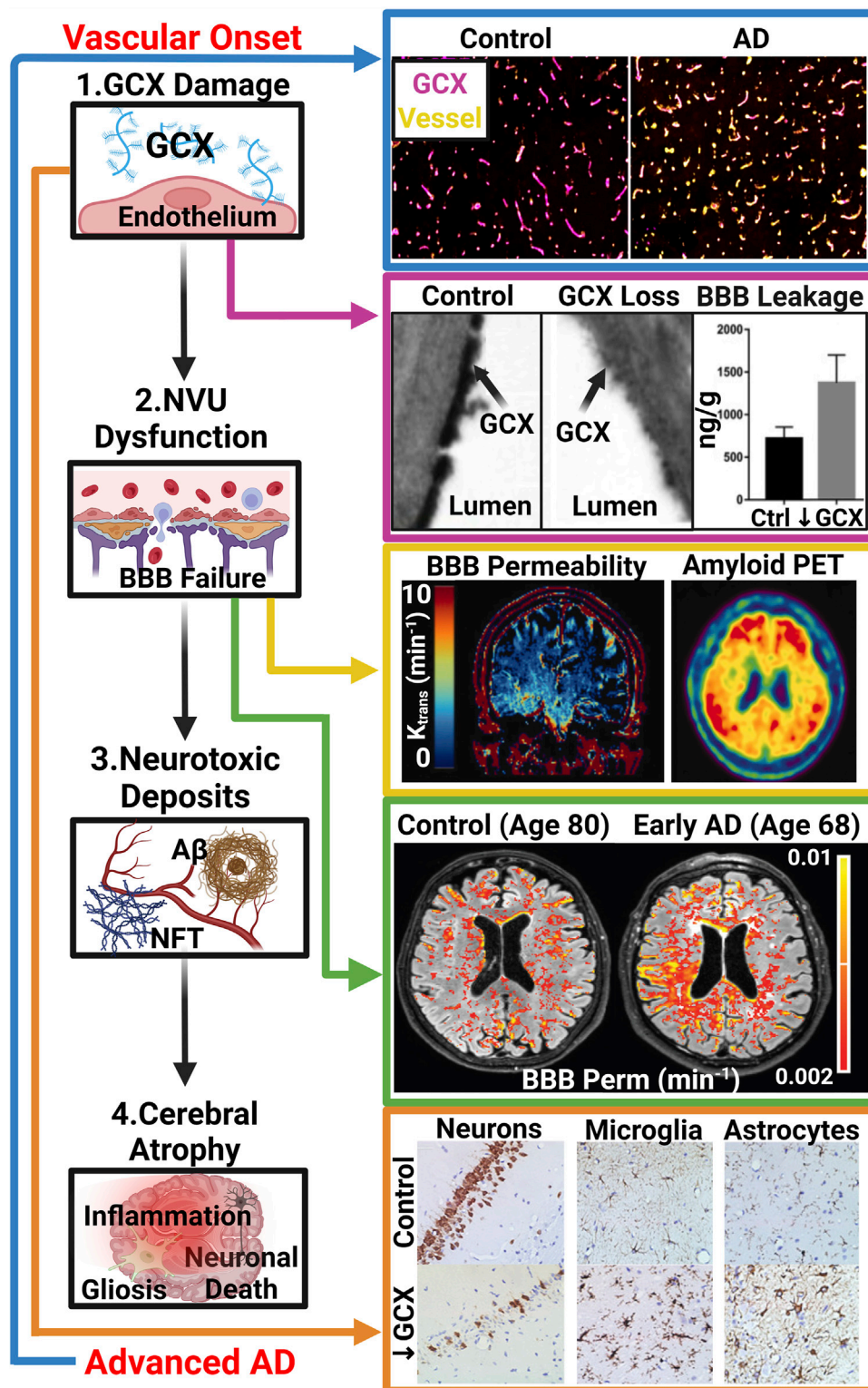


FIGURE 1

The GCV-Vascular Hypothesis of AD: Hypothesized sequence of events linking GCX degradation to AD pathology: (1.) Various vascular insults induce damage to the GCX. (2.) GCX damage initiates NVU dysfunction, notably affecting the BBB. (3.) NVU dysregulation leads to abnormal accumulation of neurotoxic deposits including Aβ and NFTs within the brain, characteristic of AD. (4.) Subsequently, these protein aggregates induce brain inflammation, gliosis, and neuronal death, facilitating cognitive decline. Several recent studies have supported this GCX-rooted hypothesis. (Blue Arrow): Smyth et al. observed a significant reduction in GCX integrity in post-mortem AD tissue compared to healthy controls, suggesting a correlation between late-stage AD and GCX integrity via immunostaining of UEA1 lectin for GCX and Collagen type IV for cerebral vasculature. Adapted from Figure 5 in Smyth LCD, et al. *Acta Neuropathologica Communications*. 2022; 10(1), Copyright (2022) by Acta Neuropathologica Communications (Smyth et al., 2022). This figure is sourced from an open-access publication. (Magenta Arrow): Zhu et al. demonstrated increased leakage of Evan's blue dye into the brain parenchyma (Continued)

FIGURE 1 (Continued)

upon GCX degradation using hyaluronidase treatment in mice, indicating GCX loss triggers NVU dysfunction. Adapted from [Figure 2](#) in Zhu J., et al., *J Cereb Blood Flow Metab.* 2018; 38(11):1979–92, Copyright (2018) by the Journal of Cerebral Blood Flow (32). Used with permission. (Yellow Arrow): Moon et al. showed a regional correlation between increased BBB permeability and AD protein aggregation in early AD patients using DCE MRI and amyloid positron emission tomography. Adapted from [Figure 1](#) in Moon Y., et al. *J Cereb Blood Flow Metab.* 2023; 43(11):1813–25, Copyright (2023) by the Journal of Cerebral Blood Flow ([Moon et al., 2023](#)). Used with permission. (Green Arrow): Furthermore, van de Haar et al. observed global increases of BBB permeability in patients suffering from early cognitive decline associated with AD compared to controls independent of age. Adapted from van de Haar HJ, et al. *Radiology.* 2016; 281(2):527–35, Copyright (2016) by the Journal of Radiology ([van de Haar et al., 2016](#)). Used with Permission. (Orange Arrow) Finally, Zhu et al. investigated the impact of GCX degradation on neuronal loss and glial cell activation through immunostaining of neurons (NeuN), microglia (Iba1), and astrocytes (GFAP), revealing significant reductions in neuron count and activated glial cells resembling cerebral pathologies in AD. Adapted from [Figure 5](#) in Zhu J., et al. *J Cereb Blood Flow Metab.* 2018; 38(11):1979–92, Copyright (2018) by the Journal of Cerebral Blood Flow ([Zhu et al., 2018](#)). Used with permission. While these studies support the proposed cascade, further research is needed to elucidate whether GCX damage is a causative factor in AD manifestation or a consequence of an already pathological state ([De La Torre, 2002](#); [van de Haar et al., 2016](#); [Zhu et al., 2018](#); [Govindpani et al., 2019](#); [Zhao et al., 2021](#); [Smyth et al., 2022](#); [Moon et al., 2023](#)). Created with [BioRender.com](#).

it remains imperative for future research to determine whether the loss of GCX precedes subsequent AD events and elucidate the underlying mechanisms. This review seeks to consolidate existing knowledge regarding the GCX's involvement in advancing neurovascular disease and eventual AD pathology, while also proposing a framework for addressing unanswered questions. In light of the limited therapeutic options available for AD, exploring the GCX for its potential as a novel target presents a source of optimism for improving outcomes in this debilitating condition.

2 The endothelial glycocalyx: a potential master regulator of neurovascular unit function

2.1 What is the cerebral vascular glycocalyx?

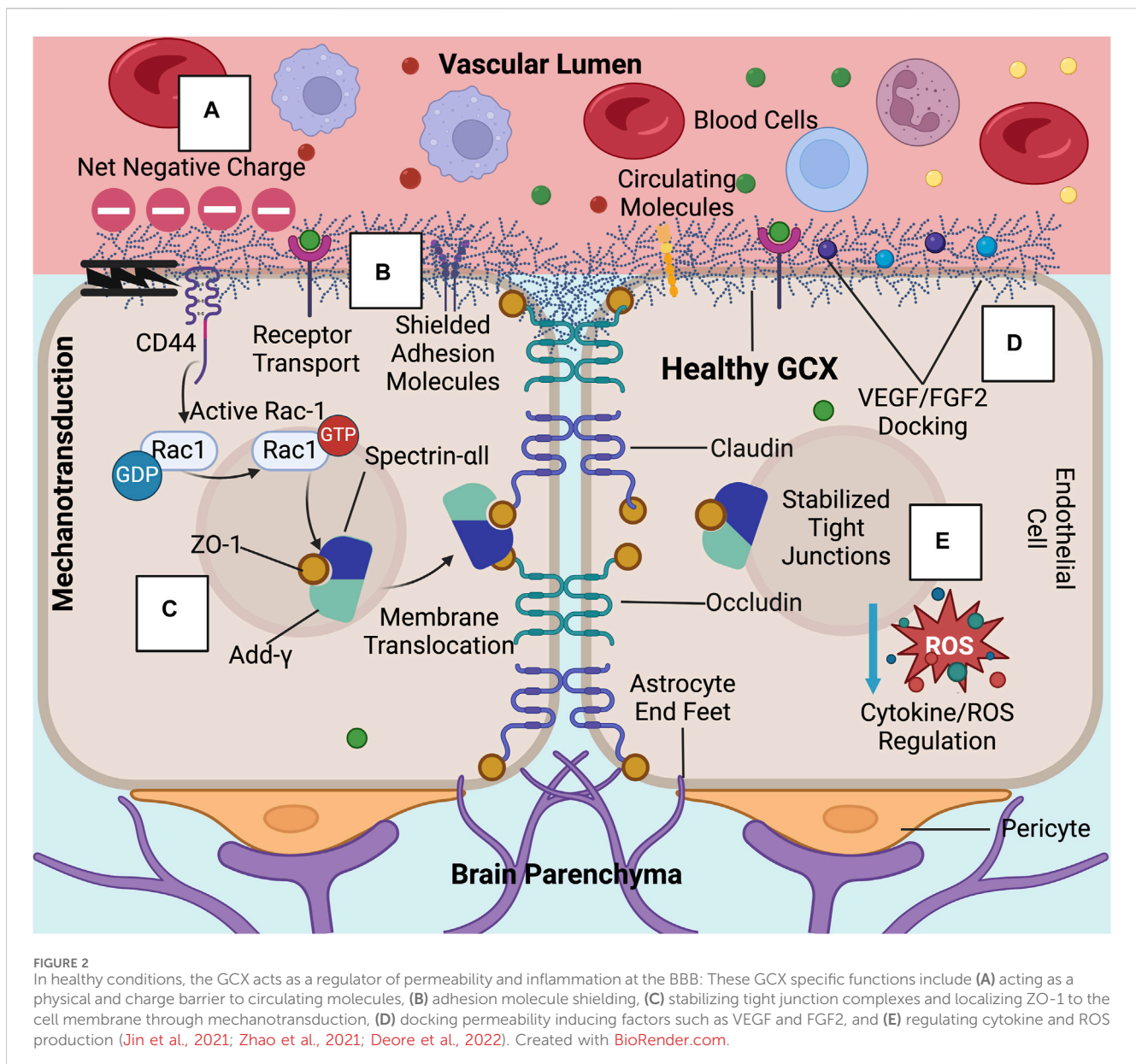
The GCX was first visualized by Luft nearly 60 years ago using electron microscopy ([Luft, 1966](#)). Over the past decade, the structure has become increasingly recognized as an essential contributor to vascular homeostasis in health and disease for its diverse roles in vessel permeability, mechanotransduction, and cellular signaling ([Alphonsus and Rodseth, 2014](#); [Uchimido et al., 2019](#); [Potje et al., 2020](#)). In light of accumulating evidence indicating that GCX damage precedes subsequent vascular pathologies, there is a growing focus on exploring the therapeutic potential of this structure upon regeneration not only for cardiovascular disease but neurological conditions as well ([Reed et al., 2019](#); [Yoon et al., 2022](#)). The GCX was only recently considered as an important component of the extended NVU due to its role in regulating neurovascular health ([Stanimirovic and Friedman, 2012](#)). The GCX has been implicated in critical processes within the NVU, including BBB regulation, inflammation control, and NO-mediated neurovascular coupling ([Reitsma et al., 2007](#); [Bartosch et al., 2017](#); [Kutuzov et al., 2018](#)). Based on the GCX's role in these processes, deterioration of the structure may be a precursor to previously described vascular etiologies of AD. Not only are all of these vascular abnormalities present in the majority of AD patients, but initial findings have also indicated that the GCX may be compromised prior to downstream neurological events in these disorders ([Reed et al., 2019](#); [Dogné and Flamion, 2020](#); [Yoon et al., 2022](#)). Protecting and restoring the GCX may therefore be a promising strategy for preventing or treating neurodegenerative diseases.

Structurally, the GCX is composed of numerous proteoglycans, glycoproteins, and associated glycosaminoglycans (GAGs) ([Reitsma et al., 2007](#); [Moore et al., 2021](#)). The major constituents of the GCX include heparan sulfate (HS) with associated core proteins syndecan and glypican, as well as hyaluronic acid (HA) and associated CD44. While these muco-poly-saccharides have been viewed as the main diagnostic markers and mechanistic contributors to GCX function, other complex carbohydrates found at the cell surface including chondroitin sulfate, keratin sulfate, dermatan sulfate, and sialic acid, are also believed to play roles in endothelial function ([Potter et al., 2009](#); [Tarbell and Cancel, 2016](#)). Further investigation is needed to fully differentiate the roles and importance of individual GCX components in regulating NVU physiology and deterring downstream AD pathology ([Pahakis et al., 2007](#); [Yang and Schmidt, 2013](#)).

The nuances of the cerebrovascular GCX compared to other vascular beds are still currently under investigation. This delayed unravelling can be ascribed to the inherent difficulties of imaging a vascular nanostructure imbedded within the skull. However, recent microscopy advances have allowed for visualization of the structure like never before. Preliminary two-photon light scanning microscopy (TPLSM) in mice has demonstrated a robust arterial and capillary GCX along the cerebral arterial tree with a thickness that varies with vessel type and did not correlate with vessel diameter ([Yoon et al., 2017](#)). Interestingly, capillaries exhibited the thickest GCX in relation to vessel diameter perhaps based on the microcirculation being the prominent location of BBB transport. Utilizing another novel imaging modality in side-stream darkfield microscopy (SDF) in human patients, Haeren et al. observed a thicker GCX in cerebral vasculature compared to sublingual vasculature, indicative of the GCX's heterogeneity throughout the body and its prospective critical role to brain physiology ([Haeren et al., 2017](#); [Haeren et al., 2018](#)). While still in its early stages, the ongoing endeavors to differentiate and unravel the intricacies of the cerebrovascular GCX offer promising prospects for future understanding.

2.2 Potential role of the endothelial vascular glycocalyx as a blood-brain barrier function controller

Mounting evidence underscores the pivotal role of the GCX in neurovascular regulation. Further understanding of this relationship



could prove pivotal in combatting AD and related neurodegenerative disorders. First, the integrity of the GCX is essential to the regulation of vascular flux throughout the body, and its role in BBB permeability is increasingly recognized (Zhao et al., 2021). Traditionally, it was believed that BBB permeability was mainly regulated through tight junctions and adherens junctions, for paracellular transport, and membrane channels, pumps, and carrier proteins, for transcellular transport pathways. However, the importance of a robust GCX is only now being appreciated for its relevance to maintaining overall BBB integrity (Zhu et al., 2018; Yang et al., 2021; Zhao et al., 2021). Research has indicated dramatic increases in vascular permeability upon GCX structure damage, strongly supporting the notion that GCX health not only plays a correlative role but a causal one in regulating overall BBB permeability and thus downstream AD pathology (Reed et al., 2019; Jin et al., 2021).

Structurally acting as a physical and charge barrier, the GCX serves as a molecular sieve to the BBB, preventing the entry of neuroinflammatory molecules into the brain while simultaneously allowing essential factors to pass through (Woodcock and Woodcock, 2012; Zhao et al., 2021). The GCX's role in deterring neurotoxic macromolecules present in the plasma, such as albumin, prothrombin, and plasminogen, may be critical to preventing the progression of AD through deterring the entry of neuroinflammatory molecules (Vink and Duling, 2000; Yang and Schmidt, 2013; Kadry et al., 2020). The GCX also regulates BBB permeability due to the high degree of net negative charge on the GAGs HS and chondroitin sulfate as well as sialic acid sugar chains (Walter et al., 2021) (Figure 2, 3). In enzymatic studies, removal of sialic acid residues on these chains resulted in an increase in albumin infiltration likely due to the reduction in electrostatic resistance (Betteridge et al., 2017). Overall, the GCX's dual functionality as a

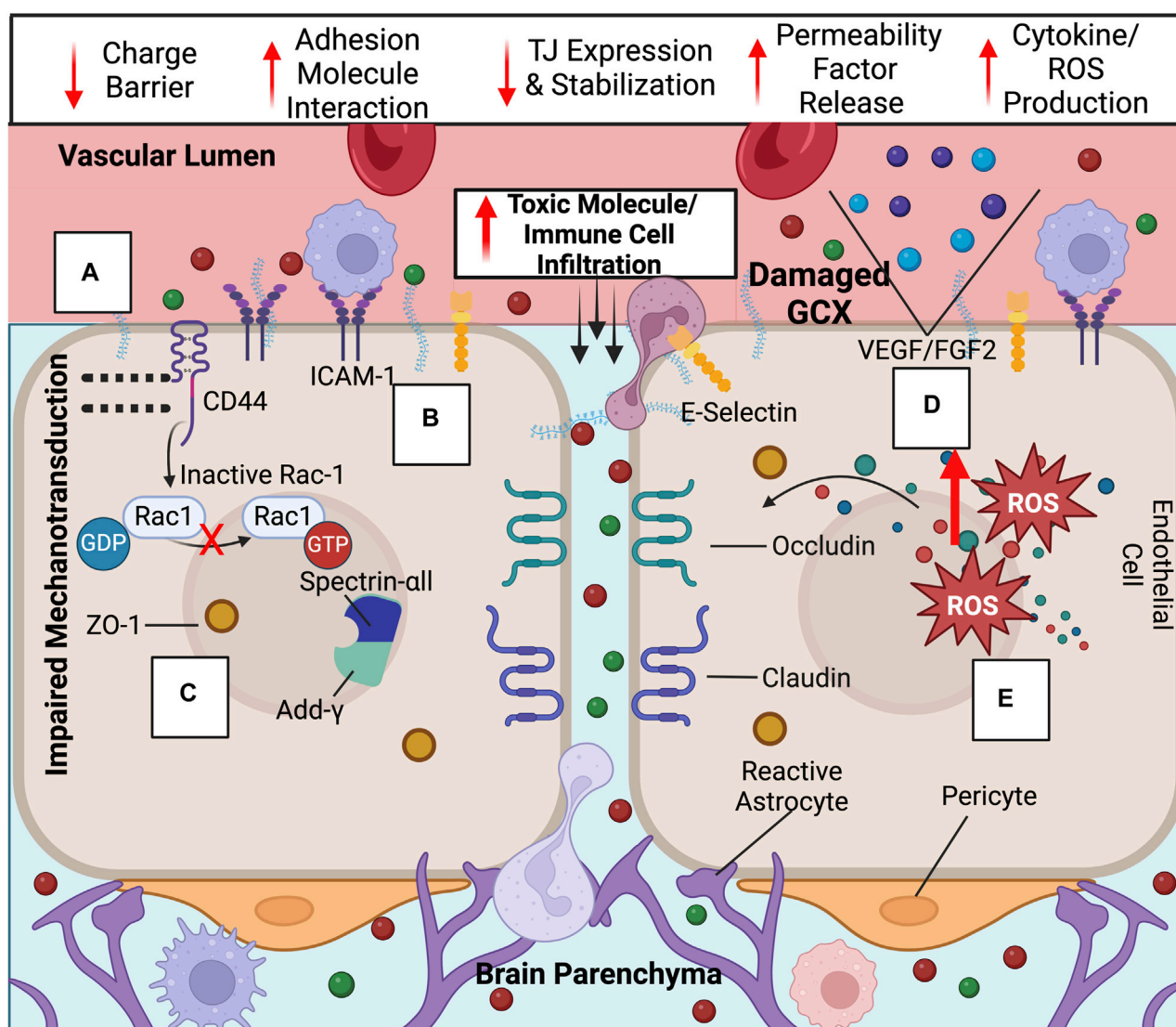


FIGURE 3 Upon GCX degradation, a variety of transport mechanisms are compromised at the BBB, leading to ultimate increased neurotoxic molecule and immune cell infiltration into the brain: Compromised endothelial functions include the loss of the (A) GCX's negative charge barrier, (B) adhesion molecule upregulation and exposure, (C) decreased tight junction expression and ZO-1 membrane localization impairment due to failed mechanotransduction, (D) permeability factor release, and (E) cytokine/ROS production. Created with [BioRender.com](#).

physical and charge barrier underscores its significance in regulating molecular access to the central nervous system (CNS).

The GCX plays a crucial role in maintaining the BBB not only through its physical structure but also by influencing cellular signaling which impacts BBB function. It is known to regulate the production and availability of reactive oxygen species (ROS) and cytokines, which are both linked to the disruption of tight junctions such as claudins and occludins at the BBB (Figure 2, 3) (Goes et al., 2001; Rochfort et al., 2014). Additionally, a thinner GCX is associated with reduced expression of crucial transcellular transporters compromised in AD, such as glucose transporter-1 and p-glycoprotein, essential for glucose transport into the brain and A β plaque clearance from it, respectively (Gomez González et al., 2011; Winkler et al., 2015; Ding et al., 2021; Santa-Maria et al., 2021). In a study directly examining the effects of GCX impairment on BBB

function, Zhu et al. found that hyaluronidase-induced degradation of HA in a rat model led to increased infiltration of Evan's blue dye into the CNS, reduced tight junction expression, elevated brain water content, and glial activation indicative of neuroinflammation (Figure 1) (Zhu et al., 2018). This highlights the potential involvement of the GCX in BBB permeability regulation and key AD promoting pathologies.

Further research is needed to determine the molecular mechanisms linking GCX loss to BBB disruption and the functions of specific components within the complex, heterogeneous structure. For example, HA removal may trigger a CD44-dependent mechanism of BBB regulation (Al-ahmad et al., 2019). CD44, the primary transmembrane receptor for HA, has been shown by Deore et al. to be critical for BBB formation (Deore et al., 2022). When CD44 is deleted through CRISPR, RAC-1 activation is suppressed whereas

RhoA becomes hyperactivated. Consequently, this prevents the initiation of a pathway that involves the recruitment of ZO-1, the actin filament capping protein adducin-1, and the cytoskeletal protein spectrin- α II to cell-cell junctions, ultimately impairing the integrity of the BBB. (Figures 2, 3). This pathway is dependent on shear-stress-based mechanotransduction, likely due to HA's role as a mechanosensor (Deore et al., 2022). The interplay of HA, CD44, shear stress, and tight junctions is crucial for maintaining a stable BBB.

Additionally, for HS, which is the most abundant GAG in the GCX, studies show that its enzymatic degradation increases monocyte infiltration into the brain (Floris et al., 2003). HS serves as a docking site for chemokines as well as various other molecules such as fibroblast growth factor 2 (FGF2) and vascular endothelial growth factor (VEGF), all involved in regulating tight junction activity (Figures 2, 3) (Chiodelli et al., 2015; Yang et al., 2021). Furthermore, HS proteoglycans, such as syndecan-1 and glypican-1, may also play critical roles in BBB permeability. Degradation of the GCX enhances syndecan-1 interaction with SRC, promoting caveolae-mediated endocytosis, while glypican-1 loss may reduce A β transport out of the brain via complex formation with low-density lipoprotein receptor-related protein 1 (LRP1) (Leite et al., 2020; Zhu et al., 2021).

Ultimately, gaining a deeper understanding of the mechanisms underlying BBB permeability induced by GCX loss and further elucidating the roles of its individual components could provide valuable insights into its relevance to the BBB-based neurodegeneration associated with AD.

2.3 Potential role of the endothelial glycocalyx as an inflammation controller for the neurovascular unit

While acting as a BBB permeability regulator, the GCX also serves as a key modulator of neuro- and vascular-inflammation. Alterations in immune cell trafficking and endothelial function may lead to AD-related pathologies including A β accumulation, oxidative stress, and neuroinflammation (Govindpani et al., 2019). A feedback loop of neurological and vascular dysfunction results in a severely diseased state of cognitive decline. Could GCX dysfunction precede these downstream events?

In physiological conditions, the GCX plays a crucial role in regulating leukocyte adhesion to the endothelium. The GCX in rat capillaries is believed to range from 200–500 nm, far exceeding the size of endothelial leukocyte receptor and adhesion molecules, such as E-selectin and intercellular adhesion molecule-1 (ICAM-1) (30–40 nm) (van den Berg et al., 2003; Lipowsky, 2012). Due to this size discrepancy, one can logically hypothesize the GCX shields the endothelium from direct interaction with circulating white blood cells (Figures 2, 3). Constantinescu et al. demonstrated that after various heparinase (an enzymatic cleaver of HS) concentrations were administered to mice, the number of adherent leukocytes increased significantly (Constantinescu et al., 2003). Not only does the GCX shield endothelial cells from leukocyte interaction with adhesion molecules, but it may also upregulate adhesion molecule expression upon shedding. In an *in vitro* flow environment, ICAM-1 levels increased by 300% upon enzymatic removal compared to static controls. This increase may be mediated

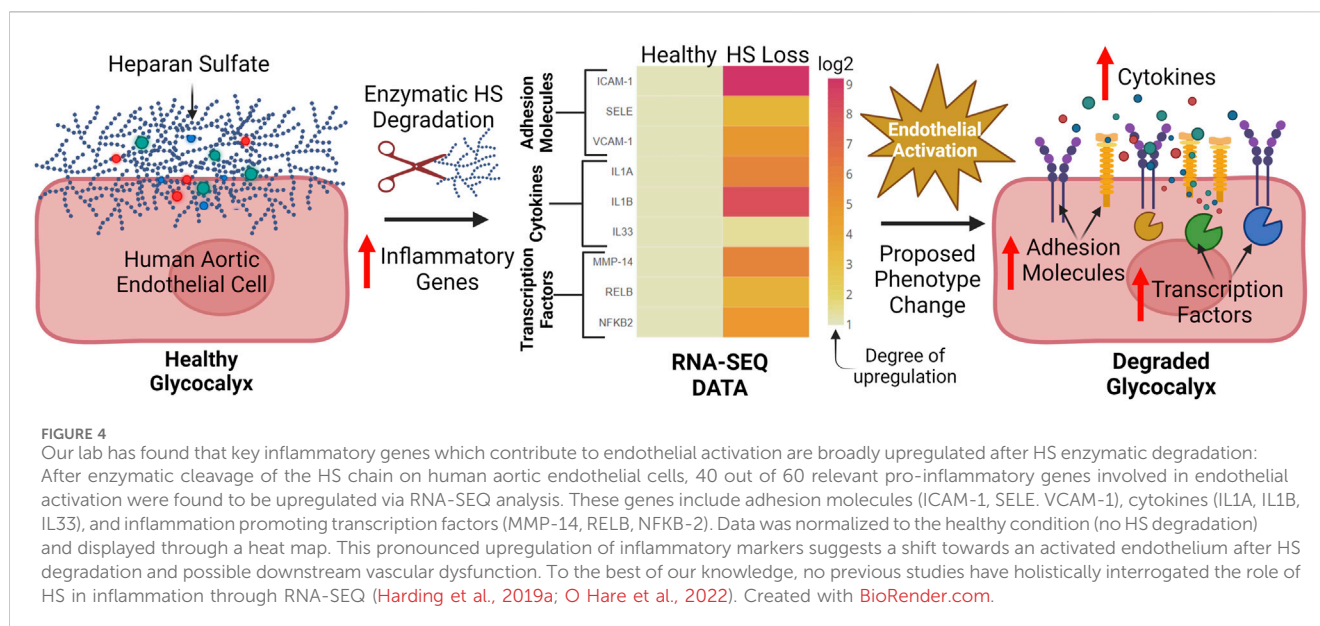
by a shear-induced NF- κ B pathway regulated by GCX components (McDonald et al., 2016).

In our lab group, we have performed broad RNA-SEQ analysis on human aortic endothelial cells to determine the effects of HS degradation on eliciting endothelial inflammation, a state associated with downstream vascular disease (Figure 4) (Harding et al., 2019a; O'Hare et al., 2022). Through analysis of 60 relevant pro-inflammatory markers, 40 of 60 were upregulated upon HS cleavage via Heparinase III treatment. To our knowledge, no study has characterized the effects of HS loss on such a wide range of inflammatory markers implicated in endothelial activation including adhesion molecules, cytokines/chemokines, and pro-inflammatory transcription factors (Figure 4). This work provides further evidence of the pronounced role HS plays in deterring endothelial dysfunction. However, the significance of HS and other GAGs within the GCX for maintaining normal endothelial function in the cerebral vasculature remains underexplored and warrants further investigation to elucidate their roles in mitigating neurovascular dysfunction associated with AD.

2.4 Potential role of the endothelial glycocalyx as a facilitator of neurovascular coupling through nitric oxide production

A final key function of the GCX which links it to AD pathology is its role in preventing neurovascular decoupling. Neurovascular decoupling, characterized by an impaired link between neuronal activity and cerebral blood flow, is a prominent vascular pathology in AD (Zhu et al., 2022). Although the brain accounts for only 2% of the body by weight, it demands 15%–20% of the body's cardiac output, requiring tightly coordinated neurovascular coupling to facilitate its extensive and dynamic nutrient demands (Williams and Leggett, 1989). In AD, there is compelling evidence indicating a notable decrease in essential nutrients reaching the brain and a rise in the accumulation of neurotoxic deposits. This is believed to stem from the vasculature's inability to meet the brain's transport demands, thus decoupling the systems (Hock et al., 1997; Park et al., 2005). Furthermore, studies aimed at recovering neurovascular coupling resulted in improved cognitive function in AD mouse models, suggesting a causal link to the disease (Tong et al., 2012; Tarantini et al., 2017). Based on this evidence, proper blood-brain signaling is essential to preventing later-stage AD.

The GCX is an essential contributor to preventing AD-associated neurovascular decoupling through regulating the mechano-physiology response of blood vessels in the cerebral vasculature. In particular, it plays a critical role in NO production, the key molecule responsible for vasodilation and subsequent neurovascular coupling (Yen et al., 2015; Dormanns et al., 2016). Endothelial NO generation relies on GCX mechanotransduction, which is compromised when the GCX is degraded (Figures 5, 6). When the GCX is intact, HS senses shear stress applied to the vascular wall and stimulates its attached core protein, glypican, to facilitate a wide range of cellular responses essential to NO production including the opening of calcium ion channels and the activation of the PI3K pathway (Tarbell and Pahakis, 2006; Kumagai et al., 2009; Ebong et al., 2014; Zeng et al., 2015). Although syndecans and glypicans bind HS, glypicans have demonstrated greater importance to the NO pathways potentially due to their propensity to reside in the caveolae, small invaginations in the cell membrane which associate



endothelial nitric oxide synthase (eNOS) (Ebong et al., 2014). With this mechanically transduced increase in Ca^{2+} , a calcium-calmodulin complex induces a conformational change to eNOS, while PI3K phosphorylates the enzyme, both processes ultimately facilitating eNOS activation (Figures 5, 6). Activated eNOS produces NO by catalyzing a reaction that converts the amino acid L-arginine and oxygen into L-citrulline and NO. Consequently, vascular tone is regulated through the release of NO, a potent vasodilator, leading to normal neurovascular coupling.

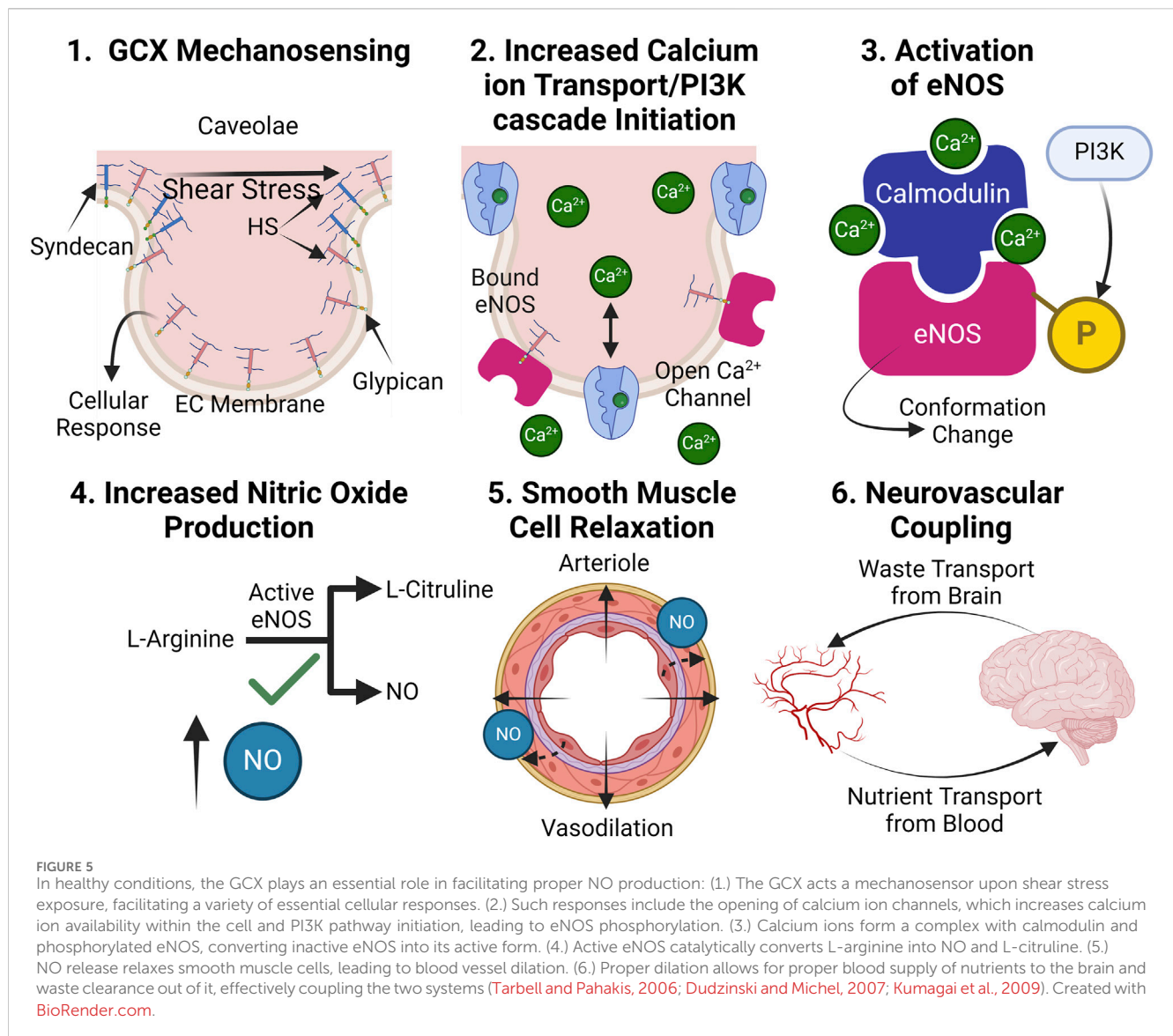
Due to the GCX's involvement in actuating NO production, studies which degrade HS have demonstrated decreased phosphorylated eNOS and subsequent reduced NO production (Ebong et al., 2014; Yen et al., 2015). Subsequent research has utilized atomic force microscopy pulling of key proteoglycans and GAGs of the GCX to identify HS and glypican-1 as being involved in the production of NO, but not syndecan-1, CD44, and HA (Bartosch et al., 2017; Bartosch et al., 2021). These works highlight the GCX's involvement in the pathway as well as the diverse functions of different components in the structure.

Further implicating previously mentioned inflammatory pathologies with NO production, the relationship between ROS, NO, and the GCX also mediates vascular dysfunction. During oxidative stress, ROS like O_2^- interact with NO, forming more precarious species like reactive nitrogen species (RNS) and peroxynitrite (Wang et al., 2018; Schenck et al., 2021). Simultaneously, NO bioavailability is reduced, and the GCX is ameliorated by superoxide dismutase (Rubio-Gayosso et al., 2006). The combination of oxidative stress, reduction in NO, and GCX deterioration creates a vicious cycle of vascular dysfunction, ultimately leading to neurovascular decoupling and the progression of AD symptoms. Future work is needed to clarify mechanisms related to GCX mechanosensing, NO production, and ultimate control of neurovascular coupling in the context of AD. However, with the structure's definitive involvement in the NO pathway, targeted regeneration of the GCX stands as a potential approach for alleviating decoupling-related AD pathology.

3 The endothelial glycocalyx: a link to Alzheimer's disease related vascular pathologies?

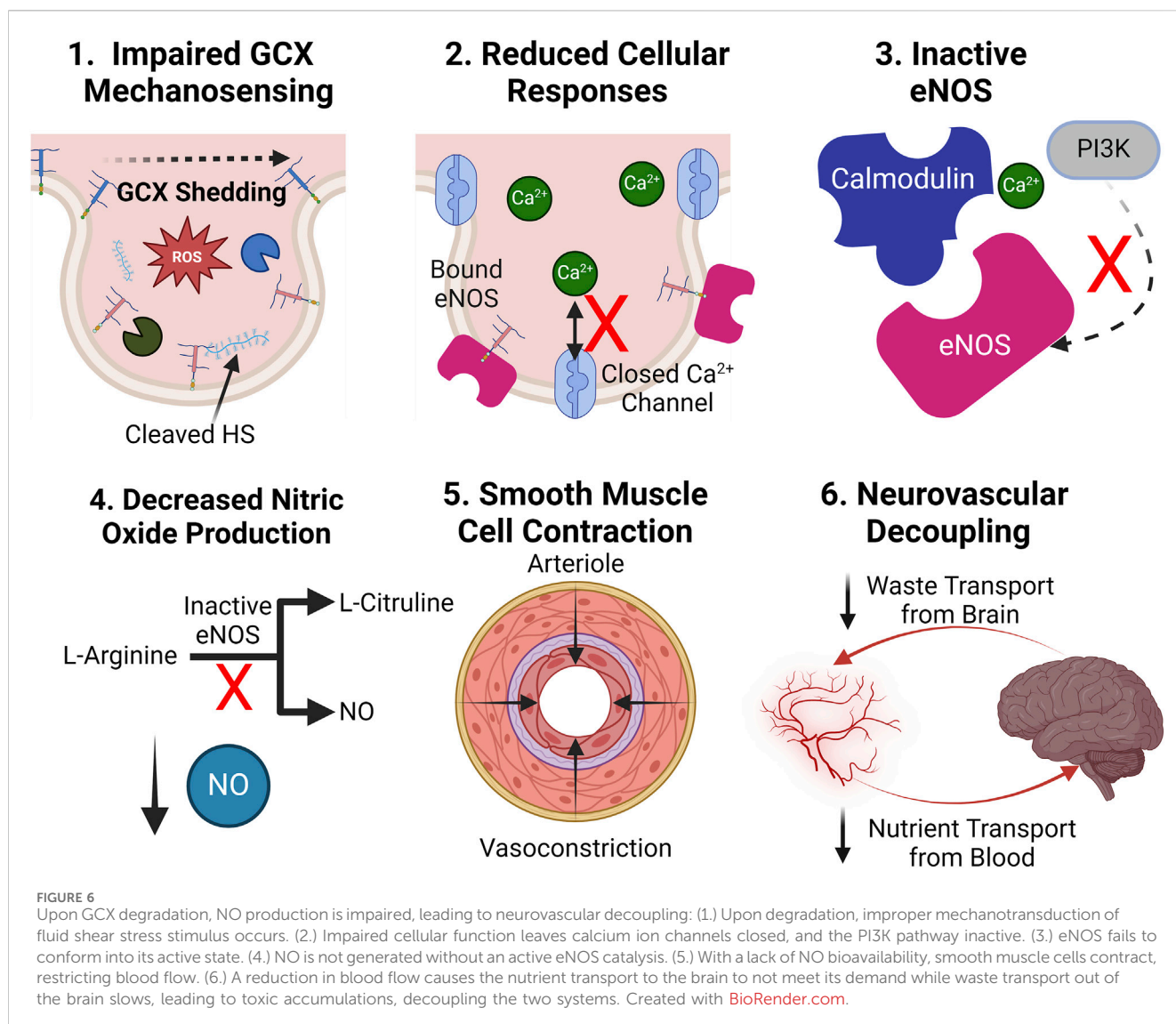
3.1 Evidence of endothelial glycocalyx degradation in Alzheimer's disease and other neurodegenerative diseases

Despite an expanding body of work ascertaining the GCX's role in regulating various vascular functions in AD, the connection between GCX shedding and the progression of AD remains inadequately explored. To establish an argument for the GCX's role in AD, foundational evidence of GCX deterioration must be demonstrated in these conditions. Currently, only a handful of studies directly examine the GCX in AD progression and other neurological disorders. Smyth et al. may have presented the most clinically-relevant evidence for the correlation between GCX shedding and AD (Figure 1). They found reduced vascular density within AD brain tissue compared to healthy controls but normalized this reduction in blood vessels to GCX abundance, further demonstrating that GCX was reduced in brain tissue regardless of the number of vessels. Their findings also elucidated a role of the GCX in deterring neutrophil attachment (Smyth et al., 2022). Others have identified a mechanism of circulating HA and HS proteoglycans in AD neuropathology as well (van Horssen et al., 2001; Reed et al., 2019; Lorente-Gea et al., 2020). Increased levels of heparinase (cleaver of HS) were found in AD brain tissue, providing another conceivable association between GCX shedding and AD progression (Garcia et al., 2017). Loss of HS likely rearranges the BBB, leading to impaired perivascular clearance and subsequent accumulation of A β (Zhang et al., 2021). These published findings provide an indication of GCX involvement in AD, although there is a lack of direct structural measurements of the GCX in AD brain microvasculature as well as mechanistic studies relating GCX loss to AD pathology.



To supplement the few studies that have examined the relationship between GCX function and AD, a growing body of work has demonstrated GCX breakdown in other neurodegenerative disorders with similar vascular pathologies. Therefore, examining the GCX's role in catalyzing a variety of neurodegenerative diseases beyond just AD, could prove widely beneficial. For example, GCX loss has been demonstrated in subcortical vascular dementia, a disease with notably similar vascular components to AD. In an extensive study examining the GCX's role in neurovascular disease, Yoon et al. reported thinning of the GCX along with increased capillary stalling in a vascular dementia animal model (Yoon et al., 2022). Additionally, after enzymatic degradation of the GCX, capillary stalling increased mainly due to leukocyte plugging and an upregulation of endothelial adhesion receptors, suggesting a causal relationship between GCX and vascular dementia pathology (Yoon et al., 2022). Researchers have also investigated the use of GCX components in plasma as an early

biomarker in other neurodegenerative diseases. In a mouse model of multiple sclerosis, HS levels increased before symptom onset, chondroitin sulfate increased prior to symptoms and remained elevated throughout, and HA levels spiked during peak disease severity (DellaValle et al., 2018). Elevated oxidative stress decreased NO levels, and increased glycoprotein deposits in cerebral tissue have also widely been attributed to GCX shedding in neurodegenerative diseases (Pacher et al., 2007; Bonne-Barkay and Wiley, 2009; Siebert et al., 2014). Although an acute event, ischemic stroke events exhibit similar GCX-related neurovascular pathologies. Ischemic stroke victims display loss of the GCX corresponding with increased neuronal and vascular inflammation (Ko et al., 2020). The initial blockage of blood flow and subsequent reperfusion initiates a rise of ROS followed by matrix metalloproteinases (MMPs) and other proteolytic enzymes which then shed the GCX (Yu et al., 2019). There is substantial evidence of increased levels of shed GCX



components like HS and syndecan in the plasma of stroke victims (Rehm et al., 2007; DellaValle et al., 2019). The deteriorated extracellular GCX structure allows for direct interaction between immune cells and the endothelium, eventually exacerbating neurological impairment (Mockl, 2020; Bettcher et al., 2021a; Bettcher et al., 2021b; Liu et al., 2023). Another acute event that occurs upstream of neurodegenerative diseases, traumatic brain injury, is also known to induce a GCX-related neuropathological cascade (Gonzalez Rodriguez et al., 2018; Zou et al., 2021; Anand et al., 2023). Increased shedding of GCX components after traumatic brain injury is associated with a negative survival rate, implicating the GCX's role in pathology. After injury, an upregulation of ROS, immune cell adhesion, and sheddases results in BBB hyperpermeability, neuroinflammation, and leukocyte attachment (Zou et al., 2021).

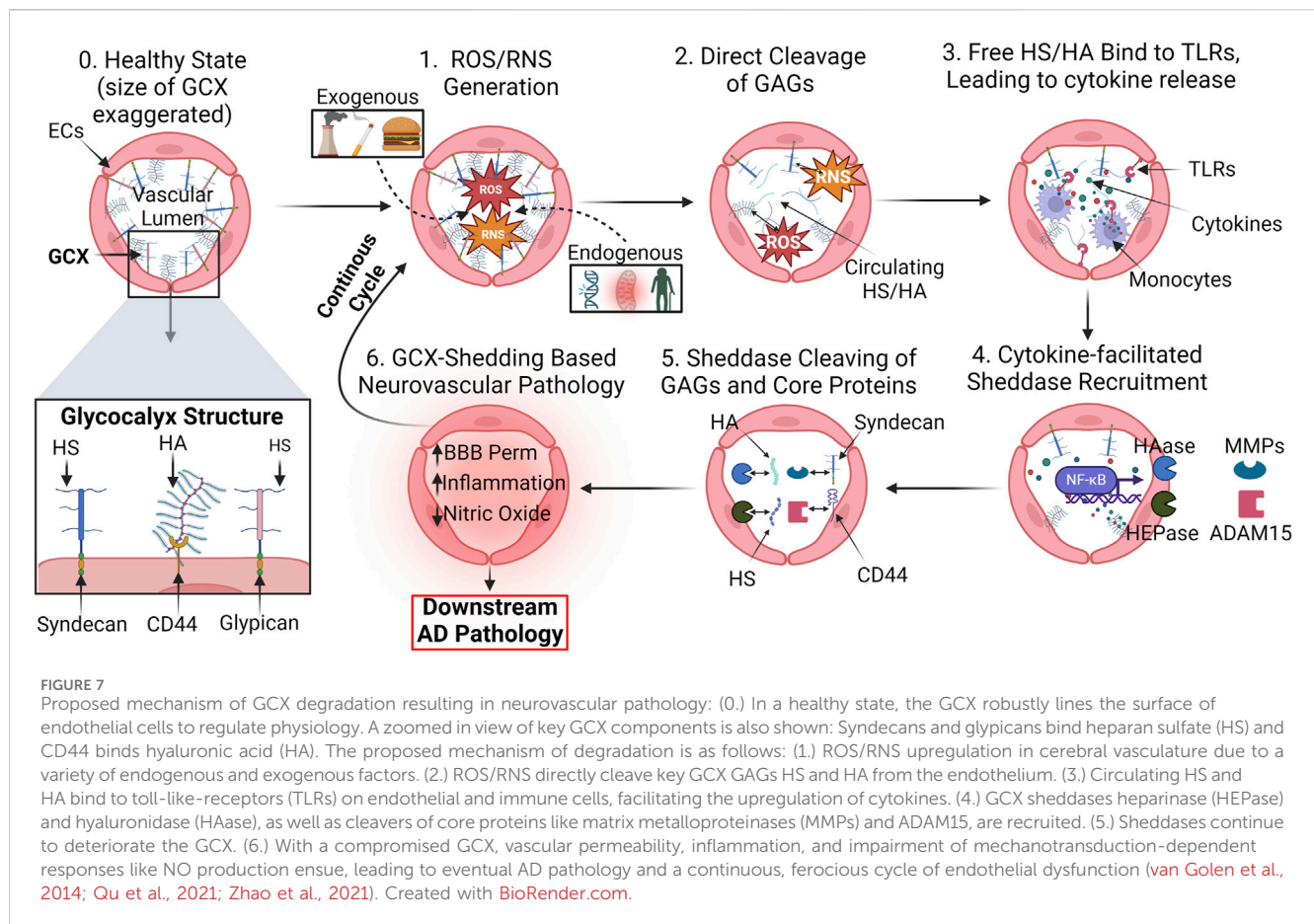
Lastly, the process of aging is worthy of mention due to age being the number one risk factor for the majority of neurodegenerative diseases (Hou et al., 2019) and known to be associated with a diminished GCX (Machin et al., 2018; Majerczak et al., 2019).

Machin et al. proposed the hypothesis that age-related GCX shedding precedes vascular dysfunction, ultimately promoting a variety of cardiovascular and neurological disease pathologies (Machin et al., 2019).

In summary, it is still emerging whether GCX shedding precedes AD and other neurological disorders characterized by vascular abnormalities. The early evidence described here indicates a correlation between GCX integrity and disease severity.

3.2 Proposed mechanism of endothelial glycocalyx shedding in Alzheimer's disease

The means by which the GCX is shed during AD pathology remains a topic of intense investigation. In physiology, GCX homeostasis is meticulously maintained through a dynamic interplay of synthesis, protection, and shear stress sensing mechanisms. Endothelial cells continually synthesize and assemble GCX components, while physiological levels of shear



stress from blood flow reinforce its structure and stimulate GAG synthesis pathways (Alphonsus and Rodseth, 2014; Banerjee et al., 2021). Endogenous factors like NO, prostacyclin, and angiotensin-1 interact with the GCX to regulate vascular tone, permeability, and stability (Becker et al., 2010; Potje et al., 2020; Qiu et al., 2022). Additionally, antioxidants such as superoxide dismutase help counteract oxidative stress-induced GCX damage, ensuring its integrity and proper function (Beresewicz et al., 1998). However, in pathology, numerous mediators, often interrelated, facilitate GCX degradation, directing a persistent cycle of endothelial dysfunction. These mediators include, but are not limited to ROS/RNS, inflammatory cytokines, sheddases, and MMPs (Masola et al., 2021; Zhao et al., 2021). Thus, understanding the mechanisms underlying the GCX dysregulation cycle is crucial for developing targeted therapeutic interventions to preserve vascular health and potentially prevent downstream neurological dysfunction (Figure 7).

ROS and RNS play a role in direct cleavage of GAGs, as well as the recruitment of other harmful compounds. Three principal reactive species that directly sever HA and HS GAG chains from core protein binding sites include hydroxyl radicals ($\bullet\text{OH}$), carbonate radical anions ($\text{CO}_3^{\bullet-}$), and hypochlorous acid (HOCl) (van Golen et al., 2014). Generation of these reactive species stems from multiple sources but one of the most pertinent endogenous routes involves their secretion by immune cells and the destabilization of the synthase that produces counteractive NO (Alderton et al., 2001; Forman and Torres, 2002). Other sources of ROS/RNS production may stem from the weakening

of free radical neutralizing systems due to aging, as well as environmental factors such as a high-fat diet, air pollution, and smoking (Pérez et al., 2009; Di Meo et al., 2016). ROS/RNS production sets off a cascade of vascular pathologies, among which cleavage of the GCX is a notable factor.

Upon initial cleavage of the HA and HS GCX chains, a cyclic inflammatory cascade promotes further GCX shedding (Figure 7). Circulating HS and low molecular weight HA bind to toll-like receptors on the surface of macrophages and endothelial cells, facilitating the release of inflammatory cytokines such as tumor necrosis factor- α (TNF- α), interleukin-1 β (IL-1 β), and IL-8 (Johnson et al., 2002; Taylor et al., 2004; Scheibner et al., 2006; Qu et al., 2021). In conjunction with ROS/RNS, cytokines recruit a variety of sheddases to the endothelial cell surface including MMPs, hyaluronidase, and heparinase (Dempsey et al., 2000; Monzon et al., 2010; Ramnath et al., 2014). These enzymes not only have the capacity to further shed GAGs but also threaten GAG-anchoring core proteins in the transmembrane domain of the cell. For example, MMP1, MMP9, and MMP14 remove the HS proteoglycan core proteins syndecan-1 and syndecan-4, respectively, while MMP9 also cleaves chondroitin sulfate (Endo et al., 2003; Sieve et al., 2018). A disintegrin and metalloproteinase 15 (ADAM15) is responsible for the scission of CD44, the core protein responsible for HA binding to the endothelial cell surface (Yang et al., 2018). Additionally, heparinases and hyaluronidases continuously remove HS and HA, further complicating GCX recovery attempts by the cell.

Understanding how the GCX degradation cascade is initiated and translating the knowledge to the development of potential avenues for reversal of GCX degradation could prove critical to the amelioration of a plethora of vascular-related cognitive diseases, including AD. Several mediators of GCX dysfunction are found at elevated levels in patients suffering from AD. Excessive generation of GCX cleavers ROS and RNS has been linked to the pathogenesis of AD, as well as variety of age-related neurodegenerative diseases (Manoharan et al., 2016). Notably, elevated levels of ROS production are found to precede late-stage AD events like A β deposits and NFTs, further supporting the notion that vascular dysfunction propagates late-stage AD events (Ahmad et al., 2017). Furthermore, postmortem AD brain tissues show an increase in cytokines IL-1 β and IL-6 (Griffin et al., 1989; Hull et al., 1996; Zheng et al., 2016), which suggests both the presence of excess circulating GCX components as well as increased immune cell infiltration and systemic inflammation processes occurring throughout disease progression. MMP-9 was also found at significantly elevated levels in the plasma of AD patients compared to controls (Lorenzl et al., 2003). Although the abovementioned mediators of GCX shedding serve diverse functions, establishing their involvement in the pathophysiology of AD supports the hypothesis of GCX-dependent contributions to the diseases.

4 Current challenges

4.1 Imaging and quantifying cerebrovascular glycofocalyx and cerebral vascular changes

To investigate the potential role of GCX integrity in neurodegenerative disease progression, it is crucial to improve both *in vitro* and *in vivo* imaging techniques of the cerebrovascular GCX. Currently, the quantification of GCX components such as HS, HA, and syndecan-1 in plasma is the primary method of assessing GCX shedding. However, additional, more direct approaches should be considered to evaluate the cerebrovascular GCX structure in preclinical, clinical, and postmortem AD tissue.

Transmission electron microscopy (TEM) is a principal technique for imaging the GCX in fixed, preserved conditions. However, one of the main challenges in TEM is preserving the sample in a way that accurately reflects the GCX ultrastructure (Haeren et al., 2016). Traditional preparation processes typically involve dehydration of the sample, causing the GCX to collapse in on itself and drastically altering its organization and thickness (Hempel et al., 2020). To address this issue, rapid freezing/freeze substitution (RF/FS) has emerged as a promising technique for sample preparation. Ebong et al. demonstrated that using RF/FS, the GCX of bovine aortic endothelial cells measured an average of 11 μ m, compared to an insubstantial 0.040 μ m using traditional TEM (Ebong et al., 2011). Despite the promise of RF/FS in accurately preserving the GCX, it remains a labor-intensive, delicate process that is unable to image specific GCX components.

To address the limitations of traditional TEM, confocal laser scanning microscopy (CLSM) is a promising method that can fluorescently label specific GCX components. While the characterization of GCX GAGs remains a challenge due to their

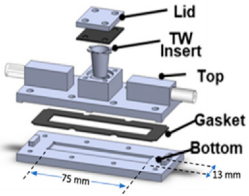
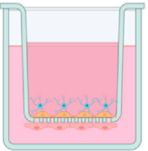

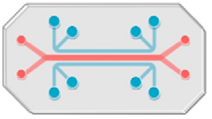
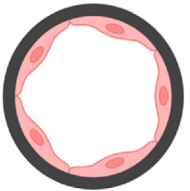
high degree of heterogeneity and lack of antigenicity, innovative antibodies and lectins (such as wheat germ agglutinin) can be utilized to tag domains of GAG components of the GCX, for fluorescent labeling and subsequent CLSM visualization (Mockl, 2020). By combining RF/FS with immunolabeling-based CLSM, Twamley et al. were able to analyze the morphology of specific GCX components (Twamley et al., 2021), advancing the state-of-the-art in labeling and quantification of the GCX.

Despite the recent advances of *in vitro* techniques, development of unique solutions to microscopic imaging of the cerebrovascular GCX *in vivo* in functional tissue remains essential for elucidating the nature and function of the structure in the body. Two-photon light scanning microscopy (TPLSM) utilizes dual-photon absorption to increase penetration depth and allow for fluorescent imaging of living tissue (Denk et al., 1990). By contrasting fluorescent dextran in the lumen with wheat germ agglutinin-tagged GCX, TPLSM has been used to assess GCX thickness, BBB permeability, and vascular geometry (Yoon et al., 2017; Kucharz et al., 2022). Results indicate that the use of *in vivo* TPLSM leads to a more robust GCX than what is observed *ex vivo* and offers a functional approach to assessing GCX thickness, BBB permeability, and vascular geometry. However, this imaging technique will likely be limited to pre-clinical animal studies for cerebrovascular GCX imaging due to its invasiveness, high cost, slow imaging speed, and the need for fluorescent contrast agents.

Another option for *in vivo* assessment of the GCX that demonstrates more clinical potential is side-stream dark field imaging (SDF). SDF measures the degree of penetration of red blood cells into the GCX through a reflected LED light. Based on the extent of penetration, computer programs like Glycocheck can correlate the perfused boundary region (the permeable part of the GCX) to a GCX thickness (Iba and Levy, 2019). A recent protocol developed by Haeren et al. was the first to utilize SDF of the cerebrovascular GCX in a clinical setting. Based on the study, SDF could effectively quantify GCX thickness in the cerebral vasculature, was straightforward to operate, and safe for the use on human patients (Haeren et al., 2018). SDF and Glycocheck offer the advantage of intraoperative measurement of GCX thickness without the need for fluorescent dyes, long processing times, and image acquisition expertise (Haeren et al., 2017; Berhouma et al., 2020). However, SDF and Glycocheck still pose several drawbacks due to indirect GCX measurement and may be affected by motion-induced blurring. With the applicability of SDF and Glycocheck, an increasing amount of data on cerebrovascular GCX integrity in neurodegenerative disease is expected to emerge in the coming years, offering valuable insights for tailored pre-clinical and clinical applications.

Finally, due to the substantial difficulties of directly quantifying the GCX *in vivo*, novel, translational imaging modalities which can broadly quantify vascular changes will be instrumental in elucidating the causal role, if any, of GCX impairment on AD progression during longitudinal studies. Some studies have utilized dynamic contrast-enhanced magnetic resonance imaging (DCE MRI) to investigate BBB leakage in early AD (Figure 1) (van de Haar et al., 2016; Moon et al., 2023). However, DCE MRI has limitations in studying BBB permeability primarily due to its inability to distinguish between blood flow and permeability changes accurately (Manning et al., 2021). To overcome this, a

TABLE 1 Choosing the Right BBB Model: Key Considerations and Comparative Analysis: This table offers a thorough evaluation of recent BBB models, examining each model against five pivotal factors essential for achieving physiological relevance as well as experimental feasibility. "Ease of fabrication" assesses the simplicity and technical expertise required for model construction. Consideration is given to the length of cell culture required for each model, impacting experimental throughput as well. "Physiological Flow" evaluates the model's ability to simulate hemodynamic flow conditions experienced by cerebral blood vessels. "Physiological geometry" examines how closely the model's structure resembles the innate architecture of the neurovasculature. "Post-experimental Analysis" assesses the ease and effectiveness of conducting post-experimental biological assays including barrier functionality, protein quantification, and fluorescent microscopy. "Model Versatility" is determined by the model's capability to adapt to different mechanical environments, culture conditions, and experimental factors, enabling diverse applications. Based on this assessment, a millifluidic, transwell-compatible model shows promise for future *in vitro* studies exploring the role of the GCX in AD.

Model type	Graphical representation	Ease of fabrication	Physiological flow	Physiological geometry	Post-experimental analysis	Versatility	Ref
Millifluidic Transwell (Ebong Model)		✓	✓		✓	✓	Harding et al. (2022)
Transwell		✓			✓		Ito et al. (2019), Li et al. (2019)
Organoid		?		✓	✓		Cho et al. (2017b), Berhouma et al. (2020)
Organ-on-a-Chip			✓		✓	✓	Brown et al. (2015), Boghdeh et al. (2022)
3D Vessel			✓	✓	?	?	Marino et al. (2021), Yan et al. (2023)

promising approach is to utilize quantitative ultra-short time-to-echo contrast-enhanced magnetic resonance imaging (QUTE-CE MRI) to holistically quantify BBB permeability changes over time more accurately. QUTE-CE MRI offers a safe, accurate, and non-invasive method of quantifying BBB leakage making it an ideal *in vivo* quantitative method for longitudinal studies (Gharagouzloo et al., 2015; Leaston et al., 2021a; Leaston et al., 2021b). Furthermore, QUTE-CE MRI's precise quantification of BBB changes facilitates targeted investigation into key regions affected in AD—like the hippocampus, thalamus, amygdala, and cerebral cortex, while still encompassing the entire brain in the study (Kapasi and Schneider, 2016; Nelson et al., 2016). Compared with traditional MRI, QUTE-CE MRI allows for more precise measurement of BBB permeability due to its ability to capture ultra-short echo times, which are sensitive to subtle changes in tissue microstructure and permeability. This enables researchers and clinicians to obtain more accurate and reliable data on BBB integrity, facilitating the possibility of prolonged longitudinal studies on a key read out for

neurovascular health. With the continued development of these revolutionary imaging methods, unprecedented insight into GCX integrity, dynamics of BBB permeability, and overall cerebral vascular health are positioned to be elucidated, heralding a transformative era in vascular and AD research.

4.2 In Vitro modeling of the BBB

Another substantial challenge with elucidating the GCX's role in AD involves the development of suitable *in vitro* models of the BBB. Access to preclinical and clinical *in vivo* settings that incorporate the complex nature of the BBB is limited. Therefore, the development of accurate yet high throughput *in vitro* models of the BBB structure remain indispensable to the field for their reproducibility, cost-effectiveness, and accessibility. *In vitro* BBB models which can accurately reproduce the interplay between the GCX, barrier function, and pathophysiology are critical to examining the

GCX-vascular hypothesis of AD. Despite significant research in this area, recent models vary widely in their fabrication methods, flow conditions, model geometry, applicability, and versatility (Table 1). Developing an *in vitro* system which balances these parameters to fit the experimental goals continues to be a priority.

Today, the field largely agrees that the primitive *in vitro* BBB model consisting of a static, brain microvascular endothelial cell monolayer cultured in a transwell insert falls short of the needed complexity to be considered a viable candidate to study GCX-BBB-AD interactions (Table 1). A primary shortcoming of this model is the lack of physiological shear stress the cells are subjected to. Hemodynamic flow conditions are increasingly recognized as essential for capturing the intricate microenvironment of the NVU *in vitro*, as endothelial cells respond dynamically to shear stress (Williams-Medina et al., 2020). Under shear stress, brain endothelial cell phenotype alterations occur, with flow models demonstrating decreased BBB permeability compared to static cultures (Santaguida et al., 2006; Cucullo et al., 2011). In specific relation to the GCX, thickness of the structure in flow conditions has been reported to increase 70%–80% compared to static conditions and approach thicknesses observed *in vivo* (Ueda et al., 2004; Tsvirkun et al., 2017; Harding et al., 2019b). Selecting a model which generates a robust GCX is essential for future studies aimed at investigating the GCX role in deterring AD pathology.

Similar to the importance of flow conditions, *in vitro* BBB models which can incorporate many cell types to recreate the complex multicellular interface are essential to accurately studying AD pathogenesis. Different cells, including primary human endothelial cells, induced pluripotent stem cell-derived (iPSC) endothelial cells, animal-derived endothelial cells, and immortalized endothelial cells, mimic the cellular lining of the brain vascular lumen (He et al., 2014; Destefano et al., 2018). Adding another layer of complexity, supportive cells such as astrocytes, pericytes, microglia, and neurons are also often incorporated and deemed essential to achieving a functional BBB model, depending on the purpose (Daneman and Prat, 2015). These diverse cell types enable the study of neurovascular function in healthy conditions, neurovascular function in neuroinflammatory and neurodegenerative conditions, therapeutic targets, and drug transport across the BBB, but it is still unclear the exact importance of them to a functional model.

In terms of fabricating a model which captures the innate geometric properties of the BBB, several innovative fabrication methods are being investigated (Table 1). Certain microfluidic systems utilize channel culturing techniques to replicate 3D blood vessels and allow for physiological flow and cell-cell interactions, providing increased physiological relevance (Bonakdar et al., 2017; Hajal et al., 2022). However, these systems can be technically complex to fabricate and operate, requiring specialized expertise and equipment. Scaffold-based approaches create three-dimensional frameworks using porous membranes or hydrogels, promoting cell-cell interactions and barrier formation but may lack the ability to precisely control spatial organization and have limited scalability (Marino et al., 2021). Novel 3D organoid models enable *in vivo* like formations of complex BBB structures (Cho CF. et al., 2017; Bergmann et al., 2018; van Dyck et al., 2023). However, organoid culturing techniques are still under development, and challenges remain in

achieving reproducibility, scalability, and mechanically accurate microenvironments. The preferred option for fabrication method often depends on research expertise, experimental design, and throughput considerations.

With the goal of taking all of these factors into consideration, our lab has developed a custom-made millifluidic device that is compatible with standard transwell inserts to develop a physiologically relevant study while maintaining high throughput for analysis of the role of the GCX in AD (Table 1) (Harding et al., 2022). This design combines standard transwell inserts with a microfluidic device featuring validated shear stress profiles. It also incorporates primary human brain endothelial cells, pericytes, and astrocytes, enhancing fidelity for studying BBB dynamics and neurological consequences of GCX impairment. The advantages of this model include its straightforward and reusable fabrication via 3D printing and insertion of transwell inserts, physiological flow rate, robust post-experimental analysis, and versatility with the ability to culture different cell types and flow rate changes. Although there are more physiological fabrication approaches which achieve 3D geometries and direct cell-cell contact, this transwell system is comparable to previous studies (Table 1). Initial studies demonstrate that GCX thickness and tight junction expression increase in tri-cultures containing endothelial cells, astrocytes, and pericytes. Furthermore, exposure to 12 dyne/cm² of shear stress increased GCX coverage, potentially supporting the lower observed permeability in flow conditions (Harding et al., 2022). This model is well suited for balancing the needed physiological relevance with ease of use required to study the GCX's role in AD.

4.3 Experimental methods of studying GCX-related Alzheimer's disease pathology

Due to the GCX's heterogeneity and complex functionality to the NVU, devising experimental strategies to study the relationship between GCX degradation and vascular-related AD pathology is a critical consideration. Traditionally, the GCX is degraded through enzymatic cleavage of its GAGs (McDonald et al., 2016; Yalcin et al., 2018). Although this technique may be sufficient for other vascular-organ interfaces, the multicellular, dynamic nature of the BBB may lead to the enzymes having several off-target effects on brain cell function, resulting in questions of causation during downstream biological analysis (Yang et al., 2021; Zhang et al., 2021).

For this reason, recent gene editing advancements offer practical means to investigate the GCX's role in AD-vascular pathology (Reitsma et al., 2007). Techniques like CRISPR/Cas9, shRNA, and siRNA effectively knockdown or knockout GCX core protein expression, facilitating the study of their functional significance (Song and Yang, 2010; Abrahimi et al., 2015). By employing these techniques *in vitro* and *in vivo*, researchers can investigate the functional consequences of depleting GCX core protein expression on cellular processes i.e., barrier integrity, inflammation control, and responsiveness to the extracellular environment. While effective *in vitro*, utilizing *in vivo* knockout models which broadly target GCX core proteins presents challenges due to their expression in cell types beyond

endothelial cells, increasing the risk of off-target effects (Couchman and Pataki, 2012). To address this issue, efforts should be directed towards generating conditional transgenic animal models with endothelial cell-specific GCX core protein knockouts (Liao et al., 2001; Fahs et al., 2014). These genomic editing approaches would contribute to a deeper understanding of the roles played by GCX core proteins in disease processes, including neurodegenerative disorders like AD.

The impact of GCX-specific knockout mice will be powerful when combined with the *in vivo* imaging techniques described in Section 4.1. For example, *in vivo* imaging techniques such as TPLSM offer the potential to track the neurovasculature and GCX over time with greater depth and precision compared to traditional techniques (Haeren et al., 2016; Kilic et al., 2020). Additionally, the use of QUTE-CE MRI provides a promising method to track neurovascular abnormalities, BBB permeability, cerebral blood flow, and neuroinflammation over the course of disease progression in a non-invasive, clinically-relevant way (Leaston et al., 2021a). Finally, post-mortem-tissue analysis utilizing RF/FS preservation techniques can visualize GCX thickness and coverage in a manner previously unobtainable with traditional preservatives. Given the relatively recent appreciation for GCX involvement in neurodegenerative disease and the development of these ground-breaking imaging modalities, the foundation is set to firmly establish a prospective relationship between GCX degradation and downstream AD pathology.

A legitimate concern with evaluating the direct relationship between GCX impairment and AD progression *in vitro* and *in vivo* is modelling complex disease in a relevant way. To generate AD-like pathology both *in vitro* and *in vivo*, researchers may employ various techniques to mimic key aspects of the disease. *In vitro*, AD-like pathology can be induced in cultured cells or blood-brain organoids by exposing them to A β peptides, tau protein aggregates, or neuroinflammatory cytokines (Sharma et al., 2021; Schreiner et al., 2022). This can lead to the formation of A β plaques, tau hyperphosphorylation, synaptic dysfunction, and neuronal cell death, resembling key features of AD pathology (Chen et al., 2021). *In vivo*, there are several commercially available transgenic rodent models of AD but are a constant subject of debate, primarily because of the disease's complex etiology and the fact that rodents cannot naturally develop it (Yokoyama et al., 2022). Some commonly deployed models for studying AD which are well-characterized for inducing neuropathological features and cognitive deficits characteristic of the disease include the mutant amyloid precursor protein and presenilin 1 (APP/PS1), Tg2576, and 5xFAD lines (Gotz et al., 2018; Sanchez-Varo et al., 2022). A major advantage of these AD models is abnormal protein folding in the brain, appreciable vascular changes, and cognitive deficits witnessed and progressing between 6 and 12 months of age in most models, setting a feasible time scale for longitudinal studies of AD (Webster et al., 2014). However, one of the persistent shortcomings of these transgenic models is their neuro-centric focus and failure to exhibit likely vascular changes present in AD. However, inducing impairment of the GCX in these models and subsequently longitudinally examining the animals for variations in cognitive function would be valuable in establishing the GCX's role as a contributor to the propagation of AD. This would be

particularly significant if AD models with GCX deficiency were to exhibit exacerbated symptoms.

Moreover, beyond studying AD models, exploring the role of the GCX in AD also involves considering the aging aspect, the number one risk factor of the disease. Aged cells and rodent models provide valuable insights into the dynamic changes occurring within the GCX as the brain matures, shedding light on its relevance to AD pathology. Aged cells exhibit physiological changes and molecular alterations that mimic aspects of aging-related neurodegeneration observed in AD while also paralleling the believed thinning of the GCX with age (Ting et al., 2021; Sun et al., 2023). *In vitro*, cell lines derived from aged individuals can be used to model age-related changes in cellular function and susceptibility to AD pathology. These cells may exhibit increased oxidative stress, protein misfolding, mitochondrial dysfunction, and altered signaling pathways associated with aging and neurodegeneration (Chen et al., 2020). Likewise, investigating aged rodents *in vivo* provides insight into the effects of aging on disease progression and its potential correlation with GCX loss. Such research, considering traditional AD amyloid-based pathology, age, and GCX alterations, not only explores the potential impact of GCX loss as a major contributing factor but also potentially informs the development of novel therapeutic interventions for AD.

To address whether GCX loss exacerbates AD pathology, specific techniques can be employed. *In vitro*, GCX loss can be induced in endothelial cells as described above, followed by exposure to AD-related stimuli. *In vivo*, genetic manipulation or pharmacological approaches targeting GCX components can be combined with AD-inducing interventions in transgenic mouse models. By assessing changes in BBB integrity, A β clearance, neuroinflammation, and cognitive function, researchers can elucidate the role of GCX loss in worsening AD pathology and identify potential therapeutic targets for intervention.

5 Future work and conclusion

Neurodegenerative diseases such as AD are among the most urgent public health concerns of the 21st century, with the demand for effective therapies expected to increase alongside the aging population. Given the complex etiology of AD involving both neurological and vascular components, it is essential to advance research on the understanding of the interplay of both systems. Targeting the vascular endothelial GCX emerges as a promising avenue, offering the potential to prolong or restore critical neurovascular functions impaired in AD. Despite the ongoing uncertainty regarding whether GCX degradation precedes vascular insult and AD pathology, recent advancements in evaluating the GCX in the cerebral vasculature open doors for future work to definitively determine its viability as a therapeutic target for neurodegenerative diseases.

After conducting an extensive literature review and considering experimental feasibility, the initial approach to determining whether the GCX could serve as a viable therapeutic target for delaying, mitigating, or preventing AD symptoms involves thoroughly assessing the functionality of the GCX in relation to countering

AD-related neurovascular pathologies in both *in vitro* and *in vivo* settings.

Tangible methods of accomplishing this task *in vitro* include: 1. Utilize a physiologically relevant, reliable, high degree of post-experimental analysis BBB model such as the one described by our group in a previous publication (Harding et al., 2022). 2. Use a highly transfectable shRNA knockdown technique to reduce the expression of individual GCX core proteins selectively and stably such as CD44, syndecan-1, and glypican-1 in brain microvascular endothelial cells. 3. Assess the effects of these GCX core protein knockdowns on NVU functionality using techniques such as dextran permeability assays, trans-endothelial electric resistance, and cell-cell communication. Additionally, analyzing the protein and gene expression of markers associated with AD-related neurovascular pathology to uncover potential mechanistic insights, including tight junctions, intracellular transporters, adhesion molecules, cytokines, and NO production mediators. This approach aims to elucidate the role of individual GCX components in maintaining physiological function.

In vivo methods of examining the role of the GCX in AD should aim to corroborate *in vitro* findings while further capturing complexities unobtainable through solely cell-based observations such as: 1. Examine distinctions among healthy mice, CD44 knockout models (Due to this knockout model's commercial availability and minimal off-target effects), and amyloid-based AD models like APP/PS1, to understand the ramifications of GCX impairment in contrast to the traditional neurocentric manifestation of AD, particularly concerning AD-related neurovascular dysfunction (Protin et al., 1999; McKallip et al., 2002). 2. Longitudinally interrogate changes in BBB permeability using translationally relevant QUTE-CE MRI until reaching an appropriate advanced age, to consider the compounded effect of aging in relation to GCX impairment and AD progression. 3. Perform immunological analysis on brain sections and plasma samples, comparing baseline samples to those obtained after aging in the three groups, and probing for similar markers as in the *in vitro* study. These findings will explore whether the knockout of a crucial GCX core protein, CD44, triggers BBB dysfunction, while also distinguishing the effects of BBB damage stemming from abnormal protein folding linked to AD.

If the data from an initial study were to show promise, further investigations could be pursued on determining the GCX's relevance in AD, involving more labor, cost, and time-intensive approaches as those highlighted in Section 4.3. If evidence were to mount indicating the significant involvement of the GCX in AD pathology, it becomes imperative to explore novel GCX-regenerating therapeutics in these models, assessing their potential to ameliorate the severe pathological symptoms of the disease (Banerjee et al., 2021). While significant efforts are still required to ascertain the role, if any, of this vascular-based structure in protecting against AD, recent advancements in biotechnology have undoubtedly opened the door to feasibly address this question like never before. As we continue to navigate the complexities of AD and the potential of a substantial vascular role, the pursuit of a deeper understanding of the GCX's relationship to the disease stands as a critical step toward effective treatments and improved public health outcomes.

Author contributions

NO'H: Conceptualization, Funding acquisition, Writing–review and editing, Data curation, Formal Analysis, Investigation, Visualization, Writing–original draft. KM: Investigation, Visualization, Writing–original draft, Writing–review and editing, Data curation, Formal Analysis. EEE: Conceptualization, Investigation, Writing–review and editing, Data curation, Funding acquisition, Project administration, Resources, Supervision.

Funding

The author(s) declare that financial support was received for the research, authorship, and/or publication of this article. This work was also funded by the National Science Foundation Graduate Research Fellowship, DGE-1938052 (to NO'H), to support PhD dissertation research focused on studying the role of the mechanically regulated endothelial glycocalyx in blood-brain barrier function and Alzheimer's Disease. We acknowledge that this work was also funded by the National Science Foundation CAREER Award, CMMI-1846962 (to EEE), to support endothelial mechanobiology research and education.

Acknowledgments

We would like to thank faculty in the chemical engineering, bioengineering, and psychology department at Northeastern University for providing invaluable input on certain aspects of this review including Dr. Abbas Yaseen, Dr. Craig Ferris, Dr. Ryan Koppes, and Dr. Guohao Dai. We acknowledge support from Kate Kryder, who is a Data Analysis & Visualization Specialist in the Northeastern University Library. Additionally, we would like to thank current and past members of the Ebong lab group for contributing with the conceptualization, focus, and editing of this review including Ian Harding, Mark Vigliotti, Ronodeep Mitra, Mohammad Hamrangsekachae, Chinedu Okorafor, and Kaleigh Pentland.

Conflict of interest

The authors declare that the research was conducted in the absence of any commercial or financial relationships that could be construed as a potential conflict of interest.

Publisher's note

All claims expressed in this article are solely those of the authors and do not necessarily represent those of their affiliated organizations, or those of the publisher, the editors and the reviewers. Any product that may be evaluated in this article, or claim that may be made by its manufacturer, is not guaranteed or endorsed by the publisher.

References

- Abrahimi, P., Chang, W. G., Kluger, M. S., Qyang, Y., Tellides, G., Saltzman, W. M., et al. (2015). Efficient gene disruption in cultured primary human endothelial cells by CRISPR/Cas9. *Circ. Res.* 117 (2), 121–128. doi:10.1161/CIRCRESAHA.117.306290
- Ahmad, W., Ijaz, B., Shabbiri, K., Ahmed, F., and Rehman, S. (2017). Oxidative toxicity in diabetes and Alzheimer's disease: mechanisms behind ROS/RNS generation. *J. Biomed. Sci.* 24 (1), 76. doi:10.1186/s12929-017-0379-z
- Al-Ahmad, A. J., Patel, R., Palecek, S. P., and Shusta, E. V. (2019). Hyaluronan impairs the barrier integrity of brain microvascular endothelial cells through a CD44-dependent pathway. *J. Cereb. Blood Flow. Metab.* 39 (9), 1759–1775. doi:10.1177/0271678X18767748
- Alderton, W. K., Cooper, C. E., and Knowles, R. G. (2001). Nitric oxide synthases: structure, function and inhibition. *Biochem. J.* 357 (Pt 3), 593–615. doi:10.1042/0264-6021:3570593
- Alphonsus, C. S., and Rodseth, R. N. (2014). The endothelial glycocalyx: a review of the vascular barrier. *Anaesthesia* 69 (7), 777–784. doi:10.1111/anae.12661
- Alzheimer's disease facts and figures (2021). Alzheimer's disease facts and figures. *Alzheimer's Dementia* 17 (3), 327–406. doi:10.1002/alz.12328
- Anand, T., Reyes, A. A., Sjoquist, M. C., Magnotti, L., and Joseph, B. (2023). Resuscitating the endothelial glycocalyx in trauma and hemorrhagic shock. *Ann. Surg. Open* 4 (3), e298. doi:10.1097/AS9.0000000000000298
- Banerjee, S., Mwangi, J. G., Stanley, T. K., Mitra, R., and Ebong, E. E. (2021). Regeneration and assessment of the endothelial glycocalyx to address cardiovascular disease. *Industrial Eng. Chem. Res.* 60 (48), 17328–17347. doi:10.1021/acs.iecr.1c03074
- Bartosch, A. M. W., Mathews, R., Mahmoud, M. M., Cancel, L. M., Haq, Z. S., and Tarbell, J. M. (2021). Heparan sulfate proteoglycan glypican-1 and PECAM-1 cooperate in shear-induced endothelial nitric oxide production. *Sci. Rep.* 11 (1), 11386. doi:10.1038/s41598-021-90941-w
- Bartosch, A. M. W., Mathews, R., and Tarbell, J. M. (2017). Endothelial glycocalyx-mediated nitric oxide production in response to selective AFM pulling. *Biophys. J.* 113 (1), 101–108. doi:10.1016/j.bpj.2017.05.033
- Becker, B. F., Chappell, D., Bruegger, D., Annecke, T., and Jacob, M. (2010). Therapeutic strategies targeting the endothelial glycocalyx: acute deficits, but great potential. *Cardiovasc. Res.* 87 (2), 300–310. doi:10.1093/cvr/cvq137
- Beresewicz, A., Czarnowska, E., and Maczewski, M. (1998). Ischemic preconditioning and superoxide dismutase protect against endothelial dysfunction and endothelium glycocalyx disruption in the posts ischemic Guinea-pig hearts. *Mol. Cell. Biochem.* 186 (1–2), 87–97. doi:10.1007/978-1-4615-4979-6_11
- Bergmann, S., Lawler, S. E., Qu, Y., Faden, C. M., Wolfe, J. M., Regan, M. S., et al. (2018). Blood-brain-barrier organoids for investigating the permeability of CNS therapeutics. *Nat. Protoc.* 13 (12), 2827–2843. doi:10.1038/s41596-018-0066-x
- Berhouma, M., Picart, T., Dumot, C., Pelissou-Guyotat, I., Meyronet, D., Ducray, F., et al. (2020). Alterations of cerebral microcirculation in peritumoral edema: feasibility of *in vivo* sidestream dark-field imaging in intracranial meningiomas. *Neuro-Oncology Adv.* 2 (1), vdaa108. doi:10.1093/oaajnl/vdaa108
- Bettcher, B. M., Tansey, M. G., Dorothee, G., and Heneka, M. T. (2021a). Peripheral and central immune system crosstalk in Alzheimer disease - a research prospectus. *Nat. Rev. Neurol.* 17 (11), 689–701. doi:10.1038/s41582-021-00549-x
- Bettcher, B. M., Tansey, M. G., Dorothee, G., and Heneka, M. T. (2021b). Publisher Correction: peripheral and central immune system crosstalk in Alzheimer disease - a research prospectus. *Nat. Rev. Neurol.* 17 (11), 724. doi:10.1038/s41582-021-00579-5
- Betteridge, K. B., Arkill, K. P., Neal, C. R., Harper, S. J., Foster, R. R., Satchell, S. C., et al. (2017). Sialic acids regulate microvessel permeability, revealed by novel *in vivo* studies of endothelial glycocalyx structure and function. *J. Physiol.* 595 (15), 5015–5035. doi:10.1111/JP274167
- Boghdeh, N. A., Risner, K. H., Barrera, M. D., Britt, C. M., Schaffer, D. K., Alem, F., et al. (2022). Application of a human blood brain barrier organ-on-a-chip model to evaluate small molecule effectiveness against Venezuelan equine encephalitis virus. *Viruses* 14 (12), 2799. doi:10.3390/v14122799
- Bonakdar, M., Graybill, P. M., and Davalos, R. V. (2017). A microfluidic model of the blood-brain barrier to study permeabilization by pulsed electric fields. *RSC Adv.* 7 (68), 42811–42818. doi:10.1039/C7RA07603G
- Bonneh-Barkay, D., and Wiley, C. A. (2009). Brain extracellular matrix in neurodegeneration. *Brain Pathol.* 19 (4), 573–585. doi:10.1111/j.1750-3639.2008.00195.x
- Braak, H., and Braak, E. (1995). Staging of Alzheimer's disease-related neurofibrillary changes. *Neurobiol. Aging* 16 (3), 271–278. ; discussion 8-84. doi:10.1016/0197-4580(95)00021-6
- Brown, J. A., Pensabene, V., Markov, D. A., Allwardt, V., Neely, M. D., Shi, M., et al. (2015). Recreating blood-brain barrier physiology and structure on chip: a novel neurovascular microfluidic bioreactor. *Biomicrofluidics* 9 (5), 054124. doi:10.1063/1.4934713
- Chen, M. B., Yang, A. C., Yousef, H., Lee, D., Chen, W., Schaum, N., et al. (2020). Brain endothelial cells are exquisite sensors of age-related circulatory cues. *Cell. Rep.* 30 (13), 4418–4432. doi:10.1016/j.celrep.2020.03.012
- Chen, X., Sun, G., Tian, E., Zhang, M., Davtyan, H., Beach, T. G., et al. (2021). Modeling sporadic Alzheimer's disease in human brain organoids under serum exposure. *Adv. Sci.* 8 (18), 2101462. doi:10.1002/adv.202101462
- Chen, Z. L., and Strickland, S. (1997). Neuronal death in the hippocampus is promoted by plasmin-catalyzed degradation of laminin. *Cell* 91 (7), 917–925. doi:10.1016/s0092-8674(00)80483-3
- Chioldi, P., Bugatti, A., Urbinati, C., and Rusnati, M. (2015). Heparin/heparan sulfate proteoglycans glycomic interactome in angiogenesis: biological implications and therapeutic use. *Molecules* 20 (4), 6342–6388. doi:10.3390/molecules20046342
- Cho, C. F., Wolfe, J. M., Faden, C. M., Calligaris, D., Hornburg, K., Chiocia, E. A., et al. (2017a). Blood-brain-barrier spheroids as an *in vitro* screening platform for brain-penetrating agents. *Nat. Commun.* 8, 15623. doi:10.1038/ncomms15623
- Cho, C.-F., Wolfe, J. M., Faden, C. M., Calligaris, D., Hornburg, K., Chiocia, E. A., et al. (2017b). Blood-brain-barrier spheroids as an *in vitro* screening platform for brain-penetrating agents. *Nat. Commun.* 8 (1), 15623. doi:10.1038/ncomms15623
- Constantinescu, A. A., Vink, H., and Spaan, J. A. E. (2003). Endothelial cell glycocalyx modulates immobilization of leukocytes at the endothelial surface. *Arteriosclerosis, Thrombosis, Vasc. Biol.* 23 (9), 1541–1547. doi:10.1161/01.ATV.0000085630.24353.3D
- Couchman, J. R., and Pataki, C. A. (2012). An introduction to proteoglycans and their localization. *J. Histochem Cytochem* 60 (12), 885–897. doi:10.1369/0022155412464638
- Cucullo, L., Hossain, M., Puvanna, V., Marchi, N., and Janigro, D. (2011). The role of shear stress in Blood-Brain Barrier endothelial physiology. *BMC Neurosci.* 12, 40. doi:10.1186/1471-2202-12-40
- Curry, F. E., and Adamson, R. H. (2012). Endothelial glycocalyx: permeability barrier and mechanosensor. *Ann. Biomed. Eng.* 40 (4), 828–839. doi:10.1007/s10439-011-0429-8
- Daneman, R., and Prat, A. (2015). The blood-brain barrier. *Cold Spring Harb. Perspect. Biol.* 7 (1), a020412. doi:10.1101/cshperspect.a020412
- De La Torre, J. C. (2002). Alzheimer disease as a vascular disorder: nosological evidence. *Stroke* 33 (4), 1152–1162. doi:10.1161/01.str.0000014421.15948.67
- de la Torre, J. C., and Mussivand, T. (1993). Can disturbed brain microcirculation cause Alzheimer's disease? *Neurol. Res.* 15 (3), 146–153. doi:10.1080/01616412.1993.11740127
- DellaValle, B., Hasseldam, H., Johansen, F. F., Iversen, H. K., Rungby, J., and Hempel, C. (2019). Multiple soluble components of the glycocalyx are increased in patient plasma after ischemic stroke. *Stroke* 50 (10), 2948–2951. doi:10.1161/STROKEAHA.119.025953
- DellaValle, B., Manresa-Arraut, A., Hasseldam, H., Stensballe, A., Rungby, J., Larsen, A., et al. (2018). Detection of glycan shedding in the blood: new class of multiple sclerosis biomarkers? *Front. Immunol.* 9, 1254. doi:10.3389/fimmu.2018.01254
- Dempsey, L. A., Brunn, G. J., and Platt, J. L. (2000). Heparanase, a potential regulator of cell-matrix interactions. *Trends Biochem. Sci.* 25 (8), 349–351. doi:10.1016/s0968-0004(00)01619-4
- Denk, W., Strickler, J. H., and Webb, W. W. (1990). Two-photon laser scanning fluorescence microscopy. *Science* 248 (4951), 73–76. doi:10.1126/science.2321027
- Deore, B. J., Partyka, P. P., Fan, F., and Galie, P. A. (2022). CD44 mediates shear stress mechanotransduction in an *in vitro* blood-brain barrier model through small GTPases RhoA and Rac1. *FASEB J.* 36 (5), e22278. doi:10.1096/fj.202100822RR
- De-Paula, V. J., Radanovic, M., Diniz, B. S., and Forlenza, O. V. (2012) *Alzheimer's disease*. Netherlands: Springer, 329–352.
- Destefano, J. G., Jamieson, J. J., Linville, R. M., and Searson, P. C. (2018). Benchmarking *in vitro* tissue-engineered blood-brain barrier models. *Fluids Barriers CNS* 15 (1), 32. doi:10.1186/s12987-018-0117-2
- Di Marco, L. Y., Venneri, A., Farkas, E., Evans, P. C., Marzo, A., and Frangi, A. F. (2015). Vascular dysfunction in the pathogenesis of Alzheimer's disease--A review of endothelium-mediated mechanisms and ensuing vicious circles. *Neurobiol. Dis.* 82, 593–606. doi:10.1016/j.nbd.2015.08.014
- Di Meo, S., Reed, T. T., Venditti, P., and Victor, V. M. (2016). Role of ROS and RNS sources in physiological and pathological conditions. *Oxid. Med. Cell. Longev.* 2016, 1245049. doi:10.1155/2016/1245049
- Ding, Y., Zhong, Y., Baldeshwiler, A., Abner, E. L., Bauer, B., and Hartz, A. M. S. (2021). Protecting P-glycoprotein at the blood-brain barrier from degradation in an Alzheimer's disease mouse model. *Fluids Barriers CNS* 18 (1), 10. doi:10.1186/s12987-021-00245-4
- Dogné, S., and Flamion, B. (2020). Endothelial glycocalyx impairment in disease: focus on hyaluronan shedding. *Am. J. Pathology* 190 (4), 768–780. doi:10.1016/j.ajpath.2019.11.016

- Dormanns, K., Brown, R. G., and David, T. (2016). The role of nitric oxide in neurovascular coupling. *J. Theor. Biol.* 394, 1–17. doi:10.1016/j.jtbi.2016.01.009
- Dudzinski, D. M., and Michel, T. (2007). Life history of eNOS: partners and pathways. *Cardiovasc. Res.* 75 (2), 247–260. doi:10.1016/j.cardiores.2007.03.023
- Ebong, E. E., Lopez-Quintero, S. V., Rizzo, V., Spray, D. C., and Tarbell, J. M. (2014). Shear-induced endothelial NOS activation and remodeling via heparan sulfate, glypican-1, and syndecan-1. *Integr. Biol. (Camb.)* 6 (3), 338–347. doi:10.1039/c3ib40199e
- Ebong, E. E., Macaluso, F. P., Spray, D. C., and Tarbell, J. M. (2011). Imaging the endothelial glycocalyx *in vitro* by rapid freezing/freezing substitution transmission electron microscopy. *Arterioscler. Thromb. Vasc. Biol.* 31 (8), 1908–1915. doi:10.1161/ATVBAHA.111.225268
- Endo, K., Takino, T., Miyamori, H., Kinsen, H., Yoshizaki, T., Furukawa, M., et al. (2003). Cleavage of syndecan-1 by membrane type matrix metalloproteinase-1 stimulates cell migration. *J. Biol. Chem.* 278 (42), 40764–40770. doi:10.1074/jbc.M306736200
- Fahs, S. A., Hille, M. T., Shi, Q., Weiler, H., and Montgomery, R. R. (2014). A conditional knockout mouse model reveals endothelial cells as the principal and possibly exclusive source of plasma factor VIII. *Blood* 123 (24), 3706–3713. doi:10.1182/blood-2014-02-555151
- Floris, S., Van Den Born, J., Van Der Pol, S. M. A., Dijkstra, C. D., and De Vries, H. E. (2003). Heparan sulfate proteoglycans modulate monocyte migration across cerebral endothelium. *J. Neuropathology Exp. Neurology* 62 (7), 780–790. doi:10.1093/jnen/62.7.780
- Forman, H. J., and Torres, M. (2002). Reactive oxygen species and cell signaling: respiratory burst in macrophage signaling. *Am. J. Respir. Crit. Care Med.* 166 (12 Pt 2), S4–S8. doi:10.1164/rccm.2206007
- Garcia, B., Martin, C., Garcia-Suarez, O., Muniz-Alonso, B., Ordiales, H., Fernandez-Menendez, S., et al. (2017). Upregulated expression of heparanase and heparanase 2 in the brains of Alzheimer's disease. *J. Alzheimers Dis.* 58 (1), 185–192. doi:10.3233/JAD-161298
- Gharagouzloo, C. A., McMahon, P. N., and Sridhar, S. (2015). Quantitative contrast-enhanced MRI with superparamagnetic nanoparticles using ultrashort time-to-echo pulse sequences. *Magnetic Reson. Med.* 74 (2), 431–441. doi:10.1002/mrm.25426
- Goes, A., Wouters, D., Pol, S. M. A., Huizinga, R., Ronken, E., Adamson, P., et al. (2001). Reactive oxygen species enhance the migration of monocytes across the blood-brain barrier *in vitro*. *FASEB J.* 15 (10), 1852–1854. doi:10.1096/fj.00-0881fj
- Gomez González, B., Larios, H. M., and Escobar, A. (2011). Increased transvascular transport of WGA-peroxidase after chronic perinatal stress in the hippocampal microvasculature of the rat. *Int. J. Dev. Neurosci.* 29 (8), 839–846. doi:10.1016/j.ijdevneu.2011.08.003
- Gonzalez Rodriguez, E., Cardenas, J. C., Cox, C. S., Kitagawa, R. S., Stensballe, J., Holcomb, J. B., et al. (2018). Traumatic brain injury is associated with increased syndecan-1 shedding in severely injured patients. *Scand. J. Trauma, Resusc. Emerg. Med.* 26 (1), 102. doi:10.1186/s13049-018-0565-3
- Gotz, J., Bodea, L. G., and Goedert, M. (2018). Rodent models for Alzheimer disease. *Nat. Rev. Neurosci.* 19 (10), 583–598. doi:10.1038/s41583-018-0054-8
- Govindpani, K., McNamara, L. G., Smith, N. R., Vinnakota, C., Waldvogel, H. J., Faull, R. L., et al. (2019). Vascular dysfunction in Alzheimer's disease: a prelude to the pathological process or a consequence of it? *J. Clin. Med.* 8 (5), 651. doi:10.3390/jcm8050651
- Griffin, W. S., Stanley, L. C., Ling, C., White, L., MacLeod, V., Perrot, L. J., et al. (1989). Brain interleukin 1 and S-100 immunoreactivity are elevated in Down syndrome and Alzheimer disease. *Proc. Natl. Acad. Sci. U. S. A.* 86 (19), 7611–7615. doi:10.1073/pnas.86.19.7611
- Haeren, R. H., van de Ven, S. E., van Zandvoort, M. A., Vink, H., van Overbeeke, J. J., Hoogland, G., et al. (2016). Assessment and imaging of the cerebrovascular glycocalyx. *Curr. Neurovasc. Res.* 13 (3), 249–260. doi:10.2174/1567202613666160504104434
- Haeren, R. H., Vink, H., Staals, J., van Zandvoort, M. A., Dings, J., van Overbeeke, J. J., et al. (2017). Protocol for intraoperative assessment of the human cerebrovascular glycocalyx. *BMJ Open* 7 (1), e013954. doi:10.1136/bmjopen-2016-013954
- Haeren, R. H. L., Rijkers, K., Schijns, O., Dings, J., Hoogland, G., van Zandvoort, M., et al. (2018). *In vivo* assessment of the human cerebral microcirculation and its glycocalyx: a technical report. *J. Neurosci. Methods* 303, 114–125. doi:10.1016/j.jneumeth.2018.03.009
- Hajal, C., Offeddu, G. S., Shin, Y., Zhang, S., Morozova, O., Hickman, D., et al. (2022). Engineered human blood-brain barrier microfluidic model for vascular permeability analyses. *Nat. Protoc.* 17 (1), 95–128. doi:10.1038/s41596-021-00635-w
- Harding, I. C., Cisneros, W., and Ebong, E. (2019a). The role of the endothelial glycocalyx in atherosclerosis development via ROS production and downstream endothelial activation. *Proc. Conf. Arteriosclerosis, Thrombosis, Vasc. Biol.* doi:10.1161/atvb.39.suppl_1.733
- Harding, I. C., Mitra, R., Mensah, S. A., Nersesyan, A., Bal, N. N., and Ebong, E. E. (2019b). Endothelial barrier reinforcement relies on flow-regulated glycocalyx, a potential therapeutic target. *Biorheology* 56 (2-3), 131–149. doi:10.3233/BIR-180205
- Harding, I. C., O'Hare, N. R., Vigliotti, M., Caraballo, A., Lee, C. I., Millican, K., et al. (2022). Developing a transwell millifluidic device for studying blood-brain barrier endothelium. *Lab a Chip* 22 (23), 4603–4620. doi:10.1039/d2lc00657j
- He, Y., Yao, Y., Tsirka, S. E., and Cao, Y. (2014). Cell-culture models of the blood-brain barrier. *Stroke* 45 (8), 2514–2526. doi:10.1161/STROKEAHA.114.005427
- Hempel, C., Kaphishnikov, S., Perez-Berna, A. J., Werner, S., Guttmann, P., Pereiro, E., et al. (2020). The need to freeze—dehydration during specimen preparation for electron microscopy collapses the endothelial glycocalyx regardless of fixation method. *Microcirculation* 27 (7), e12643. doi:10.1111/micc.12643
- Hock, C., Villringer, K., Muller-Spahn, F., Wenzel, R., Heekeren, H., Schuh-Hofer, S., et al. (1997). Decrease in parietal cerebral hemoglobin oxygenation during performance of a verbal fluency task in patients with Alzheimer's disease monitored by means of near-infrared spectroscopy (NIRS)—correlation with simultaneous rCBF-PET measurements. *Brain Res.* 755 (2), 293–303. doi:10.1016/s0006-8993(97)00122-4
- Hou, Y., Dan, X., Babbar, M., Wei, Y., Hasselbalch, S. G., Croteau, D. L., et al. (2019). Ageing as a risk factor for neurodegenerative disease. *Nat. Rev. Neurol.* 15 (10), 565–581. doi:10.1038/s41582-019-0244-7
- Hull, M., Berger, M., Volk, B., and Bauer, J. (1996). Occurrence of interleukin-6 in cortical plaques of Alzheimer's disease patients may precede transformation of diffuse into neuritic plaques. *Ann. N. Y. Acad. Sci.* 777, 205–212. doi:10.1111/j.1749-6632.1996.tb34420.x
- Hussain, B., Fang, C., and Chang, J. (2021). Blood-brain barrier breakdown: an emerging biomarker of cognitive impairment in normal aging and dementia. *Front. Neurosci.* 15, 688090. doi:10.3389/fnins.2021.688090
- Iba, T., and Levy, J. H. (2019). Derangement of the endothelial glycocalyx in sepsis. *J. Thromb. Haemost.* 17 (2), 283–294. doi:10.1111/jth.14371
- Ito, R., Umehara, K., Suzuki, S., Kitamura, K., Nunoya, K. I., Yamaura, Y., et al. (2019). A human immortalized cell-based blood-brain barrier triculture model: development and characterization as a promising tool for drug-brain permeability studies. *Mol. Pharm.* 16 (11), 4461–4471. doi:10.1021/acs.molpharmaceut.9b00519
- Jin, J., Fang, F., Gao, W., Chen, H., Wen, J., Wen, X., et al. (2021). The structure and function of the glycocalyx and its connection with blood-brain barrier. *Front. Cell. Neurosci.* 15, 739699. doi:10.3389/fncel.2021.739699
- Johnson, G. B., Brunn, G. J., Kodaira, Y., and Platt, J. L. (2002). Receptor-mediated monitoring of tissue well-being via detection of soluble heparan sulfate by Toll-like receptor 4. *J. Immunol.* 168 (10), 5233–5239. doi:10.4049/jimmunol.168.10.5233
- Kadry, H., Noorani, B., and Cucullo, L. (2020). A blood-brain barrier overview on structure, function, impairment, and biomarkers of integrity. *Fluids Barriers CNS* 17 (1), 69. doi:10.1186/s12987-020-00230-3
- Kapasi, A., and Schneider, J. A. (2016). Vascular contributions to cognitive impairment, clinical Alzheimer's disease, and dementia in older persons. *Biochim. Biophys. Acta* 1862 (5), 878–886. doi:10.1016/j.bbdis.2015.12.023
- Kilic, K., Desjardins, M., Tang, J., Thunemann, M., Sunil, S., Erdener, S. E., et al. (2020). Chronic cranial windows for long term multimodal neurovascular imaging in mice. *Front. Physiol.* 11, 612678. doi:10.3389/fphys.2020.612678
- Ko, K., Suzuki, T., Ishikawa, R., Hattori, N., Ito, R., Umehara, K., et al. (2020). Ischemic stroke disrupts the endothelial glycocalyx through activation of proHPSE via acrolein exposure. *J. Biol. Chem.* 295 (52), 18614–18624. doi:10.1074/jbc.RA120.015105
- Korczyn, A. D. (2008). The amyloid cascade hypothesis. *Alzheimer's Dementia* 4 (3), 176–178. doi:10.1016/j.jalz.2007.11.008
- Korczyn, A. D. (2012). Why have we failed to cure Alzheimer's disease? *J. Alzheimers Dis.* 29 (2), 275–282. doi:10.3233/JAD-2011-110359
- Kucharz, K., Mathiesen Janiurek, M., Christoffersen, C., and Lauritzen, M. (2022). Two-photon microscopy *in vivo* reveals brain vessel type-specific loss of glycocalyx caused by apoM/S1P signaling impairment.
- Kumagai, R., Lu, X., and Kassab, G. S. (2009). Role of glycocalyx in flow-induced production of nitric oxide and reactive oxygen species. *Free Radic. Biol. Med.* 47 (5), 600–607. doi:10.1016/j.freeradbiomed.2009.05.034
- Kumar, A., Sidhu, J., Goyal, A., and Tsao, J. W. (2022). *Alzheimer disease*. StatPearls. USA: Treasure Island (FL).
- Kutuzov, N., Flyvbjerg, H., and Lauritzen, M. (2018). Contributions of the glycocalyx, endothelium, and extravascular compartment to the blood-brain barrier. *Proc. Natl. Acad. Sci. U. S. A.* 115 (40), E9429–E9438–E38. doi:10.1073/pnas.1802155115
- Leaston, J., Ferris, C. F., Kulkarni, P., Chandramohan, D., Van De Ven, A. L., Qiao, J., et al. (2021a). Neurovascular imaging with QUTE-CE MRI in APOE4 rats reveals early vascular abnormalities. *PLOS ONE* 16 (8), e0256749. doi:10.1371/journal.pone.0256749
- Leaston, J., Qiao, J., Harding, I. C., Kulkarni, P., Gharagouzloo, C., Ebong, E., et al. (2021b). Quantitative imaging of blood-brain barrier permeability following repetitive mild head impacts. *Front. Neurology* 12, 729464. doi:10.3389/fneur.2021.729464
- Leite, D. M., Matias, D., and Battaglia, G. (2020). The role of BAR proteins and the glycocalyx in brain endothelium transcytosis. *Cells* 9 (12), 2685. doi:10.3390/cells9122685

- Li, N. C., Lee, A., Whitmer, R. A., Kivipelto, M., Lawler, E., Kazis, L. E., et al. (2010). Use of angiotensin receptor blockers and risk of dementia in a predominantly male population: prospective cohort analysis. *BMJ* 340, b5465. doi:10.1136/bmj.b5465
- Li, Y., Sun, X., Liu, H., Huang, L., Meng, G., Ding, Y., et al. (2019). Development of human *in vitro* brain-blood barrier model from induced pluripotent stem cell-derived endothelial cells to predict the *in vivo* permeability of drugs. *Neurosci. Bull.* 35 (6), 996–1010. doi:10.1007/s12264-019-00384-7
- Liao, Y., Day, K. H., Damon, D. N., and Duling, B. R. (2001). Endothelial cell-specific knockout of connexin 43 causes hypotension and bradycardia in mice. *Proc. Natl. Acad. Sci.* 98 (17), 9989–9994. doi:10.1073/pnas.171305298
- Lipowsky, H. H. (2012). The endothelial glycocalyx as a barrier to leukocyte adhesion and its mediation by extracellular proteases. *Ann. Biomed. Eng.* 40 (4), 840–848. doi:10.1007/s10439-011-0427-x
- Liu, C., Xu, S., Liu, Q., Chai, H., Luo, Y., and Li, S. (2023). Identification of immune cells infiltrating in hippocampus and key genes associated with Alzheimer's disease. *BMC Med. Genomics* 16 (1), 53. doi:10.1186/s12920-023-01458-2
- Lorente-Gea, L., Garcia, B., Martin, C., Ordiales, H., Garcia-Suarez, O., Pina-Batista, K. M., et al. (2020). Heparan sulfate proteoglycans undergo differential expression alterations in alzheimer disease brains. *J. Neuropathol. Exp. Neurol.* 79 (5), 474–483. doi:10.1093/jnen/nlaa016
- Lorenzl, S., Albers, D. S., Relkin, N., Ngyuen, T., Hilgenberg, S. L., Chirichigno, J., et al. (2003). Increased plasma levels of matrix metalloproteinase-9 in patients with Alzheimer's disease. *Neurochem. Int.* 43 (3), 191–196. doi:10.1016/s0197-0186(03)00004-4
- Luft, J. H. (1966). Fine structures of capillary and endocapillary layer as revealed by ruthenium red. *Fed. Proc.* 25 (6), 1773–1783.
- Machin, D. R., Bloom, S. I., Campbell, R. A., Phuon, T. T., Gates, P. E., Lesniewski, L. A., et al. (2018). Advanced age results in a diminished endothelial glycocalyx. *Am. J. Physiol. Heart Circ. Physiol.* 315 (3), H531–H539–H9. doi:10.1152/ajpheart.00104.2018
- Machin, D. R., Phuon, T. T., and Donato, A. J. (2019). The role of the endothelial glycocalyx in advanced age and cardiovascular disease. *Curr. Opin. Pharmacol.* 45, 66–71. doi:10.1016/j.coph.2019.04.011
- Majerczak, J., Grandys, M., Frolow, M., Szkutnik, Z., Zakrzewska, A., Nizankowski, R., et al. (2019). Age-dependent impairment in endothelial function and arterial stiffness in former high class male athletes is No different to that in men with No history of physical training. *J. Am. Heart Assoc.* 8 (18), e012670. doi:10.1161/JAHA.119.012670
- Manning, C., Stringer, M., Dickie, B., Clancy, U., Valdés Hernandez, M. C., Wiseman, S. J., et al. (2021). Sources of systematic error in DCE-MRI estimation of low-level blood-brain barrier leakage. *Magnetic Reson. Med.* 86 (4), 1888–1903. doi:10.1002/mrm.28833
- Manoharan, S., Guillemin, G. J., Abiramasundari, R. S., Essa, M. M., Akbar, M., and Akbar, M. D. (2016). The role of reactive oxygen species in the pathogenesis of Alzheimer's disease, Parkinson's disease, and huntington's disease: a mini review. *Oxid. Med. Cell. Longev.* 2016, 8590578. doi:10.1155/2016/8590578
- Marino, A., Baronio, M., Buratti, U., Mele, E., and Ciofani, G. (2021). Porous optically transparent cellulose acetate scaffolds for biomimetic blood-brain barrier *in vitro* models. *Front. Bioeng. Biotechnol.* 9, 630063. doi:10.3389/fbioe.2021.630063
- Masola, V., Zaza, G., Arduini, A., Onisto, M., and Gambaro, G. (2021). Endothelial glycocalyx as a regulator of fibrotic processes. *Int. J. Mol. Sci.* 22 (6), 2996. doi:10.3390/ijms22062996
- McDonald, K. K., Cooper, S., Danielzak, L., and Leask, R. L. (2016). Glycocalyx degradation induces a proinflammatory phenotype and increased leukocyte adhesion in cultured endothelial cells under flow. *PLOS ONE* 11 (12), e0167576. doi:10.1371/journal.pone.0167576
- McKallip, R. J., Do, Y., Fisher, M. T., Robertson, J. L., Nagarkatti, P. S., and Nagarkatti, M. (2002). Role of CD44 in activation-induced cell death: CD44-deficient mice exhibit enhanced T cell response to conventional and superantigens. *Int. Immunol.* 14 (9), 1015–1026. doi:10.1093/intimm/14.9.1015
- Mhatre, M., Nguyen, A., Kashani, S., Pham, T., Adesina, A., and Grammas, P. (2004). Thrombin, a mediator of neurotoxicity and memory impairment. *Neurobiol. Aging* 25 (6), 783–793. doi:10.1016/j.neurobiolaging.2003.07.007
- Mockl, L. (2020). The emerging role of the mammalian glycocalyx in functional membrane organization and immune system regulation. *Front. Cell. Dev. Biol.* 8, 253. doi:10.3389/fcell.2020.00253
- Montagne, A., Barnes, S. R., Sweeney, M. D., Halliday, M. R., Sagare, A. P., Zhao, Z., et al. (2015). Blood-brain barrier breakdown in the aging human hippocampus. *Neuron* 85 (2), 296–302. doi:10.1016/j.neuron.2014.12.032
- Monzon, M. E., Fregien, N., Schmid, N., Falcon, N. S., Campos, M., Casalino-Matsuda, S. M., et al. (2010). Reactive oxygen species and hyaluronidase 2 regulate airway epithelial hyaluronan fragmentation. *J. Biol. Chem.* 285 (34), 26126–26134. doi:10.1074/jbc.M110.135194
- Moon, Y., Jeon, H. J., Han, S. H., Min-Young, N., Kim, H. J., Kwon, K. J., et al. (2023). Blood-brain barrier breakdown is linked to tau pathology and neuronal injury in a differential manner according to amyloid deposition. *J. Cereb. Blood Flow. Metab.* 43 (11), 1813–1825. doi:10.1177/0271678X231180035
- Moore, K. H., Murphy, H. A., and George, E. M. (2021). The glycocalyx: a central regulator of vascular function. *Am. J. Physiol. Regul. Integr. Comp. Physiol.* 320 (4), R508–R518. doi:10.1152/ajpregu.00340.2020
- Nelson, A. R., Sweeney, M. D., Sagare, A. P., and Zlokovic, B. V. (2016). Neurovascular dysfunction and neurodegeneration in dementia and Alzheimer's disease. *Biochim. Biophys. Acta* 1862 (5), 887–900. doi:10.1016/j.bbdis.2015.12.016
- O'Hare, N. R., Harding, I. C., Herman, I. M., and Ebong, E. E. (2022). "The roles of shear stress and heparan sulfate degradation in endothelial cell activation," in *Proceeding of the Summer Biomechanics, Bioengineering, & Biotransport Conference*, China, June 28, 2023 (IEEE).
- Pacher, P., Beckman, J. S., and Liaudet, L. (2007). Nitric oxide and peroxynitrite in health and disease. *Physiol. Rev.* 87 (1), 315–424. doi:10.1152/physrev.00029.2006
- Pahakis, M. Y., Kosky, J. R., Dull, R. O., and Tarbell, J. M. (2007). The role of endothelial glycocalyx components in mechanotransduction of fluid shear stress. *Biochem. Biophysical Res. Commun.* 355 (1), 228–233. doi:10.1016/j.bbrc.2007.01.137
- Park, L., Anrather, J., Zhou, P., Frys, K., Pitstick, R., Younkin, S., et al. (2005). NADPH oxidase-derived reactive oxygen species mediate the cerebrovascular dysfunction induced by the amyloid peptide. *J. Neurosci.* 25 (7), 1769–1777. doi:10.1523/JNEUROSCI.5207-04.2005
- Pérez, V. I., Bokov, A., Remmen, H. V., Mele, J., Ran, Q., Ikeno, Y., et al. (2009). Is the oxidative stress theory of aging dead? *Biochimica Biophysica Acta (BBA) - General Subj.* 1790 (10), 1005–1014. doi:10.1016/j.bbagen.2009.06.003
- Potje, S. R., Paula, T. D., Paulo, M., and Bendhack, L. M. (2020). The role of glycocalyx and caveolae in vascular homeostasis and diseases. *Front. Physiol.* 11, 620840. doi:10.3389/fphys.2020.620840
- Potter, D. R., Jiang, J., and Damiano, E. R. (2009). The recovery time course of the endothelial cell glycocalyx *in vivo* and its implications *in vitro*. *Circulation Res.* 104 (11), 1318–1325. doi:10.1161/CIRCRESAHA.108.191585
- Prohovnik, I., Mayeux, R., Sackeim, H. A., Smith, G., Stern, Y., and Alderson, P. O. (1988). Cerebral perfusion as a diagnostic marker of early Alzheimer's disease. *Neurology* 38 (6), 931–937. doi:10.1212/wnl.38.6.931
- Protin, U., Schweighoffer, T., Jochum, W., and Hilberg, F. (1999). CD44-deficient mice develop normally with changes in subpopulations and recirculation of lymphocyte subsets. *J. Immunol.* 163 (9), 4917–4923. doi:10.4049/jimmunol.163.9.4917
- Qiu, Y., Buffon, S., Ramnath, R., Jenner, S., Fawaz, S., Arkill, K. P., et al. (2022). Endothelial glycocalyx is damaged in diabetic cardiomyopathy: angiotensin 1 restores glycocalyx and improves diastolic function in mice. *Diabetologia* 65 (5), 879–894. doi:10.1007/s00125-022-05650-4
- Qu, J., Cheng, Y., Wu, W., Yuan, L., and Liu, X. (2021). Glycocalyx impairment in vascular disease: focus on inflammation. *Front. Cell. Dev. Biol.* 9, 730621. doi:10.3389/fcell.2021.730621
- Ramnath, R., Foster, R. R., Qiu, Y., Cope, G., Butler, M. J., Salmon, A. H., et al. (2014). Matrix metalloproteinase 9-mediated shedding of syndecan 4 in response to tumor necrosis factor α : a contributor to endothelial cell glycocalyx dysfunction. *FASEB J.* 28 (11), 4686–4699. doi:10.1096/fj.14-252221
- Reed, M. J., Damodarasamy, M., Pathan, J. L., Chan, C. K., Spiekerman, C., Wight, T. N., et al. (2019). Increased hyaluronan and TSG-6 in association with neuropathologic changes of Alzheimer's disease. *J. Alzheimers Dis.* 67 (1), 91–102. doi:10.3233/JAD-180797
- Rehm, M., Bruegger, D., Christ, F., Conzen, P., Thiel, M., Jacob, M., et al. (2007). Shedding of the endothelial glycocalyx in patients undergoing major vascular surgery with global and regional ischemia. *Circulation* 116 (17), 1896–1906. doi:10.1161/CIRCULATIONAHA.106.684852
- Reitsma, S., Slaaf, D. W., Vink, H., van Zandvoort, M. A., and oude Egbrink, M. G. (2007). The endothelial glycocalyx: composition, functions, and visualization. *Pflügers Arch.* 454 (3), 345–359. doi:10.1007/s00424-007-0212-8
- Rochford, K. D., Collins, L. E., Murphy, R. P., and Cummins, P. M. (2014). Downregulation of blood-brain barrier phenotype by proinflammatory cytokines involves NADPH oxidase-dependent ROS generation: consequences for interendothelial adherens and tight junctions. *PLoS ONE* 9 (7), e101815. doi:10.1371/journal.pone.0101815
- Rubio-Gayosso, I., Platts, S. H., and Duling, B. R. (2006). Reactive oxygen species mediate modification of glycocalyx during ischemia-reperfusion injury. *Am. J. Physiol. Heart Circ. Physiol.* 290 (6), H2247–H2256. doi:10.1152/ajpheart.00796.2005
- Ruitenber, A., den Heijer, T., Bakker, S. L., van Swieten, J. C., Koudstaal, P. J., Hofman, A., et al. (2005). Cerebral hypoperfusion and clinical onset of dementia: the Rotterdam Study. *Ann. Neurol.* 57 (6), 789–794. doi:10.1002/ana.20493
- Sanchez-Varo, R., Mejias-Ortega, M., Fernandez-Valenzuela, J. J., Nunez-Diaz, C., Caceres-Palomo, L., Vegas-Gomez, L., et al. (2022). Transgenic mouse models of Alzheimer's disease: an integrative analysis. *Int. J. Mol. Sci.* 23 (10), 5404. doi:10.3390/ijms23105404
- Santaguida, S., Janigro, D., Hossain, M., Oby, E., Rapp, E., and Cucullo, L. (2006). Side by side comparison between dynamic versus static models of blood-brain barrier *in vitro*: a permeability study. *Brain Res.* 1109 (1), 1–13. doi:10.1016/j.brainres.2006.06.027

- Santa-Maria, A. R., Walter, F. R., Figueiredo, R., Kincses, A., Vigh, J. P., Heymans, M., et al. (2021). Flow induces barrier and glycocalyx-related genes and negative surface charge in a lab-on-a-chip human blood-brain barrier model. *J. Cereb. Blood Flow. Metab.* 41 (9), 2201–2215. doi:10.1177/0271678X21992638
- Schachtrup, C., Lu, P., Jones, L. L., Lee, J. K., Lu, J., Sachs, B. D., et al. (2007). Fibrinogen inhibits neurite outgrowth via beta 3 integrin-mediated phosphorylation of the EGF receptor. *Proc. Natl. Acad. Sci. U. S. A.* 104 (28), 11814–11819. doi:10.1073/pnas.0704045104
- Scheibner, K. A., Lutz, M. A., Boodoo, S., Fenton, M. J., Powell, J. D., and Horton, M. R. (2006). Hyaluronan fragments act as an endogenous danger signal by engaging TLR2. *J. Immunol.* 177 (2), 1272–1281. doi:10.4049/jimmunol.177.2.1272
- Schenck, H., Netti, E., Teernstra, O., De Ridder, I., Dings, J., Niemela, M., et al. (2021). The role of the glycocalyx in the pathophysiology of subarachnoid hemorrhage-induced delayed cerebral ischemia. *Front. Cell. Dev. Biol.* 9, 731641. doi:10.3389/fcell.2021.731641
- Schreiner, T. G., Creangă-Murariu, I., Tamba, B. I., Lucanu, N., and Popescu, B. O. (2022). *In vitro* modeling of the blood–brain barrier for the study of physiological conditions and Alzheimer's disease. *Biomolecules* 12 (8), 1136. doi:10.3390/biom12081136
- Sharma, N. S., Karan, A., Lee, D., Yan, Z., and Xie, J. (2021). Advances in modeling Alzheimer's disease *in vitro*. *Adv. NanoBiomed Res.* 1 (12), 2100097. doi:10.1002/anbr.202100097
- Sheppard, O., and Coleman, M. (2020). *Alzheimer's disease: etiology, neuropathology and pathogenesis*. China: Exon Publications, 1–22.
- Siebert, J. R., Conta Steencken, A., and Osterhout, D. J. (2014). Chondroitin sulfate proteoglycans in the nervous system: inhibitors to repair. *BioMed Res. Int.* 2014, 845323–845415. doi:10.1155/2014/845323
- Sieve, I., Munster-Kuhnel, A. K., and Hilfiker-Kleiner, D. (2018). Regulation and function of endothelial glycocalyx layer in vascular diseases. *Vasc. Pharmacol.* 100, 26–33. doi:10.1016/j.vph.2017.09.002
- Smyth, L. C. D., Murray, H. C., Hill, M., Van Leeuwen, E., Highet, B., Magon, N. J., et al. (2022). Neutrophil-vascular interactions drive myeloperoxidase accumulation in the brain in Alzheimer's disease. *Acta Neuropathol. Commun.* 10 (1), 38. doi:10.1186/s40478-022-01347-2
- Song, H., and Yang, P. C. (2010). Construction of shRNA lentiviral vector. *N. Am. J. Med. Sci.* 2 (12), 598–601. doi:10.4297/najms.2010.2598
- Soto-Rojas, L. O., Pacheco-Herrero, M., Martínez-Gómez, P. A., Campa-Córdoba, B. B., Apátiga-Pérez, R., Villegas-Rojas, M. M., et al. (2021). The neurovascular unit dysfunction in Alzheimer's disease. *Int. J. Mol. Sci.* 22 (4), 2022. doi:10.3390/ijms22042022
- Stanimirovic, D. B., and Friedman, A. (2012). Pathophysiology of the neurovascular unit: disease cause or consequence? *J. Cereb. Blood Flow. Metab.* 32 (7), 1207–1221. doi:10.1038/jcbfm.2012.25
- Sun, L., Wang, L., Ye, K. X., Wang, S., Zhang, R., Juan, Z., et al. (2023). Endothelial glycocalyx in aging and age-related diseases. *Aging Dis.* 14 (5), 1606–1617. doi:10.14336/AD.2023.0131
- Sweeney, M. D., Sagare, A. P., and Zlokovic, B. V. (2018). Blood-brain barrier breakdown in Alzheimer disease and other neurodegenerative disorders. *Nat. Rev. Neurol.* 14 (3), 133–150. doi:10.1038/nrneurol.2017.188
- Tarantini, S., Tran, C. H. T., Gordon, G. R., Ungvari, Z., and Csiszar, A. (2017). Impaired neurovascular coupling in aging and Alzheimer's disease: contribution of astrocyte dysfunction and endothelial impairment to cognitive decline. *Exp. Gerontol.* 94, 52–58. doi:10.1016/j.exger.2016.11.004
- Tarbell, J. M., and Cancel, L. M. (2016). The glycocalyx and its significance in human medicine. *J. Intern. Med.* 280 (1), 97–113. doi:10.1111/joim.12465
- Tarbell, J. M., and Pahakis, M. Y. (2006). Mechanotransduction and the glycocalyx. *J. Intern. Med.* 259 (4), 339–350. doi:10.1111/j.1365-2796.2006.01620.x
- Taylor, K. R., Trowbridge, J. M., Rudisill, J. A., Termeer, C. C., Simon, J. C., and Gallo, R. L. (2004). Hyaluronan fragments stimulate endothelial recognition of injury through TLR4. *J. Biol. Chem.* 279 (17), 17079–17084. doi:10.1074/jbc.M310859200
- Ting, K. K., Coleman, P., Zhao, Y., Vadas, M. A., and Gamble, J. R. (2021). The aging endothelium. *Vasc. Biol.* 3 (1), R35–R47. doi:10.1530/VB-20-0013
- Tong, X. K., Lecrux, C., Rosa-Neto, P., and Hamel, E. (2012). Age-dependent rescue by simvastatin of Alzheimer's disease cerebrovascular and memory deficits. *J. Neurosci.* 32 (14), 4705–4715. doi:10.1523/JNEUROSCI.0169-12.2012
- Tsvirkun, D., Grichine, A., Duperray, A., Misbah, C., and Bureau, L. (2017). Microvasculature on a chip: study of the endothelial surface layer and the flow structure of red blood cells. *Sci. Rep.* 7 (1), 45036. doi:10.1038/srep45036
- Twamley, S. G., Stach, A., Heilmann, H., Sohl-Kielczynski, B., Stangl, V., Ludwig, A., et al. (2021). Immuno-electron and confocal laser scanning microscopy of the glycocalyx. *Biol. (Basel)* 10 (5), 402. doi:10.3390/biology10050402
- Uchimido, R., Schmidt, E. P., and Shapiro, N. I. (2019). The glycocalyx: a novel diagnostic and therapeutic target in sepsis. *Crit. Care* 23 (1), 16. doi:10.1186/s13054-018-2292-6
- Ueda, A., Shimomura, M., Ikeda, M., Yamaguchi, R., and Tanishita, K. (2004). Effect of glycocalyx on shear-dependent albumin uptake in endothelial cells. *Am. J. Physiol. Heart Circ. Physiol.* 287 (5), H2287–H2294. doi:10.1152/ajpheart.00808.2003
- van de Haar, H. J., Burgmans, S., Jansen, J. F., van Osch, M. J., van Buchem, M. A., Muller, M., et al. (2016). Blood-brain barrier leakage in patients with early alzheimer disease. *Radiology* 281 (2), 527–535. doi:10.1148/radiol.2016152244
- van den Berg, B. M., Vink, H., and Spaan, J. A. (2003). The endothelial glycocalyx protects against myocardial edema. *Circ. Res.* 92 (6), 592–594. doi:10.1161/01.RES.0000065917.53950.75
- van Dyck, C. H., Swanson, C. J., Aisen, P., Bateman, R. J., Chen, C., Gee, M., et al. (2023). Lecanemab in early Alzheimer's disease. *N. Engl. J. Med.* 388 (1), 9–21. doi:10.1056/NEJMoa2212948
- van Golen, R. F., Reiniers, M. J., Vrisekoop, N., Zuurbier, C. J., Olthoff, P. B., van Rheenen, J., et al. (2014). The mechanisms and physiological relevance of glycocalyx degradation in hepatic ischemia/reperfusion injury. *Antioxid. Redox Signal* 21 (7), 1098–1118. doi:10.1089/ars.2013.5751
- van Horsen, J., Otte-Holler, I., David, G., Maat-Schieman, M. L., van den Heuvel, L. P., Wesseling, P., et al. (2001). Heparan sulfate proteoglycan expression in cerebrovascular amyloid beta deposits in Alzheimer's disease and hereditary cerebral hemorrhage with amyloidosis (Dutch) brains. *Acta Neuropathol.* 102 (6), 604–614. doi:10.1007/s004010100414
- Vink, H., and Duling, B. R. (2000). Capillary endothelial surface layer selectively reduces plasma solute distribution volume. *Am. J. Physiol. Heart Circ. Physiol.* 278 (1), H285–H289. doi:10.1152/ajpheart.2000.278.1.H285
- Walter, F. R., Santa-Maria, A. R., Meszaros, M., Veszelka, S., Der, A., and Deli, M. A. (2021). Surface charge, glycocalyx, and blood-brain barrier function. *Tissue Barriers* 9 (3), 1904773. doi:10.1080/21688370.2021.1904773
- Wang, Y., Branicky, R., Noe, A., and Hekimi, S. (2018). Superoxide dismutases: dual roles in controlling ROS damage and regulating ROS signaling. *J. Cell. Biol.* 217 (6), 1915–1928. doi:10.1083/jcb.201708007
- Webster, S. J., Bachstetter, A. D., Nelson, P. T., Schmitt, F. A., and Van Eldik, L. J. (2014). Using mice to model Alzheimer's dementia: an overview of the clinical disease and the preclinical behavioral changes in 10 mouse models. *Front. Genet.* 5, 88. doi:10.3389/fgene.2014.00088
- Williams, L. R., and Leggett, R. W. (1989). Reference values for resting blood flow to organs of man. *Clin. Phys. Physiol. Meas.* 10 (3), 187–217. doi:10.1088/0143-0815/10/3/001
- Williams-Medina, A., Deblock, M., and Janigro, D. (2020). *In vitro* models of the blood-brain barrier: tools in translational medicine. *Front. Med. Technol.* 2, 623950. doi:10.3389/fmed.2020.623950
- Winkler, E. A., Nishida, Y., Sagare, A. P., Rege, S. V., Bell, R. D., Perlmutter, D., et al. (2015). GLUT1 reductions exacerbate Alzheimer's disease vasculo-neuronal dysfunction and degeneration. *Nat. Neurosci.* 18 (4), 521–530. doi:10.1038/nn.3966
- Woodcock, T. E., and Woodcock, T. M. (2012). Revised Starling equation and the glycocalyx model of transvascular fluid exchange: an improved paradigm for prescribing intravenous fluid therapy. *Br. J. Anaesth.* 108 (3), 384–394. doi:10.1093/bja/aer515
- Yalcin, O., Jani, V. P., Johnson, P. C., and Cabrales, P. (2018). Implications enzymatic degradation of the endothelial glycocalyx on the microvascular hemodynamics and the arteriolar red cell free layer of the rat cremaster muscle. *Front. Physiol.* 9, 168. doi:10.3389/fphys.2018.00168
- Yan, L., Dwiggins, C. W., Gupta, U., and Stroka, K. M. (2023). A rapid-patterning 3D vessel-on-chip for imaging and quantitatively analyzing cell-cell junction phenotypes. *Bioeng. (Basel)* 10 (9), 1080. doi:10.3390/bioengineering10091080
- Yang, R., Chen, M., Zheng, J., Li, X., and Zhang, X. (2021). The role of heparin and glycocalyx in blood-brain barrier dysfunction. *Front. Immunol.* 12, 754141. doi:10.3389/fimmu.2021.754141
- Yang, X., Meegan, J. E., Jannaway, M., Coleman, D. C., and Yuan, S. Y. (2018). A disintegrin and metalloproteinase 15-mediated glycocalyx shedding contributes to vascular leakage during inflammation. *Cardiovasc Res.* 114 (13), 1752–1763. doi:10.1093/cvr/cvy167
- Yang, Y., and Schmidt, E. P. (2013). The endothelial glycocalyx: an important regulator of the pulmonary vascular barrier. *Tissue Barriers* 1 (1), e23494. doi:10.4161/tisb.23494
- Yen, W., Cai, B., Yang, J., Zhang, L., Zeng, M., Tarbell, J. M., et al. (2015). Endothelial surface glycocalyx can regulate flow-induced nitric oxide production in microvessels *in vivo*. *PLoS One* 10 (1), e0117133. doi:10.1371/journal.pone.0117133
- Yokoyama, M., Kobayashi, H., Tatsumi, L., and Tomita, T. (2022). Mouse models of Alzheimer's disease. *Front. Mol. Neurosci.* 15, 912995. doi:10.3389/fnmol.2022.912995
- Yoon, J. H., Lee, E. S., and Jeong, Y. (2017). *In vivo* imaging of the cerebral endothelial glycocalyx in mice. *J. Vasc. Res.* 54 (2), 59–67. doi:10.1159/000457799
- Yoon, J. H., Shin, P., Joo, J., Kim, G. S., Oh, W. Y., and Jeong, Y. (2022). Increased capillary stalling is associated with endothelial glycocalyx loss in subcortical vascular dementia. *J. Cereb. Blood Flow. Metab.* 42 (8), 1383–1397. doi:10.1177/0271678X221076568

- Yu, H., Kalogeris, T., and Korthuis, R. J. (2019). Reactive species-induced microvascular dysfunction in ischemia/reperfusion. *Free Radic. Biol. Med.* 135, 182–197. doi:10.1016/j.freeradbiomed.2019.02.031
- Zeng, Y., Liu, X. H., Tarbell, J., and Fu, B. (2015). Sphingosine 1-phosphate induced synthesis of glycocalyx on endothelial cells. *Exp. Cell. Res.* 339 (1), 90–95. doi:10.1016/j.yexcr.2015.08.013
- Zhang, X., O'Callaghan, P., Li, H., Tan, Y., Zhang, G., Barash, U., et al. (2021). Heparanase overexpression impedes perivascular clearance of amyloid- β from murine brain: relevance to Alzheimer's disease. *Acta Neuropathol. Commun.* 9 (1), 84. doi:10.1186/s40478-021-01182-x
- Zhao, F., Zhong, L., and Luo, Y. (2021). Endothelial glycocalyx as an important factor in composition of blood-brain barrier. *CNS Neurosci. Ther.* 27 (1), 26–35. doi:10.1111/cns.13560
- Zheng, C., Zhou, X.-W., and Wang, J.-Z. (2016). The dual roles of cytokines in Alzheimer's disease: update on interleukins, TNF- α , TGF- β and IFN- γ . *Transl. Neurodegener.* 5 (1), 7. doi:10.1186/s40035-016-0054-4
- Zhu, J., Li, X., Yin, J., Hu, Y., Gu, Y., and Pan, S. (2018). Glycocalyx degradation leads to blood-brain barrier dysfunction and brain edema after asphyxia cardiac arrest in rats. *J. Cereb. Blood Flow. Metab.* 38 (11), 1979–1992. doi:10.1177/0271678X17726062
- Zhu, J., Li, Z., Ji, Z., Wu, Y., He, Y., Liu, K., et al. (2021). Glycocalyx is critical for blood-brain barrier integrity by suppressing caveolin1-dependent endothelial transcytosis following ischemic stroke. *Brain Pathol.* 32, e13006. doi:10.1111/bpa.13006
- Zhu, W. M., Neuhaus, A., Beard, D. J., Sutherland, B. A., and DeLuca, G. C. (2022). Neurovascular coupling mechanisms in health and neurovascular uncoupling in Alzheimer's disease. *Brain* 145 (7), 2276–2292. doi:10.1093/brain/awac174
- Zou, Z., Li, L., Schafer, N., Huang, Q., Maegele, M., and Gu, Z. (2021). Endothelial glycocalyx in traumatic brain injury associated coagulopathy: potential mechanisms and impact. *J. Neuroinflammation* 18 (1), 134. doi:10.1186/s12974-021-02192-1



OPEN ACCESS

EDITED BY

Brian Gene Coon,
Oklahoma Medical Research Foundation,
United States

REVIEWED BY

Jorge Castorena-Gonzalez,
Tulane University, United States
Gisele Facholi Bomfim,
Federal University of Mato Grosso, Brazil

*CORRESPONDENCE

C. Javier Rendon,
✉ rendonj1@msu.edu

RECEIVED 02 April 2024

ACCEPTED 20 June 2024

PUBLISHED 12 July 2024

CITATION

Rendon CJ, Sempere L, Lauver A, Watts SW and Contreras GA (2024), Anatomical location, sex, and age modulate adipocyte progenitor populations in perivascular adipose tissues. *Front. Physiol.* 15:1411218. doi: 10.3389/fphys.2024.1411218

COPYRIGHT

© 2024 Rendon, Sempere, Lauver, Watts and Contreras. This is an open-access article distributed under the terms of the [Creative Commons Attribution License \(CC BY\)](#). The use, distribution or reproduction in other forums is permitted, provided the original author(s) and the copyright owner(s) are credited and that the original publication in this journal is cited, in accordance with accepted academic practice. No use, distribution or reproduction is permitted which does not comply with these terms.

Anatomical location, sex, and age modulate adipocyte progenitor populations in perivascular adipose tissues

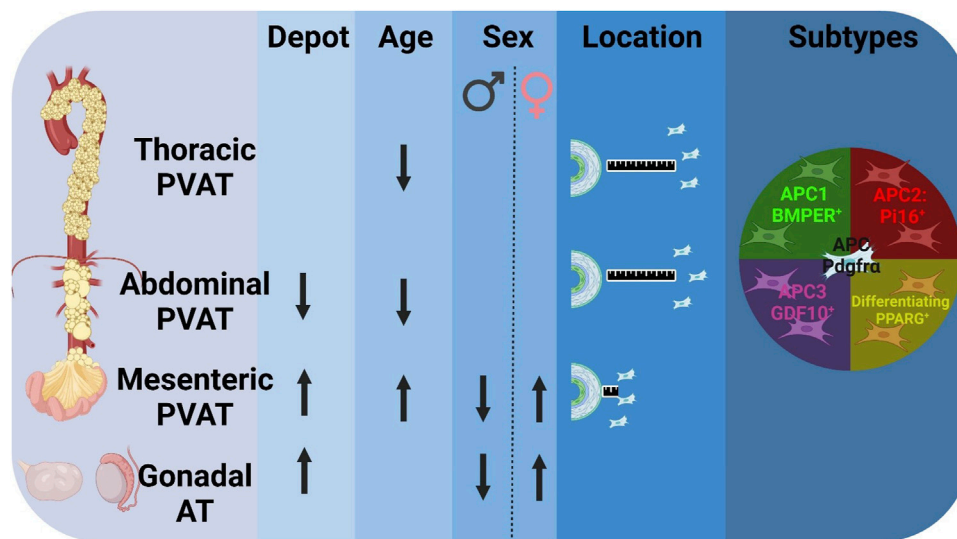
C. Javier Rendon^{1*}, Lorenzo Sempere², Adam Lauver³,
Stephanie W. Watts³ and G. Andres Contreras¹

¹Department of Large Animal Clinical Sciences, College of Veterinary Medicine, Michigan State University, East Lansing, MI, United States, ²Department of Radiology and Precision Health Program, Michigan State University, East Lansing, MI, United States, ³Department of Pharmacology and Toxicology, Michigan State University, East Lansing, MI, United States

Perivascular adipose tissue (PVAT) regulates vascular function due to its capacity to synthesize vasoactive products and its mechanical properties. PVATs most abundant cells are adipocytes, and their populations are maintained by the maturation of adipocyte progenitor cells (APC), which may play a pivotal role in the pathogenesis of cardiovascular diseases. However, the distribution of APC within PVAT depots, their potential variation in spatial location, and the influence of sex and age on their abundance remain unknown. We hypothesize that APC abundance in PVAT is affected by location, age, sex and that APC subtypes have specific spatial distributions. PVAT from thoracic and abdominal aorta, and mesenteric arteries, and AT from interscapular, gonadal, and subcutaneous depots from 13-week and 30-week-old females and males *Pdgfra-CreERT2* x *LSL-tdTomato* mice ($n = 28$) were analyzed. Abdominal aorta PVAT had fewer progenitors than mesenteric PVAT and gonadal AT. Aging reduced the abundance of APC in the thoracic aorta but increased their numbers in mesenteric PVAT. Females had more APC than males in mesenteric PVAT and gonadal AT depots. APC exhibited unique spatial distribution in the aorta and mesenteric PVAT where they localized neighboring vasa vasorum and arteries. APC subtypes (APC1, APC2, APC3, diff APC) were identified in all PVAT depots. Thoracic aorta PVAT APC3 were located in the adventitia while diff APC were in the parenchyma. This study identified variability in APC populations based on depot, age, and sex. The distinctive spatial distribution and the presence of diverse APC subtypes suggest that they may contribute differently to cardiovascular diseases-induced PVAT remodeling.

KEYWORDS

hypertension, adipocyte, remodeling, stem cell, fat, progenitors



GRAPHICAL ABSTRACT

Adipocyte Progenitor Cells (APC) from Perivascular Adipose Tissue (PVAT) is affected by depot, age, sex, and are distributed in different subtypes. Percentage of APC (Pdgfra⁺) differs by depot: fewer APC in abdominal PVAT compared to mesenteric PVAT and gonadal adipose tissue (AT). Aging reduced the APC in aortic PVAT, while increased abundance in mesenteric PVAT. Sex differences in mesenteric PVAT and gonadal AT evidence increased APC in females compared to males. More APC (white) were found farther away from aorta in aortic PVAT vs. mesenteric PVAT. APC subtypes are found in all different PVAT depots. (Arrows represent (↑) increase or (↓) decrease abundance of APC (Lin-⁺CD31-⁻/CD45-⁻/Pdgfra⁺) in total live cells in stromal vascular fraction. BMPER: Bone morphogenic protein endothelial receptor, PI16: Proteinase inhibitor, GDF10: Growth differentiation factor 10, PPARG: Peroxisome proliferator activator receptor gamma.

1 Introduction

Hypertension and other cardiovascular diseases alter the structure of conduit (e.g., thoracic and abdominal aorta) and resistance (e.g., mesenteric arteries) vessels (Khavandi et al., 2009; Van Varik et al., 2012; Lima et al., 2019; Nosalski et al., 2020; Wang et al., 2022; Zhuang et al., 2022). This remodeling process encompasses extracellular matrix deposition and the proliferation of diverse cell types in the intima, media, and adventitia tunics. However, it is less well known if the same processes occur in the tunica adiposa also known as perivascular adipose tissue (PVAT). In other AT, remodeling processes induced by catabolic or anabolic states are driven by the proliferation and differentiation of adipocyte progenitor cells (APC). Understanding the population dynamics of APC in PVAT is important since this tunica regulates blood pressure through the secretion of vasoactive compounds released by its cellular components (mainly adipocytes) and by modulating the biophysics of the vascular structure (Cao et al., 2017; Tuttle et al., 2022).

In general, AT's adipocyte populations are maintained by adipogenesis of APC. This proliferative population is a subset of stem cells that retain the pluripotent capacity to differentiate into multiple cell types other than adipocytes (Pereira et al., 1995; Krebsbach et al., 1997; Pittenger et al., 1999; Merrick et al., 2019). Platelet-derived growth factor receptor alpha (PDGFRα) is broadly expressed in PVAT and non-PVAT depots and is considered a *bona fide* marker for APC (Lee et al., 2012; Berry and Rodeheffer, 2013; Contreras et al., 2016). Multiple independent research groups have isolated cells expressing PDGFRα and demonstrated that these cells preferentially differentiate into adipocytes in several ATs *in vivo* and *in vitro* (Lee et al., 2012; Berry and Rodeheffer, 2013; Contreras et al.,

2016; Wang et al., 2018; Shin et al., 2020). Specifically, one of these studies demonstrated that transplantation of PDGFRα⁺ cells subcutaneously *in vivo* can contribute 20-fold more to the adipocyte population vs. PDGFRα⁻ cells (Lee et al., 2012). Upon differentiation, APC expresses PPARG, the key master regulator of adipogenesis that triggers many of the metabolic functions of adipocytes (Tontonoz et al., 1998; Barak et al., 1999). Physiological factors have a strong influence on progenitors' populations. One of them is sex. Estrogens, for example, promote the proliferation of progenitor cells in female animals (Zhang et al., 2016; Bjune et al., 2022). Age also impacts APC populations with reports indicating a reduction in the proliferation and differentiation capacities of these progenitors as animals get older (Kirkland et al., 1990; Park et al., 2021). However, the effect of sex, age, and PVAT's anatomical localization on APC remains unknown.

Recent single-cell transcriptomics studies identified APC phenotypic variability (Angueira et al., 2021; Burl et al., 2022; Thompson et al., 2023). In interscapular brown adipocyte tissue (BAT), three APC subtypes were described (Burl et al., 2022). APC1 is characterized by expression of bone morphogenic protein endothelial receptor (*Bmper*), APC2 expressing proteinase inhibitor 16 (*Pi16*), and APC3 that expresses growth differentiating factor 10 (*Gdf10*). Notably, APC subtypes express marker genes related to extracellular matrix deposition and cellular phenotype related to PVAT remodeling. In BAT, APC1 preferentially differentiates into adipocytes (Burl et al., 2022; Garritson et al., 2023). APC2 express markers related to TGF-β signaling, a potent fibrogenic pathway, indicating a possible preference for fibrogenic fate (Soare et al., 2020; Ohm et al., 2023). APC3 are associated with osteogenesis differentiation and ossification of carotid arteries (Hino et al., 2012; Brandt et al.,

2022). Remarkably, APC subtypes exhibit unique spatial distribution in BAT. APC1 are mainly localized in the parenchyma while APC2 are abundant in the fascia and APC3 neighboring blood vessels. The spatial distribution patterns of APCs and their subtypes in PVAT are unknown. Thus, it is relevant to elucidate how different APC could contribute to PVAT remodeling differently.

This study aimed to determine the presence of APC and their subtypes in different PVAT and AT depots and evaluate the effect of sex, age, and anatomical location on APC distribution. We hypothesize that APC abundance is modified by anatomical location, age, sex and that APC subtypes have specific spatial distributions. Our findings reveal the ubiquitous presence of APCs within PVAT depots and demonstrate their abundance varies across sexes, ages, and depots. Notably, different APC subtypes exhibit distinct spatial distributions within PVAT. These combined observations suggest heterogeneity in the APC response to hypertension, potentially influencing vascular remodeling in a sex-, age-, and anatomically-dependent manner during hypertensive states.

2 Materials and methods

2.1 Animal models and tissue collections

B6.129S-Pdgfratm1.1 (cre/ERT2)Blh/J (Pdgfra-CreERT2 mice; stock no. 032770 RRID:IMSR_JAX:032770), and B6.Cg-Gt (ROSA)26Sor_{tm9}(CAG-tdTomato)Hze/J (LSL-tdTomato; stock no. 007909 RRID:IMSR_JAX:007909) mice were purchased from Jackson Laboratory. All mice were housed at 22°C ± 2°C with a 12:12 h light-dark cycle in an AAALAC-approved animal facility at Michigan State University (East Lansing, MI). Mice were fed a standard chow diet of 18% protein *ad libitum* (Teklad, 2918). Animal protocols were approved by the Institutional Animal Care and Use Committee at Michigan State University (#PROTO202000239) and followed the “Guide for the Care and Use of Laboratory Animals,” 8th edition (Courtney et al., 2021). All mice were euthanized with carbon dioxide administration at a 30%–70% flow rate at 13 or 30 weeks of age, clinical death was confirmed after the mice stopped breathing, the corneal reflex was absent, and no heartbeat could be felt. Final confirmation of death included cervical dislocation. The 13 weeks of age was selected because animals at this age are considered young adults. In humans, this age segment is the early age at which hypertension starts to develop. The 30 weeks of age was selected because animals at this age are considered mid-age adults. In humans, the prevalence of hypertension increases twice after 50 years (mid-age) in both sexes (Flurkey et al., 2007; National Center for Health Statistics, 2018).

2.2 Cre recombination induction in transgenic mice

Cre recombination in Pdgfra-CreERT2 x LSL-tdTomato mice was induced by administering tamoxifen dissolved in corn oil (Sigma, T5648-5G, 30 mg/mL) once per day (150 µg/gr,

intraperitoneal) for 5 consecutive days. Littermates without a Pdgfra-CreERT2 allele (Pdgfra-CreERT2 ^{-/-} mice) were used as controls. To visualize APC, we employed the progeny of Pdgfra-CreERT2 x LSL-tdTomato mice. Upon tamoxifen induction, Pdgfra⁺ cells permanently express the fluorescent protein tdTomato, allowing us to effectively visualize APC populations. Euthanasia and tissue collections were performed 7 days after the first tamoxifen administration, the time when the peak of recombination occurs without affecting the proliferation or differentiation of cells (Donocoff et al., 2020; O'Rourke et al., 2016).

2.3 Blood pressure measurements

Blood pressure measurements were made using sphyngomanometry in conscious, restrained, and warmed mice. Measures were taken in healthy animals before any procedures. Animals were acclimated for 3 days before measurements were considered accurate. Animals were restrained using a device to maintain body temperature and keep animal calm. Measurements were made in the CODA system (High Throughput System, Kent Scientific, Torrington, CT, United States). Tail cuff was inflated 15 times (to a pressure of 250 mm Hg with a slow deflation over period of 20 s) with 30-s intervals between inflations. Blood pressure was obtained during each inflation cycle by a volume pressure recording sensor; the final reading was the average of ten inflations. 15 cycles were recorded. Systolic, diastolic, and mean arterial pressure are reported. Once measures were done, animals were returned to their cage.

2.4 Adipose tissue collections

Non-PVAT depots including interscapular brown AT (BAT), inguinal subcutaneous AT (SCAT), perigonadal AT (GON), and PVAT depots thoracic aorta (ATPVAT), abdominal aorta (ABPVAT) and mesenteric arteries (MESPVAT), were dissected and then immersed in Krebs-Ringer Bicarbonate Buffer (KRBB) containing NaCl 135 mM; KCl 5 mM; MgSO₄ 1 mM; KH₂PO₄ 0.4 mM; Glucose 5.5 mM; HEPES 20 mM (pH 7.4) (Teknova, Cat N° H1030) and supplemented with 100 units/mL of penicillin; 100 µg/mL of streptomycin, 0.25 µg/mL of Amphotericin B and 50 µg/mL of Gentamicin. Under a stereo microscope and on a Silastic-coated dish filled with KRBB, BAT was cleansed of adherent white fat subcutaneous tissue; PVAT was dissected from the aorta and mesenteric arteries, and GON was removed from ovaries and testis.

2.5 Adipose tissue enzymatic digestions

AT's stromal vascular fraction (SVF) was isolated as previously described (Contreras et al., 2016). Briefly, AT depots were collected and minced into small fragments (1–3 mm) and then digested for 1 h at 37°C in a rotisserie incubator using 0.5 mg/mL of LiberaseTM TL (Roche diagnostics, Cat N° 5401020001) dissolved in Hanks' balanced salt solution supplemented with 4% BSA (Bovine serum albumin; Fisher, Cat N° BP9706-100) and 10 mM HEPES. Digested material was filtered through 70 µm cell strainers (Corning, Cat N° 22363548) and then centrifuged for 5 min at 300 x g at 4°C to remove

the buoyant cells (adipocytes) from the SVF containing APCs. Pellets were resuspended in RBC lysis buffer 1X (Biolegend, Cat N° 420301), incubated at room temperature for 5 min, and then centrifuged for 5 min at 300 x g at 4°C.

2.6 Flow cytometry

SVF pellets were resuspended and incubated for 10 min at 4°C with 10 µL of FcR blocking reagent (Miltenyi Biotec, Cat N° 130-092-575) in 90 µL of FACS solution containing 1X Dulbecco's PBS, 2% FBS, 0.1% sodium azide (ThermoFisher Cat N° 26628-22-8) for non-specific antibody binding. To exclude dead cells, all samples were incubated with Biolegend Zombie NIR™ fixable viability dye (Biolegend Inc, Cat N° 423106; 1:500 in FACS). Next, cells were incubated with a pool of conjugated monoclonal primary antibodies for 30 min (Pacific Blue™ anti-mouse CD45 RRID: AB_2876534 (1:50); Brilliant Violet 785™ anti-mouse CD31 RRID: AB_2810334 (1:100)). Before conducting the experiments, the optimal concentrations of all primary antibodies were determined through titration. Following primary incubation, cells were washed, fixed with 2% paraformaldehyde in PBS, washed, and resuspended in FACS solution. In each experiment for gating selection, fluorescence minus one (FMO) control was made for all markers used using one sample. UltraComp eBeads™ (ThermoFisher, Cat N° 01-2222-41) beads were used to do single-stained control of each marker. Data acquisition and compensation were performed in Cytex® Aurora System (Cytex Biosciences, Fremont, CA) using the SpectroFlo® software (Cytex Biosciences) and analyzed in FCS express V.7 (DeNovo Software, Pasadena, CA). A gate was drawn to allow the exclusion of aggregates/doublets and another to exclude cellular debris. Gating strategies are summarized in [Supplementary Figure S1](#). Briefly, singlet events and live cells were included, while hematopoietic cells (CD45⁺) and endothelial cells (CD31⁺) were excluded. APC were defined as tdTomato⁺. Flow cytometry results are expressed as the percentage of the specified population relative to the total of live cells.

2.7 Immunohistochemistry

Aorta/mesenteric arteries with complete PVAT were cleaned of blood and paraformaldehyde-fixed for 24 h at room temperature, then embedded in paraffin blocks. Tissue sections (5 microns thick) were cut and mounted on Superfrost® Plus microscope slides (Thermo Scientific, Cat N° 12-550-15) dried at 56°C and stored at room temperature (RT) by the MSU Investigative Histopathology laboratory. To de-paraffinize, slides were washed 2 times with Histochoice Clearing Agent (VWR, Cat N° H103) and 4 times with isopropanol (VWR, Cat N° 9084-03) and 2 times with distilled water for 3 min (min) each wash. Antigen retrieval was performed by boiling slides for 30 s in Antigen Unmasking Solution (Vector Laboratories, Cat N° H3301). Slides were rinsed in distilled water and air dried. To contain the blocking serum, primary and secondary antibody solutions, circles were drawn around the sections with an ImmEdge Hydrophobic pen (Vector Laboratories, Cat N° H-4000). Slides were incubated at RT with 1.5% normal goat serum (Vector Laboratories, Cat N° S-1000) in Dulbecco's phosphate-buffered saline (PBS) (Sigma-Aldrich, Cat N° D8537) blocking solution (BS) for 1 h. Positive control sections were incubated with anti-red fluorescent protein (Rockland Lab, Cat N° 600-401-379; 1:1000) and anti-alpha

SMA-FITC (Sigma F3777; 1:500) in 1.5% normal goat serum BS, and negative control sections were incubated with BS overnight at 4°C. Negative controls were included without the addition of primary control in [Supplementary Figure S2](#). The primary antibody and BS were removed from the sections and the slides were rinsed in Dulbecco's PBS 3 times for 5 min each rinse. The slides were incubated in anti-rabbit secondary antibody AlexaFluor 568 (ThermoFisher, Cat N° A11036; 1:1000) for 1 h at RT. The secondary antibody was removed, and slides were rinsed 3 times with Dulbecco's PBS for 5 min and allowed to dry thoroughly at RT. Vectashield with DAPI (Vector Laboratories, Cat N° H-1500) was applied to the sections and coverslips mounted to the slides. The slides were allowed to dry and harden at 4°C overnight. Images were acquired at 360, 488, and 544 nm on a Nikon C1 microscope, using a ×20 objective, Nikon DS-Qi1MC camera, and NIS elements BR 4.6 software.

2.8 Automated quantification of confocal imaging

Color channels from the immunohistochemistry confocal images were exported using NIS-elements viewer v5.21. After exporting the images to QuPath v0.4.4 software ([Courtney et al., 2021](#)), color channels were split and only blue (nuclei) and red (APC) were used for the analysis. Three random regions of interest (ROI) were drawn, and only adipose tissue was included while blood vessels and adventitia were excluded. Blue objects were used for cell detection, and APCs were identified using a single measurement classifier as blue objects co-expressing red signals. Data presented is a percentage of APC in the total number of nuclei per ROI.

2.9 Spatial distribution analysis

Confocal images of immunohistochemistry sections were analyzed using PyBioProx v1.0.3 as previously described ([Dyer et al., 2020](#)). Briefly, using ImageJ confocal images were converted into RGB format. Then, each color channel was separated. A threshold was applied to the red (APC) and green (SMA/aorta) channels and a mask was created for each color. The new mask was exported to PyBioProx developed for Phyton. The distances from one object in red (APC) and the nearest object in green (SMA) were quantified by the software and then transformed to µm (0.62µm/px). The different distances were divided into 11 bins ranging from the nearest distances (0–21 µm) to the farthest distances (>201 µm). The percentage of APC on each bin was graphed and analyzed using GraphPad Prism v.9.

2.10 Multiplex immunohistochemistry (5-plex)

Tissue sections were prepared and stained in the Leica Bond-Rx station as previously described ([Sempere et al., 2020](#)). Briefly, tyramide signal amplification stain cycles were performed as followed for each marker after heat-induced epitope retrieval (20 min at 99°C with ER2 solution, EDTA pH = 9); incubation for 30 min with primary antibody, then an incubation with Goat

anti-rabbit HRP (Bio-rad, Cat N° STAR124P; dilution) or as appropriate for additional 30 min, followed by tyramide-conjugated fluorochrome (FITC, Rhodamine, DyLight 521, DyLight 594, DyLight 650). Rabbit anti-mouse primary antibodies used were anti-BMPER (1:100; ThermoFisher Cat N° BS-6910R), PI16 (1:100; Novusbio Cat N° NBP1-92254), GDF10 (1:500; ThermoFisher Cat N° BS-5720R), PPARG (1:600; ThermoFisher Cat N° MA5-14889), tdTomato/RFP (1:1000; Rockland Lab Cat N° 600-401-379). Between each stain cycle, after 15 min incubation with 3% H₂O₂ to inactivate HRP, samples were blocked with Normal rabbit serum (1:20; Jackson Lab, Cat N° 011-000-120) for 30 min each before continuing with the next stain cycle. After staining, slides were counterstained with DAPI nuclear marker for 15 min and immediately mounted and coverslipped with Prolong Gold antifade reagents with DAPI (ThermoFisher, Cat N° P36930) and imaged in the Aperio VERSA scanner (Leica Biosystems).

2.11 Co-expression quantification analysis

Multiplex (5-plex) immunofluorescence images were analyzed using the ImageScope x64 software (Leica Biosystems). Aperio Cellular IF Algorithm (Leica Biosystems, Cat N° 23CIFWL) was used for APC subtype classification based on differential marker expression. First, nuclei were identified based on the DAPI fluorescence intensity. Then cell segmentation was performed creating a mask 5 μm away from the nuclei border. We used fluorescence intensity to create a threshold to label positive cells for each channel. APC were defined as tdTomato+, while APC subtypes were defined as follows. APC1: tdTomato+/BMPER+, APC2: tdTomato+/PI16+, APC3: tdTomato+/GDF10, and diff APC (differentiating): tdTomato+/PPARG. Images of the separations of the different channels is depicted in [Supplementary Figure S3](#). The analysis was done in three regions of interest (ROI): adventitia, parenchyma, and fascia (outer layer of PVAT). The average ROI area were parenchyma: $106,943 \pm 31,138 \mu\text{m}^2$, fascia: $71,926 \pm 45,453 \mu\text{m}^2$, and adventitia: $53,524 \pm 3,659 \mu\text{m}^2$.

2.12 Statistical analysis

Data is reported as mean \pm SEM. Data were analyzed by one- or two-way ANOVA using GraphPad Prism v9 software and JMP pro16. Normality assumptions were assessed using the D'Agostino-Pearson test. Post hoc comparisons were performed using the Kruskal-Wallis test. Statistical significance was set at $p \leq 0.05$.

3 Results

3.1 Blood pressure is similar in double transgenic mice regardless of sex and age

Blood pressure measurements of healthy double transgenic Pdgfra-Cre-LSL-tdTomato are shown in [Table 1](#). Mean arterial blood pressure (MAP) between females and males at 13- and 30-weeks of age did not differ.

3.2 APC are present in PVAT, and their abundance varies by anatomical location

Flow cytometry analysis demonstrated that the percentage of APC in SVF from different AT varied by anatomical location, including PVAT depots. Combined data from both sexes and ages demonstrated that in ATPVAT, APC were $2.86\% \pm 0.31$ of the SVF population. In other PVAT depots, APC were $2.18\% \pm 0.24$ of SVF in ABPVAT and $4.71\% \pm 0.51$ in MESPVAT. In non-PVAT depots: BAT had $2.99\% \pm 0.38$ of APC, SCAT $2.55\% \pm 0.28$ and GON $4.71\% \pm 0.51$. Comparing the abundance among all different depots, we found that ABPVAT had fewer APC in total live cells than MESPVAT and GON depots ([Figure 1A](#)). To confirm the presence of APC in the different depots we used confocal microscopy to identify PDGFR α expressing cells (tdTomato+). In all depots regardless of their location, we observed APCs ([Figure 1B](#)). Quantification of the abundance of APC from the total nuclei in the confocal images from PVAT depots demonstrated that APC were more abundant in MESPVAT (13.28% of total nuclei ± 1.03) vs. ATPVAT ($5.94\% \pm 0.7$) and ABPVAT ($6.8\% \pm 1.16$) ([Figure 1C](#)).

3.3 Aging reduces APC abundance in PVAT around aorta

Next, we evaluated the effect of aging on APC populations. In ATPVAT, 30-week-old animals had lower abundance of APCs ($2.28\% \pm 0.33$) compared to 13-week-old animals ($3.36\% \pm 0.47$) ($p < 0.05$). A similar response was observed in the ABPVAT with 30-week-old mice having fewer APCs ($1.63\% \pm 0.26$) vs. 13-week-old ($2.77\% \pm 0.38$) ($p < 0.05$). In contrast, MESPVAT from 30-week-old animals had higher % of APC ($4.93\% \pm 0.78$) compared to 13-week-old mice ($2.91\% \pm 0.73$) ($p < 0.05$). Finally, no differences in APC abundance were observed in non-PVAT depots by age. ([Figure 2A](#)). Confocal imaging of PVAT depots reflected flow cytometry results, we observed fewer APCs in ATPVAT and ABPVAT from 30-week-old than 13-week-old mice. In contrast, APC populations increased with age in MESPVAT. ([Figure 2B](#)). Image analysis showed a tendency for less APC in ATPVAT between 13 weeks old ($7.2\% \pm 1.2$) vs. 30 weeks old ($5\% \pm 0.77$) ($p = 0.07$). On the other hand, more APC were found in the MESPVAT from 30-week animals ($15.29\% \pm 1.32$) vs. 13-week animals ($11.06\% \pm 1.32$) ($p < 0.05$) ([Figure 2C](#)).

3.4 Mesenteric PVAT and gonadal APC populations exhibit sexual dimorphism in 30-week-old mice

The effect of sex on APC populations was evaluated on each depot and age group separately. Thirteen-week-old mice did not show differences by sex on PVAT and other AT depots. However, in thirty-week-old animals, sex had a strong effect on MESPVAT and GON depots. MESPVAT from females had more APCs ($6.07\% \pm 0.82$) compared to males ($2.13\% \pm 0.42$). There were more APCs ($8.64\% \pm 1.16$) in GON from females vs. males ($1.69\% \pm 0.35$; [Figure 3A](#)). However, quantification of APC in confocal microscopy images showed no differences between the sexes ([Figures 3B,C](#)).

TABLE 1 Mean arterial blood pressure (MAP), systolic blood pressure (SBP), and diastolic blood pressure (DBP) of *Pdgfra-Cre-LSL-tdTomato* mice at 13- and 30-week time points. Two-way ANOVA and Bonferroni test were used. n = 6 for each group.

Groups (n = 6)	MAP (mm Hg)	SBP (mm Hg)	DBP (mm Hg)
Males 13-weeks	85.22 ± 4.9	101 ± 5.001	77.73 ± 4.9
Females 13-weeks	89.86 ± 4.3	109.7 ± 4.5	80.4 ± 3.3
Males 30 weeks	94.10 ± 10.2	104.7 ± 4.5	77.91 ± 4.5
Females 30 weeks	97.69 ± 10.5	109.5 ± 3.4	81.60 ± 4.93

3.5 Mesenteric PVAT APCs are more abundant in proximity to blood vessels compared to other PVAT depots

The spatial distribution of APCs was evaluated using confocal images from ATPVAT, ABPVAT, and MESPVAT (Figure 4A). The proximity of APC to the nearest blood vessel (stained with alpha-actin SMA) was determined using PyBioProx (Dyer et al., 2020). Near blood vessels (21–40 μm), APCs were more abundant in MESPVAT (26.85% ± 4.9) compared ATPVAT (15.11% ± 1.59) and ABPVAT (16.89% ± 1.19; *p* < 0.05) in both 13 and 30-weeks old mice. At more distant locations (61–80 μm), MESPVAT had fewer APC (3.78% ± 1.26) compared to ATPVAT (12.96% ± 0.65) and ABPVAT (13.76% ± 0.68) in 13-week-old mice. Similarly, in 30-week-old mice, there were fewer APC in MESPVAT (8.32% ± 2.05) compared to ATPVAT (11.91% ± 0.80) and ABPVAT (12.06% ± 0.74) (Figure 4B).

3.6 PVAT harbors APC subtypes regardless of sex and age

ATPVAT (Figure 5A), ABPVAT (Figure 5B), and MESPVAT (Figure 5C) depots were stained with antibodies to identify APC1, APC2, APC3, and differentiating APC subtypes. Within PVATs, parenchyma and the adventitia were analyzed for APC abundance. Diff APCs were the most abundant populations (81.85% ± 8.001) in ATPVAT parenchyma while in the adventitia, the most prevalent APC subtype was APC3 (76.23% ± 12.7) (Figure 5A). In the ABPVAT, all APC subtypes were found in the parenchyma and adventitia without differences in their spatial distribution (Figure 5B). Finally, in MESPVAT parenchyma we observed that APC2 (96.84% ± 1.5) and APC3 (97.81% ± 1.4) were the most prevalent APC. No differences between APC subtypes were observed in the adventitia (Figure 5C).

4 Discussion

4.1 Blood pressure was similar between sex and age

Our data demonstrate that blood pressure in double transgenic *Pdgfra-Cre-LSL-tdTomato* was not affected by sex and there were no differences between 13-week and 30-week-old mice. The systolic blood pressure in our study ranged from 95 to 127 mm Hg, values that can be considered normotensive [100–120 mm Hg (Ichihara et al., 2001; Ciuceis et al., 2005; Zhang et al., 2010; Lu et al., 2015)].

Interestingly, previous studies have found differences in blood pressure that vary depending on genetic backgrounds. Males C57BL/6J have higher systolic BP than females at 21 weeks of age, but these responses were not observed in FVB/N mice (Barsha et al., 2016). Our results demonstrate that there are no differences in blood pressure between sexes at two time points evaluated and that the responses of APC are not due to differences in blood pressure.

4.2 The effect of anatomical location on APC pools

Here we identified APC in PVAT and non-PVAT depots. Flow cytometry analyses indicate APC populations ranged from 0.5% to 13% of SVFs. Previous studies in rodents reported similar APC abundances ranging from 1.5% to 14% (Berry and Rodeheffer, 2013; Lee et al., 2013; Contreras et al., 2016; Angueira et al., 2021; van Kuijk et al., 2023). In non-PVAT depots such as GON and SCAT the abundance of APC is around 3% (Lee et al., 2013), in mammary AT between 2% and 5.2% (Wang et al., 2018), and in intermuscular AT around 10% of the SVF (Uezumi et al., 2010). Regarding PVAT depots, our group reported that PDGFRα⁺ cells comprise 1.5% of SVF from ATPVAT and 3% of the same cellular fraction in MESPVAT (Contreras et al., 2016). Seale et al. established that APC populations account for 5% of cells in SVF from ATPVAT. In contrast, Sluimer and colleagues reported 14% APC in SVF from ATPVAT and 8% from ABPVAT (van Kuijk et al., 2023). Different factors could contribute to the variability among studies. First, the markers used to identify progenitors were different among studies. Previous reports have used stem cell antigen 1, CD34, and/or CD24. Here, we defined APC as PDGFRα because it is a marker of committed preadipocytes and can be found across PVAT and non-PVAT depots (Contreras et al., 2016). Second, ages were different among studies, ranging from 8 to 30 weeks old. Additionally, previous studies did not evaluate sex differences, some used only males (Berry and Rodeheffer, 2013; van Kuijk et al., 2023) or combined data from males and females (Lee et al., 2013; Angueira et al., 2021). Third, flow cytometry commonly uses antibodies to detect PDGFRα on the cell surface. When using enzymatic digestions, the structure of many surface proteins can be affected, possibly reducing the sensitivity and specificity of the antibody/antigen binding. To address the latter, we used the lineage tracing model and based APC quantification on the reporter signal (td-tomato) which confers a better approach to quantifying these populations after enzymatic tissue processing.

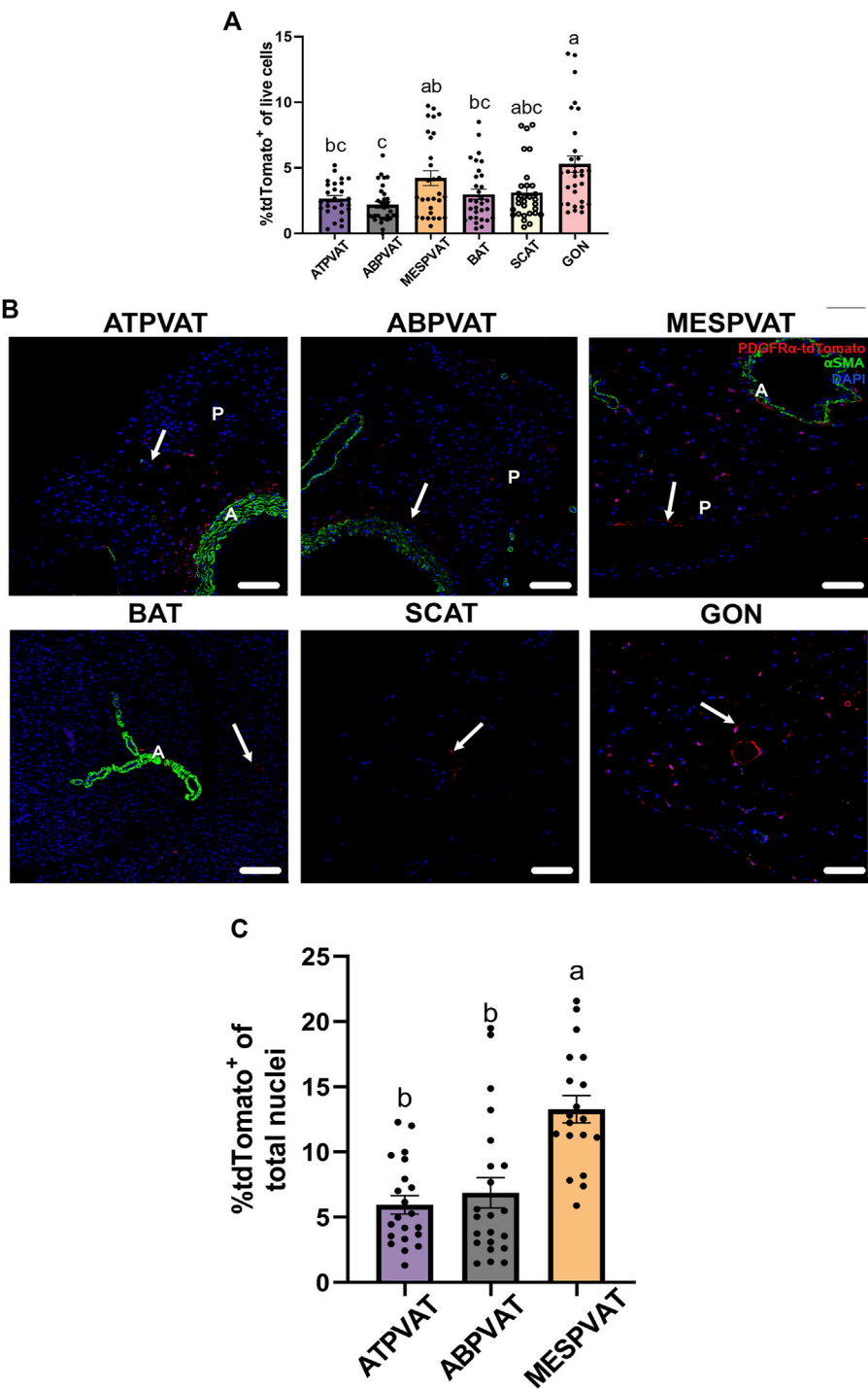


FIGURE 1
Adipocyte progenitor cells (APC) are present in PVAT. **(A)** Adipose tissue (AT) was processed for flow cytometry analysis. Difference in frequency of APCs of total live cells (100%) between AT depots of both males and females at 13-weeks and 30-weeks-old. Data are means \pm SEM. One-way ANOVA and *t*-test with Kruskal-Wallis's correction were used. Significant differences between depots are indicated by different letters a, b, and c ($p < 0.05$). **(B)** Representative images (confocal) of AT sections from PdgfraCre-LSL-tdTomato mice including non-perivascular AT interscapular (BAT), subcutaneous (SCAT), perigonadal (GON) AT and perivascular AT from thoracic aorta (ATPVAT), abdominal aorta (ABPVAT) and mesenteric arteries (MESPVAT). Antibodies against Red Fluorescent Protein (RFP/tdTomato), and alpha smooth muscle actin (α SMA) were used. Red = APC/tdTomato, green: α SMA. DAPI was used as counterstain nuclei. Arrow shows APC (tdTomato⁺). *n* = 30 mice were used. Scale bar: 100 μ m (P = Parenchyma, L = Lumen). **(C)** Quantification of confocal images of PVAT sections. APC (tdTomato⁺) percentage of total nuclei (DAPI) per region of interest (ROI). Three random areas were selected. Data are means \pm SEM. One-way ANOVA with the Kruskal-Wallis's correction test was used. Significant differences between each depot are indicated by different letters a and b ($p < 0.05$).

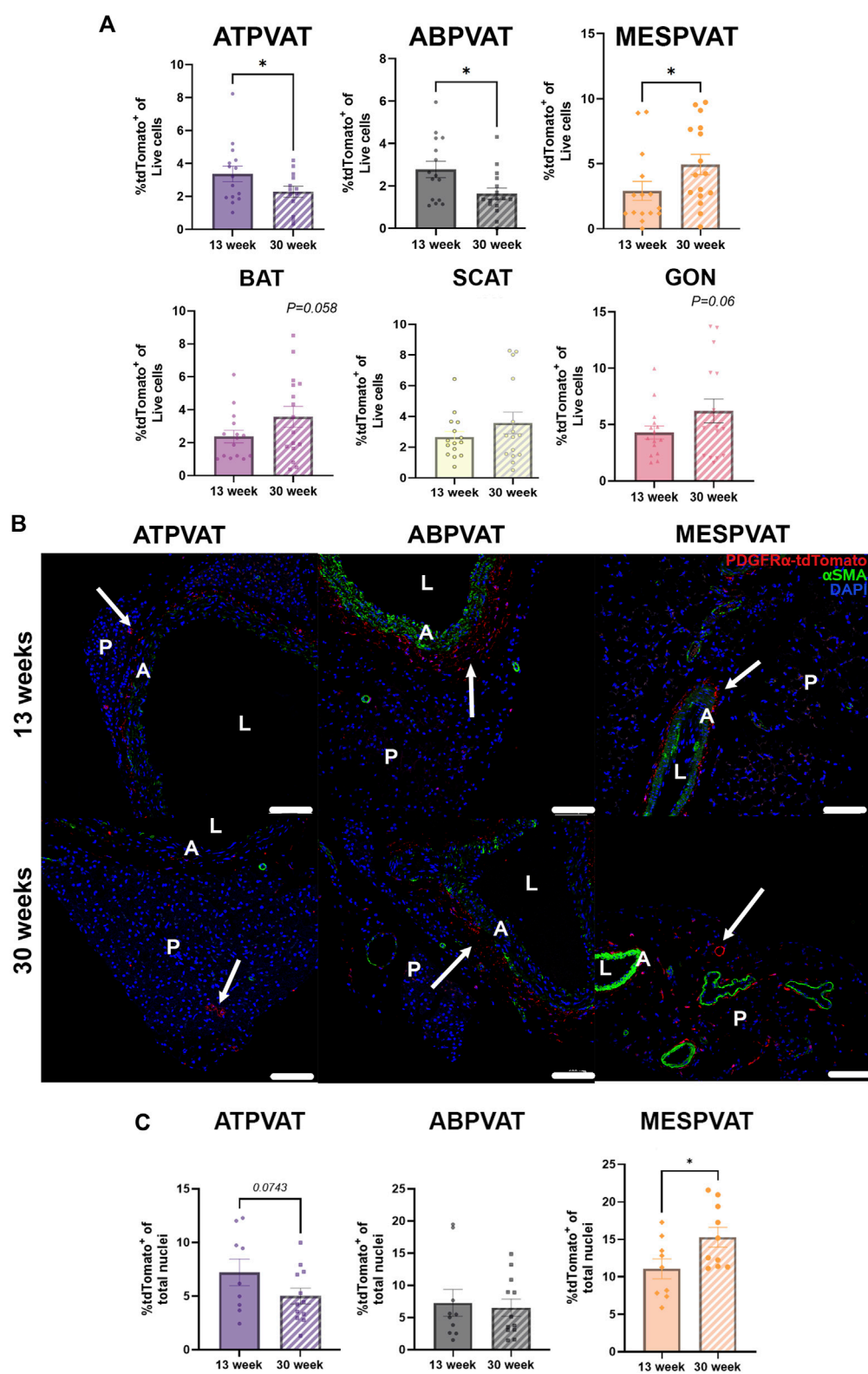


FIGURE 2
Aging reduces adipocyte progenitor cells (APC) populations aortic perivascular adipose tissues (PVAT). **(A)** Frequencies of APC (P1/ Singlets/Live/Lin⁺(CD45⁺/CD31⁺)/tdTomato⁺) in total live cells from perivascular adipose tissues (PVAT) in thoracic aorta (ATPVAT), abdominal aorta (ABPVAT), mesenteric arteries (MESPVAT) and non-PVAT interscapular (BAT), subcutaneous (SCAT), and perigonadal (GON) depots from 13-week and 30-week-old mice. Data are means \pm SEM. One-way ANOVA and *t*-test with Kruskal-Wallis's correction were used. Significant differences between ages on each depot are indicated by * (*p* < 0.05). **(B)** Representative images of ATPVAT, ABPVAT and MESPVAT. APC in red, alpha smooth muscle actin (α SMA) in green, and nuclear stain DAPI blue. Arrows shows APC (tdTomato⁺). *n* = 15 at 13-weeks and *n* = (Continued)

FIGURE 2 (Continued)

16 at 30-weeks were used. Scale bar: 100 μ m (A = aorta/arteries, L = Lumen, P = PVAT). (C) Quantification of confocal images of PVAT sections. APC (tdTomato⁺) percentage of total nuclei (DAPI) per region of interest (ROI). Data are means \pm SEM. *t*-test with Welch's correction was used. Significant differences between ages on each depot are indicated by * ($p < 0.05$).

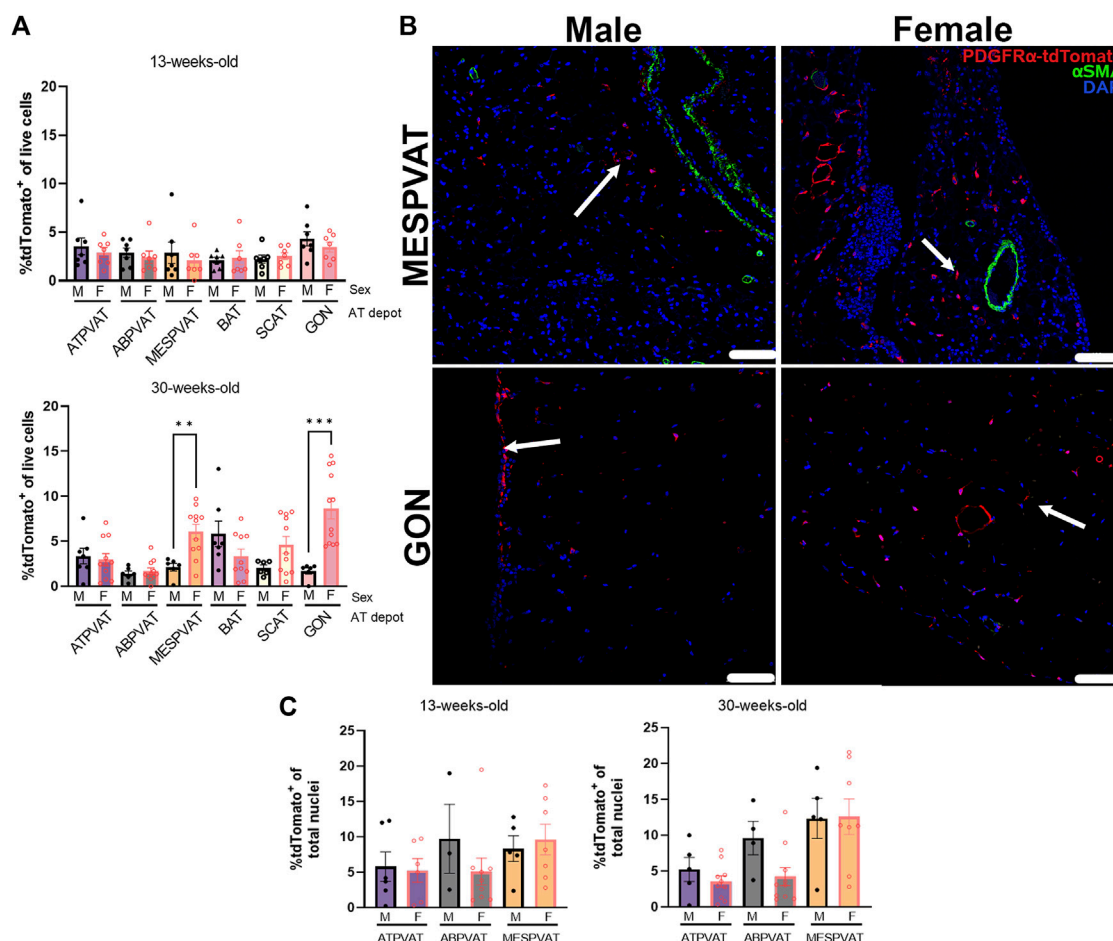


FIGURE 3

Sex differences in APCs populations appear in white AT depots at 30 weeks of age. (A) APC (tdTomato⁺) in total live cells from thoracic aortic perivascular adipose tissue (ATPVAT), abdominal aortic PVAT (ABPVAT), mesenteric arteries (MESPAT), interscapular (BAT), inguinal subcutaneous (SCAT), and perigonadal (GON) depots from males (M) and females (F) of 13-week-old (top) and 30-week-old (bottom). Data are means \pm SEM. Two-way ANOVA and *t*-test with Kruskal-Wallis's correction were used. Significant differences between sexes within each depot are indicated by ** ($p < 0.01$) and *** ($p < 0.001$). (B) Representative confocal images of mesenteric (MESPAT) and perigonadal (GON) adipose tissues comparing 30-week-old male and female mice. TdTomato in red, alpha smooth muscle actin (α SMA) in green, and nuclear stain DAPI blue. Arrow shows APC (tdTomato⁺). $n = 7$ male and $n = 7$ females in 13-weeks group, and $n = 7$ male and $n = 11$ females in 30-weeks group were used. Scale bar: 100 μ m. (C) Quantification of confocal images of PVAT sections. APC (tdTomato⁺) percentage of total nuclei (DAPI) per region of interest (ROI). Data are means \pm SEM. Two-way ANOVA and *t*-test with Welch's correction were used.

In the present study, APC abundance showed differences in an AT depot-dependent manner, with GON having more and ABPVAT having fewer APCs (Figure 1). A smaller APC population in ABPVAT could lead to reduced expansion capacity by hyperplasia and favor hypertrophy in this depot. In metabolic diseases limited preadipocyte hyperplasia is being associated with larger adipocytes and pro-inflammatory environment, changes more prevalent in abdominal PVAT (Strissel et al., 2007; Nishimura et al., 2008; Police et al., 2009; Muir et al., 2016). However, further research is needed to evaluate if low APC abundance affects PVAT remodeling during hypertension and other cardiovascular diseases.

4.3 Effects of aging on APC abundance in PVAT

Aging reduces the abundance of stem progenitor cells in tissues (Lukjanenko et al., 2019; Shcherbina et al., 2020; Von Bank et al., 2021). Previous reports evaluated the proportions of cells in PVAT with common markers of progenitors, including Sca-1⁺/CD34⁺, during aging. Pan and colleagues found no differences in stem cell abundance with aging in PVAT but reported a loss in their brown adipogenic potential (Pan et al., 2019). In the present study, we demonstrated that APCs were reduced in PVAT around the

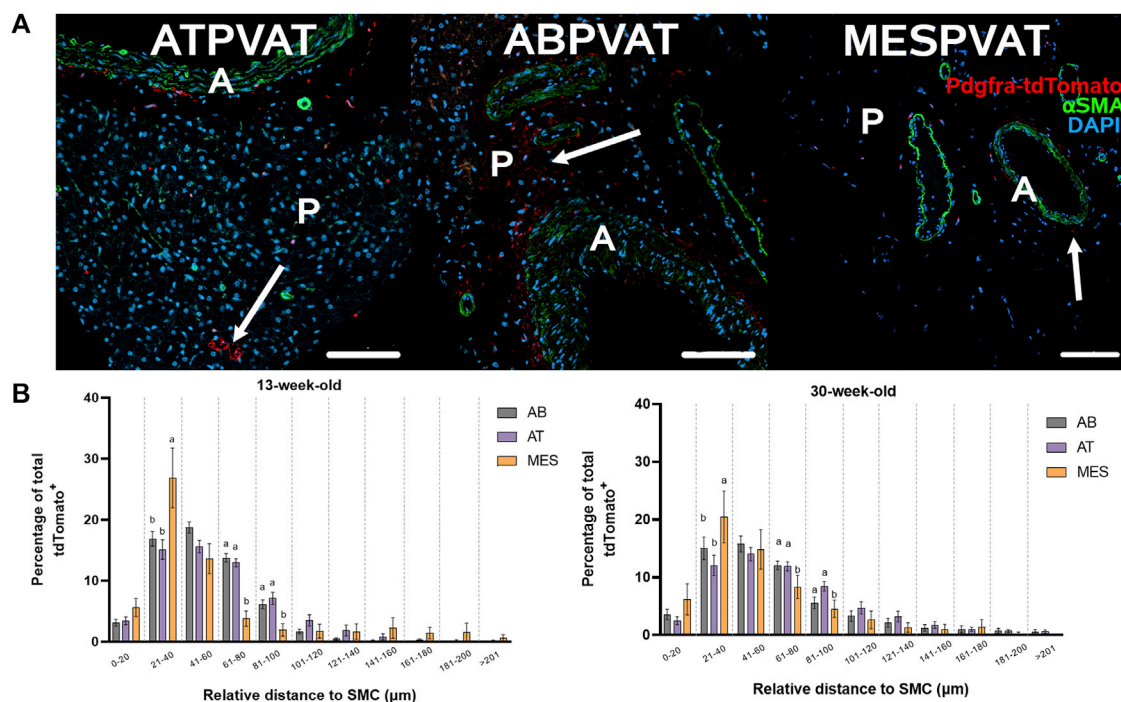


FIGURE 4

APC abundance increases near blood vessels in mesPVAT compared to other PVATs. (A) Representative images of thoracic aortic PVAT (ATPVAT), abdominal aorta PVAT (ABPVAT), and mesenteric arteries (MESPAT). tdTomato in red, alpha smooth muscle actin (αSMA) in green, and nuclear stain DAPI in blue. Scale bar: 100 μm. Arrows show APCs. (B) Distances were measured using PyBioProx on Python. Data is a percentage of APC by bins (separated by a vertical dotted line) of distances relative to the aorta or mesenteric arteries in 13-week-old and 30-week-old animals. AB: ABPVAT, AT: ATPAT, and MES: MESPAT. Data are means ± SEM. Two-way ANOVA and t-test with Welch's correction were used. $n = 7$ AT, $n = 8$ AB, and $n = 6$ MES, animals were used for both age groups. Significant differences between depots on each bin are indicated by different letters a and b ($p < 0.05$).

thoracic and abdominal aorta with aging (Figure 2A). Different mechanisms may explain these effects such as reduced proliferation, decreased viability of progenitors, or loss of self-renewal activity (Kirkland et al., 1990; Oh et al., 2014; Park et al., 2021). Fewer APCs may limit PVAT's adipocyte turnover, which can reduce the secretion of anticontractile factors, consequently promoting higher vascular stiffness, an outcome observed in aged rodents (Zemančíková and Török, 2019). On the other hand, the increased pool of APCs in MESPAT could favor adipocyte turnover, potentially increasing anticontractile factors and leading to reduced vascular stiffness. Taken together, these findings may partially explain why arterial stiffness progressively increases with age only in elastic arteries, such as the aorta, and not in muscular arteries like the mesenteric arteries (Ruitenbeek et al., 2008; Borlotti et al., 2012; Zhang et al., 2013; Leloup et al., 2015). This study further supports the established link between age and increased risk of developing hypertension (Sun, 2015; Kohler et al., 2022).

4.4 Sex dimorphism and age effects in MESPAT and GON

Results from the present study indicate that the visceral depots MESPAT and GON have higher APC abundance in 30-week-old compared to 13-week-old females (Figure 3). These differences may be attributed to age-related sex hormone dynamics. Female mice exhibit an early reproductive stage beginning around 2–3 months

(13 weeks), then a reproductive peak around 6 months (26 weeks), and a decline after 13 months (56 weeks) (Nelson et al., 1981; Nelson et al., 1982; Lamberts et al., 1997). The reproductive peak correlates here with higher abundance of APC in 30-week-old female mice. A possible explanation could be the proliferative effect of estrogen on progenitor cells (Lapid et al., 2014; Zhang et al., 2016; Bjune et al., 2022). In humans, APC population dynamics change similarly in terms of sex and age. In subcutaneous abdominal adipose depot of 29 ± 2 -year-old females, the APC abundance is 10% higher when compared to age-matched males (Tchoukalova et al., 2010). On the other hand, aging promotes a shift in fat distribution characteristic of an increased expansion of visceral vs. subcutaneous depots (Kuk et al., 2009; Ou et al., 2022). It is important to note that the present study did not include animals older than 7 months. However, our results provide evidence for the impact steroid hormones may have on APC. Future studies will need to address how sex differences may alter APC proliferations and adipogenesis during PVAT remodeling induced by hypertension, and how APC abundance change by depot in senescent animals (13–18 months).

4.5 APC are strategically located proximal to blood vessel's adventitia

Our results show that APCs are closely associated with blood vessels in MESPAT ($<60 \mu\text{m}$; Figure 4). This is a common

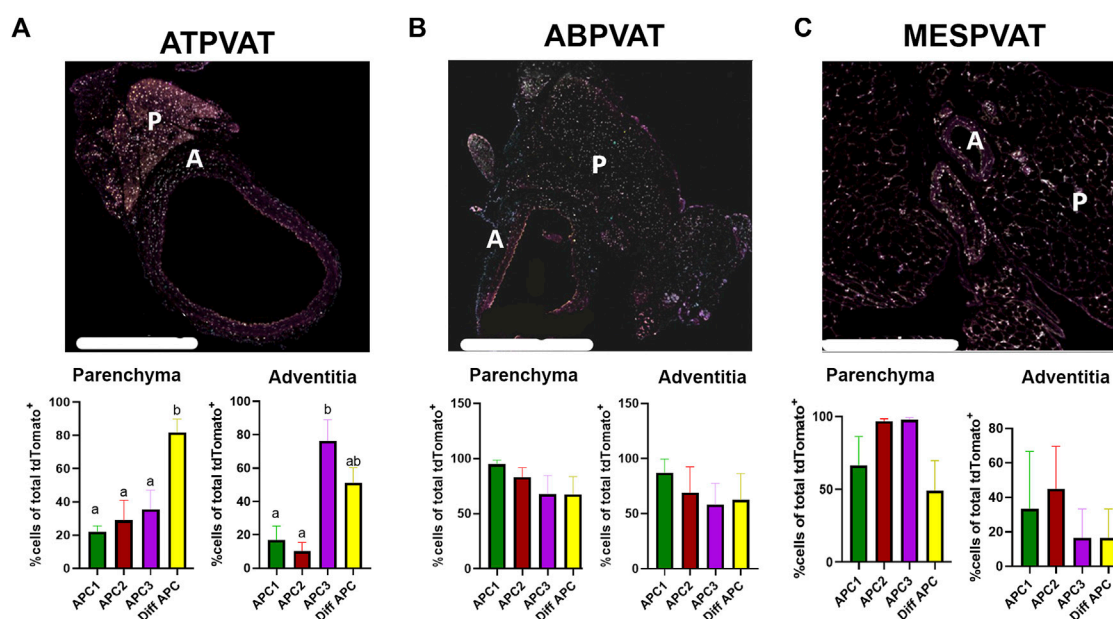


FIGURE 5

APC subtypes are present in PVAT in both sexes and age groups. 4-plex immunohistochemistry of (A) Thoracic PVAT (ATPVAT) (B) Abdominal PVAT (ABPVAT) and (C) Mesenteric arteries (MESPVAT) (Regions of interest in dotted line indicating P: Parenchyma, A: adventitia). Each depot had an analysis of the frequency of APCs of total tdTomato APCs (100%) on each subtype (APC1: BMPER, APC2: PI16, APC3: GDF10, and Diff APC: PPARG). Regions of interest (ROI): parenchyma and fascia were analyzed. Data are means \pm SEM. One-way ANOVA with Welch's correction was used. Significant differences between APC subtypes on each ROI are indicated by letters a and b ($p < 0.05$). $n = 3$ males and $n = 3$ females were analyzed for each age group. Scale bar: 200 μ m.

spatial distribution observed in PDGFR α ⁺ cells (Wang et al., 2019). However, in ATPVAT and ABPVAT, more APC were located 60 μ m away or more within the parenchyma. This spatial distribution pattern was more prominent in 30-week-old animals suggesting that adipogenesis may occur in the adventitia but also in the parenchyma of aortic PVAT in older adults. Since APCs still have the potential to differentiate into cells other than adipocytes and considering that most of them are in proximity to blood vessels in MESPVAT, this may suggest that the remodeling process starts in this area. Further experiments will need to address how hypertension modulates the fate of APCs that are closer to the blood vessels vs. those located within the parenchyma of PVAT.

4.6 APC subtypes are found in PVAT and have different spatial distribution

Previous studies identified APC subtypes in both ATPVAT and non-PVAT depots and associated these populations with specific phenotypic fates such as fibrogenesis and adipogenesis (Angueira et al., 2021; Burl et al., 2022). For instance, *Bmper*, expressed in APC1, is a positive regulator of adipogenesis and mediates the cold-induced maturation of new adipocytes that occurs in BAT (Burl et al., 2022; Garritson et al., 2023). APC2 (Pi16 populations) co-express *Dpp4*, a modulator of the TGF- β profibrogenic pathway (Soare et al., 2020; Ohm et al., 2023), while APC3 express *Gdf10*, a mediator of TGF- β and ossification

of carotid arteries (Hino et al., 2012; Brandt et al., 2022). In the parenchyma of ATPVAT, we observed high numbers of Diff APC; in contrast, we quantified higher expression of APC3 in the adventitia. This spatial distribution may indicate that regions such as adventitia may be predisposed to have ossification and fibrogenesis, while the parenchyma is more likely to be more prone to adipogenesis. In the rest of the PVAT depots we did not observe differences in APC spatial distribution. Interestingly, some APC co-expressed different markers simultaneously. Although conjecture, these results indicate that the PVAT remodeling process may occur in specific areas within the PVAT. Future experiments need to address how each APC subtype contributes differently to adipogenic and fibrogenic fates, the synthesis of ECM proteins, and the regional plasticity of PVAT remodeling during the development of hypertension.

4.7 Physiological relevance

The goal of this study was to establish how APC subpopulations in different PVAT depots, such as the aorta (conduit) and mesenteric arteries (resistant) during normotensive conditions compare to other visceral non-PVAT adipose depots. Our data demonstrate the presence of APC in all PVAT depots. For the first time, we showed uniquely defined spatial distribution of APC subtypes in ATPVAT. We also determined that females had higher APC abundance in visceral depots (MESPVAT and GON), and that age reduces

APC abundance in aortic PVAT (ATPVAT and ABPVAT) but increases it in MESPVAT mesenteric depots. The unique APC distribution, and their different subtypes with diverse spatial locations indicate that they contribute differently to hypertension-induced remodeling. The consequences of unique APC distribution and the effects of age and sex in PVAT need to be studied in detail in hypertension animal models and in human patients. Understanding the dynamic role that APC play in the remodeling process of the PVAT during hypertension will contribute to identify new therapeutic targets to treat this disease.

Data availability statement

The raw data supporting the conclusions of this article will be made available by the authors, without undue reservation.

Ethics statement

The animal study was approved by the Institutional Animal Care & Use Committee Michigan State University. The study was conducted in accordance with the local legislation and institutional requirements.

Author contributions

CR: Conceptualization, Data curation, Formal Analysis, Investigation, Methodology, Validation, Visualization, Writing—original draft, Writing—review and editing. LS: Methodology, Resources, Software, Writing—review and editing. AL: Methodology, Writing—review and editing. SW: Conceptualization, Funding acquisition, Project administration, Supervision, Writing—review and editing. GC: Conceptualization, Funding acquisition, Methodology, Project administration, Resources, Visualization, Writing—review and editing.

References

- Angueira, A. R., Sakers, A. P., Holman, C. D., Cheng, L., Arbocco, M. N., Shamsi, F., et al. (2021). Defining the lineage of thermogenic perivascular adipose tissue. *Nat. Metab.* 3 (4), 469–484. doi:10.1038/s42255-021-00380-0
- Barak, Y., Nelson, M. C., Ong, E. S., Jones, Y. Z., Ruiz-Lozano, P., Chien, K. R., et al. (1999). PPAR γ is required for placental, cardiac, and adipose tissue development. *Mol. Cell* 4 (4), 585–595. doi:10.1016/s1097-2765(00)80209-9
- Barsha, G., Denton, K. M., and Mirabito Colafella, K. M. (2016). Sex- and age-related differences in arterial pressure and albuminuria in mice. *Biol. sex Differ.* 7, 57. doi:10.1186/s13293-016-0110-x
- Berry, R., and Rodeheffer, M. S. (2013). Characterization of the adipocyte cellular lineage *in vivo*. *Nat. Cell Biol.* 15 (3), 302–308. doi:10.1038/ncb2696
- Bjune, J. I., Strömberg, P. P., Jersin, R., Mellgren, G., and Dankel, S. N. (2022). Metabolic and epigenetic regulation by estrogen in adipocytes. *Front. Endocrinol. (Lausanne)* 13, 828780. doi:10.3389/fendo.2022.828780
- Borlotti, A., Khir, A. W., Rietzschel, E. R., De Buyzere, M. L., Vermeersch, S., and Segers, P. (2012). Noninvasive determination of local pulse wave velocity and wave intensity: changes with age and gender in the carotid and femoral arteries of healthy human. *J. Appl. physiology (Bethesda, Md : 1985)* 113 (5), 727–735. doi:10.1152/japplphysiol.00164.2012
- Brandt, K. J., Burger, F., Baptista, D., Roth, A., Fernandes da Silva, R., Montecucco, F., et al. (2022). Single-cell analysis uncovers osteoblast factor growth differentiation factor 10 as mediator of vascular smooth muscle cell phenotypic modulation associated with plaque rupture in human carotid artery disease. *Int. J. Mol. Sci.* 23 (3), 1796. doi:10.3390/ijms23031796
- Burl, R. B., Rondini, E. A., Wei, H., Pique-Regi, R., and Granneman, J. G. (2022). Deconstructing cold-induced brown adipocyte neogenesis in mice. *eLife* 11, e80167. doi:10.7554/eLife.80167
- Cao, Z. F. H., Stoffel, E., and Cohen, P. (2017). Role of perivascular adipose tissue in vascular physiology and pathology. *Hypertension* 69 (5), 770–777. doi:10.1161/HYPERTENSIONAHA.116.08451
- Ciuceis, C. D., Amiri, F., Brassard, P., Endemann, D. H., Touyz, R. M., and Schiffrin, E. L. (2005). Reduced vascular remodeling, endothelial dysfunction, and oxidative stress in resistance arteries of angiotensin II-infused macrophage colony-stimulating factor-deficient mice: evidence for a role in inflammation in angiotensin-induced vascular injury. *Arteriosclerosis, thrombosis, Vasc. Biol.* 25 (10), 2106–2113. doi:10.1161/01.ATV.0000181743.28028.57
- Contreras, G. A., Thelen, K., Ayala-Lopez, N., and Watts, S. W. (2016). The distribution and adipogenic potential of perivascular adipose tissue adipocyte progenitors is dependent on sexual dimorphism and vessel location. *Physiol. Rep.* 4 (19), e12993. doi:10.14814/phy2.12993

Funding

The author(s) declare that financial support was received for the research, authorship, and/or publication of this article. This work was funded by the NIH NHLBI P01 HL152951.

Acknowledgments

The authors acknowledge the technical assistance of the Investigative Histopathology lab, the Flow Cytometry Core, the Confocal Laser Scanning Microscopy Core, Precision Health Program Tissue Analysis Core, and all the staff at GC, SW, and LS Laboratories at Michigan State University (East Lansing, MI) for the technical assistance.

Conflict of interest

The authors declare that the research was conducted in the absence of any commercial or financial relationships that could be construed as a potential conflict of interest.

Publisher's note

All claims expressed in this article are solely those of the authors and do not necessarily represent those of their affiliated organizations, or those of the publisher, the editors and the reviewers. Any product that may be evaluated in this article, or claim that may be made by its manufacturer, is not guaranteed or endorsed by the publisher.

Supplementary material

The Supplementary Material for this article can be found online at: <https://www.frontiersin.org/articles/10.3389/fphys.2024.1411218/full#supplementary-material>

- Courtney, J. M., Morris, G. P., Cleary, E. M., Howells, D. W., and Sutherland, B. A. (2021). An automated approach to improve the quantification of pericytes and microglia in whole mouse brain sections. *eNeuro* 8 (6), ENEURO.0177–21.2021. doi:10.1523/ENEURO.0177-21.2021
- Donocoff, R. S., Teteloshvili, N., Chung, H., Shoulson, R., and Creusot, R. J. (2020). Optimization of tamoxifen-induced Cre activity and its effect on immune cell populations. *Sci. Rep.* 10 (1), 15244. doi:10.1038/s41598-020-72179-0
- Dyer, J. D., Brown, A. R., Owen, A., and Metz, J. A. (2020). Quantitative measurement to describe the relative proximity of fluorescent biomarkers. *bioRxiv*. doi:10.1101/2020.12.08.416206
- Flurkey, K. M., Curren, J., and Harrison, D. E. (2007). "Chapter 20 - mouse models in aging research," in *The mouse in biomedical research*. Editors J. G. Fox, M. T. Davisson, F. W. Quimby, S. W. Barthold, C. E. Newcomer, and A. L. Smith Second Edition (Burlington: Academic Press), 637–672.
- Garrington, J. D., Zhang, J., Achenbach, A., Ferhat, M., Eich, E., Stubben, C. J., et al. (2023). BMPER is a marker of adipose progenitors and adipocytes and a positive modulator of adipogenesis. *Commun. Biol.* 6 (1), 638. doi:10.1038/s42003-023-05011-w
- Hino, J., Miyazawa, T., Miyazato, M., and Kangawa, K. (2012). Bone morphogenetic protein-3b (BMP-3b) is expressed in adipocytes and inhibits adipogenesis as a unique complex. *Int. J. Obes.* 36 (5), 725–734. doi:10.1038/ijo.2011.124
- Ichihara, S., Senbonmatsu, T., Price, E., Ichiki, T., Gaffney, F. A., and Inagami, T. (2001). Angiotensin II type 2 receptor is essential for left ventricular hypertrophy and cardiac fibrosis in chronic angiotensin II-induced hypertension. *Circulation* 104 (3), 346–351. doi:10.1161/01.cir.104.3.346
- Khavandi, K., Greenstein, A. S., Sonoyama, K., Withers, S., Price, A., Malik, R. A., et al. (2009). Myogenic tone and small artery remodeling: insight into diabetic nephropathy. *Nephrol. Dial. Transplant: official publication of the European Dialysis and Transplant Association - European Renal Association* 24 (2), 361–369. doi:10.1093/ndt/gfn583
- Kirkland, J. L., Hollenberg, C. H., and Gillon, W. S. (1990). Age, anatomic site, and the replication and differentiation of adipocyte precursors. *Am. J. physiology* 258 (2 Pt 1), C206–C210. doi:10.1152/ajpcell.1990.258.2.C206
- Kohler, I. V., Sudharsanan, N., Bandawe, C., and Kohler, H.-P. (2022). Aging and hypertension among the global poor—panel data evidence from Malawi. *PLOS Glob. Public Health* 2 (6), e0006060. doi:10.1371/journal.pgph.0006060
- Krebsbach, P. H., Kuznetsov, S. A., Satomura, K., Emmons, R. V. B., Rowe, D. W., and Robey, P. G. (1997). Bone formation in vivo: comparison of osteogenesis by transplanted mouse and human marrow stromal fibroblasts. *Transplantation* 63 (8), 1059–1069. doi:10.1097/00007890-199704270-00003
- Kuk, J. L., Saunders, T. J., Davidson, L. E., and Ross, R. (2009). Age-related changes in total and regional fat distribution. *Ageing Res. Rev.* 8 (4), 339–348. doi:10.1016/j.arr.2009.06.001
- Lamberts, S. W. J., van den Beld, A. W., and van der Lely, A.-J. (1997). The endocrinology of aging. *Sci. (New York, NY)* 278 (5337), 419–424. doi:10.1126/science.278.5337.419
- Lapid, K., Lim, A., Clegg, D. J., Zeve, D., and Graff, J. M. (2014). Oestrogen signalling in white adipose progenitor cells inhibits differentiation into brown adipose and smooth muscle cells. *Nat. Commun.* 5 (1), 5196. doi:10.1038/ncomms6196
- Lee, Y. H., Petkova, A. P., and Granneman, J. G. (2013). Identification of an adipogenic niche for adipose tissue remodeling and restoration. *Cell metab.* 18 (3), 355–367. doi:10.1016/j.cmet.2013.08.003
- Lee, Y.-H., Petkova Anelia, P., Mottillo Emilio, P., and Granneman James, G. (2012). *In vivo* identification of bipotential adipocyte progenitors recruited by β 3-adrenoceptor activation and high-fat feeding. *Cell metab.* 15 (4), 480–491. doi:10.1016/j.cmet.2012.03.009
- Leloup, A. J., Van Hove, C. E., Heykers, A., Schrijvers, D. M., De Meyer, G. R., and Franssen, P. (2015). Elastic and muscular arteries differ in structure, basal NO production and voltage-gated Ca(2+)-channels. *Front. Physiol.* 6, 375. doi:10.3389/fphys.2015.00375
- Lima, R. Sd, Silva, J. CdS., Lima, C. T., Souza, L. Ed, Silva, M. Bd, Baladi, M. G., et al. (2019). Proinflammatory role of angiotensin II in the aorta of normotensive mice. *BioMed Res. Int.* 2019, 9326896. doi:10.1155/2019/9326896
- Lu, H., Howatt, D. A., Balakrishnan, A., Moorleghen, J. J., Rateri, D. L., Cassis, L. A., et al. (2015). Subcutaneous angiotensin II infusion using osmotic pumps induces aortic aneurysms in mice. *JoVE* (103), e53191. doi:10.3791/53191
- Lukjanenko, L., Karaz, S., Stuelsatz, P., Gurriaran-Rodriguez, U., Michaud, J., Dammone, G., et al. (2019). Aging disrupts muscle stem cell function by impairing matricellular WISP1 secretion from fibro-adipogenic progenitors. *Cell Stem Cell* 24 (3), 433–446. doi:10.1016/j.stem.2018.12.014
- Merrick, D., Sakers, A., Irgebay, Z., Okada, C., Calvert, C., Morley, M. P., et al. (2019). Identification of a mesenchymal progenitor cell hierarchy in adipose tissue. *Sci. (New York, NY)* 364 (6438), eaav2501. doi:10.1126/science.aav2501
- Muir, L. A., Neeley, C. K., Meyer, K. A., Baker, N. A., Brosius, A. M., Washabaugh, A. R., et al. (2016). Adipose tissue fibrosis, hypertrophy, and hyperplasia: correlations with diabetes in human obesity. *Obesity* 24 (3), 597–605. doi:10.1002/oby.21377
- National Center for Health Statistics (2018). *Division of vital S. National Health and nutrition examination survey (NHANES): physician examination procedures manual*.
- Nelson, J. F., Felicio, L. S., Osterburg, H. H., and Finch, C. E. (1981). Altered profiles of estradiol and progesterone associated with prolonged estrous cycles and persistent vaginal cornification in aging C57BL/6J mice. *Biol. reproduction* 24 (4), 784–794. doi:10.1095/biolreprod24.4.784
- Nelson, J. F., Felicio, L. S., Randall, P. K., Sims, C., and Finch, C. E. (1982). A longitudinal study of estrous cyclicity in aging C57BL/6J mice: I. Cycle frequency, length and vaginal cytology. *Biol. reproduction* 27 (2), 327–339. doi:10.1095/biolreprod27.2.327
- Nishimura, S., Manabe, I., Nagasaki, M., Seo, K., Yamashita, H., Hosoya, Y., et al. (2008). *In vivo* imaging in mice reveals local cell dynamics and inflammation in obese adipose tissue. *J. Clin. investigation* 118 (2), 710–721. doi:10.1172/JCI33328
- Nosalski, R., Siedlinski, M., Denby, L., McGinnigle, E., Nowak, M., Cat, A. N. D., et al. (2020). T-Cell-Derived miRNA-214 mediates perivascular fibrosis in hypertension. *Circulation Res.* 126 (8), 988–1003. doi:10.1161/CIRCRESAHA.119.315428
- Oh, J., Lee, Y. D., and Wagers, A. J. (2014). Stem cell aging: mechanisms, regulators and therapeutic opportunities. *Nat. Med.* 20 (8), 870–880. doi:10.1038/nm.3651
- Ohm, M., Moneke, I., and Jungraithmayr, W. (2023). Targeting cluster of differentiation 26/dipeptidyl peptidase 4 (CD26/DPP4) in organ fibrosis. *Br. J. Pharmacol.* 180, 2846–2861. doi:10.1111/bph.15967
- O'Rourke, M., Cullen, C. L., Auderset, L., Pitman, K. A., Achatz, D., Gasperini, R., et al. (2016). Evaluating tissue-specific recombination in a Pdgfra-CreERT2 transgenic mouse line. *PLoS One* 11 (9), e0162858. doi:10.1371/journal.pone.0162858
- Ou, M.-Y., Zhang, H., Tan, P.-C., Zhou, S.-B., and Li, Q.-F. (2022). Adipose tissue aging: mechanisms and therapeutic implications. *Cell Death Dis.* 13 (4), 300. doi:10.1038/s41419-022-04752-6
- Pan, X. X., Ruan, C. C., Liu, X. Y., Kong, L. R., Ma, Y., Wu, Q. H., et al. (2019). Perivascular adipose tissue-derived stromal cells contribute to vascular remodeling during aging. *Ageing Cell* 18 (4), e12969. doi:10.1111/accel.12969
- Park, J. S., Park, G., and Hong, H. S. (2021). Age affects the paracrine activity and differentiation potential of human adipose-derived stem cells. *Mol. Med. Rep.* 23 (2), 160. doi:10.3892/mmr.2020.11799
- Pereira, R. F., Halford, K. W., O'Hara, M. D., Leeper, D. B., Sokolov, B. P., Pollard, M. D., et al. (1995). Cultured adherent cells from marrow can serve as long-lasting precursor cells for bone, cartilage, and lung in irradiated mice. *Proc. Natl. Acad. Sci.* 92 (11), 4857–4861. doi:10.1073/pnas.92.11.4857
- Pittenger, M. F., Mackay, A. M., Beck, S. C., Jaiswal, R. K., Douglas, R., Mosca, J. D., et al. (1999). Multilineage potential of adult human mesenchymal stem cells. *Sci. (New York, NY)* 284 (5411), 143–147. doi:10.1126/science.284.5411.143
- Police, S. B., Thatcher, S. E., Charnigo, R., Daugherty, A., and Cassis, L. A. (2009). Obesity promotes inflammation in periaortic adipose tissue and angiotensin II-induced abdominal aortic aneurysm formation. *Arteriosclerosis, thrombosis, Vasc. Biol.* 29 (10), 1458–1464. doi:10.1161/ATVBAHA.109.192658
- Ruitenbeek, A. G., van der Cammen, T. J., van den Meiracker, A. H., and Mattace-Raso, F. U. (2008). Age and blood pressure levels modify the functional properties of central but not peripheral arteries. *Angiology* 59 (3), 290–295. doi:10.1177/000319707035692
- Sempere, L. F., Zaluzec, E., Kenyon, E., Kiupel, M., and Moore, A. (2020). Automated Five-color multiplex co-detection of MicroRNA and protein expression in fixed tissue specimens. *Methods Mol. Biol. (Clifton, NJ)* 2148, 257–276. doi:10.1101/2020.12.08.416206
- Shcherbina, A., Larouche, J., Fraczek, P., Yang, B. A., Brown, L. A., Markworth, J. F., et al. (2020). Dissecting murine muscle stem cell aging through regeneration using integrative genomic analysis. *Cell Rep.* 32 (4), 107964. doi:10.1016/j.celrep.2020.107964
- Shin, S., Pang, Y., Park, J., Liu, L., Lukas, B. E., Kim, S. H., et al. (2020). Dynamic control of adipose tissue development and adult tissue homeostasis by platelet-derived growth factor receptor alpha. *Elife* 9, e56189. doi:10.7554/eLife.56189
- Soare, A., Györfi, H. A., Matei, A. E., Dees, C., Rauber, S., Wohlfahrt, T., et al. (2020). Dipeptidylpeptidase 4 as a marker of activated fibroblasts and a potential target for the treatment of fibrosis in systemic sclerosis. *Arthritis & rheumatology (Hoboken, NJ)* 72 (1), 137–149. doi:10.1002/art.41058
- Strissel, K. J., Stancheva, Z., Miyoshi, H., Perfield, J. W., 2nd, DeFuria, J., Jick, Z., et al. (2007). Adipocyte death, adipose tissue remodeling, and obesity complications. *Diabetes* 56 (12), 2910–2918. doi:10.2337/db07-0767
- Sun, Z. (2015). Aging, arterial stiffness, and hypertension. *Hypertension* 65 (2), 252–256. doi:10.1161/HYPERTENSIONAHA.114.03617
- Tchoukalova, Y. D., Votruba, S. B., Tchkonina, T., Giorgadze, N., Kirkland, J. L., and Jensen, M. D. (2010). Regional differences in cellular mechanisms of adipose tissue gain with overfeeding. *Proc. Natl. Acad. Sci. U. S. A.* 107 (42), 18226–18231. doi:10.1073/pnas.1005259107
- Thompson, J. M., Watts, S. W., Terrian, L., Contreras, G. A., Rockwell, C., Rendon, C. J., et al. (2023). A cell atlas of thoracic aortic perivascular adipose tissue: a focus on mechanotransducers. *bioRxiv*. 2023.10.09.561581. doi:10.1101/2023.10.09.561581

- Tontonoz, P., Nagy, L., Alvarez, J. G., Thomazy, V. A., and Evans, R. M. (1998). PPARgamma promotes monocyte/macrophage differentiation and uptake of oxidized LDL. *Cell* 93 (2), 241–252. doi:10.1016/s0092-8674(00)81575-5
- Tuttle, T., Darios, E., Watts, S. W., and Rocchianica, S. (2022). Aortic stiffness is lower when PVAT is included: a novel *ex vivo* mechanics study. *Am. J. physiology Heart circulatory physiology* 322 (6), H1003–H1013. doi:10.1152/ajpheart.00574.2021
- Uezumi, A., Fukada, S.-i., Yamamoto, N., Takeda, Si, and Tsuchida, K. (2010). Mesenchymal progenitors distinct from satellite cells contribute to ectopic fat cell formation in skeletal muscle. *Nat. Cell Biol.* 12 (2), 143–152. doi:10.1038/ncb2014
- van Kuijk, K., McCracken, I. R., Tillie, R., Asselberghs, S. E. J., Kheder, D. A., Muijtens, S., et al. (2023). Human and murine fibroblast single-cell transcriptomics reveals fibroblast clusters are differentially affected by ageing and serum cholesterol. *Cardiovasc. Res.* 119 (7), 1509–1523. doi:10.1093/cvr/cvad016
- Van Varik, B., Rennenberg, R., Reutelingsperger, C., Kroon, A., de Leeuw, P., and Schurgers, L. (2012). Mechanisms of arterial remodeling: lessons from genetic diseases. *Front. Genet.* 3, 290. doi:10.3389/fgene.2012.00290
- Von Bank, H., Kirsh, C., and Simcox, J. (2021). Aging adipose: depot location dictates age-associated expansion and dysfunction. *Ageing Res. Rev.* 67, 101259. doi:10.1016/j.arr.2021.101259
- Wang, Q. A., Song, A., Chen, W., Schwalie, P. C., Zhang, F., Vishvanath, L., et al. (2018). Reversible de-differentiation of mature white adipocytes into preadipocyte-like precursors during lactation. *Cell metab.* 28 (2), 282–288. doi:10.1016/j.cmet.2018.05.022
- Wang, Y., Xu, J., Meyers, C. A., Gao, Y., Tian, Y., Broderick, K., et al. (2019). PDGFR α marks distinct perivascular populations with different osteogenic potential within adipose tissue. *Stem Cells (Dayton, Ohio)* 38 (2), 276–290. doi:10.1002/stem.3108
- Wang, Z., Lu, H., Garcia-Barrio, M., Guo, Y., Zhang, J., Chen, Y. E., et al. (2022). RNA sequencing reveals perivascular adipose tissue plasticity in response to angiotensin II. *Pharmacol. Res.* 178, 106183. doi:10.1016/j.phrs.2022.106183
- Zemančíková, A., and Török, J. (2019). Influence of age on anticontractile effect of perivascular adipose tissue in normotensive and hypertensive rats. *Oxid. Med. Cell Longev.* 2019, 9314260. doi:10.1155/2019/9314260
- Zhang, R., Zhang, Y. Y., Huang, X. R., Wu, Y., Chung, A. C. K., Wu, E. X., et al. (2010). C-reactive protein promotes cardiac fibrosis and inflammation in angiotensin II-induced hypertensive cardiac disease. *Hypertension* 55 (4), 953–960. doi:10.1161/HYPERTENSIONAHA.109.140608
- Zhang, W., Schmult, S., Du, M., Liu, J., Lu, Z., Zhu, H., et al. (2016). Estrogen receptor α and β in mouse: adipose-derived stem cell proliferation, migration, and Brown adipogenesis *in vitro*. *Cell. Physiology Biochemistry* 38 (6), 2285–2299. doi:10.1159/000445583
- Zhang, Y., Agnoletti, D., Protogerou, A. D., Topouchian, J., Wang, J. G., Xu, Y., et al. (2013). Characteristics of pulse wave velocity in elastic and muscular arteries: a mismatch beyond age. *J. Hypertens.* 31 (3), 554–559. doi:10.1097/HJH.0b013e32835d4aec
- Zhuang, R., Chen, J., Cheng, H. S., Assa, C., Jamaïyar, A., Pandey, A. K., et al. (2022). Perivascular fibrosis is mediated by a KLF10-IL-9 signaling Axis in CD4 $^{+}$ T cells. *Circulation Res.* 130 (11), 1662–1681. doi:10.1161/CIRCRESAHA.121.320420



OPEN ACCESS

EDITED BY

Brian Gene Coon,
Oklahoma Medical Research Foundation,
United States

REVIEWED BY

Roland Pittman,
Virginia Commonwealth University,
United States
Nicolas Baeyens,
Université libre de Bruxelles, Belgium

*CORRESPONDENCE

Etienne Roux,
✉ etienne.roux@u-bordeaux.fr

RECEIVED 14 February 2024

ACCEPTED 17 June 2024

PUBLISHED 12 July 2024

CITATION

Nicolas N, de Tilly A and Roux E (2024), Blood shear stress during the cardiac cycle and endothelial cell orientation and polarity in the carotid artery of male and female mice. *Front. Physiol.* 15:1386151. doi: 10.3389/fphys.2024.1386151

COPYRIGHT

© 2024 Nicolas, de Tilly and Roux. This is an open-access article distributed under the terms of the [Creative Commons Attribution License \(CC BY\)](#). The use, distribution or reproduction in other forums is permitted, provided the original author(s) and the copyright owner(s) are credited and that the original publication in this journal is cited, in accordance with accepted academic practice. No use, distribution or reproduction is permitted which does not comply with these terms.

Blood shear stress during the cardiac cycle and endothelial cell orientation and polarity in the carotid artery of male and female mice

Nabil Nicolas¹, Alexandre de Tilly² and Etienne Roux^{1*}

¹Biologie des Maladies Cardiovasculaires, INSERM, U1034, University of Bordeaux, Pessac, France,

²Hemovis, Fontenay-sous-Bois, France

Introduction: Blood flow produces fluid shear stress (SS), a frictional force parallel to the blood flow, on the endothelial cell (EC) layer of the lumen of the vessels. ECs themselves are sensitive to this frictional force in terms of directionality and intensity. The aim of this study was to determine the physiological shear stress value during the cardiac cycle and EC polarity and orientation from blood flow in healthy male and female mouse carotid artery.

Methods: Experimentation is done on anesthetized male and female 8-week-old C5BL/6J mice. *In vivo* measurements of maximum blood velocity and vessel diameter in diastole and systole were performed on the right common carotid artery by Doppler ultrasound imaging. Blood viscosity (total and plasmatic) and hematocrit were determined on blood samples. For SS calculation, we developed a new method assuming heterogenous blood flow, i.e., a red cell central plug flow surrounded by a peripheral plasma sheath flow, and computing SS from vessel diameter and hemodynamical measurements (maximal blood velocity, hematocrit and plasmatic viscosity).

Results: Results were compared with the classical method assuming a homogenous blood flow with constant apparent total blood viscosity. EC polarity and orientation were determined *ex vivo* on the carotid endothelium by confocal imaging after labeling of the EC nucleus and Golgi apparatus. Diastolic and systolic SS were 6 ± 2.5 Pa and 30 ± 6.5 Pa, respectively. Total blood and plasmatic viscosity was 4 ± 0.5 cP and 1.27 cP, respectively. ECs were polarized and significantly oriented against blood flow. No sex difference was identified.

KEYWORDS

ultrasound imaging, blood viscosity, Fahreaus-Lindqvist-effect, carotid artery, sex effect

Introduction

Blood flow produces fluid shear stress, a frictional force parallel to the blood flow, on the endothelial cell (EC) layer of the walls of the vessels, the wall shear stress (WSS). Due to hemodynamic variations during the cardiac cycle, the WSS is not a constant but varies between diastole and systole. ECs themselves are sensitive to this frictional force in terms of directionality and intensity, inducing local short-term (vasomotricity) and long-term (remodeling) alteration of the vessel, which in turn modifies the

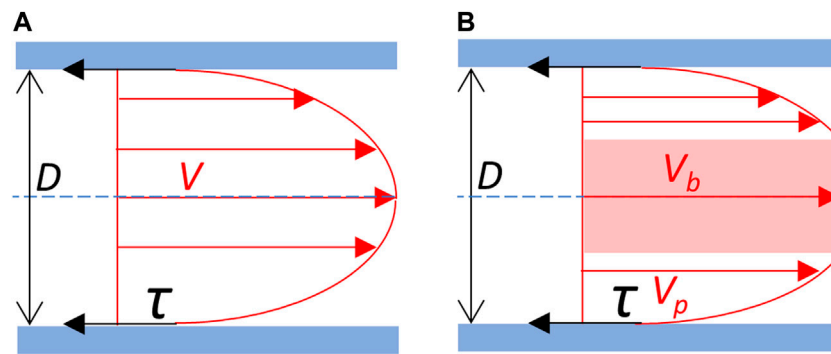


FIGURE 1

Blood flow velocity profile and wall shear stress. (A) Newtonian schematic representation of the velocity profile of the blood flow. Blood is considered as an homogeneous fluid which velocity profile (V) follows a parabolic curve, the maximal velocity being at the center of the vessel. (B) Schematic representation of the separation between red blood cells plug flow and plasma sheath flow on the velocity profile of the blood flow. Blood is considered as non-homogeneous. Cellular elements of the blood constitute a central blood plug (in pink), which velocity (V_b) corresponds to the maximal velocity, in fact the velocity of the plug flow. The plasma forms a peripheral sheath which velocity profile (V_p) depends on its thickness. Red arrows: velocity (V). τ (black arrows): shear stress exerted on the vessel wall (in blue). D : vessel diameter. Blue dot line: central axis of the vessel.

hemodynamical characteristics of the blood flow (Baeyens et al., 2016). It has been shown that this feedback loop contributes to the maintenance of the shear stress value in a narrow physiological range, the so-called WSS homeostasis, in which EC planar polarity plays a key role. Theoretical and experimental investigation have shown that this WSS homeostasis contributes the functional efficiency of the vascular network, and loss of WSS homeostasis robustness or homeostasis disruption is involved in vascular impairment and disease (Ong et al., 2020; Roux et al., 2020). A large number of publications have been dedicated to the investigation of the effect of WSS on ECs and vessel morphogenesis and remodeling (McCue et al., 2006; Chen and Tzima, 2009; Poduri et al., 2017; John et al., 2018; Lee et al., 2022). However, the availability in the literature of WSS physiological values is limited, in mice, an animal model largely used in biomedical research. The aim of this study is to determine *in vivo* physiological WSS value during the cardiac cycle in healthy male and female mouse carotid artery by *in vivo* measurement of blood flow velocity and vessel diameter combined with blood viscosity determination, and EC polarity and orientation from blood flow.

For a given fluid, the shear stress depends on the viscosity of the fluid and the shear rate it generates. On this basic principle, several methods exist for the calculation of the WSS, both *in vivo* and *in vitro*, depending, on the one hand, on the parameters that can be experimentally determined and, on the other hand, on theoretical hemodynamic assumptions about blood flow grounding the mathematical formulation of WSS calculation. Classically, calculation of WSS is based on the assumption that blood can be considered as a “Newtonian” fluid, i.e., a homogenous fluid with constant viscosity, following the Poiseuille’s law (Roux et al., 2020). However, it is known, since the primary work of Fahraeus and Lindqvist, that in narrow vessels (diameter inferior to 0.3 mm) the hemodynamic flow follows a structure of a plug flow of the red cells surrounded by a sheath flow of plasma, the so-called “Fahraeus-Lindqvist” effect (Fahraeus, 1929; Fahraeus and Lindqvist, 1931; Barbee and Cokelet, 1971). Fahraeus and Lindqvist showed that in such narrow vessels the Poiseuille’s law, relative to whole blood

viscosity, is not valid. In this case, the WSS depends on the plasma layer, i.e., plasma thickness and viscosity, and on the suspension state of the red cells, i.e., the plug flow thickness, and the vessel radius. Though the Fahraeus-Lindqvist effect occurs in narrow vessels, it has been evidenced that “Fahraeus-type” heterogenous blood behavior, i.e., with a red cell central plug flow surrounded by a peripheral plasma sheath flow, actually occurs for vessel diameter superior to 0.3 mm (Aarts et al., 1984; Aarts et al., 1988; Yeleswarapu et al., 1998; Hoskins, 2011; Secomb and Pries, 2013). Additionally, recent work of Thurston and Tilly showed that such a central plug/peripheral plasma sheath effect appears well in vessel-like geometries, namely, glass and polydimethylsiloxane capillaries, allowing the development of a new device for the measurement of total blood and plasmatic viscosities (de Tilly et al., 2023). One specific objective of this study was hence to propose a method based on the blood plug and sheath flow separation principle that grounded both the mathematical formulation of the shear stress exerted on the vessel wall and the obtention of experimental data for blood viscosity, compared to the classical one assuming Poiseuille’s law Newtonian fluid properties of the blood.

Materials and methods

Animal preparation

Experiments were done on male and female 8-week-old C5BL/6J mice, in accordance with National and European Union guidelines for experimental animal use, using procedures approved by the local Ethical Committee and authorized by National institution [#32550-2021100615085247 v4]. Food and water were available *ad libitum*, with a 12 h dark/light cycle. Mice were anaesthetized by gas (Vetflurane® 1,000 mg/g, Virbac). They were placed on their backs and their legs taped to a 38°C heating platform. Thoracic hair was removed using a depilatory cream (Veet Minima™ Sensitive Skin Depilatory Cream, Reckitt, Slough, United States). An ultrasound gel (neojelly®us, Asept InMed®, Quint-Conserves, France) was applied to the thoracic area. After ultrasound recording,

an 850 μL blood sample was taken intravenously via the retro-orbital route using a piece of capillary pipette (ringcaps[®] 50 μL , HIRSCHMANN, Eberstadt, Germany) in an EDTA tube (4 mL EDTA K2 (7.2 mg) Tube BD[®] Vacutainer[®], Becton, Dickinson and Company, United States). Mice were then euthanized without recovery by intraperitoneal injection, using a 25G needle, of 300 μL of sodium pentobarbital (Exagon[®] à 400 mg/mL, Axience, Pantin, France) diluted in physiological solution.

In vivo measurement of carotid diameter and blood flow velocity

After thoracic depilation, *in vivo* measurement of blood flow and vessel diameter of the right common carotid artery are performed on anesthetized mice by Doppler ultrasound imaging, using a Vevo 2,100 Imaging Platform ultrasound scanner (VisualSonics, Toronto, Canada).

The diameter of the right common carotid artery was measured on series of images of the artery acquired in B mode with a gain of 27 dB, an image frequency of 78, a depth of 13 mm, a width of 10.36 mm, and a focal zone framing the carotid artery. The diameter was measured (in mm) in diastole and systole over the same cycle. Measurements were repeated on three different cycles, located at a distance from the inspiration, and the average of the three was automatically calculated by the device.

The velocity of the circulating blood was measured in the middle of the right common carotid artery between the first rib and the bifurcation between the right internal and external carotid arteries, in the center of the carotid artery to obtain the maximum blood velocity. Maximum blood velocity was recorded as a function of time in Pulse Wave mode with a gain of 30 dB, a beam angle of 0° and a 1,000 Hz filter, and with a flow measurement zone located at a depth of 8 mm, a size of 0.27 mm and oriented in the direction of blood flow at an angle of 80°. The maximum blood velocity measured over time was automatically adjusted to a sensitivity of x6. Maximum blood velocity (in $\text{mm}\cdot\text{s}^{-1}$) was measured in diastole and systole over 5 consecutive cycles, and averaged manually.

Measurement of hemodynamic viscosity and hematocrit

Hemodynamic viscosity was determined on blood samples using a newly developed setup and methodology (Hemovis, Fontenay-sous-Bois, France). A situation similar to the *in vivo* red blood cells and plasma plug flow separation effect is replicated in the device developed by Hemovis (de Tilly et al., 2023) allowing whole blood and plasma viscosity measurements and the plasma thickness estimation. Briefly, whole blood viscosity (η_b) was measured, for each mouse, on 800 μL of blood at 3 kPa pressure in a 380 μm diameter tube (shear rate = $1,200\text{ s}^{-1}$) using Hemovis device. Then, all same sex mice blood samples were pooled and centrifugated at 2,000 g for 10 min to separate the plasma and the cellular elements of blood. Plasma viscosity (η_p) was measured, for same sex mice pooled blood, using Hemovis device.

Hematocrit (Ht) was measured, for each mouse, on 50 μL of blood using scil Vet abc Plus + device (Scil Animal Care Company, Altorf, France).

Calculation of carotid wall shear stress

The experimental data, i.e., carotid inner diameter, maximal blood flow velocity and parameters related to blood viscosity (total blood viscosity, plasmatic viscosity and hematocrit), have been used to calculate the carotid diastolic and systolic WSS using 2 different methods, the classical one, assuming Poiseuille's law Newtonian fluid properties of the blood, and our own method based on the "Fahraeus-type" separation between red blood cells plug flow and plasma sheath flow, called in this article N-method and F-method, respectively (Figure 1). In both cases, WSS calculation was grounded on the basic principle according to which the WSS (τ) is the product of the viscosity η and the shear rate (σ) (Roux et al., 2020):

$$\tau = \eta \times \sigma \quad (1)$$

The shear rate depends on the geometry of the vessel segment and the characteristics of the fluid flow, and the 2 methods differed (i) in the value chosen for η and (ii) in the way σ was calculated.

Calculation of WSS (τ) according to the N-method was based on the general equation:

$$\tau = \eta \times \frac{8 \times V_m}{D} \quad (2)$$

where η is the blood viscosity, V_m is the mean blood velocity, and D the vessel inner diameter. Since Doppler measurement provides not the mean velocity but the maximal one (V_{max}), WSS calculation should consider the relationship between V_m and V_{max} , determined by the profile of blood velocity from the centre of the vessel, where the velocity is maximal, to the edges of the vessel. Under the assumption that blood behaves as a Newtonian fluid, the velocity profile is parabolic, and the ratio of V_{max} to V_m is 2, so the WSS is given by the following equation:

$$\tau_t = \eta_b \times \frac{4 \times V_{max}}{D} \quad (3)$$

where τ_t is the theoretical WSS, η_b is the total blood viscosity, V_{max} is the maximal blood velocity, and D the carotid inner diameter. Eq. 3 was applied to calculate the WSS according to the so-called "theoretical N-method," using, for each animal, individual values of vessel diameter, maximal blood velocity, and blood viscosity.

However, it has been shown that in small arteries, the V_{max} to V_m ratio is usually between 1.39 and 1.54, i.e., less than the theoretical value 2 (Reneman et al., 2006), and the apparent blood viscosity is lower than in larger vessels. These differences from the theoretical values are due to the fact that blood cells concentrate in the central core of blood flow, surrounded by a fluid peripheral sheath of plasma with some blood cells in suspension, known as the Fahraeus-Lindqvist effect, but this heterogenous blood behavior can be considered in an approximate way with a corrected Newtonian-based equation, as follows:

$$\tau_c = \eta \times \frac{5,5 \times V_{max}}{D} \quad (4)$$

where τ_c is the corrected WSS, η is the fluid viscosity, V_{max} is the maximal blood velocity, and D the carotid inner diameter, assuming a V_{max}/V_m ratio equal to 1.45. Eq. 4 has been applied to calculate the WSS according to the so-called “corrected N-method,” using, for each animal, individual values of vessel diameter, maximal blood velocity, and 3 different values for η : the average plasmatic viscosity calculated on the pooled plasma of each animal group (η_p), the individual total blood viscosity (η_b), and a apparent viscosity ($\eta_{app.}$) obtained using a correcting factor for η_p . In accordance with the literature, we set the correcting factor at 1.78 ($\eta_{app.} = 1.78 \times \eta_p$) (Secomb, 2017).

By contrast with the N-method, calculation of WSS according to the F-method (τ_F) considers a non-homogenous behavior of the blood flow, with a central solid-like blood plug, constituted by the cellular elements of the blood, circled by a peripheral plasmatic sheath responsible for the actual WSS, which hence depends on the plasmatic viscosity and the shear rate (σ_F):

$$\tau_F = \eta_p \times \sigma_F \quad (5)$$

As for σ_F , it depends on (i) the velocity of the central blood plug, corresponding to V_{max} , (ii) the vessel diameter, (iii) the thickness of the plasmatic sheath, and (iv) the velocity profile within the plasmatic sheath. Based on a previous 2D model (de Tilly, 2015), applying the physical formulation of the blood plug and sheath flow separation model to the real vessel, we developed a 3D equation allowing to calculate σ_F from the maximal blood velocity (V_{max}), the vessel radius ($R = D/2$) and hematocrit (Ht) (see [Supplementary Material](#)):

$$\sigma_F = \frac{2V_{max}}{R} \times \frac{(1 - Ht)}{Ht \times (1 - 2 \ln \sqrt{Ht}) - 1} \quad (6)$$

The WSS can be calculated as follows:

$$\tau_F = \eta_p \times \frac{4V_{max}}{D} \times \frac{(1 - Ht)}{Ht \times (1 - \ln Ht) - 1} \quad (7)$$

In this equation, σ_F is negative, the direction of the shear stress vector being opposite to that of the blood flow. To present the WSS as positive, as it is usual done, and to make easy comparison with the N-method equation, the absolute value of σ_F was calculated from Eq. 7 as follows:

$$\tau_F \vee \eta_p \times \frac{4V_{max}}{D} \times \frac{(Ht - 1)}{Ht \times (1 - \ln Ht) - 1} \quad (8)$$

where η_p is the blood plasma viscosity, V_{max} is the maximal blood velocity, D the carotid inner diameter and Ht the hematocrit. Eq. 8 has been applied to calculate the WSS according to the so-called “F-method,” using, for each animal, individual values of vessel diameter, maximal blood velocity and hematocrit, and the average plasmatic viscosity calculated on the pooled plasma of each animal group.

Endothelial cells planar polarity and orientation

Carotid preparation

After euthanasia, a sternotomy was carried out to catheterize the left ventricle. A perfusion of physiological solution at 80 mm Hg

pressure for 3 min was done to remove the blood from the vasculature. A second perfusion of 4% formalin (10% neutral buffered formalin, DiaPath, Martinengo, Italy) was done for 5 min to fix the tissues. The right common carotid artery was then carefully harvested with its bifurcation, to determine the direction of blood flow, and gently opened in two to allow better penetration of the immunostaining products. It was then placed in 4% formalin for 30 min at room temperature.

Carotid *in toto* immunostaining

To study the orientation and polarity of right common carotid artery ECs, Golgi apparatus immunostaining and nuclear labelling were performed on carotid arteries *in toto* in a 350 μ L flat-bottom 96-well plate (Dutscher, Bernolsheim, France). For each bath or wash, the carotids were placed in 200 μ L of the solution. The plate was placed on a shaker with horizontal agitation at 300 rpm.

Following the formalin fixation, the carotid arteries were washed twice with PBS1X for 7 min each at room temperature. Antigen retrieval was performed for 4 min at 95°C in an Eppendorf tube containing a solution of 1M Tris (TRIS Base Ultrapure, Euromedex, Souffelweyersheim, France)/ 0.5M EDTA (EDTA, Euromedex, Souffelweyersheim, France) at pH 8 to reveal the antigenic sites for the primary antibody. Three 5-min washes with PBS1X were performed. Non-specific binding sites were saturated for 1 h at room temperature using a saturation solution containing 10% donkey serum (Donkey Normal Serum (UP77719A K), Interchim Uptima, Montluçon, France), 0.5% Triton X-100 (Triton X-100 (T8532), Sigma-Aldrich, Missouri, United States), 0.01% Deoxycholic Acid Sodium Salt (BP 349-100), ThermoFisher Scientific, Massachusetts, United States) in PBS1X. Incubation with rabbit primary antibody anti-mouse Golgi integral membrane protein 4 [Recombinant Anti-GOLPH4/GPP130 antibody (EPR13439) (ab197595), abcam, Cambridge, United States] was carried out overnight at 4°C with horizontal agitation at 70 rpm. The following day, three 10-min washes with PBS1X were performed at room temperature. Incubation with Donkey secondary antibody anti-rabbit IgG coupled to a green-emitting fluorochrome (Donkey anti-Rabbit IgG (H + L) Highly Cross-Adsorbed Secondary Antibody, Alexa Fluor™ 488 (A21206), ThermoFisher Scientific, Massachusetts, United States) was performed for 2 h at room temperature. A final 10-min wash at room temperature was performed.

The right common carotid artery was mounted between glass slide and coverslip using a mounting medium containing DAPI (Fluoromount-GTM, with DAPI (00-4959-52), ThermoFisher Scientific, Massachusetts, United States), for nuclei labelling. The right common carotid artery was oriented so that the endothelium was in contact with the coverslip and the bifurcation was at the top of the slide. It was stored in an opaque box at room temperature for at least 2 days until the images were acquired.

Image acquisition

2D images of the nuclei and Golgi apparatus of the endothelium of the right common carotid artery were acquired by confocal microscopy using an LSM 900 system (Jena, Germany) equipped an Axiocam 305 mono camera and a 40×/1 Plan-Apochromat objective. The tissue was illuminated consecutively by a with

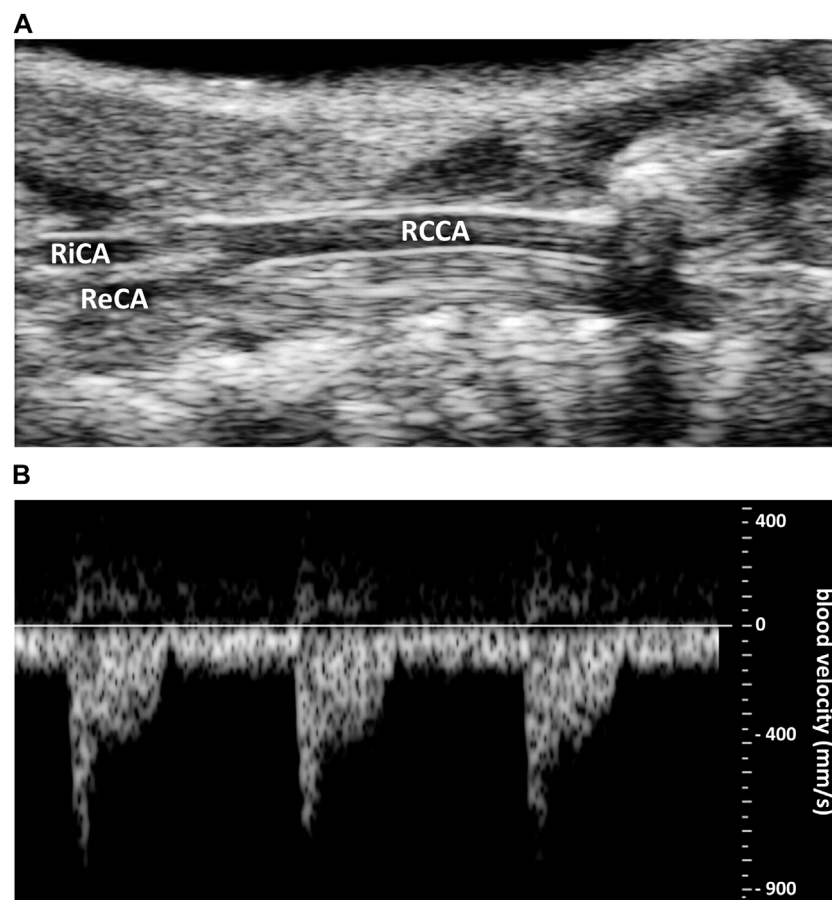


FIGURE 2
Representative original traces of carotid ultrasound imaging. **(A)** Right common coronary artery (RCCA) diameter. RiCA, right internal carotid artery. ReCA, right external carotid artery. **(B)** Blood velocity profile (in $\text{mm}\cdot\text{s}^{-1}$).

405 nm laser to observe nuclei, and a 488 nm laser to observe Golgi apparatus. The pinhole was set at 3.03 Airy for the 405 nm laser and 2.81 Airy for the 488 nm laser, allowing acquisition of a section 1.5 μm thick. The laser power was set at 1.5% of the maximum power, and the gain at 600. The fluorescence wavelength emitted was collected at 452 nm to image the nuclei, and 520 nm for the Golgi apparatus. Imaging is performed by sampling an area measuring $160 \times 160 \mu\text{m}$. The spatial resolution of the system is 156 nm in (x, y). The final pixel size is 78 nm in (x, y). At the end of acquisition, the images obtained are in 8-bit format.

Image processing

Image processing was performed using the open-source ImageJ/Fiji software [ImageJ 2.1.0/1.53h/Java 1.8.0_66 (64 bit)]. Segmentation was used to obtain binarized images of the nuclei and Golgi apparatus. A threshold, based on the Gaussian distribution of the background voxel grey-level histogram technique, was calculated for each image by adapting previously developed thresholding technique for vascular network (Nicolas et al., 2023). Threshold was set at the mean + 3.89xSD to eliminate the background and 99.995% of the unlabeled vascular tissue voxel population. After binarization of the segmented images, a median

filter set at 3 voxels for (x, y) was applied to suppress artefactual isolated voxels. After segmentation and filtering of the Golgi apparatus and nuclei images, the two images were merged into a single RGB image, with the nuclei in blue and the Golgi apparatus in green. After merging the images, some artefacts remain, corresponding to small blue and green objects that are neither nuclei nor Golgi apparatus. To identify only the nuclei and Golgi apparatus, two successive segmentations based on the color and size of the objects were carried out. Segmentation based on color identified all objects of the same color. Nuclei and associated artefacts were thresholded on blue, and Golgi apparatus and associated artefacts were thresholded on green. Size segmentation was used to exclude small artefacts that corresponded neither to nuclei nor to Golgi apparatus, so that only nuclei and Golgi apparatus could be identified and numbered. The thresholds for identifying nuclei and Golgi apparatus by size are $10 \mu\text{m}^2$ and $2 \mu\text{m}^2$ respectively.

Data analysis

At the end of the nuclei and Golgi apparatus identification stage, a unique ID number was obtained for each object (nucleus and Golgi apparatus), with the orthonormal coordinates of its center in (x,y),

TABLE 1 Hemodynamic parameters. Values are given as mean \pm standard deviation (SD), for 8-week old C57BL6/J male (S♂) and female (S♀) mice. bpm: beats per minute; WSS: wall shear stress. Shear stress data in italics are calculated from the experimental data using (Eq. 3) for theoretical N-method (Eq. 4), for corrected N-method, with apparent viscosity = 2.24 (♂) and 2.26 (♀), applying 1.78 as correcting factor to plasmatic viscosity, and (Eq. 8) for F-method.

	S♂ (n = 6–8)		S♀ (n = 7–8)	
Hematocrit	0.43 \pm 0.02		0.43 \pm 0.03	
Total blood viscosity (cP)	4.1 \pm 0.4		3.9 \pm 0.6	
Plasma viscosity (cP)	1.26		1.27	
Heart frequency (bpm)	455 \pm 36		429 \pm 62	
	Diastole	Systole	Diastole	Systole
Diameter (mm)	0.387 \pm 0.05	0.484 \pm 0.05	0.376 \pm 0.04	0.466 \pm 0.05
Blood velocity (mm.s ⁻¹)	157 \pm 43	999 \pm 183	167 \pm 54	1,015 \pm 258
Theoretical N-method WSS (Pa)	<i>6.1 \pm 1.5</i>	<i>34.7 \pm 8.1</i>	<i>6.9 \pm 2.9</i>	<i>33.4 \pm 9.4</i>
Corrected N-method WSS (Pa)	<i>5.2 \pm 1.9</i>	<i>25.9 \pm 5.9</i>	<i>5.6 \pm 2.3</i>	<i>27.2 \pm 7.0</i>
F-method WSS (Pa)	5.9 \pm 2.3	29.7 \pm 6.5	6.3 \pm 2.5	30.4 \pm 6.9

and the length (in μm) of its major and minor axes. These data were processed, using Microsoft Excel with the Kutools extension, to calculate the orientation and the polarity of ECs as follows.

For each EC orientation, the “nucleus-Golgi apparatus” (N-G) vector was first identified by the coordinates of its starting point (center of the nucleus) and its ending point (center of the nearest Golgi apparatus). The angle between each N-G vector and the direction of the blood flow was then calculated (in degree, reported on a semicircle) and used to define the orientation of each EC from blood flow, 0° and 180° being the orientations similar and opposite to the blood flow, respectively. Three classes of orientation were then defined according to the N-G vector angle: (i) a dromic orientation (in the direction of the flow) when the angle range was [0°; 60°]; (ii) a perpendicular orientation (to the direction of the flow) when it was [60°; 120°]; (iii) an antidromic orientation (in the opposite direction to the flow) when it was [120°; 180°]. The frequency of angle distribution was studied for each carotid. In the case of an equiprobable distribution, corresponding to the absence of orientation, the angle frequency is one-third per class.

The polarity of the ECs of the right common carotid artery was defined by two parameters, the length (in μm) of the N-G vector and the elongation coefficient of the nucleus corresponding to the ratio between the lengths of the major and minor axes of the nucleus.

Statistical analysis

All statistical analyses were done using GraphPad Prism® software (Prism 9.0.1 version), (San Diego, CA, United States), and results were considered as statistically significant for $p < 0.05$. Hematocrit, viscosity, and shear stress parameters are expressed as mean \pm standard deviation (SD). Statistical comparisons between male and female were done with Mann-Whitney non-parametric test. Hematocrit versus blood viscosity was analyzed by linear regression. Cell orientation parameters were analyzed using a contingency table with three outcomes, and

compared with χ^2 test. Polarity parameters were expressed as mean \pm SEM. Statistical comparisons were done with one-sample Wilcoxon signed-rank test (nucleus elongation index) and Mann-Whitney non-parametric test (male versus female).

Results

Blood flow velocity and vessel diameter

Representative original traces of right common carotid artery diameter and blood flow velocity measurements are shown in Figure 2. Systolic and diastolic arterial diameters and maximum blood velocities are given in Table 1 and presented in Figure 3. For all parameters, differences between male and female were very low, less than 6%, and were not statistically significant. Average mean diastolic diameter was around 0.380 mm, with around 25% increase in systole. Average mean diastolic maximum blood velocity was around 160 mm.s⁻¹, with more than 500% increase in systole.

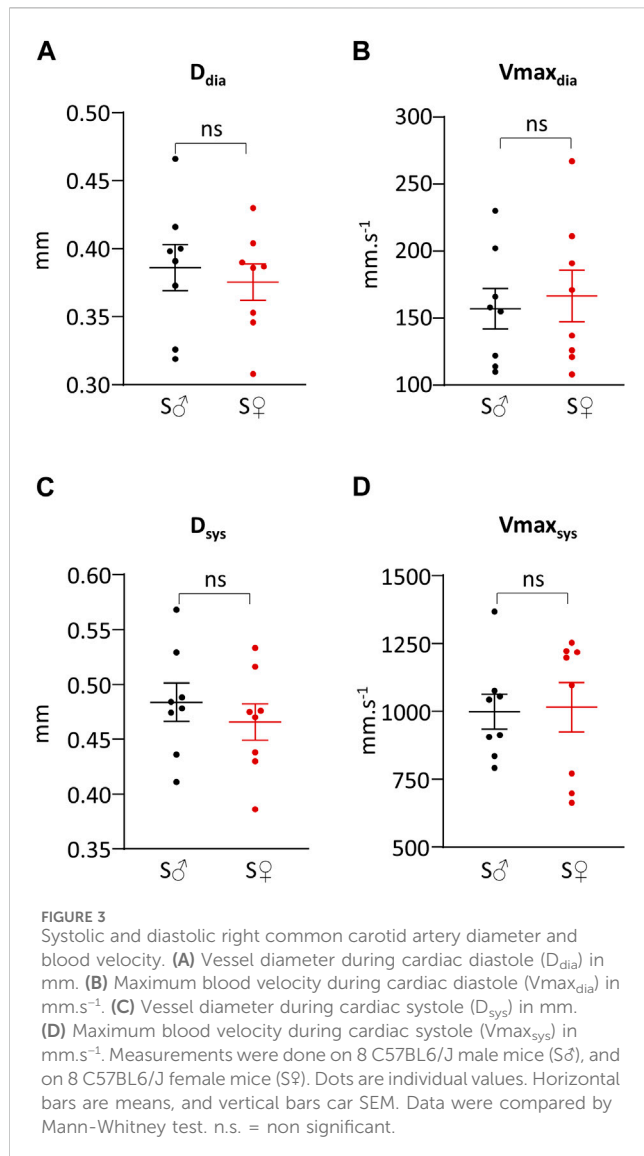
Hemodynamic viscosity and hematocrit

Total blood viscosity and hematocrit are given in Table 1 and presented in Figures 4A, B, respectively. Differences between male and female blood viscosity were very low, equal to 5%, and were not statistically different. Individual hematocrit varied between 38% and 46%, without difference in mean value between male and female.

The relationship between total blood viscosity and hematocrit was evaluated by plotting blood viscosity (η_b) against the hematocrit (Ht) (Figure 4C) with linear regression analysis, providing the following equation ($R^2 = 0.35$):

$$\eta_b = (0.01258 \times Ht) - 0.001443 \quad (9)$$

Plasma viscosity was measured, for each sex, on pooled blood of each sex group. Male plasma viscosity was equal to 1.26 cP, and female plasma viscosity was equal to 1.27 cP.

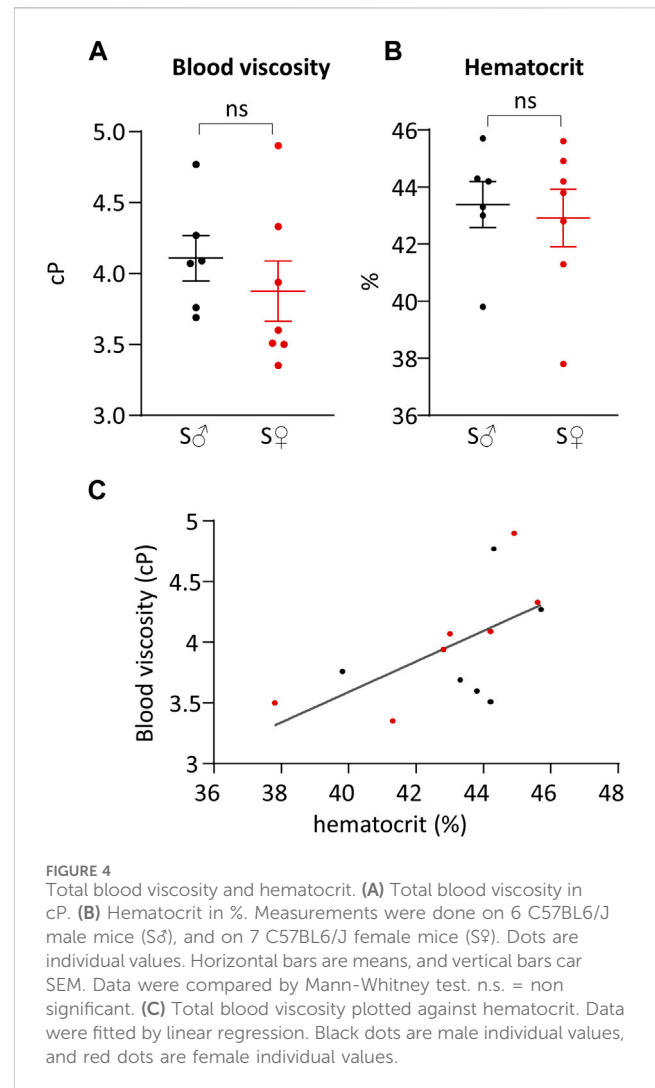


Shear stress

Systolic and diastolic shear stress values were calculated by the theoretical N-method (tN-method), corrected N-method (cN-method), and F-method (Table 1; Figure 5). Regarding sex difference, whatever the calculation method used, differences between male and female mice for systolic and diastolic WSS values were very small, ranging from less than 1% to 13%, and were not statistically different.

cN-method generated identical WSR values but very different WSS ones depending on the viscosity value, as shown in Figures 5B, E, with a 3-fold difference between plasmatic and total blood viscosity, the value obtained with apparent viscosity (corrected from plasmatic viscosity) being in between. WSS values with plasmatic and total blood viscosity were very different from that obtained using the tN- and F-methods. By contrast, cN-method with corrected apparent viscosity provided WSS values close to that obtained from tN-method and F-method, themselves being very similar for both diastolic (6% difference) and systolic (14% difference) WSS values.

Beyond the calculation of WSS with our own experimental results, we have used Eqs 3, 8 to perform a comparative sensitivity analysis of



the tN-method and F-methods to vessel diameter, blood flow velocity, and hematocrit. For this, we generated WSS predictions of the tN-method and F-methods changing each of these parameters, the others being set constant. Since no sex difference was seen, data from each sex were pooled for these comparisons. Since the Fahraeus-Lindqvist effect is usually considered to occur in small vessels (diameter <0.3 mm), we have first analyzed the relationship between vessel diameter ranging from 0.1 to 1 mm (with 0.1 mm step) and WSS predicted by the tN- and F-methods, respectively, for our average diastolic and systolic V_{max} . Whatever the diameter, the difference between tN- and F-methods was 13.03% (Figures 6A, B). A similar approach was used to analyze the relationship between blood maximal velocity (ranging from 100 to 1,100 $mm.s^{-1}$) for our average diastolic and systolic diameters, with identical results (13.03% difference) whatever the blood maximal velocity (data not shown). For the analysis of hematocrit variation, since this parameter is not formally present in the tN-method, we have implemented Eq. 3 with the linear Eq. 9 obtained from the regression analysis of the hematocrit-viscosity analysis, as follows:

$$\tau_t = ((0.01258 \times Ht) - 0.001443) \times \frac{4 \times V_{max}}{D} \quad (10)$$

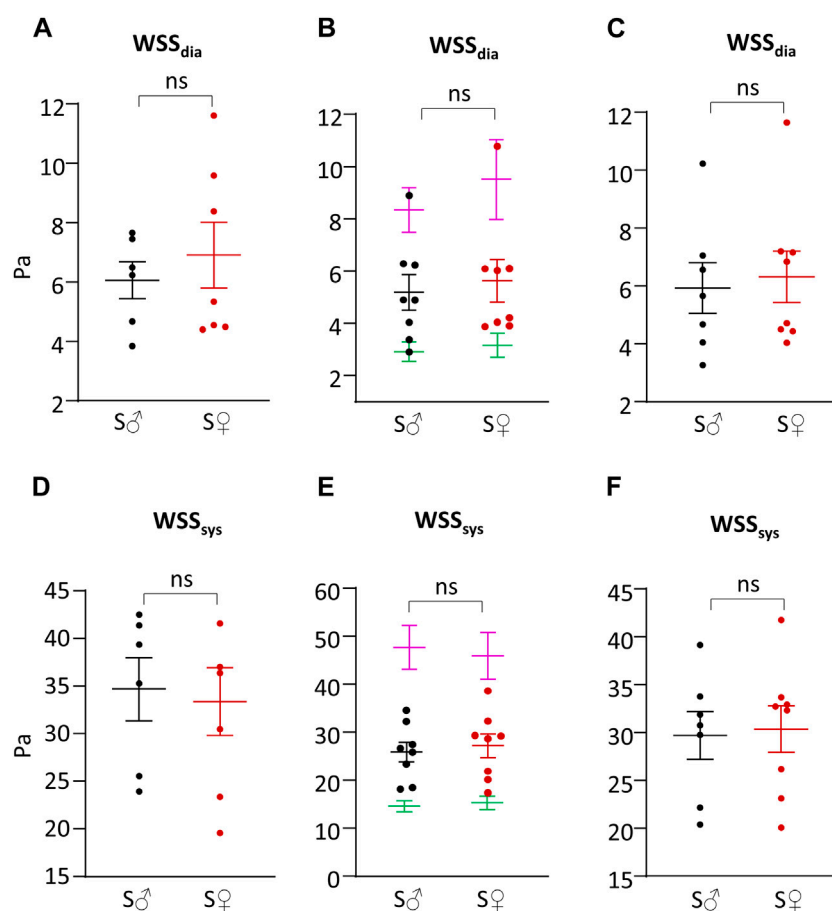


FIGURE 5

Shear stress. (A) Wall shear stress value during cardiac diastole (WSS_{dia}) in Pa, calculated with theoretical N-method (Eq. 3). (B) Wall shear stress value during cardiac diastole (WSS_{dia}) in Pa, calculated with corrected N-method with plasmatic (green), total blood (purple) and apparent (≈ 1.78 plasmatic) (female, red/male, black) viscosity (Eq. 4). (C) Wall shear stress value during cardiac diastole (WSS_{dia}) in Pa, calculated with F-method (Eq. 8). (D) Wall shear stress value during cardiac systole (WSS_{sys}) in Pa, calculated with theoretical N-method (Eq. 3). (E) Wall shear stress value during cardiac systole (WSS_{sys}) in Pa, calculated with corrected N-method with plasmatic (green), total blood (purple) and apparent (≈ 1.78 plasmatic) (female, red/male, black) viscosity (Eq. 4). (F) Wall shear stress value during cardiac systole (WSS_{sys}) in Pa, calculated with F-method (Eq. 8). Measurements were done on 6–8 C57BL6/J male mice (S_{δ}), and on 7–8 C57BL6/J female mice (S_{η}). Dots are individual values. Horizontal bars are means, and vertical bars car SEM. Data were compared by Mann-Whitney test. n.s. = non significant.

The relationship between hematocrit, ranging from 38% to 48% mm (the range observed in our own experiments) and WSS predicted by the tN- and F-methods, respectively, calculated for our average diastolic V_{max} and D , is shown in Figure 6C. The difference in the predicted values by the 2 methods depended on the Ht value, the difference increasing with increasing hematocrit, ranging from 7% to 16% for hematocrit ranging from 38% to 48% (Figure 6D). Identical results were obtained for average systolic V_{max} and D (data not shown).

EC polarity and orientation

A representative image of nucleus and Golgi apparatus automated identification is shown in Figure 7A. The percentage of antidromic, dromic and lateral EC orientation (angle between N-G vector and blood flow direction, see Figure 7B) is presented in Figure 7C. For both sex, ECs were mainly oriented against blood

flow, with more than 50% of antidromic ECs (statistically different from random orientation). Differences between male and female ECs orientation were very low, inferior to 15%, and were not statistically different.

Regarding EC polarization, nuclei were elongated with a nucleus elongation ratio statistically different from 1, for both sexes. EC polarization was similar in both sexes, since differences between male and female for the N-G vector length and nucleus elongation ratio were very low, less than 4%, and not statistically different. The length of the N-G vector and the elongation of the nuclei are presented in Figures 7D, E, respectively.

Discussion

Our results showed that mouse common coronary artery diameter varies between 350 μm and 550 μm , approximatively, between cardiac diastole and systole. While being more than ten-

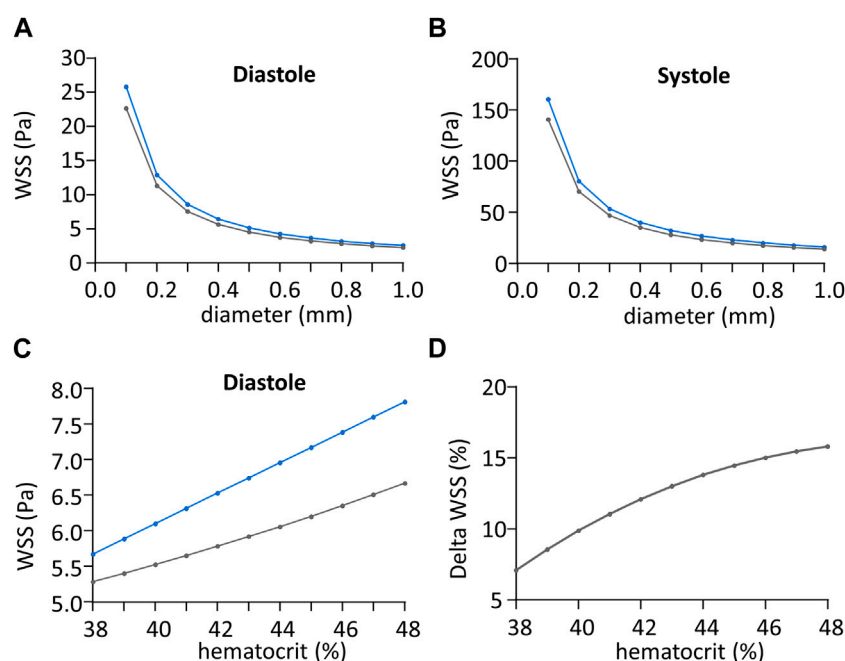


FIGURE 6

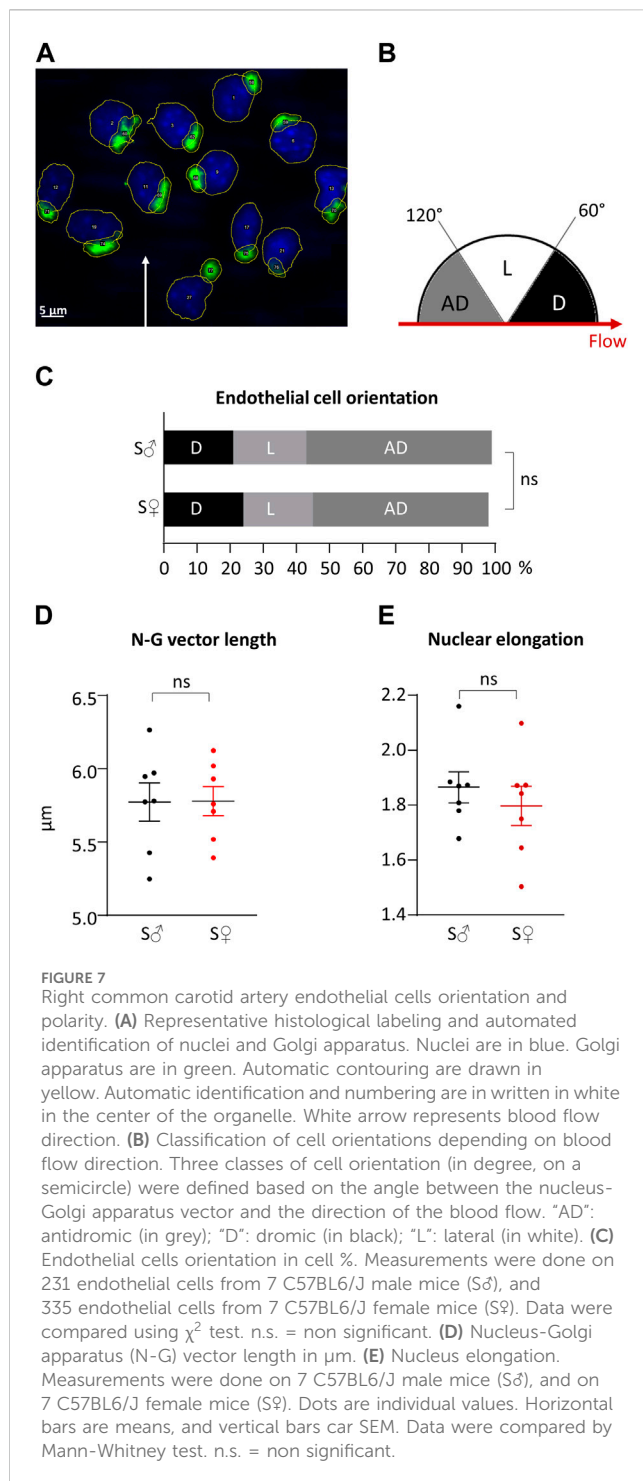
Impact of shear stress calculation method regarding vessel diameter. (A) Wall shear stress value (WSS) during cardiac diastole in Pa, regarding vessel diameter in mm, calculated with theoretical N-method (in blue) and F-method (in grey). (B) Wall shear stress (WSS) value during cardiac systole in Pa, regarding vessel diameter in mm, calculated with theoretical N-method (in blue) and F-method (in grey). (C) Wall shear stress (WSS) value during cardiac diastole in Pa, regarding hematocrit in %, calculated with theoretical N-method (in blue) and F-method (grey). (D) Difference between theoretical N-method and F-method wall shear stress (WSS) values normalized to the mean WSS from the two methods, in Pa, plotted against hematocrit in %.

fold thinner than average human carotid artery diameter (Roux et al., 2020), our results are in accordance with mouse literature values (Panteleev et al., 2021). Regarding the maximum blood velocity, our values vary between 150 mm.s^{-1} (diastole) and $1,000 \text{ mm.s}^{-1}$ (systole). Compared to literature on mouse carotid artery that shows a variation between 250 mm.s^{-1} and $1,800 \text{ mm.s}^{-1}$ (Parzy et al., 2009), our own values are a little bit lower. However, this difference can be correlated to the heart beat effect, as it can be seen that the higher the heart beats are, the higher the blood velocity values are too, and vice versa (Chérin et al., 2006; Parzy et al., 2009).

Our results showed that mouse average hematocrit is around 43%, which is in accordance with average values found in literature around 40%–42% (Vogel et al., 2003; Windberger et al., 2003). While it has been already shown for humans that hematocrit values are higher for man compared to woman (Grau et al., 2018), to our study showed that there were no difference between male and female hematocrit in mice. Average total blood viscosity in our study was found around 4 cP. It has been shown that mouse total blood apparent viscosity decreases from 30 cP to 4 cP when the shear rate value increases from 0 s^{-1} to $1,000 \text{ s}^{-1}$, following an exponential decay (Vogel et al., 2003; Windberger et al., 2003; Alexy et al., 2022). As we measured this apparent blood viscosity at $1,200 \text{ s}^{-1}$, our average value is in accordance with literature observation. Our results also confirmed previous observation regarding the linear relationship between the total blood viscosity and the hematocrit (Vogel et al., 2003). Our values for mouse plasma viscosity are in accordance with literature values (Vogel et al., 2003; Windberger et al., 2003).

WSS calculations were done under 2 different and opposite assumptions regarding the rheological properties of blood flow, both being idealized representations of actual blood flow. Importantly, they produced similar results, the differences between methods being small and not statistically significant, suggesting that these methods are similarly relevant.

In the so-called “Newtonian” method, blood is considered as a homogenous fluid following Poiseuille’s law Newtonian fluid properties, whereas the so-called « Fahraeus-Lindqvist » method considers that the blood flow is heterogeneous, with a central plug of blood cells separated from the plasma sheath, equivalent to the phenomenon initially described by Fahraeus in small tubes, and known as the “Fahraeus-Lindqvist effect.” It is generally accepted that this effect occurs in vessels of less than $300 \mu\text{m}$ diameter, close but inferior to the inner diastolic and systolic diameters of the mouse common carotid. It could be hence hypothesized that blood flow had an intermediate behavior in our model, the reason why we tested an empirical adaptation of the theoretical « Newtonian » approach, the so-called « corrected » N-method. Though opposite in their theoretical assumptions and different in their mathematical formulations, the theoretical N- and F-methods provided very similar results, that may be explained by the fact that the measured total blood viscosity, used for tN-method, is an apparent one assuming that blood is a homogenous fluid. This was also true for the corrected N-method when a correcting factor was applied to the plasmatic velocity to obtain the apparent viscosity. By contrast, the corrected N-method results with uncorrected blood viscosity, either plasmatic or total blood ones, were very different, being much lower and much higher,



respectively, then that obtained with the other methods. Though it is known that the peripheral sheath directly in contact with the vessel wall is cell-free plasma (Secomb and Pries, 2013), taking into account the plasmatic viscosity produced irrelevant results. This is due to the fact that correction of the N-method, supposedly more realistic, remains an idealized representation of the blood as a Newtonian fluid and hence requires to rectify the plasmatic viscosity using a correcting factor. The key question is hence the choice of the correcting factor, in particular because the corrected N-method is highly sensitive to the viscosity value, and the

correcting factor is not directly obtained from our experimental results. Additionally, the velocity profile could not be experimentally determined due to technical limitation, so that the V_{max}/V_m ratio was also extrapolated from studies done in conditions different from that of the present study. Though supposedly being realistic, taking into account the experimental data obtained in our study, this kind of approach is not really realistic, since it is highly sensitive to parameters that cannot be experimentally determined. By contrast, the F-method proposed in this study does not require such corrections and allows the calculation of shear rate and shear stress using non corrected experimental values for the different parameters of the corresponding equation. It is based on an idealization of the blood behavior, considering that all the blood cells constitutes the central core, and the peripheral sheath as cell-free plasma, whereas blood cells are actually present in suspension in the plasma sheath, except its peripheral layer directly in contact with the vessel wall (Secomb, 2017). However, comparison with *in vitro* measurement of blood flow (Yeleswarapu et al., 1998) shows that the theoretical velocity profile hypothesized in the F-method is realistically relevant.

Regarding the theoretical N- versus the F-method, the relative difference in their predictions remains identical under variation of the vessel diameter below and above the « threshold » value under which the Fahraeus-Lindqvist effect is supposed to occur. This may be surprising considering the actual blood flow behavior, but is mathematically logical since for both methods, the mathematical dependence of WSS on vessel diameter is identical, as it is for the maximal velocity (see Eqs 3, 8). This is not the case for the effect of the hematocrit on WSS value, since hematocrit is a parameter of the F-method but not the N-one. As discussed above, the total blood viscosity is indeed dependent on the hematocrit, but the empirical correlation is weak and hence of poor predictive value. Moreover, the total blood viscosity needed for the calculation of the WSS with the tN-method is an apparent one which value depends not only on the hematocrit but also the shear rate, which is not the case for the plasmatic viscosity (Vogel et al., 2003). Since the shear rate varies between diastole and systole, unbiased calculation of WSS using the total blood viscosity should consider different viscosity values for diastolic and systolic WSS, which is not the case for the F-method that used the plasmatic viscosity. Whatever the method used, our results showed highly oscillatory SS values during the cardiac cycle. Although these values are around 10-fold higher than those measured in the human common carotid artery (Roux et al., 2020), they are consistent with those found in the literature in mice (De Wilde et al., 2016).

Our results showed that mouse ECs were polarized and mainly oriented against the blood flow. This is in accordance with previous studies that showed that, physiologically, ECs are elongated (Urschel et al., 2021) and oriented against the blood flow (Franco et al., 2015; Vion et al., 2021). According to the literature, these characteristics of EC planar cell polarity are related to the high wall shear stress. ECs exposed to low WSS tend to show a "cobble-stone like shape" (Urschel et al., 2021), and more likely oriented with the blood flow direction (Baeyens et al., 2015; Vion et al., 2021).

In conclusion, our study provides, for both male and female mice, hemodynamic values for blood flow velocity and vessel diameter, combined with *in vitro* hematocrit and viscosity measurements on each mouse, allowing individual calculation of WSS variation during the cardiac cycle. We propose a new method

for WSS calculation, alternative to the classical one based on the Poiseuille's law, considering the so-called "Fahraeus-Lindqvist effect." Comparison with experimental characterization of blood flow behavior indicates that this methodology is relevant to compute WSS in the macrovasculature, i.e., for vessel diameter above 100 μm . For small vessels, with diameter around 10 μm or lower, characterization of blood flow properties at microscale level requires further investigation. Additionally, regarding the potential influence of sex on WSS and EC sensitivity to blood flow direction, a comparison that, to the best of our knowledge, it has not been yet done in previous studies, it showed that WSS homeostasis was similar in male and female mice.

Data availability statement

The original contributions presented in the study are included in the article/**Supplementary Material**, further inquiries can be directed to the corresponding author.

Ethics statement

The animal study was approved by the Bordeaux local Ethical Committee. The study was conducted in accordance with the local legislation and institutional requirements.

Author contributions

NN: Data curation, Formal Analysis, Investigation, Methodology, Resources, Validation, Visualization, Writing—original draft, Writing—review and editing. AdT: Methodology, Resources, Software, Validation, Writing—review

and editing. ER: Conceptualization, Data curation, Formal Analysis, Investigation, Methodology, Project administration, Resources, Supervision, Validation, Visualization, Writing—original draft, Writing—review and editing.

Funding

The author(s) declare that no financial support was received for the research, authorship, and/or publication of this article.

Conflict of interest

The authors declare that the research was conducted in the absence of any commercial or financial relationships that could be construed as a potential conflict of interest.

Publisher's note

All claims expressed in this article are solely those of the authors and do not necessarily represent those of their affiliated organizations, or those of the publisher, the editors and the reviewers. Any product that may be evaluated in this article, or claim that may be made by its manufacturer, is not guaranteed or endorsed by the publisher.

Supplementary material

The Supplementary Material for this article can be found online at: <https://www.frontiersin.org/articles/10.3389/fphys.2024.1386151/full#supplementary-material>

References

- Aarts, P. A., van den Broek, S. A., Prins, G. W., Kuiken, G. D., Sixma, J. J., and Heethaar, R. M. (1988). Blood platelets are concentrated near the wall and red blood cells, in the center in flowing blood. *Arterioscler. Off. J. Am. Heart Assoc. Inc.* 8, 819–824. doi:10.1161/01.ATV.8.6.819
- Aarts, P. A. M. M., van Broek, J. A., Th, M., Kuiken, G. D. C., Sixma, J. J., and Heethaar, R. M. (1984). Velocity profiles in annular perfusion chamber measured by laser-Doppler velocimetry. *J. Biomech.* 17, 61–63. doi:10.1016/0021-9290(84)90081-2
- Alexy, T., Deterich, J., Connes, P., Toth, K., Nader, E., Kenyeres, P., et al. (2022). Physical properties of blood and their relationship to clinical conditions. *Front. Physiol.* 13, 906768. doi:10.3389/fphys.2022.906768
- Baeyens, N., Bandyopadhyay, C., Coon, B. G., Yun, S., and Schwartz, M. A. (2016). Endothelial fluid shear stress sensing in vascular health and disease. *J. Clin. Invest.* 126, 821–828. doi:10.1172/JCI83083
- Baeyens, N., Nicoli, S., Coon, B. G., Ross, T. D., Van den Dries, K., Han, J., et al. (2015). Vascular remodeling is governed by a VEGFR3-dependent fluid shear stress set point. *eLife* 4, e04645. doi:10.7554/eLife.04645
- Barbee, J. H., and Cokelet, G. R. (1971). The Fahraeus effect. *Microvasc. Res.* 3, 6–16. doi:10.1016/0026-2862(71)90002-1
- Chen, Z., and Tzima, E. (2009). PECAM-1 is necessary for flow-induced vascular remodeling. *Arterioscler. Thromb. Vasc. Biol.* 29, 1067–1073. doi:10.1161/ATVBAHA.109.186692
- Chérin, E., Williams, R., Needles, A., Liu, G., White, C., Brown, A. S., et al. (2006). Ultrahigh frame rate retrospective ultrasound microimaging and blood flow visualization in mice *in vivo*. *Ultrasound Med. Biol.* 32, 683–691. doi:10.1016/j.ultrasmedbio.2005.12.015
- de Tilly, A. (2015). A method of determining a viscosity index of a complex fluid. Available at: <https://patentscope.wipo.int/search/en/detail.js?docId=W0201517768>.
- de Tilly, A., Jouenne, S., Heurteux, G., and Santanach Carreras, E. (2023). Measurement system for a liquid. Available at: [https://patents.google.com/patent/WO2023111614A1/en?q=\(tilly+jouenne\)&ox=tilly+jouenne](https://patents.google.com/patent/WO2023111614A1/en?q=(tilly+jouenne)&ox=tilly+jouenne).
- De Wilde, D., Trachet, B., De Meyer, G., and Segers, P. (2016). The influence of anesthesia and fluid–structure interaction on simulated shear stress patterns in the carotid bifurcation of mice. *J. Biomech.* 49, 2741–2747. doi:10.1016/j.jbiomech.2016.06.010
- Fahraeus, R. (1929). The suspension stability of the blood. *Physiol. Rev.* 9, 241–274. doi:10.1152/physrev.1929.9.2.241
- Fåhræus, R., and Lindqvist, T. (1931). The viscosity of the blood in narrow capillary tubes. *Am. J. Physiol.-Leg. Content* 96, 562–568. doi:10.1152/ajplegacy.1931.96.3.562
- Franco, C. A., Jones, M. L., Bernabeu, M. O., Geudens, L., Mathivet, T., Rosa, A., et al. (2015). Dynamic endothelial cell rearrangements drive developmental vessel regression. *PLoS Biol.* 13, e1002125. doi:10.1371/journal.pbio.1002125
- Grau, M., Cremer, J. M., Schmeichel, S., Kunkel, M., and Bloch, W. (2018). Comparisons of blood parameters, red blood cell deformability and circulating nitric oxide between males and females considering hormonal contraception: a longitudinal gender study. *Front. Physiol.* 9, 1835. doi:10.3389/fphys.2018.01835
- Hoskins, P. R. (2011). Estimation of blood velocity, volumetric flow and wall shear rate using Doppler ultrasound. *Ultrasound* 19, 120–129. doi:10.1258/ult.2011.011015
- John, L., Ko, N. L., Gokin, A., Gokina, N., Mandalà, M., and Osol, G. (2018). The Piezo1 cation channel mediates uterine artery shear stress mechanotransduction and vasodilation during rat pregnancy. *Am. J. Physiol.-Heart Circ. Physiol.* 315, H1019–H1026. doi:10.1152/ajpheart.00103.2018

- Lee, H.-W., Shin, J. H., and Simons, M. (2022). Flow goes forward and cells step backward: endothelial migration. *Exp. Mol. Med.* 54, 711–719. doi:10.1038/s12276-022-00785-1
- McCue, S., Dajnowiec, D., Xu, F., Zhang, M., Jackson, M. R., and Langille, B. L. (2006). Shear stress regulates forward and reverse planar cell polarity of vascular endothelium *in vivo* and *in vitro*. *Circ. Res.* 98, 939–946. doi:10.1161/01.RES.0000216595.15868.55
- Nicolas, N., Dinet, V., and Roux, E. (2023). 3D imaging and morphometric descriptors of vascular networks on optically cleared organs. *iScience* 26, 108007. doi:10.1016/j.isci.2023.108007
- Ong, C. W., Wee, I., Syn, N., Ng, S., Leo, H. L., Richards, A. M., et al. (2020). Computational fluid dynamics modeling of hemodynamic parameters in the human diseased aorta: a systematic review. *Ann. Vasc. Surg.* 63, 336–381. doi:10.1016/j.avsg.2019.04.032
- Pantelev, M. A., Korin, N., Reesink, K. D., Bark, D. L., Cosemans, J. M. E. M., Gardiner, E. E., et al. (2021). Wall shear rates in human and mouse arteries: standardization of hemodynamics for *in vitro* blood flow assays: communication from the ISTH SSC subcommittee on biorheology. *J. Thromb. Haemost.* 19, 588–595. doi:10.1111/jth.15174
- Parzy, E., Miraux, S., Jean-Michel, F., and Thiaudière, E. (2009). *In vivo* quantification of blood velocity in mouse carotid and pulmonary arteries by ECG-triggered 3D time-resolved magnetic resonance angiography. *NMR Biomed.* 22, 532–537. doi:10.1002/nbm.1365
- Poduri, A., Raftrey, B., Chang, A. H., Rhee, S., Van, M., and Red-Horse, K. (2017). Endothelial cells respond to the direction of mechanical stimuli through SMAD signaling to regulate coronary artery size. *Dev. Dev.* 144, 3241–3252. doi:10.1242/dev.150904
- Reneman, R. S., Arts, T., and Hoeks, A. P. G. (2006). Wall shear stress—an important determinant of endothelial cell function and structure—in the arterial system *in vivo*. Discrepancies with theory. *J. Vasc. Res.* 43, 251–269. doi:10.1159/000091648
- Roux, E., Bougaran, P., Dufourcq, P., and Couffignal, T. (2020). Fluid shear stress sensing by the endothelial layer. *Front. Physiol.* 11, 861. doi:10.3389/fphys.2020.00861
- Secomb, T. W. (2017). Blood flow in the microcirculation. *Annu. Rev. Fluid Mech.* 49, 443–461. doi:10.1146/annurev-fluid-010816-060302
- Secomb, T. W., and Pries, A. R. (2013). Blood viscosity in microvessels: experiment and theory. *Comptes Rendus Phys.* 14, 470–478. doi:10.1016/j.crhy.2013.04.002
- Urschel, K., Tauchi, M., Achenbach, S., and Dietel, B. (2021). Investigation of wall shear stress in cardiovascular research and in clinical practice—from bench to bedside. *Int. J. Mol. Sci.* 22, 5635. doi:10.3390/ijms22115635
- Vion, A.-C., Perovic, T., Petit, C., Hollfinger, I., Bartels-Klein, E., Frampton, E., et al. (2021). Endothelial cell orientation and polarity are controlled by shear stress and VEGF through distinct signaling pathways. *Front. Physiol.* 11, 623769. doi:10.3389/fphys.2020.623769
- Vogel, J., Kiessling, I., Heinicke, K., Stallmach, T., Ossent, P., Vogel, O., et al. (2003). Transgenic mice overexpressing erythropoietin adapt to excessive erythrocytosis by regulating blood viscosity. *Blood* 102, 2278–2284. doi:10.1182/blood-2003-01-0283
- Windberger, U., Bartholovitsch, A., Plasenzotti, R., Korak, K. J., and Heinze, G. (2003). Whole blood viscosity, plasma viscosity and erythrocyte aggregation in nine mammalian species: reference values and comparison of data. *Exp. Physiol.* 88, 431–440. doi:10.1113/eph8802496
- Yeleswarapu, K. K., Kameneva, M. V., Rajagopal, K. R., and Antaki, J. F. (1998). The flow of blood in tubes: theory and experiment. *Mech. Res. Commun.* 25, 257–262. doi:10.1016/S0093-6413(98)00036-6



OPEN ACCESS

EDITED BY

Markus Hecker,
Heidelberg University, Germany

REVIEWED BY

Thomas Korff,
Heidelberg University, Germany
Andreas H. Wagner,
Heidelberg University, Germany

*CORRESPONDENCE

Julia J. Mack,
✉ jmack@mednet.ucla.edu

RECEIVED 13 May 2024

ACCEPTED 01 July 2024

PUBLISHED 24 July 2024

CITATION

Hong S-G, Kennelly JP, Williams KJ,
Bensinger SJ and Mack JJ (2024), Flow-
mediated modulation of the endothelial
cell lipidome.

Front. Physiol. 15:1431847.

doi: 10.3389/fphys.2024.1431847

COPYRIGHT

© 2024 Hong, Kennelly, Williams, Bensinger and Mack. This is an open-access article distributed under the terms of the [Creative Commons Attribution License \(CC BY\)](#). The use, distribution or reproduction in other forums is permitted, provided the original author(s) and the copyright owner(s) are credited and that the original publication in this journal is cited, in accordance with accepted academic practice. No use, distribution or reproduction is permitted which does not comply with these terms.

Flow-mediated modulation of the endothelial cell lipidome

Soon-Gook Hong^{1,2}, John P. Kennelly^{2,3}, Kevin J. Williams^{4,5},
Steven J. Bensinger^{5,6} and Julia J. Mack^{1,2*}

¹Department of Medicine, Division of Cardiology, University of California, Los Angeles, Los Angeles, CA, United States, ²Molecular Biology Institute, University of California, Los Angeles, Los Angeles, CA, United States, ³Department of Pathology and Laboratory Medicine, University of California, Los Angeles, Los Angeles, CA, United States, ⁴Department of Biological Chemistry, University of California, Los Angeles, Los Angeles, CA, United States, ⁵UCLA Lipidomics Lab, University of California, Los Angeles, Los Angeles, CA, United States, ⁶Department of Microbiology, Immunology and Molecular Genetics, University of California, Los Angeles, Los Angeles, CA, United States

The luminal surface of the endothelium is exposed to dynamic blood flow patterns that are known to affect endothelial cell phenotype. While many studies have documented the phenotypic changes by gene or protein expression, less is known about the role of blood flow pattern on the endothelial cell (EC) lipidome. In this study, shotgun lipidomics was conducted on human aortic ECs (HAECs) exposed to unidirectional laminar flow (UF), disturbed flow (DF), or static conditions for 48 h. A total of 520 individual lipid species from 17 lipid subclasses were detected. Total lipid abundance was significantly increased for HAECs exposed to DF compared to UF conditions. Despite the increase in the total lipid abundance, HAECs maintained equivalent composition of each lipid subclass (% of total lipid) under DF and UF. However, by lipid composition (% of total subclass), 28 lipid species were significantly altered between DF and UF. Complimentary RNA sequencing of HAECs exposed to UF or DF revealed changes in transcripts involved in lipid metabolism. Shotgun lipidomics was also performed on HAECs exposed to pro-inflammatory agonists lipopolysaccharide (LPS) or Pam3CSK4 (Pam3) for 48 h. Exposure to LPS or Pam3 reshaped the EC lipidome in both unique and overlapping ways. In conclusion, exposure to flow alters the EC lipidome and ECs undergo stimulus-specific lipid reprogramming in response to pro-inflammatory agonist exposure. Ultimately, this work provides a resource to profile the transcriptional and lipidomic changes that occur in response to applied flow that can be accessed by the vascular biology community to further dissect and extend our understanding of endothelial lipid biology.

KEYWORDS

shear stress, flow pattern, endothelial cell, lipid profile, inflammation

1 Introduction

Endothelial cells (ECs) line the luminal surface of the vasculature and are constantly exposed to mechanical forces generated by blood flow (Galley and Webster, 2004). Due to variations in vessel geometry and curvature, the arterial endothelium experiences different blood flow patterns, including unidirectional laminar flow (UF) generated in linear regions of the vasculature and oscillatory disturbed flow (DF) in regions of the vasculature that are highly curved or bifurcated (Malek et al., 1999). Different levels of hemodynamic shear stress (the frictional force acting on ECs) are present and range from high arterial shear stress

(>15 dyne/cm²) induced by UF to low time-averaged shear stress (4 dyne/cm²) and oscillating flow direction induced by DF.

These distinct blood flow patterns are known to induce different EC phenotypes. While UF promotes a state of endothelial quiescence and an anti-inflammatory phenotype, a pro-inflammatory phenotype is associated with ECs exposed to DF (Chiu and Chien, 2011). Therefore, exposure to DF presents as a local risk factor for vascular inflammation and disease progression (Davis et al., 2001; Yurdagul et al., 2016). Furthermore, the endothelium exposed to DF is more susceptible to the development of chronic inflammatory diseases such as atherosclerosis (Malek et al., 1999; Yurdagul et al., 2016).

Lipids are a major class of biological molecules that are essential for cellular function. Lipids are involved in many bioenergetic, biochemical, and biophysical processes (Muro et al., 2014) and so maintaining lipid homeostasis is critical to cellular health. All cellular membranes are composed of lipids, predominantly phospholipids including glycerophospholipids and sphingolipids (Mutlu et al., 2021; Sakuragi and Nagata, 2023). Neutral lipids, including triglycerides (TG) and cholesteryl esters, are also stored in cytosolic lipid droplets surrounded by a monolayer of phospholipids (Goodman, 2008). In ECs, it has been demonstrated previously that mechanical forces due to applied flow affect the membrane lipid order and fluidity (Yamamoto and Ando, 2013) and alter membrane cholesterol levels (Yamamoto et al., 2020). However, a comprehensive assessment of the changes that occur to the EC lipidome in response to mechanical stress is lacking. In the last decades, many studies have set out to understand the mechanisms of EC inflammatory activation and to identify molecular pathways and potential therapeutic targets to alleviate vascular inflammation (Immanuel and Yun, 2023). However, the role of membrane lipids in the context of EC signaling and vascular inflammation has been less studied.

Here, we conducted complementary studies to characterize the transcriptional and lipidomic profiles of human aortic ECs (HAECs) exposed to the physiological flow conditions of UF and DF. We further compared these datasets to the lipidomic signatures of HAECs exposed to pro-inflammatory agonists. Our results provide a resource to examine how blood flow pattern affects the EC lipid profile and enable the identification of lipid species involved in endothelial inflammation and vascular disease.

2 Methods

2.1 Cell culture and flow application

Primary HAECs (Cell Applications #S304-05a, Lot#1487(s); healthy normal human aorta from 21-year-old Caucasian male) were used from P4 to P12. For cell culture experiments, MCDB-131 complete media (VEC Technologies #MCDB-131 Complete) was supplemented with 10% FBS (Omega USDA certified FBS #FB-11). For plating cells on cell culture dishes, 0.1% gelatin (Stemcell #07903) coating was first applied. Cells were cultured in a 37 °C incubator with 5% CO₂. For application of shear stress, HAECs were seeded in ibidi μ -Slide 0.2 (ibidi #80166) or 0.6 (ibidi #80186) Luer ibiTreat. Unidirectional laminar flow (20 dyn/cm²) or disturbed flow (\pm 4 dyn/cm², 2 Hz) was applied to confluent monolayers using the ibidi pump system (ibidi #10902).

2.2 RNA sequencing analysis

HAECs were seeded on ibidi μ -Slides and subjected to unidirectional laminar flow (20 dyn/cm²) or disturbed flow (\pm 4 dyn/cm², 2 Hz) using the ibidi pump system for 48 h in a 37°C incubator with 5% CO₂. After 48 h, cells were washed with 1X PBS (Gibco #14190-144) and then lysed using RLT lysis buffer (QIAGEN #79216) plus 1% 2-Mercaptoethanol (Sigma Aldrich #M6250). For each condition, four μ -Slides were combined as one flow-exposed sample for a total of 12 slides for n = 3 samples. RNA extraction, library construction, and sequencing were conducted by the UCLA Technology Center for Genomics & Bioinformatics (TCGB) core facility.

Briefly, libraries for RNA sequencing were prepared with KAPA Stranded mRNA-Seq Kit (KAPA Biosystems #KK8421). Briefly, the workflow consisted of mRNA enrichment and fragmentation, first strand cDNA synthesis using random priming followed by second strand synthesis converting cDNA:RNA hybrid to double-stranded cDNA (ds-cDNA), and incorporation of dUTP into the second cDNA strand. cDNA generation was followed by end repair to generate blunt ends, A-tailing, adaptor ligation and PCR amplification. Different adaptors were used for multiplexing samples in one lane. Sequencing was performed on Illumina HiSeq 3,000 for SE 1 \times 65bp run. Data quality check was done on Illumina SAV. Demultiplexing was performed with Illumina Bcl2fastq v2.19.1.403 software. The alignment was performed with Spliced Transcripts Alignment to a Reference (STAR) (Dobin et al., 2013) using the human reference genome assembly GRCh38. The Ensembl Transcripts release GRCh38.107 GTF was used for gene feature annotation. For normalization of transcript counts, normalized counts were generated by counts per million (CPM) normalization.

For graphical display of differential expression, Heatmapper (Babicki et al., 2016) was used to create a heatmap of gene expression. Average linkage was used as Clustering Method, and Kendall's Tau was used as Distance Measurement Method. VolcanoR was used to generate the Volcano plot of gene expression. Log₂ (fold change; FC) as X-variables and -log₁₀ (p-value) as Y-variables were used. ShinyGO 0.77 (Ge et al., 2020) was used for gene enrichment analysis with false discovery rate (FDR) of 0.05 as cut-off. The Database for Annotation, Visualization and Integrated Discovery (DAVID, NIH) was used to identify the biological pathways enriched under DF *versus* UF. Principal component analysis (PCA) was conducted using ClustVis (Metsalu and Vilo, 2015).

Gene Set Enrichment Analysis (GSEA) 4.3.2 software was used to identify biological pathways enriched in response to DF. Genes used for GSEA were those that were differentially expressed in HAECs under DF *versus* UF. The Hallmarks gene set database was used with the following analysis parameters: Number of permutations: 1,000; Collapse/Remap to Gene Symbols: No Collapse; Permutation type: Gene Set; Chip Platform: Human Gene Symbol with Remapping MSigDB.v2023.1. Hs.chip; Enrichment Statistic: Weighted; Metric for Ranking Genes: Signal2Noise; Gene List Sorting Mode: Real; Gene List Ordering Mode: Descending; Max Size: Exclude Larger Sets: 500; Min Size: Exclude Smaller Sets: 15.

From the Gene Ontology (GO) database, lists of genes involved in lipid catabolic process (GO:0016042), neutral lipid catabolic process (GO:004646), and fatty acid catabolic process (GO:

0009062) were identified, and gene expression levels analyzed, from the RNAseq dataset.

2.3 Lipidomics analysis

For flow experiments, HAECs were seeded on ibidi μ -Slides and subjected to unidirectional laminar flow (20 dyn/cm²) or disturbed flow (± 4 dyn/cm², 2 Hz) using the ibidi pump system for 48 h in a 37°C incubator with 5% CO₂. After 48 h, cells were washed with ice-cold 1X PBS and subjected to trypsinization for cell detachment from the slide. For each flow condition, 3 μ -Slides were combined as one sample for a total of 9 slides for $n = 3$ samples. For inflammatory agonist treatments, HAECs were seeded to confluence on 6-well plates (Corning #353046) and treated with either LPS (50 ng/mL; Invivogen, #tlrl-smlps), Pam3 (200 ng/mL; Invivogen #tlrl-pms), or vehicle control for 48 h. Cells were collected and resuspended after centrifugation at 900 rpm for 5 min at 4°C. Cell number was assessed by hemocytometer. Lipid extraction and analysis were conducted by the UCLA Lipidomics Lab.

Cells were transferred to extraction tubes with 1X PBS. A modified Bligh and Dyer extraction (Hsieh et al., 2021) was carried out on samples. Prior to biphasic extraction, a standard mixture of 75 lipid standards (Avanti #330820, 861809, 330729, 330727, 791642) was added to each sample. Following two successive extractions, pooled organic layers were dried down in a Thermo SpeedVac SPD300DDA using ramp setting 4 at 35°C for 45 min with a total run time of 90 min. Lipid samples were resuspended in 1:1 methanol/dichloromethane with 10 mM ammonium acetate and transferred to robovials (Thermo #10800107) for analysis.

Samples were analyzed by direct infusion on a Sciex 5,500 with Differential Mobility Device (DMS) —comparable to the Sciex Lipidizer platform—with a targeted acquisition list consisting of 1,450 lipid species across 17 subclasses. The DMS was tuned with EquiSPLASH LIPIDOMIX (Avanti #330731). Data analysis was performed with in-house data analysis workflow. All instrument settings, MRM lists, and analysis methods are available (Su et al., 2021). Quantitative values were normalized to cell counts.

Heatmaps were generated using Heatmapper (Babicki et al., 2016) and ClustVis (Metsalu and Vilo, 2015). Principal component analysis (PCA) was conducted using ClustVis. X and Y -axis show principal component 1 (PC1) and principal component 2 (PC2), respectively. PCA loadings were extracted from the ClustVis, and the top 20 loadings for PC1 were identified. Cross analysis of the datasets was conducted using InteractiVenn (Heberle et al., 2015) to identify lipid species that were changed under DF and pro-inflammatory agonist exposure.

2.4 Gene expression analysis

For gene expression analysis using qPCR, total RNA was extracted from HAECs using RNeasy Mini kit (QIAGEN #74104). RNA was converted to cDNA by reverse transcription, and cDNA was quantified using a Nano-Drop 8,000 (Thermo Fisher). Target genes were quantified using iTaq universal SYBR Green Supermix (BioRad #1725125) and the appropriate primer pairs. Samples were run on a QuantStudio 6 Flex 384-well qPCR apparatus (Applied Biosystems). Each target gene was normalized to HPRT. Primer sequences (5'–3') are listed below.

KLF2 CATCTGAAGGCGCATCTG CGTGTGCTTTCGGTAGTGG.
KLF4 AGAGTTCCCATCTCAAGGCA GTCAGTTCATCTGAGCGGG.
HPRT GCCCTGGCGTCGTGATTAGT AGCAAGACGTTTCAGTCTGTC.
NOS3 GGATGTGGCTGTCTGCATGGAC TGGTCCACGATGGTGACTTTGG.

2.5 Immunostaining and confocal imaging

For immunostaining, HAECs were fixed with 4% PFA for 5 min followed by multiple washes with 1X PBS. Samples were then blocked for 1 h with 5% Normal donkey serum (Jackson Immuno Research Laboratories #017-000-121) in 1X PBS. Then, samples were permeabilized with 0.1% Triton X-100 (Fisher Scientific #A16046-0F) for 5 min followed by blocking with 5% Normal donkey serum for 1 h. Primary antibodies were incubated overnight at 4 °C in blocking buffer and secondary antibodies applied for 1 h at room temperature. Primary antibodies used: NOS3 (Santa Cruz #sc-376751), ICAM-1 (Santa Cruz #sc-107), NF- κ B p65 (Cell Signaling #8242S), VE-Cadherin (R&D #AF938). Imaging was performed on a Zeiss LSM 900 confocal microscope equipped with 405nm, 488nm, 561nm and 640 nm laser lines using Plan-Apochromat objectives and Airyscan2 GaAsP-PMT detector. Identical laser intensity settings were applied to samples being compared with equivalent Z thickness. After acquisition, a maximum intensity projection of the Z-stack was applied using ZEN Blue 3.5 software (ZEISS). Image processing and quantification of parameters was performed with ImageJ (NIH).

2.6 Drawings

Schematics in figures were created using [BioRender.com](https://www.biorender.com).

2.7 Statistical analysis

Statistical analysis was performed using GraphPad Prism software. The results are presented as mean \pm SD. The Shapiro-Wilk normality test was conducted to measure normal distribution of dependent variables. For normally distributed data, two-tailed independent t -test was used to determine statistically significant differences between two groups. For data that did not pass the normality test, nonparametric one-tailed Mann-Whitney U test was conducted to examine statistical significance between 2 experimental conditions. $p < 0.05$ was considered statistically significant for all analyses.

3 Results

3.1 Disturbed flow alters genes associated with lipid metabolism

HAECs were exposed to UF (20 dyn/cm²) or DF (± 4 dyn/cm², 2 Hz) for 48 h and subjected to RNA sequencing (RNAseq) and shotgun lipidomics (Figure 1A). We confirmed the expected difference in cell morphology of HAECs after exposure to UF

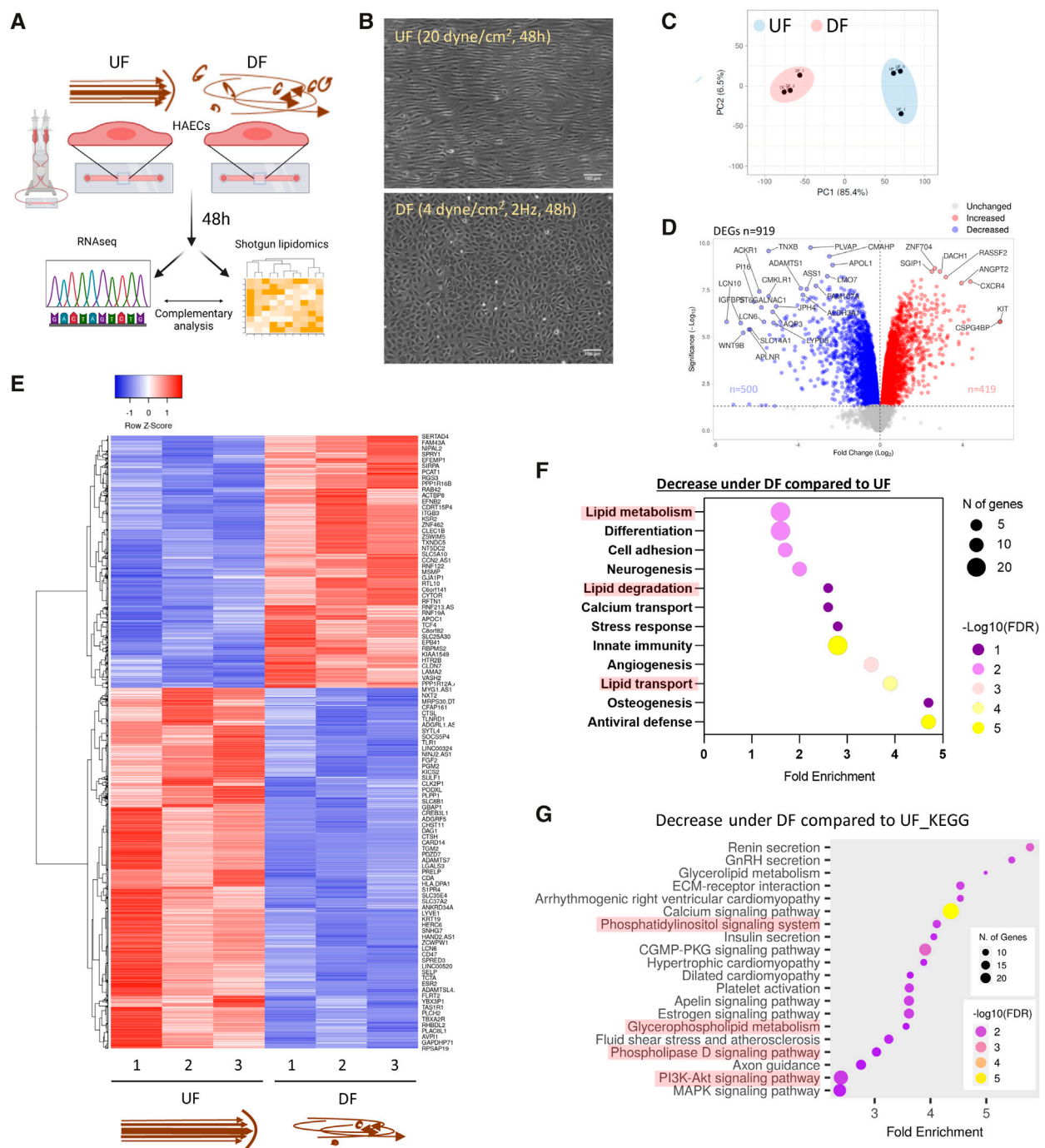


FIGURE 1

Flow pattern affects the transcriptional signature of HAECs and alters the expression of genes related to lipid metabolism (A) Schematic diagram of the experimental procedure. (B) Brightfield micrographs of HAEC monolayers exposed to UF and DF for 48 h. (C) PCA plot of RNA sequencing (RNAseq) data. (D) Volcano plot of differentially expressed genes (DEGs). (E) Heatmap of DEGs. (F) Pathway analysis using DAVID (UniProt database) showing the biological processes downregulated under DF vs. UF. (G) Pathway analysis using ShinyGO (KEGG database) to show reduced biological pathways under DF. UF = Unidirectional laminar flow. DF = Disturbed flow.

or DF for 48 h (Figure 1B). To confirm that our *in vitro* flow system generated the expected EC phenotypes under the applied flow conditions, we validated gene and protein expression. The expression levels of known flow-responsive genes, including Kruppel-like Factor 2 (*KLF2*), Kruppel-like Factor 4 (*KLF4*),

and Nitric Oxide Synthase 3 (*NOS3*) showed a significant upregulation under UF (Supplementary Figure S1A). In addition, confocal imaging of HAEC monolayers confirmed the increase in eNOS protein expression under UF (Supplementary Figure S1B).

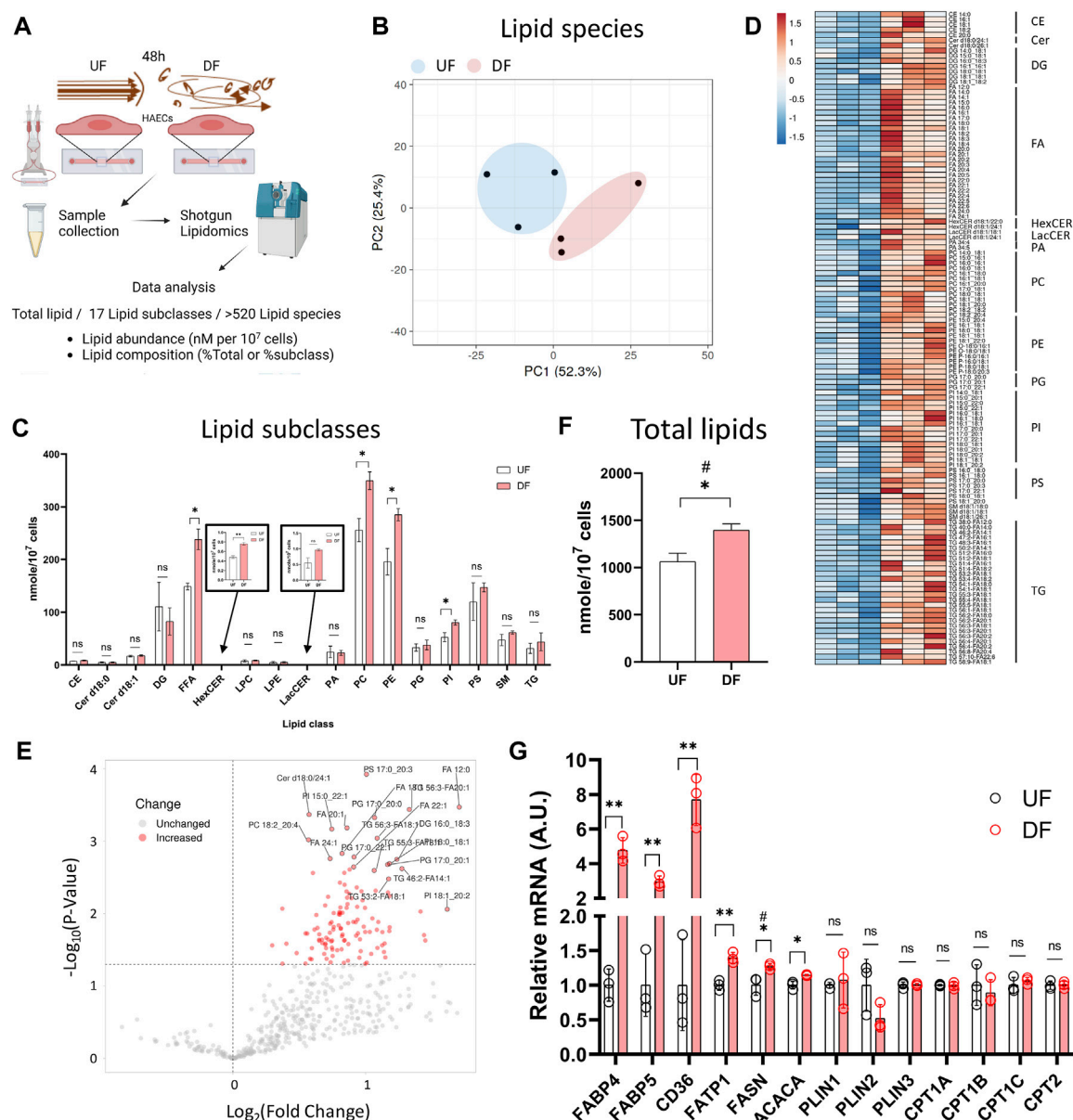


FIGURE 2

Lipid abundance is elevated in HAECs exposed to DF compared to UF (A) Schematic diagram of the lipidomics analysis. (B) PCA plot of lipidomics data. (C) Abundance of each lipid subclasses under UF vs. DF (n = 3). (D) Heatmap of altered lipid species for DF vs. UF. (E) Volcano plot showing altered lipid species under DF vs. UF. (F) Total lipid abundance (nmole per 10⁷ cells) under UF vs. DF. Total lipid abundance was calculated from lipidomics results (n = 3). (G) Expression of the genes involved in fatty acid synthesis, uptake and transport from the RNAseq data (n = 3). Bar graph shown as mean ± SD. *p < 0.05, **p < 0.01, ns = not significant by two-tailed unpaired t-test. #p < 0.05 by one-tailed Mann-Whitney U test.

Consistent with previous reports (Tamargo et al., 2023), our RNAseq analysis showed that DF resulted in dramatic changes in the gene expression profile compared to HAECs exposed to UF (Figures 1C–E). Pro-inflammatory genes known to be induced by DF, such as Angiopoietin 2 (*ANGPT2*), Endothelin 1 (*EDN1*), C-C Motif Chemokine Ligand 2 (*CCL2*), NADPH Oxidase 4 (*NOX4*), 6-phosphofructo-2-kinase/fructose-2,6-biphosphatase 3 (*PFKFB3*), and Hypoxia-Inducible-Factor 1A (*HIF1A*) (Doddaballapur et al., 2015; Wu et al., 2017; Maurya et al., 2021), were significantly elevated in HAECs exposed to DF

(Supplementary Figure S1C). Additionally, we confirmed the pro-inflammatory phenotype of HAECs exposed to DF by confocal imaging. HAECs exposed to DF had increased nuclear NF-κB p65 localization and ICAM-1 protein expression compared to HAECs exposed to UF (Supplementary Figures S1D, S1E). Pathway analysis of differentially expressed genes for HAECs exposed to DF versus UF revealed changes in transcripts associated with lipid metabolism, lipid degradation, lipid transport, and lipid signaling (Figures 1F, G).

3.2 Exposure to disturbed flow increases total cellular lipid content

Based on the observation that genes associated with lipid metabolism were altered in DF compared to UF, we hypothesized that the applied flow pattern may affect the EC lipidome. Therefore, we compared the lipid profiles of HAECs exposed to UF and DF for 48 h (Figure 2A).

Shotgun lipidomics detected a total of 520 individual lipid species from 17 lipid subclasses (Figure 2A). As visualized by principal component analysis (PCA), the lipid profile was distinct between HAECs exposed to UF and DF (Figure 2B). Of the 17 lipid subclasses measured, 5 lipid subclasses were significantly elevated in HAECs exposed to DF compared to UF (Figure 2C). The lipid subclasses that were higher in DF included free fatty acids (FFA), hexosylceramides (HexCER), phosphatidylcholines (PC), phosphatidylethanolamines (PE), and phosphatidylinositols (PI). PC and PE were the most abundant lipid subclasses detected for HAECs under both flow profiles (Figure 2C). A comparison of individual lipid species showed that 66 species were significantly elevated under DF *versus* UF (Figures 2D, E). Furthermore, the total lipid abundance per cell was higher for HAECs exposed to DF compared to UF (Figure 2F).

Further analysis indicated an increase in the abundance of unesterified fatty acids for HAECs exposed to DF (Supplementary Figures S2A, S2B). Fatty acyl chains for phospholipid and glycerolipid synthesis are obtained via import or endogenous synthesis (He et al., 2023) and the fatty acid abundance in cells is affected by proteins that regulate the uptake, synthesis, and transport of fatty acids, as well as proteins that hydrolyze fatty acids from neutral lipids and phospholipids (Supplementary Figure S2D). Cross analysis of the RNAseq data indicated that genes involved in fatty acid synthesis (*ACACA*, *FASN*), fatty acid uptake (*CD36*) and fatty acid transport (*FABP4*, *FABP5*, *FATP1*) were upregulated under DF (Figure 2G). Interestingly, genes involved in lipid catabolic processes, neutral lipid catabolic processes, and fatty acid catabolic processes tended to be reduced in the presence of DF (Supplementary Figures S3A–D). Additionally, GSEA analysis revealed an increase in transcripts related to cholesterol biosynthesis under DF (Supplementary Figure S3E), further suggesting that flow modulates lipid metabolic pathways in HAECs. Together, gene expression analysis indicated a shift towards a program of increased lipid biosynthesis and import, with reduced lipid turnover for HAECs exposed to DF.

Comparing HAECs under static conditions revealed a lipid profile quite distinct from HAECs exposed to either DF or UF (Supplementary Figures S4, S5). PCA of the lipidomics data showed that cells exposed to UF or DF were clearly separated from cells in static conditions on PC1, and cells exposed to DF or static conditions were separated from cells exposed to UF on PC2 (Supplementary Figure S6A). The top 20 lipid species responsible for the separation along PC1 and PC2 are listed in Supplementary Figure S6B. Furthermore, HAECs exposed to DF had more lipid content per cell than HAECs exposed to either UF or static conditions (Supplementary Figure S6C). A heatmap of differentially expressed lipid species showed clear effects of applied flow on the lipid profile of HAECs (Supplementary Figure S6D).

3.3 Specific lipid species are altered by disturbed flow

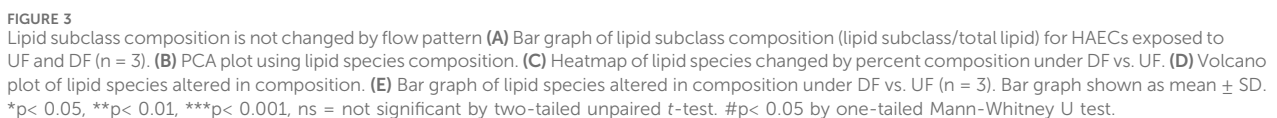
We next analyzed the lipid composition of cells exposed to DF or UF by expressing each lipid subclass as a percent (%) of total cellular lipids. Despite the increase in total lipid mass per cell in the DF condition, the percent composition of each lipid subclass remained unchanged for HAECs exposed to DF or UF (e.g., PCs accounted for ~25% total cellular lipids in both DF and UF) (Figure 3A). Therefore, we examined whether there was a shift in the contribution of specific lipid species as a fraction of its total subclass. Twenty-three lipid species were increased, and five lipid species were decreased under DF compared to UF (Figures 3B–E). A closer look at the lipid species indicated that phospholipids containing mono-unsaturated fatty acids (MUFA) at the sn-2 position were increased in DF compared to UF (e.g., PE 18:1_18:1, PG 16:0_18:1, PG 18:1_18:1, PI 18:0_18:1, PI 18:0_20:1). Conversely, phospholipid species containing polyunsaturated fatty acids (e.g., PC 18:0_20:4, PE 18:0_20:4, PE 18:0_22:4) were decreased under DF.

3.4 Endothelial lipid profile is altered in response to pro-inflammatory signals

Since DF results in an inflammatory phenotype (Supplementary Figures S1C–E), we asked if specific pro-inflammatory signals also altered the lipid composition of ECs. To address this, we performed shotgun lipidomics on statically cultured HAECs in the absence or presence of the pro-inflammatory agonists Pam3CSK4 (Pam3; Toll-like receptor 1/2 agonist) or lipopolysaccharides (LPS; Toll-like receptor 4 agonist) for 48 h. We first confirmed that exposure to LPS and Pam3 for 48 h at the dosages applied resulted in an inflammatory phenotype by staining for ICAM-1 and NF- κ B p65. As expected, HAECs exposed to LPS or Pam3 had increased ICAM-1 and nuclear localization of NF- κ B p65 compared to control HAECs (Supplementary Figures S7A–D). As we observed for HAECs exposed to DF, the total lipid abundance per cell was significantly elevated in response to LPS and Pam3 compared to vehicle treated control cells (Figure 4A). Cellular lipidomes were distinct between HAECs treated with pro-inflammatory agonists *versus* control HAECs (Figures 4B, C, E, F). In summary, a total of twelve lipid subclasses were elevated in response to LPS and eight lipid subclasses were elevated in response to Pam3 (Figure 4D). We noted that cholesteryl ester (CE) and sphingomyelin (SM) subclasses were reduced in Pam3-treated HAECs, while CE and SM were increased in response to LPS (Figure 4D). In addition, PCA and hierarchical clustering showed that exposure to inflammatory agonists led to dramatic differences in the cellular lipid composition (Supplementary Figures S7E–I).

3.5 Specific lipid species are elevated in response to disturbed flow and inflammatory agonists

Cross-analysis of the datasets identified lipid species that were altered in the presence of DF and inflammatory agonist



further noted that four out of the five lipids that increased in absolute mass and percent of total lipid class by DF, LPS, and Pam3 were PI species. This observation was consistent with pathway enrichment scores for PI signaling and metabolism from the RNASeq data for HAECs exposed to DF (Supplementary Figure S9).

We subsequently investigated the acyl tail compositions of fatty acids incorporated at the sn-2 position in phospholipids for cells

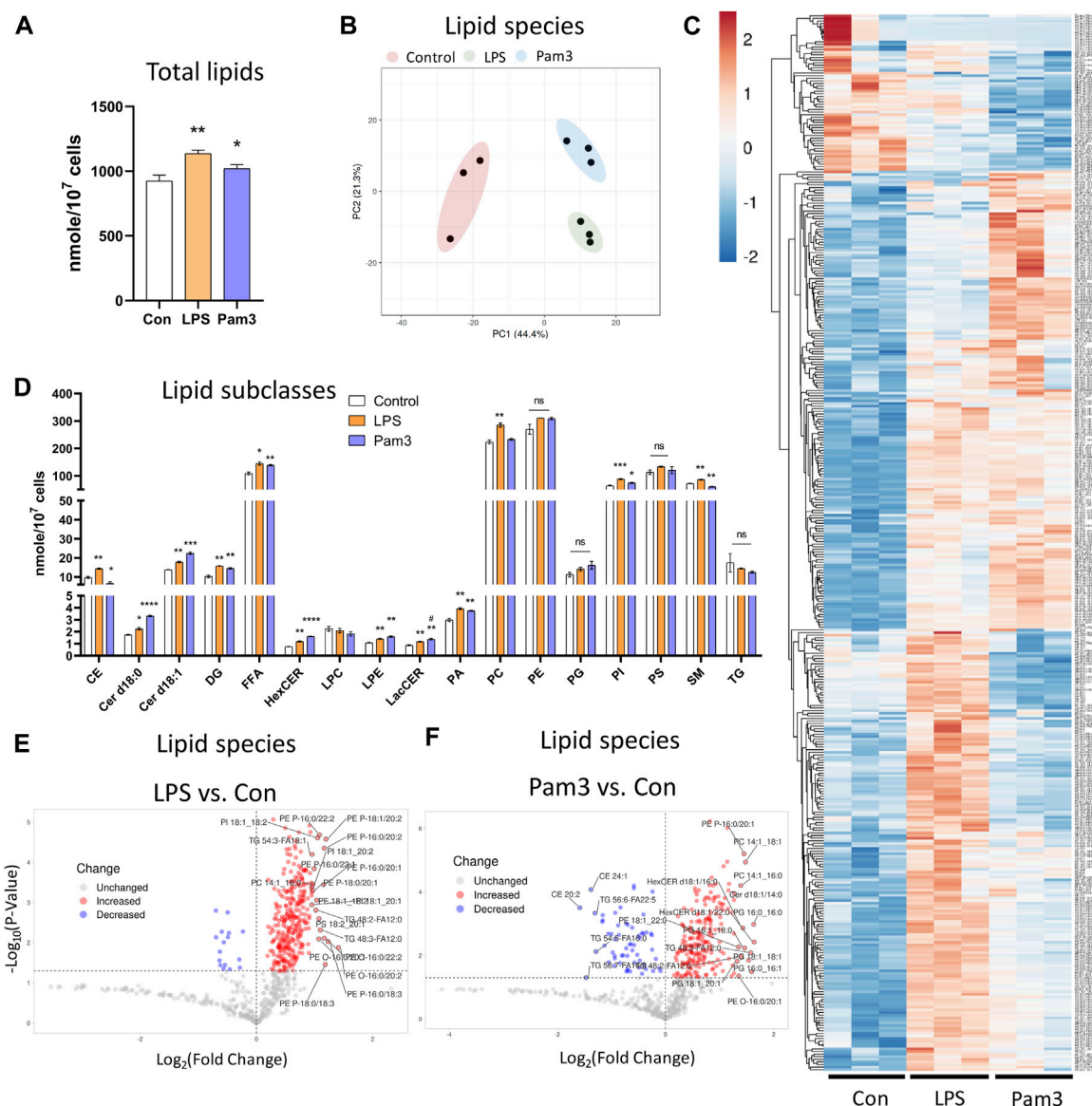


FIGURE 4

Lipid profile is altered in response to inflammatory agonist exposure (A) Total lipid abundance (nM per 10⁷ cells) in HAECs treated with vehicle (control), LPS, and Pam3. Total lipid abundance was calculated from lipidomics results (n = 3). (B) PCA plot. Red = control HAECs, Green = LPS-treated HAECs, Blue = Pam3-treated HAECs. (C) Heatmap of altered lipid species in composition in response to vehicle, LPS, and Pam3. (D) Bar plot of lipid subclass abundance in control, LPS, and Pam3 groups (n = 3). (E) Volcano plot of lipid species changed in LPS vs. control. (F) Volcano plot of lipid species changed in Pam3 vs. control. Bar graph shown as mean ± SD. *p < 0.05, **p < 0.01, ***p < 0.001, ns = not significant by two-tailed unpaired t-test. #p < 0.05 by one-tailed Mann-Whitney U test.

exposed to DF and UF. Comparing the altered phospholipid species by abundance, we found that ~61% of the phospholipids contained MUFAs at the sn-2 position, while ~24% contained a saturated fatty acid (SFA) and ~14% contained a polyunsaturated fatty acid (PUFA) (Figures 6A, B). Over half of the phospholipids that were significantly changed in DF by composition contained a MUFA and 42% contained a PUFA at the sn-2 position (Figures 6B, C).

Phospholipids are produced by *de novo* synthesis and their fatty acyl chains can subsequently be remodeled by Land's cycle, which involves removing a fatty acid from the sn-2 position by phospholipase A2 before re-acylating it by lysophospholipid

acyltransferases (LPLATs) (Shindou et al., 2013) (Figure 6D). Therefore, the observed changes in phospholipid composition of membranes under DF compared to UF could be due to (1) altered uptake or synthesis of fatty acids for *de novo* phospholipid production or (2) changes in phospholipid remodeling.

From the RNASeq data, we observed higher expression of the fatty acid transporter *CD36*, a major route of fatty acid uptake, for HAECs under DF (Figure 2H). Additionally, the sequencing data indicated that genes involved in SFA and MUFA synthesis, including *FASN*, *ACACA*, and Stearoyl-CoA Desaturase 5 (*SCD5*) were significantly increased for HAECs exposed to DF

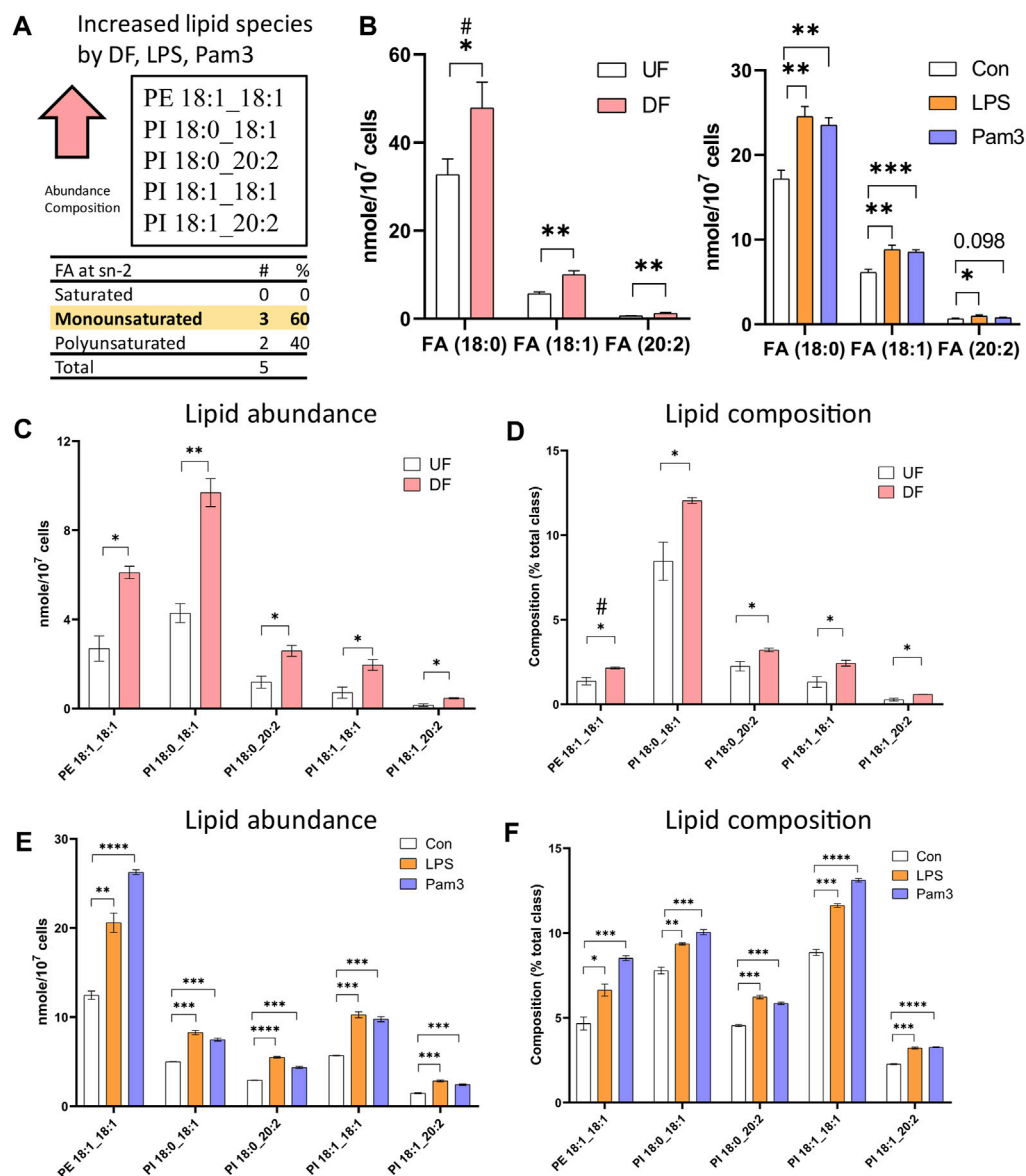


FIGURE 5

Specific lipid species are increased in HAECS exposed to disturbed flow or inflammatory agonists (A) Summary of cross analysis from the lipidomics datasets. Five lipid species (PE 18:1_18:1, PI 18:0_18:1, PI 18:0_20:2, PI 18:1_18:1, PI 18:1_20:2) were significantly elevated in abundance and percent composition for HAECS exposed to either DF or inflammatory agonist treatment. (B) Abundance of fatty acids incorporated into the lipid species identified in (A) for HAECS under UF and DF or HAECS exposed to vehicle (control), LPS, and Pam3 treatments (n = 3). (C) Lipid abundance of the shared lipid species in HAECS under UF vs. DF (n = 3). (D) Lipid composition of the shared lipid species in HAECS under UF vs. DF (n = 3). (E) Lipid abundance of the shared lipid species in HAECS in response to vehicle, LPS, and Pam3 (n = 3). (F) Lipid composition of the commonly shared lipid species for HAECS in response to vehicle, LPS, and Pam3 (n = 3). Bar graph shown as mean ± SD. *p < 0.05, **p < 0.01, ***p < 0.001, ****p < 0.0001, ns = not significant by two-tailed unpaired t-test. #p < 0.05 by one-tailed Mann-Whitney U test.

(Figure 6G). The RNASeq data suggests that higher *de novo* MUFA synthesis could contribute to the increased abundance of MUFA-containing phospholipids under DF. The data also showed that the expression levels of select LPLATs were changed under DF compared to UF (Figure 6E). Specifically, gene expression of the membrane bound O-acyltransferase domain-containing 7 (*MBOAT7*)/lysophosphatidylcholine acyltransferase 1 (*LPIAT1*), an enzyme involved in PI remodeling (Shindou et al., 2009; Shindou et al., 2013; Tanaka et al., 2021), and lysophosphatidylcholine

acyltransferase 2 (*LPCAT2*), which remodels platelet-activating factor (PAF) and PC (Shindou et al., 2009; Shindou et al., 2013), were significantly upregulated under DF. Together, the observations suggest that changes in fatty acid import and synthesis, combined with changes in the phospholipid remodeling machinery (Figure 6F), could contribute to the changes in phospholipid species composition for HAECS exposed to DF compared to UF.

The top 20 phospholipid species used for the PCA loadings for PC1 are listed in Supplementary Figures S10A, S10B. Notably,

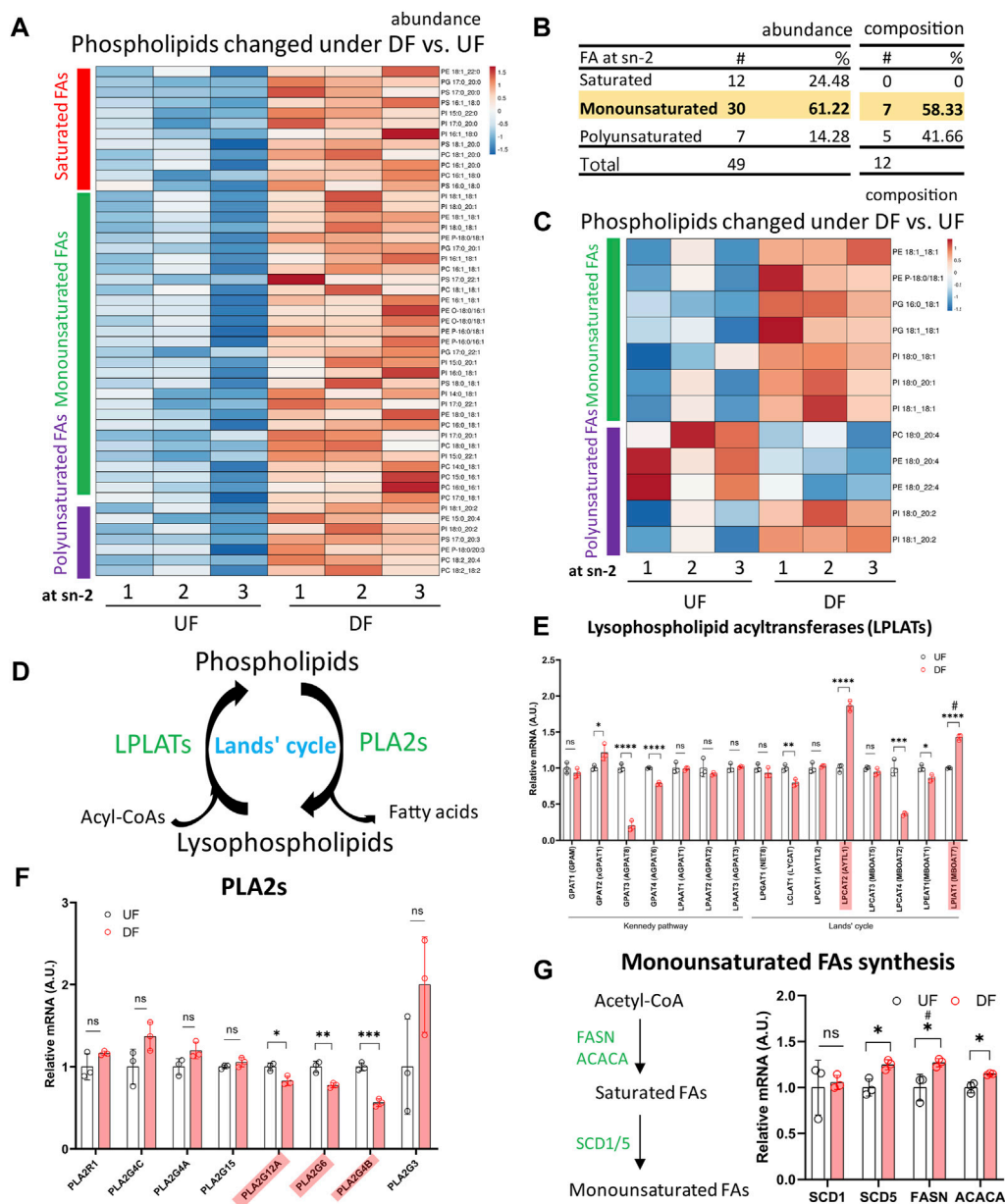


FIGURE 6 Incorporation of monounsaturated fatty acids into phospholipids at the sn-2 position was enhanced under DF. (A) Heatmap of phospholipids altered in abundance under DF vs. UF. (B) Table listing the fatty acid incorporated at the sn-2 position of altered phospholipids. Values of abundance from (A) and values of composition from (C). (C) Heatmap of phospholipids changed in composition under DF vs. UF. (A, C) Color bars represent fatty acid type located at the sn-2 position. Red = saturated, Green = monounsaturated, Purple = polyunsaturated. (D) Schematic diagram of Lands' cycle. Data from RNAseq dataset for HAECS under DF vs. UF showing (E) gene expression of Lysophospholipid acyltransferases (LPLATs), (F) gene expression of Phospholipase A2 (PLA2s) isoforms and (G) genes associated with monounsaturated fatty acid synthesis ($n = 3$). Bar graph shown as mean \pm SD. * $p < 0.05$, ** $p < 0.01$, *** $p < 0.001$, **** $p < 0.0001$, ns = not significant by two-tailed unpaired t -test. # $p < 0.05$ by one-tailed Mann-Whitney U test.

MUFAs were the dominant acyl tails incorporated at the sn-2 position of the top 20 phospholipid species under both DF (65%) and LPS/Pam3 stimulation (45%), as assessed by PCA analysis. Additionally, the abundance of MUFAs in phospholipids was significantly increased after exposure to DF and pro-inflammatory agonists (Supplementary Figures S10C–H), suggesting a shift towards a program of increased MUFA synthesis and/or FA import.

4 Discussion

In this study, we found that the applied flow pattern (DF *versus* UF) distinctively alters the EC transcriptome and lipidome. While previous reports have shown that laminar shear stress alters the lipidome of pulmonary artery ECs (Hirata et al., 2021), this is the first report to correlate how flow pattern affects metabolic gene expression and lipidomic profiles of arterial ECs. Using RNA

sequencing and shotgun lipidomics, we found that HAECs exposed to DF have an inflammatory transcriptional signature and increased cellular lipid content compared to HAECs exposed to UF. By exposing HAECs to inflammatory agonists, Pam3 or LPS, we confirmed that the EC inflammatory state is associated with higher lipid accumulation. Increased lipid accumulation has previously been reported in other cell types exposed to stress conditions, including viral infection-mediated inflammation (Prado et al., 2023). Furthermore, in human microvascular ECs, the expression of the FA transporter CD36 increased in response to viral infection (Sato and Coburn, 2017). Analysis of our RNA sequencing data for DF versus UF revealed that genes involved in fatty acid synthesis (*FASN* and *ACACA*), and fatty acid transport (*CD36* and *FATP1*), were upregulated, while genes involved in lipid and fatty acid catabolic processes were reduced. These transcriptional changes suggest that DF may induce changes in the rate of lipid uptake and synthesis to supply more fatty acids for phospholipid and neutral lipid synthesis.

Considering the increased lipid load, it is interesting to consider whether altering lipogenesis in the presence of an inflammatory stimulus would alter the EC phenotype. Previous studies have shown that increasing *de novo* MUFA synthesis by Stearoyl-CoA Desaturases (SCDs) can modulate vascular inflammation, where an attenuation of MUFA synthesis by inhibition of endothelial SCD1 activity stimulated the secretion of pro-inflammatory cytokines and elevated inflammation in the mouse aorta (MacDonald et al., 2009; Cavallero et al., 2024). Therefore, it is conceivable that inhibition of *de novo* lipogenesis, a step upstream of SCDs, by pharmacological inhibition or by deletion of Fatty Acid Synthase could also alter the EC phenotype in response to DF. However, we note the critical role of *de novo* lipogenesis in the context of angiogenesis, eNOS activity, and permeability (Wei et al., 2011; Bruning et al., 2018), therefore, inhibition of lipogenesis could have broad consequences. It is also likely that a major contributor to the increase in EC fatty acid content in an inflammatory setting is the increase in CD36, which transports fatty acids into cells. Inhibition of lipogenesis alone may not be sufficient to block the increase in cellular fatty acids after exposure to DF. Future studies are needed to dissect the impact of the observed elevation of lipids in response to inflammatory stimuli in ECs. Additionally, experiments using stable isotope tracing to measure the contribution of long chain SFA and MUFA synthesis for the observed altered phospholipid composition in response to DF will enable quantification of EC lipid uptake and synthesis.

Exposure of HAECs to DF or an inflammatory agonist, either LPS or Pam3, led to an increase in the abundance of MUFA-containing phospholipids. We noted that genes involved in SFA and MUFA synthesis, including *FASN*, *ACACA* and *SCD5*, were elevated under DF. Stearoyl Coenzyme A (CoA) desaturases incorporate a Δ^9 -cis-double bond into SFA-CoA to make MUFAs (Igal and Sinner, 2021), and MUFAs have been reported to counteract membrane stress induced by SFAs (Hardy et al., 2000; Koeberle et al., 2016). Furthermore, MUFAs have been shown to play a role in the modulation of various stress signaling pathways (Koeberle et al., 2015; Koeberle et al., 2016; Magtanong et al., 2019; Tesfay et al., 2019; Igal and Sinner, 2021). In fact, a recent study in macrophages found that Toll-like receptor-agonist exposure increased *de novo* MUFA synthesis and that attenuating MUFA

synthesis with inhibition of SCDs led to heightened inflammation (Hsieh et al., 2020). Therefore, the observed increase in MUFA-containing phospholipid content in response to DF in ECs could be a compensatory mechanism to alleviate the DF-induced inflammatory state. Examination of the mechanisms by which MUFA-containing phospholipid content is increased in response to inflammatory agonists or DF, and the specific pathways that are modulated by MUFA-containing phospholipids, is warranted.

The lipidomics data revealed an increase in the major membrane lipids PC and PE for HAECs exposed to DF compared to UF. Notably, the total unesterified fatty acid content of cells exposed to DF was higher. This increase in PC and PE content could be driven by increased fatty acid import via CD36 or higher *de novo* fatty acid synthesis, since fatty acid availability drives phospholipid synthesis (Pelech et al., 1983). Another possible explanation for the increased pool size of PC and PE is the expansion of cellular organelle volume and/or organelle number in ECs under DF. In fact, athero-susceptible shear stress has been reported to induce ER stress and ER expansion, thereby leading to EC dysfunction and inflammation (Bailey et al., 2017). However, future studies are required to investigate these possible scenarios and the functional importance of increased PC and PE content in ECs exposed to DF.

Finally, we identified five lipid species (PE 18:1_18:1, PI 18:0_18:1, PI 18:0_20:2, PI 18:1_18:1, PI 18:1_20:2) that were significantly elevated in abundance and percent composition for HAECs exposed to DF and inflammatory agonist treatment. We noted that the total abundance of the fatty acids incorporated into those lipid species— stearic acid, oleic acid and eicosadienoic acid— were elevated in cells exposed to DF and exposure to inflammatory agonists. By RNA sequencing, we observed altered expression of genes related to PI signaling and metabolism under DF. While the role of PI metabolism on cellular stress signaling has not been examined in detail in ECs, a recent study showed that the SCD1-derived 'lipokine' PI 18:1_18:1 suppressed stress signaling in fibroblasts (Thurmer et al., 2022). The results in fibroblasts indicated that PI 18:1_18:1 was elevated in response to cytotoxic stressors and prevented p38 MAPK activation and impeded the unfolded protein response (Thurmer et al., 2022). Future studies are needed to determine how our observed changes in the abundance of PI species in response to DF affects signaling in ECs.

We note that our *in vitro* flow system using parallel plate flow chambers does not recapitulate the physiological oscillatory disturbed flow patterns of the aortic arch. However, considering the limitations of *in vitro* models, we confirmed that using the ibidi μ -slide flow chambers under continuous unidirectional laminar flow (20 dyn/cm²) and oscillatory flow (4 dyn/cm², 2 Hz) effectively provided athero-protective and athero-prone phenotypes as evidenced by EC cell morphology, gene expression, and protein expression. We also note that HAECs from one single healthy donor were used throughout this study. The choice of a single donor was to provide technical replicates for the changes in gene expression and lipids across treatments. Future work is certainly warranted to investigate how variations in genetics affect the gene expression and lipid responses across multiple donor HAECs in the context of aging and genetic backgrounds.

5 Conclusion

In conclusion, we provide transcriptomic and lipidomic datasets of HAECs under athero-protective UF and athero-prone DF patterns. Additionally, we map the lipidome of HAECs after exposure to the inflammatory agonists LPS and Pam3. We anticipate that these datasets will be a useful resource for the vascular biology community to be further dissected and advance our understanding of how flow pattern influences the EC phenotype.

Data availability statement

The RNA sequencing data has been deposited in NCBI's Gene Expression Omnibus repository (GSE266437). Normalized RNA sequencing data and the lipidomics data are provided as an Excel file in the [Supplementary Material](#).

Ethics statement

Ethical approval was not required for the studies on humans in accordance with the local legislation and institutional requirements because only commercially available cell lines were used.

Author contributions

S-GH: Conceptualization, Data curation, Formal Analysis, Investigation, Methodology, Project administration, Validation, Visualization, Writing—original draft, Writing—review and editing. JK: Visualization, Writing—review and editing. KW: Data curation, Formal Analysis, Investigation, Methodology, Writing—review and editing. SB: Methodology, Resources, Supervision, Writing—review and editing. JM: Conceptualization, Funding acquisition, Investigation, Project administration, Supervision, Writing—original draft, Writing—review and editing.

References

- Babicki, S., Arndt, D., Marcu, A., Liang, Y., Grant, J. R., Maciejewski, A., et al. (2016). Heatmapper: web-enabled heat mapping for all. *Nucleic Acids Res.* 44, W147–W153. doi:10.1093/nar/gkw419
- Bailey, K. A., Haj, F. G., Simon, S. I., and Passerini, A. G. (2017). Atherosusceptible shear stress activates endoplasmic reticulum stress to promote endothelial inflammation. *Sci. Rep.* 7, 8196. doi:10.1038/s41598-017-08417-9
- Bruning, U., Morales-Rodriguez, F., Kalucka, J., Goveia, J., Taverna, F., Queiroz, K. C. S., et al. (2018). Impairment of angiogenesis by fatty acid synthase inhibition involves mTOR malonylation. *Cell. Metab.* 28, 866–880. doi:10.1016/j.cmet.2018.07.019
- Cavallero, S., Roustaei, M., Satta, S., Cho, J. M., Phan, H., Baek, K. I., et al. (2024). Exercise mitigates flow recirculation and activates metabolic transducer SCD1 to catalyze vascular protective metabolites. *Sci. Adv.* 10, ead7481. doi:10.1126/sciadv.ad7481
- Chiu, J. J., and Chien, S. (2011). Effects of disturbed flow on vascular endothelium: pathophysiological basis and clinical perspectives. *Physiol. Rev.* 91, 327–387. doi:10.1152/physrev.00047.2009
- Davis, M. E., Cai, H., Drummond, G. R., and Harrison, D. G. (2001). Shear stress regulates endothelial nitric oxide synthase expression through c-Src by divergent signaling pathways. *Circ. Res.* 89, 1073–1080. doi:10.1161/hh2301.100806
- Dobin, A., Davis, C. A., Schlesinger, F., Drenkow, J., Zaleski, C., Jha, S., et al. (2013). STAR: ultrafast universal RNA-seq aligner. *Bioinformatics* 29, 15–21. doi:10.1093/bioinformatics/bts635
- Doddaballapur, A., Michalik, K. M., Manavski, Y., Lucas, T., Houtkooper, R. H., You, X., et al. (2015). Laminar shear stress inhibits endothelial cell metabolism via KLF2-mediated repression of PFKFB3. *Arterioscler. Thromb. Vasc. Biol.* 35, 137–145. doi:10.1161/ATVBAHA.114.304277
- Galley, H. F., and Webster, N. R. (2004). Physiology of the endothelium. *Br. J. Anaesth.* 93, 105–113. doi:10.1093/bja/aeh163
- Ge, S. X., Jung, D., and Yao, R. (2020). ShinyGO: a graphical gene-set enrichment tool for animals and plants. *Bioinformatics* 36, 2628–2629. doi:10.1093/bioinformatics/btz931
- Goodman, J. M. (2008). The gregarious lipid droplet. *J. Biol. Chem.* 283, 28005–28009. doi:10.1074/jbc.R800042200
- Hardy, S., Langelier, Y., and Prentki, M. (2000). Oleate activates phosphatidylinositol 3-kinase and promotes proliferation and reduces apoptosis of MDA-MB-231 breast cancer cells, whereas palmitate has opposite effects. *Cancer Res.* 60, 6353–6358.
- Heberle, H., Meirelles, G. V., Da Silva, F. R., Telles, G. P., and Minghim, R. (2015). InteractiVenn: a web-based tool for the analysis of sets through Venn diagrams. *BMC Bioinforma.* 16, 169. doi:10.1186/s12859-015-0611-3

Funding

The author(s) declare that financial support was received for the research, authorship, and/or publication of this article. This work was funded by the National Center for Advancing Translational Sciences UCLA CTSI Grant UL1TR001881 and NIH grant P30 DK063491. S-GH was supported as a Jim Easton CDF Investigator; JK was supported by AHA Postdoctoral Fellowship 903306; SB was supported by NIH grant R01HL157710; JM was supported by American Heart Association Career Development Award 19CDA34760007.

Acknowledgments

The content of this manuscript has previously appeared online as a preprint on bioRxiv, the preprint server for biology (Hong et al., 2024).

Conflict of interest

The authors declare that the research was conducted in the absence of any commercial or financial relationships that could be construed as a potential conflict of interest.

Publisher's note

All claims expressed in this article are solely those of the authors and do not necessarily represent those of their affiliated organizations, or those of the publisher, the editors and the reviewers. Any product that may be evaluated in this article, or claim that may be made by its manufacturer, is not guaranteed or endorsed by the publisher.

Supplementary material

The Supplementary Material for this article can be found online at: <https://www.frontiersin.org/articles/10.3389/fphys.2024.1431847/full#supplementary-material>

- He, Q., Chen, Y., Wang, Z., He, H., and Yu, P. (2023). Cellular uptake, metabolism and sensing of long-chain fatty acids. *Front. Biosci.* 28, 10. doi:10.31083/j.fbl2801010
- Hirata, T., Yamamoto, K., Ikeda, K., and Arita, M. (2021). Functional lipidomics of vascular endothelial cells in response to laminar shear stress. *FASEB J.* 35, e21301. doi:10.1096/fj.202002144R
- Hong, S.-G., Kennelly, J. P., Williams, K. J., Bensinger, S. J., and Mack, J. J. (2024). Flow-mediated modulation of the endothelial cell lipidome. *bioRxiv* 2024.
- Hsieh, W. Y., Williams, K. J., Su, B., and Bensinger, S. J. (2021). Profiling of mouse macrophage lipidome using direct infusion shotgun mass spectrometry. *Star. Protoc.* 2, 100235. doi:10.1016/j.xpro.2020.100235
- Hsieh, W. Y., Zhou, Q. D., York, A. G., Williams, K. J., Scumpia, P. O., Kronenberger, E. B., et al. (2020). Toll-like receptors induce signal-specific reprogramming of the macrophage lipidome. *Cell. Metab.* 32, 128–143. doi:10.1016/j.cmet.2020.05.003
- Igal, R. A., and Sinner, D. I. (2021). Stearoyl-CoA desaturase 5 (SCD5), a Delta-9 fatty acyl desaturase in search of a function. *Biochim. Biophys. Acta Mol. Cell. Biol. Lipids* 1866, 158840. doi:10.1016/j.bbalip.2020.158840
- Immanuel, J., and Yun, S. (2023). Vascular inflammatory diseases and endothelial phenotypes. *Cells* 12, 1640. doi:10.3390/cells12121640
- Koeberle, A., Loser, K., and Thurmer, M. (2016). Stearoyl-CoA desaturase-1 and adaptive stress signaling. *Biochim. Biophys. Acta* 1861, 1719–1726. doi:10.1016/j.bbalip.2016.08.009
- Koeberle, A., Pergola, C., Shindou, H., Koeberle, S. C., Shimizu, T., Laufer, S. A., et al. (2015). Role of p38 mitogen-activated protein kinase in linking stearyl-CoA desaturase-1 activity with endoplasmic reticulum homeostasis. *FASEB J.* 29, 2439–2449. doi:10.1096/fj.14-268474
- Macdonald, M. L., Van Eck, M., Hildebrand, R. B., Wong, B. W., Bissada, N., Ruddle, P., et al. (2009). Despite antiatherogenic metabolic characteristics, SCD1-deficient mice have increased inflammation and atherosclerosis. *Arterioscler. Thromb. Vasc. Biol.* 29, 341–347. doi:10.1161/ATVBAHA.108.181099
- Magtanong, L., Ko, P. J., To, M., Cao, J. Y., Forcina, G. C., Tarangelo, A., et al. (2019). Exogenous monounsaturated fatty acids promote a ferroptosis-resistant cell state. *Cell. Chem. Biol.* 26, 420–432. doi:10.1016/j.chembiol.2018.11.016
- Malek, A. M., Alper, S. L., and Izumo, S. (1999). Hemodynamic shear stress and its role in atherosclerosis. *JAMA* 282, 2035–2042. doi:10.1001/jama.282.21.2035
- Maurya, M. R., Gupta, S., Li, J. Y., Ajami, N. E., Chen, Z. B., Shyy, J. Y., et al. (2021). Longitudinal shear stress response in human endothelial cells to atheroprone and atheroprotective conditions. *Proc. Natl. Acad. Sci. U S A* 118, e2023236118. doi:10.1073/pnas.2023236118
- Metsalu, T., and Vilo, J. (2015). ClustVis: a web tool for visualizing clustering of multivariate data using Principal Component Analysis and heatmap. *Nucleic Acids Res.* 43, W566–W570. doi:10.1093/nar/gkv468
- Muro, E., Atilla-Gokcumen, G. E., and Eggert, U. S. (2014). Lipids in cell biology: how can we understand them better? *Mol. Biol. Cell.* 25, 1819–1823. doi:10.1091/mbc.E13-09-0516
- Mutlu, A. S., Duffy, J., and Wang, M. C. (2021). Lipid metabolism and lipid signals in aging and longevity. *Dev. Cell.* 56, 1394–1407. doi:10.1016/j.devcel.2021.03.034
- Pelech, S. L., Pritchard, P. H., Brindley, D. N., and Vance, D. E. (1983). Fatty acids promote translocation of CTP:phosphocholine cytidyltransferase to the endoplasmic reticulum and stimulate rat hepatic phosphatidylcholine synthesis. *J. Biol. Chem.* 258, 6782–6788. doi:10.1016/s0021-9258(18)32290-7
- Prado, L. G., Camara, N. O. S., and Barbosa, A. S. (2023). Cell lipid biology in infections: an overview. *Front. Cell. Infect. Microbiol.* 13, 1148383. doi:10.3389/fcimb.2023.1148383
- Sakuragi, T., and Nagata, S. (2023). Regulation of phospholipid distribution in the lipid bilayer by flippases and scramblases. *Nat. Rev. Mol. Cell. Biol.* 24, 576–596. doi:10.1038/s41580-023-00604-z
- Sato, H., and Coburn, J. (2017). *Leptospira interrogans* causes quantitative and morphological disturbances in adherens junctions and other biological groups of proteins in human endothelial cells. *PLoS Negl. Trop. Dis.* 11, e0005830. doi:10.1371/journal.pntd.0005830
- Shindou, H., Hishikawa, D., Harayama, T., Eto, M., and Shimizu, T. (2013). Generation of membrane diversity by lysophospholipid acyltransferases. *J. Biochem.* 154, 21–28. doi:10.1093/jb/mvt048
- Shindou, H., Hishikawa, D., Harayama, T., Yuki, K., and Shimizu, T. (2009). Recent progress on acyl CoA: lysophospholipid acyltransferase research. *J. Lipid Res.* 50, S46–S51. doi:10.1194/jlr.R800035-JLR200
- Su, B., Bettcher, L. F., Hsieh, W. Y., Hornburg, D., Pearson, M. J., Blomberg, N., et al. (2021). A DMS shotgun lipidomics workflow application to facilitate high-throughput, comprehensive lipidomics. *J. Am. Soc. Mass Spectrom.* 32, 2655–2663. doi:10.1021/jasms.1c00203
- Tamargo, I. A., Baek, K. I., Kim, Y., Park, C., and Jo, H. (2023). Flow-induced reprogramming of endothelial cells in atherosclerosis. *Nat. Rev. Cardiol.* 20, 738–753. doi:10.1038/s41569-023-00883-1
- Tanaka, Y., Shimanaka, Y., Caddeo, A., Kubo, T., Mao, Y., Kubota, T., et al. (2021). LPIAT1/MBOAT7 depletion increases triglyceride synthesis fueled by high phosphatidylinositol turnover. *Gut* 70, 180–193. doi:10.1136/gutjnl-2020-320646
- Tesfay, L., Paul, B. T., Konstorum, A., Deng, Z., Cox, A. O., Lee, J., et al. (2019). Stearoyl-CoA desaturase 1 protects ovarian cancer cells from ferroptotic cell death. *Cancer Res.* 79, 5355–5366. doi:10.1158/0008-5472.CAN-19-0369
- Thurmer, M., Gollowitzer, A., Pein, H., Neukirch, K., Gelmez, E., Waltl, L., et al. (2022). PI(18:1/18:1) is a SCD1-derived lipokine that limits stress signaling. *Nat. Commun.* 13, 2982. doi:10.1038/s41467-022-30374-9
- Wei, X., Schneider, J. G., Shenouda, S. M., Lee, A., Towler, D. A., Chakravarthy, M. V., et al. (2011). *De novo* lipogenesis maintains vascular homeostasis through endothelial nitric-oxide synthase (eNOS) palmitoylation. *J. Biol. Chem.* 286, 2933–2945. doi:10.1074/jbc.M110.193037
- Wu, D., Huang, R. T., Hamanaka, R. B., Krause, M., Oh, M. J., Kuo, C. H., et al. (2017). HIF-1α is required for disturbed flow-induced metabolic reprogramming in human and porcine vascular endothelium. *Elife* 6, e25217. doi:10.7554/eLife.25217
- Yamamoto, K., and Ando, J. (2013). Endothelial cell and model membranes respond to shear stress by rapidly decreasing the order of their lipid phases. *J. Cell. Sci.* 126, 1227–1234. doi:10.1242/jcs.119628
- Yamamoto, K., Nogimori, Y., Imamura, H., and Ando, J. (2020). Shear stress activates mitochondrial oxidative phosphorylation by reducing plasma membrane cholesterol in vascular endothelial cells. *Proc. Natl. Acad. Sci. U S A* 117, 33660–33667. doi:10.1073/pnas.2014029117
- Yurdagul, A., JR, Finney, A. C., Woolard, M. D., and Orr, A. W. (2016). The arterial microenvironment: the where and why of atherosclerosis. *Biochem. J.* 473, 1281–1295. doi:10.1042/BJ20150844



OPEN ACCESS

EDITED BY

Nicolas Baeyens,
Université libre de Bruxelles, Belgium

REVIEWED BY

Daisuke Yoshino,
Tokyo University of Agriculture and
Technology, Japan
Julian Albarran Juarez,
Aarhus University, Denmark

*CORRESPONDENCE

J. S. Fang,
✉ jfang5@tulane.edu

[†]These authors have contributed equally to
this work

RECEIVED 06 May 2024

ACCEPTED 10 July 2024

PUBLISHED 29 July 2024

CITATION

Martier A, Chen Z, Schaps H, Mondrinos MJ and
Fang JS (2024), Capturing physiological
hemodynamic flow and mechanosensitive cell
signaling in vessel-on-a-chip platforms.
Front. Physiol. 15:1425618.
doi: 10.3389/fphys.2024.1425618

COPYRIGHT

© 2024 Martier, Chen, Schaps, Mondrinos and
Fang. This is an open-access article distributed
under the terms of the [Creative Commons
Attribution License \(CC BY\)](#). The use,
distribution or reproduction in other forums is
permitted, provided the original author(s) and
the copyright owner(s) are credited and that the
original publication in this journal is cited, in
accordance with accepted academic practice.
No use, distribution or reproduction is
permitted which does not comply with these
terms.

Capturing physiological hemodynamic flow and mechanosensitive cell signaling in vessel-on-a-chip platforms

A. Martier¹, Z. Chen², H. Schaps², M. J. Mondrinos^{1,3†} and
J. S. Fang^{2,3†*}

¹Department of Biomedical Engineering, School of Science and Engineering, Tulane University, New Orleans, LA, United States, ²Department of Cell and Molecular Biology, School of Science and Engineering, Tulane University, New Orleans, LA, United States, ³Department of Physiology, School of Medicine, Tulane University, New Orleans, LA, United States

Recent advances in organ chip (or, “organ-on-a-chip”) technologies and microphysiological systems (MPS) have enabled *in vitro* investigation of endothelial cell function in biomimetic three-dimensional environments under controlled fluid flow conditions. Many current organ chip models include a vascular compartment; however, the design and implementation of these vessel-on-a-chip components varies, with consequently varied impact on their ability to capture and reproduce hemodynamic flow and associated mechanosensitive signaling that regulates key characteristics of healthy, intact vasculature. In this review, we introduce organ chip and vessel-on-a-chip technology in the context of existing *in vitro* and *in vivo* vascular models. We then briefly discuss the importance of mechanosensitive signaling for vascular development and function, with focus on the major mechanosensitive signaling pathways involved. Next, we summarize recent advances in MPS and organ chips with an integrated vascular component, with an emphasis on comparing both the biomimicry and adaptability of the diverse approaches used for supporting and integrating intravascular flow. We review current data showing how intravascular flow and fluid shear stress impacts vessel development and function in MPS platforms and relate this to existing work in cell culture and animal models. Lastly, we highlight new insights obtained from MPS and organ chip models of mechanosensitive signaling in endothelial cells, and how this contributes to a deeper understanding of vessel growth and function *in vivo*. We expect this review will be of broad interest to vascular biologists, physiologists, and cardiovascular physicians as an introduction to organ chip platforms that can serve as viable model systems for investigating mechanosensitive signaling and other aspects of vascular physiology.

KEYWORDS

organ chips, microphysiological systems, vessel-on-a-chip, fluid shear stress, wall shear stress, mechanotransduction, hemodynamic flow

Introduction

The blood vasculature is an extensive organ system comprised of hierarchically organized blood vessels that circulate blood from the heart to all tissues of the body. The mechanical forces that blood flow exerts on vascular cells is a key mechanical signal for vascular cell function and homeostasis. Yet, the contribution of hemodynamic flow signaling to healthy and diseased vascular cell function can be difficult to capture experimentally, in part due to the nature of currently available *in vitro* and *in vivo* models of the blood vasculature. Here, we review the importance of hemodynamic flow in the blood vasculature and discuss how increasingly sophisticated microphysiological models of the vasculature, or so-called vessel-on-a-chip systems, may enable new study of flow-sensitive signaling and mechanotransduction in the blood vasculature.

Research on the biology of the blood vasculature has traditionally taken advantage of two general types of model systems. First, many studies use *in vitro* two-dimensional (2D) or three-dimensional (3D) cultures, with the latter often entailing co-culture of endothelial cells with vascular support cells, including fibroblasts, vascular smooth muscle cells, and/or pericytes. The simplicity and high throughput capacity of 2D cultures has enabled discovery of many fundamental aspects of endothelial cell biology, including response to shear stress in 2D cultures of endothelial cells in parallel plate flow chambers (James et al., 1995; Sedlak and Clyne, 2023). 3D cultures in hydrogels composed of natural ECM proteins are useful tools for modeling vasculogenesis and the impact of culture parameters on vascular network architecture. Vascular organoids generated with induced pluripotent stem cell derivatives are powerful tools for modeling key aspects of vascular niche formation including pericyte interactions and basement membrane synthesis (Mondrinos et al., 2014; Wimmer et al., 2019). Collectively, these evolving 2D and 3D culture models have advanced our understanding of vascular biology and the pharmacodynamics of drugs targeting the vasculature (Cochrane et al., 2019; Haas et al., 2020).

Regarding hemodynamics and more complex aspects of vascular physiology, most of the aforementioned *in vitro* cell culture systems fail to simultaneously capture the 3D architecture and flow perfusion of blood vessels *in vivo*. On the other hand, studies of intact blood vessels can be performed either *in vivo* in research animals (e.g., mice, rats, hamsters, etc.) or in *ex vivo* blood vessel explants. However, *in vivo* models can be expensive, time-consuming, and potentially incompatible with certain experimental approaches. Modeling the effects of different flow conditions in a reductionist manner while simultaneously controlling for other system elements is challenging unless isolated *ex vivo* vessel preparations are used (Adamson et al., 1994). Furthermore, differences between human and research animal physiology may further complicate interpretation of data for clinical translation (Seok et al., 2013).

In the last 20 years, new *in vitro* models—termed organ chip (or, “organ-on-a-chip”) technology and so-called microphysiological systems (MPS)—have emerged as powerful tools to complement existing *in vitro* and *in vivo* tissue models. MPS, which were originally conceived as “human surrogates” to serve as platforms for modeling pharmacokinetics and pharmacodynamics *in vitro* (Viravaidya and Shuler, 2004; Edington et al., 2018), can fill the

gap between traditional culture systems and animal models by situating human cells in a more physiologically-relevant context with controlled biochemical and biophysical parameters (Bhatia and Ingber, 2014).

Early MPS designs focused on the use of printed microfluidic features to interconnect cultures of multiple human cell types and enable real-time communication *via* the transport of soluble factors. In 2004, Viravaidya et al. developed a “microscale cell culture analog” system in which a series of culture chambers containing lung and liver cells were connected by patterned microfluidic channels to “mimic the circulatory system.” (Viravaidya et al., 2004) While in this model an acellular circuit of microfluidic channels accomplishes the essential macroscale transport functions of the circulatory system, the endothelium is in itself an organ that influences tissue-specific and systemic physiology (Augustin and Koh, 2017). Thus, development of systems that faithfully recapitulate the vascular niche of intact blood vessels has long been considered a critical requirement for improving the physiological relevance of MPS (Ewald et al., 2021). In 2010, Huh and colleagues integrated a cellularized vascular compartment in their lung-on-a-chip model of the alveolar-capillary tissue-tissue interface. In this model, a lower tissue channel is lined with primary vascular endothelial cells to form an endothelial monolayer cultured under pump-driven flow and separated from an overlying lung epithelial monolayer by a porous elastomeric membrane that enables inter-tissue exchange of growth factors and nutrients (Huh, 2015). This pioneering microphysiological model of the blood-air interface of the lung has since been used to capture a variety of complex tissue interactions, including immune responses to respiratory virus infection (Huh, 2015; Si et al., 2021).

In the years since these early proof-of-concept prototypes, there has been a proliferation of unique organ chip models—all varying in their platform design and target tissue, as well as presence (or absence) of a vascular tissue component. These include (but are not limited to) working organ chip models of the gut and associated microbiome (Langer et al., 2019; Pocevičute and Ismagilov, 2019), the female reproductive system (Xiao et al., 2017), the pancreatic islet (Bender et al., 2024), the blood-brain barrier (Phan et al., 2017; Campisi et al., 2018), and cancer growth and metastasis (Jeon et al., 2015; Sobrino et al., 2016; Chen et al., 2017; Hachey et al., 2021; Hachey et al., 2024) among many others. Ongoing efforts to engineer body-on-a-chip systems will likely require capturing the physiology of a continuous intact vasculature under physiological flow to model systemic processes and pharmacokinetics (Vogt, 2022). In this review, we will focus on the importance of hemodynamic flow as a regulator of vascular physiology and disease, and explore the challenges of integrating these physiological flow forces in next-generation vessel-on-a-chip designs.

The blood vasculature and hemodynamic flow

Several specialized blood vessel types support efficient systemic circulation, including muscularized arteries and arterioles that constrict and dilate to control local and systemic blood flow; thinly-walled veins and venules that function as elastic

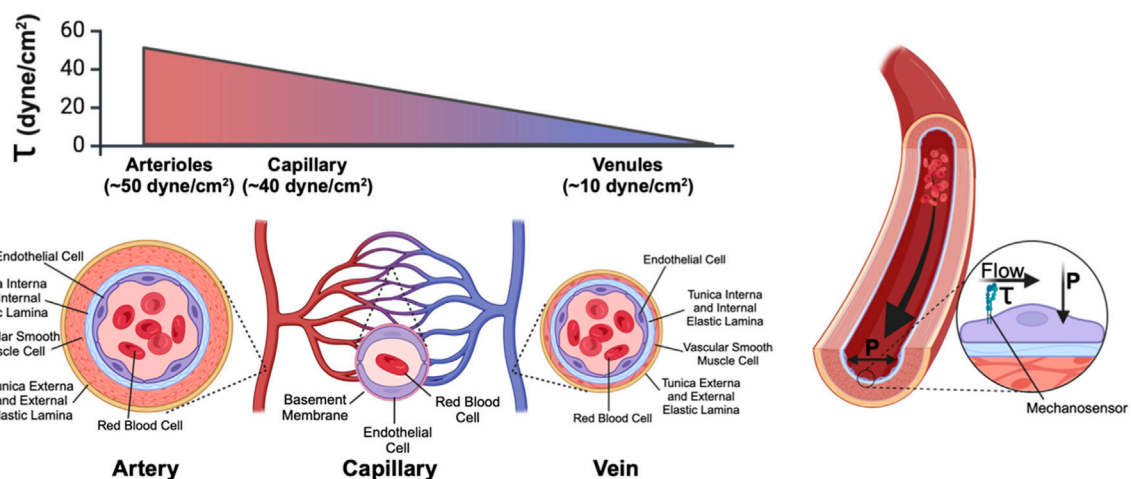


FIGURE 1

Anatomy of a blood vessel. Blood vessels are lined on their luminal surface by the vascular endothelium, which consists of a single continuous layer of endothelial cells. Surrounding the vascular endothelium is an extracellular matrix layer (tunica interna) which separates the endothelium from the medial layer, which consists of vascular smooth muscle cells (arteries/arterioles, and veins/venules) or pericytes (capillaries). The outermost layer of blood vessels is the tunica externa, another collagen-rich extracellular matrix layer. Within a microvascular network (in which blood flows from arteriole to capillary to venule) fluid shear stress (τ) (the frictional force of fluid flow along the luminal face of the vasculature and that is sensed by endothelial-expressed cell surface mechanoreceptors) is high in the arteriole and low in the venule. Transmural pressure (P), generated by the hydrostatic pressure imparted by fluid in the vessel, acts perpendicular to the endothelium.

capacitance reservoirs for excess blood volume, and intervening small-caliber capillaries (typically 8–10 μm in diameter) that connect the arteriolar and venous sides of the circulatory system and that function as the primary site of oxygen, nutrient, and waste exchange between blood and surrounding tissue. All blood vessels are lined on their luminal surface by endothelial cells—specialized epithelial cell types that form a continuous barrier between circulating blood and surrounding tissue. The apical, lumen-facing surface of vascular endothelium is enriched for proteoglycans and glycoproteins, which forms a protective and immunoregulatory layer known as the glycocalyx that interfaces directly with circulating blood (Figure 1). The basolateral side of endothelial cells, on the other hand, rests upon the tunica interna—a collagen-, laminin-, and fibronectin-rich basement membrane supported by an elastin-rich internal elastic lamina that confers radial elasticity onto the blood vessel. Beyond the tunica interna, perivascular cells—including contractile smooth muscle cells and vessel-stabilizing pericytes—form a medial layer that stabilizes blood vessels and—in the case of smooth muscle—constricts and relaxes to establish local vessel tone and regulate downstream blood flow. On the outer surface of the blood vessel is the tunica externa, a collagen-rich layer of extracellular matrix that confers additional vascular elasticity to the vessel. Mural cells are physically separated from the vascular endothelium by the tunica interna except *via* pores in the intervening extracellular matrix layer (termed myoendothelial junctions (Heberlein et al., 2009)) that enable endothelial-mural cell contact and intracellular exchange of signaling molecules.

Endothelial cells critically drive both the development and function of the blood vasculature (Garcia and Larina, 2014). During embryonic development, primordial endothelial cells coalesce into a primitive and lumenized vascular plexus (vasculogenesis), which subsequently expands by sprouting

angiogenesis to establish new blood vessels in surrounding avascular tissue. Once blood vessels are established in the post-natal animal, vascular endothelium is highly specialized to perform key functions including to regulate blood flow distribution through local control of vessel tone; to mediate vascular-stromal exchange of oxygen, nutrients, and waste; and to regulate inflammation and immune cell responses. Under some physiological (e.g., menstruation) and pathological (e.g., cancer neovascularization, wet age-related macular degeneration, diabetes, etc.) conditions, the vascular endothelium may also reactivate pro-angiogenic signaling pathways to grow new blood vasculature.

As the interface between circulating blood and surrounding tissue, vascular endothelium is exposed to hemodynamic flow that exerts (and is thus sensed by primary mechanosensory cell surface receptors (Figure 1) as) mechanical friction forces (i.e., wall shear stress, WSS or τ) onto the lumen-facing (apical) surface of endothelial cells. Local WSS depends upon both vessel diameter and the flow characteristics of circulating blood. WSS can be calculated (Papaioannou and Stefanadis, 2005; Khankin et al., 2021) as:

$$\text{WSS} = 4\eta Q/\pi r^3$$

In this equation, η is blood viscosity, Q is fluid velocity, and r is vessel diameter—all are critical parameters that determine local WSS. Importantly, of these parameters, both fluid velocity and vessel diameter can vary significantly across the systemic circulation. While fluid velocity is directly correlated with shear, this equation underscores how even small changes in vessel diameter—such as what occurs in the hierarchal branching of the vascular tree—can produce large effects in WSS (Table 1). Endothelial cells of the aorta, for example, experience high-velocity pulsatile flow at magnitudes of ~ 20 dynes/cm² (~ 2 Pa) (Callaghan and Grieve, 2018). Pulsatile flow is defined as flow that oscillates between periods of high and low pressure, which

TABLE 1 Flow characteristics and average wall shear stress forces in human vasculature.

	Flow type	Wall shear stress (dynes/cm ²)	Reference
Aorta	Pulsatile	5–22	Callaghan and Grieve (2018)
			Chatterjee (2018)
Artery	Laminar	3–13	Reneman and Hoeks (2008)
			Chatterjee (2018)
Arteriole	Laminar	10–60	Reneman and Hoeks (2008)
			Hoesseinzadegan and Tafti (2017)
			Chatterjee (2018)
Microvessels	Intermittent	28–955 (Average: 40)	Koutsiaris et al. (2007)
Venule	Laminar	10	Ballerman et al. (1998)
			Chatterjee (2018)
Vein	Laminar	1–5	Ballerman et al. (1998)
			Chatterjee (2018)

*All values are approximate ranges based on referenced studies and reviews.

corresponds to systole and diastole; flow pulsatility is quickly lost as the vessel wall dampens the pressure oscillations leading to steady downstream laminar flow. By contrast, WSS values for the microvessels are on average 40 dynes/cm², but flow through these vessels is intermittent due to dynamic, moment-to-moment vasomotor changes that alter precapillary vessel diameter to control whether downstream capillary networks are perfused. Shearing forces are further compounded by the movement of circulating red blood cells as they squeeze through—and thus drag along the inner wall of—small caliber capillaries (Figure 1). Thus, capillary flow and WSS can vary by as much as 3–96 dynes/cm² (0.3Pa–9.6Pa). Importantly, normal vascular WSS values are also species-specific: mice, for example, can experience WSS of ~600 dynes/cm² in the aorta, whereas such WSS forces are rarely found in humans (Suo et al., 2007).

WSS is a key biophysical signal for endothelial cells, and influences many aspects of vascular biology by altering endothelial cell shape, proliferation (Guo et al., 2007; Fang et al., 2017), migration (Hsu et al., 2001), gene expression and signaling activation (Guo et al., 2007; Fang et al., 2017; Chung et al., 2022; Mendez et al., 2022), and junctional permeability (Baeyens et al., 2016). During blood vessel development, WSS is a critical signal for proper vascular morphogenesis, and onset of systemic blood flow from the heart drives reorganization, remodeling, and mural cell recruitment to transform this plexus into a mature vascular network that includes arteries, capillaries, and veins (Lucitti et al., 2007; Garcia and Larina, 2014). For example, exposure of endothelial cells to arterial levels of flow drives expression of the arterial identity gene Cx40, and knockout of this gene leads to disrupted arteriogenesis (Buschmann et al., 2010; Fang et al., 2017). By contrast, vascular malformations in the congenital disease Hereditary Hemorrhagic Telangiectasia (HHT) occur primarily in high flow vessels (Larrivee et al., 2012), and appear to arise from defects in flow-sensitive endothelial cell migration (Jin et al., 2017). In post-natal vasculature, healthy vascular endothelial cell function remains tightly regulated

by flow, especially in regard to vascular barrier function where flow induces profound changes in expression of junctional proteins [e.g., cadherins (Miao et al., 2005), gap junctions (Fang et al., 2017), and tight junctions (Yang et al., 2020)]. Flow also controls cell-cell signaling [e.g., Notch (Fang et al., 2017; Mack et al., 2017)], activates vasodilatory signals [e.g., eNOS (Sahni et al., 2023)], suppresses anti-inflammatory KLF2 signaling and increases production of circulating cytokines (Fledderus et al., 2007; Chen et al., 2021), and induces endothelial cell cycle arrest and specification (Fang et al., 2017). Abnormal WSS signaling is associated with endothelial cell dysfunction, and is a major contributor to the pathophysiology of vascular diseases such as atherosclerosis (Zhou et al., 2023). In the lymphatic circulation, WSS is similarly critical for lymphatic vascular development and function (Angeli and Lim, 2023).

Notably, endothelial cells are exposed to transmural blood-pressure mediated hydrostatic pressure (P, Figure 1) in addition to WSS. The innate pulsatile flow of blood throughout the cardiovascular system imparts a significant force against vascular walls. Like WSS, this additional pressure is a known modulator of endothelial cell behavior, both on the individual and tissue scales. Externally applied hydrostatic pressure in culture models has been shown to regulate endothelial cell proliferation, focal adhesion complexes, and integrin expression (Schwartz et al., 1999; Prystopiuk et al., 2018). Tuning the applied hydrostatic pressure to match known physiological ranges protects against barrier damage in endothelial perturbation studies (Muller-Marschhausen et al., 2008). Moreover, hydrostatic pressure has been shown to induce angiogenesis *via* YAP1 signaling in damaged lung tissues (Mammoto et al., 2022) and to promote vascular tube formation *in vitro* *via* Ras-ERK signaling (Yoshino et al., 2020). Hence, hydrostatic pressure in the vascular system is an important mechanical signal sensed by the endothelium *in vivo* and within the context of *in vitro* systems. Controlling and monitoring hydrostatic pressure should be considered along with applied shear

stress in the design and implementation of vessel-on-a-chip systems. Technology for studying the effects of hydrostatic pressure relevant to vessel-on-a-chip systems include microfluidic culture devices with embedded pressure sensors designed to grant independent control of applied pressures and shear stresses (Liu et al., 2013). This review focuses on modeling and interrogating endothelial mechanosensing of shear forces associated with applied fluid flow.

Diversity in flow-sensitive signaling across endothelial cells

Endothelial cells exhibit distinct responses to the magnitude of WSS forces, indicating exquisite mechanosensing capabilities. Cleavage of the Notch intracellular domain, for example, is maximal in endothelial cells at 18 dynes/cm², but reduced at either higher or lower shear, or under static conditions (Fang et al., 2017). By contrast, Smad1/5 phosphorylation occurs at low (1 dynes/cm²) shear stress, but this is suppressed at higher (3 dynes/cm²) shear (Mendez et al., 2022). In microfluidic channel models of the vasculature, only application of fluid flow above a minimum threshold induces angiogenic sprouting in an MMP1-dependent manner (Galie et al., 2014). Taken together, the findings that many mechanosensitive signals respond differently to different magnitudes of flow have led to the hypothesis that distinct endothelial cells maintain themselves at a specific fluid shear stress “setpoint” (Baeyens et al., 2015; Baeyens et al., 2016), and that this may be established in an organotypic and vessel-specific manner. Furthermore, the homeostatic regulation of setpoint signaling appears to be a key determinant for endothelial cell biology in health and disease (Baeyens et al., 2015), and may moreover differ across distinct endothelial cell subtypes. Indeed, recent next-generation sequencing analysis of the murine vasculature reveals profound heterogeneity in endothelial cell identity and gene expression (Kalucka et al., 2020), suggesting that fluid shear stress “setpoint” and mechanosensitive responses may also vary widely within an individual blood vessel, between blood vessels of different identity and caliber within a single network, and across distinct tissue-specific blood vasculatures. Lastly, heterogeneity of the endothelium is also heavily influenced by tissue-specific paracrine and ECM signals that function in concert with hemodynamic signals to confer local phenotypes (Aird, 2012; Gunawardana et al., 2021).

Several cell surface proteins have been reported to function as primary mechanosensors that sense and transduce WSS signals into biological cell signaling responses (Figure 1). Of these, the junctional complex comprised of VE-Cadherin/CD31/VEGFR2/3 (Tzima et al., 2005; Coon et al., 2015) has been well characterized and plays a critical role as a mechanosensor of WSS in endothelial cells. The non-selective Piezo1 cation channel (Hyman et al., 2017), Notch1 (Mack et al., 2017), S1PR1 (Cantalupo et al., 2017), and primary cilia structures have also been proposed to be flow mechanosensors (Luu et al., 2018), although how and under what circumstances these mechanosensory proteins and cell structures (individually and collectively) translate WSS signals to control endothelial cell biology in health and disease remains the subject of active research. The ability to precisely control and measure applied shear stress in vessel-on-a-chip systems can allow

researchers to investigate shear sensing mechanisms in a physiologically relevant format using human cells. In summary, efforts to mimic the physiology of living blood vasculature in microphysiological systems will require careful consideration of applied flow and the resultant shear stresses that regulate endothelial cell forms and functions.

History of vessel-on-a-chip systems

Early efforts to harness microfluidic technologies for vascular engineering largely focused on integrating an artificially engineered circulatory system into bulk-engineered tissue constructs. Methods of patterning a template of channels included micromachining a series of channels in a rigid polymer bulk, or by manipulating the 3D architecture of more compliant extracellular matrix-derived substrates (Figure 2). In the latter approach, a sacrificial material (often made of sugar, alginate, or gelatin) was embedded within a bulk hydrogel in the pattern of the desired vascular structures. Subsequent dissolution of this matrix produced a network of perfusable channels to enable fluid circulation (Golden and Tien, 2007; Bellan et al., 2009; Norotte et al., 2009; Miller et al., 2012; Zervantonakis et al., 2012; Wang et al., 2014). Alternatively, photolithography-based methods could be used to generate micropatterned hydrogels with internal channels approximating vascular structures (Shevkoplyas et al., 2003; Moon et al., 2009; Du et al., 2011; Zheng et al., 2012). Further engineered efforts combined both micromachining and 3D matrix micromolding (Bertassoni et al., 2014). Overall, while such models were able to generate channel networks to perfuse bulk tissues, these printed channel designs were often not endothelialized and lacked many key biological characteristics such as structural heterogeneity of the native vasculature and the presence of stromal support cells.

In recent years, considerable efforts have been dedicated to engineering MPS models of the vasculature, either as a stand-alone vessel-on-a-chip platform or in the presence of organ-specific parenchymal cells (Torisawa et al., 2014; Huh, 2015; Blundell et al., 2016; Jang et al., 2019; Pocericiute and Ismagilov, 2019). Contemporary vessel-on-a-chip platforms vary widely in their design and ability to recapitulate aspects of the intact vascular niche (Table 2). A commonly used single vessel-on-a-chip platform involves fabrication of an extracellular matrix-comprised hydrogel cast within a mold fabricated from polydimethylsiloxane (PDMS) in the presence of a stainless steel needle or similar template (Figure 2). Subsequent withdrawal of the needle produces a templated channel that can then be seeded with endothelial cells to form a complete circumferential monolayer on the inner surface of the channel (Chrobak et al., 2006; Price et al., 2008; Seto et al., 2010; Wong et al., 2010; Sadr et al., 2011; Kusuma et al., 2013; Linville et al., 2016; Polacheck et al., 2017; Polacheck et al., 2019). This approach produces perfusable vessels as small as 160 µm in diameter (Polacheck et al., 2017; Polacheck et al., 2019)—within the range of small peripheral vessels in humans. Linville and colleagues showed that controlled patterns of interstitial pressure, stiffer hydrogel matrices, and high cAMP can enhance the generation of small diameter biomimetic vessels *via* this method (Linville et al., 2016). Hypothesis-driven studies using the needle withdrawal model have yielded insights into endothelial cell

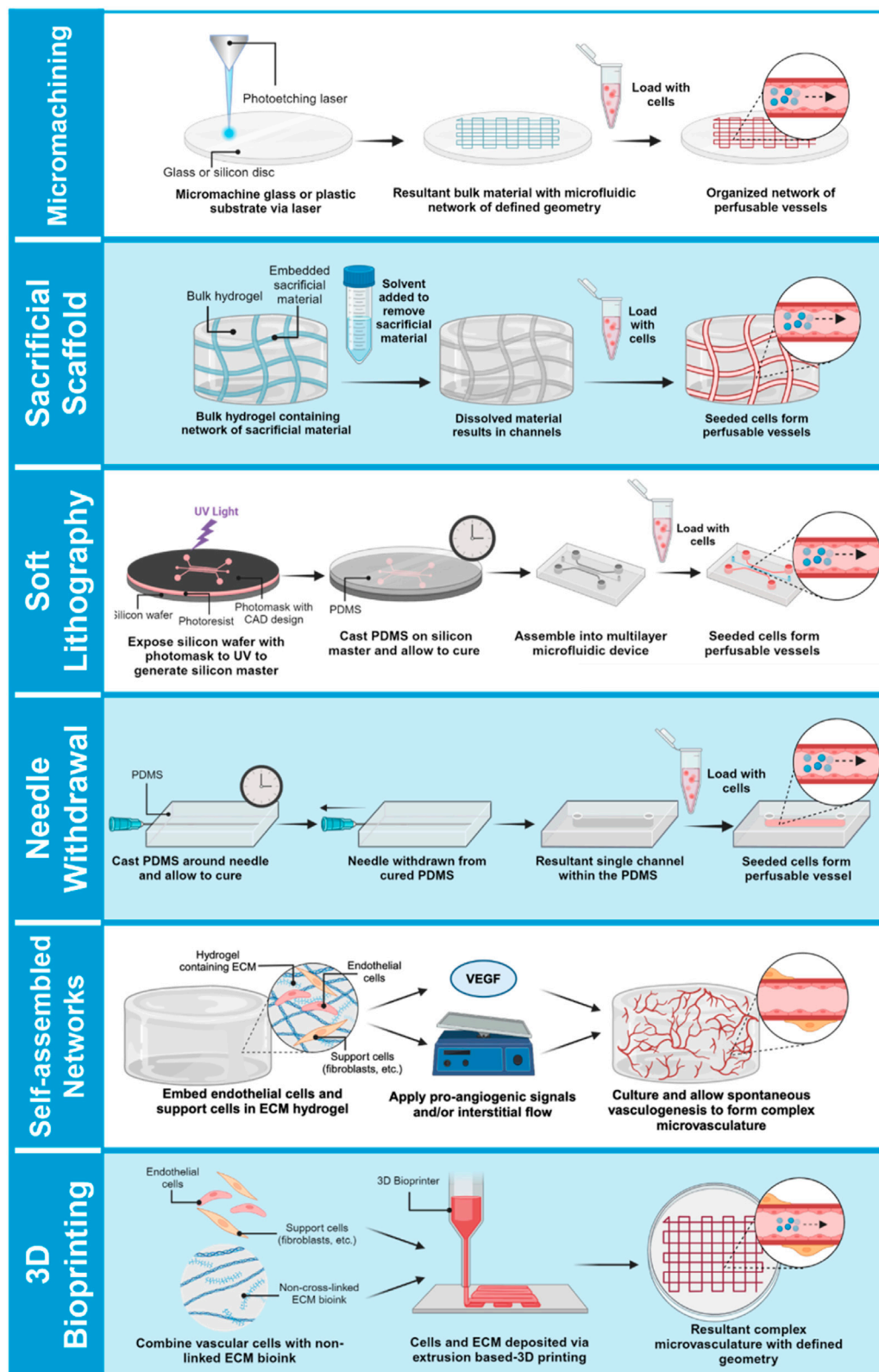


FIGURE 2

Approaches for bioengineering vessel-on-a-chip models. Micromachined or acellular gel-imprinted microfluidic channels circulate flow between distinct tissue compartments. Alternatively, complex microfluidic channel designs can be formed in a 3D hydrogel by soft lithography printing, or by a needle withdrawal method to generate a single-channel vessel-on-a-chip. Microvessel networks can be formed in organ chips either by embedding endothelial cells with support cells into a 3D hydrogel and inducing network self-assembly by application of interstitial flow, or vessel networks can be bioprinted onto a minimal scaffold, and then exposed to interstitial flow to promote lumenization.

TABLE 2 Characteristics and Functions of *In Vivo* Vasculature and Examples of their Representation in MPS.

<i>In Vivo</i> vascular characteristic	Example(s) of representation in MPS	Reference
Vasculogenesis	Endothelial cells are induced to self-organized into an interconnected vascular network	Campisi et al. (2018)
Sprouting Angiogenesis	Established vessel networks are induced to sprout into an adjacent avascular hydrogel	Chan et al. (2012), Kpeli et al. (2024)
Vessel lumenization	Establishing an empty tube in hydrogel (e.g., by viscous finger patterning or other approaches), which is then endothelialized on the inner luminal surface	Bischel et al. (2012), Polacheck et al. (2019)
Hierarchical and branching network organization	Endothelial cells are induced to self-organized into an interconnected vascular network; microvessels are patterned onto a bioprinted extracellular matrix comprised of a branching architecture	Sobrinho et al. (2016), Kolesky et al. (2014)
Vessel barrier maturation	Establishment of an endothelialized tube to study transmural transport; Integration of neural cell types to model the barrier function of the blood-brain barrier	Polacheck et al. (2019), Campisi et al. (2018)
Perfusion and blood flow	Gravity-driven or motorized circulation of media through lumenized vessels	Figure 2, and associated text
Basement membrane formation	Porous elastomeric tissue-tissue interfaces to provide physical separation; artificial ECM analogs	Huh (2015)
Mural cell coverage, i.e., pericytes, smooth muscle)	Vascular mural cells co-seeded with endothelial cells	Sobrinho et al. (2016), Campisi et al. (2018)
Conducted vasomotor changes	None reported	
Tissue-specific endothelial cell identity	Co-seeding with tissue-specific EC or stroma derived either from donor tissue or iPSC.	Campisi et al. (2018)
Immune cell transmigration	A chemotactic gradient drives immune cell extravasation across a bioengineered vessel wall	van Os et al. (2023)
Cancer cell metastasis	Cancer cells are circulated in the vascular compartment to measure vascular transmigration	Ozer et al. (2023)

signaling mechanisms that control vessel barrier function (Wong et al., 2010; Polacheck et al., 2017; Polacheck et al., 2019). However, this vessel-on-a-chip is limited by difficulties in incorporating a well-organized outer mural cell layer. The single vessel format with constant diameter also lacks the morphology of fractal branching and tapered diameters that contribute to heterogenous flow patterns and gradients of WSS that are present in native vascular beds (Saqr et al., 2020).

Organ chip models of entire vascular beds have been developed in attempts to create more biomimetic systems for investigating vascular physiology, drug delivery, and pathophysiological processes such as tumor cell metastasis (Haase et al., 2020; Del Piccolo et al., 2021; Chen et al., 2023) (Figure 1). In brief, human donor-derived (i.e., primary or iPSC-derived) endothelial and vascular support cells (e.g., fibroblasts, pericytes, vascular smooth muscle) are co-seeded in extracellular matrix hydrogels loaded in organ chip devices. These organ chips typically entail a “3-lane” design in which a central channel loaded with the 3D hydrogel mixture containing vascular cells is flanked by side channels that can be seeded with a confluent endothelial layer to aid anastomosis with the internal bulk vasculature (Wang et al., 2016). Various approaches have been reported to enhance anastomosis, such as the subsequent application of pro-angiogenic signals (e.g., exogenous VEGF) and/or interstitial flow that drives cytoskeletal rearrangement and increases nitric oxide (NO) synthesis, (Kim et al., 2016). Collectively, numerous approaches can facilitate the self-organization of vascular cells into a patent and perfusable microvascular bed, although defining the mechanism of anastomosis to achieve greater control will require further investigation. Most importantly, the resultant models exhibit organotypic vascular organization (i.e., appropriate lumen size, branching architecture, mural cell wrapping) and grant

the ability to precisely control biophysical and biochemical signals for tuned mimicry of *in vivo* blood vessels (Nakatsu and Hughes, 2008; Newman et al., 2011; Chan et al., 2012; Kim et al., 2013). Reports of microvasculature-on-a-chip models outperforming conventional 2D and 3D models in their recapitulation of *in vivo* drug responses are a testament to the translational potential of these platforms (Hachey et al., 2021; Hachey et al., 2024).

Organ chip models of vascular beds that rely on vascular cell self-organization may be difficult to standardize due to variations in cell sourcing, purity, and quality. Recently, some groups have incorporated cutting-edge 3D bioprinting approaches to circumvent this requirement by artificially depositing vascular cells into pre-determined architectures within an extracellular matrix (Kolesky et al., 2014; Gao et al., 2017; Zhang G. et al., 2020; Zhang et al., 2021; Orellano et al., 2022; Zhang et al., 2022), and these models are capable of generating perfused vascular networks supported by minimal scaffolding material (Kolesky et al., 2014; Lee et al., 2014; Jia et al., 2016; Cao et al., 2019; Freeman et al., 2019; Gold et al., 2021). Unlike other models described thus far, bioprinted vessel characteristics are dependent on the mechanical properties of both the bioinks used as well as the surrounding hydrogel scaffold. For example, changing flow rate and print-head speed affects resulting bioprinted vessel lumen size (Attalla et al., 2016). Inclusion of solid frames within the hydrogel scaffold produces tensile forces that also influence vessel morphology (Zhang G. et al., 2020; Zhang et al., 2021; Zhang et al., 2022). While bioprinted platforms have the potential to precisely control 3D architecture, the complexity and technical demands of the approach currently limits its broad adoption by basic scientists and preclinical researchers. Organ chip models and MPS allow researchers to utilize familiar 2D and 3D cell culture methods

using fluidic device platforms with increasing commercial availability as “off the shelf” products to a wide-range of end users (Zhang and Radisic, 2017).

As with all MPS, engineering organ-specific vessel-on-a-chip models require precise control of cell type, microtissue architecture, extracellular matrix composition, and mechanical forces such as substrate stiffness and the shear stress applied by microfluidic flow. Importantly, these parameters are key signals for microvessel-on-a-chip network formation—which underscores the importance of these signals in the function of native vasculature—and are critical for capturing endothelial cell physiology in an *in vitro* setting. In a recent study by Hatch et al. to develop a COVID-on-a-chip vascular model, for example, endothelial cell expression of SARS-CoV2 target ACE2 was reported to be flow-dependent, and a SARS-CoV2 pseudovirus failed to efficiently infect primary endothelial cells except within a vessel-on-a-chip platform under flow (Hatch et al., 2024).

Optimization of chip biomaterials, organotypic cell combinations, extracellular matrix composition is a unique tissue engineering problem within each specific organ chip application. Most organ chips are fabricated out of optically transparent, biocompatible elastomers—most commonly PDMS. Pure PDMS has a relatively low elastic modulus (1.3–3 MPa) and tensile strength (3.5–5.1 MPa) (Ariati et al., 2021), meaning that it is a relatively soft and elastic elastomer when compared to other inorganic materials. Furthermore, the mechanical properties of PDMS can be controlled either by altering the curing conditions of pure PDMS or by including fillers to create PDMS composites that can vary widely in their mechanical properties (Ariati et al., 2021). Nonetheless, pure PDMS is inherently less elastic and more stiff than biological tissues (including intact vessel wall), and most PDMS composites increase—not decrease—these properties (Ebrahimi, 2009). The difference in PDMS stiffness relative to intact basement membrane will affect the resulting shear stress that is generated by fluid flow and sensed by endothelial cells—particularly with regard to organ chips in which endothelial cells are seeded directly onto PDMS-based (or other elastomeric) surfaces and where the PDMS provides direct mechanical support for the engineered endothelium.

Alternatively, blood vessels can be generated within extracellular matrix hydrogels seeded into microfluidic tissue compartments, such that the PDMS of the tissue chamber is not directly in contact with engineered blood vessels and is not directly contributing to mechanical wall stiffness. In these types of vessel-on-a-chip designs, the elastic modulus of vascular mural cells and surrounding hydrogel typically falls within the compliant range of soft tissues—i.e., 1 kPa or less—providing a more physiologically relevant microenvironment that better approximates the mechanical properties of intact blood vasculature. As has been previously shown to be the case in simpler 3D angiogenesis models (Newman et al., 2011), the presence of fibroblasts is essential for network formation. In the absence of perivascular support cells, networks fail to form or regress rapidly (Nakatsu et al., 2003; Newman et al., 2011; Whisler et al., 2014). More research is needed to determine the optimal types and ratios of support cells to produce coveted organ-specific endothelial phenotypes. Extracellular matrix protein composition and density also affects vascular network formation and maturation, likely through combined effects on cell-matrix signaling and matrix

stiffness. For example, increased fibrinogen concentration increases the average diameter of resulting vessels (Whisler et al., 2014), and extent of gelatin methacrylate methylation dictates vessel outgrowth potential and vasculogenesis (Chen et al., 2012). Externally applied mechanical load alone also controls vessel architecture (Krishnan et al., 2008; Rosenfeld et al., 2016), suggesting that both cell-matrix signaling and mechanical properties of the extracellular space contribute to vascular morphogenesis in these models.

In summary, MPS research has delivered the foundation for accurate biomimicry of vascular beds, but future efforts will be needed to develop and implement protocols for the creation of organ-specific models of healthy and diseased vasculature.

Integrating physiological fluid flow into vessel-on-a-chip platforms

Of greatest relevance to this review, vessel-on-a-chip models enable study of bioengineered blood vessels *under controlled flow*, which promises to significantly advance our understanding of how hemodynamic flow contributes to healthy and diseased vascular biology in intact blood vessels. Thus, vessel-on-a-chip design and implementation demands careful attention to the method of introducing circulating flow, which entails a balance between ease of use and the degree to which researchers wish to mimic the *in vivo* milieu for a given application. This is especially important when considered in the context of the aforementioned “fluid shear setpoint” hypothesis advanced by Baeyens et al. (Baeyens et al., 2016). There is also inherent applied hydrostatic pressure that will vary with the total liquid volume, reservoir height, and layout of the fluidic channel circuit in each vessel-on-a-chip design. Within replicates of a single design exposed to the same fluid flow conditions, the applied hydrostatic pressure is relatively uniform, which allows for isolation of applied shear stress as an experimental variable by varying the flow rate (Alonzo et al., 2015; Lam et al., 2018). Altered hydrostatic pressure should be considered when moving between vessel chip platforms as changes to system parameters such as channel geometry, total liquid volume, and method of generating flow will impart varying hydrostatic pressure profiles.

Varying WSS experienced by endothelial cells in a vessel-on-a-chip platform is achieved *via* control of applied fluid flow. The primary strategies for controlling fluid flow in vessel-on-a-chip systems include: 1) motorized pumping, 2) motorized rocking of the platform to reset gravity-driven flow, or 3) non-motorized gravity-driven flow with manual reset (Figure 3). Motorized syringe pumps have the advantage of being able to readily achieve high circulating fluid velocity (and thus, correspondingly higher levels of WSS within the ranges seen *in vivo*, Table 1). In addition, motorized pumps (unlike gravity-driven models) allow users to program defined patterns of continuous, oscillatory, and/or pulsatile flow, which may be critical if modeling blood vessel structures in which complex flow profiles are typically observed *in vivo*. However, pump-based systems are mechanically complex, and require numerous accessory components to maintain flow through the pump system. This significantly increases the required volume of circulating media, limits the number of devices that can be run in parallel, and introduces points of

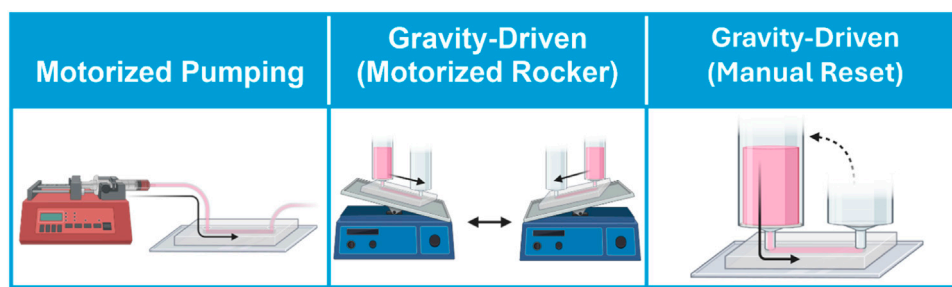


FIGURE 3

Approaches for circulating flow on vessel-on-a-chip models. Flow is circulated through vessel-on-a-chip platform through motorized pumping, or by gravity-driven flow in which motorized rockers automate hydrostatic pressure reset, or by manual pressure head reset.

potential device failure through fluid leak or microbial contamination. While syringe pumps are often used to provide programmable flow control, peristaltic pumps have become an attractive alternative that offer increased simplicity, lowered cost, and decreased risk of contamination due to the closed nature of recirculating peristaltic systems (Abello et al., 2022; Mohammed et al., 2019; Schneider et al., 2021; Zhang X. et al., 2020; O'Grady et al., 2018). A limitation of such pumps is the inherently pulsatile nature of the produced fluid flow. It is well documented that endothelial cells respond differentially to laminar versus pulsatile flow (Eskin et al., 1984; Helmlinger et al., 1991; Miao et al., 2005; Guo et al., 2007; Mohammed et al., 2019; Liu et al., 2021), thus pulsatile flow patterns will not impart physiological shear forces to small vessels which naturally feature continuous laminar flow in intact microvasculature. Efforts have been made to generate laminar flow *via* peristaltic pumps using pulse dampeners (Voyvodic et al., 2012; Pech et al., 2020; Abello et al., 2022). The transition from pulsatile flow in the macrovasculature to continuous flow in the microvascular beds *in vivo* should be considered when choosing a mechanical pumping approach for specific vessel-on-a-chip applications.

On the other hand, pumpless gravity-driven models are mechanically simpler, and thus potentially easier to scale in studies in which large numbers of devices must be run in parallel (Figure 3). Nonetheless, gravity-driven models also have unique drawbacks. Gravity-driven flow depends upon the hydrostatic pressure gradient generated between two coupled media reservoirs. Thus, gravity-driven flow is initially high when the hydrostatic pressure gradient is largest, but this driving force decreases over time as the volumes of the two reservoirs equilibrate. Not only does this produce a changing flow profile over time, but also necessitates frequent reset of the hydrostatic pressure heads within the two media reservoirs to maintain flow through the system. This process can be performed manually through pipetting, or can be automated using a motorized rocker. Of these two strategies, motorized rockers typically produce bi-directional (i.e., alternating flow direction) gravity-driven fluid circulation, which does not accurately reflect the unidirectionality of blood flow in the intact vasculature. A recent pumpless gravity-driven system corrects this problem using a platform with additional supporting channels and valve features to create continuous unidirectional flow with rocking, although it is not yet in widespread use (Wang and Shuler, 2018). Alternatively,

hydrostatic pressure heads can be manually reset through pipetting. While manual pipetting can be tedious, time-consuming, and inconsistent, it is likely that automated robotic pipetting will solve this problem for high-throughput applications, particularly in industrial settings (Langer and Joensson, 2020).

In addition to the above challenges, gravity-driven strategies are also typically limited by media reservoir size, which physically constrains the size of the hydrostatic pressure gradient that can be generated by this approach. As a result, it can be challenging to produce sufficiently high fluid velocity to capture high fluid flow and WSS using gravity-driven approaches. Since WSS depends heavily on vessel diameter, pump-driven models in which high fluid flow rates are introduced in large-diameter vessel compartments, the high fluid velocity may still be insufficient to produce physiological levels of WSS in some models. By contrast, the small vessel sizes (e.g., 25–30 μm in diameter) (Fang et al., 2024) that are often achievable in self-assembled microvasculature-on-a-chip models can bring even gravity-driven models into physiological ranges of WSS (Fang et al., 2024). Precise control of hemodynamic flow, regardless of the mode in which it is applied, in vessel-on-a-chip models is also constrained by the lack of widely adaptable tools for the study of real-time fluid flow. Precise measurement of flow rates and local fluid velocities within a 3D vascular architecture will be necessary for robust quality control and precise determination of WSS effects in functional assays. Fluid velocity can be measured in vessel-on-a-chip models by particle velocimetry, i.e., time-lapse imaging of perfused fluorescent particles from which particle trajectories and velocities can be used to calculate flow patterns and estimate applied WSS based on defined vessel geometry (Pitts and Fenech, 2013). Alternatively, fluid velocity and WSS can be estimated using *in silico* modeling based on the size and shape of bioengineered vessels (Fang et al., 2024; Hatch et al., 2024) using approaches similar to have been previously applied in intact tissue (Bernabeu et al., 2014), but this still presupposes that the pumping or rocking method used generates the desired flow rates within an engineered vessel or vascular bed. Empirical and computational approaches to quantify applied WSS will likely be combined in industrial settings, but these strategies currently present challenges to implementation in most research labs that use vessel-on-a-chip systems. Developing new tools for adaptable and scalable automation of real-time flow monitoring in MPS with complex 3D vasculature will enable modeling of hemodynamics *in vitro* with unprecedented biomimicry.

Another issue for vessel-on-a-chip models is endothelial cell source, particularly with regard to capturing tissue-specific endothelial cell mechanosensitive signaling. Early vessel-on-a-chip models including many described in this review rely on “generic” primary human endothelial cells selected for their ease-of-use and non-specific endothelial cell identity (e.g., human umbilical vein endothelial cells (HUVEC); circulating endothelial progenitor cells (EPC), *etc.*), with the idea that these “generic” endothelial cells would acquire more specialized identities when co-seeded with tissue-specific stromal cells in organ chip platforms. However, with recent studies further underscoring the broad heterogeneity of vascular endothelial cells (Kalucka et al., 2020)—with likely important implications for heterogeneity in mechanosensitive signaling—recent organ chip work has increasingly focused on integrating tissue-specific primary endothelial cells into organ chip settings, with these endothelial cells either isolated directly from tissue-specific vascular beds (e.g. (Park et al., 2019)) or generated from iPSC (e.g. (Vatine et al., 2019)). These latest efforts are more likely to recapitulate tissue-specific flow-sensitive signaling relative to platforms that were developed using “generic” endothelial cells. However, tissue-specific endothelial cells may lose their specialized endothelial cell identities with time in culture, and/or may have compromised vessel self-assembly properties that may limit their integration into platforms that rely upon this property to form vessel-on-a-chip networks. Ongoing work in the field is focused on addressing these various challenges.

A final consideration when incorporating physiological flow into vessel-on-a-chip platforms is the composition of the circulating media. Current vessel-on-a-chip models typically circulate growth factor-rich endothelial growth medium. However, endothelial growth medium often contains higher levels of pro-angiogenic growth factors and other supplements than is typically found in circulating blood. This alone would be hypothesized to drive endothelial cells in vessel-on-a-chip platforms towards a more activated, pro-inflammatory, and pro-angiogenic state more representative of disease, whereas endothelial cells in established and healthy (i.e., uninjured) blood vessels are typically non-proliferative and quiescent (Langille et al., 1986). In addition, the cell culture media typically circulated through vessel-on-a-chip models lacks the higher viscosity of blood and colloidal properties imparted by circulating blood cells—both properties that greatly influence vascular WSS experienced *in vivo*. Additional work remains to be done to improve our current “blood surrogates” to better mimic the biophysical and biochemical properties of *in vivo* blood (Marx et al., 2016). This will in turn further enhance the physiological relevance of circulating fluid flow in vessel-on-a-chip platforms to better recapitulate the effect of hemodynamic forces on intact vasculature.

Conclusion

Vascularized MPS (i.e., vessel-on-a-chip systems) are powerful *in vitro* models that enable precise control of cell type composition, 3D tissue architecture and layering, extracellular matrix composition, and intravascular fluid flow that regulates biotransport processes and mechanical forces such as applied shear stresses. Current vessel-on-a-chip systems take varied approaches to model the *in vivo* vascular

niche, and have successfully recapitulated many of the hallmarks of intact blood vessels that remain elusive in conventional 2D cell culture, while still retaining many of the ease-of-use advantages of *in vitro* experimentation. Balancing complexity and ease-of-use by the widest range of possible end users will be a critical dimension of efforts to maximize translational impact of vessel-on-a-chip technologies. Studies using vessel-on-a-chip models have already produced novel insights into the role of fluid flow and WSS as key signals in vascular health and disease. However, efforts to fully capture the physiological hemodynamics in vascularized MPS remain challenging due to engineering considerations such as controlling and monitoring intravascular fluid flow. Future vessel-on-a-chip platforms must continue to consider how important parameters that determine WSS—including vessel diameter, flow velocity, and fluid viscosity—are represented in their chip designs to ensure that resulting on-chip flow fully captures the biomechanical properties of circulating blood and its corresponding signaling to regulate vascular physiology and function.

Author contributions

AM: Visualization, Writing–review and editing, Writing–original draft, Conceptualization. ZC: Writing–review and editing. HS: Writing–review and editing. MM: Writing–review and editing, Writing–original draft, Funding acquisition, Conceptualization. JF: Writing–review and editing, Writing–original draft, Visualization, Funding acquisition, Conceptualization.

Funding

The author(s) declare that financial support was received for the research, authorship, and/or publication of this article. This work was funded in part by a grant from the Eye, Ear, Nose and Throat Foundation of New Orleans (EE221102 to JF and MM).

Acknowledgments

The authors would like to acknowledge members of the Fang and Mondrinos labs for their collegiality and scientific discussions.

Conflict of interest

The authors declare that the research was conducted in the absence of any commercial or financial relationships that could be construed as a potential conflict of interest.

Publisher’s note

All claims expressed in this article are solely those of the authors and do not necessarily represent those of their affiliated organizations, or those of the publisher, the editors and the reviewers. Any product that may be evaluated in this article, or claim that may be made by its manufacturer, is not guaranteed or endorsed by the publisher.

References

- Abello, J., Raghavan, S., Yien, Y. Y., and Stratman, A. N. (2022). Peristaltic pumps adapted for laminar flow experiments enhance *in vitro* modeling of vascular cell behavior. *J. Biol. Chem.* 298, 102404. doi:10.1016/j.jbc.2022.102404
- Adamson, R. H., Lenz, J. F., and Curry, F. E. (1994). Quantitative laser scanning confocal microscopy on single capillaries: permeability measurement. *Microcirculation* 1, 251–265. doi:10.3109/10739689409146752
- Aird, W. C. (2012). Endothelial cell heterogeneity. *Cold Spring Harb. Perspect. Med.* 2, a006429. doi:10.1101/cshperspect.a006429
- Alonzo, L. F., Moya, M. L., Shirure, V. S., and George, S. C. (2015). Microfluidic device to control interstitial flow-mediated homotypic and heterotypic cellular communication. *Lab. Chip* 15, 3521–3529. doi:10.1039/c5lc00507h
- Angeli, V., and Lim, H. Y. (2023). Biomechanical control of lymphatic vessel physiology and functions. *Cell Mol. Immunol.* 20, 1051–1062. doi:10.1038/s41423-023-01042-9
- Ariati, R., Sales, F., Souza, A., Lima, R. A., and Ribeiro, J. (2021). Polydimethylsiloxane composites characterization and its applications: a review. *Polym. (Basel)* 13, 4258. doi:10.3390/polym13234258
- Attalla, R., Ling, C., and Selvelganapathy, P. (2016). Fabrication and characterization of gels with integrated channels using 3D printing with microfluidic nozzle for tissue engineering applications. *Biomed. Microdevices* 18, 17–12. doi:10.1007/s10544-016-0042-6
- Augustin, H. G., and Koh, G. Y. (2017). Organotypic vasculature: from descriptive heterogeneity to functional pathophysiology. *Science* 357, eaal2379. doi:10.1126/science.aal2379
- Baeyens, N., Bandyopadhyay, C., Coon, B. G., Yun, S., and Schwartz, M. A. (2016). Endothelial fluid shear stress sensing in vascular health and disease. *J. Clin. Invest.* 126, 821–828. doi:10.1172/JCI83083
- Baeyens, N., Nicoli, S., Coon, B. G., Ross, T. D., Van den Dries, K., Han, J., et al. (2015). Vascular remodeling is governed by a VEGFR3-dependent fluid shear stress set point. *Elife* 4, e04645. doi:10.7554/eLife.04645
- Ballermann, B. J., Dardik, A., Eng, E., and Liu, A. (1998). Shear stress and the endothelium. *Kidney Int. Suppl.* 67, S100–S108. doi:10.1046/j.1523-1755.1998.06720.x
- Bellan, L. M., Singh, S. P., Henderson, P. W., Porri, T. J., Craighead, H. G., and Spector, J. A. (2009). Fabrication of an artificial 3-dimensional vascular network using sacrificial sugar structures. *Soft Matter* 5, 1354–1357. doi:10.1039/b819905a
- Bender, R. H. F., O'Donnell, B. T., Shergill, B., Pham, B. Q., Tahmoures, S., Sanchez, C. N., et al. (2024). A vascularized 3D model of the human pancreatic islet forex vivostudy of immune cell-islet interaction. *Biofabrication* 16, 025001. doi:10.1088/1758-5090/ad17d0
- Bernabeu, M. O., Jones, M. L., Nielsen, J. H., Kruger, T., Nash, R. W., Groen, D., et al. (2014). Computer simulations reveal complex distribution of haemodynamic forces in a mouse retina model of angiogenesis. *J. R. Soc. Interface* 11, 20140543. doi:10.1098/rsif.2014.0543
- Bertassoni, L. E., Cecconi, M., Manoharan, V., Nikkhah, M., Hjortnaes, J., Cristino, A. L., et al. (2014). Hydrogel bioprinted microchannel networks for vascularization of tissue engineering constructs. *Lab. Chip* 14, 2202–2211. doi:10.1039/c4lc00030g
- Bhatia, S. N., and Ingber, D. E. (2014). Microfluidic organs-on-chips. *Nat. Biotechnol.* 32, 760–772. doi:10.1038/nbt.2989
- Bischel, L. L., Lee, S. H., and Beebe, D. J. (2012). A practical method for patterning lumens through ECM hydrogels via viscous finger patterning. *J. Lab. Autom.* 17, 96–103. doi:10.1177/2211068211426694
- Blundell, C., Tess, E. R., Schanzer, A. S., Coutifaris, C., Su, E. J., Parry, S., et al. (2016). A microphysiological model of the human placental barrier. *Lab. Chip* 16, 3065–3073. doi:10.1039/c6lc00259e
- Buschmann, I., Pries, A., Styp-Rekowska, B., Hillmeister, P., Loufrani, L., Henrion, D., et al. (2010). Pulsatile shear and Gja5 modulate arterial identity and remodeling events during flow-driven arteriogenesis. *Development* 137, 2187–2196. doi:10.1242/dev.045351
- Callaghan, F. M., and Grieve, S. M. (2018). Normal patterns of thoracic aortic wall shear stress measured using four-dimensional flow MRI in a large population. *Am. J. Physiol. Heart Circ. Physiol.* 315, H1174–H1181. doi:10.1152/ajpheart.00017.2018
- Campisi, M., Shin, Y., Osaki, T., Hajal, C., Chiono, V., and Kamm, R. D. (2018). 3D self-organized microvascular model of the human blood-brain barrier with endothelial cells, pericytes and astrocytes. *Biomaterials* 180, 117–129. doi:10.1016/j.biomaterials.2018.07.014
- Cantalupo, A., Gargiulo, A., Dautaj, E., Liu, C., Zhang, Y., Hla, T., et al. (2017). S1PR1 (Sphingosine-1-Phosphate receptor 1) signaling regulates blood flow and pressure. *Hypertension* 70, 426–434. doi:10.1161/HYPERTENSIONAHA.117.09088
- Cao, X., Ashfaq, R., Cheng, F., Maharjan, S., Li, J., Ying, G., et al. (2019). A tumor-on-a-chip system with bioprinted blood and lymphatic vessel pair. *Adv. Funct. Mater.* 29, 1807173. doi:10.1002/adfm.201807173
- Chan, J. M., Zervantonakis, I. K., Rimchala, T., Polacheck, W. J., Whisler, J., and Kamm, R. D. (2012). Engineering of *in vitro* 3D capillary beds by self-directed angiogenic sprouting. *PLoS One* 7, e50582. doi:10.1371/journal.pone.0050582
- Chatterjee, S. (2018). Endothelial mechanotransduction, redox signaling and the regulation of vascular inflammatory pathways. *Front. Physiol.* 9, 524. doi:10.3389/fphys.2018.00524
- Chen, C., Chen, J., Tao, X., Fu, M., Cheng, B., and Chen, X. (2021). Activation of GPR30 with G1 inhibits oscillatory shear stress-induced adhesion of THP-1 monocytes to HAECS by increasing KLF2. *Aging (Albany NY)* 13, 11942–11953. doi:10.18632/aging.202897
- Chen, M. B., Whisler, J. A., Fröse, J., Yu, C., Shin, Y., and Kamm, R. D. (2017). On-chip human microvasculature assay for visualization and quantification of tumor cell extravasation dynamics. *Nat. Protoc.* 12, 865–880. doi:10.1038/nprot.2017.018
- Chen, S. W., Blazeski, A., Zhang, S., Shelton, S. E., Offeddu, G. S., and Kamm, R. D. (2023). Development of a perfusable, hierarchical microvasculature-on-a-chip model. *Lab. Chip* 23, 4552–4564. doi:10.1039/d3lc00512g
- Chen, Y.-C., Lin, R.-Z., Qi, H., Yang, Y., Bae, H., Melero-Martin, J. M., et al. (2012). Functional human vascular network generated in photocrosslinkable gelatin methacrylate hydrogels. *Adv. Funct. Mater.* 22, 2027–2039. doi:10.1002/adfm.201101662
- Chrobak, K. M., Potter, D. R., and Tien, J. (2006). Formation of perfused, functional microvascular tubes *in vitro*. *Microvasc. Res.* 71, 185–196. doi:10.1016/j.mvr.2006.02.005
- Chung, J., Kim, K. H., Yu, N., An, S. H., Lee, S., and Kwon, K. (2022). Fluid shear stress regulates the landscape of microRNAs in endothelial cell-derived small extracellular vesicles and modulates the function of endothelial cells. *Int. J. Mol. Sci.* 23, 1314. doi:10.3390/ijms23031314
- Cochrane, A., Albers, H. J., Passier, R., Mummery, C. L., van den Berg, A., Orlova, V. V., et al. (2019). Advanced *in vitro* models of vascular biology: human induced pluripotent stem cells and organ-on-chip technology. *Adv. Drug Deliv. Rev.* 140, 68–77. doi:10.1016/j.addr.2018.06.007
- Coon, B. G., Baeyens, N., Han, J., Budatha, M., Ross, T. D., Fang, J. S., et al. (2015). Intramembrane binding of VE-cadherin to VEGFR2 and VEGFR3 assembles the endothelial mechanosensory complex. *J. Cell Biol.* 208, 975–986. doi:10.1083/jcb.201408103
- Del Piccolo, N., Shirure, V. S., Bi, Y., Goedegebuure, S. P., Gholami, S., Hughes, C. C. W., et al. (2021). Tumor-on-chip modeling of organ-specific cancer and metastasis. *Adv. Drug Deliv. Rev.* 175, 113798. doi:10.1016/j.addr.2021.05.008
- Du, Y., Ghodousi, M., Qi, H., Haas, N., Xiao, W., and Khademhosseini, A. (2011). Sequential assembly of cell-laden hydrogel constructs to engineer vascular-like microchannels. *Biotechnol. Bioeng.* 108, 1693–1703. doi:10.1002/bit.23102
- Ebrahimi, A. P. (2009). Mechanical properties of normal and diseased cerebrovascular system. *J. Vasc. Interv. Neurol.* 2, 155–162.
- Edington, C. D., Chen, W. L. K., Geishecker, E., Kassis, T., Soenksen, L. R., Bhushan, B. M., et al. (2018). Interconnected microphysiological systems for quantitative biology and pharmacology studies. *Sci. Rep.* 8, 4530. doi:10.1038/s41598-018-22749-0
- Eskin, S. G., Ives, C. L., McIntire, L. V., and Navarro, L. T. (1984). Response of cultured endothelial cells to steady flow. *Microvasc. Res.* 28, 87–94. doi:10.1016/0026-2862(84)90031-1
- Ewald, M. L., Chen, Y. H., Lee, A. P., and Hughes, C. C. W. (2021). The vascular niche in next generation microphysiological systems. *Lab. Chip* 21, 3244–3262. doi:10.1039/d1lc00530h
- Fang, J. S., Coon, B. G., Gillis, N., Chen, Z., Qiu, J., Chittenden, T. W., et al. (2017). Shear-induced Notch-Cx37-p27 axis arrests endothelial cell cycle to enable arterial specification. *Nat. Commun.* 8, 2149. doi:10.1038/s41467-017-01742-7
- Fang, J. S., Hatch, C. J., Andrejcsk, J., van Trigt, W., Juat, D. J., Chen, Y.-H., et al. (2024). A microphysiological HHT-on-a-chip platform recapitulates patient vascular lesions. *bioRxiv*. doi:10.21203/rs.3.rs-4578507/v1
- Fledderus, J. O., van Thienen, J. V., Boon, R. A., Dekker, R. J., Rohlena, J., Volger, O. L., et al. (2007). Prolonged shear stress and KLF2 suppress constitutive proinflammatory transcription through inhibition of ATF2. *Blood* 109, 4249–4257. doi:10.1182/blood-2006-07-036020
- Freeman, S., Ramos, R., Alexis Chando, P., Zhou, L., Reeser, K., Jin, S., et al. (2019). A bioink blend for rotary 3D bioprinting tissue engineered small-diameter vascular constructs. *Acta Biomater.* 95, 152–164. doi:10.1016/j.actbio.2019.06.052
- Galie, P. A., Nguyen, D. H., Choi, C. K., Cohen, D. M., Janmey, P. A., and Chen, C. S. (2014). Fluid shear stress threshold regulates angiogenic sprouting. *Proc. Natl. Acad. Sci. U. S. A.* 111, 7968–7973. doi:10.1073/pnas.1310842111
- Gao, Q., Liu, Z., Lin, Z., Qiu, J., Liu, Y., Liu, A., et al. (2017). 3D bioprinting of vessel-like structures with multilevel fluidic channels. *ACS Biomaterials Sci. Eng.* 3, 399–408. doi:10.1021/acsbmaterials.6b00643
- Garcia, M. D., and Larina, I. V. (2014). Vascular development and hemodynamic force in the mouse yolk sac. *Front. Physiol.* 5, 308. doi:10.3389/fphys.2014.00308
- Gold, K. A., Saha, B., Rajeeva Pandian, N. K., Walther, B. K., Palma, J. A., Jo, J., et al. (2021). 3D bioprinted multicellular vascular models. *Adv. Healthc. Mater.* 10, 2101141. doi:10.1002/adhm.202101141

- Golden, A. P., and Tien, J. (2007). Fabrication of microfluidic hydrogels using molded gelatin as a sacrificial element. *Lab. Chip* 7, 720–725. doi:10.1039/b618409j
- Gunawardana, H., Romero, T., Yao, N., Heidt, S., Mulder, A., Elashoff, D. A., et al. (2021). Tissue-specific endothelial cell heterogeneity contributes to unequal inflammatory responses. *Sci. Rep.* 11, 1949. doi:10.1038/s41598-020-80102-w
- Guo, D., Chien, S., and Shyy, J. Y. (2007). Regulation of endothelial cell cycle by laminar versus oscillatory flow: distinct modes of interactions of AMP-activated protein kinase and Akt pathways. *Circ. Res.* 100, 564–571. doi:10.1161/01.RES.0000259561.23876.c5
- Haas, M. J., Feng, V., Gonzales, K., Onstead-Haas, L., and Mooradian, A. D. (2020). High-throughput analysis identifying drugs that reduce oxidative and ER stress in human coronary artery endothelial cells. *Eur. J. Pharmacol.* 879, 173119. doi:10.1016/j.ejphar.2020.173119
- Haase, K., Offeddu, G. S., Gillrie, M. R., and Kamm, R. D. (2020). Endothelial regulation of drug transport in a 3D vascularized tumor model. *Adv. Funct. Mater.* 30, 2002444. doi:10.1002/adfm.202002444
- Hachey, S. J., Hatch, C. J., Gaebler, D., Mocherla, A., Nee, K., Kessenbrock, K., et al. (2024). Targeting tumor-stromal interactions in triple-negative breast cancer using a human vascularized micro-tumor model. *Breast Cancer Res.* 26, 5. doi:10.1186/s13058-023-01760-y
- Hachey, S. J., Movsesyan, S., Nguyen, Q. H., Burton-Sojo, G., Tankanzyan, A., Wu, J., et al. (2021). An *in vitro* vascularized micro-tumor model of human colorectal cancer recapitulates *in vivo* responses to standard-of-care therapy. *Lab. Chip* 21, 1333–1351. doi:10.1039/d0lc01216e
- Hatch, C. J., Piombo, S. D., Fang, J. S., Gach, J. S., Ewald, M. L., Van Trigt, W. K., et al. (2024). SARS-CoV-2 infection of endothelial cells, dependent on flow-induced ACE2 expression, drives hypercytokinemia in a vascularized microphysiological system. *Front. Cardiovasc. Med.* 11, 1360364. doi:10.3389/fcvm.2024.1360364
- Heberlein, K. R., Straub, A. C., and Isakson, B. E. (2009). The myoendothelial junction: breaking through the matrix? *Microcirculation* 16, 307–322. doi:10.1080/10739680902744404
- Helmlinger, G., Geiger, R. V., Schreck, S., and Nerem, R. M. (1991). Effects of pulsatile flow on cultured vascular endothelial cell morphology. *J. Biomech. Eng.* 113, 123–131. doi:10.1115/1.2891226
- Hosseinizadegan, H., and Tafti, D. K. (2017). Modeling thrombus formation and growth. *Biotechnol. Bioeng.* 114, 2154–2172. doi:10.1002/bit.26343
- Hsu, P. P., Li, S., Li, Y. S., Usami, S., Ratcliffe, A., Wang, X., et al. (2001). Effects of flow patterns on endothelial cell migration into a zone of mechanical denudation. *Biochem. Biophys. Res. Commun.* 285, 751–759. doi:10.1006/bbrc.2001.5221
- Huh, D. D. (2015). A human breathing lung-on-a-chip. *Ann. Am. Thorac. Soc.* 12 (Suppl. 1), S42–S44. doi:10.1513/AnnalsATS.201410-442MG
- Hyman, A. J., Tumova, S., and Beech, D. J. (2017). Piezo1 channels in vascular development and the sensing of shear stress. *Curr. Top. Membr.* 79, 37–57. doi:10.1016/bbs.ctm.2016.11.001
- James, N. L., Harrison, D. G., and Nerem, R. M. (1995). Effects of shear on endothelial cell calcium in the presence and absence of ATP. *FASEB J.* 9, 968–973. doi:10.1096/fasebj.9.10.7615166
- Jang, K. J., Otieno, M. A., Ronxhi, J., Lim, H. K., Ewart, L., Kodella, K. R., et al. (2019). Reproducing human and cross-species drug toxicities using a Liver-Chip. *Sci. Transl. Med.* 11, eaax5516. doi:10.1126/scitranslmed.aax5516
- Jeon, J. S., Bersini, S., Gilardi, M., Dubini, G., Charest, J. L., Moretti, M., et al. (2015). Human 3D vascularized organotypic microfluidic assays to study breast cancer cell extravasation. *Proc. Natl. Acad. Sci. U. S. A.* 112, 214–219. doi:10.1073/pnas.1417115112
- Jia, W., Gungor-Ozkerim, P. S., Zhang, Y. S., Yue, K., Zhu, K., Liu, W., et al. (2016). Direct 3D bioprinting of perfusable vascular constructs using a blend bioink. *Biomaterials* 106, 58–68. doi:10.1016/j.biomaterials.2016.07.038
- Jin, Y., Muhl, L., Burmakin, M., Wang, Y., Duchez, A. C., Betsholtz, C., et al. (2017). Endoglin prevents vascular malformation by regulating flow-induced cell migration and specification through VEGFR2 signalling. *Nat. Cell Biol.* 19, 639–652. doi:10.1038/ncb3534
- Kalucka, J., de Rooij, L., Goveia, J., Rohlenova, K., Dumas, S. J., Meta, E., et al. (2020). Single-cell transcriptome atlas of murine endothelial cells. *Cell* 180, 764–779. doi:10.1016/j.cell.2020.01.015
- Khankin, E. V., Ko, N. L., Mandala, M., Karumanchi, S. A., and Osol, G. (2021). Normalization of wall shear stress as a physiological mechanism for regulating maternal uterine artery expansive remodeling during pregnancy. *FASEB Bioadv.* 3, 702–708. doi:10.1096/fba.2021-00019
- Kim, S., Chung, M., Ahn, J., Lee, S., and Jeon, N. L. (2016). Interstitial flow regulates the angiogenic response and phenotype of endothelial cells in a 3D culture model. *Lab. Chip* 16, 4189–4199. doi:10.1039/c6lc00910g
- Kim, S., Lee, H., Chung, M., and Jeon, N. L. (2013). Engineering of functional, perfusable 3D microvascular networks on a chip. *Lab. Chip* 13, 1489–1500. doi:10.1039/c3lc41320a
- Kolesky, D. B., Truby, R. L., Gladman, A. S., Busbee, T. A., Homan, K. A., and Lewis, J. A. (2014). 3D bioprinting of vascularized, heterogeneous cell-laden tissue constructs. *Adv. Mater.* 26, 3124–3130. doi:10.1002/adma.201305506
- Koutsiaris, A. G., Tachmitzi, S. V., Batis, N., Kotoula, M. G., Karabatsas, C. H., Tsironi, E., et al. (2007). Volume flow and wall shear stress quantification in the human conjunctival capillaries and post-capillary venules *in vivo*. *Biorheology* 44, 375–386.
- Kpeli, G. W., Conrad, K. M., Bralower, W., Byrne, C. E., Boue, S. M., Burow, M. E., et al. (2024). Xenohormetic phytochemicals inhibit neovascularization in microphysiological models of vasculogenesis and tumor angiogenesis. *Adv. Biol. (Weinh)* 8, e2300480. doi:10.1002/adbi.202300480
- Krishnan, L., Underwood, C. J., Maas, S., Ellis, B. J., Kode, T. C., Hoving, J. B., et al. (2008). Effect of mechanical boundary conditions on orientation of angiogenic microvessels. *Cardiovasc. Res.* 78, 324–332. doi:10.1093/cvr/cvn055
- Kusuma, S., Shen, Y. I., Hanjaya-Putra, D., Mali, P., Cheng, L., and Gerech, S. (2013). Self-organized vascular networks from human pluripotent stem cells in a synthetic matrix. *Proc. Natl. Acad. Sci. U. S. A.* 110, 12601–12606. doi:10.1073/pnas.1306562110
- Lam, S. F., Shirure, V. S., Chu, Y. E., Soetikno, A. G., and George, S. C. (2018). Microfluidic device to attain high spatial and temporal control of oxygen. *PLOS ONE* 13, e0209574. doi:10.1371/journal.pone.0209574
- Langer, K., and Joensson, H. N. (2020). Rapid production and recovery of cell spheroids by automated droplet microfluidics. *SLAS Technol.* 25, 111–122. doi:10.1177/2472630319877376
- Langer, V., Vivi, E., Regensburger, D., Winkler, T. H., Waldner, M. J., Rath, T., et al. (2019). IFN- γ drives inflammatory bowel disease pathogenesis through VE-cadherin-directed vascular barrier disruption. *J. Clin. Invest.* 129, 4691–4707. doi:10.1172/JCI124884
- Langille, B. L., Reidy, M. A., and Kline, R. L. (1986). Injury and repair of endothelium at sites of flow disturbances near abdominal aortic coarctations in rabbits. *Arteriosclerosis* 6, 146–154. doi:10.1161/01.atv.6.2.146
- Larriee, B., Prahst, C., Gordon, E., del Toro, R., Mathivet, T., Duarte, A., et al. (2012). ALK1 signaling inhibits angiogenesis by cooperating with the Notch pathway. *Dev. Cell* 22, 489–500. doi:10.1016/j.devcel.2012.02.005
- Lee, V. K., Kim, D. Y., Ngo, H., Lee, Y., Seo, L., Yoo, S.-S., et al. (2014). Creating perfused functional vascular channels using 3D bio-printing technology. *Biomaterials* 35, 8092–8102. doi:10.1016/j.biomaterials.2014.05.083
- Linville, R. M., Boland, N. F., Covarrubias, G., Price, G. M., and Tien, J. (2016). Physical and chemical signals that promote vascularization of capillary-scale channels. *Cell. Mol. Bioeng.* 9, 73–84. doi:10.1007/s12195-016-0429-8
- Liu, M. C., Shih, H. C., Wu, J. G., Weng, T. W., Wu, C. Y., Lu, J. C., et al. (2013). Electrofluidic pressure sensor embedded microfluidic device: a study of endothelial cells under hydrostatic pressure and shear stress combinations. *Lab. Chip* 13, 1743–1753. doi:10.1039/c3lc41414k
- Liu, Z., Ruter, D. L., Quigley, K., Tanke, N. T., Jiang, Y., and Bautch, V. L. (2021). Single-cell RNA sequencing reveals endothelial cell transcriptome heterogeneity under homeostatic laminar flow. *Arterioscler. Thromb. Vasc. Biol.* 41, 2575–2584. doi:10.1161/ATVBAHA.121.316797
- Lucitti, J. L., Jones, E. A., Huang, C., Chen, J., Fraser, S. E., and Dickinson, M. E. (2007). Vascular remodeling of the mouse yolk sac requires hemodynamic force. *Development* 134, 3317–3326. doi:10.1242/dev.02883
- Luu, V. Z., Chowdhury, B., Al-Omran, M., Hess, D. A., and Verma, S. (2018). Role of endothelial primary cilia as fluid mechanosensors on vascular health. *Atherosclerosis* 275, 196–204. doi:10.1016/j.atherosclerosis.2018.06.818
- Mack, J. J., Mosquero, T. S., Archer, B. J., Jones, W. M., Sunshine, H., Faas, G. C., et al. (2017). NOTCH1 is a mechanosensor in adult arteries. *Nat. Commun.* 8, 1620. doi:10.1038/s41467-017-01741-8
- Mammoto, T., Hunyenyiwa, T., Kyi, P., Hendee, K., Matus, K., Rao, S., et al. (2022). Hydrostatic pressure controls angiogenesis through endothelial YAP1 during lung regeneration. *Front. Bioeng. Biotechnol.* 10, 823642. doi:10.3389/fbioe.2022.823642
- Marx, U., Andersson, T. B., Bahinski, A., Beilmann, M., Beken, S., Cassee, F. R., et al. (2016). Biology-inspired microphysiological system approaches to solve the prediction dilemma of substance testing. *ALTEX* 33, 272–321. doi:10.14573/altex.1603161
- Mendez, P. L., Obendorf, L., Jatzlau, J., Burdzinski, W., Reichenbach, M., Nageswaran, V., et al. (2022). Atheroprone fluid shear stress-regulated ALK1-Endoglin-SMAD signaling originates from early endosomes. *BMC Biol.* 20, 210. doi:10.1186/s12915-022-01396-y
- Miao, H., Hu, Y. L., Shiu, Y. T., Yuan, S., Zhao, Y., Kaunas, R., et al. (2005). Effects of flow patterns on the localization and expression of VE-cadherin at vascular endothelial cell junctions: *in vivo* and *in vitro* investigations. *J. Vasc. Res.* 42, 77–89. doi:10.1159/000083094
- Miller, J. S., Stevens, K. R., Yang, M. T., Baker, B. M., Nguyen, D.-H. T., Cohen, D. M., et al. (2012). Rapid casting of patterned vascular networks for perfusable engineered three-dimensional tissues. *Nat. Mater.* 11, 768–774. doi:10.1038/nmat3357
- Mohammed, M., Thurgood, P., Gilliam, C., Nguyen, N., Pirogova, E., Peter, K., et al. (2019). Studying the response of aortic endothelial cells under pulsatile flow using a

compact microfluidic system. *Anal. Chem.* 91, 12077–12084. doi:10.1021/acs.analchem.9b03247

Mondrinos, M. J., Jones, P. L., Finck, C. M., and Lelkes, P. I. (2014). Engineering *de novo* assembly of fetal pulmonary organoids. *Tissue Eng. Part A* 20, 2892–2907. doi:10.1089/ten.TEA.2014.0085

Moon, J. J., Hahn, M. S., Kim, I., Nsiah, B. A., and West, J. L. (2009). Micropatterning of poly(ethylene glycol) diacrylate hydrogels with biomolecules to regulate and guide endothelial morphogenesis. *Tissue Eng. Part A* 15, 579–585. doi:10.1089/ten.tea.2008.0196

Muller-Marschhausen, K., Waschke, J., and Drenckhahn, D. (2008). Physiological hydrostatic pressure protects endothelial monolayer integrity. *Am. J. Physiol. Cell Physiol.* 294, C324–C332. doi:10.1152/ajpcell.00319.2007

Nakatsu, M. N., and Hughes, C. C. (2008). An optimized three-dimensional *in vitro* model for the analysis of angiogenesis. *Methods Enzymol.* 443, 65–82. doi:10.1016/S0076-6879(08)02004-1

Nakatsu, M. N., Sainson, R. C. A., Aoto, J. N., Taylor, K. L., Aitkenhead, M., Pérez-del-Pulgar, S., et al. (2003). Angiogenic sprouting and capillary lumen formation modeled by human umbilical vein endothelial cells (HUVEC) in fibrin gels: the role of fibroblasts and Angiopoietin-1. *Microvasc. Res.* 66, 102–112. doi:10.1016/s0026-2862(03)00045-1

Newman, A. C., Nakatsu, M. N., Chou, W., Gershon, P. D., and Hughes, C. C. (2011). The requirement for fibroblasts in angiogenesis: fibroblast-derived matrix proteins are essential for endothelial cell lumen formation. *Mol. Biol. Cell* 22, 3791–3800. doi:10.1091/mbc.E11-05-0393

Norotte, C., Marga, F. S., Niklason, L. E., and Forgacs, G. (2009). Scaffold-free vascular tissue engineering using bioprinting. *Biomaterials* 30, 5910–5917. doi:10.1016/j.biomaterials.2009.06.034

O'Grady, B. J., Wang, J. X., Faley, S. L., Balikov, D. A., Lippmann, E. S., Bellan, L. M., et al. (2018). A customizable, low-cost perfusion system for sustaining tissue constructs. *SLAS Technol.* 23, 592–598. doi:10.1177/2472630318775059

Orellano, I., Thomas, A., Herrera, A., Brauer, E., Wulsten, D., Petersen, A., et al. (2022). Engineering vascular self-assembly by controlled 3D-printed cell placement. *Adv. Funct. Mater.* 32, 2208325. doi:10.1002/adfm.202208325

Ozer, L. Y., Fayed, H. S., Ericsson, J., and Al Haj Zen, A. (2023). Development of a cancer metastasis-on-chip assay for high throughput drug screening. *Front. Oncol.* 13, 1269376. doi:10.3389/fonc.2023.1269376

Papaioannou, T. G., and Stefanadis, C. (2005). Vascular wall shear stress: basic principles and methods. *Hell. J. Cardiol.* 46, 9–15.

Park, T. E., Mustafaoglu, N., Herland, A., Hasselkus, R., Mannix, R., FitzGerald, E. A., et al. (2019). Hypoxia-enhanced Blood-Brain Barrier Chip recapitulates human barrier function and shuttling of drugs and antibodies. *Nat. Commun.* 10, 2621. doi:10.1038/s41467-019-10588-0

Pech, S., Richter, R., and Lienig, J. (2020). "Peristaltic pump with continuous flow and programmable flow pulsation," in 2020 IEEE 8th electronics system-integration technology conference, ESTC, Norway, 15-18 September 2020 (IEEE) 1–5.

Phan, D. T., Bender, R. H. F., Andrejczek, J. W., Sobrino, A., Hachey, S. J., George, S. C., et al. (2017). Blood-brain barrier-on-a-chip: microphysiological systems that capture the complexity of the blood-central nervous system interface. *Exp. Biol. Med.* (Maywood) 242, 1669–1678. doi:10.1177/1535370217694100

Pitts, K. L., and Fenech, M. (2013). Micro-particle image velocimetry for velocity profile measurements of micro blood flows. *J. Vis. Exp.* 10, e50314. doi:10.3791/50314

Poceviciute, R., and Ismagilov, R. F. (2019). Human-gut-microbiome on a chip. *Nat. Biomed. Eng.* 3, 500–501. doi:10.1038/s41551-019-0425-0

Polacheck, W. J., Kutys, M. L., Tefft, J. B., and Chen, C. S. (2019). Microfabricated blood vessels for modeling the vascular transport barrier. *Nat. Protoc.* 14, 1425–1454. doi:10.1038/s41596-019-0144-8

Polacheck, W. J., Kutys, M. L., Yang, J., Eyckmans, J., Wu, Y., Vasavada, H., et al. (2017). A non-canonical Notch complex regulates adherens junctions and vascular barrier function. *Nature* 552, 258–262. doi:10.1038/nature24998

Price, G. M., Chrobak, K. M., and Tien, J. (2008). Effect of cyclic AMP on barrier function of human lymphatic microvascular tubes. *Microvasc. Res.* 76, 46–51. doi:10.1016/j.mvr.2008.02.003

Prystopiuk, V., Fels, B., Simon, C. S., Liashkovich, I., Pasrednik, D., Kronlage, C., et al. (2018). A two-phase response of endothelial cells to hydrostatic pressure. *J. Cell Sci.* 131, jcs206920. doi:10.1242/jcs.206920

Reneman, R. S., and Hoeks, A. P. (2008). Wall shear stress as measured *in vivo*: consequences for the design of the arterial system. *Med. Biol. Eng. Comput.* 46, 499–507. doi:10.1007/s11517-008-0330-2

Rosenfeld, D., Landau, S., Shandalov, Y., Raindel, N., Freiman, A., Shor, E., et al. (2016). Morphogenesis of 3D vascular networks is regulated by tensile forces. *PNAS* 113, 3215–3220. doi:10.1073/pnas.1522273113

Sadr, N., Zhu, M., Osaki, T., Kakegawa, T., Yang, Y., Moretti, M., et al. (2011). SAM-based cell transfer to photopatterned hydrogels for microengineering vascular-like structures. *Biomaterials* 32, 7479–7490. doi:10.1016/j.biomaterials.2011.06.034

Sahni, J., Arshad, M., Schake, M. A., Brooks, J. R., Yang, R., Weinberg, P. D., et al. (2023). Characterizing nuclear morphology and expression of eNOS in vascular endothelial cells subjected to a continuous range of wall shear stress magnitudes and directionality. *J. Mech. Behav. Biomed. Mater.* 137, 105545. doi:10.1016/j.jmbbm.2022.105545

Saqr, K. M., Tupin, S., Rashad, S., Endo, T., Niizuma, K., Tominaga, T., et al. (2020). Physiologic blood flow is turbulent. *Sci. Rep.* 10, 15492. doi:10.1038/s41598-020-72309-8

Schneider, S., Bubeck, M., Rogal, J., Weener, H. J., Rojas, C., Weiss, M., et al. (2021). Peristaltic on-chip pump for tunable media circulation and whole blood perfusion in PDMS-free organ-on-chip and Organ-Disc systems. *Lab. Chip* 21, 3963–3978. doi:10.1039/d1lc00494h

Schwartz, E. A., Bizios, R., Medow, M. S., and Gerritsen, M. E. (1999). Exposure of human vascular endothelial cells to sustained hydrostatic pressure stimulates proliferation. Involvement of the αV integrins. *Circ. Res.* 84, 315–322. doi:10.1161/01.res.84.3.315

Sedlak, J., and Clyne, A. (2023). Application of shear stress to endothelial cells using a parallel plate flow chamber. *Methods Mol. Biol.* 2600, 81–90. doi:10.1007/978-1-0716-2851-5_5

Seok, J., Warren, H. S., Cuenca, A. G., Mindrinos, M. N., Baker, H. V., Xu, W., et al. (2013). Genomic responses in mouse models poorly mimic human inflammatory diseases. *Proc. Natl. Acad. Sci. U. S. A.* 110, 3507–3512. doi:10.1073/pnas.1222878110

Seto, Y., Inaba, R., Okuyama, T., Sassa, F., Suzuki, H., and Fukuda, J. (2010). Engineering of capillary-like structures in tissue constructs by electrochemical detachment of cells. *Biomaterials* 31, 2209–2215. doi:10.1016/j.biomaterials.2009.11.104

Shevkoplyas, S. S., Gifford, S. C., Yoshida, T., and Bitensky, M. W. (2003). Prototype of an *in vitro* model of the microcirculation. *Microvasc. Res.* 65, 132–136. doi:10.1016/s0026-2862(02)00034-1

Si, L., Bai, H., Rodas, M., Cao, W., Oh, C. Y., Jiang, A., et al. (2021). A human-airway-on-a-chip for the rapid identification of candidate antiviral therapeutics and prophylactics. *Nat. Biomed. Eng.* 5, 815–829. doi:10.1038/s41551-021-00718-9

Sobrino, A., Phan, D. T., Datta, R., Wang, X., Hachey, S. J., Romero-Lopez, M., et al. (2016). 3D microtumors *in vitro* supported by perfused vascular networks. *Sci. Rep.* 6, 31589. doi:10.1038/srep31589

Suo, J., Ferrara, D. E., Sorescu, D., Guldborg, R. E., Taylor, W. R., and Giddens, D. P. (2007). Hemodynamic shear stresses in mouse aortas: implications for atherogenesis. *Arterioscler. Thromb. Vasc. Biol.* 27, 346–351. doi:10.1161/01.ATV.0000253492.45717.46

Torisawa, Y. S., Spina, C. S., Mammoto, T., Mammoto, A., Weaver, J. C., Tat, T., et al. (2014). Bone marrow-on-a-chip replicates hematopoietic niche physiology *in vitro*. *Nat. Methods* 11, 663–669. doi:10.1038/nmeth.2938

Tzima, E., Irani-Tehrani, M., Kiesses, W. B., Dejana, E., Schultz, D. A., Engelhardt, B., et al. (2005). A mechanosensory complex that mediates the endothelial cell response to fluid shear stress. *Nature* 437, 426–431. doi:10.1038/nature03952

van Os, L., Yeoh, J., Witz, G., Ferrari, D., Krebs, P., Chandorkar, Y., et al. (2023). Immune cell extravasation in an organ-on-chip to model lung inflammation. *Eur. J. Pharm. Sci.* 187, 106485. doi:10.1016/j.ejps.2023.106485

Vatine, G. D., Barrille, R., Workman, M. J., Sances, S., Barriga, B. K., Rahnama, M., et al. (2019). Human iPSC-derived blood-brain barrier chips enable disease modeling and personalized medicine applications. *Cell Stem Cell* 24, 995–1005. doi:10.1016/j.stem.2019.05.011

Viravaidya, K., and Shuler, M. L. (2004). Incorporation of 3T3-L1 cells to mimic bioaccumulation in a microscale cell culture analog device for toxicity studies. *Biotechnol. Prog.* 20, 590–597. doi:10.1021/bp034238d

Viravaidya, K., Sin, A., and Shuler, M. L. (2004). Development of a microscale cell culture analog to probe naphthalene toxicity. *Biotechnol. Prog.* 20, 316–323. doi:10.1021/bp0341996

Vogt, N. (2022). Modeling multi-organ systems on a chip. *Nat. Methods* 19, 641. doi:10.1038/s41592-022-01533-z

Voyvodic, P. L., Min, D., and Baker, A. B. (2012). A multichannel dampened flow system for studies on shear stress-mediated mechanotransduction. *Lab. Chip* 12, 3322–3330. doi:10.1039/c2lc40526a

Wang, X., Phan, D. T., Sobrino, A., George, S. C., Hughes, C. C., and Lee, A. P. (2016). Engineering anastomosis between living capillary networks and endothelial cell-lined microfluidic channels. *Lab. Chip* 16, 282–290. doi:10.1039/c5lc01050k

Wang, X.-Y., Jin, Z.-H., Gan, B.-W., Lv, S.-W., Xie, M., and Huang, W.-H. (2014). Engineering interconnected 3D vascular networks in hydrogels using molded sodium alginate lattice as the sacrificial template. *Lab. Chip* 14, 2709–2716. doi:10.1039/c4lc00069b

Wang, Y. I., and Shuler, M. L. (2018). UniChip enables long-term recirculating unidirectional perfusion with gravity-driven flow for microphysiological systems. *Lab. Chip* 18, 2563–2574. doi:10.1039/c8lc00394g

Whisler, J. A., Chen, M. B., and Kamm, R. D. (2014). Control of perfusable microvascular network morphology using a multiculture microfluidic system. *Tissue Eng. - Part C. Methods* 20, 543–552. doi:10.1089/ten.TEC.2013.0370

- Wimmer, R. A., Leopoldi, A., Aichinger, M., Wick, N., Hantusch, B., Novatchkova, M., et al. (2019). Human blood vessel organoids as a model of diabetic vasculopathy. *Nature* 565, 505–510. doi:10.1038/s41586-018-0858-8
- Wong, K. H., Truslow, J. G., and Tien, J. (2010). The role of cyclic AMP in normalizing the function of engineered human blood microvessels in microfluidic collagen gels. *Biomaterials* 31, 4706–4714. doi:10.1016/j.biomaterials.2010.02.041
- Xiao, S., Coppeta, J. R., Rogers, H. B., Isenberg, B. C., Zhu, J., Olalekan, S. A., et al. (2017). A microfluidic culture model of the human reproductive tract and 28-day menstrual cycle. *Nat. Commun.* 8, 14584. doi:10.1038/ncomms14584
- Yang, F., Zhang, Y., Zhu, J., Wang, J., Jiang, Z., Zhao, C., et al. (2020). Laminar flow protects vascular endothelial tight junctions and barrier function via maintaining the expression of long non-coding RNA MALAT1. *Front. Bioeng. Biotechnol.* 8, 647. doi:10.3389/fbioe.2020.00647
- Yoshino, D., Funamoto, K., Sato Kenry, K., Sato, M., and Lim, C. T. (2020). Hydrostatic pressure promotes endothelial tube formation through aquaporin 1 and Ras-ERK signaling. *Commun. Biol.* 3, 152. doi:10.1038/s42003-020-0881-9
- Zervantonakis, I. K., Hughes-Alford, S. K., Charest, J. L., Condeelis, J. S., Gertler, F. B., and Kamm, R. D. (2012). Three-dimensional microfluidic model for tumor cell intravasation and endothelial barrier function. *Proc. Natl. Acad. Sci. U. S. A.* 109, 13515–13520. doi:10.1073/pnas.1210182109
- Zhang, B., and Radisic, M. (2017). Organ-on-a-chip devices advance to market. *Lab. Chip* 17, 2395–2420. doi:10.1039/c6lc01554a
- Zhang, G., Cao, G., Gu, C., Fu, Y., Jin, G., Tang, L., et al. (2022). Regulation of vascular branch formation in 3D bioprinted tissues using confining force. *Appl. Mater. Today* 26, 101240. doi:10.1016/j.apmt.2021.101240
- Zhang, G., Varkey, M., Wang, Z., Xie, B., Hou, R., and Atala, A. (2020a). ECM concentration and cell-mediated traction forces play a role in vascular network assembly in 3D bioprinted tissue. *Biotechnol. Bioeng.* 117, 1148–1158. doi:10.1002/bit.27250
- Zhang, G., Wang, Z., Han, F., Jin, G., Xu, L., Xu, H., et al. (2021). Mechano-regulation of vascular network formation without branches in 3D bioprinted cell-laden hydrogel constructs. *Biotechnol. Bioeng.* 118, 3787–3798. doi:10.1002/bit.27854
- Zhang, X., Bishawi, M., Zhang, G., Prasad, V., Salmon, E., Breithaupt, J. J., et al. (2020b). Modeling early stage atherosclerosis in a primary human vascular microphysiological system. *Nat. Commun.* 11, 5426. doi:10.1038/s41467-020-19197-8
- Zheng, Y., Chen, J., Craven, M., Choi, N. W., Totorica, S., Diaz-Santana, A., et al. (2012). *In vitro* microvessels for the study of angiogenesis and thrombosis. *PNAS* 109, 9342–9347. doi:10.1073/pnas.1201240109
- Zhou, M., Yu, Y., Chen, R., Liu, X., Hu, Y., Ma, Z., et al. (2023). Wall shear stress and its role in atherosclerosis. *Front. Cardiovasc. Med.* 10, 1083547. doi:10.3389/fcvm.2023.1083547



OPEN ACCESS

EDITED BY

Julia J. Mack,
UCLA Health System, United States

REVIEWED BY

Federica Piani,
University of Bologna, Italy
Gulnaz Begum,
University of Pittsburgh, United States

*CORRESPONDENCE

Volodymyr I. Lushchak,
✉ volodymyr.lushchak@pnu.edu.ua

RECEIVED 04 June 2024

ACCEPTED 23 July 2024

PUBLISHED 05 August 2024

CITATION

Dmytriv TR, Duve KV, Storey KB and Lushchak VI (2024), Vicious cycle of oxidative stress and neuroinflammation in pathophysiology of chronic vascular encephalopathy. *Front. Physiol.* 15:1443604. doi: 10.3389/fphys.2024.1443604

COPYRIGHT

© 2024 Dmytriv, Duve, Storey and Lushchak. This is an open-access article distributed under the terms of the [Creative Commons Attribution License \(CC BY\)](#). The use, distribution or reproduction in other forums is permitted, provided the original author(s) and the copyright owner(s) are credited and that the original publication in this journal is cited, in accordance with accepted academic practice. No use, distribution or reproduction is permitted which does not comply with these terms.

Vicious cycle of oxidative stress and neuroinflammation in pathophysiology of chronic vascular encephalopathy

Tetiana R. Dmytriv ^{1,2}, Khrystyna V. Duve ³,
Kenneth B. Storey ² and Volodymyr I. Lushchak ^{1,2*}

¹Department of Biochemistry and Biotechnology, Vasyl Stefanyk Precarpathian National University, Ivano-Frankivsk, Ukraine, ²Research and Development University, Ivano-Frankivsk, Ukraine,

³Department of Neurology, I. Horbachevsky Ternopil National Medical University, Ternopil, Ukraine

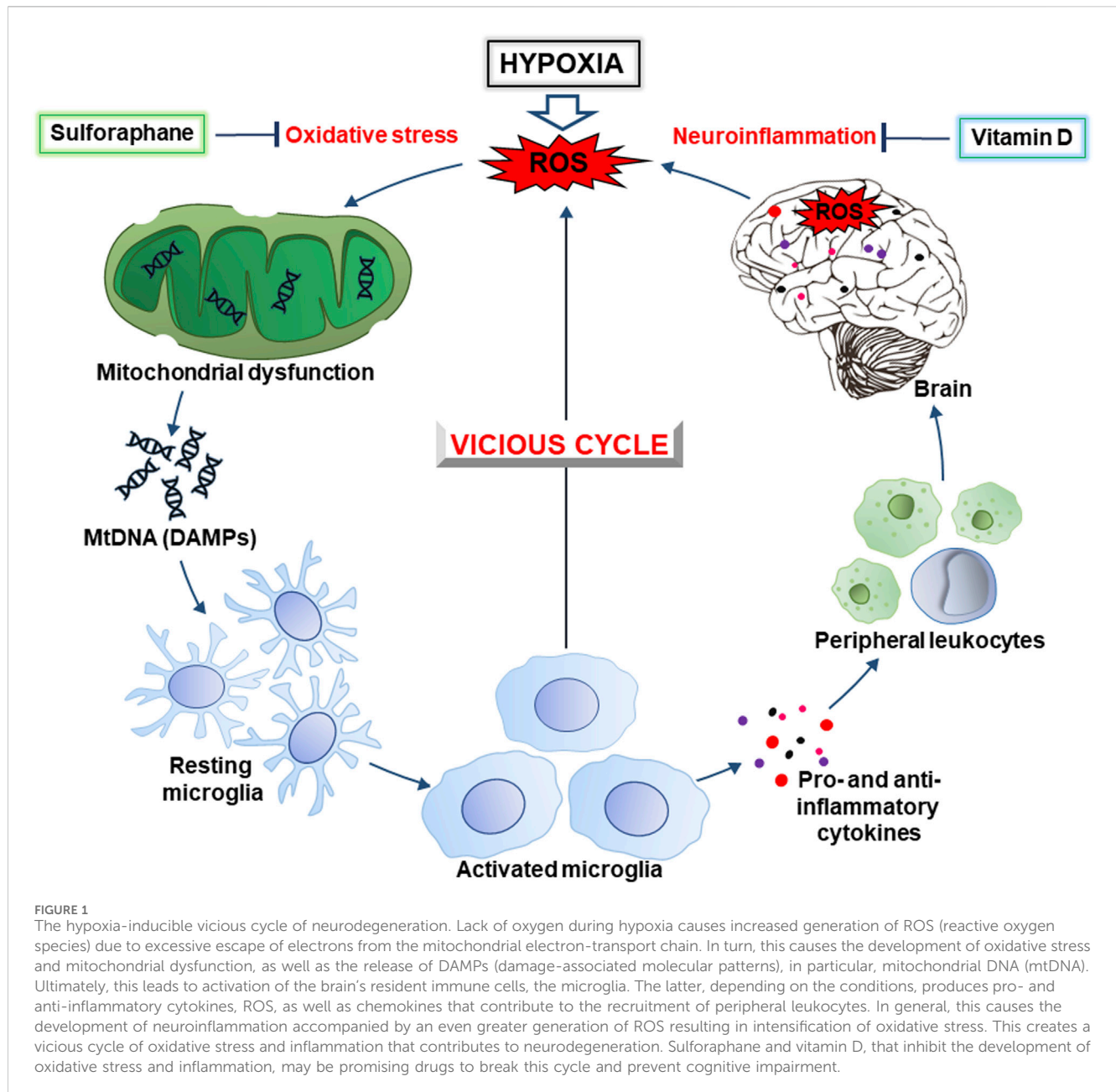
Chronic vascular encephalopathy (CVE) is a frequent cause of vascular mild cognitive impairment and dementia, which significantly worsens the quality of life, especially in the elderly population. CVE is a result of chronic cerebral hypoperfusion, characterized by prolonged limited blood flow to the brain. This causes insufficient oxygenation of the brain leading to hypoxia. The latter can trigger a series of events associated with the development of oxidative/reductive stresses and neuroinflammation. Addressing the gap in knowledge regarding oxidative and reductive stresses in the development of vascular disorders and neuroinflammation can give a start to new directions of research in the context of CVE. In this review, we consider the hypoxia-induced molecular challenges involved in the pathophysiology of CVE, focusing on oxidative stress and neuroinflammation, which are combined in a vicious cycle of neurodegeneration. We also briefly describe therapeutic approaches to the treatment of CVE and outline the prospects for the use of sulforaphane, an isothiocyanate common in cruciferous plants, and vitamin D to break the vicious cycle and alleviate the cognitive impairments characteristic of patients with CVE.

KEYWORDS

ROS, DAMPs, microglia, NF- κ B, inflammasome, vicious cycle

1 Introduction

Scientific data suggests that more than 16% of individuals over the age of 60 suffer from moderate to severe cognitive disorders caused by cerebrovascular diseases (Owolabi et al., 2018). In particular, vascular encephalopathy is increasingly recognized as the cause of such symptoms as inappropriate behavior, decreased motivation, memory defects, coordination problems, and others. These brain disorders are associated with a violation of brain blood supply leading to the development of cerebral hypoperfusion, hypoxia, ischemia, and reoxygenation, with functional consequences for the brain. Long-term chronic low perfusion in the whole brain or local brain regions causes chronic vascular encephalopathy (CVE). Depending on the severity of the impairment, this is divided into mild vascular cognitive impairment and vascular dementia (Jellinger, 2013). The causes of these problems are varied and complex, making the pathogenetic mechanisms underlying the disease controversial. Dysregulation of cerebral blood flow, resulting in inadequate



blood supply to the brain is one common factor among all of these causes (Yu et al., 2022). As a result, the impaired blood supply to the brain disrupts memory, cognition, and behavior, affecting neural networks and their functionality (Jellinger, 2013).

Inflammation and oxidative stress are among the key factors in the pathophysiology of vascular cognitive impairment and dementia. Brain hypoxia and ischemia, caused by chronic cerebral hypoperfusion in CVE, are fundamental factors that induce a series of pathological processes, including induction of oxidative stress and activation of the resident immune cells in the brain. In turn, this contributes to the development of neuroinflammation to maintain the stability of the microenvironment. However, excessive activation of the inflammatory response can cause significant damage to the brain by reactive oxygen species (ROS) due to their enhanced generation

and contribute in this way to neurological dysfunction (Tian et al., 2022). Neuroinflammation is usually tightly connected with the development of oxidative stress. This results from an imbalance between ROS generation and elimination in favor of the first with various physiological consequences (Lushchak and Storey, 2021). ROS cause numerous oxidative modifications of biomolecules, including oxidation of proteins, lipids and DNA, that eventually lead to apoptotic death, contributing to the progression of cognitive impairment (Poh et al., 2022; Butterfield, 2023; Dmytriv et al., 2023).

Various substances of natural origin can potentially be used for the prevention and relief of neuroinflammation and oxidative stress in CVE. For example, sulforaphane, an isothiocyanate from cruciferous vegetables, is a promising neuroprotectant that prevents and alleviates the symptoms of many neurological disorders (Klomprens and Ding, 2019). In addition, vitamin D

may also be promising in this direction. In particular, vitamin D receptor signaling in microglia inhibits neuroinflammation (Cui et al., 2023). Understanding the molecular mechanisms of the above-mentioned pathological processes will provide a valuable theoretical basis for the prevention and treatment of CVE. This review aims to shed light on oxidative and reductive stresses induced by hypoxia and reoxygenation and the development of neuroinflammation in CVE. In particular, we combine oxidative stress and neuroinflammation into a vicious cycle of neurodegeneration (Figure 1) that may underlie the pathophysiology of CVE and outline the potential of using sulforaphane and vitamin D to break this vicious cycle.

2 Hypoxia-inducible challenges in chronic vascular encephalopathy: focusing on oxidative stress

Hypoxia is one of the most important features of CVE and is much more dangerous when combined with reoxygenation (the so-called “oxygen paradox”). There are several mechanisms for developing hypoxia and related vascular dysfunctions and compromised oxygen delivery to the brain (Dhillon et al., 2022). Below we list some of the key ways in which hypoxia can be developed in the context of CVE:

1. Vascular insufficiency caused by chronic vascular changes, such as stenosis (narrowing) or occlusion of blood vessels supplying the brain, which can lead to reduced blood flow and oxygen delivery (cerebral hypoperfusion).
2. Systemic dysfunction of endothelial cells lining blood vessels. Endothelial cells perform several important functions: (i) regulation of vascular tone, (ii) control of blood flow and clotting, and (iii) production of cytokines and adhesion molecules that regulate and direct the inflammatory process. Under homeostatic conditions, the endothelium maintains normal vascular tone and blood flow, and pro-inflammatory factors are practically absent. However, numerous risk factors such as hyperglycemia, hypercholesterolemia, hypertension, smoking, obesity, and others can initiate a chronic inflammatory process, that is accompanied by a loss of vasodilator and antithrombotic factors and an increase in vasoconstrictors and prothrombotic products, contributing to cardiovascular diseases (Widlansky et al., 2003). The presence of risk factors for cardiovascular diseases with subsequent damage to cerebral vessels is associated with an increased risk of developing cognitive impairment in elderly patients, and increased levels of markers of endothelial damage are associated with an increased risk of developing vascular dementia (Quinn et al., 2011; Sabayan et al., 2014). The latter emphasizes the importance of endothelial dysfunction in the pathophysiology of CVE.
3. Microvascular disease related to damage of small vessels, capillaries, and arterioles in the brain. These disrupt the microcirculation of blood in the brain.
4. Ischemic events such as transient ischemic attacks or small ischemic strokes may temporarily or permanently disrupt blood flow to specific brain regions.
5. Chronic inflammation may cause vascular dysfunction and hypoxia. This impairs blood vessel function, compromises the blood-brain barrier (BBB), and exacerbates vascular pathology.
6. BBB disruption that may also compromise the entry of substances, including inflammatory cells and molecules, into the brain, that can cause vascular dysfunction.
7. Mitochondrial dysfunction leading to impaired cellular energy production and the development of oxidative stress contributing to vascular damage.
8. Increased production of reactive oxygen species (ROS), for example, by xanthine oxidase (XO), may lead to vascular dysfunction. XO, together with xanthine dehydrogenase (XDH), are interconverting isoforms of the same enzyme known as xanthine oxidoreductase (XOR). XDH catalyzes the conversion of xanthine and hypoxanthine into uric acid producing NADH, whereas XO catalyzes the same reaction producing ROS such as superoxide anions and hydrogen peroxide as byproducts (Houston et al., 1999; Burrage et al., 2023). In addition, XO secondarily leads to peroxynitrite formation, a highly reactive compound produced by the reaction of nitric oxide and superoxide radicals, that is considered to be a marker of oxidative and nitrosative stresses. Under physiological conditions, XOR is mainly found in the dehydrogenase form, whereas in inflammatory situations XOR is usually found as XO (Sabán-Ruiz et al., 2013). The latter has a high affinity for glycosaminoglycans on the vascular endothelium, where its immobilization induces endothelial dysfunction via ROS production (Houston et al., 1999; Burrage et al., 2023), that can potentially lead to hypoxia.

Overall, the development of hypoxia in CVE involves a combination of vascular, inflammatory, and metabolic abnormalities disrupting oxygen delivery and its utilization by the brain, contributing to neuronal dysfunction and cognitive impairment. Short-term hypoxia is called acute hypoxia, whereas prolonged oxygen limitation is called chronic hypoxia (Figure 2). As mentioned above, a hypoxic period may be changed to normoxia by restoration of blood flow that can result from the opening of occluded or narrowed vessels. This leads to reoxygenation and also frequently results in damage to vessel walls. This is due to enhanced ROS generation and the whole complex of events with damaging consequences has been called “oxygen paradox”. Now we will consider molecular events induced by hypoxia and reoxygenation that are related to brain damage due to ROS and induction of inflammation, termed neuroinflammation, since it occurs in the brain (Figure 2). Reduced oxygen levels under hypoxia not only lead to decreased production of ATP in mitochondria but also increase the levels of electrons in the electron transport chain of mitochondria. This state where the reductivity of intracellular space is increased has been called “reductive stress” (Lushchak, 2011). Excess “reductive force” or reducing substances (e.g., RedS) disrupts many cellular processes particularly due to the interaction of reducing equivalents with various cellular components (proteins, nucleic acids, etc.) leading to the production of so-called damage-associated molecular patterns (DAMPs).

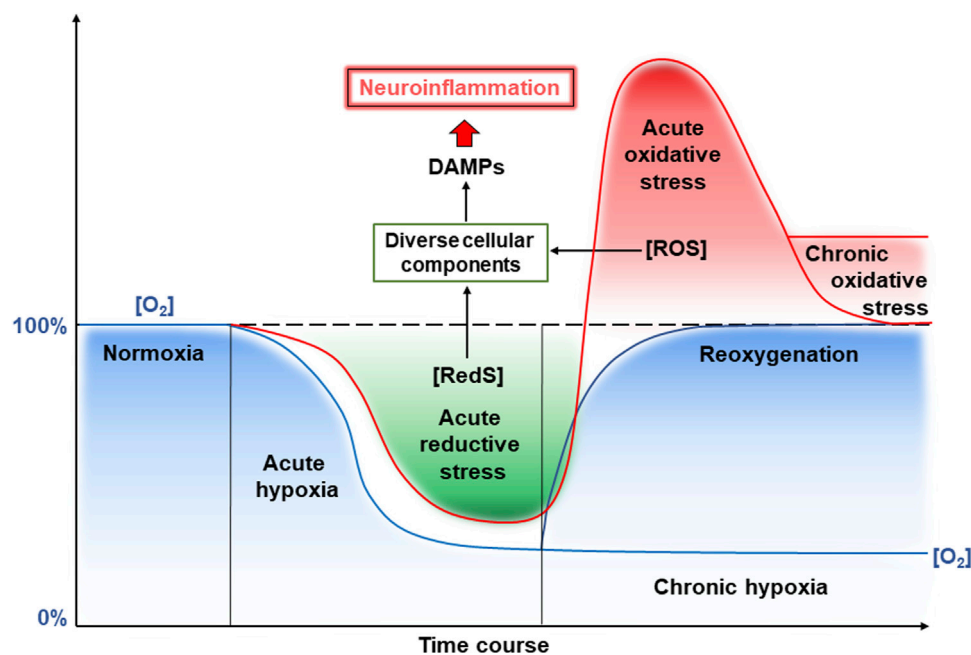


FIGURE 2
Reductive and oxidative stresses and neuroinflammation induced by hypoxia and reoxygenation. See a detailed description in the text.
Abbreviations: RedS – reductive substrates, ROS – reactive oxygen species.

Hypoxic conditions can also lead to mitochondrial dysfunction, with impaired operation of the electron transport chain (ETC) and ATP production. In certain cases, hypoxia-induced dysfunction can enhance the generation of ROS causing various forms of damage. These processes lead to the production of mitochondrial-derived DAMPs, mainly ROS-modified mitochondrial DNA (mtDNA) and mitochondrial proteins (Dmytriv et al., 2023). These DAMPs may be released from cells and trigger the production of proinflammatory cytokines, thereby contributing to oxidative stress. The latter is an imbalance between oxidants and antioxidants in living organisms in favor of OXIDANTS with certain changes in physiological processes (Lushchak, 2014). This imbalance can occur due to decreased oxygen availability (hypoxia), or impairing the function of oxygen-related antioxidant enzymes such as superoxide dismutase and catalase. Hence, reductive stress also can cause tissue damage and activate inflammatory pathways via the production of DAMPs. The stress induced by hypoxia is accompanied by damage that leads to the activation of proinflammatory pathways due to production of proinflammatory cytokines, chemokines, and other proinflammatory mediators. Again, the inflammatory processes may also contribute to the production of DAMPs from damaged cell constituents, amplifying reductive stress through activation of redox-sensitive signaling pathways. Collectively, these events form a vicious cycle of worsening hypoxia-induced damage (Figure 1).

Hypoxia can also induce endoplasmic reticulum stress due to the disruption of protein folding and leads to the accumulation of misfolded proteins (Díaz-Bulnes et al., 2020). The latter, together with heat shock proteins (HSPs) and high-mobility group box 1 (HMGB1) protein, may operate as DAMPs, contributing further to inflammation and reductive stress. If

hypoxia is prolonged or becomes more severe, this can result in cell death via apoptosis or necrosis. Released intracellular components and DAMPs further contribute to tissue damage via exacerbating inflammatory and reductive stress responses associated with hypoxia.

To this end, hypoxia-induced stress production of DAMPs may be enhanced due to activation of glycolysis and production of such side products as methylglyoxal (Garaschuk et al., 2018). However, this can worsen the situation due to the induction of reductive stress that can enhance CVE severity via provoking mitochondrial dysfunction, proinflammatory responses, endoplasmic reticulum stress, and cellular damage (Semchyshyn, 2021). Understanding these molecular mechanisms may be useful in developing targeted therapeutic strategies to mitigate the detrimental effects of hypoxia and oxidative/reductive stress in CVE.

Hypoxia-induced temporary partial or full closure of blood vessels may be crucially changed by opening the vascular lumen. However, the expected potential positive result is, in fact, the opposite, because this substantially enhances the generation of ROS and causes massive damage to tissues. Such an effect of reoxygenation has been called the “oxygen paradox” (Hearse et al., 1978). Generally, the oxygen paradox defines a phenomenon where reoxygenation (restoration of oxygen supply) following a period of hypoxia or ischemia can lead to a substantial increase of ROS generation and induction of oxidative stress leading to tissue damage (Lushchak, 2011). There are several reasons for such a “paradoxical response” that can occur under various conditions, such as during organ transplantation, or ischemia-reperfusion injury in the brain or other organs. Such processes is believed to contribute the most to damage to the brain at reoxygenation.

As mentioned above, under hypoxic conditions, a highly reduced state of the mitochondrial ETC can develop and is called reductive stress (Lushchak, 2011). During reoxygenation, “excessive electrons” escape the mitochondrial ETC and interact with molecular oxygen due to increased oxygen availability. This gives rise to a burst of ROS production. Furthermore, ROS such as superoxide anion radicals, hydrogen peroxide, and hydroxyl radicals, can attack cellular components causing oxidative damage to macromolecules including lipids, proteins, and DNA. These processes are augmented by the accompanied disruption of mitochondrial function related to ETC dysfunction, also resulting in increased ROS production within mitochondria. ROS migration out of the mitochondria will then contribute to cell damage. Hence, mitochondrial dysfunction further exacerbates oxidative stress and contributes to cell death pathways.

Both pathways described in the previous paragraph collectively trigger inflammatory responses, activating immune cells and the release of pro-inflammatory cytokines and chemokines. In the brain, under these conditions, microglia are activated (Dmytriv et al., 2023). Inflammation amplifies oxidative stress by promoting ROS generation and impairing antioxidant defenses and, together, they form a vicious cycle that worsens the situation (Figure 1).

Homeostasis of calcium is also substantially challenged during reoxygenation (Hearse et al., 1978). Induction of oxidative stress and inflammation can lead to intracellular calcium overload, disruption of calcium homeostasis, and activation of calcium-dependent enzymes, such as phospholipases and proteases (Mattson, 2007). Again, calcium overload may contribute to cell death pathways and oxidative stress and in some way be incorporated into the above-mentioned vicious cycles.

Reactive nitrogen species (RNS) are also important players in reoxygenation. Nitric oxide ($\bullet\text{NO}$) is very important for blood vessel operation because it causes vasodilation. During reoxygenation, $\bullet\text{NO}$ production can be enhanced and this can improve blood supply to the brain due to vasodilation (Li and Jackson, 2002). However, $\bullet\text{NO}$ is a free radical that can interact with many components in the brain. Moreover, at high levels, $\bullet\text{NO}$ can interact with superoxide anion radicals ($\text{O}_2^{\bullet-}$), that are plentiful during reoxygenation and form peroxynitrite, a highly reactive molecule that causes oxidative damage to biomolecules and exacerbates tissue injury (Lushchak and Lushchak, 2021). Finally, ROS and RNS formed during reoxygenation in excessive amounts may activate redox-sensitive signaling pathways, such as nuclear factor kappa B (NF- κB) and mitogen-activated protein kinase (MAPK) pathways (Kruk et al., 2019). Collectively, these regulate inflammatory and cell survival/death responses and dysregulation of these pathways contributes to oxidative stress and brain damage at CVE.

Hence, hypoxia followed by reoxygenation induces intensive oxidative stress via a complex interplay between oxygen availability, ROS and RNS generation, inflammatory responses, and cellular signaling pathways. Strategies to mitigate the fluctuations in redox processes may involve antioxidant therapies, modulation of inflammatory responses, and preservation of mitochondrial function to alleviate damage and improve tissue outcomes.

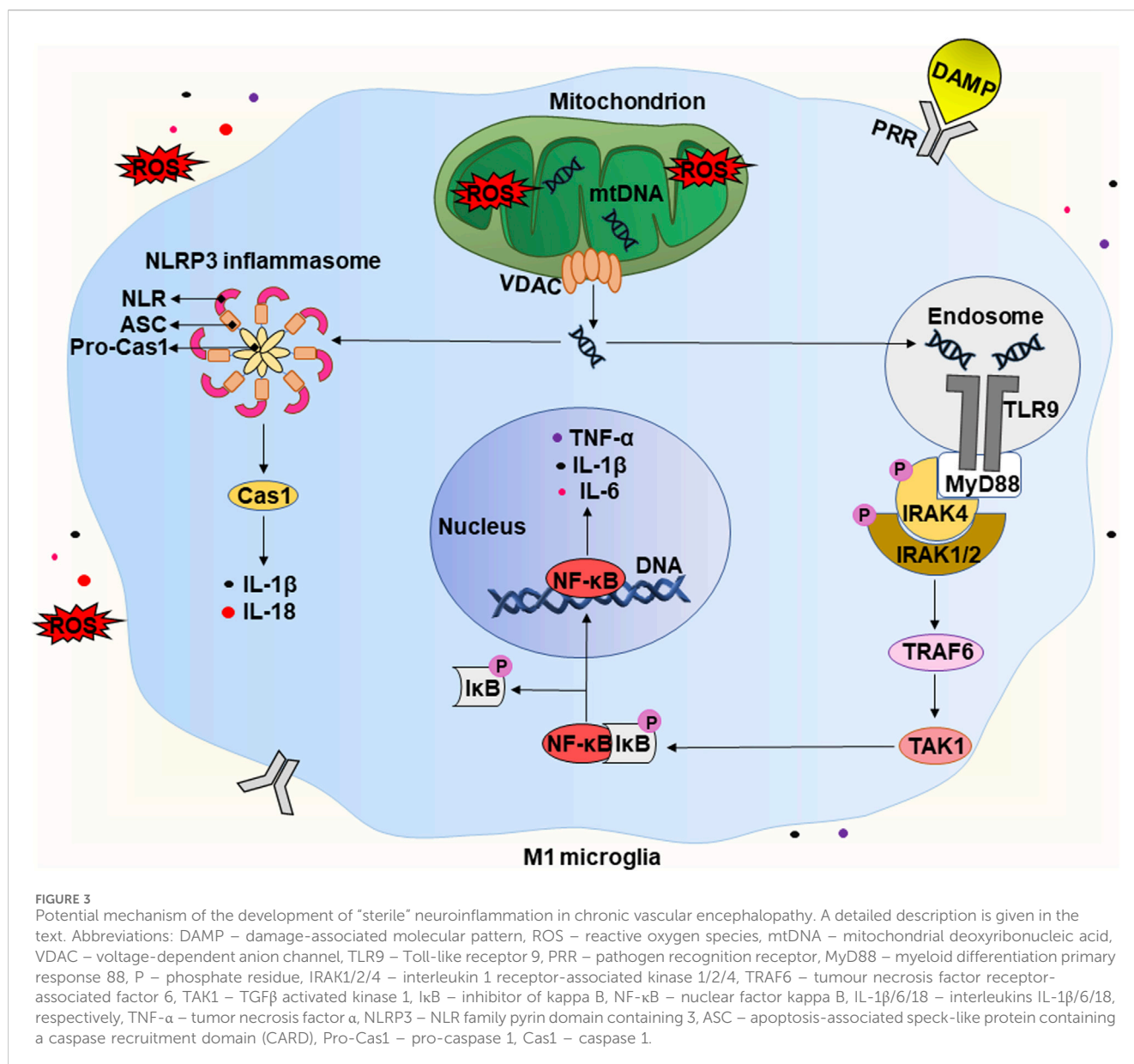
3 Neuroinflammation in chronic vascular encephalopathy

Inflammation is a protective response of the immune system that acts in response to aseptic injury, for example, sterile surgical interventions and non-aseptic interventions (viral or bacterial invasion). Activation of the inflammatory response leads to the migration of tissue leukocytes, in particular, monocytes, to the site of inflammation where they differentiate into macrophages, providing phagocytosis and control of the local microenvironment. Although inflammation is essentially a beneficial defense mechanism, an excessive pro-inflammatory response causes tissue damage and has negative functional consequences (Lyman et al., 2014).

Several experimental studies have shown a relationship between neuroinflammation and cognitive disorders (Sun et al., 2015; Tan et al., 2015; Tian et al., 2015; Hajiluian et al., 2017). In particular, chronic neuroinflammation is observed in patients suffering from vascular cognitive impairment at various stages of vascular dementia, including pre-clinical, clinical, and severe stages (Poh et al., 2022). Animal studies show that chronic cerebral hypoperfusion, that is a key factor of CVE, can cause short- and long-term neuroinflammation, damaging the myelin sheath, the BBB, and the grey matter (Liu et al., 2013; Miyanohara et al., 2018; Poh et al., 2021). Therefore, neuroinflammation appears to play a significant role in cognitive decline. Typically, it includes features such as activation of microglia, resident immune cells of the central nervous system (CNS), increased levels of proinflammatory cytokines and chemokines, recruitment of peripheral immune cells, and local brain damage (Moyse et al., 2022; Tian et al., 2022).

Microglia play a central role in the development of neuroinflammation. They make up about 10%–20% of the cell population of the CNS and provide primary immune surveillance. In a healthy brain under physiological conditions, microglial cells show the so-called “resting” morphology, that is characterized by a small cell body with numerous long, thin and highly branched processes. The latter are constantly moving, checking the surrounding space for signs of pathogen- or damage-related molecules, in particular, PAMPs and DAMPs (DiSabato et al., 2016; Raffaele and Fumagalli, 2022; Garaschuk and Verkhratsky, 2024). Transcriptome analysis of “resting” microglia shows that they significantly express genes associated with steady-state brain functions, including maintenance of homeostasis, neuronal maturation, and synaptic integrity. However, recognition of DAMPs activates microglial cells, changing their morphology and transcriptional profile (Wendimu and Hooks, 2022). Below we consider the details of the potential mechanisms of the development of the so-called “sterile” neuroinflammation in CVE (Figure 3).

As mentioned in Section 2 above, CVE is often accompanied by acute and chronic hypoxia that can lead to increased levels of reducing equivalents and ROS, causing the development of reductive and oxidative stress, respectively (Figure 2). The latter have various consequences for cells, including the release of endogenous DAMPs. Under physiological conditions, limited production of ROS is necessary for maintaining the biological functions of cells. However, at high concentrations, ROS are recognized as DAMPs and activate the innate immune system of



the brain (Koenig and Buskiewicz-Koenig, 2022). In addition, the increase in ROS levels can overwhelm defense systems causing numerous oxidative modifications of biomolecules and contributing to the increase of other types of DAMPs. It is worth mentioning that mtDNA is the first and closest target for the harmful effects of mtROS (Roh and Sohn, 2018; Dmytriv et al., 2023). An increase in the level of mtROS leads to mitochondrial dysfunction, which is characterized by swelling of these intracellular organelles, an increase in inner membrane permeability, and a release of mtDNA (Figure 3) (Lin et al., 2022). The latter occurs with the participation of voltage-dependent anion channels (VDACs). This is the most common protein of the outer mitochondrial membrane and plays the role of a channel to transport ATP, Ca^{2+} , and other metabolites between mitochondria and cytosol (Kmita et al., 2023). However, under stressful conditions, VDACs oligomerize to form macropores that provide the release of mtDNA (Kim et al., 2023).

The release of endogenous DAMPs, including mtDNA, contributes to the development of “sterile” inflammation that is not associated with pathogens. The brain contains a significant number of DAMP sensors, in particular, pathogen recognition receptors (PRRs). There are several subfamilies of PRRs, including Toll-like receptors (TLRs), C-type lectin receptors (CLRs), RIG-like receptors (RLRs), and Nod-like receptors (NLRs). RLRs and NLRs are expressed inside cells and recognize intracellular inflammation-related molecules. Generally, CLR and TLR are transmembrane receptors that contribute to the surveillance of the extracellular environment (Kigerl et al., 2014). However, there are some exceptions. For example, TLR9 is expressed intracellularly on the endoplasmic reticulum and under certain conditions migrates to endosomal membranes (De Gaetano et al., 2021). Thus, microglial cells can recognize DAMPs both intracellularly and extracellularly. This interaction activates receptors and morphologically transforms the branched state of these cells into

an amoeboid state with a large cell body and almost no processes (Figure 1) (Wendimu and Hooks, 2022). Below, we take a closer look at the molecular mechanisms involved in the initiation of a pro-inflammatory response due to the release of mtDNA.

Released mtDNA is recognized by several intracellular receptors, for example, TLR9 and NLR (Figure 3). TLR9 interacts with mtDNA with a 2:2 stoichiometry (2 TLR9 monomers and two mtDNA molecules). This interaction leads to the activation of the first downstream target, the adapter protein MyD88 (myeloid differentiation primary response 88) (De Gaetano et al., 2021). The latter forms a complex with IRAK4 (interleukin one receptor-associated kinase 4), that recruits IRAK1 and IRAK2 resulting in their phosphorylation. Phosphorylated IRAKs interact with TRAF6 (tumor necrosis factor receptor-associated factor 6), that activates TAK-1 (TGF β activated kinase 1) to mediate activation of the transcription factor NF- κ B (Zheng et al., 2020). Under non-stress conditions, NF- κ B is in a complex with I κ B (inhibitor of NF- κ B) and remains in the cytoplasm. Phosphorylation of I κ B by the IKK complex (I κ B kinase) leads to polyubiquitination of I κ B with its subsequent proteasomal degradation (Christian et al., 2016). TAK1 also carries out an alternative phosphorylation of I κ B, promoting the release of NF- κ B. The latter translocates into the nucleus and activates the transcription of pro-inflammatory cytokines, in particular, IL-1 β , IL-6, and TNF- α (Zheng et al., 2020).

In addition, some NLRs, when recognizing DAMPs, form a multi-protein complex called the “inflammasome”. It consists of NLR, an adapter protein (ASC), and a precursor of caspase 1 (pro-caspase 1). Assembly of the inflammasome triggers the autocleavage of pro-caspase one and the formation of functionally active caspase one that then cleaves pro-IL-1 β and pro-IL-18 into their active forms (IL-1 β and IL-18). The release of pro-inflammatory cytokines activates the pro-inflammatory microglial phenotype, that is called M1 (Galizzi and Di Carlo, 2023). M1 microglia actively produce IL-1 β , IL-6, TNF- α , chemokines, and others. They also significantly express the enzyme NADPH oxidase, that produces ROS, in particular, the superoxide anion radical, and inducible nitric oxide synthase (iNOS) producing \cdot NO (Guo et al., 2022). In this way, microglial cells can damage nearby neurons and astrocytes. Potentially, this can lead to cognitive decline and brain damage, which are observed in patients with CVE. Production of pro-inflammatory cytokines and chemokines promotes the recruitment of peripheral immune cells, including monocytes and macrophages. These events initiate a number of pathophysiological processes, including both the production of pro-inflammatory cytokines and tissue damage, and the production of anti-inflammatory cytokines and healing. As a result, this can lead to demyelination, loss of synapses and death of neurons (Ising and Heneka, 2018; Fard and Stough, 2019).

Synapses are sites of cell–cell contact that transmit signals between neurons. They provide a molecular mechanism by which information is encoded, processed, and stored within the brain (Bailey and Kandel, 2008). Until recently, synapses were considered as simple connections between neurons. However, disruption of these connections causes significant violations of behavior, cognition, and memory (Adams et al., 2023). Loss of synapses is often a consequence of inflammation and has been found in many neurodegenerative diseases. It correlates with the severity of

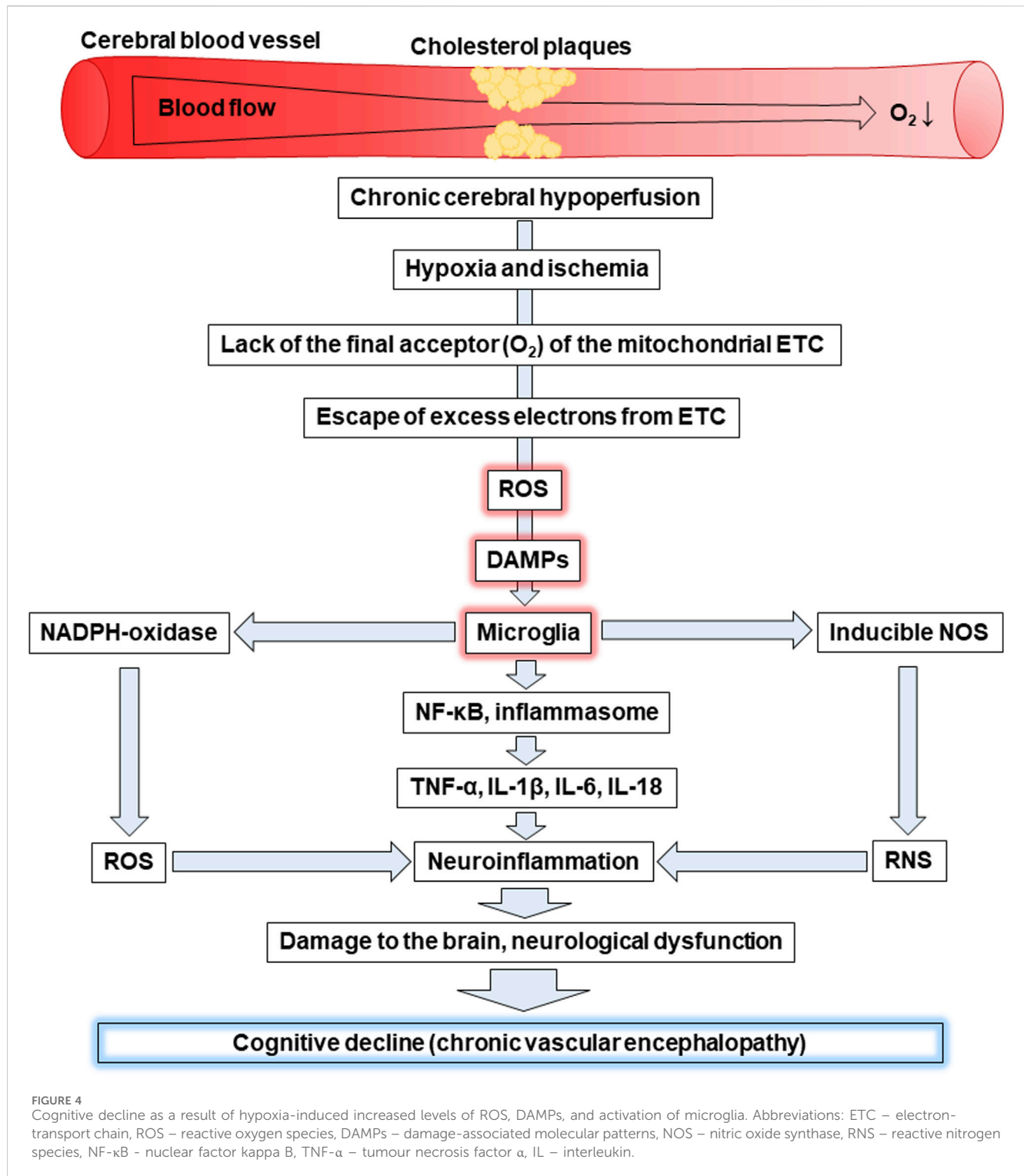
cognitive decline and contributes to cognitive impairment even in the absence of gross atrophy (Griffiths and Grant, 2023). Thus, even a small loss of synapses caused by the development of neuroinflammation in CVE can potentially lead to cognitive decline and subsequent dementia.

It is also worth mentioning the role of astrocytes, the most abundant type of glial cells in the CNS. Under homeostatic conditions, astrocytes provide baseline trophic support for neurons, coordinate the formation and functioning of synapses, and participate in forming the BBB. In addition, they are also immunocompetent cells that can recognize danger signals in their extracellular environment (Colombo and Farina, 2016). In particular, the release of pro-inflammatory mediators and ROS by microglial cells can cause a change in the morphological and functional characteristics of astrocytes to adopt a so-called “reactive” phenotype. Unlike typical astrocytes, that promote neuronal survival, reactive astrocytes downregulate accessory functions and begin to secrete neurotoxic factors, including complement components and chemokines, that promote the recruitment of immune cells across the BBB into the CNS (Lawrence et al., 2023). Potentially, this can lead to dysfunction of cerebral blood vessels, neurotoxicity, and the development of CVE. Reactive astrocytes proliferate, become hypertrophied, and increase the expression of intermediate filament proteins, cytokines, and chemokines. They are grouped into polarized bundles and connect with components of the extracellular matrix, forming astrocytic scars. The latter forms a physical barrier limiting inflammation (Cekanaviciute and Buckwalter, 2016). However, as far as we know, there is currently no information on astrocytic scars in patients with CVE.

4 Therapeutic approaches for the treatment of chronic vascular encephalopathy

Known therapeutic approaches for treating CVE face many obstacles, including polypharmacy, disease specificity, and complications such as neuroinflammation, excessive BBB permeability, ionic imbalance, etc. It should be noted that strategies for CVE treatment mostly focus on controlling its symptoms as well as the underlying cardiovascular and cerebrovascular risk factors (O'Brien et al., 2017). Next, we will consider several therapeutic and nutraceutical interventions based on counteracting ionic imbalance, BBB dysfunction, and inflammation in CVE.

Chronic cerebral hypoperfusion, one of the main pathological changes occurring in vascular dementia, also disrupts ion homeostasis decreasing K⁺ and increasing Ca²⁺ and Na⁺ levels (Poh et al., 2022). Multiple ion transporters and their regulatory kinases play crucial roles in the reactive astrogliosis process, so the use of their pharmacological inhibitors represents promising drugs for CVE (Rahman et al., 2024). For instance, bumetanide, a specific inhibitor of Na-K-Cl cotransporter 1, attenuates chronic hypoperfusion-induced white matter damage and cognitive impairment in a mouse model of vascular cognitive impairment and dementia (Yu et al., 2018). Chronic administration of nimodipine, a central nervous system-selective dihydropyridine



calcium channel blocking agent provides an effective preventive treatment for stroke and cognitive decline in cerebral small vessel disease (Yang et al., 2024).

Zhang et al. (2024) demonstrated that vascular cell adhesion molecule 1 (VCAM1) is involved in BBB dysfunction in chronic cerebral hypoperfusion. In particular, VCAM1 expression directly correlates with the severity of BBB impairment, whereas blocking VCAM1 reduces BBB leakage and protects white matter integrity. In

such a way, the use of inhibitors of VCAM1 may offer a new therapeutic approach to CVE treatment.

An analgesic neurotrophin alleviates cognitive impairment by inhibiting the TLR4/MyD88/NF- κ B signaling pathway in a mouse model of vascular dementia. In particular, it promotes cerebral blood flow, weakens damage to the white matter, reduces the loss of neurons, and improves cognitive functions (Zou et al., 2023). Pharmacological inhibition of NLRP3 inflammasome also has

therapeutic potential in this field (Xu et al., 2023). In addition, preclinical studies of rodents strongly suggest that intermittent fasting (a dietary pattern alternating between eating and fasting periods within a 24-h cycle) attenuates pathological mechanisms, including inflammation, involved in vascular cognitive impairment (Rajeev et al., 2024).

Various substances of natural origin can also be used for CVE treatment. For example, sulforaphane is a powerful activator of the nuclear factor erythroid 2-related factor 2 (Nrf2), which upregulates the expression of a number of genes coding antioxidant and anti-inflammatory proteins/enzymes (Lushchak, 2014). Mao et al. (2019) found that sulforaphane-mediated neuroprotection in a rat model of vascular cognitive impairment was associated with enhanced activation of Nrf2 and upregulation of heme oxygenase 1. Thus, the use of sulforaphane increases the antioxidant potential of cells, inhibiting the development of oxidative stress and neuroinflammation (Townsend and Johnson, 2016; Zhou et al., 2016; Subedi et al., 2019).

Vitamin D may also be promising for CVE treatment. The vitamin D receptor (VDR) is a DNA-binding transcription factor and a member of the nuclear steroid hormone receptor family. VDR signaling in microglia inhibits neuroinflammation, whereas VDR knockout promotes a proinflammatory phenotype characterized by the production of proinflammatory cytokines (Cui et al., 2023).

5 Conclusion and perspectives

CVE is a frequent cause of cognitive impairment, including mild vascular cognitive impairment and dementia. It occurs as a result of chronic disorders of the blood supply to the brain, in particular, chronic cerebral hypoperfusion, which causes hypoxia and ischemia. ROS and DAMPs are among the key players in the pathophysiology of CVE. Figure 4 shows a scheme that connects all of these concepts into one chain of sequential events that leads to the cognitive decline characteristic of CVE.

Chronic cerebral hypoperfusion is associated with insufficient blood supply to the brain. For example, the deposition of cholesterol plaques on the walls of cerebral vessels can cause reduced blood flow to the brain, leading to hypoxia and ischemia. Oxygen is the final acceptor of electrons in the mitochondrial ETC and its lack is primarily associated with a decrease in ATP production, as well as increased generation of ROS. The latter is a consequence of excess electrons escaping from the ETC causing the formation of ROS. This leads to the development of oxidative stress as witnessed by oxidative modifications of proteins, lipids, and nucleic acids.

Mitochondria, as the site of the ETC are the first target for the harmful effects of mtROS. As a result, they swell, become more permeable and release mtDNA, which together with mtROS are recognized as DAMPs. Microglial cells can face DAMPs released as a result of apoptosis or necrosis of neighbouring cells and recognize them through transmembrane PRRs or recognize their own endogenous DAMPs, including mtROS and mtDNA through intracellular PRRs, for example, TLR9. Oxidative stress can be the cause of both events. The interaction of DAMPs and PRRs leads to the activation of microglia characterized by enhanced expression of NADPH oxidase, which produces the superoxide anion radical, and inducible NOS, which generates $^{\bullet}\text{NO}$. In

general, this promotes an increase in ROS and RNS levels resulting in the induction of oxidative and nitrosative stress, respectively. In addition, activated microglia are associated with the activation of the transcription factor NF- κ B and the inflammasome. Both contribute to the production of pro-inflammatory cytokines, including TNF- α , IL-1 β , IL-6, IL-18 inducing neuroinflammation. In addition, microglia release chemokines that ensure the recruitment of peripheral leukocytes. In general, all of the events listed above can lead to neuronal degradation, demyelination, and loss of synapses causing the significant cognitive decline characteristic of CVE. Thus, oxidative stress caused by the increase of ROS and neuroinflammation caused by the release of DAMPs, which are recognized by microglia, play a crucial role in the progression of CVE.

Most neurodegenerative diseases are currently considered incurable, so the search for various methods for their prevention and treatment remains relevant. For example, the use of sulforaphane, an isothiocyanate of the cruciferous family, and vitamin D as dietary supplements may be promising for the relief of CVE symptoms. Potentially, they can be used to break the vicious cycle (Figure 1) of neurodegeneration associated with oxidative stress and neuroinflammation. For example, the inhibition of NLRP3, a key player in inflammation (Figure 3), slows neurodegeneration and alleviates cognitive impairment (Dempsey et al., 2017; Liang et al., 2022). In addition, a decrease in IL-1 β production alleviates hypoperfusion-induced brain injury (Poh et al., 2021). Together, this indicates the essential role of neuroinflammation in the progression of CVE.

Sulforaphane inhibits neuroinflammation and associated oxidative stress. In particular, it activates the transcription factor Nrf2 and the expression of its target genes in microglia. The latter include NQO1 (NAD(P)H quinone dehydrogenase 1) and HMOX1 (heme oxygenase 1) (Townsend and Johnson, 2016). NQO1 catalyzes the two-electron reduction of quinones and many other compounds in the cytosol. This minimizes the formation of reactive semiquinones resulting from one-electron reduction as well as ROS (Dinkova-Kostova and Talalay, 2010). HMOX1 is the enzyme responsible for the degradation of heme into three products: carbon monoxide, iron ions, and biliverdin. The latter is successively transformed into a powerful antioxidant bilirubin by biliverdin reductase (Consoli et al., 2021). In addition, Nrf2 upregulates the expression of SOD1 (superoxide dismutase 1) (Daněk et al., 2022), that scavenges the superoxide anion radical leading to the formation of hydrogen peroxide, that is further neutralized by catalase and peroxidases (Bayliak et al., 2023). In general, the increase in antioxidant enzyme activities enhances the antioxidant potential and capability to degrade ROS. In turn, this suppresses neuroinflammation. In particular, sulforaphane decreases levels of pro-inflammatory cytokines, including IL-1 β and IL-6, as well as reduces the expression of iNOS. This indicates that it is a potentially beneficial dietary supplement that can reduce microglia-mediated oxidative stress and neuroinflammation (Townsend and Johnson, 2016). In addition, increased expression of Nrf2 blocks the induction of astrocyte reactive gene expression by counteracting NF- κ B, whereas the absence of Nrf2 conversely promotes the activation of reactive astrocytes. Thus, the use of Nrf2 activators such as sulforaphane can potentially prevent astrocyte reactivity, suppressing neuroinflammation (Nakano-Kobayashi et al., 2023).

Vitamin D can also be used in this direction. It downregulates the expression of NF- κ B, a crucial neuroinflammatory factor (Figure 3), and markedly suppresses IL-6 and IL-17 levels (Hajiluian et al., 2017). In turn, this prevents excessive permeability of the BBB and cognitive dysfunction. Thus, both sulforaphane and vitamin D may be promising supplements for the prevention and treatment of CVE, particularly for breaking the vicious cycle of oxidative stress and neuroinflammation (Figure 1) that underlies neurodegeneration.

Taking into account all of the above, the following directions for future research in the field of CVE can be outlined:

1. Systemic investigation of the role of oxidative stress induced by hypoxia and reoxygenation in neurodegeneration.
2. Research on reductive stress under hypoxic conditions.
3. The use of sulforaphane and vitamin D for the treatment of CVE.
4. The potential of antioxidant therapy in patients with CVE.

Author contributions

TD: Conceptualization, Formal Analysis, Investigation, Visualization, Writing—original draft, Writing—review and editing. KD: Conceptualization, Investigation, Visualization, Writing—original draft, Writing—review and editing. KS: Conceptualization, Writing—original draft, Writing—review and editing. VL: Conceptualization, Funding acquisition, Methodology, Supervision, Writing—original draft, Writing—review and editing.

References

- Adams, N. E., Jafarian, A., Perry, A., Rouse, M. A., Shaw, A. D., Murley, A. G., et al. (2023). Neurophysiological consequences of synapse loss in progressive supranuclear palsy. *Brain* 146, 2584–2594. doi:10.1093/brain/awac471
- Bailey, C. H., and Kandel, E. R. (2008). Synaptic remodeling, synaptic growth and the storage of long-term memory in Aplysia. *Prog. Brain Res.* 169, 179–198. doi:10.1016/S0079-6123(07)00010-6
- Bayliak, M. M., Gospodaryov, D. V., and Lushchak, V. I. (2023). Homeostasis of carbohydrates and reactive oxygen species is critically changed in the brain of middle-aged mice: molecular mechanisms and functional reasons. *BBA Adv.* 3, 100077. doi:10.1016/j.bbadva.2023.100077
- Burrage, E. N., Coblenz, T., Prabhu, S. S., Childers, R., Bryner, R. W., Lewis, S. E., et al. (2023). Xanthine oxidase mediates chronic stress-induced cerebrovascular dysfunction and cognitive impairment. *J. Cereb. Blood Flow. Metab.* 43, 905–920. doi:10.1177/0271678X231152551
- Butterfield, D. A. (2023). Oxidative stress in brain in amnesic mild cognitive impairment. *Antioxidants* 12, 462. doi:10.3390/antiox12020462
- Cekanaviciute, E., and Buckwalter, M. S. (2016). Astrocytes: integrative regulators of neuroinflammation in stroke and other neurological diseases. *Neurotherapeutics* 13, 685–701. doi:10.1007/s13311-016-0477-8
- Christian, F., Smith, E. L., and Carmody, R. J. (2016). The regulation of NF- κ B subunits by phosphorylation. *Cells* 5, 12. doi:10.3390/cells5010012
- Colombo, E., and Farina, C. (2016). Astrocytes: key regulators of neuroinflammation. *Trends Immunol.* 37, 608–620. doi:10.1016/j.it.2016.06.006
- Consoli, V., Sorrenti, V., Grosso, S., and Vanella, L. (2021). Heme oxygenase-1 signaling and redox homeostasis in physiopathological conditions. *Biomolecules* 11, 589. doi:10.3390/biom11040589
- Cui, P., Lu, W., Wang, J., Wang, F., Zhang, X., Hou, X., et al. (2023). Microglia/macrophages require vitamin D signaling to restrain neuroinflammation and brain injury in a murine ischemic stroke model. *J. Neuroinflammation* 20, 63. doi:10.1186/s12974-023-02705-0
- Daněš, J., Danačíková, Š., Kala, D., Svoboda, J., Kapoor, S., Pošta, A., et al. (2022). Sulforaphane ameliorates metabolic changes associated with status epilepticus in immature rats. *Front. Cell. Neurosci.* 16, 855161. doi:10.3389/fncel.2022.855161
- De Gaetano, A., Solodka, K., Zanini, G., Selleri, V., Mattioli, A. V., Nasi, M., et al. (2021). Molecular mechanisms of mtDNA-mediated inflammation. *Cells* 10, 2898. doi:10.3390/cells10112898
- Dempsey, C., Rubio Araiz, A., Bryson, K. J., Finucane, O., Larkin, C., Mills, E. L., et al. (2017). Inhibiting the NLRP3 inflammasome with MCC950 promotes non-phlogistic clearance of amyloid- β and cognitive function in APP/PS1 mice. *Brain Behav. Immun.* 61, 306–316. doi:10.1016/j.bbi.2016.12.014
- Dhillon, S. K., Gunn, E. R., Lear, B. A., King, V. J., Lear, C. A., Wassink, G., et al. (2022). Cerebral oxygenation and metabolism after hypoxia-ischemia. *Front. Pediatr.* 10, 925951. doi:10.3389/fped.2022.925951
- Díaz-Bulnes, P., Saiz, M. L., López-Larrea, C., and Rodríguez, R. M. (2020). Crosstalk between hypoxia and ER stress response: a key regulator of macrophage polarization. *Front. Immunol.* 10, 2951. doi:10.3389/fimmu.2019.02951
- Dinkova-Kostova, A. T., and Talalay, P. (2010). NAD(P)H:quinone acceptor oxidoreductase 1 (NQO1), a multifunctional antioxidant enzyme and exceptionally versatile cytoprotector. *Arch. Biochem. Biophys.* 501, 116–123. doi:10.1016/j.abb.2010.03.019
- DiSabato, D. J., Quan, N., and Godbout, J. P. (2016). Neuroinflammation: the devil is in the details. *J. Neurochem.* 139, 136–153. doi:10.1111/jnc.13607
- Dmytriv, T. R., Tsiumpala, S. A., Semchyshyn, H. M., Storey, K. B., and Lushchak, V. I. (2023). Mitochondrial dysfunction as a possible trigger of neuroinflammation at post-traumatic stress disorder (PTSD). *Front. Physiol.* 14, 1222826. doi:10.3389/fphys.2023.1222826
- Fard, M. T., and Stough, C. A. (2019). A review and hypothesized model of the mechanisms that underpin the relationship between inflammation and cognition in the elderly. *Front. Aging Neurosci.* 11, 56. doi:10.3389/fnagi.2019.00056
- Galizzi, G., and Di Carlo, M. (2023). Mitochondrial DNA and inflammation in Alzheimer's disease. *Curr. Issues Mol. Biol.* 45, 8586–8606. doi:10.3390/cimb45110540
- Garaschuk, O., Semchyshyn, H. M., and Lushchak, V. I. (2018). Healthy brain aging: interplay between reactive species, inflammation and energy supply. *Ageing Res. Rev.* 48, 26–45. doi:10.1016/j.arr.2018.02.003
- Garaschuk, O., and Verkhatsky, A. (2024). Sleep, calcium and microglia - an (un) expected liaison. *Cell Calcium* 119, 102872. doi:10.1016/j.ceca.2024.102872

Funding

The author(s) declare that financial support was received for the research, authorship, and/or publication of this article. This work was partially supported by a grant from the Ministry of Education and Science of Ukraine (#0122U000894) to VL.

Acknowledgments

The authors dedicate this article to the defenders of Ukraine, the warriors who sacrifice their health and lives to protect the Motherland from russian aggressors.

Conflict of interest

The authors declare that the research was conducted in the absence of any commercial or financial relationships that could be construed as a potential conflict of interest.

Publisher's note

All claims expressed in this article are solely those of the authors and do not necessarily represent those of their affiliated organizations, or those of the publisher, the editors and the reviewers. Any product that may be evaluated in this article, or claim that may be made by its manufacturer, is not guaranteed or endorsed by the publisher.

- Griffiths, J., and Grant, S. G. N. (2023). Synapse pathology in Alzheimer's disease. *Semin. Cell. Dev. Biol.* 139, 13–23. doi:10.1016/j.semcdb.2022.05.028
- Guo, S., Wang, H., and Yin, Y. (2022). Microglia polarization from M1 to M2 in neurodegenerative diseases. *Front. Aging Neurosci.* 14, 815347. doi:10.3389/fnagi.2022.815347
- Hajiluan, G., Nameni, G., Shahabi, P., Mesgari-Abbasi, M., Sadigh-Eteghad, S., and Farhangi, M. A. (2017). Vitamin D administration, cognitive function, BBB permeability and neuroinflammatory factors in high-fat diet-induced obese rats. *Int. J. Obes.* 41, 639–644. doi:10.1038/ijo.2017.10
- Hearse, D. J., Humphrey, S. M., and Bullock, G. R. (1978). The oxygen paradox and the calcium paradox: two facets of the same problem? *J. Mol. Cell. Cardiol.* 10, 641–668. doi:10.1016/s0022-2828(78)80004-2
- Houston, M., Estevez, A., Chumley, P., Aslan, M., Marklund, S., Parks, D. A., et al. (1999). Binding of xanthine oxidase to vascular endothelium. Kinetic characterization and oxidative impairment of nitric oxide-dependent signaling. *J. Biol. Chem.* 274, 4985–4994. doi:10.1074/jbc.274.8.4985
- Ising, C., and Heneka, M. T. (2018). Functional and structural damage of neurons by innate immune mechanisms during neurodegeneration. *Cell. Death Dis.* 9, 120. doi:10.1038/s41419-017-0153-x
- Jellinger, K. A. (2013). Pathology and pathogenesis of vascular cognitive impairment—a critical update. *Front. Aging Neurosci.* 5, 17. doi:10.3389/fnagi.2013.00017
- Kigerl, K. A., de Rivero Vaccari, J. P., Dietrich, W. D., Popovich, P. G., and Keane, R. W. (2014). Pattern recognition receptors and central nervous system repair. *Exp. Neurol.* 258, 5–16. doi:10.1016/j.expneurol.2014.01.001
- Kim, J., Kim, H. S., and Chung, J. H. (2023). Molecular mechanisms of mitochondrial DNA release and activation of the cGAS-STING pathway. *Exp. Mol. Med.* 55, 510–519. doi:10.1038/s12276-023-00965-7
- Klomparens, E., and Ding, Y. (2019). The neuroprotective mechanisms and effects of sulforaphane. *Brain Circ.* 5, 74–83. doi:10.4103/bc.bc_7_19
- Kmita, H., Messina, A. A., and De Pinto, V. (2023). VDAC as a cellular hub: docking molecules and interactions. *Int. J. Mol. Sci.* 24, 6649. doi:10.3390/ijms24076649
- Koenig, A., and Buskiewicz-Koenig, I. A. (2022). Redox activation of mitochondrial DAMPs and the metabolic consequences for development of autoimmunity. *Antioxid. Redox Signal.* 36, 441–461. doi:10.1089/ars.2021.0073
- Kruk, J., Aboul-Enein, H. Y., Kladna, A., and Bowser, J. E. (2019). Oxidative stress in biological systems and its relation with pathophysiological functions: the effect of physical activity on cellular redox homeostasis. *Free Radic. Res.* 53, 497–521. doi:10.1080/10715762.2019.1612059
- Lawrence, J. M., Schardien, K., Wigdahl, B., and Nonnemacher, M. R. (2023). Roles of neuropathology-associated reactive astrocytes: a systematic review. *Acta Neuropathol. Commun.* 11, 42. doi:10.1186/s40478-023-01526-9
- Li, C., and Jackson, R. M. (2002). Reactive species mechanisms of cellular hypoxia-reoxygenation injury. *Am. J. Physiol. Cell. Physiol.* 282, 227–241. doi:10.1152/ajpcell.00112.2001
- Liang, T., Zhang, Y., Wu, S., Chen, Q., and Wang, L. (2022). The role of NLRP3 inflammasome in Alzheimer's disease and potential therapeutic targets. *Front. Pharmacol.* 13, 845185. doi:10.3389/fphar.2022.845185
- Lin, M.-M., Liu, N., Qin, Z.-H., and Wang, Y. (2022). Mitochondrial-derived damage-associated molecular patterns amplify neuroinflammation in neurodegenerative diseases. *Acta Pharmacol. Sin.* 43, 2439–2447. doi:10.1038/s41401-022-00879-6
- Liu, Q., He, S., Groysman, L., Shaked, D., Russin, J., Cen, S., et al. (2013). White matter injury due to experimental chronic cerebral hypoperfusion is associated with C5 deposition. *PLoS One* 8, e84802. doi:10.1371/journal.pone.0084802
- Lushchak, V. I. (2011). Adaptive response to oxidative stress: bacteria, fungi, plants and animals. *Comp. Biochem. Physiol. C. Toxicol. Pharmacol.* 153, 175–190. doi:10.1016/j.cbpc.2010.10.004
- Lushchak, V. I. (2014). Free radicals, reactive oxygen species, oxidative stresses and their classifications. *Ukr. Biochem. J.* 87, 11–18. doi:10.1016/j.cbi.2014.10.016
- Lushchak, V. I., and Lushchak, O. V. (2021). Interplay between reactive oxygen and nitrogen species in living organisms. *Chem. Biol. Interact.* 349, 109680. doi:10.1016/j.cbi.2021.109680
- Lushchak, V. I., and Storey, K. B. (2021). Oxidative stress concept updated: definitions, classifications, and regulatory pathways implicated. *EXCLI J.* 20, 956–967. doi:10.17179/excli2021-3596
- Lyman, M., Lloyd, D. G., Ji, X., Vizcaychipi, M. P., and Ma, D. (2014). Neuroinflammation: the role and consequences. *Neurosci. Res.* 79, 1–12. doi:10.1016/j.neures.2013.10.004
- Mao, L., Yang, T., Li, X., Lei, X., Sun, Y., Zhao, Y., et al. (2019). Protective effects of sulforaphane in experimental vascular cognitive impairment: contribution of the Nrf2 pathway. *J. Cereb. Blood Flow. Metab.* 39, 352–366. doi:10.1177/0271678X18764083
- Mattson, M. R. (2007). Calcium and neurodegeneration. *Aging Cell* 6, 337–350. doi:10.1111/j.1474-9726.2007.00275.x
- Miyahara, J., Kakae, M., Nagayasu, K., Nakagawa, T., Mori, Y., Arai, K., et al. (2018). TRPM2 channel aggravates CNS inflammation and cognitive impairment via activation of microglia in chronic cerebral hypoperfusion. *J. Neurosci.* 38, 3520–3533. doi:10.1523/JNEUROSCI.2451-17.2018
- Moyse, E., Krantic, S., Djellouli, N., Roger, S., Angoulvant, D., Debacq, C., et al. (2022). Neuroinflammation: a possible link between chronic vascular disorders and neurodegenerative diseases. *Front. Aging Neurosci.* 14, 827263. doi:10.3389/fnagi.2022.827263
- Nakano-Kobayashi, A., Canela, A., Yoshihara, T., and Hagiwara, M. (2023). Astrocyte-targeting therapy rescues cognitive impairment caused by neuroinflammation via the Nrf2 pathway. *Proc. Natl. Acad. Sci. U. S. A.* 120, e2303809120. doi:10.1073/pnas.2303809120
- O'Brien, J. T., Holmes, C., Jones, M., Jones, R., Livingston, G., McKeith, I., et al. (2017). Clinical practice with anti-dementia drugs: a revised (third) consensus statement from the British Association for Psychopharmacology. *J. Psychopharmacol.* 31, 147–168. doi:10.1177/0269881116680924
- Owolabi, M., Ojagbemi, A., Kalaria, R., Sarfo, F. S., and Akinyemi, R. (2018). Behavioural and cognitive effects of cerebrovascular diseases. *Behav. Neurol.* 2018, 7516032. doi:10.1155/2018/7516032
- Poh, L., Fann, D. Y., Wong, P., Lim, H. M., Foo, S. L., Kang, S. W., et al. (2021). AIM2 inflammasome mediates hallmark neuropathological alterations and cognitive impairment in a mouse model of vascular dementia. *Mol. Psychiatry.* 26, 4544–4560. doi:10.1038/s41380-020-00971-5
- Poh, L., Sim, W. L., Jo, D. G., Dinh, Q. N., Drummond, G. R., Sobey, C. G., et al. (2022). The role of inflammasomes in vascular cognitive impairment. *Mol. Neurodegener.* 17, 4. doi:10.1186/s13024-021-00506-8
- Quinn, T. J., Gallacher, J., Deary, I. J., Lowe, G. D., Fenton, C., and Stott, D. J. (2011). Association between circulating hemostatic measures and dementia or cognitive impairment: systematic review and meta-analyses. *J. Thromb. Haemost.* 9, 1475–1482. doi:10.1111/j.1538-7836.2011.04403.x
- Raffaele, S., and Fumagalli, M. (2022). Dynamics of microglia activation in the ischemic brain: implications for myelin repair and functional recovery. *Front. Cell. Neurosci.* 16, 950819. doi:10.3389/fncel.2022.950819
- Rahman, M. S., Islam, R., and Bhuiyan, M. I. H. (2024). Ion transporter cascade, reactive astroglia and cerebrovascular diseases. *Front. Pharmacol.* 15, 1374408. doi:10.3389/fphar.2024.1374408
- Rajeev, V., Tabassum, N. I., Fann, D. Y., Chen, C. P., Lai, M. K. P., and Arumugam, T. V. (2024). Intermittent metabolic switching and vascular cognitive impairment. *J. Obes. Metab. Syndr.* 33, 92–107. doi:10.7570/jomes24010
- Roh, J. S., and Sohn, D. H. (2018). Damage-associated molecular patterns in inflammatory diseases. *Immune Netw.* 18, e27. doi:10.4110/in.2018.18.e27
- Sabán-Ruiz, J., Alonso-Pachó, A., Fabregate-Fuente, M., and de la Puerta González-Quevedo, C. (2013). Xanthine oxidase inhibitor febuxostat as a novel agent postulated to act against vascular inflammation. *Antinflamm. Antiallergy Agents Med. Chem.* 12, 94–99. doi:10.2174/1871523011312010011
- Sabayan, B., Westendorp, R. G., van der Grond, J., Stott, D. J., Sattar, N., van Osch, M. J. P., et al. (2014). Markers of endothelial dysfunction and cerebral blood flow in older adults. *Neurobiol. Aging* 35, 373–377. doi:10.1016/j.neurobiolaging.2013.08.020
- Semchyshyn, H. (2021). Is carbonyl/AGE/RAGE stress a hallmark of the brain aging? *Pflugers. Arch.* 473, 723–734. doi:10.1007/s00424-021-02529-y
- Subedi, L., Cho, K., Park, Y. U., Choi, H. J., and Kim, S. Y. (2019). Sulforaphane-enriched broccoli sprouts pretreated by pulsed electric fields reduces neuroinflammation and ameliorates scopolamine-induced amnesia in mouse brain through its antioxidant ability via Nrf2-HO-1 activation. *Oxid. Med. Cell. Longev.* 2019, 3549274. doi:10.1155/2019/3549274
- Sun, J., Zhang, S., Zhang, X., Zhang, X., Dong, H., and Qian, Y. (2015). IL-17A is implicated in lipopolysaccharide-induced neuroinflammation and cognitive impairment in aged rats via microglial activation. *J. Neuroinflammation* 12, 165. doi:10.1186/s12974-015-0394-5
- Tan, H., Bi, J., Wang, Y., Zhang, J., and Zuo, Z. (2015). Transfusion of old rbc induces neuroinflammation and cognitive impairment. *Crit. Care Med.* 43, e276–e286. doi:10.1097/CCM.0000000000001023
- Tian, A., Ma, H., Cao, X., Zhang, R., Wang, X., and Wu, B. (2015). Vitamin D improves cognitive function and modulates Th17/Treg cell balance after hepatectomy in mice. *Inflammation* 38, 500–509. doi:10.1007/s10753-014-9956-4
- Tian, Z., Ji, X., and Liu, J. (2022). Neuroinflammation in vascular cognitive impairment and dementia: current evidence, advances, and prospects. *Int. J. Mol. Sci.* 23, 6224. doi:10.3390/ijms23116224
- Townsend, B. E., and Johnson, R. W. (2016). Sulforaphane induces Nrf2 target genes and attenuates inflammatory gene expression in microglia from brain of young adult and aged mice. *Exp. Gerontol.* 73, 42–48. doi:10.1016/j.exger.2015.11.004
- Wendimu, M. Y., and Hooks, S. B. (2022). Microglia phenotypes in aging and neurodegenerative diseases. *Cells* 11, 2091. doi:10.3390/cells11132091
- Widlansky, M. E., Gokke, N., Keaney Jr, J. F., and Vita, J. A. (2003). The clinical implications of endothelial dysfunction. *J. Am. Coll. Cardiol.* 42, 1149–1160. doi:10.1016/s0735-1097(03)00994-x

- Xu, Y., Yang, Y., Chen, X., Jiang, D., Zhang, F., Guo, Y., et al. (2023). NLRP3 inflammasome in cognitive impairment and pharmacological properties of its inhibitors. *Transl. Neurodegener.* 12, 49. doi:10.1186/s40035-023-00381-x
- Yang, Z., Lange, F., Xia, Y., Chertavian, C., Cabolis, K., Sajic, M., et al. (2024). Nimodipine protects vascular and cognitive function in an animal model of cerebral small vessel disease. *Stroke* 55, 1914–1922. doi:10.1161/STROKEAHA.124.047154
- Yu, W., Li, Y., Hu, J., Wu, J., and Huang, Y. (2022). A study on the pathogenesis of vascular cognitive impairment and dementia: the chronic cerebral hypoperfusion hypothesis. *J. Clin. Med.* 11, 4742. doi:10.3390/jcm11164742
- Yu, Y., Fu, P., Yu, Z., Xie, M., Wang, W., and Luo, X. (2018). NKCC1 inhibition attenuates chronic cerebral hypoperfusion-induced white matter lesions by enhancing progenitor cells of oligodendrocyte proliferation. *J. Mol. Neurosci.* 64, 449–458. doi:10.1007/s12031-018-1043-0
- Zhang, H., Shang, J., Li, W., Gao, D., and Zhang, J. (2024). Increased expression of VCAM1 on brain endothelial cells drives blood-brain barrier impairment following chronic cerebral hypoperfusion. *ACS Chem. Neurosci.* 15, 2028–2041. doi:10.1021/acschemneuro.4c00039
- Zheng, C., Chen, J., Chu, F., Zhu, J., and Jin, T. (2020). Inflammatory role of TLR-MyD88 signaling in multiple sclerosis. *Front. Mol. Neurosci.* 12, 314. doi:10.3389/fnmol.2019.00314
- Zhou, Q., Chen, B., Wang, X., Wu, L., Yang, Y., Cheng, X., et al. (2016). Sulforaphane protects against rotenone-induced neurotoxicity *in vivo*: involvement of the mTOR, Nrf2, and autophagy pathways. *Sci. Rep.* 6, 32206. doi:10.1038/srep32206
- Zou, H., Chen, X., Lu, J., Zhou, W., Zou, X., Wu, H., et al. (2023). Neurotrophin alleviates cognitive impairment by inhibiting TLR4/MyD88/NF- κ B inflammation signaling pathway in mice with vascular dementia. *Neurochem. Int.* 171, 105625. doi:10.1016/j.neuint.2023.105625



OPEN ACCESS

EDITED BY

Julia J Mack,
UCLA Health System, United States

REVIEWED BY

Vicente Andres,
Spanish National Centre for Cardiovascular
Research, Spain
G.W. Gant Luxton,
University of California, United States

*CORRESPONDENCE

George A. Truskey,
✉ gtruskey@duke.edu

RECEIVED 14 July 2024

ACCEPTED 13 August 2024

PUBLISHED 22 August 2024

CITATION

Shores KL and Truskey GA (2024)
Mechanotransduction of the vasculature in
Hutchinson-Gilford Progeria Syndrome.
Front. Physiol. 15:1464678.
doi: 10.3389/fphys.2024.1464678

COPYRIGHT

© 2024 Shores and Truskey. This is an open-access article distributed under the terms of the [Creative Commons Attribution License \(CC BY\)](#). The use, distribution or reproduction in other forums is permitted, provided the original author(s) and the copyright owner(s) are credited and that the original publication in this journal is cited, in accordance with accepted academic practice. No use, distribution or reproduction is permitted which does not comply with these terms.

Mechanotransduction of the vasculature in Hutchinson-Gilford Progeria Syndrome

Kevin L. Shores and George A. Truskey*

Department of Biomedical Engineering, Duke University, Durham, NC, United States

Hutchinson-Gilford Progeria Syndrome (HGPS) is a premature aging disorder that causes severe cardiovascular disease, resulting in the death of patients in their teenage years. The disease pathology is caused by the accumulation of progerin, a mutated form of the nuclear lamina protein, lamin A. Progerin binds to the inner nuclear membrane, disrupting nuclear integrity, and causes severe nuclear abnormalities and changes in gene expression. This results in increased cellular inflammation, senescence, and overall dysfunction. The molecular mechanisms by which progerin induces the disease pathology are not fully understood. Progerin's detrimental impact on nuclear mechanics and the role of the nucleus as a mechanosensor suggests dysfunctional mechanotransduction could play a role in HGPS. This is especially relevant in cells exposed to dynamic, continuous mechanical stimuli, like those of the vasculature. The endothelial (ECs) and smooth muscle cells (SMCs) within arteries rely on physical forces produced by blood flow to maintain function and homeostasis. Certain regions within arteries produce disturbed flow, leading to an impaired transduction of mechanical signals, and a reduction in cellular function, which also occurs in HGPS. In this review, we discuss the mechanics of nuclear mechanotransduction, how this is disrupted in HGPS, and what effect this has on cell health and function. We also address healthy responses of ECs and SMCs to physiological mechanical stimuli and how these responses are impaired by progerin accumulation.

KEYWORDS

progeria, progerin, lamin a, mechanotransduction, endothelial cell, vascular smooth muscle cell, atherosclerosis

Introduction

Mechanotransduction is the translation of mechanical stimuli into biochemical signals through numerous mechanosensitive cellular components such as stretch-activated ion channels, G protein-coupled receptors (GPCRs), integrins, and cytoskeletal filaments. The cellular response to mechanical forces is critical for tissue development and homeostasis (Humphrey et al., 2014; Davis et al., 2023). By decoupling nuclear and cytoplasmic responses to external mechanical stresses, a role for the nucleus as a mechanosensor has been identified (Kirby and Lammerding, 2018). Nuclear mechanotransduction involves the generation and regulation of signals transmitted through the cytoskeleton or modulation of gene expression by nuclear deformation. How the nucleus senses mechanical stimuli and what effect that has on cellular function is of particular interest in the context of various diseases, specifically those that affect nuclear architecture like laminopathies. These are genetic disorders that cause mutations in proteins of the nuclear

lamina, leading to structural disruption of the nucleus or gene mis-regulation (Maraldi et al., 2011). Some of the most studied laminopathies include Emery-Dreifuss muscular dystrophy, dilated cardiomyopathy, and the accelerated aging disorder, Hutchinson-Gilford Progeria Syndrome (HGPS) (Maurer and Lammerding, 2019). Of these, HGPS is the most severe, resulting in the premature death of patients in their early teens due to extreme cardiovascular disease caused by progerin, a truncated and farnesylated form of the lamin A protein (Gordon et al., 2014). Cells that are exposed to high, continuous mechanical stresses are often the most affected in HGPS. These include bone (Schmidt et al., 2012), skin (Sagelius et al., 2008), and vascular cells, particularly the smooth muscle cells (SMCs) within larger arteries (Murtada et al., 2023; Olive et al., 2010). Vascular cells are constantly exposed to varying mechanical stresses from blood flow and intraluminal pressure, and thus are highly sensitive to perturbations in these forces (Davis et al., 2023). Disturbances in mechanical loads within the vasculature, which occur within curved or branched arteries, can promote cellular dysfunction, leading to manifestation of disease (Chiu and Chien, 2011). Impairment of cellular responsiveness to physiological mechanical signaling may contribute to cellular dysfunction and disease in HGPS (Hennekam, 2006). Here, we discuss the influence of progerin expression on cellular mechanotransduction to fluid and solid stresses acting on vascular cells and evaluate how this might contribute to the vascular pathology seen in HGPS.

Pathophysiology of Hutchinson-Gilford Progeria Syndrome

HGPS is a rare and fatal disease that results in premature aging of children. Common symptoms of the disease include delayed growth, alopecia, bone dysplasia, joint contracture, scleroderma, lipodystrophy, and severe atherosclerosis (Olive et al., 2010; Gordon et al., 2007; Merideth et al., 2008; Ullrich and Gordon, 2015). The atherosclerosis, manifested as vascular stiffening, calcification, and fibrotic thickening of the vessel wall, leads to myocardial infarction or stroke. The disease develops rapidly with patients only surviving into their mid-teens (Olive et al., 2010; Hennekam, 2006; Gordon et al., 2014).

In over 90% of the affected population, the disease pathology is caused by a point mutation in the *LMNA* gene (c. 1824C>T) (Eriksson et al., 2003; De Sandre-Giovannoli et al., 2003). This mutation disrupts the post-translational processing of pre-lamin A, a major component of the nuclear lamina, by activating a cryptic splice site, causing an in-frame deletion of 50 amino acids near the C-terminus. Under healthy conditions, prelamin A is post-translationally modified by two transfer reactions, adding a farnesyl and carboxymethyl group, and two proteolytic cleavages that remove these groups to form mature lamin A (Musich and Zou, 2009). The mutated protein in HGPS, called progerin, lacks sites for endoproteolytic cleavage and remains farnesylated and carboxymethylated (Ahmed et al., 2018; Eriksson et al., 2003). At the cellular level, this leads to increased inflammation (Osorio et al., 2012), accelerated senescence (Cao et al., 2011; Wheaton et al., 2017; Benson et al., 2010), and stem cell dysfunction (Scaffidi and Misteli,

2008; Espada et al., 2008; Rosengarten et al., 2011). Progerin accumulates in the nuclear lamina causing abnormal nuclear shapes and protrusions (“blebs”) (Goldman et al., 2004), defects in DNA repair mechanisms (Gonzalo and Kreienkamp, 2015), epigenetic alterations (Shumaker et al., 2006), loss of heterochromatin (Goldman et al., 2004; McCord et al., 2013), and nuclear stiffening (Booth et al., 2015). While it is not yet fully understood how progerin causes cellular and nuclear dysfunction, a disruption to mechanotransduction appears to play a significant role.

Nuclear mechanotransduction and the impact of laminopathies

Mechanotransduction within the nucleus occurs through the nuclear envelope. This structure is comprised of the outer nuclear membrane (ONM), the inner nuclear membrane (INM), the perinuclear space between the ONM and INM, nuclear pore complexes (NPCs), and the nuclear lamina (Kalukula et al., 2022). The nuclear envelope is connected to the cytoskeleton via the linker of nucleoskeleton and cytoskeleton (LINC) complex. Actin filaments, microtubules, or intermediate filaments in the cytoplasm bind directly or indirectly to nesprin proteins that are localized to the ONM (Figure 1). Within the perinuclear space, these nesprins bind SUN (Sad1p, UNC-84) domain-containing proteins that span the INM and connect to the lamins of the nuclear lamina, NPCs, or directly to chromatin (Crisp et al., 2006; Kalukula et al., 2022). The nuclear lamina, comprised of A-type lamins (lamin A and C) and B-type lamins (lamin B1 and B2) bind with NPCs, LINC complex proteins, and chromatin (Burke and Stewart, 2013; de Leeuw et al., 2018). These elements provide a direct link from the cytoskeleton to DNA and facilitate changes in gene expression that occur in response to mechanical stimuli. The role of the LINC complex in vascular mechanotransduction was recently reviewed (Bougaran and Bautch, 2024) and only key features will be noted here.

The nuclear lamina is essential for maintaining nuclear structure and organization of the genome (Gruenbaum and Foisner, 2015). Lamins provide a structural scaffold, anchoring chromatin and transcription factors to the nuclear periphery. This anchoring facilitates the compartmentalization of the genome, which is essential for accurate DNA transcription, replication, and repair. Furthermore, lamin expression levels are directly associated with nuclear mechanical stability, as well as tissue rigidity and plasticity. Higher amounts of lamin A and C correlate with increased nuclear stiffness, while lower amounts result in more deformable and fragile nuclei (Maurer and Lammerding, 2019). Lamins recruit DNA damage response machinery and regulate transcription factor binding. They also modulate heterochromatin, domains of densely packed DNA that are transcriptionally repressed and anchor it to the nuclear periphery (Camozzi et al., 2014). Specifically, lamin A interacts with INM proteins to regulate the location of heterochromatin based on extracellular mechanical stresses (Capanni et al., 2009; Maraldi et al., 2011; Solovei et al., 2013). Lamins also bind and anchor transcription factors to the nuclear periphery, regulating expression of the genes associated with these factors (Gruenbaum and Foisner, 2015). Dysfunctional lamin

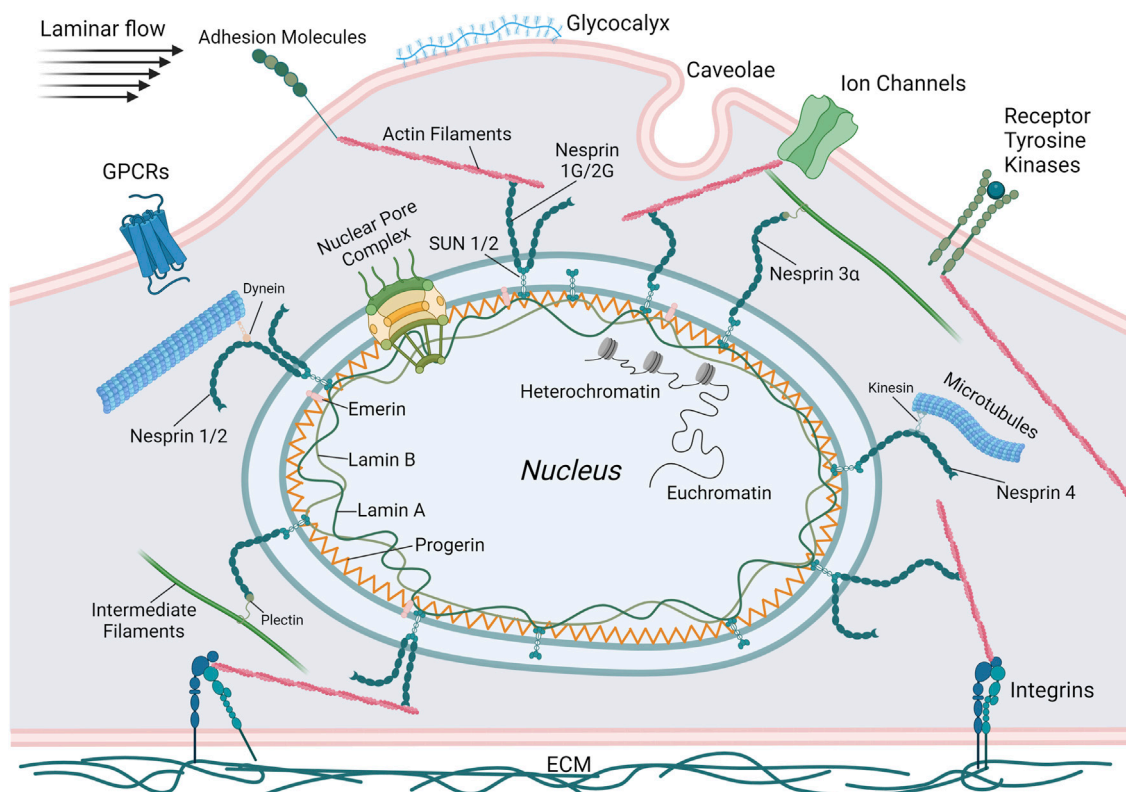


FIGURE 1 Schematic illustrating the primary mechanosensing elements of ECs including G-protein coupled receptors (GPCRs), adhesion molecules, ion channels, receptor tyrosine kinases, integrins, caveolae, and the glycocalyx. Also depicted are the components of the LINC complex. Lamins and, in the case of HGPS, progerin, are localized to the nuclear periphery and bind DNA or transcription factors. SUN proteins bridge the nuclear membrane, connecting intranuclear lamins with extranuclear KASH proteins (nesprins 1–4). These nesprins then bind to the cytoskeletal elements actin, microtubules, and intermediate filaments that are connected to or influenced by the various mechanosensors. Thus, the complete mechanotransductive pathway that regulates gene expression in response to external mechanical stresses can be visualized. This figure was generated using BioRender.

A, like that seen in HGPS, can detrimentally alter its ability to maintain appropriate nuclear mechanical properties and regulate gene expression.

In addition to lamins regulating gene expression through the organization of heterochromatin and transcription factors, there are several other ways that mechanical forces influence the activation or repression of genes. Mechanical stresses can induce nuclear deformations that result in immediate stretching of chromatin through the connections of the cytoskeleton and LINC complex (Tajik et al., 2016). While not completely understood, the prevailing theory is that chromatin opening reveals previously inaccessible areas of the genome, resulting in rapid transcription of mechanosensitive genes (Dupont and Wickström, 2022; Kirby and Lammerding, 2018). In addition to the direct stretching of chromatin, these nuclear deformations can also stretch the NPCs localized within the nuclear envelope. NPCs allow the exchange of macromolecules between the nucleus and cytoplasm. NPCs are governed by the binding of soluble nuclear transport factors and transport signals (e.g., nuclear localization sequences or nuclear export sequences) to macromolecules that then allow docking to and transport through the NPC (Strambio-De-Castilla et al., 2010). Stretching of the nuclear membrane increases the diameter of the NPC opening, allowing import of mechanoresponsive

transcriptional regulators like YAP (Yes-associated protein) (Elosegui-Artola et al., 2017). Depending on the nature of the mechanical force and the resultant deformation of the nuclear membrane, NPC stretching can promote nuclear export, or the NPC opening can constrict, inhibiting exchange of macromolecules (Kalukula et al., 2022). The nuclear membrane also controls stretch-sensitive ion channels that can be opened during nuclear deformations induced by mechanical stresses. These channels allow increased uptake of calcium into the nucleus, altering chromatin organization (Nava et al., 2020). Finally, external forces can induce conformational changes and increase phosphorylation of lamins (Buxboim et al., 2014b; Swift et al., 2013). Lamin conformational changes can expose residues, altering interactions with other proteins and downstream signaling (Ihalainen et al., 2015), while lamin phosphorylation influences their nucleo-cytoskeletal coupling (Guilluy et al., 2014), chromatin binding (Liu and Ikegami, 2020), and regulation of nuclear stiffness through lamin disassembly (Buxboim et al., 2014a). Due to truncation of amino acids, progerin lacks some of the major phosphorylation sites found on lamin A (Ao et al., 2023). This reduces its rate of phosphorylation in response to mechanical stimuli (Cho et al., 2018) and promotes cellular senescence (Ao et al., 2023).

Laminopathies like HGPS result from mutations that alter lamin function or expression. There are two prevailing hypotheses as to how these dysfunctional lamins cause disease: (1) mutant lamins make the nucleus more fragile, resulting in greater nuclear ruptures and cell death, particularly in tissues exposed to high mechanical stresses, and (2) lamin mutations alter gene expression through impaired chromatin interactions or inhibition of transcription factor binding (Maurer and Lammerding, 2019). Nuclear mechanotransduction can influence both proposed mechanisms. Cells with lamin A mutations or deletions exhibit increases in nuclear ruptures following mechanical loading that leads to greater cell death (Lammerding et al., 2004; Kim et al., 2021; Earle et al., 2020; Kim et al., 2024; Sears and Roux, 2022). Of note, decreased levels of lamin A correspond to more deformable nuclei with increased fragility, making them more susceptible to rupture (Lammerding et al., 2004). In contrast, some lamin A mutations, like those that produce progerin, increase nuclear stiffness (Dahl et al., 2006), reducing its compliance and ability to deform under mechanical loading, resulting in a greater susceptibility to rupture (Kim et al., 2021; Yue et al., 2023; Verstraeten et al., 2008). Preceding cell death, nuclear rupture can also promote senescence and the production of pro-inflammatory cytokines known as the senescence-associated secretory phenotype (SASP). Genomic DNA released into the cytosol following nuclear rupture binds to cyclic GMP-AMP synthase (cGAS), which triggers SASP production (Dou et al., 2017; Glück et al., 2017). HGPS and other laminopathies also cause DNA damage. This can occur through dysfunctional nuclear-cytoskeletal coupling, in the form of nuclear membrane rupture (Kalukula et al., 2022), that causes impaired recruitment (Liu et al., 2005) or cytoplasmic mislocalization (Xia et al., 2018) of DNA damage response factors.

Progerin can change the epigenetic landscape by altering the state of histone methylation, specifically reducing methylation of histone 3 on lysine 9 (H3K9) and H3K27, while increasing methylation of H4K20 (Shumaker et al., 2006; Columbaro et al., 2005). Progerin is also involved in the regulation of histone deacetylases (HDACs), with HGPS cells showing a loss of HDAC1 that correlated with heterochromatin defects (Pegoraro et al., 2009). While these epigenetic changes seen with HGPS have yet to be directly correlated with aberrant nuclear mechanotransduction, there is evidence for their regulation in response to mechanical stimuli under other conditions (Kalukula et al., 2022). Changes to nuclear mechanics induced by progerin accumulation may contribute to the apparent epigenetic alterations. H3K9me3 is suppressed in cardiomyocytes and dissociates from the nuclear periphery during environmental stiffening that reduces nuclear deformations, presumably increasing nuclear stiffness (Seelbinder et al., 2021). A similar mechanism of epigenetic alteration could be imagined in HGPS, where progerin accumulation leads to nuclear stiffening and an impairment of its response to mechanical stimuli (Booth et al., 2015), leading to a reduction in histone methylation. These detriments to nuclear structure and genome stability seen in HGPS are especially prevalent in cells under constant biomechanical stress, like those of the vasculature. Moreover, progerin accumulation within the nucleus can alter mechanotransduction pathways leading to cellular dysfunction.

Mechanotransduction in healthy endothelial cells

The arterial endothelium is exposed to two primary stresses (force per unit area) in the body: shear stress from the flow of blood and circumferential stress due to stretching of arteries from increases in blood pressure (Hahn and Schwartz, 2009). Responses to these forces modulate critical homeostatic functions such as inflammation, vasomotor tone, and vascular remodeling (Chiu and Chien, 2011). ECs sense these forces in a variety of ways such as ion channels (e.g., Piezo1, TRPV4, inner-rectifier K⁺ channel), G protein-coupled receptors (GPCRs), tyrosine kinase receptors (e.g., VEGFR2), caveolae, the glycocalyx, and integrins (Figure 1). (See (Davis et al., 2023) for an extensive review). Increases in laminar shear stress, brought on by increasing blood flow due to altered physical activity such as exercise, induce ECs to generate prostacyclin and nitric oxide (NO). These molecules promote relaxation of smooth muscle cells (SMCs) in the vascular media, providing control over vasomotor tone and ultimately blood pressure (Davies, 1995). Prostacyclin, additionally, promotes SMC health and function by increasing transcription of transgelin (SM22 α), which results in a more contractile SMC phenotype (Tsai et al., 2009). NO is generated in response to shear stress through the platelet/endothelial cell adhesion molecule 1 (PECAM1)/vascular endothelium (VE)-cadherin/vascular endothelial growth factor receptor 2 (VEGFR2) complex. Initially, PECAM1 is phosphorylated in response to flow and activates a Src family kinase. VE-cadherin associates with VEGFR2 (also known as FLK1) and brings it into proximity with PECAM1. VEGFR2 is then activated by the Src family kinase and proceeds to recruit and activate phosphoinositide 3-kinase (PI3K). PI3K then phosphorylates endothelial nitric oxide synthase (eNOS) in an Akt-dependent manner. This phosphorylated eNOS, through a series of redox reactions, produces NO to relax SMCs and dilate the vessel (Tzima et al., 2005). ECs can also modulate vascular tone by releasing potassium through calcium-sensitive potassium channels that transport the potassium to the SMCs, triggering hyperpolarization and relaxation (Garland and Dora, 2017).

In addition to generating NO, shear forces also cause ECs to align in the direction of flow. This reorganization of the cytoskeleton is mediated by the PECAM1/VE-cadherin/VEGFR2 complex as well. Specifically, PI3K promotes conformational activation of integrins that, in turn, activate small GTPases (Rac, Rho, and CDC42), which regulate cell-cell junctions and remodeling of the actin cytoskeleton to elongate and align ECs in the flow direction (Osborn et al., 2006; Hahn and Schwartz, 2009). The cytoskeleton is critical for EC sensing and reacting to external stimuli as inhibiting actin, microtubules, or intermediate filaments block many EC responses to flow (Hahn and Schwartz, 2009).

Shear stresses have a direct effect on the nucleus and LINC complex in ECs. Cytoskeletal reorganization under flow leads to protrusion of the nucleus, exposing it to higher shear stresses than the rest of the cell (Tkachenko et al., 2013; Barbee et al., 1994; Barbee et al., 1995). Like the cell body cytoskeleton, the nucleus elongates in the direction of flow, providing a visual confirmation for its mechanosensing capacity (Danielsson et al., 2022b; Nava et al., 2020; Deguchi et al., 2005). Within the nuclear envelope, the LINC complex proteins exhibit essential functions in regulating

TABLE 1 Summary of the major findings from studies showing a disrupted mechanotransduction pathway in ECs expressing progerin.

Model	Major findings	Reference
<i>in vitro</i> (HUVECs expressing progerin)	<ul style="list-style-type: none">• Significant EC loss and increase in apoptosis markers under physiological shear stress• EC death was rescued by FTI treatment or pre-aligning HUVECs to flow direction	Danielsson et al. (2022a)
<i>in vitro</i> (HUVECs expressing progerin)	<ul style="list-style-type: none">• Physiological shear stress had no effect on chromatin dynamics, possibly due to increased nuclear stiffness	Booth et al. (2015)
<i>in vitro</i> (iPSC-derived ECs from HGPS patients)	<ul style="list-style-type: none">• Lower eNOS expression under physiological flow• Increased E-selectin and VCAM1 expression	Atchison et al. (2020)
<i>in vivo</i> (EC-specific progerin expression mouse model)	<ul style="list-style-type: none">• Elevated levels of ICAM1 in lung endothelium• Reduced eNOS levels and NO production• Significantly reduced Sirt7 levels• Treatment with AAV encoding Sirt7 increased average lifespan by 76%	Sun et al. (2020)
<i>in vivo</i> (EC-specific progerin expression mouse model)	<ul style="list-style-type: none">• ECs in descending aorta did not align with blood flow• Reduced levels of eNOS, likely from accumulation of MRTFA at nuclear periphery, and NO production• Treatment with MRTFA inhibitor rescued eNOS levels	Osmanagic-Myers et al. (2019)

HUVECs, human umbilical vein endothelial cells; FTI, farnesyltransferase inhibitor; iPSC, induced pluripotent stem cell; VCAM1, vascular cell adhesion molecule 1; ICAM1, intercellular adhesion molecule 1; eNOS, endothelial nitric oxide synthase; NO, nitric oxide; AAV, adeno-associated virus; MRTFA, myocardin-related transcription factor A.

many EC mechanotransductive pathways. SUN1 and 2 regulate nesprin-1 interactions with microtubules, which influences signaling of the small GTPase Ras homology family (Rho) proteins that alter cell-cell junctions or induce expression of EC tight junction proteins, leading to increased barrier function (Yang et al., 2020; Buglak et al., 2023).

In ECs, many transcription factors and transcriptional coactivators are upregulated in response to laminar shear stresses. These, along with the alteration of histone acetylation and phosphorylation induced by flow (Chen et al., 2008; Wang et al., 2010; Chen et al., 2010), modulate gene expression. Krüppel-like Factor (KLF) 2 and 4 and nuclear factor erythroid 2-related factor 2 (NRF2) are transcription factors critical to maintaining EC homeostasis. KLF2 expression is upregulated by phosphorylation and nuclear export of histone deacetylase 5 (HDAC5) in response to shear. Specifically, KLF2 induces eNOS expression and inhibits pro-inflammatory signaling through suppression of vascular cell adhesion molecule 1 (VCAM1) and E-selectin. KLF2 recruits the histone acetyltransferase p300 and outcompetes nuclear factor-κB (NF-κB), which promotes the expression of inflammatory genes (SenBanerjee et al., 2004; Dekker et al., 2002). In addition to increased recruitment, hemodynamic shear stress increases the activity of the transcriptional coactivator p300, which leads to increased eNOS transcription (Chen et al., 2008). YAP is another transcriptional coactivator that regulates many functions in ECs. Its phosphorylation leads to its proteasomal degradation in the cytosol, while dephosphorylation results in nuclear localization and activation of genes (Dupont et al., 2011). YAP nuclear localization is increased by the resultant NPC opening from mechanically stretching cells (Elosegui-Artola et al., 2017). Its translocation is also dependent on nuclear compression. Nuclei that became softer after silencing of lamin A/C experienced greater compression and elevated YAP nuclear localization (Koushki et al., 2023). Laminar flow promotes YAP phosphorylation in ECs, inhibiting its nuclear localization,

through activation of G-protein-integrin interactions and RhoA inhibition (Wang et al., 2016a). YAP suppression downregulates pro-inflammatory gene expression such as monocyte chemoattractant protein-1 (MCP1), intercellular adhesion molecule-1 (ICAM1), and vascular cell adhesion molecule-1 (VCAM1) (Liu et al., 2019; Xu et al., 2016; Wang et al., 2016b). In contrast, YAP activation promotes inflammation and proliferation in ECs (Wang et al., 2016a). How the shear stress response of ECs is disrupted in HGPS is not completely understood, but several studies have started to reveal possible mechanisms that relate EC dysfunction with an impaired mechanosensing ability.

Disruption of mechanotransduction in HGPS endothelial cells

Many of the homeostatic functions of ECs discussed in the previous section are diminished or even reversed under disturbed flow that generates low, oscillatory shear stresses around vessel branches or in curved arteries (Andueza et al., 2020; Jiang et al., 2014; Lee et al., 2012) (Table 1). When exposed to disturbed flow, ECs lose their ability to regulate vasomotor tone by inducing SMC relaxation and vessel dilation (Chiu and Chien, 2011). This is caused by a reduction in KLF2/4, which activates eNOS and NO production under physiological laminar shear (Andueza et al., 2020; Jiang et al., 2014). Phosphorylation of eNOS is also reduced due to inhibition of the mechanosensitive adenosine monophosphate-activated protein kinase (AMPK) pathway (Guo et al., 2007). Disturbed flow increases EC inflammation due to reduced KLF2 expression (SenBanerjee et al., 2004), increased YAP/TAZ nuclear localization (Wang et al., 2016a; Wang et al., 2016b), and enhanced NF-κB activity (Nagel et al., 1999). It also reduces autophagic flux (Vion et al., 2017) and increases endoplasmic reticulum stress (Civelek et al., 2009). Additionally, ECs lose their migratory capacity and exhibit impaired alignment with the flow direction due to, in part, a

disruption of nuclear-cytoskeletal coupling by loss of nesprin-1 (Chancellor et al., 2010; Denis et al., 2021; King et al., 2014). Moreover, low shear stresses (5 dynes/cm²) decrease nesprin -2 and lamin A in ECs, which leads to an increase in apoptosis (Han et al., 2015).

When exposed to the more uniform laminar flow conditions in straight regions of blood vessels, HGPS ECs mirror the dysfunction seen under disturbed flow, indicating an inability to respond to external mechanical stimuli, presumably because of progerin accumulation within the nucleus. Several *in vitro* studies have shown HGPS EC dysfunction in response to laminar shear stress. Danielsson and colleagues expressed progerin in human umbilical vein endothelial cells (HUVECs) and exposed them to physiological shear (12 dynes/cm²) for 3 days. They found significant cell loss and increased markers of apoptosis compared to control HUVECs (Danielsson et al., 2022a). These responses were rescued by treatment with a farnesyltransferase inhibitor (FTI), that prevents progerin accumulation at the nuclear periphery (Yang et al., 2006), or, interestingly, by pre-aligning the HUVECs to flow prior to inducing progerin expression (Danielsson et al., 2022a). This suggests that progerin accumulation inhibits ECs ability to respond to flow, and that this impairment can result in increased EC apoptosis. HGPS ECs have lower eNOS expression after exposure to steady laminar shear stress for 24 h (Atchison et al., 2020; Gete et al., 2021), increased inflammation (Atchison et al., 2020; Osmanagic-Myers et al., 2019; Sun et al., 2020), and an inability to properly align under physiological flow (Osmanagic-Myers et al., 2019; Danielsson et al., 2022a). Treatment of HGPS ECs with the FTI lonafarnib or the rapamycin analog Everolimus restored eNOS and KLF2 expression (Abutaleb et al., 2023).

Another study measured chromatin dynamics under 20 dynes/cm² shear stress in HUVECs treated with exogenously expressed progerin (Booth et al., 2015). External forces had no effect on chromatin dynamics in HUVECs expressing progerin compared to untreated HUVECs, possibly due to the increased nuclear stiffness caused by progerin accumulation (Verstraeten et al., 2008). This suggests a disruption in the nuclear mechanotransduction pathway that can alter chromatin organization, and possibly inhibit the regulation of critical mechanoresponsive genes.

Tissue-engineered blood vessels (TEBVs) prepared using induced pluripotent stem cell (iPSC)-derived ECs and SMCs from HGPS patients (viECs) (Atchison et al., 2020) showed suppressed dilation in response to acetylcholine (ACh) and increases in E-selectin and VCAM1 expression (Atchison et al., 2020). These results suggest a disruption in the mechanosensing pathway, inhibiting eNOS upregulation and promoting a pro-inflammatory response under laminar flow conditions.

Two *in vivo* studies using HGPS mouse models corroborated some of the findings from *in vitro* experiments. In both models, mice solely express progerin in ECs, allowing the investigation of their effects on HGPS vascular pathology without the influence from other vascular cells. Using single-cell transcriptomics analysis, Sun and colleagues found significant increases in the inflammatory response in the lung endothelium of EC-specific progerin expressing mice, with elevated levels of ICAM1 (Sun et al., 2020). They supported these findings by overexpressing progerin in HUVECs and showing significantly elevated levels of

inflammatory genes. Relative to controls, progerin-expressing ECs exhibited significantly attenuated relaxation of the thoracic aorta in response to ACh and reduced eNOS levels. Sodium nitroprusside treatment, which induces SMC relaxation in an EC-independent manner (Bonaventura et al., 2008), was unaffected, suggesting the dysfunction is due to progerin-expressing ECs. In progerin-expressing ECs, levels of Sirtuin 7 (Sirt7), a nicotinamide adenine dinucleotide (NAD⁺)-dependent deacylase were reduced significantly. Further, enhanced interactions of Sirt7 and progerin compared to lamin A resulted in increased polyubiquitination of the Sirt7. Treatment with an adeno-associated viral vector encoding Sirt7 resulted in a 76% increase in average lifespan (Sun et al., 2020). While EC response to mechanical stimuli was not directly measured in this study, the detrimental effects of progerin expression, such as increased inflammation and reduced eNOS and NO production, suggest dysfunctional mechanosensing.

In another EC-specific progerin expressing mouse model (Osmanagic-Myers et al., 2019), ECs within the descending aorta were not aligned with the direction of blood flow. Progerin-expressing ECs exposed to 12 dynes/cm² shear stress *in vitro* did not align with flow or exhibit nuclear elongation. Progerin-expressing ECs also showed reduced levels of eNOS, which resulted in lower systemic NO levels. To determine possible mechanisms for this dysfunctional response to shear stresses, the authors found upregulation of both SUN1 and 2 as well as an increase in actin polymerization, which may have been caused by a mislocalization of emerin (a nuclear envelope protein that regulates expression of mechanosensitive genes) into discrete aggregates (Osmanagic-Myers et al., 2019).

SUN1 expression also increased in another HGPS mouse model and human HGPS fibroblasts (Chen et al., 2012). This led to increases in nuclear defects and cellular senescence, with the reduction in heterochromatin due to increased SUN1 expression appearing to play a role. SUN1 knockdown significantly decreased cellular senescence in HGPS fibroblasts and more than doubled the lifespan of progeroid mice (Chen et al., 2012). The upregulation of SUN1 in progerin-expressing ECs, seen by Osmanagic-Myers and colleagues (Osmanagic-Myers et al., 2019), may have contributed to the dysfunctional cell response to mechanical stimuli. Additionally, a recent study evaluating the effects of cyclic stretch on mesenchymal stromal cells from a *Zmpste24*^{-/-} mouse model supports the contribution of increased SUN2 expression and actin polymerization in promoting cellular dysfunction (Yue et al., 2023). The *Zmpste24*^{-/-} model lacks the metalloprotease needed to cleave the farnesyl group from prelamin A during posttranslational processing. This results in a permanently farnesylated prelamin A that accumulates at the nuclear envelope, similarly to progerin, leading to misshapen nuclei, increased nuclear stiffness, and elevated cellular senescence (Mu et al., 2020). This model exhibited increases in SUN2 expression, actin polymerization, and nuclear stiffness that correlated with increased DNA damage and cellular senescence. SUN2 suppression reduced DNA damage and senescence following mechanical loading. This response was potentially mediated by nuclear decoupling and softening as polymerized actin levels and nuclear stiffness also decreased with SUN2 knockdown (Yue et al., 2023). Though not directly measured, an increased nuclear stiffness due to elevated SUN2 expression and subsequent actin polymerization may have influenced the impaired

shear response of ECs (Booth et al., 2015; Danielsson et al., 2022a) seen by Osmanagic-Myers and colleagues (Osmanagic-Myers et al., 2019). These authors also found increased accumulation of myocardin-related transcription factor A (MRTFA) at the nuclear periphery, associated with progerin. MRTFA binds to the eNOS promoter region and reduces its expression (Fang et al., 2011). The enhanced localization of MRTFA at the nuclear periphery in progerin-expressing ECs appeared to increase its association with eNOS leading to eNOS suppression. Treating ECs with a small molecule MRTFA inhibitor (CCG-203971) rescued eNOS levels. Importantly, MRTFA is a mechanosensitive transcription factor whose nuclear localization is increased by emerin expression and subsequent actin polymerization (Osmanagic-Myers et al., 2019). Collectively, this study provides evidence for the impact of progerin expression on the ability of ECs to properly respond to mechanical stimuli. Understanding what other mechanotransduction pathways might be affected in ECs will be an important next step for determining how to mitigate their dysfunctional response.

Mechanotransduction in healthy vascular smooth muscle cells

Vascular SMCs are exposed to intraluminal stresses caused by changes in blood pressure that lead to stretch that depends on the extent of vessel dilation and cell orientation (Davis et al., 2023). A phenomenon known as the myogenic response causes SMCs in arterioles to constrict in response to increases in luminal pressure. This response does not require an intact endothelium or innervation, although it can be influenced by them (Davis and Hill, 1999). The myogenic response has several physiological functions, primarily establishing a basal vascular tone and responding to changes in blood flow. Ion channels are most likely involved in the force sensing mechanism (see Ref (Davis et al., 2023) for an extensive review). Ion channels are activated by mechanosensing GPCRs such as angiotensin II type 1 receptor (AT1R). Cell stretching changes GPCR conformation, allowing it to activate an associated G protein (Zou et al., 2004). The activated ion channels cause a depolarization of the SMC plasma membrane, which stimulates voltage-gated calcium channels, leading to an increase in intracellular calcium. The increased calcium activates myosin light chain 20 (MLC20), resulting in vasoconstriction (Davis et al., 2023). In addition to ion channels, GPCRs activate enzymes such as Ras homology family A (RhoA). This enzyme controls the activity of several downstream effector proteins that impact SMC proliferation, migration, differentiation, and contractility. For example, the effector protein, Rho associated coiled-coil containing protein kinase 2 (ROCK2) alters contractility by promoting phosphorylation of MLC20 (de Godoy and Rattan, 2011).

Mechanical forces significantly influence gene expression and phenotype changes in SMCs, particularly under pathological conditions (Owens et al., 2004). *In vitro*, physiological stretching of cells ($\leq 10\%$) results in maintenance of a contractile phenotype (Mao et al., 2012; Reusch et al., 1996; Yao et al., 2014; Huang et al., 2015), while supraphysiological stretching decreases the expression of contractile genes encoding proteins such as calponin, transgelin, α -smooth muscle actin, and myosin heavy chain 11 (Wang et al., 2018; Wan et al., 2015; Hu et al., 2014). Upregulation of contractile

proteins under physiological loading appears to be matrix-dependent, with SMCs cultured on basement membrane laminin showing the greatest upregulation and those cultured on fibronectin showing no upregulation (Reusch et al., 1996). Correspondingly, cyclic stretching regulates integrin expression to influence interactions with extracellular matrix (ECM) and downstream mechanotransduction pathways (Mao et al., 2012).

Transforming growth factor β and sirtuin pathways are implicated in the regulation and maintenance of a contractile SMC phenotype (Yao et al., 2014; Huang et al., 2015). HDACs also contribute to SMC phenotype regulation, with HDAC7 being upregulated and HDACs 3 and 4 being downregulated in a more contractile, quiescent phenotype (Yan et al., 2009). Changes to the SMC phenotype were influenced by both matrix stiffness and stretching through regulation of RhoA-ROCK2 and calcium influx pathways, respectively (Swiatlowska et al., 2022). Discoidin domain receptor-1 (DDR1) is a membrane protein that acts as a mechanosensor after binding to collagen (Ngai et al., 2020). Increased stiffness of the ECM, which occurs as HGPS progresses, leads to increased expression and activation of DDR1. This leads to YAP activation (Ngai et al., 2022) and stress fiber formation and expression of genes involved in calcification. Further, YAP activation leads to further DDR1 expression creating a positive feedback loop promoting vessel stiffness (Ngai et al., 2022).

Disruption of mechanotransduction in HGPS smooth muscle cells

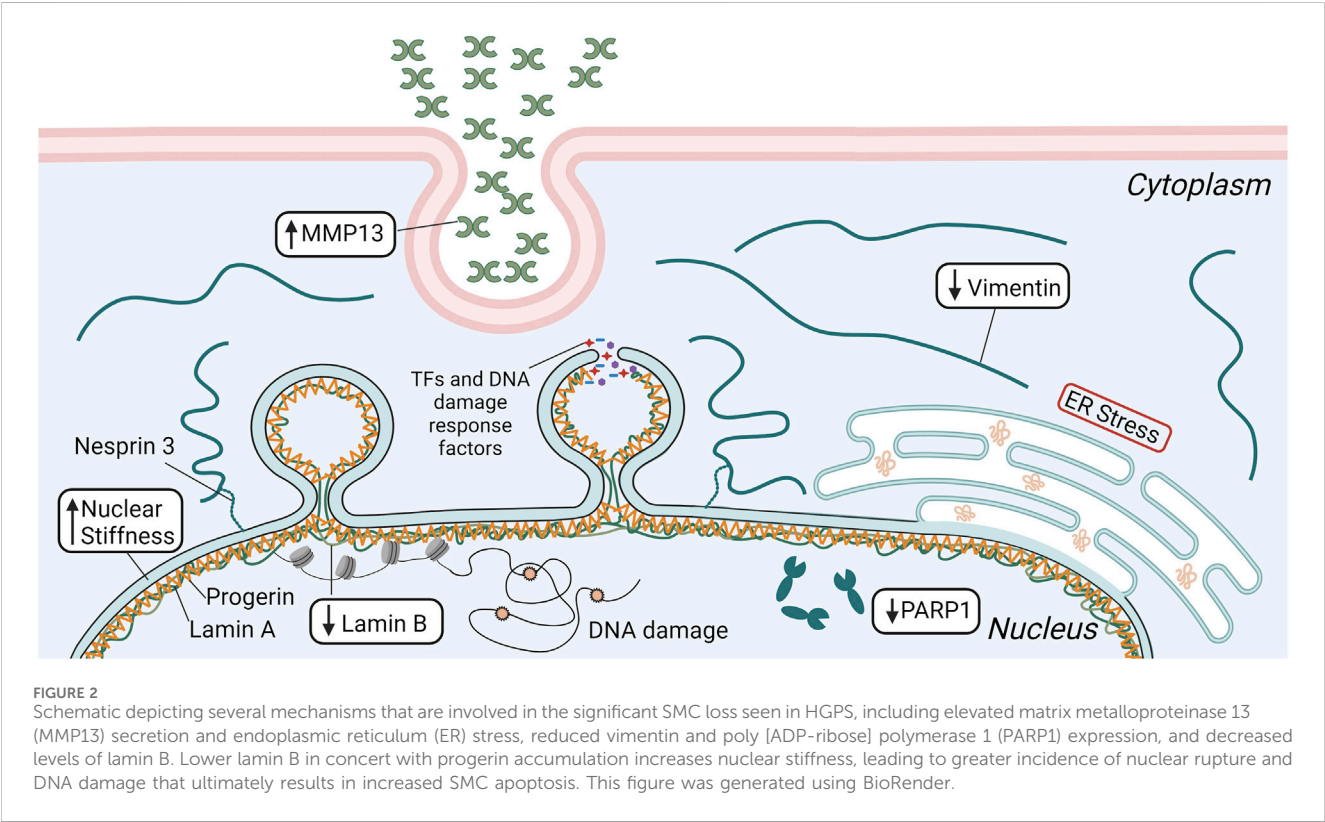
While HGPS ECs clearly show some level of dysfunction in response to physiological shear stresses, the substantial decrease in the number of SMCs within the medial layer of large arteries (Varga et al., 2006) is believed to be the driver of the cardiovascular dysfunction in HGPS. As such, many studies have attempted to determine the mechanism behind this significant reduction in cellular content unique to the vascular media. Although the loss of SMCs is the predominant feature associated with HGPS pathology, there is also an SMC dysfunction that appears to be attributed, at least in part, to altered mechanotransduction, including increased inflammation (Ribas et al., 2017), elevated DNA damage (Kim et al., 2021), and reduced contractile response (de Godoy and Rattan, 2011; Murtada et al., 2020) (Table 2). While HGPS SMCs do manifest a dysfunctional contractile response (Del Campo et al., 2020; Murtada et al., 2020), the myogenic response and SMC phenotype switching in HGPS have not been examined.

Exposing SMCs derived from iPSCs of HGPS donors to 16% cyclic stretch for 24 h resulted in an increased inflammatory response, through upregulation of IL-1 β and IL-6, as well as elevated levels of DNA damage (Ribas et al., 2017). While 16% stretch is generally considered pathological (Jensen et al., 2021), these deleterious results were not seen in non-HGPS controls, indicating the HGPS SMCs have a comparatively dysfunctional mechanoreponse to cyclic stretching. Treatment of these SMCs with an FTI or statin attenuated the inflammatory response to mechanical forces, suggesting progerin expression plays a role in this response. While no direct mechanism was determined for the increased inflammation, HGPS cells cultured under static conditions

TABLE 2 Summary of the major findings from studies showing a disrupted mechanotransduction pathway in SMCs expressing progerin.

Model	Major findings	Reference
<i>in vitro</i> (iPSC-derived SMCs from HGPS patients)	<ul style="list-style-type: none">Increased IL-1β and IL-6 expression and elevated levels of DNA damage after 16% cyclic stretch for 24 hTreatment with FTI or statin reduced inflammatory response under cyclic stretching	Ribas et al. (2017)
<i>in vivo</i> (G608G BAC mouse model of HGPS that expresses human progerin)	<ul style="list-style-type: none">At 12 months, significant SMC loss in ascending aorta but not descending aortaReduction of intermediate filament protein vimentin in SMCs of ascending aorta	Song et al. (2014)
<i>in vivo</i> (G609G mouse model of HGPS that expresses mouse progerin)	<ul style="list-style-type: none">Fewer SMCs at regions of disturbed flow within the aortaDisrupting the LINC complex increased SMC content in the ascending aorta by 65%	Kim et al. (2018)
<i>in vitro</i> (mouse aortic SMCs expressing human progerin)	<ul style="list-style-type: none">Increasing lamin B1 led to 80% reduction in nuclear membrane ruptures, lower DNA damage levels, and increased cell survival after stretchingElevated lamin B1 decreases nuclear stiffness by 23%	Kim et al. (2021)

FTI, farnesyltransferase inhibitor; iPSC, induced pluripotent stem cell.



did not express the inflammatory markers (Ribas et al., 2017). Several *in vivo* studies using HGPS mouse models have also shown increased SMC dysfunction, though not always in the context of impaired mechanotransduction. One study that focused on the biomechanical changes of the vasculature with disease progression found, in addition to significant SMC loss, there was a total loss of vessel constriction capacity (Murtada et al., 2020) in response to phenylephrine (PE), as opposed to increased luminal pressure. However, PE mediates contraction through the RhoA-ROCK pathway, which is reduced in HGPS models (Hale et al., 2008), and, as noted, RhoA-ROCK suppression induces a more synthetic phenotype in SMCs (de Godoy and Rattan, 2011). In addition, mice in which only SMCs express progerin, exhibited significantly lower vessel constriction by PE or KCl compared with control mice that did not express progerin

(Del Campo et al., 2020). Such a response was not observed in mice that expressed progerin in ECs alone.

In vivo studies observed significant SMC loss and vascular remodeling in the ascending aorta of a mouse model expressing human progerin after 12 months (Song et al., 2014). Interestingly, SMC loss did not occur in the descending aorta. The authors hypothesized this was due to the increased mechanical stresses within the ascending aorta, determining that the reduction in lumen diameter due to vascular remodeling of the ascending aorta could lead to significantly higher mechanical stresses not experienced by the descending aorta or within the ascending aorta of healthy controls (Song et al., 2014). Others have also seen differences in disease severity between different vascular regions, with the areas exposed to the highest mechanical forces being most affected (Murtada et al., 2023). In addition to significant SMC loss, there

was also a reduction in intermediate filament proteins, particularly vimentin (Song et al., 2014) (Figure 2). These are important to many mechanotransduction pathways and help disperse mechanical stresses in cells (Hu et al., 2019). The descending aorta did not show the same vimentin reduction. In an *ex vivo* experiment using a microfluidic system, the descending aortas of WT and HGPS mice were exposed to high levels of shear stress (75 dynes/cm²). The WT samples did not show any changes in vimentin expression, but HGPS samples had a substantial reduction (Song et al., 2014). This study suggests that SMC loss seen in HGPS is dependent on the magnitude of pathological mechanical forces and that a potential mechanism involves the reduction in mechanotransduction related proteins.

Another *in vivo* study found a connection among components of the nucleoskeleton, pathological biomechanical forces, and loss of SMCs in an HGPS mouse model (Kim et al., 2018). The HGPS phenotype (e.g., greater ECM deposition and adventitial thickening with fewer SMCs) was more severe at regions of disturbed flow within the aorta. To determine if HGPS led to increased sensitivity to irregular mechanical stresses, progerin-expressing SMCs were stretched *in vitro* for 24 h. Stretching caused 40% of the SMCs to detach from the flexible membrane and these were determined non-viable, whereas WT SMCs were unaffected by the same mechanical regimen. The authors hypothesized that this response to mechanical forces may be due to the low levels of lamin B1 in SMCs combined with progerin expression, while WT SMCs are protected by their high levels of lamin A. They disrupted the connection between the nuclear and cytoskeleton by overexpressing the KASH domain of nesprin-2 (a component of the LINC complex). Since nesprins interact with SUN proteins through KASH domains, overexpressing the KASH domain of nesprin2 occupies SUN protein binding sites, preventing the connection between the nuclear and cytoskeleton and reducing the transmission of external forces to the nucleus (Kim et al., 2018). This disruption of the LINC complex greatly improved progerin-expressing SMC survival after stretching. *In vivo*, KASH overexpression increased SMC content to 65% of WT mice in the outer curvature of the ascending aorta, and, interestingly, adventitial fibrosis was eliminated. Improvements were also seen in the inner curvature of the ascending aorta, albeit, not as pronounced, where the pathology is more severe (Kim et al., 2018). This study suggests that the resilience of the nucleus to external mechanical forces is impaired by progerin expression, leading to nuclear damage and cell death. While the exact mechanism is unknown, the authors speculate it is due to the increased nuclear rigidity imparted by progerin accumulation in conjunction with the low levels of lamin B1 seen in SMCs (Kim et al., 2018).

Increasing lamin B1 in progerin-expressing SMCs leads to an 80% reduction in nuclear membrane ruptures, lower amounts of DNA damage, and increased cell survival after 2 hours of stretching. Elevated lamin B1 decreases nuclear stiffness by 23% (Kim et al., 2021). This suggests that in HGPS SMCs, lower nuclear compliance due to reduced lamin B1 and elevated progerin leads to greater incidence of nuclear membrane ruptures and cell death. *In vivo*, progerin expression increases with age, while lamin B1 decreases, and this correlates with increased nuclear membrane ruptures in the aortic SMCs of older HGPS mice (Kim et al., 2021). In healthy SMCs, lamin A forms an organized network on the nuclear membrane with openings of mean size around 0.085 μm^2 (Kim et al., 2024). However, when the SMCs express progerin, the network is less organized with larger openings through which blebs formed

(Figure 2). The blebs were associated with low levels of lamin B1. Overexpressing lamin B1 normalized the meshwork and reduced bleb formation. Collectively, these *in vivo* studies suggest that progerin accumulation leads to a dysfunction in the components of the nucleoskeleton of SMCs that impairs their ability to resist damage caused by elevated or disturbed external mechanical forces, leading to nuclear/DNA damage and cell death.

Future directions and conclusion

It is clear from *in vitro* and *in vivo* studies that the progerin accumulation negatively impacts mechanotransduction pathways in both ECs and SMCs. To what extent this impaired mechanoresponse influences the cellular dysfunction seen in HGPS needs additional study.

For ECs, it would be interesting to investigate the effect of modulating LINC complex proteins on their response to physiological flow, such as cell alignment, inflammation, and elevated expression of homeostatic proteins like eNOS, KLF2, and NRF2. Additionally, other mechanotransduction pathways important to EC homeostasis are disrupted in non-endothelial HGPS cells (Son et al., 2024; Kubben et al., 2016). As mentioned, in ECs, the mechanosensitive AMPK pathway activates eNOS to produce NO (Guo et al., 2007). This pathway was inhibited in HGPS fibroblasts and activating it rescued the HGPS phenotype, reducing progerin expression and DNA damage, while restoring heterochromatin marks (Son et al., 2024). Similarly, NRF2, which provides antioxidant protection and suppresses inflammation in ECs (Chen et al., 2006), is mislocalized in HGPS fibroblasts to the nuclear periphery by progerin, preventing its activation. Providing activated NRF2 prevented nuclear defects, lowered progerin expression, and reduced oxidative stress (Kubben et al., 2016). These pathways should be investigated in the context of EC mechanotransduction as they may also be inhibited by progerin expression. This could provide additional explanation for the impaired mechanoresponse of HGPS ECs. Also, understanding how nuclear mechanics change in ECs with progerin accumulation and how this might differ from SMCs could provide insight into ECs ability to survive the high shear stresses in larger arteries while SMCs cannot.

While it is unclear what causes the characteristic loss of SMCs in HGPS, progerin accumulation may decrease nuclear compliance leading to increased nuclear ruptures and cell death. Song and colleagues attributed this to the loss of vimentin in SMCs of the ascending aorta that are exposed to high shear stresses (Song et al., 2014). In support of this hypothesis, others have found vimentin to be necessary for nuclear resistance to deformation under mechanical strains (Neelam et al., 2015; Patteson et al., 2019). The nuclear elasticity imparted by vimentin reduces the incidence of nuclear rupture and DNA damage (Patteson et al., 2019). Studies with cultured cells indicate that loss of vimentin is compensated by increased ECM synthesis and stiffening of the ECM (Grolleman et al., 2023), which could then explain changes in the vessel wall composition and stiffness in HGPS. Moreover, increased endoplasmic reticulum stress (Hamczyk et al., 2019), elevated matrix metalloproteinase 13 expression (Pitrez et al., 2020), and increased poly (ADP-ribose) polymerase 1 expression (Zhang et al., 2014) influence SMC loss and treatment of the specific condition resulted in improved SMC survival.

Vascular dysfunction in HGPS is likely caused by multiple factors, with impaired mechanotransduction having an influence. Progerin accumulation not only affects the mechanosensing of the cell through disruption of the nuclear-cytoskeletal coupling, but can sequester transcription factors at the nuclear periphery, affecting their activity, and alter the epigenome. The long lifetime of progerin in large arteries can amplify any of these pathways (Hasper et al., 2023). While some studies involving HGPS SMCs suggest it is mainly the change in nuclear stiffness that promotes the pathological features, ones focused on ECs show protein mislocalization (e.g., MRTFA) or destabilization (e.g., Sirt7) having a prominent influence. Understanding how these two mechanisms of progerin accumulation alter cellular function in each of these vascular cells can influence what treatment methods may be required for improving the cardiovascular disease caused by HGPS.

Author contributions

KS: Investigation, Writing—original draft, Writing—review and editing. GT: Conceptualization, Funding acquisition, Investigation, Resources, Supervision, Writing—review and editing.

Funding

The author(s) declare that financial support was received for the research, authorship, and/or publication of this article. Supported by

NIH grant HL138252 (GAT) and an NIH predoctoral fellowship to KS (F31HL172589).

Acknowledgments

Figures were created using BioRender.

Conflict of interest

The authors declare that the research was conducted in the absence of any commercial or financial relationships that could be construed as a potential conflict of interest.

The author(s) declared that they were an editorial board member of Frontiers, at the time of submission. This had no impact on the peer review process and the final decision.

Publisher's note

All claims expressed in this article are solely those of the authors and do not necessarily represent those of their affiliated organizations, or those of the publisher, the editors and the reviewers. Any product that may be evaluated in this article, or claim that may be made by its manufacturer, is not guaranteed or endorsed by the publisher.

References

- Abutaleb, N. O., Atchison, L., Choi, L., Bedapudi, A., Shores, K., Gete, Y., et al. (2023). Lonafarnib and everolimus reduce pathology in iPSC-derived tissue engineered blood vessel model of Hutchinson-Gilford Progeria Syndrome. *Sci. Rep.* 13, 5032. doi:10.1038/s41598-023-32035-3
- Ahmed, M. S., Ikram, S., Bibi, N., and Mir, A. (2018). Hutchinson-0067ilford progeria syndrome: a premature aging disease. *Mol. Neurobiol.* 55, 4417–4427. doi:10.1007/s12035-017-0610-7
- Andueza, A., Kumar, S., Kim, J., Kang, D. W., Mumme, H. L., Perez, J. I., et al. (2020). Endothelial reprogramming by disturbed flow revealed by single-cell RNA and chromatin accessibility study. *Cell Rep.* 33, 108491. doi:10.1016/j.celrep.2020.108491
- Ao, Y., Wu, Z., Liao, Z., Lan, J., Zhang, J., Sun, P., et al. (2023). Role of C-terminal phosphorylation of lamin A in DNA damage and cellular senescence. *Cells* 12, 639. doi:10.3390/cells12040639
- Atchison, L., Abutaleb, N. O., Snyder-Mounts, E., Gete, Y., Ladha, A., Ribar, T., et al. (2020). iPSC-derived endothelial cells affect vascular function in a tissue-engineered blood vessel model of hutchinson-gilford progeria syndrome. *Stem Cell Rep.* 14, 325–337. doi:10.1016/j.stemcr.2020.01.005
- Barbee, K. A., Davies, P. F., and Lal, R. (1994). Shear stress-induced reorganization of the surface topography of living endothelial cells imaged by atomic force microscopy. *Circulation Res.* 74, 163–171. doi:10.1161/01.res.74.1.163
- Barbee, K. A., Mundel, T., Lal, R., and Davies, P. F. (1995). Subcellular distribution of shear stress at the surface of flow-aligned and nonaligned endothelial monolayers. *Am. J. Physiology-Heart Circulatory Physiology* 268, H1765–H1772. doi:10.1152/ajpheart.1995.268.4.H1765
- Benson, E. K., Lee, S. W., and Aaronson, S. A. (2010). Role of progerin-induced telomere dysfunction in HGPS premature cellular senescence. *J. Cell Sci.* 123, 2605–2612. doi:10.1242/jcs.067306
- Bonaventura, D., Lunardi, C. N., Rodrigues, G. J., Neto, M. A., and Bendhack, L. M. (2008). A novel mechanism of vascular relaxation induced by sodium nitroprusside in the isolated rat aorta. *Nitric Oxide* 18, 287–295. doi:10.1016/j.niox.2008.02.004
- Booth, E. A., Spagnol, S. T., Alcoser, T. A., and Dahl, K. N. (2015). Nuclear stiffening and chromatin softening with progerin expression leads to an attenuated nuclear response to force. *Soft Matter* 11, 6412–6418. doi:10.1039/c5sm00521c
- Bougaran, P., and Bautch, V. L. (2024). Life at the crossroads: the nuclear LINC complex and vascular mechanotransduction. *Front. Physiol.* 15, 1411995. doi:10.3389/fphys.2024.1411995
- Buglak, D. B., Bougaran, P., Kulikauskas, M. R., Liu, Z., Monaghan-Benson, E., Gold, A. L., et al. (2023). Nuclear SUN1 stabilizes endothelial cell junctions via microtubules to regulate blood vessel formation. *Elife* 12, e83652. doi:10.7554/eLife.83652
- Burke, B., and Stewart, C. L. (2013). The nuclear lamins: flexibility in function. *Nat. Rev. Mol. Cell Biol.* 14, 13–24. doi:10.1038/nrm3488
- Buxboim, A., Swift, J., Irianto, J., Spinler, K. R., Dingal, P. C., Athirasala, A., et al. (2014a). Matrix elasticity regulates lamin-A/C phosphorylation and turnover with feedback to actomyosin. *Curr. Biol.* 24, 1909–1917. doi:10.1016/j.cub.2014.07.001
- Buxboim, A., Swift, J., Irianto, J., Spinler, K. R., Dingal, P. D. P., Athirasala, A., et al. (2014b). Matrix elasticity regulates lamin-A, C phosphorylation and turnover with feedback to actomyosin. *Curr. Biol.* 24, 1909–1917. doi:10.1016/j.cub.2014.07.001
- Camozzi, D., Capanni, C., Cenni, V., Mattioli, E., Columbaro, M., Squarzone, S., et al. (2014). Diverse lamin-dependent mechanisms interact to control chromatin dynamics. Focus on laminopathies. *Nucleus* 5, 427–440. doi:10.4161/nuc.36289
- Cao, K., Blair, C. D., Faddah, D. A., Kieckhafer, J. E., Olive, M., Erdos, M. R., et al. (2011). Progerin and telomere dysfunction collaborate to trigger cellular senescence in normal human fibroblasts. *J. Clin. Invest.* 121, 2833–2844. doi:10.1172/JCI43578
- Capanni, C., Del Coco, R., Mattioli, E., Camozzi, D., Columbaro, M., Schena, E., et al. (2009). Emerin-prelamin A interplay in human fibroblasts. *Biol. Cell* 101, 541–554. doi:10.1042/BC20080175
- Chancellor, T. J., Lee, J., Thodeti, C. K., and Lele, T. (2010). Actomyosin tension exerted on the nucleus through nesprin-1 connections influences endothelial cell adhesion, migration, and cyclic strain-induced reorientation. *Biophys. J.* 99, 115–123. doi:10.1016/j.bpj.2010.04.011
- Chen, C. Y., Chi, Y. H., Mutalif, R. A., Starost, M. F., Myers, T. G., Anderson, S. A., et al. (2012). Accumulation of the inner nuclear envelope protein Sun1 is pathogenic in progeric and dystrophic laminopathies. *Cell* 149, 565–577. doi:10.1016/j.cell.2012.01.059
- Chen, X. L., Dodd, G., Thomas, S., Zhang, X., Wasserman, M. A., Rovin, B. H., et al. (2006). Activation of Nrf2/ARE pathway protects endothelial cells from oxidant injury and inhibits inflammatory gene expression. *Am. J. Physiol. Heart Circ. Physiol.* 290, H1862–H1870. doi:10.1152/ajpheart.00651.2005
- Chen, W., Bacanamwo, M., and Harrison, D. G. (2008). Activation of p300 histone acetyltransferase activity is an early endothelial response to laminar shear stress and is essential for stimulation of endothelial nitric-oxide synthase mRNA transcription. *J. Biol. Chem.* 283, 16293–16298. doi:10.1074/jbc.M801803200

- Chen, Z., Peng, I. C., Cui, X., Li, Y. S., Chien, S., and Shyy, J. Y. (2010). Shear stress, SIRT1, and vascular homeostasis. *Proc. Natl. Acad. Sci. U. S. A.* 107, 10268–10273. doi:10.1073/pnas.1003833107
- Chiu, J. J., and Chien, S. (2011). Effects of disturbed flow on vascular endothelium: pathophysiological basis and clinical perspectives. *Physiol. Rev.* 91, 327–387. doi:10.1152/physrev.00047.2009
- Cho, S., Abbas, A., Irianto, J., Ivanovska, I. L., Xia, Y., Tewari, M., et al. (2018). Progerin phosphorylation in interphase is lower and less mechanosensitive than lamin-A/C in iPS-derived mesenchymal stem cells. *Nucleus* 9, 230–245. doi:10.1080/19491034.2018.1460185
- Civelek, M., Manduchi, E., Riley, R. J., Stoeckert, C. J., and Davies, P. F. (2009). Chronic endoplasmic reticulum stress activates unfolded protein response in arterial endothelium in regions of susceptibility to atherosclerosis. *Circ. Res.* 105, 453–461. doi:10.1161/CIRCRESAHA.109.203711
- Columbaro, M., Capanni, C., Mattioli, E., Novelli, G., Parnaik, V., Squarzone, S., et al. (2005). Rescue of heterochromatin organization in Hutchinson-Gilford progeria by drug treatment. *Cell. Mol. Life Sci.* 62, 2669–2678. doi:10.1007/s00018-005-5318-6
- Crisp, M., Liu, Q., Roux, K., Rattner, J. B., Shanahan, C., Burke, B., et al. (2006). Coupling of the nucleus and cytoplasm: role of the LINC complex. *J. Cell Biol.* 172, 41–53. doi:10.1083/jcb.200509124
- Dahl, K. N., Scaffidi, P., Islam, M. F., Yodh, A. G., Wilson, K. L., and Misteli, T. (2006). Distinct structural and mechanical properties of the nuclear lamina in Hutchinson-Gilford progeria syndrome. *Proc. Natl. Acad. Sci.* 103, 10271–10276. doi:10.1073/pnas.0601058103
- Danielsson, B. E., Peters, H. C., Bathula, K., Spear, L. M., Noll, N. A., Dahl, K. N., et al. (2022a). Progerin-expressing endothelial cells are unable to adapt to shear stress. *Biophys. J.* 121, 620–628. doi:10.1016/j.bpj.2022.01.004
- Danielsson, B. E., Tieu, K. V., Spagnol, S. T., Vu, K. K., Cabe, J. I., Raisch, T. B., et al. (2022b). Chromatin condensation regulates endothelial cell adaptation to shear stress. *Mol. Biol. Cell* 33, ar101. doi:10.1091/mbc.E22-02-0064
- Davies, P. F. (1995). Flow-mediated endothelial mechanotransduction. *Physiol. Rev.* 75, 519–560. doi:10.1152/physrev.1995.75.3.519
- Davis, M. J., Earley, S., Li, Y.-S., and Chien, S. (2023). Vascular mechanotransduction. *Physiol. Rev.* 103, 1247–1421. doi:10.1152/physrev.00053.2021
- Davis, M. J., and Hill, M. A. (1999). Signaling mechanisms underlying the vascular myogenic response. *Physiol. Rev.* 79, 387–423. doi:10.1152/physrev.1999.79.2.387
- DE Godoy, M. A., and Rattan, S. (2011). Role of rho kinase in the functional and dysfunctional tonic smooth muscles. *Trends Pharmacol. Sci.* 32, 384–393. doi:10.1016/j.tips.2011.03.005
- Deguchi, S., Maeda, K., Ohashi, T., and Sato, M. (2005). Flow-induced hardening of endothelial nucleus as an intracellular stress-bearing organelle. *J. Biomechanics* 38, 1751–1759. doi:10.1016/j.jbiomech.2005.06.003
- Dekker, R. J., VAN Soest, S., Fontijn, R. D., Salamanca, S., DE Groot, P. G., Vanbavel, E., et al. (2002). Prolonged fluid shear stress induces a distinct set of endothelial cell genes, most specifically lung Krüppel-like factor (KLF2). *Blood* 100, 1689–1698. doi:10.1182/blood-2002-01-0046
- Del Campo, L., Sánchez-López, A., González-Gómez, C., Andrés-Manzano, M. J., Dorado, B., and Andrés, V. (2020). Vascular smooth muscle cell-specific progerin expression provokes contractile impairment in a mouse model of hutchinson-gilford progeria syndrome that is ameliorated by nitrite treatment. *Cells* 9, 656. doi:10.3390/cells9030656
- DE Leeuw, R., Gruenbaum, Y., and Medalia, O. (2018). Nuclear lamins: thin filaments with major functions. *Trends Cell Biol.* 28, 34–45. doi:10.1016/j.tcb.2017.08.004
- Denis, K. B., Cabe, J. I., Danielsson, B. E., Tieu, K. V., Mayer, C. R., and Conway, D. E. (2021). The LINC complex is required for endothelial cell adhesion and adaptation to shear stress and cyclic stretch. *Mol. Biol. Cell* 32, 1654–1663. doi:10.1091/mbc.E20-11-0698
- DE Sandre-Giovannoli, A., Bernard, R., Cau, P., Navarro, C., Amiel, J., Boccaccio, I., et al. (2003). Lamin A truncation in Hutchinson-Gilford progeria. *Science* 300, 2055. doi:10.1126/science.1084125
- Dou, Z., Ghosh, K., Vizioli, M. G., Zhu, J., Sen, P., Wangenstein, K. J., et al. (2017). Cytoplasmic chromatin triggers inflammation in senescence and cancer. *Nature* 550, 402–406. doi:10.1038/nature24050
- Dupont, S., Morsut, L., Aragona, M., Enzo, E., Giulitti, S., Cordenonsi, M., et al. (2011). Role of YAP/TAZ in mechanotransduction. *Nature* 474, 179–183. doi:10.1038/nature10137
- Dupont, S., and Wickström, S. A. (2022). Mechanical regulation of chromatin and transcription. *Nat. Rev. Genet.* 23, 624–643. doi:10.1038/s41576-022-00493-6
- Earle, A. J., Kirby, T. J., Fedorchak, G. R., Isermann, P., Patel, J., Iruvanti, S., et al. (2020). Mutant lamins cause nuclear envelope rupture and DNA damage in skeletal muscle cells. *Nat. Mater.* 19, 464–473. doi:10.1038/s41563-019-0563-5
- Elosegui-Artola, A., Andreu, I., Beedle, A. E. M., Lezamiz, A., Uroz, M., Kosmalska, A. J., et al. (2017). Force triggers YAP nuclear entry by regulating transport across nuclear pores. *Cell* 171, 1397–1410. doi:10.1016/j.cell.2017.10.008
- Eriksson, M., Brown, W. T., Gordon, L. B., Glynn, M. W., Singer, J., Scott, L., et al. (2003). Recurrent *de novo* point mutations in lamin A cause Hutchinson-Gilford progeria syndrome. *Nature* 423, 293–298. doi:10.1038/nature01629
- Espada, J., Varela, I., Flores, I., Ugalde, A. P., Cadiñanos, J., Pendás, A. M., et al. (2008). Nuclear envelope defects cause stem cell dysfunction in premature-aging mice. *J. Cell Biol.* 181, 27–35. doi:10.1083/jcb.200801096
- Fang, F., Yang, Y., Yuan, Z., Gao, Y., Zhou, J., Chen, Q., et al. (2011). Myocardin-related transcription factor A mediates OxLDL-induced endothelial injury. *Circ. Res.* 108, 797–807. doi:10.1161/CIRCRESAHA.111.240655
- Garland, C. J., and Dora, K. A. (2017). EDH: endothelium-dependent hyperpolarization and microvascular signalling. *Acta Physiol.* 219, 152–161. doi:10.1111/apha.12649
- Gete, Y. G., Koblan, L. W., Mao, X., Trappio, M., Mahadik, B., Fisher, J. P., et al. (2021). Mechanisms of angiogenic incompetence in Hutchinson-Gilford progeria via downregulation of endothelial NOS. *Aging Cell* 20, e13388. doi:10.1111/accel.13388
- Glück, S., Guey, B., Gulen, M. F., Wolter, K., Kang, T.-W., Schmacke, N. A., et al. (2017). Innate immune sensing of cytosolic chromatin fragments through cGAS promotes senescence. *Nat. cell Biol.* 19, 1061–1070. doi:10.1038/ncb3586
- Goldman, R. D., Shumaker, D. K., Erdos, M. R., Eriksson, M., Goldman, A. E., Gordon, L. B., et al. (2004). Accumulation of mutant lamin A causes progressive changes in nuclear architecture in Hutchinson-Gilford progeria syndrome. *Proc. Natl. Acad. Sci. U. S. A.* 101, 8963–8968. doi:10.1073/pnas.0402943101
- Gonzalo, S., and Kreienkamp, R. (2015). DNA repair defects and genome instability in Hutchinson-Gilford Progeria Syndrome. *Curr. Opin. Cell Biol.* 34, 75–83. doi:10.1016/j.ccb.2015.05.007
- Gordon, L. B., Massaro, J., D'Agostino, R. B. S. R., Campbell, S. E., Brazier, J., Brown, W. T., et al. (2014). Impact of farnesylation inhibitors on survival in Hutchinson-Gilford progeria syndrome. *Circulation* 130, 27–34. doi:10.1161/CIRCULATIONAHA.113.008285
- Gordon, L. B., McCarten, K. M., Giobbie-Hurder, A., Machan, J. T., Campbell, S. E., Berns, S. D., et al. (2007). Disease progression in Hutchinson-Gilford progeria syndrome: impact on growth and development. *Pediatrics* 120, 824–833. doi:10.1542/peds.2007-1357
- Grolleman, J., VAN Engeland, N. C. A., Raza, M., Azimi, S., Conte, V., Sahlgren, C. M., et al. (2023). Environmental stiffness restores mechanical homeostasis in vimentin-depleted cells. *Sci. Rep.* 13, 18374. doi:10.1038/s41598-023-44835-8
- Gruenbaum, Y., and Foisner, R. (2015). Lamins: nuclear intermediate filament proteins with fundamental functions in nuclear mechanics and genome regulation. *Annu. Rev. Biochem.* 84, 131–164. doi:10.1146/annurev-biochem-060614-034115
- Guilluy, C., Osborne, L. D., VAN Landeghem, L., Sharek, L., Superfine, R., Garcia-Mata, R., et al. (2014). Isolated nuclei adapt to force and reveal a mechanotransduction pathway in the nucleus. *Nat. Cell Biol.* 16, 376–381. doi:10.1038/ncb2927
- Guo, D., Chien, S., and Shyy, J. Y. (2007). Regulation of endothelial cell cycle by laminar versus oscillatory flow: distinct modes of interactions of AMP-activated protein kinase and Akt pathways. *Circ. Res.* 100, 564–571. doi:10.1161/01.RES.0000259561.23876.c5
- Hahn, C., and Schwartz, M. A. (2009). Mechanotransduction in vascular physiology and atherogenesis. *Nat. Rev. Mol. Cell Biol.* 10, 53–62. doi:10.1038/nrm2596
- Hale, C. M., Shrestha, A. L., Khatau, S. B., Stewart-Hutchinson, P. J., Hernandez, L., Stewart, C. L., et al. (2008). Dysfunctional connections between the nucleus and the actin and microtubule networks in laminopathic models. *Biophys. J.* 95, 5462–5475. doi:10.1529/biophysj.108.139428
- Hamczyk, M. R., Villa-Bellosta, R., Quesada, V., Gonzalo, P., Vidak, S., Nevado, R. M., et al. (2019). Progerin accelerates atherosclerosis by inducing endoplasmic reticulum stress in vascular smooth muscle cells. *EMBO Mol. Med.* 11, e9736. doi:10.15252/emmm.201809736
- Han, Y., Wang, L., Yao, Q. P., Zhang, P., Liu, B., Wang, G. L., et al. (2015). Nuclear envelope proteins Nesprin2 and LaminA regulate proliferation and apoptosis of vascular endothelial cells in response to shear stress. *Biochim. Biophys. Acta* 1853, 1165–1173. doi:10.1016/j.bbamcr.2015.02.013
- Hasper, J., Welle, K., Swovick, K., Hryhorenko, J., Ghaemmaghami, S., and Buchwalter, A. (2023). Long lifetime and tissue-specific accumulation of lamin A/C in Hutchinson-Gilford progeria syndrome. *J. Cell Biol.* 223, e202307049. doi:10.1083/jcb.202307049
- Hennekam, R. C. M. (2006). Hutchinson-Gilford progeria syndrome: review of the phenotype. *Am. J. Med. Genet. Part A* 140A, 2603–2624. doi:10.1002/ajmg.a.31346
- Huang, K., Yan, Z. Q., Zhao, D., Chen, S. G., Gao, L. Z., Zhang, P., et al. (2015). SIRT1 and FOXO mediate contractile differentiation of vascular smooth muscle cells under cyclic stretch. *Cell Physiol. Biochem.* 37, 1817–1829. doi:10.1159/000438544
- Hu, B., Song, J. T., Qu, H. Y., Bi, C. L., Huang, X. Z., Liu, X. X., et al. (2014). Mechanical stretch suppresses microRNA-145 expression by activating extracellular signal-regulated kinase 1/2 and upregulating angiotensin-converting enzyme to alter vascular smooth muscle cell phenotype. *PLoS One* 9, e96338. doi:10.1371/journal.pone.0096338
- Hu, J., Li, Y., Hao, Y., Zheng, T., Gupta, S. K., Parada, G. A., et al. (2019). High stretchability, strength, and toughness of living cells enabled by hyperelastic vimentin

intermediate filaments. *Proc. Natl. Acad. Sci. U. S. A.* 116, 17175–17180. doi:10.1073/pnas.1903890116

Humphrey, J. D., Dufresne, E. R., and Schwartz, M. A. (2014). Mechanotransduction and extracellular matrix homeostasis. *Nat. Rev. Mol. Cell Biol.* 15, 802–812. doi:10.1038/nrm3896

Ihalainen, T. O., Aires, L., Herzog, F. A., Schwartlander, R., Moeller, J., and Vogel, V. (2015). Differential basal-to-apical accessibility of lamin A/C epitopes in the nuclear lamina regulated by changes in cytoskeletal tension. *Nat. Mater.* 14, 1252–1261. doi:10.1038/nmat4389

Jensen, L. F., Bentzon, J. F., and Albarrán-Juárez, J. (2021). The phenotypic responses of vascular smooth muscle cells exposed to mechanical cues. *Cells* 10, 2209. doi:10.3390/cells10092209

Jiang, Y. Z., Jiménez, J. M., Ou, K., McCormick, M. E., Zhang, L. D., and Davies, P. F. (2014). Hemodynamic disturbed flow induces differential DNA methylation of endothelial Kruppel-Like Factor 4 promoter *in vitro* and *in vivo*. *Circ. Res.* 115, 32–43. doi:10.1161/CIRCRESAHA.115.303883

Kalukula, Y., Stephens, A. D., Lammerding, J., and Gabriele, S. (2022). Mechanics and functional consequences of nuclear deformations. *Nat. Rev. Mol. Cell Biol.* 23, 583–602. doi:10.1038/s41580-022-00480-z

Kim, P. H., Chen, N. Y., Heizer, P. J., Tu, Y., Weston, T. A., Fong, J. L., et al. (2021). Nuclear membrane ruptures underlie the vascular pathology in a mouse model of Hutchinson-Gilford progeria syndrome. *JCI Insight* 6, e151515. doi:10.1172/jci.insight.151515

Kim, P. H., Kim, J. R., Tu, Y., Jung, H., Jeong, J. Y. B., Tran, A. P., et al. (2024). Progerin forms an abnormal meshwork and has a dominant-negative effect on the nuclear lamina. *Proc. Natl. Acad. Sci.* 121, e2406946121. doi:10.1073/pnas.2406946121

Kim, P. H., Luu, J., Heizer, P., Tu, Y., Weston, T. A., Chen, N., et al. (2018). Disrupting the LINC complex in smooth muscle cells reduces aortic disease in a mouse model of Hutchinson-Gilford progeria syndrome. *Sci. Transl. Med.* 10, eaat7163. doi:10.1126/scitranslmed.aat7163

King, S. J., Nowak, K., Suryavanshi, N., Holt, I., Shanahan, C. M., and Ridley, A. J. (2014). Nesprin-1 and nesprin-2 regulate endothelial cell shape and migration. *Cytoskelet. Hob.* 71, 423–434. doi:10.1002/cm.21182

Kirby, T. J., and Lammerding, J. (2018). Emerging views of the nucleus as a cellular mechanosensor. *Nat. Cell Biol.* 20, 373–381. doi:10.1038/s41556-018-0038-y

Koushki, N., Ghaghe, A., Srivastava, L. K., Molter, C., and Ehrlicher, A. J. (2023). Nuclear compression regulates YAP spatiotemporal fluctuations in living cells. *Proc. Natl. Acad. Sci. U. S. A.* 120, e2301285120. doi:10.1073/pnas.2301285120

Kubben, N., Zhang, W., Wang, L., Voss, T. C., Yang, J., Qu, J., et al. (2016). Repression of the antioxidant NRF2 pathway in premature aging. *Cell* 165, 1361–1374. doi:10.1016/j.cell.2016.05.017

Lammerding, J., Schulze, P. C., Takahashi, T., Kozlov, S., Sullivan, T., Kamm, R. D., et al. (2004). Lamin A/C deficiency causes defective nuclear mechanics and mechanotransduction. *J. Clin. Invest* 113, 370–378. doi:10.1172/JCI19670

Lee, D. Y., Lee, C. I., Lin, T. E., Lim, S. H., Zhou, J., Tseng, Y. C., et al. (2012). Role of histone deacetylases in transcription factor regulation and cell cycle modulation in endothelial cells in response to disturbed flow. *Proc. Natl. Acad. Sci. U. S. A.* 109, 1967–1972. doi:10.1073/pnas.1121214109

Liu, S. Y., and Ikegami, K. (2020). Nuclear lamin phosphorylation: an emerging role in gene regulation and pathogenesis of laminopathies. *Nucleus* 11, 299–314. doi:10.1080/19491034.2020.1832734

Liu, B., Wang, J., Chan, K. M., Tjia, W. M., Deng, W., Guan, X., et al. (2005). Genomic instability in laminopathy-based premature aging. *Nat. Med.* 11, 780–785. doi:10.1038/nm1266

Liu, D., Lv, H., Liu, Q., Sun, Y., Hou, S., Zhang, L., et al. (2019). Atheroprotective effects of methotrexate via the inhibition of YAP/TAZ under disturbed flow. *J. Transl. Med.* 17, 378. doi:10.1186/s12967-019-02135-8

Mao, X., Said, R., Louis, H., Max, J. P., Bourhim, M., Challande, P., et al. (2012). Cyclic stretch-induced thrombin generation by rat vascular smooth muscle cells is mediated by the integrin $\alpha v \beta 3$ pathway. *Cardiovasc Res.* 96, 513–523. doi:10.1093/cvr/cvs274

Maraldi, N. M., Capanni, C., Cenni, V., Fini, M., and Lattanzi, G. (2011). Laminopathies and lamin-associated signaling pathways. *J. Cell Biochem.* 112, 979–992. doi:10.1002/jcb.22992

Maurer, M., and Lammerding, J. (2019). The driving force: nuclear mechanotransduction in cellular function, fate, and disease. *Annu. Rev. Biomed. Eng.* 21, 443–468. doi:10.1146/annurev-bioeng-060418-052139

Mccord, R. P., Nazario-Toole, A., Zhang, H., Chines, P. S., Zhan, Y., Erdos, M. R., et al. (2013). Correlated alterations in genome organization, histone methylation, and DNA-lamin A/C interactions in Hutchinson-Gilford progeria syndrome. *Genome Res.* 23, 260–269. doi:10.1101/gr.138032.112

Merideth, M. A., Gordon, L. B., Claus, S., Sachdev, V., Smith, A. C., Perry, M. B., et al. (2008). Phenotype and course of Hutchinson-Gilford progeria syndrome. *N. Engl. J. Med.* 358, 592–604. doi:10.1056/NEJMoa0706898

Murtada, S.-I., Kawamura, Y., Caulk, A. W., Ahmadzadeh, H., Mikush, N., Zimmerman, K., et al. (2020). Paradoxical aortic stiffening and subsequent cardiac

dysfunction in Hutchinson-Gilford progeria syndrome. *J. R. Soc. Interface* 17, 20200066. doi:10.1098/rsif.2020.0066

Murtada, S. I., Kawamura, Y., Cavinato, C., Wang, M., Ramachandra, A. B., Spronck, B., et al. (2023). Biomechanical and transcriptional evidence that smooth muscle cell death drives an osteochondrogenic phenotype and severe proximal vascular disease in progeria. *Biomech. Model. Mechanobiol.* 22, 1333–1347. doi:10.1007/s10237-023-01722-5

Musich, P. R., and Zou, Y. (2009). Genomic instability and DNA damage responses in progeria arising from defective maturation of prelamin A. *Aging (Albany NY)* 1, 28–37. doi:10.18632/aging.100012

Mu, X., Tseng, C., Hambright, W. S., Matre, P., Lin, C. Y., Chanda, P., et al. (2020). Cytoskeleton stiffness regulates cellular senescence and innate immune response in Hutchinson-Gilford Progeria Syndrome. *Aging Cell* 19, e13152. doi:10.1111/accel.13152

Nagel, T., Resnick, N., Dewey, C. F., and Gimbrone, M. A. (1999). Vascular endothelial cells respond to spatial gradients in fluid shear stress by enhanced activation of transcription factors. *Arterioscler. Thromb. Vasc. Biol.* 19, 1825–1834. doi:10.1161/01.atv.19.8.1825

Nava, M. M., Miroshnikova, Y. A., Biggs, L. C., Whitefield, D. B., Metge, F., Boucas, J., et al. (2020). Heterochromatin-driven nuclear softening protects the genome against mechanical stress-induced damage. *Cell* 181, 800–817. doi:10.1016/j.cell.2020.03.052

Neelam, S., Chancellor, T. J., Li, Y., Nickerson, J. A., Roux, K. J., Dickinson, R. B., et al. (2015). Direct force probe reveals the mechanics of nuclear homeostasis in the mammalian cell. *Proc. Natl. Acad. Sci. U. S. A.* 112, 5720–5725. doi:10.1073/pnas.1502111112

Ngai, D., Lino, M., Rothenberg, K. E., Simmons, C. A., Fernandez-Gonzalez, R., and Bendeck, M. P. (2020). DDR1 (discoidin domain receptor-1)-RhoA (Ras homolog family member A) Axis senses matrix stiffness to promote vascular calcification. *Arteriosclerosis, Thrombosis, Vasc. Biol.* 40, 1763–1776. doi:10.1161/ATVBAHA.120.314697

Ngai, D., Mohabeer, A. L., Mao, A., Lino, M., and Bendeck, M. P. (2022). Stiffness-responsive feedback autoregulation of DDR1 expression is mediated by a DDR1-YAP/TAZ axis. *Matrix Biol.* 110, 129–140. doi:10.1016/j.matbio.2022.05.004

Olive, M., Harten, I., Mitchell, R., Beers, J. K., Djabali, K., Cao, K., et al. (2010). Cardiovascular pathology in hutchinson-gilford progeria: correlation with the vascular pathology of aging. *Arteriosclerosis, Thrombosis, Vasc. Biol.* 30, 2301–2309. doi:10.1161/ATVBAHA.110.209460

Osborn, E. A., Rabodzey, A., Dewey, C. F., and Hartwig, J. H. (2006). Endothelial actin cytoskeleton remodeling during mechanostimulation with fluid shear stress. *Am. J. Physiol. Cell Physiol.* 290, C444–C452. doi:10.1152/ajpcell.00218.2005

Osmanagic-Myers, S., Kiss, A., Manakanatas, C., Hamza, O., Sedlmayer, F., Szabo, P. L., et al. (2019). Endothelial progerin expression causes cardiovascular pathology through an impaired mechanoresponse. *J. Clin. Invest* 129, 531–545. doi:10.1172/JCI121297

Osorio, F. G., Bárcena, C., Soria-Valles, C., Ramsay, A. J., DE Carlos, F., Cobo, J., et al. (2012). Nuclear lamina defects cause ATM-dependent NF- κ B activation and link accelerated aging to a systemic inflammatory response. *Genes Dev.* 26, 2311–2324. doi:10.1101/gad.197954.112

Owens, G. K., Kumar, M. S., and Wamhoff, B. R. (2004). Molecular regulation of vascular smooth muscle cell differentiation in development and disease. *Physiol. Rev.* 84, 767–801. doi:10.1152/physrev.00041.2003

Patteson, A. E., Vahabikashi, A., Pogoda, K., Adam, S. A., Mandal, K., Kittisopikul, M., et al. (2019). Vimentin protects cells against nuclear rupture and DNA damage during migration. *J. Cell Biol.* 218, 4079–4092. doi:10.1083/jcb.201902046

Pegoraro, G., Kubben, N., Wickert, U., Göhler, H., Hoffmann, K., and Misteli, T. (2009). Ageing-related chromatin defects through loss of the NURD complex. *Nat. cell Biol.* 11, 1261–1267. doi:10.1038/ncb1971

Pitrez, P. R., Estronca, L., Monteiro, L. M., Colell, G., Vazão, H., Santinha, D., et al. (2020). Vulnerability of progeroid smooth muscle cells to biomechanical forces is mediated by MMP13. *Nat. Commun.* 11, 4110. doi:10.1038/s41467-020-17901-2

Reusch, P., Wagdy, H., Reusch, R., Wilson, E., and Ives, H. E. (1996). Mechanical strain increases smooth muscle and decreases nonmuscle myosin expression in rat vascular smooth muscle cells. *Circ. Res.* 79, 1046–1053. doi:10.1161/01.res.79.5.1046

Ribas, J., Zhang, Y. S., Pitrez, P. R., Leijten, J., Miscuglio, M., Rouwkema, J., et al. (2017). Biomechanical strain exacerbates inflammation on a progeria-on-a-chip model. *Small* 13. doi:10.1002/smll.201603737

Rosengarten, Y., McKenna, T., Grochová, D., and Eriksson, M. (2011). Stem cell depletion in Hutchinson-Gilford progeria syndrome. *Aging Cell* 10, 1011–1020. doi:10.1111/j.1474-9726.2011.00743.x

Sagelius, H., Rosengarten, Y., Hanif, M., Erdos, M. R., Rozell, B., Collins, F. S., et al. (2008). Targeted transgenic expression of the mutation causing Hutchinson-Gilford progeria syndrome leads to proliferative and degenerative epidermal disease. *J. Cell Sci.* 121, 969–978. doi:10.1242/jcs.022913

Scaffidi, P., and Misteli, T. (2008). Lamin A-dependent misregulation of adult stem cells associated with accelerated ageing. *Nat. Cell Biol.* 10, 452–459. doi:10.1038/ncb1708

- Schmidt, E., Nilsson, O., Koskela, A., Tuukkanen, J., Ohlsson, C., Rozell, B., et al. (2012). Expression of the Hutchinson-Gilford progeria mutation during osteoblast development results in loss of osteocytes, irregular mineralization, and poor biomechanical properties. *J. Biol. Chem.* 287, 33512–33522. doi:10.1074/jbc.M112.366450
- Sears, R. M., and Roux, K. J. (2022). Mechanisms of A-type lamin targeting to nuclear ruptures are disrupted in LMNA- and BANF1-associated progerias. *Cells* 11, 865. doi:10.3390/cells11050865
- Seelbinder, B., Ghosh, S., Schneider, S. E., Scott, A. K., Berman, A. G., Goergen, C. J., et al. (2021). Nuclear deformation guides chromatin reorganization in cardiac development and disease. *Nat. Biomed. Eng.* 5, 1500–1516. doi:10.1038/s41551-021-00823-9
- Senbanerjee, S., Lin, Z., Atkins, G. B., Greif, D. M., Rao, R. M., Kumar, A., et al. (2004). KLF2 Is a novel transcriptional regulator of endothelial proinflammatory activation. *J. Exp. Med.* 199, 1305–1315. doi:10.1084/jem.20031132
- Shumaker, D. K., Dechat, T., Kohlmaier, A., Adam, S. A., Bozovsky, M. R., Erdos, M. R., et al. (2006). Mutant nuclear lamin A leads to progressive alterations of epigenetic control in premature aging. *Proc. Natl. Acad. Sci.* 103, 8703–8708. doi:10.1073/pnas.0602569103
- Solovei, I., Wang, A. S., Thanisch, K., Schmidt, C. S., Krebs, S., Zwerger, M., et al. (2013). LBR and lamin A/C sequentially tether peripheral heterochromatin and inversely regulate differentiation. *Cell* 152, 584–598. doi:10.1016/j.cell.2013.01.009
- Son, S. M., Park, S. J., Breusegem, S. Y., Larrieu, D., and Rubinstein, D. C. (2024). p300 nucleocytoplasmic shuttling underlies mTORC1 hyperactivation in Hutchinson-Gilford progeria syndrome. *Nat. Cell Biol.* 26, 235–249. doi:10.1038/s41556-023-01338-y
- Song, M., San, H., Anderson, S. A., Cannon, R. O., and Orlic, D. (2014). Shear stress-induced mechanotransduction protein deregulation and vasculopathy in a mouse model of progeria. *Stem Cell Res. Ther.* 5, 41. doi:10.1186/scrt429
- Strambio-DE-Castillia, C., Niepel, M., and Rout, M. P. (2010). The nuclear pore complex: bridging nuclear transport and gene regulation. *Nat. Rev. Mol. Cell Biol.* 11, 490–501. doi:10.1038/nrm2928
- Sun, S., Qin, W., Tang, X., Meng, Y., Hu, W., Zhang, S., et al. (2020). Vascular endothelium-targeted Sirt7 gene therapy rejuvenates blood vessels and extends life span in a Hutchinson-Gilford progeria model. *Sci. Adv.* 6, eaay5556. doi:10.1126/sciadv.aay5556
- Swiatlowska, P., Sit, B., Feng, Z., Marhuenda, E., Xanthis, I., Zingaro, S., et al. (2022). Pressure and stiffness sensing together regulate vascular smooth muscle cell phenotype switching. *Sci. Adv.* 8, eabm3471. doi:10.1126/sciadv.abm3471
- Swift, J., Ivanovska, I. L., Buxboim, A., Harada, T., Dingal, P. D. P., Pinter, J., et al. (2013). Nuclear lamin-A scales with tissue stiffness and enhances matrix-directed differentiation. *Science* 341, 1240104. doi:10.1126/science.1240104
- Tajik, A., Zhang, Y., Wei, F., Sun, J., Jia, Q., Zhou, W., et al. (2016). Transcription upregulation via force-induced direct stretching of chromatin. *Nat. Mater.* 15, 1287–1296. doi:10.1038/nmat4729
- Tkachenko, E., Gutierrez, E., Saikin, S. K., Fogelstrand, P., Kim, C., Groisman, A., et al. (2013). The nucleus of endothelial cell as a sensor of blood flow direction. *Biol. Open* 2, 1007–1012. doi:10.1242/bio.20134622
- Tsai, M.-C., Chen, L., Zhou, J., Tang, Z., Hsu, T.-F., Wang, Y., et al. (2009). Shear stress induces synthetic-to-contractile phenotypic modulation in smooth muscle cells via peroxisome proliferator-activated receptor α /delta activations by prostacyclin released by sheared endothelial cells. *Circulation Res.* 105, 471–480. doi:10.1161/CIRCRESAHA.109.193656
- Tzima, E., Irani-Tehrani, M., Kiosses, W. B., Dejana, E., Schultz, D. A., Engelhardt, B., et al. (2005). A mechanosensory complex that mediates the endothelial cell response to fluid shear stress. *Nature* 437, 426–431. doi:10.1038/nature03952
- Ullrich, N. J., and Gordon, L. B. (2015). Hutchinson-Gilford progeria syndrome. *Handb. Clin. Neurol.* 132, 249–264. doi:10.1016/B978-0-444-62702-5.00018-4
- Varga, R., Eriksson, M., Erdos, M. R., Olive, M., Harten, I., Kolodgie, F., et al. (2006). Progressive vascular smooth muscle cell defects in a mouse model of Hutchinson-Gilford progeria syndrome. *Proc. Natl. Acad. Sci. U. S. A.* 103, 3250–3255. doi:10.1073/pnas.0600012103
- Verstraeten, V. L. R. M., Ji, J. Y., Cummings, K. S., Lee, R. T., and Lammerding, J. (2008). Increased mechanosensitivity and nuclear stiffness in Hutchinson-Gilford progeria cells: effects of farnesyltransferase inhibitors. *Aging Cell* 7, 383–393. doi:10.1111/j.1474-9726.2008.00382.x
- Vion, A.-C., Kheloufi, M., Hammoutene, A., Poisson, J., Lasselin, J., Devue, C., et al. (2017). Autophagy is required for endothelial cell alignment and atheroprotection under physiological blood flow. *Proc. Natl. Acad. Sci.* 114, E8675–E8684. doi:10.1073/pnas.1702223114
- Wan, X. J., Zhao, H. C., Zhang, P., Huo, B., Shen, B. R., Yan, Z. Q., et al. (2015). Involvement of BK channel in differentiation of vascular smooth muscle cells induced by mechanical stretch. *Int. J. Biochem. Cell Biol.* 59, 21–29. doi:10.1016/j.biocel.2014.11.011
- Wang, K.-C., Yeh, Y.-T., Nguyen, P., Limqueco, E., Lopez, J., Thorossian, S., et al. (2016a). Flow-dependent YAP/TAZ activities regulate endothelial phenotypes and atherosclerosis. *Proc. Natl. Acad. Sci.* 113, 11525–11530. doi:10.1073/pnas.1613121113
- Wang, L., Luo, J. Y., Li, B., Tian, X. Y., Chen, L. J., Huang, Y., et al. (2016b). Integrin-YAP/TAZ-JNK cascade mediates atheroprotective effect of unidirectional shear flow. *Nature* 540, 579–582. doi:10.1038/nature20602
- Wang, W., Ha, C. H., Jhun, B. S., Wong, C., Jain, M. K., and Jin, Z. G. (2010). Fluid shear stress stimulates phosphorylation-dependent nuclear export of HDAC5 and mediates expression of KLF2 and eNOS. *Blood* 115, 2971–2979. doi:10.1182/blood-2009-05-224824
- Wang, Y., Cao, W., Cui, J., Yu, Y., Zhao, Y., Shi, J., et al. (2018). Arterial wall stress induces phenotypic switching of arterial smooth muscle cells in vascular remodeling by activating the YAP/TAZ signaling pathway. *Cell Physiol. Biochem.* 51, 842–853. doi:10.1159/000495376
- Wheaton, K., Campuzano, D., Ma, W., Sheinis, M., Ho, B., Brown, G. W., et al. (2017). Progerin-induced replication stress facilitates premature senescence in hutchinson-gilford progeria syndrome. *Mol. Cell Biol.* 37, e716-006599. doi:10.1128/MCB.00659-16
- Xia, Y., Ivanovska, I. L., Zhu, K., Smith, L., Irianto, J., Pfeifer, C. R., et al. (2018). Nuclear rupture at sites of high curvature compromises retention of DNA repair factors. *J. Cell Biol.* 217, 3796–3808. doi:10.1083/jcb.201711161
- Xu, S., Koroleva, M., Yin, M., and Jin, Z. G. (2016). Atheroprotective laminar flow inhibits Hippo pathway effector YAP in endothelial cells. *Transl. Res.* 176, 18–28. doi:10.1016/j.trsl.2016.05.003
- Yan, Z. Q., Yao, Q. P., Zhang, M. L., Qi, Y. X., Guo, Z. Y., Shen, B. R., et al. (2009). Histone deacetylases modulate vascular smooth muscle cell migration induced by cyclic mechanical strain. *J. Biomech.* 42, 945–948. doi:10.1016/j.jbiomech.2009.01.012
- Yang, S. H., Meta, M., Qiao, X., Frost, D., Bauch, J., Coffinier, C., et al. (2006). A farnesyltransferase inhibitor improves disease phenotypes in mice with a Hutchinson-Gilford progeria syndrome mutation. *J. Clin. Invest* 116, 2115–2121. doi:10.1172/JCI28968
- Yang, F., Zhang, Y., Zhu, J., Wang, J., Jiang, Z., Zhao, C., et al. (2020). Laminar flow protects vascular endothelial tight junctions and barrier function via maintaining the expression of long non-coding RNA MALAT1. *Front. Bioeng. Biotechnol.* 8, 647. doi:10.3389/fbioe.2020.00647
- Yao, Q. P., Zhang, P., Qi, Y. X., Chen, S. G., Shen, B. R., Han, Y., et al. (2014). The role of SIRT6 in the differentiation of vascular smooth muscle cells in response to cyclic strain. *Int. J. Biochem. Cell Biol.* 49, 98–104. doi:10.1016/j.biocel.2014.01.016
- Yue, X., Cui, J., Sun, Z., Liu, L., Li, Y., Shao, L., et al. (2023). Nuclear softening mediated by Sun2 suppression delays mechanical stress-induced cellular senescence. *Cell Death Discov.* 9, 167. doi:10.1038/s41420-023-01467-1
- Zhang, H., Xiong, Z. M., and Cao, K. (2014). Mechanisms controlling the smooth muscle cell death in progeria via down-regulation of poly(ADP-ribose) polymerase 1. *Proc. Natl. Acad. Sci. U. S. A.* 111, E2261–E2270. doi:10.1073/pnas.1320843111
- Zou, Y., Akazawa, H., Qin, Y., Sano, M., Takano, H., Minamino, T., et al. (2004). Mechanical stress activates angiotensin II type 1 receptor without the involvement of angiotensin II. *Nat. Cell Biol.* 6, 499–506. doi:10.1038/ncb1137



OPEN ACCESS

EDITED BY

Nicolas Baeyens,
Université libre de Bruxelles, Belgium

REVIEWED BY

George Davis,
Morsani College of Medicine, USF Health,
United States
Maud Martin,
Université libre de Bruxelles, Belgium
Julien Vermot,
Imperial College London, United Kingdom

*CORRESPONDENCE

M. Luisa Iruela-Arispe,
✉ arispe@northwestern.edu

RECEIVED 30 April 2024

ACCEPTED 20 August 2024

PUBLISHED 10 September 2024

CITATION

Moise K, Arun KM, Pillai M, Salvador J, Mehta AS,
Goyal Y and Iruela-Arispe ML (2024) Endothelial
cell elongation and alignment in response to
shear stress requires acetylation
of microtubules.
Front. Physiol. 15:1425620.
doi: 10.3389/fphys.2024.1425620

COPYRIGHT

© 2024 Moise, Arun, Pillai, Salvador, Mehta,
Goyal and Iruela-Arispe. This is an open-access
article distributed under the terms of the
[Creative Commons Attribution License \(CC BY\)](https://creativecommons.org/licenses/by/4.0/).
The use, distribution or reproduction in other
forums is permitted, provided the original
author(s) and the copyright owner(s) are
credited and that the original publication in this
journal is cited, in accordance with accepted
academic practice. No use, distribution or
reproduction is permitted which does not
comply with these terms.

Endothelial cell elongation and alignment in response to shear stress requires acetylation of microtubules

Katiannah Moise¹, Keerthana M. Arun², Maalavika Pillai^{1,2},
Jocelynda Salvador¹, Aarya S. Mehta¹, Yogesh Goyal^{1,2} and
M. Luisa Iruela-Arispe^{1*}

¹Department of Cell and Development Biology, Northwestern University, Feinberg School of Medicine, Chicago, IL, United States, ²Center for Synthetic Biology, Northwestern University, Chicago, IL, United States

The innermost layer of the vessel wall is constantly subjected to recurring and relenting mechanical forces by virtue of their direct contact with blood flow. Endothelial cells of the vessel are exposed to distension, pressure, and shear stress; adaptation to these hemodynamic forces requires significant remodeling of the cytoskeleton which includes changes in actin, intermediate filaments, and microtubules. While much is known about the effect of shear stress on the endothelial actin cytoskeleton; the impact of hemodynamic forces on the microtubule network has not been investigated in depth. Here we used imaging techniques and protein expression analysis to characterize how pharmacological and genetic perturbations of microtubule properties alter endothelial responses to laminar shear stress. Our findings revealed that pharmacological suppression of microtubule dynamics blocked two typical responses to laminar shear stress: endothelial elongation and alignment. The findings demonstrate the essential contribution of the microtubule network to changes in cell shape driven by mechanical forces. Furthermore, we observed a flow-dependent increase in microtubule acetylation that occurred early in the process of cell elongation. Pharmacological manipulation of microtubule acetylation showed a direct and causal relationship between acetylation and endothelial elongation. Finally, genetic inactivation of aTAT1, a microtubule acetylase, led to significant loss of acetylation as well as inhibition of cell elongation in response to flow. In contrast, loss of HDAC6, a microtubule deacetylase, resulted in robust microtubule acetylation with cells displaying faster kinetics of elongation and alignment. Taken together, our findings uncovered the critical contributions of HDAC6 and aTAT1, that through their roles in the regulation of microtubule acetylation, are key mediators of endothelial mechanotransduction.

KEYWORDS

cytoskeleton, hemodynamics, mechanotransduction, mechanosensing, vascular biology

Introduction

The inner surface of the entire circulatory system is covered by a monolayer of endothelial cells (EC) directly exposed to the physical stressors of blood flow, namely: stretch, pressure, and shear stress (Chien, 2007; Baeyens and Schwartz, 2016). In response to shear stress, endothelial cells elongate in the direction of flow and transduce mechanical stimuli into sequential biochemical reactions that enable homeostatic regulation of vascular function (Bevan et al., 1990; Langille, 1992). In addition, endothelial cells significantly alter their transcriptome and epigenome affecting their inflammatory status. It has been very well documented that the type of flow, laminar or disturbed, can have profound effects on endothelial gene expression (Chiu and Chien, 2011). In this manner, regions associated with non-uniform shear stresses like areas of bifurcations induce a pro-inflammatory status on the endothelium and are prone to the development of early atherosclerotic lesions. In contrast, regions of the vessel wall exposed to uniform laminar flow are anti-inflammatory and athero-protective.

The realization that physical forces regulate the inflammatory status of the endothelium by affecting gene expression stimulated interest in clarifying the mechanisms associated with mechanosensing and mechanotransduction. To identify the molecular players involved in the cellular responses to mechanical stress, endothelial cells have been cultured under flow-controlled conditions and subjected to uniform, disturbed, pulsatile and oscillatory types of shear stresses to mimic *in vivo* environments. In this manner, a large array of mechanosensing receptors, ion channels, and cell adhesion molecules have been identified as playing important roles in flow responses and their respective contributions have been studied in depth (Coste et al., 2010; Mack et al., 2017; Fleming et al., 2005; Mendoza et al., 2010; Mohan et al., 1997; Zhang et al., 2006; Tzima et al., 2005; Fan et al., 2017). More recently, the potential impact of shear stress patterns in the development of site-specific vascular malformations added further attention to the cross talk between physical forces and signal transduction in the emergence of vascular pathology (Rodel et al., 2019).

Perhaps the most well recognized effect of laminar shear stress relates to its impact on endothelial cell shape (Campinho et al., 2020). Confluent endothelial monolayers subjected to physiological levels of laminar shear stress elongate in direction to flow within 24 h. The transition in cell shape from polygonal to elongated implies significant remodeling of the cytoskeleton contingent upon exposure to flow. Measurements obtained using live cell microscopy revealed that shear stress induces heterogeneous patterns of mechanical strain on the intermediate filament network at the basal surface of endothelial cells, and that this affects focal adhesions (Helmke et al., 2003). Lateral strain caused by shear stress on PECAM homotypic interactions was shown to impact vimentin and actin. These collective dynamic structural changes can also concentrate mechanical stimuli in cellular compartments where biochemical transduction occurs. For example, mean traction force against the substrate and Rho GTPase activity were found to be increased in endothelial cells shortly after onset of shear stress (Shiu et al., 2004; Collins et al., 2012). Furthermore, activation of Rho followed by Rac triggered robust cellular changes in the actin

cytoskeleton with the formation of stress fibers and reorganization of focal adhesions (Mott and Helmke, 2007). Finally, the microtubule (MT) network is also affected by shear stress. Using subconfluent endothelial cells, Zielinski and colleagues showed a rapid reorganization of microtubules upon application of shear stress (Zielinski et al., 2018). Importantly, laminar shear stress was also shown to promote microtubule stability by increasing acetylation downstream of GSK-3 β (McCue et al., 2006). This last study indicated that microtubules were altered in response to shear stress, but the biological impact of this alteration on individual and collective endothelial cell responses has not been systematically examined.

In this study, we sought to investigate the requirement of the MT network to endothelial cells responses to shear stress and gain additional molecular insight on mechanisms. We found that MT dynamics were essential to enable elongation and alignment following application of laminar shear stress on endothelial monolayers. We confirmed that shear stress promotes rapid and robust microtubule acetylation and that this effect was sustained over 48 h *in vitro*. We demonstrated that MT acetylation is higher in areas of laminar shear than in regions of disturbed flow *in vivo*. We further showed that flow-mediated increase in acetylation is driven by a rapid decrease in HDAC6 protein. Finally, we demonstrated that pharmacological or genetic perturbations in microtubule acetylation blocked the ability of endothelial cells to elongate and align in response to laminar shear stress.

Materials and methods

Cell culture

Human arterial endothelial cells (HAECs) were purchased from the American Type Culture Collection (ATCC, #PCS-100-011, Manassas, VA) and Lonza (Lonza, #CC-2535, Morrisville, NC). HAECs were cultured on 0.1% gelatin coated dishes and used between passages 4 and 8. Human Umbilical Vein Endothelial cells (HUVEC) were isolated from three separate patients and used between passages 4 and 9. Patients were informed and gave their consent for the research. Both HAECs and HUVECs were cultured in commercial MCDB-131 media (MCDB131-WOFBS, VEC Technologies, Inc.) or in commercial EBM -2 Basal media (Lonza, #CC-3121) supplemented with EGM-2 BulletKit (Lonza, #CC-4176) containing 10% fetal bovine serum (FBS; Omega Scientific Inc.) with antibiotics. Cultures were maintained in a 5% CO₂ incubator at 37°C. Human embryonic kidney cells (HEK293T) (ATCC, #CRL-3216) were cultured with DMEM media with 10% FBS (Fisher Scientific #MT10017CV). All cells were characterized with cell-specific antibodies and tested negative for *mycoplasma*.

In vitro simulation of laminar shear stress

Orbital shaker method

Confluent endothelial cells (HAEC and HUVEC) were cultured in gelatin-coated 6-well glass bottom plates with 4% Dextran media with 1% or 10% FBS and subjected to constant fluid shear stress (20 dynes/cm²) on a Benchmark Orbi-Shaker Jr Mini orbital shaker

TABLE 1 Lentiviral constructs.

Nickname	Construct	Guide sequences	Length of region of deletion	Vector size
HDAC6KO	pLV[2CRISPR]hCas9:T2A:Puro-U6>hHDAC6 [gRNA#1780]-U6>hHDAC6 [gRNA#2152]	TCCATCCACCGCTACGAGCA, ATGATC CGCAAGATGCGCTG	1,693	12,124 bp
αTAT1KO	pLV[2CRISPR]hCas9:T2A:Puro-U6>hATAT1 [gRNA#170]-U6>hATAT1[gRNA#221]	GAGCATGTGGCACTCACGGT, CATGAGTCTGTGCAACGCCA	378	12,047 bp

(130 rpm, 19 mm radius, Sycamore Life Sciences) inside an incubator with 5% CO₂ and at 37°C incubator. Dextran (Leuconostoc spp. Mr 450,000-650,000, Millipore Sigma, #31392) was added to the media at a w/v of 4% to create a viscosity similar to blood and delivered the adequate shear stress.

Ibidi pump system method

For some experiments, we also used an Ibidi pump system (Ibidi #10902) to deliver laminar shear stress at 20 dynes/cm². For this, 100,000 endothelial cells were seeded into a 0.4 mm deep u-slide I Luer (Ibidi #80176) microfluidic slide 24 h prior to experiments. A media change was performed prior to connecting the slide to the fluidic unit.

Microtubule targeting agents (MTAs)

Taxol (10 nM, Tocris #1097), Nocodazole (100 nM, Selleck Chemicals #S2775), and Colchicine (10 nM, Selleck Chemicals #S2284) were applied to endothelial monolayers either under static or flow conditions, as indicated. The concentrations were selected by using EB3-GFP transfections. The lowest concentration able to achieve microtubule disturbance in the absence of cell death was selected.

Pharmacological perturbation of acetylation

Confluent HAECs seeded on glass bottom plates were treated with the TAK1 inhibitor, 5Z-7-Oxozeaenol (5Z-7; 1uM; Fisher Scientific #HY-12686) to suppress acetylation mediated by alpha-TAT1 (Shah et al., 2018). Tubacin (Tub; 5uM; Tocris #3402) was used to inhibit HDAC6 activity. DMSO was used as a control.

Immunofluorescence

To visualize microtubules, post-translational modifications of microtubules, and cell-cell junctions, two methods of fixation and staining were employed. Endothelial cultures were washed with 1x PBS buffer and fixed with ice-cold methanol for 10 min at -20°C to visualize microtubules. Wells were permeabilized with 0.1% Triton X-100 in 1x PBS buffer for 10 min at room temperature. Depending on the fixation, methanol-fixed cells were stained using monoclonal rabbit Acetylated-α-tubulin (Lys40) (D20G3) (Cell Signaling #5335, RRID:AB_10544694, 1:1,000), monoclonal mouse anti-Acetylated

α-tubulin (Millipore Sigma #T7451, RRID:AB_609894, 1:1,000), monoclonal mouse anti-Acetylated (Lys40) (6-11B-1) α-tubulin (Cell Signaling #12152s, RRID:AB_2797830, 1:1,000), monoclonal mouse DM1a (Cell Signaling #3873s, RRID:AB_1904178, 1:1,000), polyclonal rabbit anti-detyrosinated tubulin (Millipore Sigma #AB3201, RRID:AB_117350 1:1,000), monoclonal mouse anti-polyglutamylated Tubulin, clone B3 (Sigma-Aldrich #T9822,RRID:AB_477598, 1:1,000), monoclonal rat Anti-Tubulin Antibody, clone YL1/2 (Tyrosinated-tubulin) (Millipore Sigma #MAB1864, RRID:AB_1679330, 1:1,000) and DAPI for nuclear staining (4', 6-Diamidino-2-Phenylindole, Dihydrochloride) (Thermo Fisher Scientific, #D1306, RRID:AB_2629482, 5 mg/mL). Primary antibodies were incubated for 1 h at room temperature. Cell-cell junctions were visualized using a 647-conjugated Hec1/VE-cadherin supernatant gifted by William Muller (Northwestern University, Chicago, IL, 1:500) for 30 min at room temperature. Conjugation of the antibody was done using a Pierce Dylight Antibody labeling Kit (Fisher Scientific #PI84535). For time-lapse visualization of microtubules under laminar flow, a red live dye was used by ABBERIOR (2.5 uM, #LVRED-0141050UG). Secondary antibodies were used at 1: 400 concentration for Donkey anti-mouse IgG (H&L) (Alexa Fluor 568) (Abcam, #ab175472, RRID:AB_2636996), Donkey anti-mouse IgG (H&L) (Alexa Fluor 488) (Abcam, #b150105; RRID:AB_2732856), Donkey anti-rabbit IgG (H&L) Alexa Fluor 568 (Thermo Fisher Scientific, #A10042; RRID:AB_2534017) and incubated for 1 h at room temperature. For methanol fixed samples, all antibodies were diluted in Wash Buffer Solution (1% BSA, 10% of 1x TBS, 0.1% of Triton X-100 in ddH2O) and all washes were done using the Wash Buffer solution.

For PFA-fixed endothelial cultures, cells were stained using DAPI and polyclonal goat human VE-Cadherin (R&D Systems, #AF938, 1:500) as primary antibodies with overnight incubation at 4°C. For secondary antibodies, all were used at 1:400 dilution using Donkey-anti-goat IgG Alexa 647 pre-adsorbed (Abcam, #ab150135; RRID:AB_2687955) Secondaries were incubated for 2 h at room temperature. Antibodies were diluted in a buffer solution containing 3% normal donkey serum (Jackson ImmunoResearch), 0.3% Triton X-100 (Sigma-Aldrich), 0.05% Tween20 (Sigma-Aldrich) in 1xPBS. Washes were done with 1x PBS. Immunostaining of whole-mount aorta was performed as previously described (McDonald et al., 2018).

Images were taken at ×20 magnification using an Olympus PlanApochromat 20x/0.8 N.A. objective on the ECHO Revolve scope (ECHO, San Diego, CA). Other images were taken at ×68 magnification using a CFI60 PlanApochromat Lambda D



(Continued)

FIGURE 1 (Continued)

relative positioning of a cell to the median angle of a monolayer of cells. (G) Cell shape analysis was performed by segmenting images using the “cyto2” model in CellPose 2.0, a pre-trained neural network-based algorithm, to quantify cell dimensions (H) Radial graphs comparing control and MTA treated cells. Values are shown between 0 to 360 degrees. $n = 100$ cells per condition, 3 biological replicates. Coefficients of variation for static (left to right) are 0.5, 0.56, 0.51, 0.6 and for flow (left to right) are 0.29, 0.5, 0.52, and 0.56 (Supplementary Figure S2). (I) Quantification of elongation factor. $n = 300$ per condition, 3 biological replicates. Values are shown as mean \pm SD; $n = 300$ cells per condition; Kruskal-Wallis Test with Dunn's correction. * $p < 0.05$, ** $p < 0.01$, *** $p < 0.001$, **** $p < 0.0001$.

40x/1.25 N.A. silicone oil objective on a Nikon Eclipse Ti2 spinning disk confocal microscope with CSU-W1 Yokogawa Confocal Scanner unit with LIVESR for acquisition. Images taken on the Nikon confocal microscope were post-processed using the deconvolution feature with the Richardson-Lucy method. Additional image processing and quantification was done using Imaris Software 9.9 and 10.0 (Bitplane).

Immunoblotting

Cultures were washed twice with 1xPBS buffer and protein extracts were collected with cell scrapers in mRIPA lysis buffer (40 mM Tris-HCL pH 7.5, 10% glycerol, 5mM MgCl₂, 4%SDS), containing phosphatase and protease inhibitors. Lysates were spun down and the supernatant was removed for determination of protein concentration (using a Bradford Assay) and storage. For Western blots, equal concentrations of protein lysates were loaded onto the wells of 4%–15% Mini-Protean TGXTM gels (BioRad #4561096) or 4%–20% Criterion TGX Stain-Free Protein Gels (BioRad #5678093) and subjected to electrophoresis under reducing conditions. Gels were transferred onto nitrocellulose membranes (BioRad Laboratories) and blocked for 1 h at room temperature with 2% dry skim milk-1xTBS buffer with 0.1% Tween-20. Primary antibodies monoclonal rabbit Acetylated α -tubulin (Lys40) (D20G3) (Cell Signaling #5335, RRID:AB_10544694, 1:1,000), monoclonal mouse anti-Acetylated α -tubulin (Millipore Sigma #T7451, RRID:AB_609894, 1:1,000), monoclonal mouse anti-Acetylated (Lys40) (6-11B-1) α -tubulin (Cell Signaling #12152s, RRID:AB_2797830, 1:1,000), monoclonal mouse DM1a (Cell Signaling #3873s, RRID:AB_1904178, 1:1,000), polyclonal rabbit anti-detyrosinated tubulin (Millipore Sigma #AB3201, RRID:AB_117350 1:1,000), monoclonal mouse anti-polyglutamylated tubulin, clone B3 (Sigma-Aldrich #T9822,RRID:AB_477598, 1:1,000), monoclonal rat Anti-Tubulin Antibody, clone YL1/2 (Tyrosinated-tubulin) (Millipore Sigma #MAB1864, RRID:AB_1679330, 1:1,000), mouse monoclonal GAPDH (Millipore Sigma #MAB374, RRID:AB_2107445, 1:1,000), monoclonal rat α -tubulin (YOL1/34) (Invitrogen #MA1-80189, RRID:AB_2210200, 1:1,000) and monoclonal rabbit HDAC6 (D2E5) antibody (Cell Signaling #7558s, RRID:AB_10891804, 1:1,000) were used. Blots were incubated overnight at 4°C with primaries. Membranes were washed with 1xTBS with Tween-20 buffer before adding secondary horseradish peroxidase-conjugated anti-rabbit, anti-mouse or anti-rat antibodies. Visualization of bands was done using enhanced luminol-based chemiluminescence (SuperSignal West Femto Maximum Sensitivity Substrate) (Fisher Scientific #PI34096) or (SuperSignal West Pico Chemiluminescent Substrate) (Fisher Scientific #PI34580). Densitometry was performed to quantify

protein amount using Image Lab (Bio rad). Normalization of protein levels was performed against housekeeping genes: GAPDH or α -tubulin.

Generation of HDAC6 and aTAT1 CRISPR-KO endothelial cells

HUVECs between a passage of 4 and 7 were seeded in antibiotic-free culture media with 10% FBS with a final concentration of 8ug/mL of polybrene and MOI 10 of lentivirus. Constructs containing CAS9 and guide RNAs (as in Table 1) were packaged with a second generation system using 0.08 mg/mL of PEI, VSV. G, psPAX2, and transfer plasmids in OPTIMEM I reduced serum medium. For generation of virus, transfection was performed by adding dropwise the mixed solution onto a 15 cm plastic tissue culture dish of HEK293Ts at 90% confluency cultured in antibiotic free DMEM media with 10% FBS. Lentiviral supernatants were collected 1 day after transfection. Transduced HUVECs were selected for positive genetic inactivation by puromycin selection for 2 weeks.

Transfection of EB3-GFP plasmid

Transfections of endothelial cells were performed using a Lipofectamine 3000 kit (Thermo Fisher Scientific # L3000015). EB3-GFP plasmid (Addgene, Plasmid #190164), Lipofectamine 3000 Reagent and P3000 Reagent were diluted in Opti-MEM I reduced serum medium (Fisher Scientific # 31985070) combined, and incubated at room temperature for 10–15 min. In a 6-well plastic bottom plate, 1.75 mL of antibiotic-free media with 3% FBS were added to each well. Confluent cells were trypsinized (Thermo Fisher Scientific Cat#15090046) and neutralized with full serum media, spun down, and counted for a cell concentration of 200,000 cells/mL. Incubated transfection reagent was added to each well, after which, the appropriate volume of cells was added to plates. The next day, a media change was performed using EGM-2 media with 10% FBS and antibiotics.

Time-lapse live-imaging of EB3-GFP transfected endothelial cells

24 h prior to live-imaging, 120,000 transfected endothelial cells are seeded into 0.4 mm deep u-slide I Luer microfluidic slides. Cells were used between 1-2 days after transfection to ensure the best

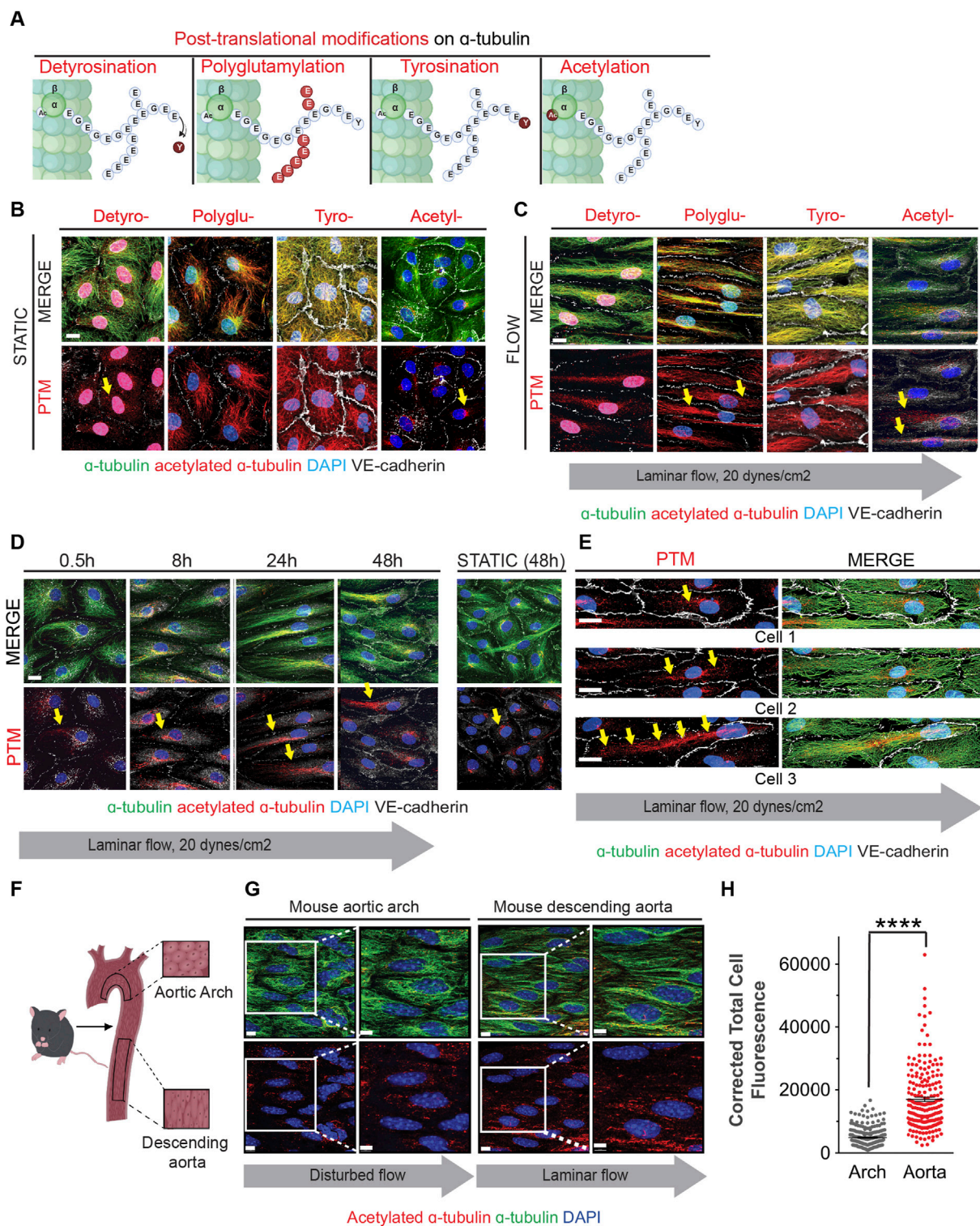


FIGURE 2

Fluid shear stress increases MT acetylation as endothelial cells undergo elongation and alignment in response to flow. (A) Schematic of post-translational modifications (PTMs) on the C-terminal end of α -tubulin (marked and labeled in red); detyrosination (detyro-), polyglutamylation (polyglu-), tyrosination (tyro-) and acetylation (acetyl-). (B) Immunofluorescence staining of post-translational modifications (red) and tubulin of HAECS exposed to static for 48 hours. Nuclei stained with DAPI. Scale bar: 20 μ m. (C) Immunofluorescence staining of post-translational modifications (red) and tubulin of HAECS exposed to laminar shear stress for 48 h. Nuclei stained with DAPI. Scale bar: 20 μ m. (D) Time course of acetylation in HAECS exposed to laminar flow at indicated time points. Yellow arrows show localization of acetylation. Scale bar: 20 μ m. (E) Staining of acetylated α -tubulin within three different endothelial cells exposed to flow. Yellow arrows point to localization of acetylation. (F) Schematic of the mouse aorta and arch. (G) Enface staining of the aortic arch and descending aorta with acetylated α -tubulin (red), α -tubulin (green), and for nuclei (DAPI). Scale bar: 10 μ m. (H) Quantification of acetylation of the aorta and arch. Data shown as mean \pm SD. Mann-Whitney U test. **** p < 0.0001.

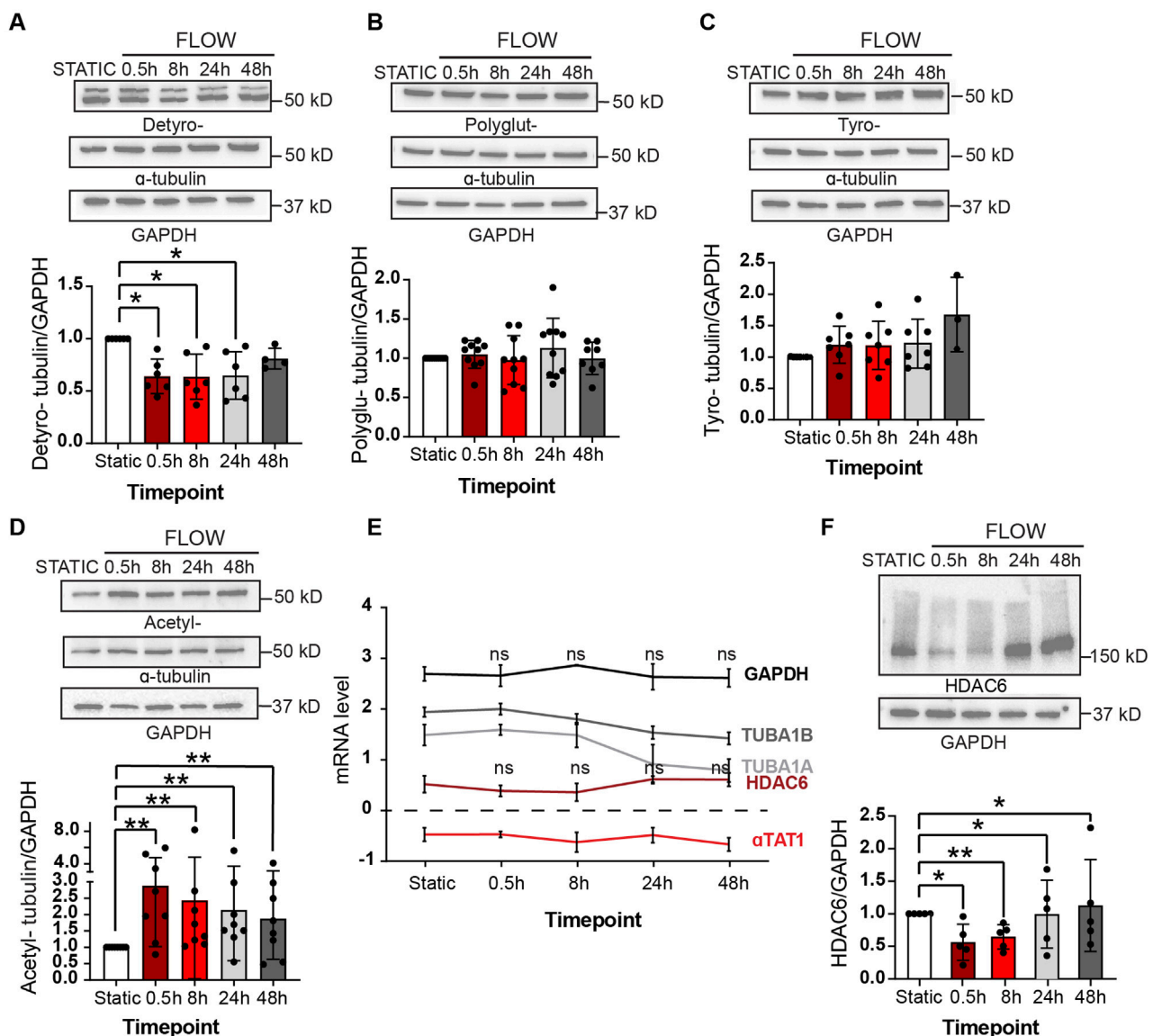


FIGURE 3

Shear stress alters post-translational modifications under shear stress Protein expression of PTMs at static (48 h), 0.5, 8, 24 and 48 h of shear stress.

(A) Detyrosination (B) Polyglutamylation (C) Tyrosination (D) Acetylation. One sample Wilcoxon test. $n =$ at least 3 technical replications with 3 biological replicates. (E) Transcriptomic data showing mRNA levels of various genes over 48 h of shear stress. Mann-Whitney U test. $n = 4$ biological replicates. (F) Protein expression of HDAC6 levels at indicated time course of static and laminar flow. Proteins were normalized to GAPDH. $n = 5$ technical replicates. One sample t-test. Data shown as mean \pm SD. * $p < 0.05$, ** $p < 0.01$.

transfection efficiency. Cells within the chamber are allowed to attach overnight. A Nikon Eclipse Ti2 spinning disk confocal microscope was used for live-imaging. A temperature-controlled enclosure with a heated stage tabletop incubator (Ibidi, Cat# 12720) was used. The attached u-slide is placed into the stage top incubator at 35°C for the lid and 37°C for the stage. To follow EB3 comets, cells were visualized using the Perfect Focus feature. Using the ND multipoint acquisition, multiple cells were chosen to be imaged simultaneously. Images were taken at intervals of 2s for a duration of 2 min with 200 ms exposure time and a 15% power of the 488 nm-laser line. Once the time-lapse videos were acquired, movies were post-processed using denoise (Denoise.ai) on NIS Elements for all frames.

Elongation factor and alignment analysis

All images were segmented using the “cyto2” model in CellPose 2.0, a pre-trained neural network-based cell segmentation algorithm. CellPose (Stringer et al., 2021) uses a U-net architecture to estimate spatial flow, combined with an energy function for each mask (i.e. the region covered by the outlines of a cell). Although CellPose is pre-trained on many diverse datasets, it is a semi-supervised model and requires certain user-defined parameters for ensuring accurate segmentation. Three main parameters that can be modified in this model are the average cell diameter, flow, and cell probability threshold. The average cell diameter (in pixels) can either be user

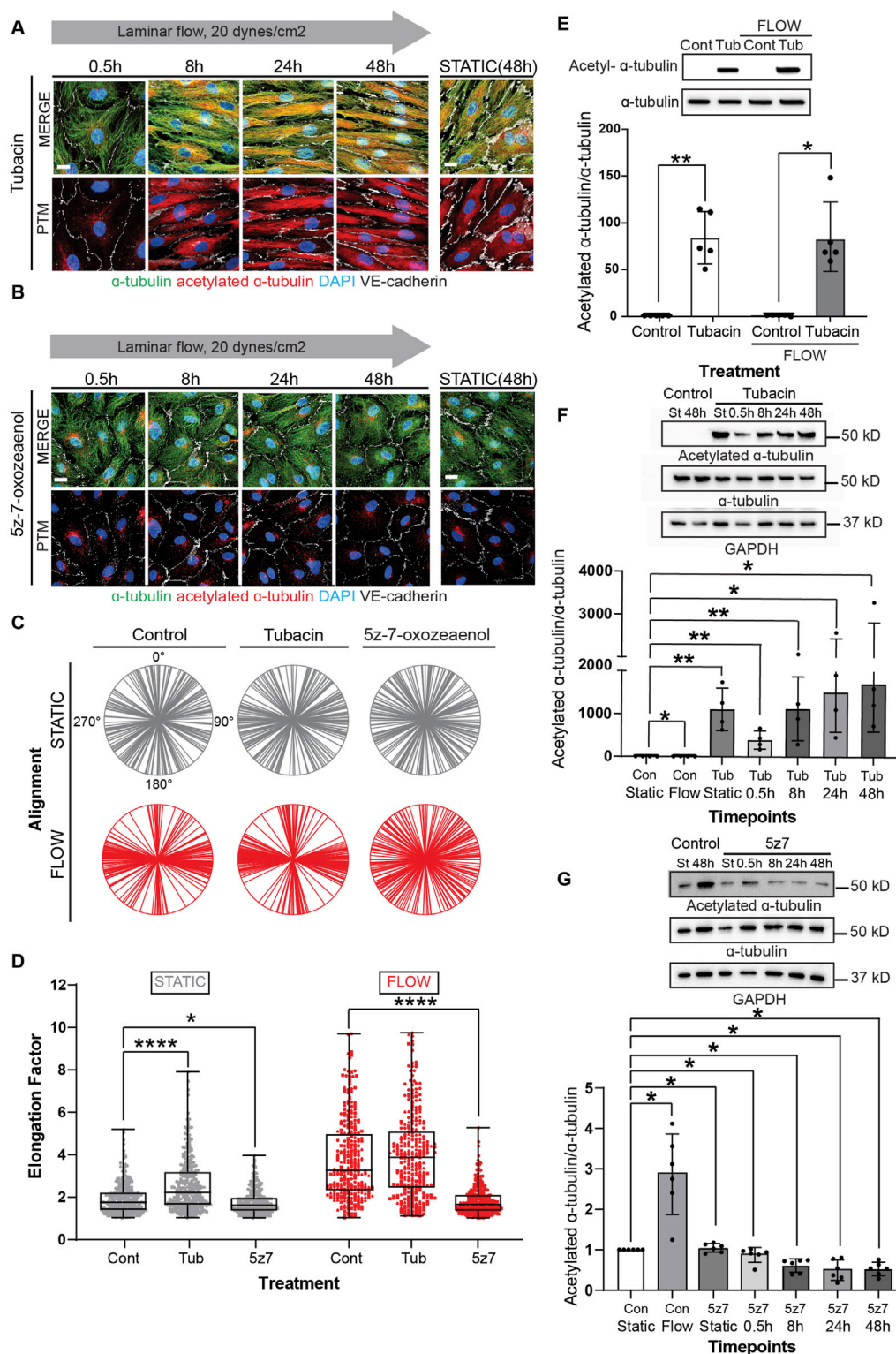


FIGURE 4

Modulation of MT acetylation by Tubacin and 5z-7-oxozeaenol impairs EC alignment and elongation under shear stress. (A, B) Immunofluorescence images of a time course of endothelial cells treated with Tubacin or 5z-7-oxozeaenol, respectively. Cells were stained for α-tubulin (green), acetylated α-tubulin (red), nuclei (DAPI) and VE-cadherin (white). Scale bar: 20 μm. (C) Radial graphs. *n* = 100 cells per condition, 3 biological replicates. Coefficients of variations for static (left to right) 0.53, 0.5, 0.48 and flow (left to right) are 0.17, 0.13 and 0.58 (Supplementary Figure S2). (D) Elongation Factor. *n* = 300 cells per condition, 3 biological replicates. Kruskal-Wallis Test with Dunn's correction. (E) Protein expression of acetylated α-tubulin and α-tubulin comparing control and Tubacin-treated cells with and without flow. *n* = 5 technical replicates with 3 biological replicates. One sample Wilcoxon test. (F) Representative blot and quantification of a time course of endothelial cells treated with Tubacin with control cells exposed to static and laminar flow. *n* = (Continued)

FIGURE 4 (Continued)

4 technical replicates. Unpaired t-test. (G) Protein quantification of a time course of endothelial cells treated with 5z-7-oxozeaenol with control cells exposed to static and laminar flow for 48 hours. $n = 6$ technical replicates. One sample Wilcoxon test. Data shown as mean \pm SD. * $p < 0.05$, ** $p < 0.01$, *** $p < 0.001$, **** $p < 0.0001$.

defined or algorithmically estimated. The flow is defined as the model fit threshold, and it determines whether a mask is consistent with the real cell's signal. Increasing the flow generates more masks. The cell probability threshold determines whether a region is a cell based on the channel intensity. By setting a high cell probability threshold, dim areas of the image can be detected as masks. Conversely, setting a low probability threshold avoids detection of dim areas as masks. Various properties of the mask (such as area, orientation, major axis length, etc.) are identified using the `region_props` function in the `scikit-image` package, which is commonly used to measure region properties of labeled images. Following segmentation, the masks were quality-checked to avoid false-positive segmentations. Very small segmentations (less than 20% of the largest cell), oddly shaped segments (major to minor axis ratio greater than 10) and partial cells present on the border of the image were removed during this process. The masks were used to estimate the longest diameter, which is the major axis of the cell. The chord perpendicular to the major axis and passing through the centroid of the mask is called the minor axis of the cell. The elongation factor is calculated as the ratio of the major axis to the minor axis. The orientation is estimated as the angle of the major axis from a horizontal line (x -axis). Since cells can be oriented along any axis (not necessarily the x -axis), we subtracted each value from the median orientation of cells in that image, to obtain the deviation from the median value (which is transformed to 0). The cell orientations are then represented as a diameter in a cell using a radial plot.

Illustrations

Illustrations were made with Biorender.

Statistical analysis

Statistical analyses across conditions were performed using GraphPad Prism 9 (San Diego, United States). For normally distributed data, two-tailed unpaired t-test was used to determine statistically significant differences between two groups. For nonparametric data, a two-tailed Mann-Whitney U test was conducted. For groups with three or more conditions, Kruskal-Wallis test was performed. For Western blot analyses, non-normal data was performed using a Wilcoxon sign rank test, while normally distributed data utilized a one sample t-test. All samples were done with at least 3 technical replicates, identified biological replicates are disclosed within each individual figure legend. $p < 0.05$ was considered statistically significant for all analyses.

Results

Active microtubule remodeling is required for EC elongation and alignment in response to laminar shear stress

In response to laminar shear stress, endothelial cells progressively alter their shape, transitioning from polygonal to elongated morphology, and aligning in the direction of flow (Figure 1A). This process is gradual but noticeable by 24–48 h in confluent monolayers. Importantly, exposure of subconfluent cells to laminar shear stress, show that cell-cell contacts were not necessary for elongation but were required for alignment (orientation of cells in relation to each other) (Supplementary Figure S1A–C). Changes in elongation and alignment are the most basic responses to shear stress and are known to be associated with changes in all three major elements of the cytoskeleton (Zielinski et al., 2018). Significant emphasis has been placed on understanding the effects of flow dynamics on actin, while information associated with changes in the microtubular network has lagged. To capture information associated with microtubule remodeling, we first used *siTubulin* to facilitate live cell labeling of MTs. Using this approach, we observed changes in orientation and structure of MTs that indicated a complex and progressive response following exposure of endothelial monolayers to laminar flow (Figure 1B). Still images collected at specific time points revealed rapid expansion of the MT network as cells elongate and increase in the abundance of polymerized MTs (Figure 1B). Importantly, under subconfluent conditions, elongation was noted, but not alignment (Supplementary Figure S1A–C), indicating that cell-cell interactions were necessary for alignment.

To clarify the significance of the flow induced MT dynamics, we exposed endothelial cultures to well-known pharmacological drugs that either promote (colchicine, nocodazole) or prevent (taxol) depolymerization of MTs (Figure 1C). MT-disruptive agents (MTAs) were titrated using EB3-GFP transfections (Supplementary Figure S1D, Video S1). The lowest dose that affected EB3-GFP movement was selected to evaluate their effect on elongation. Interestingly all MT-disrupting agents blocked the ability of endothelial cells to respond to laminar shear stress (Figure 1D). The effects on elongation (length over width) and alignment (mean angle of cell orientation in relation to each other) (Figures 1E, F) were quantified on confluent monolayers using several biological replicates and endothelial cell subtypes (aortic and vein) by combining machine learning and artificial intelligence (AI) strategies to process hundreds of individual images (Figure 1G). Radial plots were used to represent cell alignment, whereby polarity in two directions indicated positive alignment and broad circular distribution represented lack of alignment. This robust assembly of quantification methods indicated that all three pharmacological

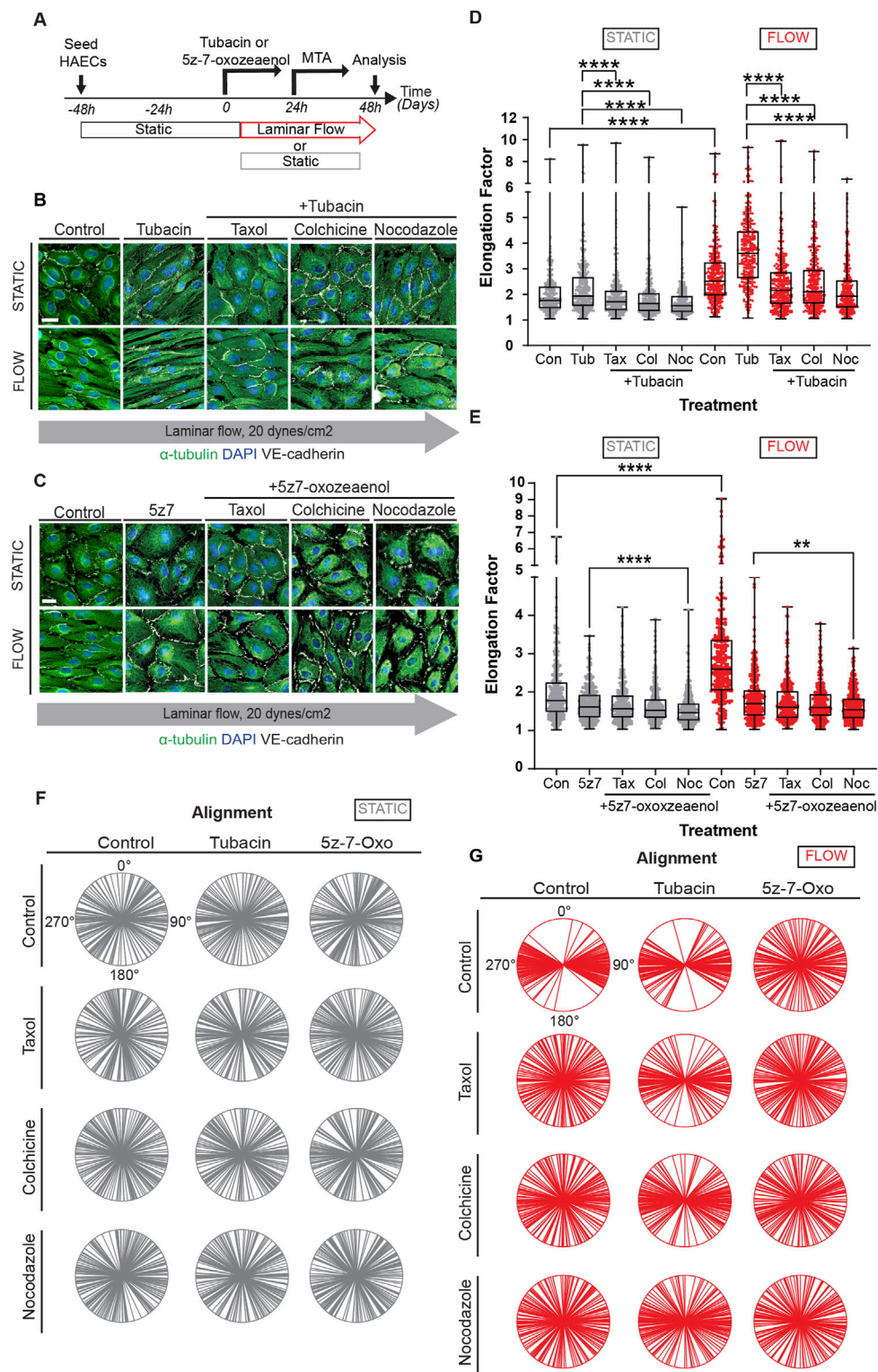


FIGURE 5

Constant microtubule dynamics and controlled acetylation is required for proper EC responses to flow. **(A)** HAECS were pre-treated with pharmacological inhibitors, Tubacin and 5z-7-oxozeaenol, and then treated with MTAs (taxol, nocodazole, or colchicine) under static or flow. Immunofluorescence images of cells sequentially treated with **(B)** Tubacin **(C)** 5z-7-oxozeaenol and then with MTAs under static or shear stress conditions. Images show staining for α -tubulin (green), nuclei (DAPI) and VE-cadherin (white). Scale bar: 20 μ m. **(D-E)** Analysis of elongation factor of **(B)** and **(C)**. Data are shown as mean \pm SD; $n = 300$ cells per condition, 3 biological replicates. Kruskal-Wallis Test with Dunn's correction. **(F, G)** Radial graphs of **(B)** and **(C)**. Coefficients of variations of **(F)** for static (column by column) are 0.57, 0.58, 0.58, 0.52, 0.63, 0.55, 0.61, 0.57, 0.59, 0.58, 0.62 and 0.59. Coefficients of variations of **(G)** for flow (column by column) are 0.28, 0.53, 0.48, 0.54, 0.28, 0.36, 0.54, 0.52, and 0.5, 0.52, 0.57 and 0.56 (**Supplementary Figure S2**). $n = 100$ cells per condition, 3 biological replicates. ** $p < 0.01$, *** $p < 0.001$, **** $p < 0.0001$.

treatments disrupted endothelial cell alignment and elongation under confluent conditions (Figures 1H, I).

Figure 1I includes findings from three biological replicates from each treatment (coefficient of variation included in the legend and shown in Supplementary Figure S2), while Supplementary Figure S3 provides the data per biological replicate. Despite some intrinsic individual variability, the outcomes were consistent in independent biological replicates (Supplementary Figure S3A–D). The effect of MTAs nullified the ability of endothelial cells to respond to shear stress by morphological reorganization. Combined these findings strongly support the hypothesis that active remodeling of the MT network is essential for endothelial cell alignment and elongation responses to laminar shear stress.

Flow-induced microtubule acetylation is necessary for EC elongation

As MTs are subjected to several types of post-translational modifications, we next inquired whether some of these modifications were altered by exposure of endothelial cells to shear stress. Specifically, we assessed MT detyrosination, polyglutamination, tyrosination, and acetylation (Figure 2A). Initially we examined the distribution and relative abundance of these modifications by immunocytochemistry (Figure 2B). This first-pass evaluation indicated that MT acetylation was increased after exposure to shear stress and that its distribution was also altered over time (Figures 2B, C). In fact, MT acetylation under laminar shear stress expanded rapidly from a Golgi-centric pattern to an elongated pattern in which microtubules extended toward one or both cellular poles (Figures 2D, E). Importantly, while MT filled the entire cytoplasm, only a subset of MT in the center of the cell were acetylated (Figure 2E).

To ascertain whether acetylation of microtubules was associated with laminar shear stress *in vivo*, we evaluated endothelial cells from aortic arch regions exposed to either disturbed or laminar blood flow. The lesser curvature of the aortic arch experiences oscillatory and disturbed flow patterns associated with the rhythmic cycles of systole and diastole; in this region, ECs are polygonal and do not align in the direction of flow (Figures 2F, G). In contrast, ECs in the descending aorta are exposed to laminar shear stress and are both elongated and aligned in the direction of blood flow (Figure 2G). Furthermore, levels of acetylated alpha-tubulin were higher in the descending aorta when compared to the aortic arch (Figure 2H).

A more expansive assessment of microtubule post-translational modifications was conducted by immunoblot analyses with multiple biological replicates (Figures 3A–D). Upon initiation of flow, we observed a statistically significant decrease in alpha-tubulin detyrosination which returned to static levels after 48 h (Figure 3A). No changes were noted in the levels of polyglutamination or tyrosination (Figures 3B, C). However, a rapid increase in acetylated alpha-tubulin was observed over the same time course when compared to static conditions. Significantly, alpha-tubulin experienced a 2.5 fold increase in acetylation over the first 30 min after initiation of flow (Figure 3D; Supplementary Figure S4 for uncropped individual blots).

The observed response of MT-acetylation to flow was fast and robust and we then explored the potential mechanism associated with such change. Steady-state acetylation of proteins is reached by

the net effect of acetylases and deacetylases. In the case of microtubules, this is accomplished by the acetylase alpha TAT1 and the deacetylase HDAC6 (Kalebic et al., 2013; Haggarty et al., 2003; Hubbert et al., 2002; You et al., 2020; North et al., 2007). One potential explanation to the increase in MT acetylation would be either the transcriptional increase of alpha TAT1 or the decrease of HDAC6 by flow. However, we found that both transcripts were fairly stable upon flow induction (Figure 3E). In contrast, levels of HDAC6 protein declined precipitously upon exposure of endothelial cultures to flow conditions (Figure 2F). This reduction of HDAC6 protein explains the significant accumulation of MT acetylation at early time points.

Next, we explored the biological implications of pharmacological blockade of acetylases and deacetylases to endothelial cell elongation and alignment under flow conditions. Tubacin is a highly selective and reversible HDAC6 inhibitor that permeates the cell membrane and leads to rapid increase in tubulin acetylation (Hideshima et al., 2016; Itoh et al., 2007). In contrast, 5z-7-oxozeanol, an inhibitor of TAK1 prevents TAT-1 mediated acetylation of microtubules (Shah et al., 2018). Prior to exposing cells to tubacin and 5z-7-oxozeanol, we titrated the levels of these inhibitors to reach changes in acetylation while maintaining cellular function and MT dynamics. For this, we again used EB3-GFP to monitor MT activity (Supplementary Figure S1E, Video S2) while also assessing efficient modifications on MT acetylation.

Treatment of confluent endothelial cultures with tubacin resulted in abundant acetylation of MT with accelerated elongation (Figure 4A). In contrast, blockade of MT acetylation with 5z-7-oxozeanol prevented endothelial cell elongation in response to laminar shear stress (Figure 4B). Evaluation of cell alignment in confluent cultures showed that tubacin enhanced parallel organization of cells in direction to flow, while 5z-7-oxozeanol impaired this collective response to flow (Figure 4C). The alignment of individual biological replicates under each treatment is shown in Supplementary Figure S5A–D. Importantly, quantification of endothelial elongation revealed that even under static conditions, tubacin promoted cell elongation, an effect that was more pronounced under flow conditions (Figure 4D). Increased MT acetylation by tubacin was confirmed by immunoblots revealing an increase of approximately 80-fold over control-treated cultures (Figure 4E; Supplementary Figure S6 for uncropped blots). The effect of tubacin on microtubule acetylation is gradual but extremely robust and noted as early as 30 min by immunoblot (Figure 4F). Importantly, flow-mediated induction in acetylation was significantly blocked by 5z-7-oxozeanol (Figure 4G). Interestingly, base-line acetylation was retained in the presence of the TAK1 inhibitor (Figures 4B, G) implying that 5z-7-oxozeanol only blocks the acetylation that is induced by flow. Note that for these experiments, treatment with 5z-7-oxozeanol was done concurrently with application of flow, but even after 48h, base-line acetylation was retained.

Maintenance of elongation requires MT remodeling despite prior increases in acetylation

Acetylation of microtubules is thought to increase their stability. Interestingly, we found that levels of MT acetylation were drastically

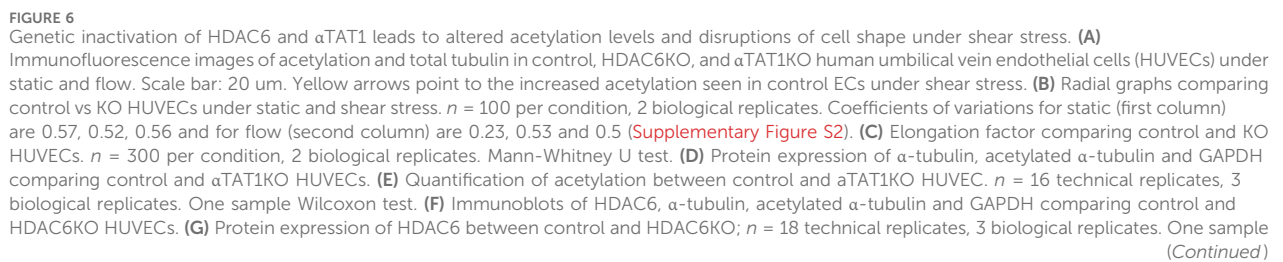


FIGURE 6 (Continued)

Wilcoxon test. (H) Protein expression of acetylated α -tubulin from control compared to HDAC6KO HUVECs. $n = 14$ technical replicates, 3 biological replicates. One sample Wilcoxon test. Data shown as mean \pm SD, except (D) which is shown at mean \pm SEM. * $p < 0.05$ ** $p < 0.01$, *** $p < 0.0001$.

increased when endothelial cells were exposed to taxol (Supplementary Figure S7), indicating that status of MT dynamics feedbacks on acetylation. Along these lines, it is unclear if shear-induced elongation of endothelial cells is a stable phenotype or if microtubule remodeling is continuously necessary to maintain this phenotype. Thus, we performed experiments in which cells were exposed to flow for 24 h, in the presence or absence of tubacin or 5z-7-oxozeaenol, followed by an additional 24 h of laminar flow with MT disrupting agents (Figure 5A). Evaluation of such cultures by immunocytochemistry revealed that cell elongation was reversed by MTA drugs even when in the presence of tubacin (Figure 5B), while no change was observed when similar experiments were done with 5z-7-oxozeaenol (Figure 5C). Quantification of cell elongation in the presence of tubacin under static conditions further showed a statistically significant difference between tubacin alone and tubacin in the presence of MTAs (Figure 5D). Under flow conditions, cells lost their elongated phenotype and became polygonal when exposed to inhibitors of MT dynamics even in the context of shear stress (Figure 5D). When exposed to 5z-7-oxozeaenol in the presence of MTAs, a statistically significant difference was only observed when in the presence of nocodazole (Figure 5E). Despite these changes, intercellular contacts were retained under all conditions (Figures 5B, C).

Alignment was also evaluated in these experiments. As expected, no changes in alignment were observed under static conditions (Figure 5F and individual biological replicates in Supplementary Figure S8). Cultures under laminar shear stress and treated with tubacin tended to show a different trend for alignment than for elongation when exposed to inhibitors of MT dynamics (Figure 5G). In fact, cultures exposed to tubacin were more resistant to becoming randomized in their alignment when exposed to taxol and colchicine than cultures not exposed to tubacin (Figure 5G). This effect was more pronounced in some biological replicates than in others (Supplementary Figure S8). The findings are consistent with the notion that acetylation increases MT stability making them more resistant to depolymerization. In addition, these results underline the constant requirement of MT dynamics to mechanotransduction.

HDAC6 and alpha-TAT1 regulate MT acetylation during EC responses to laminar shear stress

To mitigate the potential off-target effects of pharmacological inhibitors (tubacin and 5z-7-oxozeaenol) on the emerging conclusions, we performed experiments where HDAC6 and alpha-TAT1 were inactivated by CRISPR on endothelial cells. It has been well-accepted that HDAC6 is the enzyme that removes acetyl groups from tubulin (Haggarty et al., 2003), while alpha-

TAT1 can acetylate tubulin on lysine 40 (Kalebic et al., 2013). Although these two enzymes are not the only ones that can have this function on MT. We indeed found that CRISPR-mediated inactivation of alpha TAT1 results in a very efficient blockade of MT-acetylation (Figure 6A). Furthermore, elongation and alignment were inhibited when this enzyme was absent in endothelial cells (Figures 6A–C). In contrast, inactivation of HDAC6 resulted in robust microtubule acetylation, promoted endothelial cell elongation and alignment (Figures 6A–C; Supplementary Figure S9A–C for individual biological replicates). Similarly to tubacin exposure, inactivation of HDAC6 resulted in a statistically significant increase in endothelial cell elongation even under static conditions (Figure 6C). Biochemical evaluation of the changes in microtubule acetylation was also conducted using immunoblots. Inactivation of alpha alpha TAT1 blocked microtubule acetylation (Figures 6D, E; Supplementary Figures S9D–H for uncropped blots). In contrast, the absence of HDAC6 resulted in a robust increase (nearly 100-fold) in microtubule acetylation (Figures 6F–H). The impressive elevation of acetylation in HDAC6 null cultures underlines the essential impact of this enzyme in controlling steady-state levels of MT acetylation.

DISCUSSION

Using a combination of pharmacological inhibitors and genetic manipulations, this study demonstrates the essential requirement of MT dynamics on endothelial cell mechanotransduction in response to laminar shear stress. Specifically, endothelial cell elongation and alignment were blocked in the presence of agents that either inhibit polymerization or depolymerization of MT. We also showed that acetylation of microtubules increases rapidly when endothelial cells are exposed to laminar shear stress *in vitro* and *in vivo* (Figure 7A). Furthermore, genetic or pharmacological prevention of this post-translational modification hinders cell elongation and alignment in response to laminar shear stress (Figure 7B). Together, these findings highlight the contributions of microtubules to the most basic responses of endothelial cells to fluid flow.

The cytoskeleton is a common denominator in a growing array of cellular responses to mechanical force. All three major components of the cytoskeleton have been implicated in responses to physical force, including actin, intermediate filaments, and microtubules (Chien, 2007; Campinho et al., 2020). Thus, it is not surprising that endothelial responses to shear stress have been linked with an expanding number of alterations in these proteins and an expanding appreciation for the role of cytoskeletal regulators in their highly varied physiologic contexts. In fact, remodeling of the endothelial actin cytoskeleton

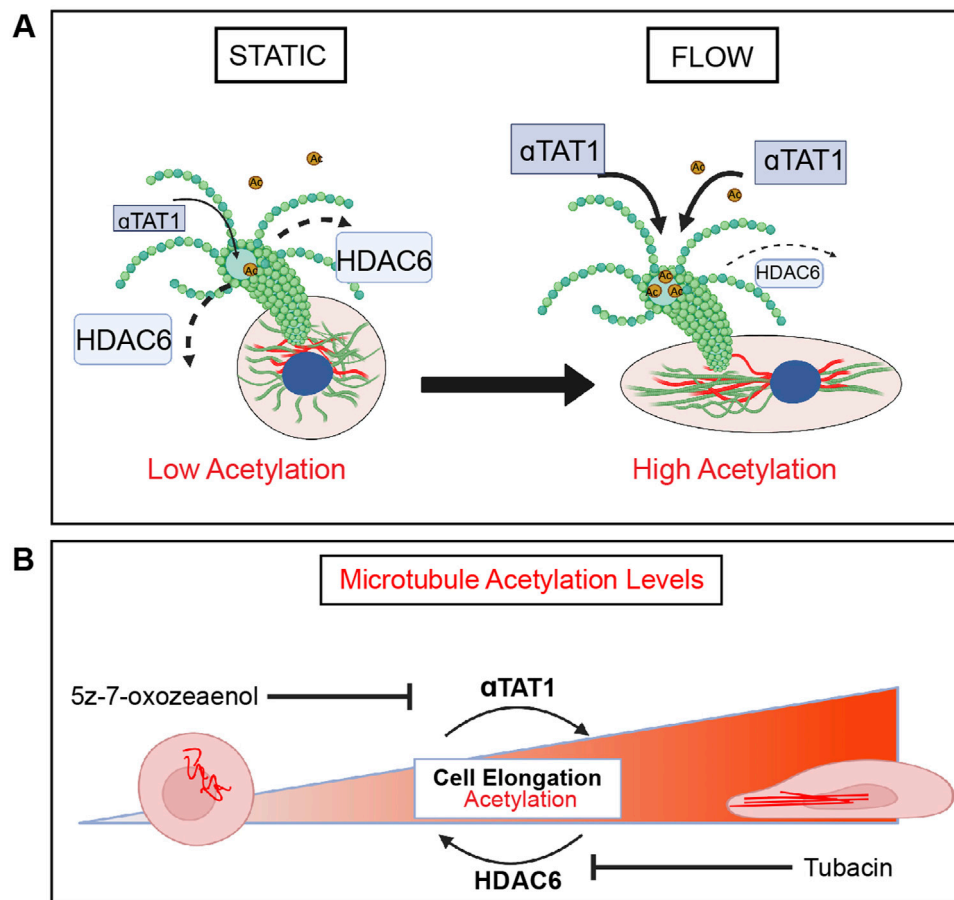


FIGURE 7

HDAC6 and α TAT1 are key mediators of EC mechanotransduction through regulation of microtubule acetylation. **(A)** In response to shear stress, endothelial cells elongate and align in the direction of flow through remodeling of the cytoskeleton which includes reorganization of microtubules. There is a flow-dependent increase in acetylation that corresponds to endothelial cell elongation and alignment. HDAC6 and α TAT1 regulate the timing (kinetics) and localization of acetylation on α -tubulin in response to shear stress in endothelial cells. HDAC6 is found at its lowest at the onset of flow. **(B)** Disruption of HDAC6 and α TAT1, the key regulators of MT acetylation by pharmacological inhibition or through genetic inactivation results in impairment of endothelial cell mechanotransduction. Loss of HDAC6 leads to significant acetylation and faster kinetics in elongation. Inactivation of α TAT1 leads to significant reduction in acetylation with reduced elongation.

and focal adhesions have been described in detail (Helmke et al., 2003; Noria et al., 2004; Mott and Helmke, 2007; Gegenfurtner et al., 2018). Intermediate filaments, and in particular vimentin has been implicated in the transmission of forces sensed by PECAM in response to shear stress (Collins et al., 2012). Conspicuously absent from this framework was the role of microtubules relatively few studies reporting microtubule network elongation in response to shear stress (Zielinski et al., 2018). Importantly, previous investigators recognized an increase in MT acetylation in response to shear stress, although those studies did not address the kinetics, deacetylases and acetylases involved, mechanisms, or effects on alignment (McCue et al., 2006).

Unexpectedly and in broad strokes, the contribution of the three major cytoskeletal proteins in sensing and responding to shear stress appears to be largely not-overlapping. For example, genomic inactivation of vimentin, the main and highly abundant intermediate filament in endothelial cells has no impact on endothelial cell elongation in response to flow (Salvador et al., 2022). This is not to negate other roles of

vimentin in mechanotransduction. Nonetheless it is clear that cell elongation in response to flow is not part of its portfolio of vimentin activities. In contrast, the actin cytoskeleton owns a unique position in the regulation of EC polarity, cell-cell and cell-matrix through its interactions with focal adhesions and cell adhesion molecules, like cadherin complexes (Wojciak-Stohard and Ridley, 2003; Noria et al., 2004) both in the presence and absence of flow. Furthermore, the actin cytoskeleton is critical at counterbalancing excessive intracellular tension through cross talk with phosphoinositide (PI) 3-kinase (Thodeti et al., 2009). At present, microtubules stand alone in regulating cell shape changes in response to shear stress, a function that couples well with its roles in intracellular transport. While not tested here, it is possible that microtubule acetylation, known to alter affinity for motor proteins could contribute to elongation by playing a formative role in delivering key components needed for polarized membrane expansion and resorption. Along these lines, it is interesting that actin displays interactions specifically

with acetylated microtubules, through Arp2/3 regulation of cargo trafficking (Yoshimura et al., 2021).

We also found that the MT network adapts differently in regions of the arterial tree responding to different types of flow stress. ECs on the inner curvature of the aortic arch are exposed to disturbed blood flow, are polygonal in morphology, and exhibit lower levels of acetylated MTs. In contrast, ECs found in the descending aorta are exposed to unidirectional (laminar) blood flow. ECs in descending aorta are elongated in the direction of flow and express a MT network that is directionally organized and displaying increased levels of acetylated- α -tubulin in the region of the cell facing into the flow, upstream of the nucleus. A potential function of increased acetylation of α -tubulin could be the acquisition of additional resilience to mechanical strain, helping to buttress cellular responses to shear stress. Along these lines, it is interesting that acetylation of microtubules is known to augment their stability, enhance flexibility and resistance against repeated mechanical stresses (Xu et al., 2017; Prokop et al., 2022; Saunders et al., 2022). An unexpected finding from our studies was that treatment with taxol alone, resulted in a remarkable increase in MT acetylation. Interestingly despite this high acetylation (similar to levels seen with tubacin), presence of taxol blocked endothelial cells from responding flow. The findings imply that microtubule dynamics are continuously required for endothelial responses to flow, as high acetylation cannot override the need for microtubule remodeling. Importantly, acetylation of α -tubulin protects long-lived MTs from mechanical aging by making them less susceptible to stress-induced damage while preventing pre-existing MT lattice defects from spreading (Portran et al., 2017). Whereas accumulation of stress-induced damage was observed in deacetylated MTs subjected to continuous stress (Portran et al., 2017). Cilia are structures highly enriched for acetylated tubulin, however in agreement with previous literature (Dinsmore and Reiter, 2016) we found that only a low percentage of cells under laminar shear stress had cilia.

The potential links between MT acetylation and TGF- β signaling in the context of shear stress did not escape us. As demonstrated here, α -TAT1 is the critical acetyltransferase responsible for microtubule acetylation in response to shear stress. Interestingly, TGF- β activated kinase (TAK1) phosphorylates α -TAT1 at Ser237 promoting its activation and, in turn, MT acetylation (Shah et al., 2018; Zhu et al., 2021). These molecular and functional relationships link TGF- β signaling to MT acetylation and endothelial cell elongation. In fact, the use of 5z-7 oxozeanol, an inhibitor of TAK1, clearly shows the relevance of this kinase in microtubule acetylation in response to flow. Interestingly, 5z-7 oxozeanol blocked flow-induced MT acetylation; however, base-line acetylation of MT in proximity to the Golgi was retained, as noted by staining and immunoblotting. The findings imply that base-line acetylation in might be regulated by a distinct subset of acetylases. It is peculiar that a clear consequence in endothelial cells that lack endoglin or Smad4 is the loss of endothelial cell elongation in response to shear stress (Poduri et al., 2017; Sugden et al., 2017). The implication is that inadequate MTacetylation in response to flow might impact endothelial cell shape and perhaps contribute to the development of

hereditary hemorrhagic telangiectasia in patients with mutations in those genes.

In summary, our data expands our current understanding of how endothelial cells respond to shear stress and bring microtubule acetylation at the forefront of cell shape remodeling in the context of physical forces.

LIMITATIONS: There are several limitations of the study, particularly in relation to the specificity of acetylation and possible confounding effects of pharmacological and genetic inactivation on other targets. In fact, HDAC6 deacetylates multiple other cytoplasmic targets, some of these highly relevant to endothelial cell biology such as cortactin. The same can be stated for α -TAT1. Alternative approaches would be to mutate the lysine associated with the acetylation. Unfortunately, this is also problematic in the case of microtubules, as lysine 40 is also a site for methylation. Thus, mutating this site will also be confounded by how absence of methylation impacts MT function in the context of shear stress. Despite these limitations, the combination of pharmacological and genetic inhibition of HDAC6 does bring to light the constant activity of this enzyme on endothelial MT and its regulation is likely to be the rate-limiting step in the maintenance and distribution of acetylated microtubules. Future studies evaluating HDAC6 regulation and control, as well as the impact of MT acetylation in transport of cargo are likely important next steps to fully understand endothelial polarity in response to shear stress.

Data availability statement

The raw data presented in the study are deposited in the BioImage Archive, accession number S-BIAD1345 (<https://www.ebi.ac.uk/biostudies/BioImages/studies/S-BIAD1345>). The code used for elongation and alignment analyses are deposited in Github (<https://github.com/GoyalLab/EndothelialCellAnalysis>).

Ethics statement

The animal study was approved by IACUC Northwestern University, Feinberg School of Medicine. The study was conducted in accordance with the local legislation and institutional requirements.

Author contributions

KM: Visualization, Writing–review and editing, Writing–original draft, Validation, Methodology, Investigation, Formal Analysis, Data curation. KA: Writing–review and editing, Visualization, Software, Methodology, Formal Analysis. MP: Writing–review and editing, Software, Formal Analysis. JS: Writing–review and editing, Visualization, Data curation. ASM: Writing–review and editing, Validation, Visualization, Formal analysis. YG: Writing–review and editing, Supervision, Software. MLI-A: Writing–review and editing, Writing–original draft, Supervision, Resources, Investigation, Funding acquisition, Conceptualization.

Funding

The author(s) declare that financial support was received for the research, authorship, and/or publication of this article. This work was supported by the National Institutes of Health R35HL140014 to MLIA.

Acknowledgments

The author team would like to acknowledge the contributions of Sanna Vattulainen-Collanus who provided some of the preliminary data for this work while in the Arispe lab at UCLA. We most sincerely appreciate the gift of the EB3-GFP construct from the Gelfand laboratory (Dept. of Cell and Dev. Biology, Northwestern University) and their insight on microtubules. We also would like to thank the CAM core at Northwestern University, Feinberg School of Medicine. We also would like to acknowledge the Carson Stringer and Marius Pachitariu. (Howard Hughes Medical Institute (HHMI) Janelia Research Campus) providing the software tools for analyzing cell-segmentation data in CellPose.

References

- Baeyens, N., and Schwartz, M. A. (2016). Biomechanics of vascular mechanosensation and remodeling. *Mol. Biol. Cell* 27, 7–11. doi:10.1091/mbc.E14-11-1522
- Bevan, J. A., Garcia-Roldan, J. L., and Joyce, E. H. (1990). Resistance artery tone is influenced independently by pressure and by flow. *Blood Vess* 27, 202–207. doi:10.1159/000158811
- Campinho, P., Vilfan, A., and Vermont, J. (2020). Blood flow forces in shaping the vascular system: a focus on endothelial cell behavior. *Front. Physiol.* 11, 552–557. doi:10.3389/fphys.2020.00552
- Chien, S. (2007). Mechanotransduction and endothelial cell homeostasis: the wisdom of the cell. *Am. J. Physiol. Heart Circ. Physiol.* 292, H1209–H1224. doi:10.1152/ajpheart.01047.2006
- Chiu, J. J., and Chien, S. (2011). Effects of disturbed flow on vascular endothelium: pathophysiological basis and clinical perspectives. *Physiol. Rev.* 91, 327–387. doi:10.1152/physrev.00047.2009
- Collins, C., Guilly, C., Welch, C., O'Brien, E. T., Hahn, K., Superfine, R., et al. (2012). Localized tensional forces on PECAM-1 elicit a global mechanotransduction response via the integrin-RhoA pathway. *Curr. Biol.* 22, 2087–2094. doi:10.1016/j.cub.2012.08.051
- Coste, B., Mathur, J., Schmidt, M., Earley, T. J., Ranade, S., Petrus, M. J., et al. (2010). Piezo1 and Piezo2 are essential components of distinct mechanically activated cation channels. *Science* 330, 55–60. doi:10.1126/science.1193270
- Dinsmore, C., and Reiter, J. F. (2016). Endothelial primary cilia inhibit atherosclerosis. *EMBO Rep.* 17, 156–166. doi:10.15252/embr.201541019
- Fan, Y., Lu, H., Liang, W., Hu, W., Zhang, J., and Chen, Y. E. (2017). Krüppel-like factors and vascular wall homeostasis. *J. Mol. Cell Biol.* 9, 352–363. doi:10.1093/jmcb/mjx037
- Fleming, I., Fisslthaler, B., Dixit, M., and Busse, R. (2005). Role of PECAM-1 in the shear-stress-induced activation of Akt and the endothelial nitric oxide synthase (eNOS) in endothelial cells. *J. Cell Sci.* 118, 4103–4111. doi:10.1242/jcs.02541
- Gegenfurtner, F. A., Jahn, B., Wagner, H., Ziegenhain, C., Enard, W., Geistlinger, L., et al. (2018). Micropatterning as a tool to identify regulatory triggers and kinetics of actin-mediated endothelial mechanosensing. *J. Cell Sci.* 131, 212886. doi:10.1242/jcs.212886
- Haggarty, S. J., Joeller, K. M., Wong, J. C., Grozinger, C. M., and Schreiber, S. L. (2003). Domain-selective small-molecule inhibitor of histone deacetylase 6 (HDAC6)-mediated tubulin deacetylation. *Proc. Natl. Acad. Sci. U. S. A.* 100, 4389–4394. doi:10.1073/pnas.0430973100
- Helmke, B. P., Rosen, A. B., and Davies, P. F. (2003). Mapping mechanical strain of an endogenous cytoskeletal network in living endothelial cells. *Biophys. J.* 84, 2691–2699. doi:10.1016/S0006-3495(03)75074-7
- Hideshima, T., Qi, J., Paranal, R. M., Bradner, J. E., Greenberg, E., West, N., et al. (2016). Discovery of selective small-molecule HDAC6 inhibitor for overcoming proteasome inhibitor resistance in multiple myeloma. *Proc. Nat. Acad. Sci. U. S. A.* 113, 13162–13167. doi:10.1073/pnas.1608067113
- Hubbert, C., Guardiola, A., Shao, R., Kawaguchi, Y., Ito, A., Nixon, A., et al. (2002). HDAC6 is a microtubule-associated deacetylase. *Nature* 417, 455–458. doi:10.1038/417455a
- Itoh, Y., Suzuki, T., Kouketsu, A., Suzuki, N., Maeda, S., Yoshida, M., et al. (2007). Design, synthesis, structure-selectivity relationship and effect on human cancer cells of a novel series of histone deacetylase 6-selective inhibitors. *J. Med. Chem.* 50, 5425–5438. doi:10.1021/jm7009217
- Kalebic, N., Sorrentino, S., Perlas, E., Bolasco, G., Martinez, C., and Heppenstall, P. A. (2013). α TAT1 is the major α -tubulin acetyltransferase in mice. *Nat. Comm.* 4, 1962. doi:10.1038/ncomms2962
- Langille, B. L. (1992). Blood flow-induced remodeling of arteries in health and disease. *Cardiovasc. Pathol.* 1, 245–251. doi:10.1016/1054-8807(92)90034-L
- Mack, J. J., Mosquero, T. S., Archer, B. J., Jones, W. M., Sunshine, H., Faas, G. C., et al. (2017). NOTCH1 is a mechanosensor in adult arteries. *Nat. Commun.* 8, 1620. doi:10.1038/s41467-017-01741-8
- McCue, S., Dajnowiec, D., Xu, F., Zhang, M., Jackson, M. R., and Langille, B. L. (2006). Shear stress regulates forward and reverse planar cell polarity of vascular endothelium *in vivo* and *in vitro*. *Circ. Res.* 98, 939–946. doi:10.1161/01.RES.0000216595.15868.55
- McDonald, A. I., Shirali, A. S., Aragón, R., Ma, F., Hernandez, G., Vaughn, D. A., et al. (2018). Endothelial regeneration of large vessels is a biphasic process driven by local cells with distinct proliferative capacities. *Cell Stem Cell* 23, 210–225. doi:10.1016/j.stem.2018.07.011
- Mendoza, S. A., Fang, J., Gutterman, D. D., Wilcox, D. A., Bubolz, A. H., Li, R., et al. (2010). TRPV4-mediated endothelial Ca^{2+} influx and vasodilation in response to shear stress. *Am. J. Physiol. Heart Circ. Physiol.* 298, H466–H476. doi:10.1152/ajpheart.00854.2009
- Mohan, S., Mohan, N., and Sprague, E. A. (1997). Differential activation of NF-kappa B in human aortic endothelial cells conditioned to specific flow environments. *Am. J. Physiol.* 273, C572–C578. doi:10.1152/ajpcell.1997.273.2.C572
- Mott, R. E., and Helmke, B. P. (2007). Mapping the dynamics of shear stress-induced structural changes in endothelial cells. *Am. J. Physiol. Cell Physiol.* 293, C1616–C1626. doi:10.1152/ajpcell.00457.2006
- Noria, S., Xu, F., McCue, S., Jones, M., Gotlieb, A. I., and Langille, B. L. (2004). Assembly and reorientation of stress fibers drives morphological changes to endothelial cells exposed to shear stress. *Am. J. Pathol.* 164, 1211–1223. doi:10.1016/S0002-9440(10)63209-9
- North, B. J., Sadoul, K., Pabion, M., and Khochbin, S. (2007). HDAC6, at the crossroads between cytoskeleton and cell signaling by acetylation and ubiquitination. *Oncogene* 26, 5468–5476. doi:10.1038/sj.onc.1210614

Conflict of interest

The authors declare that the research was conducted in the absence of any commercial or financial relationships that could be construed as a potential conflict of interest.

Publisher's note

All claims expressed in this article are solely those of the authors and do not necessarily represent those of their affiliated organizations, or those of the publisher, the editors and the reviewers. Any product that may be evaluated in this article, or claim that may be made by its manufacturer, is not guaranteed or endorsed by the publisher.

Supplementary material

The Supplementary Material for this article can be found online at: <https://www.frontiersin.org/articles/10.3389/fphys.2024.1425620/full#supplementary-material>

- Poduri, A., Chang, A. H., Raftrey, B., Rhee, S., Van, M., and Red-Horse, K. (2017). Endothelial cells respond to the direction of mechanical stimuli through SMAD signaling to regulate coronary artery size. *Development* 144, 3241–3252. doi:10.1242/dev.150904
- Portran, D., Schaedel, L., Xu, Z., Théry, M., and Nachury, M. V. (2017). Tubulin acetylation protects long-lived microtubules against mechanical ageing. *Nat. Cell Biol.* 19, 391–398. doi:10.1038/ncb3481
- Prokop, A. (2022). Microtubule regulation: transcending the tenet of K40 acetylation. *Curr. Biol.* 32, R126–R128. doi:10.1016/j.cub.2021.12.018
- Rödel, C. J., Otten, C., Donat, S., Lourenço, M., Fischer, D., Kuropka, B., et al. (2019). Blood flow suppresses vascular anomalies in a zebrafish model of cerebral cavernous malformations. *Circ. Res.* 125, e43–e54. doi:10.1161/CIRCRESAHA.119.315076
- Salvador, J., Hernandez, G. E., Ma, F., Abrahamson, C. W., Pellegrini, M., Goldman, R., et al. (2022). Transcriptional evaluation of the ductus arteriosus at the single-cell level uncovers a requirement for vim (vimentin) for complete closure. *Arter. Thromb. Vasc. Biol.* 42, 732–742. doi:10.1161/ATVBAHA.121.317172
- Saunders, H. A. J., Johnson-Schlitz, D. M., Jenkins, B. V., Volkert, P. J., Yang, S. Z., and Wildonger, J. (2022). Acetylated α -tubulin K394 regulates microtubule stability to shape the growth of axon terminals. *Curr. Biol.* 32, 614–630.e5. doi:10.1016/j.cub.2021.12.012
- Shah, N., Kumar, S., Zaman, N., Pan, C. C., Bloodworth, J. C., Lei, W., et al. (2018). TAK1 activation of α -TAT1 and microtubule hyperacetylation control AKT signaling and cell growth. *Nat. Commun.* 9, 1696. doi:10.1038/s41467-018-04121-y
- Shiu, Y.-T., Li, S., Marganski, W. A., Usami, S., Schwartz, M. A., Wang, Y.-L., et al. (2004). Rho mediates the shear-enhancement of endothelial cell migration and traction force generation. *Biophys. J.* 86, 2558–2565. doi:10.1016/S0006-3495(04)74311-8
- Stringer, C., Wang, T., Michaelos, M., and Pachitariu, M. (2021). Cellpose: a generalist algorithm for cellular segmentation. *Nat. Methods* 18, 100–106. doi:10.1038/s41592-020-01018-x
- Sugden, W. W., Meissner, R., Aegerter-Wilmsen, T., Tsaryk, R., Leonard, E. V., Bussmann, J., et al. (2017). Endoglin controls blood vessel diameter through endothelial cell shape changes in response to haemodynamic cues. *Nat. Cell Biol.* 19, 653–665. doi:10.1038/ncb3528
- Thodeti, C. K., Matthews, B., Ravi, A., Mammoto, A., Ghosh, K., Bracha, A. L., et al. (2009). TRPV4 channels mediate cyclic strain-induced endothelial cell reorientation through integrin-to-integrin signaling. *Circ. Res.* 104, 1123–1130. doi:10.1161/CIRCRESAHA.108.192930
- Tzima, E., Irani-Tehrani, M., Kiosses, W. B., Dejana, E., Schultz, D. A., Engelhardt, B., et al. (2005). A mechanosensory complex that mediates the endothelial cell response to fluid shear stress. *Nature* 437, 426–431. doi:10.1038/nature03952
- Wojciak-Stothard, B., and Ridley, A. J. (2003). Shear stress-induced endothelial cell polarization is mediated by Rho and Rac but not Cdc42 or PI 3-kinases. *J. Cell Biol.* 161, 429–439. doi:10.1083/jcb.200210135
- Xu, Z., Schaedel, L., Portran, D., Aguilar, A., Gaillard, J., Marinkovich, M. P., et al. (2017). Microtubules acquire resistance from mechanical breakage through intraluminal acetylation. *Science* 356, 328–332. doi:10.1126/science.aai8764
- Yoshimura, A., Miserey-Lenkei, S., Coudrier, E., and Goud, B. (2021). Branched actin maintains acetylated microtubule network in the early secretory pathway. *Cells* 11, 15. doi:10.3390/cells11010015
- You, E., Ko, P., Jeong, J., Keum, S., Kim, J. W., Seo, Y. J., et al. (2020). Dynein-mediated nuclear translocation of yes-associated protein through microtubule acetylation controls fibroblast activation. *Cell Mol. Life Sci.* 77, 4143–4161. doi:10.1007/s00018-019-03412-x
- Zhang, Y., Lee, T. S., Kolb, E. M., Sun, K., Lu, X., Sladek, F. M., et al. (2006). AMP-activated protein kinase is involved in endothelial NO synthase activation in response to shear stress. *Arterioscler. Thromb. Vasc. Biol.* 26, 1281–1287. doi:10.1161/01.ATV.0000221230.08596.98
- Zhu, L., Lama, S., Tu, L., Disting, G. J., Wang, J.-H., and Liu, G.-S. (2021). TAK1 signaling is a potential therapeutic target for pathological angiogenesis. *Angiogenesis* 24, 453–470. doi:10.1007/s10456-021-09787-5
- Zielinski, A., Linnartz, C., Pleschka, C., Dreissen, G., Springer, R., Merkel, R., et al. (2018). Reorientation dynamics and structural interdependencies of actin, microtubules and intermediate filaments upon cyclic stretch application. *Cytoskeleton* 75, 385–394. doi:10.1002/cm.21470

Frontiers in Physiology

Understanding how an organism's components work together to maintain a healthy state

The second most-cited physiology journal, promoting a multidisciplinary approach to the physiology of living systems - from the subcellular and molecular domains to the intact organism and its interaction with the environment.

Discover the latest Research Topics

[See more →](#)

Frontiers

Avenue du Tribunal-Fédéral 34
1005 Lausanne, Switzerland
frontiersin.org

Contact us

+41 (0)21 510 17 00
frontiersin.org/about/contact

